AN ANALYSIS OF BETA CEPHEI STARS IN NGC 3293 AND THE EFFECTS OF STELLAR ROTATION

CA Engelbrecht

AN ANALYSIS OF BETA CEPHEI STARS IN NGC 3293 AND THE EFFECTS OF STELLAR ROTATION

by

Christian Albertus Engelbrecht

Thesis Presented for the Degree of

DOCTOR OF PHILOSOPHY

in the Department of Astronomy

UNIVERSITY OF CAPE TOWN

March 1994

Acknowledgements

Thanks are due to my two supervisors, Dr Luis Balona and Professor Brian Warner, for their continued support and patience while this work was being completed. I would like to thank Luis especially for suggesting the topic of this thesis and for providing insightful corrective criticism at various stages of its development, and Brian for valuable suggestions to improve its content.

Professors Erie Reynhardt and Wynand Verwoerd of the Department of Physics at the University of South Africa deserve sincere thanks for allowing me to test their patience to alarming lengths, while they never failed to provide encouragement and support in numerous forms. The Dean of Science, Professor Casper Schutte, is also thanked for his continued interest and support.

My father and mother sowed the seeds of scientific interest in my mind in various ways, and without their input this would not have been written. I wish to thank all of my parents, biological as well as acquired, for their unwavering encouragement and support, in tangible as well as intangible form, over a far longer period than they had anticipated. Their support was more valuable than they probably realised.

Those who were forced to sacrifice most are my wife Elsabé and our daughters Lezette and Linda. I can never replace the countless lost hours and opportunities devoured by the process of sculpting this thesis. These words displace a portion of their joys and pleasures, yet their encouragement could always be counted on. Whatever worth these pages may hold, I dedicate to them.

Abstract

An intensive photometric study in the Johnson B band of ten β Cephei stars in the open cluster NGC 3293 is presented. High sampling rates of the stars' light curves allow the identification of many formerly unknown pulsation frequencies in these stars, by means of Fourier periodogram analysis. All of the stars are found to be multiperiodic, with up to five frequencies identified for individual stars. Physical parameters of the stars are determined from previous photometric results in the literature. These parameters are used to make a comparison of the observed frequencies with theoretical predictions, including the effects of rotation. The results imply a preference for first and second overtone quadrupole ($\ell = 2$) pulsation in these stars, while a weak relationship between stellar mass and pulsation overtone is identified.

One of the stars is identified as a member of an eclipsing binary system, only the second β Cephei star to be identified as such. Physical parameters of the system are determined.

The effects of rapid rotation (specifically, the distortion of the stellar profile from a perfect sphere) on alternative methods of pulsation mode identification are investigated for a model β Cephei star. Ratios between light and velocity amplitudes show extreme differences between rotationally distorted and undistorted models, but these ratios show high sensitivity to other parameters as well.

Thermally broadened spectral line profiles are calculated for the same model, for modes with $\ell = 0$ to 4 and equatorial rotation velocities up to 400 km/s. Neglect of rotational distortion is shown to lead to underestimation of true equatorial rotation velocities by as much as 25%. This result confirms that observed B stars are probably rotating at break–up velocities.

In summary, various aspects of the behaviour of the β Cephei stars in NGC 3293 in particular, and of β Cephei stars in general, including rapid rotators, are illuminated and augmented by this study.

CONTENTS

CHAPTER 1. INTRODUCTION

1.1 The β Cephei Stars 1
1.2 Motivation for this Study 16
1.3 Outline of Thesis 17

CHAPTER 2. DATA COLLECTION

2.1 Instrumentation 19
2.2 Observing Programme 21

CHAPTER 3. METHODOLOGY OF DATA ANALYSIS

3.1 Log of Observations 27
3.2 Light Curves 28
3.3 Fourier Analysis 29
3.4 Periodogram Analysis 32

CHAPTER 4. FREQUENCIES AND AMPLITUDES OF PULSATIONS OBSERVED IN BETA CEPHEI STARS IN NGC 3293

4.1 Fourier Fitting of Frequencies to Data 39
4.2 Results 39
4.3 The Star 3293–5 44
4.4 The Star 3293–10 49
4.5 The Star 3293–11 54
4.6 The Star 3293–14 59
4.7 The Star 3293–16 63
4.8 The Star 3293–18 69
4.9 The Star 3293–23 74
4.10 The Star 3293–24 80
4.11 The Star 3293–27 85
4.12 The Star 3293–65 90

CHAPTER 5. STELLAR PULSATION THEORY

5.1 Introduction 95
5.2 Differential Equations 95
5.3 Linearisation 96
5.4 Separation into Space and Time Coordinates 97
5.5 Modal Structure of Eigensolutions 98
5.6 Effects of Stellar Rotation 100

CHAPTER 6. IDENTIFICATION OF PULSATION MODES OF β CEPHEI STARS IN NGC 3293

6.1 The Case for Nonradial Pulsations 103
6.2 Comparison of Numerically Calculated Pulsation Frequencies with Observations 104
6.3 Rotational Splitting of Eigenfrequencies 117

CHAPTER 7. CALCULATING GEOMETRICAL EFFECTS ON OBSERVATIONAL CHARACTERISTICS OF RAPIDLY ROTATING BETA CEPHEI STARS

7.1 Introduction 133
7.2 The Light Curve of a Rapidly Rotating β Cephei Star 139
7.3 The Radial Velocity of a Rapidly Rotating β Cephei Star 150
7.4 Transforming to the Observer's Coordinates 153
7.5 Input Paameters for Calculation 156

CHAPTER 8. RELATIVE AMPLITUDES OF MAGNITUDE AND RADIAL VELOCITY VARIATIONS 161

CHAPTER 9. SPECTRAL LINE PROFILES

9.1 Introduction 189
9.2 Calculating Raw Profiles 192
9.3 Broadening the Profiles 193
9.4 Results 195

CHAPTER 10. THE ECLIPSING BINARY SYSTEM CONTAINING 3293–5 229

CHAPTER 11. SUMMARY AND DISCUSSION 237

REFERENCES 243

APPENDIX 1 249

APPENDIX 2 269

APPENDIX 3 325

CHAPTER 1

INTRODUCTION

1.1 THE β CEPHEI STARS

The history of the β Cephei variable stars starts in 1902, when Frost (1902) detected short–period (less than half a day) variability in the radial velocity of the star β Cephei. The following years saw the slow development of a short list of stars displaying similar behaviour: σ Scorpii, β Canis Majoris and 12 Lacertae (Campbell 1908, Selga 1916, Young 1918, Slipher 1904). Variations in observed magnitude (or "light", for short) were found to occur alongside the variations in radial velocity, although lagging by about one quarter–period in phase behind the latter (Struve 1955). Henroteau (1918) announced the discovery of variations in the appearance of the spectral lines themselves, while Meyer (1934) published the important discovery that the variations in β Canis Majoris could be described by a combination of two sine curves with slightly different amplitudes and periods. Interference between the two sine waves gives rise to the so–called **beat phenomenon** which is frequently found among the β Cephei stars: a slow (typically of the order of several days) periodic variation in the amplitude of the total observed variation.

Despite many efforts to add more stars to this list, Otto Struve (acknowledged as the leading researcher on the β Cephei stars in the 1950's) would include only ten stars as definite members of this class in 1955 (Struve 1955). At that time, there were a number of known β Cephei stars with single periods and an approximately equal number with multiple periods. Furthermore, a definite period–luminosity relationship was believed

to exist and the observed variations were attributed to stellar **pulsation**.

Ledoux (1951) introduced the possibility of **non–radial** pulsations (see chapter 5 for an explanation of the terminology associated with stellar pulsation) as an explanation for β Cephei variability, although this topic only started receiving substantial attention from the late 1960's onward. In this landmark paper, Ledoux deduced that the difference between the two frequencies giving rise to the beats of β CMa was too small to be reconciled with radial pulsations of the star. He proposed that the star is pulsating in two **nonradial** modes, the frequencies of which are "separated" due to rotation of the star. Further references to this paper appear below.

Phase differences in the variations in spectral lines for different chemical elements – the so–called **Van Hoof effect** – were established in 1951 (Van Hoof & Struve 1953), and a time lag in the light variations, from the blue to the red part of the visual spectrum, in 1952 (Stebbins & Kron 1954). The rotation velocity of these stars was a subject of discussion and uncertainty for many years, until a wide range of velocities was eventually confirmed. The emerging theory of stellar evolution introduced a new dimension into the study of β Cephei stars, and attention was focussed on their age and structure. Today these stars are known to be relatively young giants of early spectral type (B0.5 – B2). Sterken & Jerzykiewicz (1991) pointed out that there are currently two definitions of a β Cephei star in circulation: Many researchers consider any early B star showing regular light or radial velocity variations with periods of the order of 0.1 to 0.3 days as a β Cephei star. A more stringent definition allows only those early B stars which clearly show the presence of a **radial** pulsation mode (see chapter 5) to be classified as such. The former, broader definition is adopted in this thesis. Since the 1970's, discussion and investigation of the β Cephei stars has predominantly involved the following:

(a) The extent of the supposed β Cephei **instability strip** in the H–R diagram

(b) The **evolutionary state** of the β Cephei stars

(c) The nature of the physical **mechanism** driving the pulsations

(d) The detailed **modes** of pulsation

(e) **Identification** of additional β Cephei variables

The paths leading to the present perspectives on these five aspects are briefly summarised as follows:

1.1.1 The β Cephei Instability Strip and Evolutionary State

(a) and (b) are so closely related that their development has to be treated as a unit: A review by Lesh & Aizenman (1978) placed the instability strip for β Cephei stars squarely on the so–called "S–bend" region of the evolutionary tracks for stars of $7 - 15$ $M_{\odot}$; see figure 1.1, taken from their paper. This implied that these stars could be in one of three possible evolutionary stages: The end of initial core hydrogen–burning; the stage of secondary (ie following the end of core H–burning) gravitational contraction; the start of hydrogen–burning in a shell surrounding the core. Various arguments by Percy (1981) suggested that the first of these alternatives was to be preferred, actually including the whole phase from shortly after leaving the main sequence until close to the end of core H–burning. Balona & Engelbrecht (1983) clearly identified the ten β Cephei stars in the open cluster NGC 3293 as positioned in the late stages of core H–burning, by comparison with other cluster members (see figure 1.2, taken from their paper). A significant discovery was the detection of six β Cephei stars in the open cluster NGC 6231, by Shobbrook (1979), Balona (1983) and Balona & Engelbrecht (1985), all of which were clearly placed very close to the main sequence, at a significantly earlier age than any other β Cephei stars identified so far. This seemed to identify the β Cephei stars as core H–burners without any doubt. Further H–R diagrams for the class were

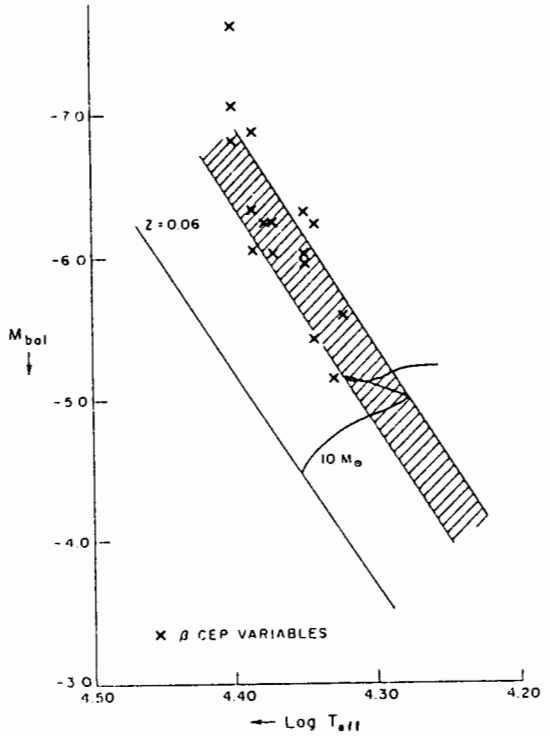

Figure 2 Location of the β Cephei stars in the theoretical HR diagram. The zero-age main sequence for a composition of ($X = 0.69$, $Y = 0.25$, $Z = 0.06$) and the evolutionary track for a 10 $M_\odot$ model are shown. The hatched area is the region traversed three times by a star in the course of its early post-main sequence evolution. After Lesh & Aizenman (1973a).

Figure 1.1. From Lesh & Aizenman (1978)

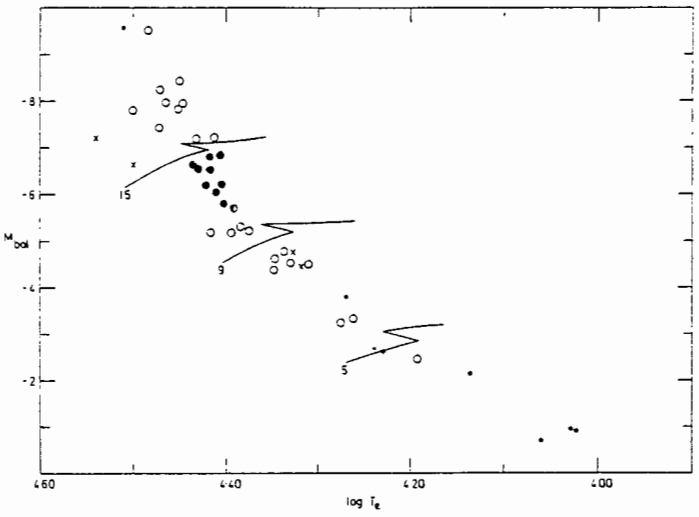

Figure 1. The theoretical H–R diagram for stars in NGC 3293. The evolutionary tracks are labelled according to stellar mass in solar units. Filled circles: β Cep variables, crosses: other variables, open circles: constant stars, small symbols: stars not monitored for variability.

Figure 1.2. From Balona & Engelbrecht (1983)

published by Shobbrook (1985), displaying 47 β Cephei stars, and by Sterken & Jerzykiewicz (1990), showing 49 stars in a diagram based on Strömgren photometry. However, Sterken & Jerzykiewicz argued that the strong propensity for cluster β Cephei stars to be found in the core H–burning phase did not exclude the possibility, at least, that some of the **field** β Cephei stars are in a phase after core hydrogen exhaustion. Chapellier's (1985) study of the rates of change of the pulsation periods observed in β Cephei stars also indicated an evolutionary age near the end of core H–burning. Shobbrook (1985) pointed out that stars which appear to lie at higher luminosities than the luminosity defined by the bulk of the instability strip could simply be unresolved **binaries**, a conclusion which would again favour an evolutionary age younger than the end of core H–burning.

The apparent resolution of the puzzle surrounding the **physical cause** of β Cephei variability (extensively discussed in section 1.1.2 below) has finally provided clear grounds for the existence of the observed β Cephei instability strip, occurring within sharply defined ranges of stellar luminosity and temperature. Specifically, the instability strip can now be defined on the basis of **theoretical** understanding, as against the phenomenological definition, based purely on **observation**, which existed up to 1990. Dziembowski & Pamyatnykh (1993) found that theoretically determined areas of pulsational instability occurred either predominantly in the entire "S–bend" region menitoned above, for solar values of stellar metallicity, or predominantly in the initial post main–sequence evolution (while H–burning in the core is still taking place) for higher metallicities. Gautschy & Saio (1993) obtained similar results. Briefly stated, the β Cephei instability strip is constrained by the necessity that the region of highest heavy–element opacity within a star occurs at a position which enables it to drive sustained eigenmodes of pulsation for the star, and that these modes should be sufficiently active at the stellar surface that they will be observable.

1.1.2 The Driving Mechanism behind β Cephei Pulsations

Many papers on the driving mechanism behind the pulsations have appeared in the last twenty–odd years. Reviews can be found in Percy (1981), Osaki (1982), Cox (1987) and Cox et al. (1992). Vibrational instability analyses for radial as well as nonradial pulsation modes (Davey 1973, Osaki 1975) indicated that small random perturbations in models of β Cephei stars were not amplified to form sustained pulsations. These findings were obviously in conflict with observation, and possible mechanisms for exciting the observed pulsations were keenly sought, both in the stellar envelope and in the deep interior. Osaki (1982) argued that the increasing area in the H–R diagram in which variables were at that stage being found supported an **envelope** mechanism, since the stellar structure in the envelope is not as sensitive to variations in temperature and luminosity as that in the interior. Among envelope mechanisms, the "opacity bump" mechanism introduced by Stellingwerf (1978, 1979), involving the second ionization of helium, was hailed as the most promising, but still fell short of driving the pulsations on its own (Lee and Osaki 1982). Among the deep **interior** mechanisms, nuclear energy generation, so–called "wave trapping" due to the μ–gradient zone in the deep interior, and a mechanism linked to semi–convection were all tried, but without success (Osaki 1975, Shibahashi and Osaki 1976). In the light of these failures, a few unusual driving mechanisms were also proposed. Cox (1981) invoked a "jolt" mechanism in which repeated structural adjustments, linked to changes in the energy generation process, took place. Osaki (1974) suggested that a rapidly spinning convective core could excite nonradial pulsations through resonant coupling. Ando (1981) investigated Kelvin–Helmholtz instability in a differentially rotating star. These mechanisms were all based on ad–hoc assumptions which were difficult to defend.

The necessary breakthrough gently materialised around 1990. The relatively sharp

definition of an instability strip for the β Cephei stars, as discussed above, was noted by Waelkens et al. (1991) as a strong argument in favour of some sort of **opacity mechanism** causing pulsations in these stars, similar to the situation obtaining in classical Cepheids and Mira variables. The nearly successful attempt by Stellingwerf at pinpointing such a mechanism has been discussed above. A revision of calculated opacities in stellar material at temperatures of 10^5 to 10^6 K was prompted by suggestions from Simon (1982). Such calculations were performed by Iglesias et al. (1987, 1990), indicating that the opacity due to **iron** had been greatly underestimated in previous calculations. Taking the more accurate opacities into account solved the 30–year puzzle of the β Cephei pulsations at a stroke. Cox & Morgan (1990) appear to have presented the first discussion of the implications of these exciting results for the β Cephei stars, followed by a flurry of papers following suit. Waelkens et al. (1991) were quick to point out that the extreme sensitivity of the opacity on the **iron abundance** implies that β Cephei variability should be very closely correlated with a star's **metal content**. A search for β Cephei stars in the Large Magellanic Cloud was an immediate response, since the low metallicity typical of the LMC would test this scenario very effectively. The discovery of β Cephei stars with low metallicity would invalidate this newly proposed opacity mechanism at once. Searches of the LMC were conducted by Sterken & Jerzykiewicz (1988) and Balona (1992, 1993), with no β Cephei stars being found. Waelkens & Cuypers (1985) linked the anomalous (earlier than normal) evolutionary age of the β Cephei stars in NGC 6231, mentioned earlier in this discussion, to the possible higher metallicity of the cluster resulting from to its relative proximity to the Galactic centre. Waelkens et al.'s (1991) study of the newly identified probable β Cephei star HD 166540, including an analysis of other β Cephei stars towards the Galactic centre (GC), appears to substantiate this argument, finding clear evidence of a blueward shift of the instability strip for stars closer to the GC.

Interestingly, Delgado & Alfaro (1990) appear to some extent to have pre–empted these conclusions by arguing that the β Cephei instability strip for any particular open cluster is determined by the chemical composition of the cluster. They even derived a numerical relationship between metallicity, and position of the β Cephei instability strip in a Strömgren $\beta/(u–b)_0$ diagram:

$$[Fe/H] = 0.003 + 7.374\Delta(u–b)_0 - 5.415[\Delta(u–b)_0]^2$$

(1.1)

where $\Delta(u–b)_0$ describes the shift of the β Cephei instability strip relative to the classical strip, as determined by β Cephei stars in the solar neighbourhood. They finally proposed that this relationship could be used to infer the metallicity of a cluster from observation of sufficient numbers of β Cephei stars in it.

Returning to recent papers on the opacity issue, Cox et al. (1992) did a detailed study of the specific mechanism by which the opacity gradient brings about sustained pulsation. For the sophisticated $12M_\odot$ model star they used, sustainable pulsations (henceforth termed **instability**) were only obtained in the very last stages of core hydrogen–burning (when the abundance $X_{core} = 0.047$), assuming a (solar) metallicity of $Z = 0.02$. However, they pointed out that the iron content in the critical region could be enhanced by levitation from deeper layers. The shearing forces arising from nonradial pulsation would eventually mix the enhanced iron back into the surrounding layers of the star, the combination of these two effects resulting in β Cephei pulsations "switching on and off" in a star, reminiscent of the observed demise of β Cephei pulsations in α Vir and β CMa, and the initiation of β Cephei variation in 27 CMa (Balona & Rozowsky 1991).

Addressing the observed characteristics of β Cephei stars in open clusters, Cox et al.

stated that increased metallicity could allow the opacity mechanism to maintain pulsations within a larger region within a star, and consequently at an earlier evolutionary age of the star, as witnessed in NGC 6231, for instance.

In a practically simultaneous paper, Kiriakidis et al. (1992) performed a study of a $15M_{\odot}$ model star, with Z = 0.02 and 0.03 respectively. Figure 1.3, taken from their paper, clearly illustrates the change in opacity calculations, including the strong correlation with metallicity. In contrast with Cox et al., these authors found that the new opacities were still not sufficient to drive pulsations when Z = 0.02. Only the higher metallicity of Z = 0.03 rendered the model pulsationally unstable. Kiriakidis et al. claimed that their method provided more accurate results than that of Cox et al..

The next analysis, of a $12M_{\odot}$ model with Z = 0.03 and Z = 0.04 respectively, was done by Moskalik & Dziembowski (1992). Their results also suggested that a metallicity not much lower than Z = 0.03 was required for pulsational instability. This paper was followed up by Dziembowski & Pamyatnykh (1993) with a study of instability in the mass range $7 - 16\ M_{\odot}$, for values of the spherical harmonic degree ℓ from 0 to 8 (see chapter 5). Using the very latest improvements to the opacity tables of Iglesias et al. (1992), these authors found that instability did occur in a model β Cephei star at a metallicity of Z = 0.02. They concluded by indicating that the next question to be addressed was why only some, and not all, of the modes found to be unstable are actually observed in real β Cephei stars.

Finally, Gautschy & Saio (1993) performed their stability analyses on a range of stellar models from $5.2M_{\odot}$ to $12.1M_{\odot}$, all with Z = 0.03 and using the latest improved iron opacities. They found a temperature dependence in agreement with Dziembowski & Pamyatnykh (above), where modes with longer periods became excited towards lower

temperatures. They also found a theoretical instability strip significantly broader than the observationally defined strip, suggesting that the theoretical understanding of the opacity mechanism still needs further refinement.

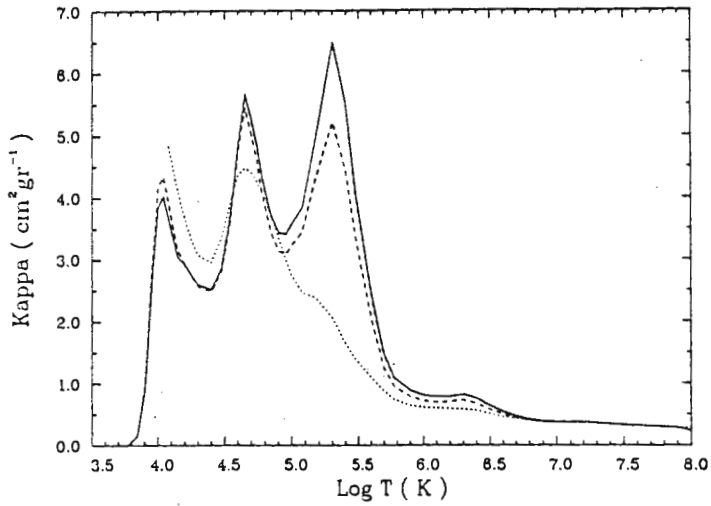

Figure 1. Rosseland mean opacities versus temperature for log $R = -4$ with $R = \rho/T_6^3$ (ρ is the density, T_6 the temperature in units of 10^6 K). For a solar mixture with $(X, Y, Z) = (0.70, 0.28, 0.02)$ (Anders & Grevesse 1989), LAOL and OPAL opacities are represented by the dotted and dashed line, respectively. OPAL opacities for the composition $(X, Y, Z) = (0.67, 0.30, 0.03)$ are given by the full line.

Figure 1.3. From Kiriakidis et al. (1992)

(LAOL refers to old opacities; OPAL to new opacities)

1.1.3 Identification of Pulsation Modes in β Cephei Stars

A review of pulsation mode identifications appeared in Lesh (1981). Three major approaches have been followed in this regard:

- comparison of **theoretically** expected pulsation frequencies with those actually **observed**
- the **ratios** of observed **amplitudes** of **magnitude** variations in ultraviolet and visible wavelengths respectively, combined with the ratios of amplitudes of variations in specific wavelengths and amplitudes of **radial velocity** variations
- analyses of the variations in the **profiles** of spectral lines

The first method outlined above can primarily be used to determine the **overtone** (or order) of a pulsation mode. The second method can primarily be used to distinguish between radial and nonradial modes, while the third method allows the identification of both the spherical harmonic degree (signified by the index ℓ) and the azimuthal index (m in the standard Legendre polynomial notation).

Initial results of the first approach suggested first overtone pulsations of pressure modes (radial or nonradial) as the most probable among the β Cephei stars, with fundamental or second overtone modes as secondary possibilities (Lesh and Aizenman 1974, Jones and Shobbrook 1974, Balona and Feast 1975). Lesh & Aizenman (1978), however, concluded that radial **second** overtone, together with nonradial second overtone modes with $\ell = 2$ were dominant, allowing first overtone modes as a possibility for some stars. Shobbrook (1985), using highly accurate Strömgren photometry, coupled with statistical arguments, also recognised the radial first overtone as the dominant pulsation in the β Cephei stars, acknowledging the presence of radial fundamental and higher overtone modes in some stars.

The second approach was employed by Stamford & Watson (1977, 1979), who concluded that the comparison of light and colour variations (ie comparison of the amplitudes of variations in the Johnson V band (A_V) and the amplitudes of variations in the differential between Johnson U and B bands), was more useful as a mode discriminant than ratios of radial velocity amplitude (A_{rv}) to A_V. Their results indicated that certain β Cephei stars are radial pulsators while others are low–order nonradial pulsators. Balona & Stobie (1979b) calculated A_{rv}/A_V for 17 modes occurring in 13 β Cephei stars. They also required ratios of light and colour variations, the observed values of which seemed to point towards radial pulsation in about half of the stars. The method requires accurate and simultaneous measurements of the radial velocity and the

magnitude in various wavelengths, however, and has not been widely used.

Watson (1988) published an extensive investigation which included **phase** differences between light and colour variations as well, following earlier work in this regard by Balona & Stobie (1980). Application of his results to 19 β Cephei stars again split these stars fairly evenly into radial and nonradial $\ell = 2$ pulsators respectively. His mode identifications for specific β Cephei stars were totally consistent with identifications made by Campos & Smith (1980), using line profile variations (see below).

Recently, Heynderickx (1991) compared light amplitudes in various bands of the Walraven photometric system to determine the spherical harmonic degree ℓ of pulsations in 29 β Cephei stars. Of the 49 modes analysed, 17 were identified as radial ($\ell = 0$) modes, 11 as ($\ell = 1$) modes, 15 as ($\ell = 2$) modes and 6 as ($\ell = 4$) modes, with 17 of the 29 stars showing at least one radial mode.

The third approach has received the most attention in recent years. Osaki (1971) pioneered the more recent interest in this method. Following up Ledoux's (1951) investigation of the nonradial quadrupole ($\ell = 2$) mode, he concluded that stars showing significant variations in spectral line broadening could be favourably regarded as pulsating in this mode, with $m = -1$ or -2. Kubiak (1978) analysed radial velocity curves and line profile changes for modes with values of ℓ from 1 to 4, excepting the $(\ell,m) = (2,-2)$ mode considered by Osaki. His conclusion was that the behaviour of β Cephei stars classically regarded as radial pulsators could also be understood as the result of pulsation in nonradial modes of low degree ($\ell = 1$ or 2) with $m = 0$. Work by Jerzykiewicz (1978) and Campos and Smith (1980) also favoured a quadrupole mode for those stars which have been identified as nonradial pulsators.

A few mode identifications by this method have been attempted for specific β Cephei stars. Gies & Kullavanijaya (1988) identified modes with m = –3, –4, –5 and –6 in ϵ Per, probably indicating $\ell = 3$ to 6. Borisova et al. (1991) identified modes with $\ell = 2$ and $\ell = 6$ in 19 Mon, and Aerts et al. (1992), using Balona's moment method (Balona 1986*a*, 1986*b*, 1987), identified δ Cet as a radial pulsator. Most published work has concentrated on compilations of **predicted** line profiles for various nonradial pulsation modes, however. Examples are to be found in Kambe & Osaki (1988) ($\ell = 5$, 6, 7 and 8), Lee & Saio (1990) ($\ell = 5$ & 9), Lee at al. (1992) ($\ell = 8$), Cugier (1993) ($\ell = 0$) and Aerts & Waelkens (1993) ($\ell = 2$, 3, 4 and 8).

These findings may be compared to the identity of the specific modes predicted to be unstable by the stability calculations discussed in section 1.1.2 above:

Cox et al. (1992), using the new iron opacities, found instability for g–modes of low order (ie overtone) and low degree (spherical harmonic index ℓ). Specifically, they found instability for modes with $\ell = 0$ to 8. The periods of unstable modes clustered around a value of 0.3 days. In particular, they found that for each value of ℓ showing instability, there was a mode with a period close to the radial fundamental pulsation period, suggesting that those β Cephei stars displaying three closely spaced frequencies could well be pulsating in modes with $\ell = 0$, 1, and 2 respectively. They predicted that modes with higher ℓ would become unstable in stars with higher metallicity. Cox et al. concluded that the β Cephei variables are pulsating in radial fundamental and nonradial gravity modes (or g –modes for short), in contrast to the observation–based opinion in favour of radial first overtone pulsation and nonradial pressure modes (or p –modes). This concluded preference for g–modes over p–modes followed mainly from the greater depth in the star of the driving region indicated by the new opacity mechanism.

Kiriakidis et al.'s (1992) treatment of the new opacities predicted instability for the radial fundamental mode and nonradial p_1–mode, including values of ℓ from 0 to at least 4. In agreement with Cox et al., they found that the eigenfrequencies for the various unstable modes were all very similar. They favoured the possibility that the g–modes could also be unstable, but differed from Cox et al. in predicting that the p_1–mode would be much stronger, attributing this discrepancy to deficiencies in Cox et al.'s approach.

Moskalik & Dziembowski (1992) likewise determined that the radial fundamental mode was unstable, with no instability for any radial overtones. Their analysis did not include nonradial modes. Dziembowski & Pamyatnykh (1993), using the very latest improvements to the opacity tables of Iglesias et al. (1992), found sustained pulsation not only for the radial fundamental mode, but for the first two radial overtones as well, in contrast with the three papers mentioned immediately above. They also found sustainable pulsations for modes with ℓ from 1 to 8, for both g–modes and p–modes. Specifically, they found that different modes became unstable at different stellar effective temperatures. In addition, they noted that higher overtones became unstable as the stellar mass (or luminosity) increased. For low values of ℓ, the unstable modes were of low order, with high overtones of the g–modes starting to appear at $\ell = 6$.

Gautschy & Saio (1993) also found instability for the radial fundamental as well as the first two overtones, and, for $\ell = 2$ specifically, instability for only the p_1 and p_2–modes during the evolution of the star towards the end of core H–burning. At the cooler temperatures after the end of this stage, the p–modes were found to stabilize, with the g–modes then becoming unstable, although they argued that even these modes should strictly be regarded as p–modes, due to the so–called "avoided crossing" phenomenon in the modal eigenfrequency spectrum.

Finally, a few studies of β Cephei stars which are members of **binary** systems have led to pulsation mode identifications. One such example is discussed in chapter 10 of this thesis, favouring either the radial first and second overtones, or two pulsations with $(\ell,m) = (2,+2)$ and $(2,-2)$ respectively. Chapellier & Valtier (1992) concluded that the binary σ Sco is a nonradially pulsating star.

Summarising briefly, the very latest improvements to the recalculated opacities point toward a rich spectrum of unstable pulsation modes in the β Cephei stars, including at least the first three radial eigenmodes and nonradial pressure modes, increasing in number with higher degree ℓ. The discussion of identifications of actually observed pulsation modes in β Cephei stars, presented above, appears to suggest a mix of radial and low–degree nonradial modes, mostly in the first overtone.

1.1.4 Identifying β Cephei stars

Specific searches for β Cephei stars were conducted by Hill (1967), Percy (1970, 1971), Percy & Madore (1972), Percy & Lane (1977), Balona (1977), Jerzykiewicz & Sterken (1977) and Jerzykiewicz (1993). These searches, together with serendipitous discoveries, have allowed confident identifications of β Cephei stars to have risen in number, from Struve's 10 in 1955, to 21 in the mid–seventies (Lesh & Aizenman 1978) to 57 at the start of the nineties (Sterken & Jerzykiewicz 1990). A recent discovery, which is interesting in the light of previous opinion that the β Cephei stars and the Be stars were mutually exclusive classes, is the identification of 27 CMa as a β Cephei star by Balona & Rozowsky (1991). Further improvements in photoelectric detectors, coupled with continued search campaigns, should lead to the discovery of many more of these potentially important stars.

1.2 MOTIVATION FOR THIS STUDY

The study of β Cephei stars in general is motivated by the many important roles they may potentially play in the future development of astrophysics. Their high intrinsic brightness and apparent sensitivity to metallicity suggest their use as probes of distances to, and chemical compositions of, both nearby and distant stellar systems. In addition, their apparently rich structure of pulsation modes set them up as potential testbeds for stellar evolution theory. Although the problem of identifying the physical mechanism responsible for pulsation finally appears to have been solved, much still remains to be learned about the properties of the pulsations as such. In the context of the currently emerging research field of asteroseismology, the precise determination of the full spectrum of pulsation modes obtaining in these stars will allow penetrating insights into their detailed interior structure. As stated by Sterken & Jerzykiewicz (1990), the accurate knowledge of pulsation modes of β Cephei stars is a prerequisite for successfully addressing the questions surrounding the mechanism of pulsation mode **selection** and the processes limiting the **amplitudes** of pulsation. The intensive photometry conducted on the stars in NGC 3293 in particular, as described in the chapters to follow, has allowed some progress to be made towards these goals.

The study of β Cephei stars in **open clusters** specifically could make a potentially very valuable contribution to a more accurate understanding of these stars, for two reasons. More meaningful **comparisons** between stars are possible because of the homogeneity in composition and age of members of a single cluster, and a more accurate determination of their **physical parameters** is possible as a result of the more precisely known **distance** which can be assigned to clusters than to individual distant stars. Hill (1967), Balona (1977), Jakate (1978), Shobbrook (1979), Delgado et al. (1984, 1992) and Alfaro et al. (1985) have applied themselves to this task in recent decades, and the investigations

presented in this thesis extend this work.

A prominent subject of research in recent years has been the development of more efficient **methods** of determining the modal content of a star's pulsations from its observed behaviour. Various approaches to this problem are also pursued in this study, hopefully shedding light on the more productive paths to follow in future.

1.3 OUTLINE OF THESIS

I now turn to a more sharply focussed summary of this thesis. Among those open clusters known to contain β Cephei stars, NGC 3293 has displayed the greatest number. A total of ten of these variables has been found in this cluster by Balona and Engelbrecht (Balona 1977, Balona & Engelbrecht 1981, Balona & Engelbrecht 1983), and a detailed study of their characteristics is presented in the following chapters. The following matters in particular are addressed:

(a) The precise **periods** and **amplitudes** of the pulsations

(b) The specific **modes** in which these stars are pulsating

(c) The effect of **stellar rotation** on observations of the pulsations of β Cephei stars in general

(d) The merits of various **methods** of pulsation mode identification

After a description of the instrumentation and methods used to obtain the observational data, the observational results are presented. An analysis of the periods appearing in the data is followed by an application of the theory of nonradial pulsation and of stellar rotation to the stars being studied. Their general characteristics (mass, radius, etc.) are also discussed.

A detailed attempt at identifying the modes obtaining in the β Cephei stars in NGC 3293, through pulsation period analysis, leads on to an investigation into the implications of rapid rotation on observable characteristics of β Cephei stars in general. An eclipsing binary found among the ten variables in NGC 3293 is discussed in a separate chapter, and finally the implications of this investigation are summarized.

CHAPTER 2

DATA COLLECTION

2.1 INSTRUMENTATION

2.1.1 Telescopes

The 0.5 m, 0.75 m and 1.0 m Cassegrain reflectors at the Sutherland observing station of the South African Astronomical Observatory were used to obtain the basic observational data, consisting of photometric integrations for previously identified β Cephei stars in the open cluster NGC 3293.

2.1.2 Equipment

All three telescopes were connected to EMI photomultipliers with S13 cathodes. Observations were made through Johnson B filters, as well as apertures of the following sizes for the respective telescopes:

(a) 0.5 m : 23 arc seconds.

(b) 0.75 m : 23 arc seconds.

(c) 1.0 m : 16 and 21 arc seconds, depending on the seeing.

The choice of aperture size was a compromise between the need to prevent loss of starlight outside the aperture on nights of relatively bad seeing and the need to exclude neighbouring stars from the aperture. Due to the proximity of the stars to each other and the fact that differential photometry was being performed using constant stars

within the cluster, no correction of the natural B magnitudes to the standard Johnson system was necessary.

2.1.3 Data collection

In each instance, the signal from the photomultiplier was amplified by a SSR amplifier and sent to a Data General Nova mini computer which calculated a magnitude m_B according to the following formula:

$$m_B = -2{,}5log(N) - E \cdot A - Z \qquad (2.1)$$

where N = counts per second for star, minus counts per second for sky,

E = extinction coefficient of the B filter,

A = air mass at the time of integration,

and Z = zero point correction (arbitrary in this case, since only **variations** are of interest).

The number of counts obtained per second was corrected for the finite detection time of the cathode in the photomultiplier by applying a so–called **dead–time correction** in the following manner:

$$N_{\text{true}} = N_{\text{observed}} \cdot (1 - D \cdot N_{\text{observed}})^{-1} \qquad (2.2)$$

where N = number of counts per second

and D = dead–time coefficient (typically 55 nanoseconds).

The values of the extinction coefficient used on different nights are given in Table 2.1.

Table 2.1

Data reduction parameters on different nights

Date	E	Telescope
1–3 March 1983	0.27	1.0 m
4–6 March 1983	0.32	1.0 m
19 March 1983	0.30	0.75 m
20–21 March 1983	0.32	0.75 m
22–24 March 1983	0.32	1.0 m
25–26 March 1983	0.29	1.0 m
28 March 1983	0.29	1.0 m
10–12 May 1983	0.27	0.5 m
14–20 Feb 1984	0.27	1.0 m
13–16 March 1984	0.27	1.0 m
19 March 1984	0.27	1.0 m
10–14 April 1984	0.27	1.0 m
16–20 April 1984	0.27	1.0 m
22 April 1984	0.27	1.0 m

2.2 OBSERVING PROGRAMME

The ten β Cephei stars in the open cluster NGC 3293 (see section 1.3) were observed in two seasons: five stars in 1983 and the other five in 1984. With a few exceptions, an observation of a constant comparison star was sandwiched between observations of the variables, to ensure that changes in extinction and sky brightness would be followed accurately.

When the relative positions of stars was such that an undue amount of time would be lost in maintaining this observing procedure, two or three variables were observed in a row before turning to a comparison star again. The longest interval between observations of comparison stars was about 8 minutes, and generally the interval was 2 to 4 minutes in length. These intervals were short enough to keep track of any changes in extinction and sky brightness. Each observation consisted of two succesive integrations of 25 seconds (1983) or 20 seconds (1984) each, with an integration of the sky brightness at least every 15 minutes, depending on the rate at which the motion of the moon caused it to change. Since the variables and comparison stars were all quite bright (faintest $m_V = 10.2$), small changes in the sky background could be ignored.

The comparison stars were chosen to satisfy the following criteria:

(a) They had to be bright, with no close companion stars visible.
(b) Previous observations of these stars on at least two full nights were required to confirm their constancy.
(c) They had to be as close as possible to the variables being studied.

Table 2.2 contains details of the variables and comparison stars observed in the two seasons. The numbering system of Feast (1958), supplemented by Turner et al.(1980), is used throughout this thesis. When referring to a particular star, eg star no 5 as named by Feast, the notation 3293–5 will be used. In table 2.2, however, only the suffix number is indicated.

Table 2.2

Details of observing seasons

Variables: 5, 14, 18, 24, 27

Comparisons: 7, 13, 20

Date	Telescope
1 – 8 March 1983	1.0 m
15–22 March 1983	0.75 m
22–29 March 1983	1.0 m
10–17 May 1983	0.5 m

Variables: 10, 11, 16, 23, 65

Comparisons: 2*, 7, 13, 20, 22

Date	Telescope
14–21 Febr. 1984	1.0 m
13–20 March 1984	1.0 m
10–24 April 1984	1.0 m

* Despite fulfilling requirement (b) on the previous page, 3293–2 showed variations with a period of about one day. After this was discovered, 3293–7 was substituted as a comparison star, while 3293–2 was observed for the rest of the season as a matter of interest.

A chart of the cluster NGC 3293 appears in Figure 2.1. Stars 3293–2 & 3293–11 only appear in Figure 2.1(b). A typical example of the original form of the collected data is

shown in Table 2.3, which covers one cycle of stars. The first two lines of each block show the star's name and equatorial coordinates, the next two the starting time of the photometer integration, length of the integration, three control numbers and a photon count number. The observation of 3293–20 includes a sky observation. The final line of a block contains the fractional heliocentric Julian date, the air mass and the B magnitude, with its uncertainty due to photon shot noise, calculated as follows:

If N = counts obtained in a length of time T, the photon–statistical uncertainty in N is given by:

$$N = (N + nT/t)^{1/2} \tag{2.3}$$

where n = counts of the sky background obtained in a length of time t.

In magnitudes, the uncertainty is given by (Balona et al. 1979):

$$\Delta B = 1{,}1\ \Delta N/N. \tag{2.4}$$

On a typical night of eight hours' observing, about 30 observations were obtained for each variable star. The following chapters describe the analysis of the collected data.

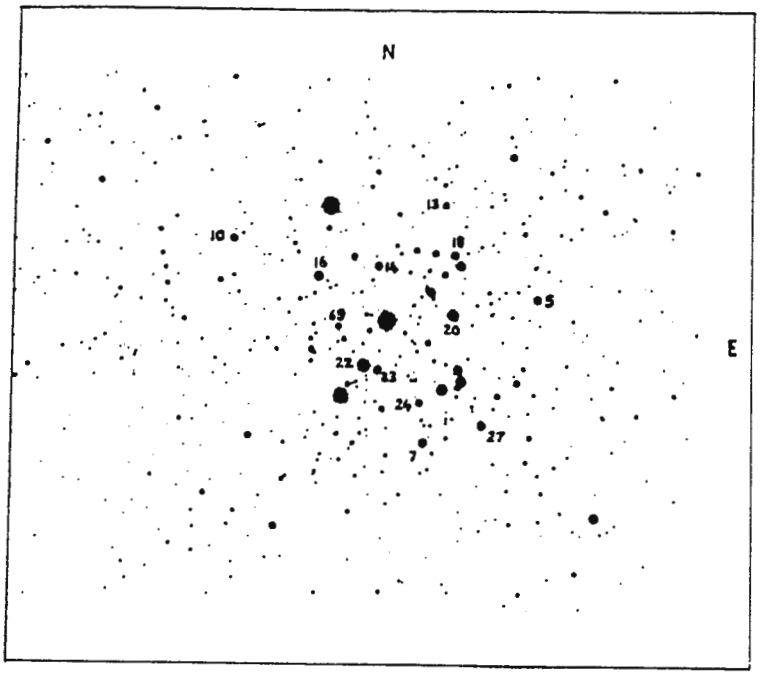

Figure 2.1 (a): Identification of β Cephei stars and standard stars in NGC 3293

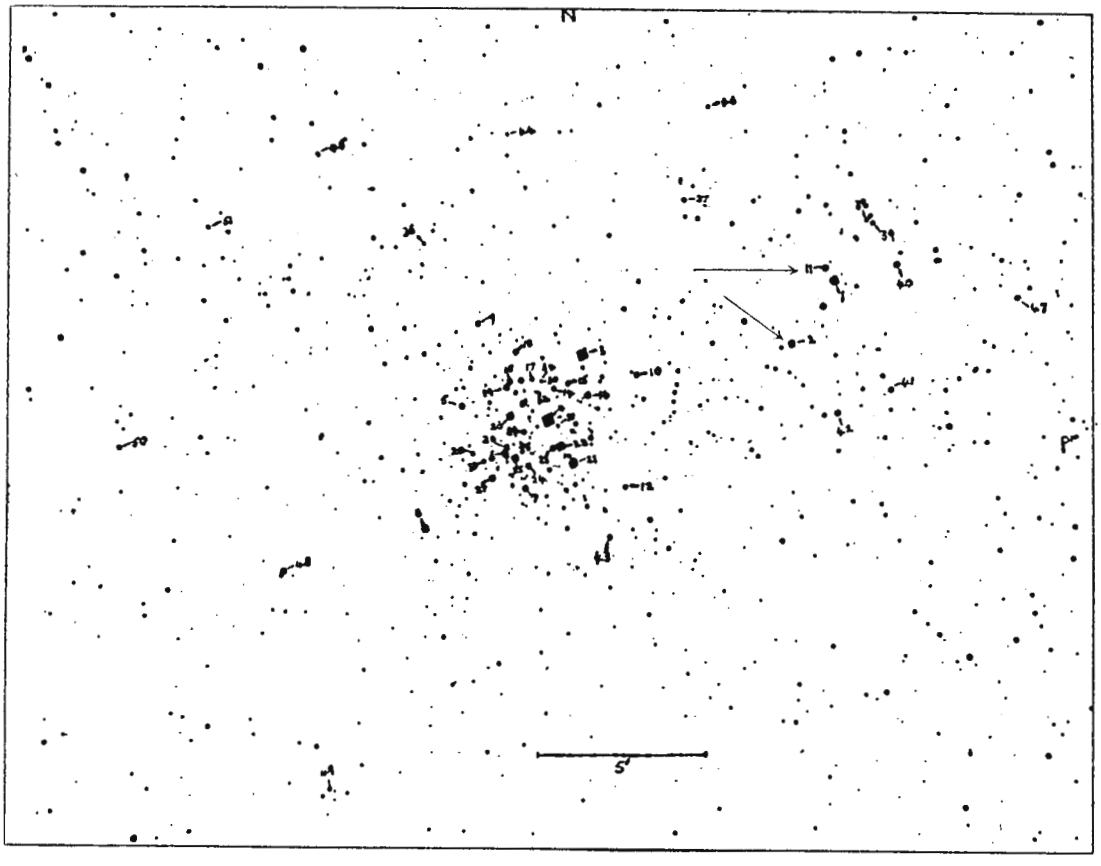

Figure 2.1 (b): As for (a), but on a larger scale, to include 3293–2 & 3293–11 (arrowed)

Table 2.3

Example of raw data table

```
+3293N11
   +1035.1   -5808.0
202041 20 1 12 1   776117
202101 20 2 12 1   777765
+.26751 +1.1215 :   +9.236 +.001 [01]

+3293N2
   +1035.1   -5808.0
202153 20 1 12 1  1226397
202213 20 2 12 1  1222184
+.26834 +1.1209 :   +8.736 +.001 [01]

+3293N10
   +1035.1   -5808.0
202339 20 1 12 1   902610
202359 20 2 12 1   900071
+.26957 +1.1201 :   +9.073 +.001 [01]

+3293N13
   +1035.1   -5808.0
202515 20 1 12 1   546026
202535 20 2 12 1   544103
+.27068 +1.1194 :   +9.628 +.001 [01]

+3293N16
   +1035.1   -5808.0
202642 20 1 12 1  1964058
202702 20 2 12 1  1965040
+.27169 +1.1187 :   +8.217 +.001 [01]

+3293N20
   +1035.1   -5808.0
202758 20 1 12 1  3662946
202818 20 2 12 1  3651463
202856 10 3 12 0     4953
202906 10 4 12 0     5032
+.27257 +1.1182 :   +7.535 +.001 [01]

+3293N65
   +1035.1   -5808.0
203003 20 1 12 1   691151
203023 20 2 12 1   694369
+.27401 +1.1173 :   +9.363 +.001 [01]

+3293N22
   +1035.1   -5808.0
203130 20 1 12 1  4897380
203150 20 2 12 1  4901551
+.27502 +1.1168 :   +7.213 +.001 [01]

+3293N23
   +1035.1   -5808.0
203227 20 1 12 1  1236296
203247 20 2 12 1  1235752
+.27568 +1.1164 :   +8.726 +.001 [01]

+3293N7
   +1035.1   -5808.0
203331 20 1 12 1  2136144
203351 20 2 12 1  2137469
+.27642 +1.1160 :   +8.126 +.001 [01]
```

CHAPTER 3

METHODOLOGY OF DATA ANALYSIS

3.1 LOG OF OBSERVATIONS

A log of the observations obtained of the β Cephei stars in NGC 3293 appears in Table 3.1. The columns respectively show the date of each week–long observing run, Heliocentric Julian Dates for the epoch 2440000 on which observations were obtained, the average number of observations of each star on the night, the average number of hours of observation, the standard deviation (in magnitude) of a single observation on the night and the telescope used.

Table 3.1

Log of observations

Variable stars: 5, 14, 18, 24, 27
Standard stars: 7, 13, 20

Date	HJD	N	Hrs	σ(mag)	Telescope
1 – 8 Mar 1983	5397	22	5.9	0.003	1.0 m
	5398	18	6.3	0.004	
	5399	22	8.1	0.003	
	5400	33	8.7	0.004	
15–22 Mar 1983	5413	23	8.0	0.002	0.75 m
	5414	4	0.9	0.002	
	5415	23	7.9	0.002	
22–29 Mar 1983	5416	26	7.5	0.002	1.0 m
	5417	24	6.4	0.002	
	5418	22	7.8	0.004	
	5419	27	8.0	0.004	
	5420	24	8.1	0.002	
	5422	28	7.8	0.002	
10–17 May 1983	5465	13	3.8	0.002	0.5 m
	5466	20	5.1	0.002	
	5467	23	5.5	0.003	
Total	16	352	106		

Table 3.1 (continued)

Variable stars: 10, 11, 16, 23, 65
Standard stars: 7, 13, 20, 22

Date	HJD	N	Hrs	σ(mag)	Telescope
14–21 Feb 1984	5745	20	6.8	0.003	1.0 m
	5746	23	7.4	0.003	
	5747	27	7.0	0.002	
	5748	28	7.7	0.003	
	5749	17	5.2	0.003	
	5750	12	3.1	0.002	
	5751	17	5.3	0.002	
13–20 Mar 1984	5773	29	8.6	0.004	1.0 m
	5774	30	8.1	0.003	
	5775	32	8.4	0.003	
	5776	32	8.4	0.004	
	5779	20	7.9	0.006	
10–24 Apr 1984	5801	19	6.2	0.002	1.0 m
	5802	24	6.6	0.002	
	5803	26	7.1	0.003	
	5804	17	4.6	0.002	
	5805	26	7.0	0.002	
	5807	21	5.7	0.003	
	5808	24	7.0	0.003	
	5809	25	6.4	0.002	
	5810	25	6.3	0.002	
	5811	24	6.6	0.003	
	5813	9	2.3	0.003	
Total	23	527	150		

3.2 LIGHT CURVES

The magnitudes obtained during each night were used to draw light curves for each star. Transparency curves for each night were obtained from the standard stars' light curves, by doing a linear interpolation for each successive set of four points in the curves and then computing the average curve for the standard stars. Light curves for all stars observed on a particular night were corrected for changes in atmospheric extinction by subtraction of the relevant transparency curve.

Although four standard stars were observed on each night, data for only two of them were used to compile the transparency curves, since the data for the other standards showed considerably more noise than the data for these two. The two standards used were 3293–20 and 3293–7.

The light curves for the β Cephei stars in NGC 3293 are shown in Appendix 1, as they appear after being corrected for extinction. During the analysis of data for 3293–5, it became clear that certain sharp changes in the light curves of this star were not due to short–period pulsation, and the possibility that an eclipsing companion to the β Cephei star might be present was investigated. This suspicion was confirmed, and a detailed discussion of the binary nature of 3293–5 appears in chapter 10.

3.3 FOURIER ANALYSIS

A discrete Fourier analysis method for unequally–spaced data, based on the work of Deeming (1975), was applied to the set of light curves for each star. Briefly, this involved the following:

(a) For a given pulsation frequency of ν cycles per day, let

$$\sigma = 2\pi\nu. \tag{3.1}$$

Let σ now represent the pulsation frequency (in radians per day) of a particular star. Assuming harmonic variations in the star's luminosity, the observed magnitude y_i of the star at time t_i may be written as:

$$y_i = A\cos(\sigma t_i + \varphi) + B - \epsilon_i \quad (i = 1,2,...,n) \tag{3.2}$$

where y_i = magnitude observed,

A = amplitude of the light curve (magnitude variation),

t_i = time of observation,

φ = an appropriate phase factor,

B = mean magnitude of the star,

and ϵ_i = error of the measured magnitude (relative to the true magnitude).

The actual frequencies (if any) present in the set of light curves of a star are obtained as follows: Equation 3.2 can be written as:

$$y_i + \epsilon_i = A\cos(\sigma t_i)\cos\varphi - A\sin(\sigma t_i)\sin\varphi + B. \tag{3.3}$$

Take averages over all data and identify these averages by angular brackets:

$$\langle y_i \rangle + \langle \epsilon_i \rangle = A\langle \cos\sigma t_i \rangle \cos\varphi - A\langle \sin\sigma t_i \rangle \sin\varphi + B.$$

(3.4)

Multiply eq. 3.3 by $\cos(\sigma t_i)$ on each side and take averages:

$$\begin{aligned}\langle y_i \cos\sigma t_i \rangle + \langle \epsilon_i \cos\sigma t_i \rangle = {} & A\langle \cos^2\sigma t_i \rangle \cos\varphi \\ & - A\langle \sin(\sigma t_i)\cos\sigma t_i \rangle \sin\varphi \\ & + B\langle \cos\sigma t_i \rangle.\end{aligned} \tag{3.5}$$

Multiply eq. 3.3 by $\sin(\sigma t_i)$ on each side and take averages:

$$\begin{aligned}\langle y_i \sin\sigma t_i \rangle + \langle \epsilon_i \sin\sigma t_i \rangle = {} & A\langle \sin(\sigma t_i)\cos\sigma t_i \rangle \cos\varphi \\ & - A\langle \sin^2\sigma t_i \rangle \sin\varphi \\ & + B\langle \sin\sigma t_i \rangle.\end{aligned} \tag{3.6}$$

In the least squares approximation:

$$\begin{aligned}\langle \epsilon_i \cos\sigma t_i \rangle &= 0, \\ \langle \epsilon_i \sin\sigma t_i \rangle &= 0, \\ \text{and } \langle \epsilon_i \rangle &= 0.\end{aligned} \tag{3.7}$$

The following approximations hold for large numbers of observations, and are subsequently used here:

$$<cos(\sigma t_i)sin\sigma t_i> = 0,$$

$$<cos^2\sigma t_i> = 1/2,$$

$$<sin^2\sigma t_i> = 1/2,$$

$$<cos\sigma t_i> = 0,$$

$$\text{and } <sin\sigma t_i> = 0. \tag{3.8}$$

These expressions change the equations above to the following forms:

$$<y_i> = B,$$

$$<y_i cos\sigma t_i> = (A/2)cos\varphi,$$

$$\text{and } <y_i sin\sigma t_i> = (-A/2)sin\varphi. \tag{3.9}$$

Therefore:

$$(1/4)A^2 = <y_i cos\sigma t_i>^2 + <y_i sin\sigma t_i>^2. \tag{3.10}$$

Since y_i and t_i are contained in the data, the value of A can be calculated for each specific frequency σ. Furthermore,

$$\begin{aligned} <\epsilon_i y_i> + <\epsilon_i^2> = & \; Acos\varphi<\epsilon_i cos\sigma t_i> \\ & - Asin\varphi<\epsilon_i sin\sigma t_i> \\ & + B<\epsilon_i>, \end{aligned} \tag{3.11}$$

so that:

$$<\epsilon_i^2> = -<\epsilon_i y_i>,$$

$$\text{and } <y_i^2> - <\epsilon_i^2> = <y_i^2> + <\epsilon_i y_i>$$

$$= Acos\varphi<y_i cos\sigma t_i> - Asin\varphi<y_i sin\sigma t_i> + B<y_i>$$

$$= (1/2)A^2cos^2\varphi + (1/2)A^2sin^2\varphi + <y_i>^2. \tag{3.12}$$

Therefore:

$$<\epsilon_i^2> = <y_i^2> - <y_i>^2 - (1/2)A^2,$$

$$\text{so that } (1/2)A^2 = \sigma_y^2 - <\epsilon_i^2>, \tag{3.13}$$

$$\text{where } \sigma_y^2 = <y_i^2> - <y_i>^2.$$

Obviously, the smaller $<\epsilon_i^2>$ is, the larger A will be, since $<\epsilon_i^2>$ is less than σ_y^2 for

real values of A.

The magnitude of A thus serves as an indication of the degree of accuracy with which the frequency σ represents a harmonic variation in the data. Since the β Cephei stars usually have pulsation frequencies between 3 and 10 cycles per day, the value of A was calculated for values of σ from 0 to 20 cycles per day, in increments of 0.01 cycles per day. When a local maximum of A had been identified, the frequency space immediately surrounding this maximum was sampled in increments of 0.001 cycles per day, to determine the peak frequncy more precisely. The results of these calculations are represented in the form of periodograms, as discussed in the following section.

3.4 PERIODOGRAM ANALYSIS

The aim of the analysis described below is to determine, for each star, those frequencies which best represent its light curve as a sum of cosine waves. The degree of success achieved in this attempt will of course depend on the mathematical form of the physical light curve itself.

The β Cephei stars in NGC 3293 are all multiperiodic, with the result that their periodograms are quite complex. The analysis of these periodograms, to determine the presence of harmonic variations in the sample stars, proceeded by means of successive 'prewhitening' of the data, consisting of the following steps:

(i) Determining the value of the frequency which shows the highest peak in the periodogram. Since the data collection for β Cephei stars under discussion was done over a period of about 70 days, a difference greater than 1/70 cycles per day between successive sampling frequencies would cause a large number of frequencies (including

some which may be good representations of the data, thus causing peaks in the periodogram) to be overlooked in the calculation of the periodogram. Frequency sampling was therefore done at intervals of less than 1/70 cycles per day. The amount of data and the spacing thereof allowed a precision of slightly less than 0.01 cycles per day in the calculation of the periodogram.

(ii) Fitting the best cosine function with this frequency to the data by taking equation (3.2) for the given frequency σ and minimizing the errors ϵ_i with respect to A and φ. In other words, impose the following requirements:

$$\frac{\partial \Sigma \epsilon_i^2}{\partial A} = 0$$

$$\text{and} \quad \frac{\partial \Sigma \epsilon_i^2}{\partial \varphi} = 0, \tag{3.14}$$

where ϵ_i now represents the difference between the observed magnitude at time t_i and the magnitude calculated for given values of σ, A and φ. The data are then **prewhitened** by the frequency σ by subtracting this cosine function from the data.

(iii) Calculating a new periodogram for the 'prewhitened' data.

(iv) Repeating (i) to (iii) until no peak remains above the detection limit. This limit is found by Scargle's (1982) criterion: the detection limit above which a frequency peak has a 99% probability of being real is given by

$$z = 4.6 + ln(N), \tag{3.15}$$

where z = the amplitude of the peak

and N = the number of frequencies searched for a maximum.

This translates to an amplitude signal–to–noise ratio of:

$$s/n = 2\sqrt{z/N}. \tag{3.16}$$

Since more than 350 observations were obtained for each of the variable stars, and N

was of the order of 1000, this equation implies that $s/n < 1$. The mean noise level in the periodograms of 3293–20 and 3293–7 (the adopted standards for this work) is approximately 0.0004 mag. In practice it was found that the periodograms of the variables become noisy below about 0.002 mag., and this was value was therefore adopted as the minimum level for a confident identification of a harmonic variation in the data. This limit is much higher than that suggested by Scargle's method, and a high degree of confidence can be attached to all the frequencies found in this analysis.

As successive frequencies are identified in the data, prewhitening has to be done for an increasing number of frequencies to continue the periodogram analysis. When a periodogram has to be prewhitened by more than one frequency, the least squares calculation of amplitudes and phases (described earlier) has to be done for all frequencies **simultaneously**, to prevent the appearance of false peaks in the periodogram due to an accumulation of small errors. Instead of equation (3.2), one uses:

$$y_i = B + \sum_j A_j cos(\sigma_j t_i + \varphi_j) - \epsilon_i \qquad (3.17)$$

where the sum is over the number of frequencies being prewhitened, and equation (3.14) becomes:

$$\frac{\partial \Sigma \epsilon_i^2}{\partial A_j} = 0$$

$$\text{and} \quad \frac{\partial \Sigma \epsilon_i^2}{\partial \varphi_j} = 0, \qquad (3.18)$$

with the sum as above. The functions $A_j cos(\sigma_j t_i + \varphi_j)$ are added together, the best fit is calculated and subtracted from the data, and a new periodogram is calculated. These calculations were done with LA Balona's computer programs which are in use at the SA Astronomical Observatory.

This technique has its pitfalls, among which "aliasing" is foremost. Due to discontinuities (daylight and non–photometric nights) in the process of data collection, the exact number of pulsation cycles spanning a set of nights is uncertain. The severity of this uncertainty is expressed quantitatively by a so–called **spectral window**. Each distribution of sampling dates (times when the star was observed) has a unique spectral window associated with it, which is calculated as follows:

(i) Set all observed magnitudes equal to a fixed value, say zero.

(ii) Calculate the periodogram for these (zero) magnitudes at the sampling dates.

(iii) Normalise the amplitudes with respect to that at zero frequency.

Since all magnitudes are set to a constant value, they lie along a horizontal line – corresponding to an infinitely long period, or a frequency of zero. The spectral window therefore peaks at zero frequency. Frequencies corresponding to the gaps appearing regularly in the time dimension of the data also have large amplitudes in the spectral window. For instance, a high amplitude is found at frequencies of one and two cycles per day respectively, marking the interruption of the observing programme (for instance by a cloudy night) and the onset of daytime respectively.

Figure 3.1 shows a spectral window corresponding to all data collected in the 1983 observing season. The spectral window for 1984 is very similar. The main peak is at zero frequency, the rest of the spectrum being normalised to this value. Note the tall side peaks at 1 and 2 cycles per day. If a frequency ν_1, say, was present in the data with an amplitude A in the periodogram, then frequencies (ν_1+1) and (ν_1-1) respectively would have an amplitude of $0{,}84A$, while frequencies (ν_2+2) and (ν_2-2) would each have an amplitude of about $0{,}4A$. The periodogram obtained for a particular star is a convolution of the true power distribution of frequencies present in the data with the spectral window of the latter, so instead of isolated peaks, 'families' of peaks, in groups of 3, 5, 7,etc, depending on when they become submerged under the noise level, appear

in the periodogram.

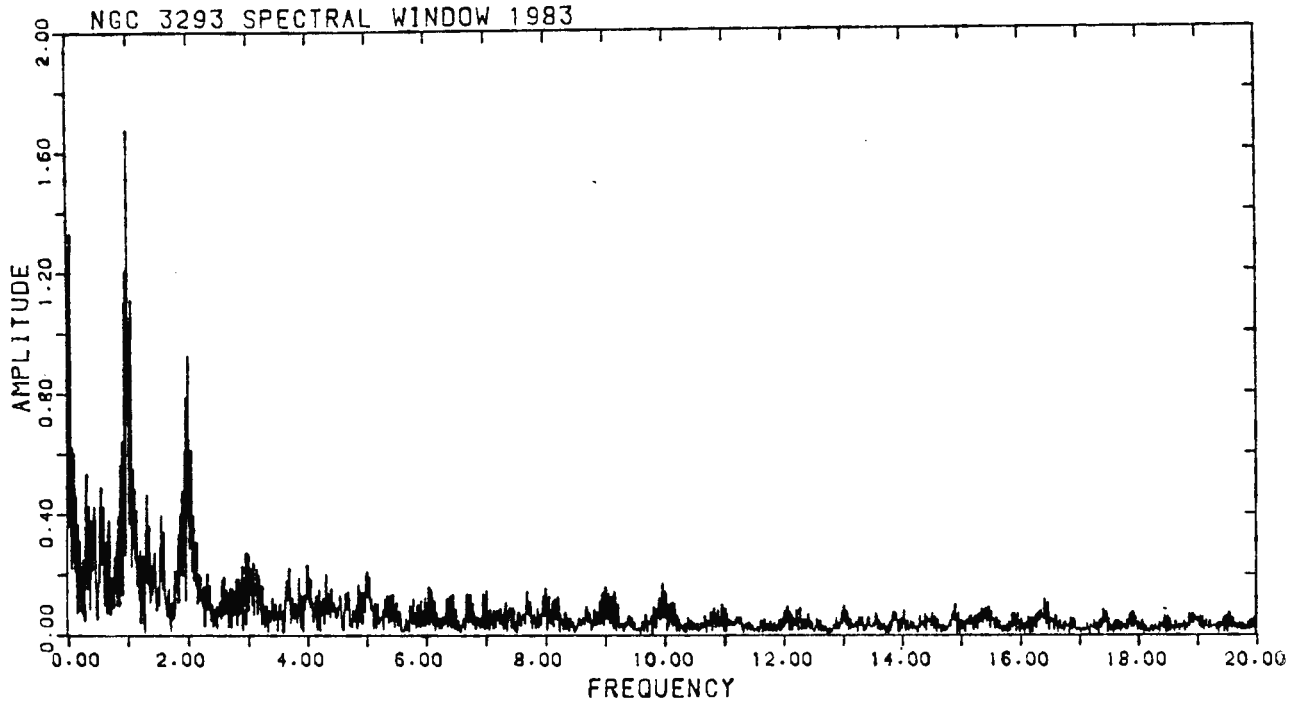

Figure 3.1: Spectral window for observations of stars in NGC 3293 collected in 1983

In mathematical terms, the aliasing can be understood as follows: Let $\sigma = 2\pi\nu$ represent frequency, in radians per day. Since $cos(\sigma t \pm 2\pi) = cos\sigma t$, the frequency $\sigma \pm (2\pi/t)$ represents the data just as well as σ itself, or in terms of ν: $(\nu \pm 1/t)$ (where t represents the sampling interval) represents the data just as well as ν itself. When data are collected on a daily basis, $t = 1$ day, and aliases are expected at $\nu \pm 1$ cycles per day. Furthermore, frequencies ν and $-\nu$ lead to the same result, and "reflected" peaks will appear in the periodogram at frequencies smaller than 1 cycle per day. For example, if a frequency of 0.8 cycles per day is actually present in the data, it is equally well represented by $\nu = -0.8$ cycles per day. The alias of this frequency will then appear in the periodogram at 0.2 cycles per day.

However, since the one–day sampling interval is only approximate (many individual observations are made within a night, and the exact times of observation differ from night to night), the "side peaks" have smaller amplitudes than the principal peak.

The results of the periodogram analysis of the β Cephei stars in NGC 3293 are presented in chapter 4.

CHAPTER 4

FREQUENCIES AND AMPLITUDES OF PULSATIONS OBSERVED IN BETA CEPHEI STARS IN NGC 3293

4.1 FOURIER FITTING OF FREQUENCIES TO DATA

The periodogram analysis described in the previous chapter produced a set of pulsation frequencies for each of the β Cephei stars in NGC 3293, with a corresponding amplitude and phase for each of the individually identified frequencies. Fourier fits of these frequencies to the observed light curves were constructed as follows: For each star, the sum of the functions

$$x_j = A_j cos(\omega_j t + \varphi_j) \qquad (j = 1,...,m) \qquad (4.1)$$

was added to the mean magnitude B, and the result superimposed on the data in a composite diagram, as shown in the next section.

4.2 RESULTS

The results of the periodogram analyses and the Fourier fitting procedures described above, are presented in this section. For each β Cephei star, periodograms for distinct observing runs are given first, followed by periodograms for the entire data set, to indicate the degree of consistency of the frequencies determined. Identified pulsation frequencies are then tabulated in order of decreasing amplitude. Finally, the best Fourier fits of the identified frequencies to the observed light curves are shown. The divisions on the vertical magnitude represent intervals of 0.02 magnitudes throughout.

The frequency determination process was complicated for many of the stars by the presence of tall peaks at low frequencies (corresponding to periods of longer than a day) in the periodograms, which may have been caused by the following factors:

(a) The actual presence of variations with relatively long periods in the observed magnitudes, due to binary motion, rotation of a star with a non–homogeneous surface or other physical factors.

(b) A deterioration of observing conditions on some nights, with a subsequent increase in the scatter of measured magnitudes about the true values. This could cause a spurious amount of power at frequencies of 1, 1/2, 1/3, etc cycles per day, depending on the spacing and regularity of such occasions. Since the influence of changes in the seeing varied with the density of stars in the cluster, some stars were more prone to this effect than others.

When low (less than 1 cycle per day) frequencies had significant power in a periodogram, the data were also prewhitened for these frequencies, to eliminate their influence on the frequency determination. These frequencies were omitted from the tables containing pulsation frequencies, however, since they were much lower than the typical β Cephei pulsation frequencies of 3–7 cycles per day. Note that the amplitudes of most frequencies appear to have changed from one observing run to the next. This could be a mathematical effect due to the poor resolution over such short intervals, especially for the stars observed in 1983, but on a few occasions (3293–10 and 3293–11) the dominant frequency also switched from one observing run to another. The 1.0 cycle per day frequency appearing in the periodogram for 3293–10 is quite strong, and could have a physical rather than an observational cause.

There are many instances of one–day aliases appearing in the analyses of successive observing runs shown in the tables that follow. The frequencies determined for the full observing runs may be clearly distinguished from their aliases in the periodograms, and may be accepted with confidence. As stated in chapter 3, the final frequencies obtained for the full observing runs are accurate to less than 0.01 cycles per day. The successful representation of the observations by these frequencies supports their reliability. The resolution frequency for a week's observing is 0.14 cycles per day, while that for a fortnight is 0.07 cycles per day. This accounts for the apparent variation in the values of the tabulated frequencies from one season to another.

Fourier fits to the observations, as seen in the diagrams, generally appear to match the observed light curves very well, although the amplitudes do not match exactly on a number of occasions (e.g. nights 5750, 5802, 5803 and 5807 for 3293–10; 5803 and 5805 for 3293–16; 5745 for 3293–65). However, the **frequencies** consistently match the observations with the exception of 3293–18, for which the match is poor on some nights, but excellent on others. Possibly this star has some peculiarities in its light output causing irregular disturbances. Star 3293–23 was analysed with the data for nights 5774 and 5804 deleted, after it was noticed that the mean magnitude of the star on these nights was fainter than usual. Superposition of the results onto the observed light curves clearly demonstrates the star's behaviour, for which the most probable explanation is that the star is an eclipsing binary. The Fourier fit to the observed light curves of 3293–5 on nights 5399, 5416 and 5466 can be found in Chapter 10, where the binary nature of this star is discussed.

The periodograms for the two standard stars, 3293–20 and 3293–7, appear in Figure 4.1, for comparison with the periodograms for the variable stars.

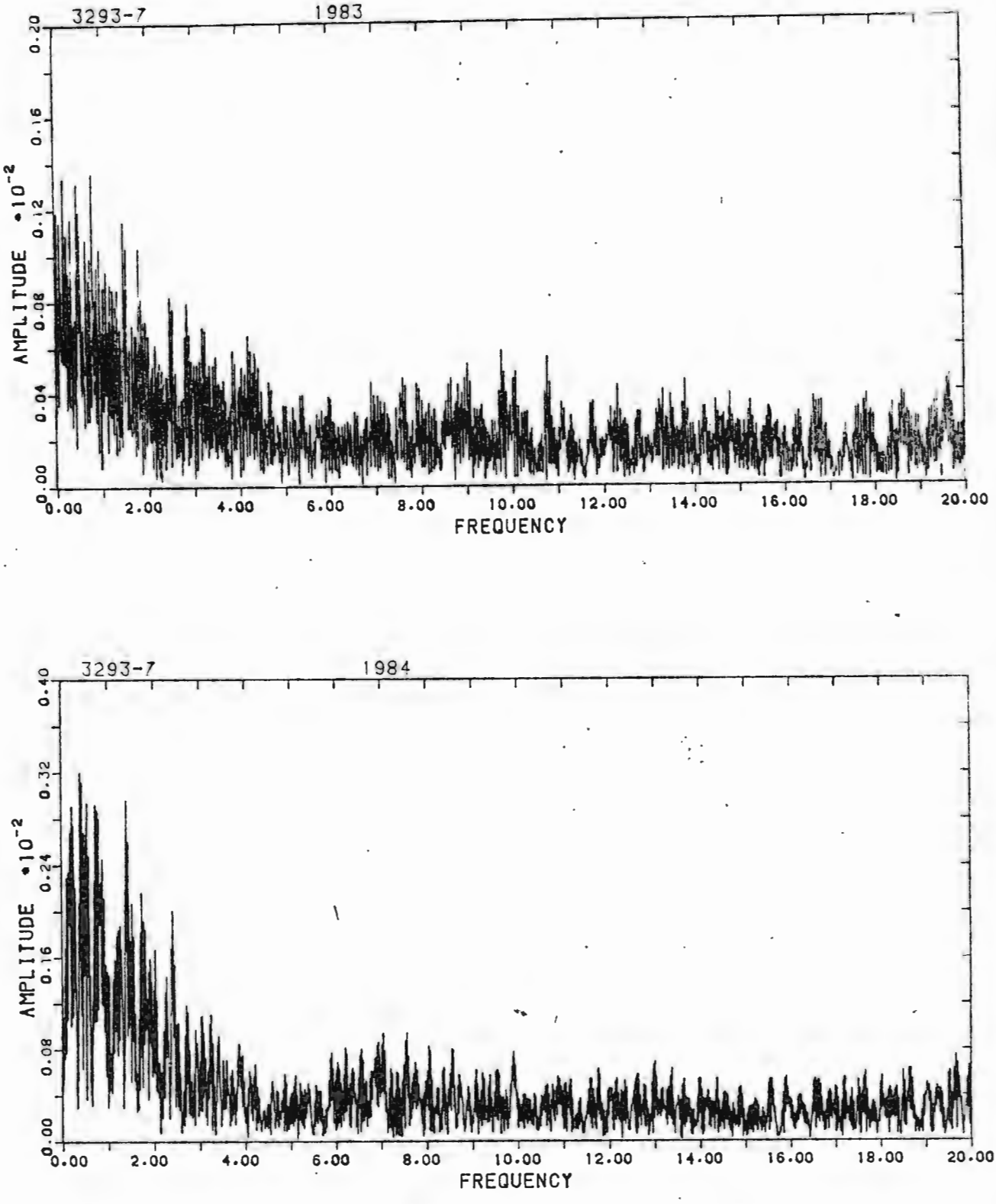

(a)

Figure 4.1: Periodograms of standard stars in NGC 3293, for the observing seasons in 1983 and 1984 respectively. (a) 3293–7

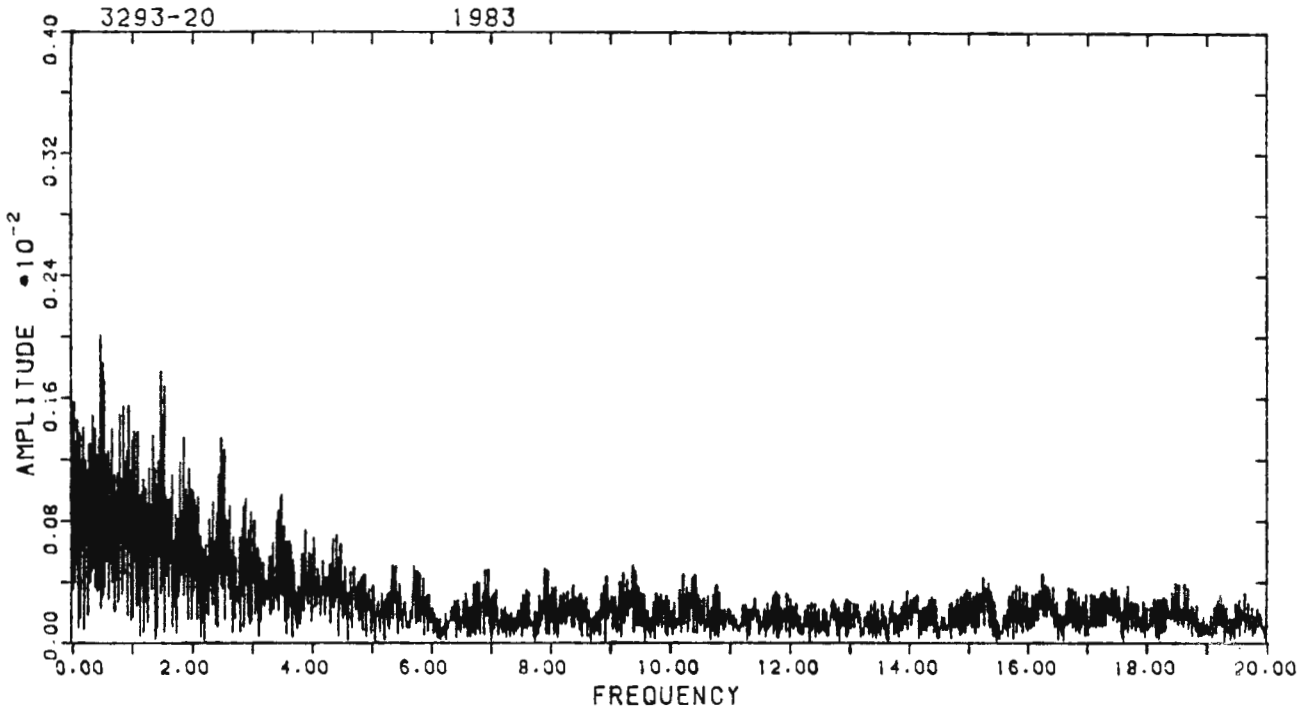

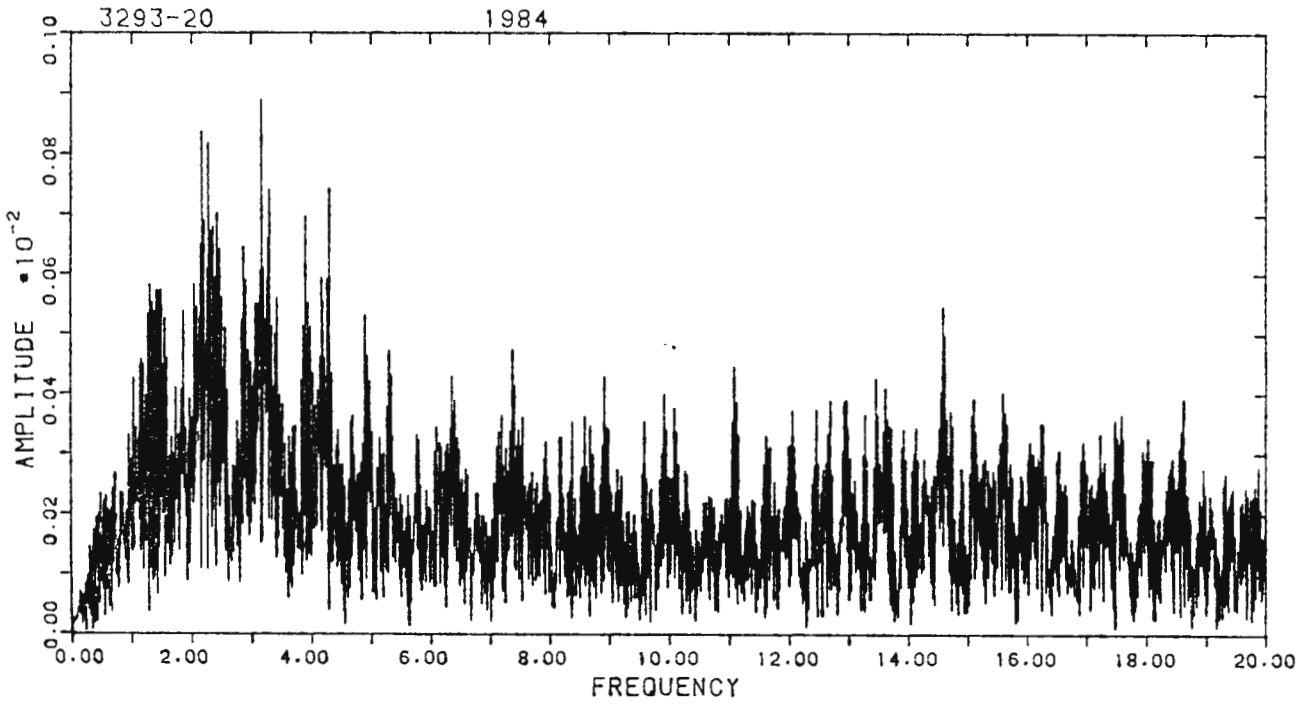

(b)

Figure 4.1 (continued): (b) 3293–20

4.3 THE STAR 3293–5

4.3.1 Periodograms

The periodograms for this star are dominated by low frequencies, due to the occurence of eclipses of, and by, the β Cephei star's companion while observations were being made. In order not to distort the frequency determination, data obtained on three nights in the 1983 observing season when eclipses were observed, were deleted from the data set before the periodogram for this star was calculated. The periodogram for the whole data set appears in Figure 4.2(a), to demonstrate the effect of the eclipses.

4.3.2 Pulsation frequencies identified

Table 4.1(a)

Pulsation frequencies of 3293–5

Frequency (cycles per day)	Amplitude (B magnitude)	Date
7.14	0.0055	1 – 8 Mar 1983
4.61	0.0044	
5.64	0.0108	15–29 Mar 1983
7.72	0.0035	
3.28	0.0032	
3.38	0.0025	
9.26	0.0021	
6.15	0.0091	10–17 May 1983
7.50	0.0034	
5.64	0.0087	March–May 1983
6.66	0.0039	
7.17	0.0029	

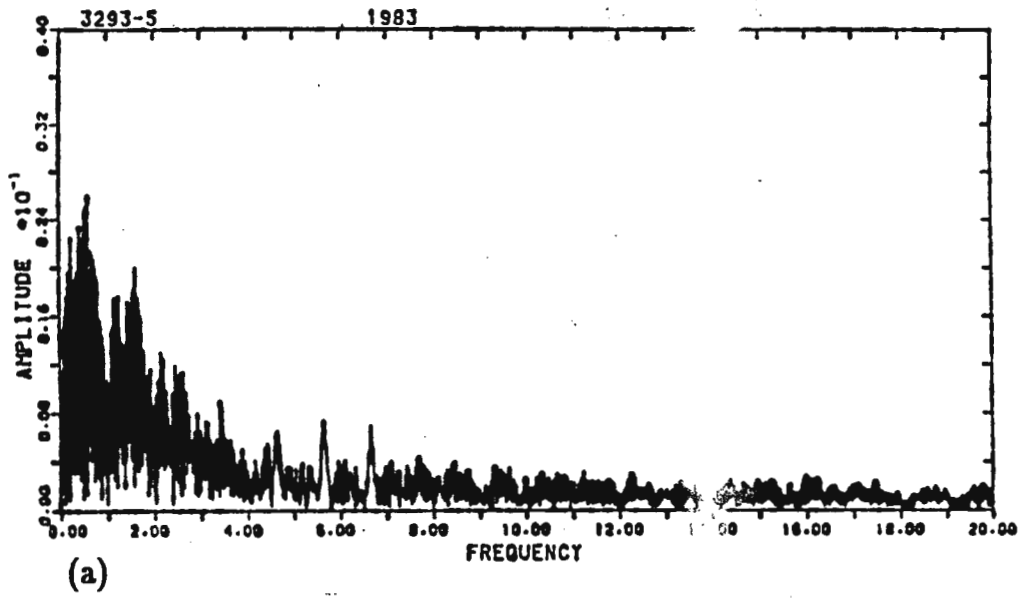

(a)

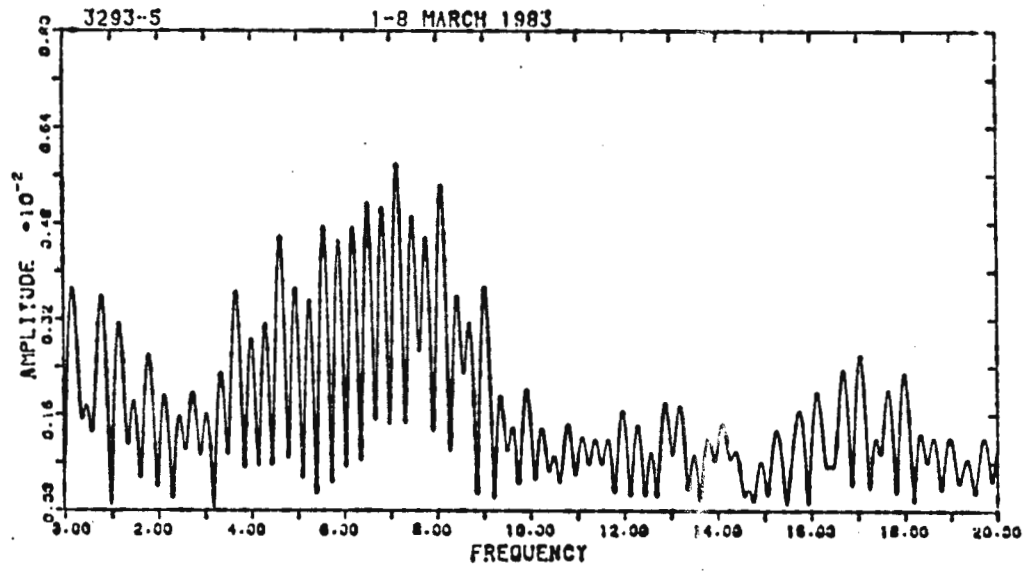

(b)

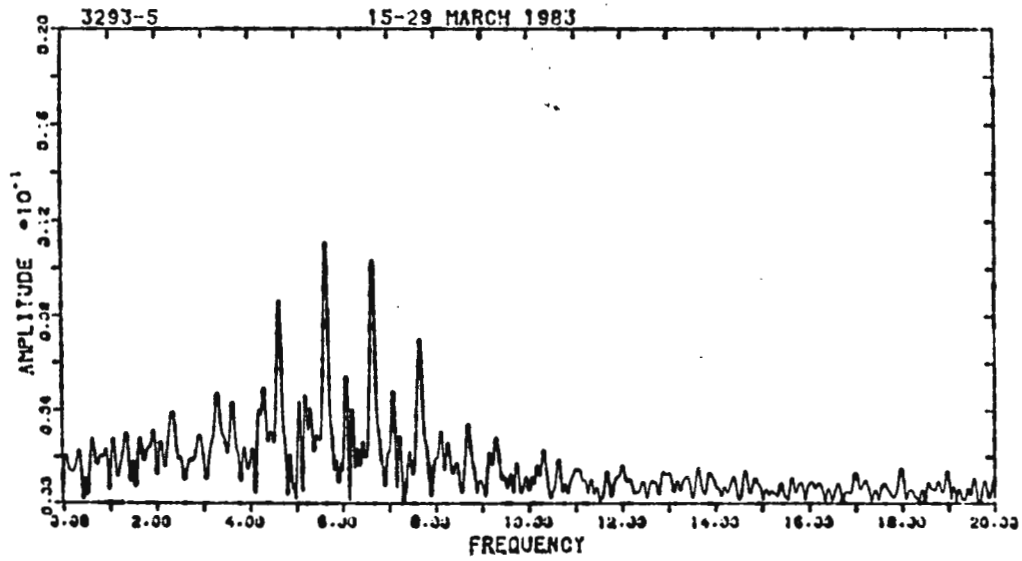

(c)

Figure 4.2: Periodograms of 3293–5
(a) Including eclipses. (b) 1–8 March 1983. (c) 15–29 March 1983

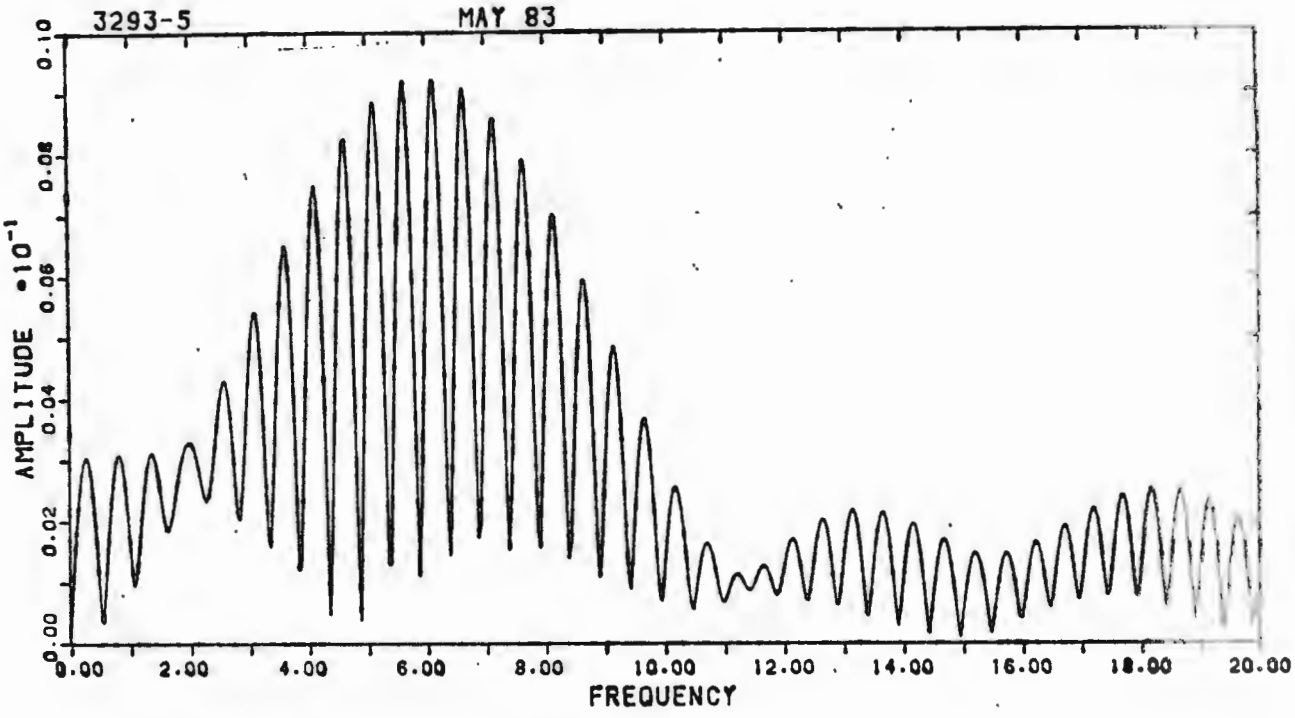

(d)

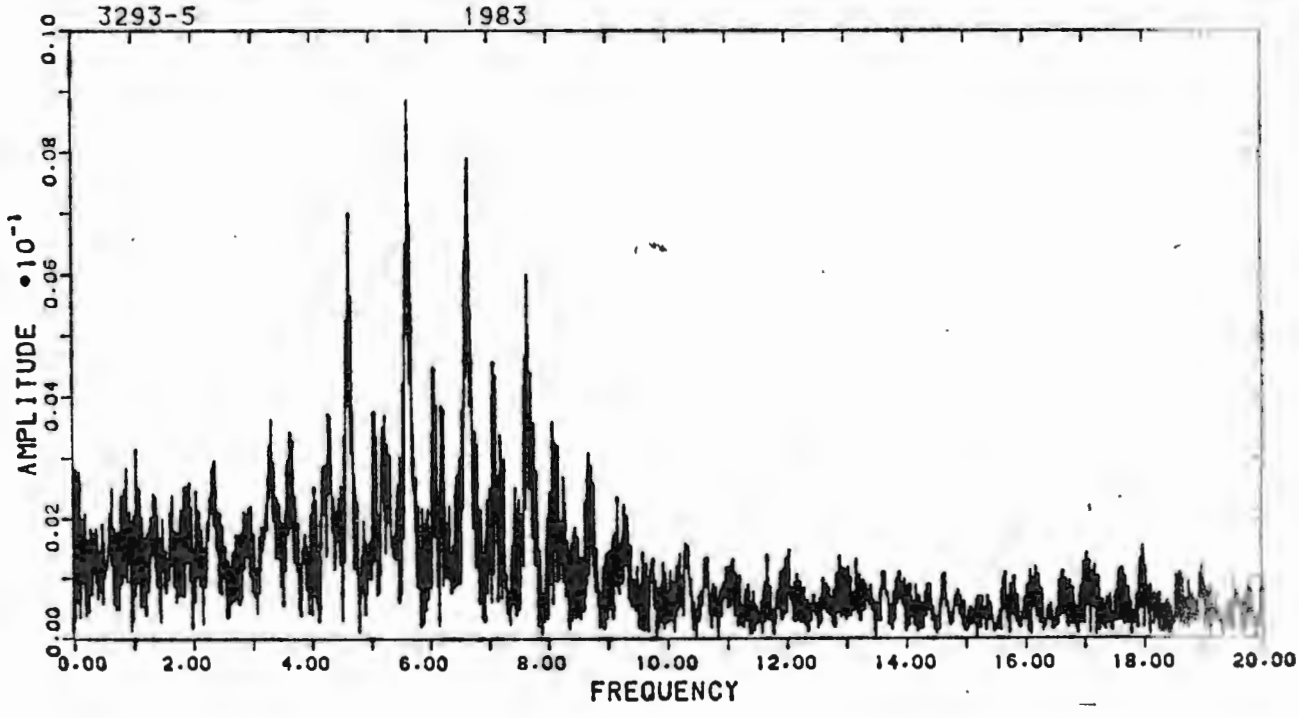

(e)

Figure 4.2 (continued):
(d) 10–17 May 1983. (e) March to May 1983 (excluding eclipses).

4.3.3 Fourier fit

Table 4.1 (b)
Fourier parameters for 3293–5

Frequency (cycles per day)	Amplitude (B magnitude)
5.64	0.0074
6.66	0.0050
7.17	0.0028

Standard error of a single observation:
$0^{m}.0055$

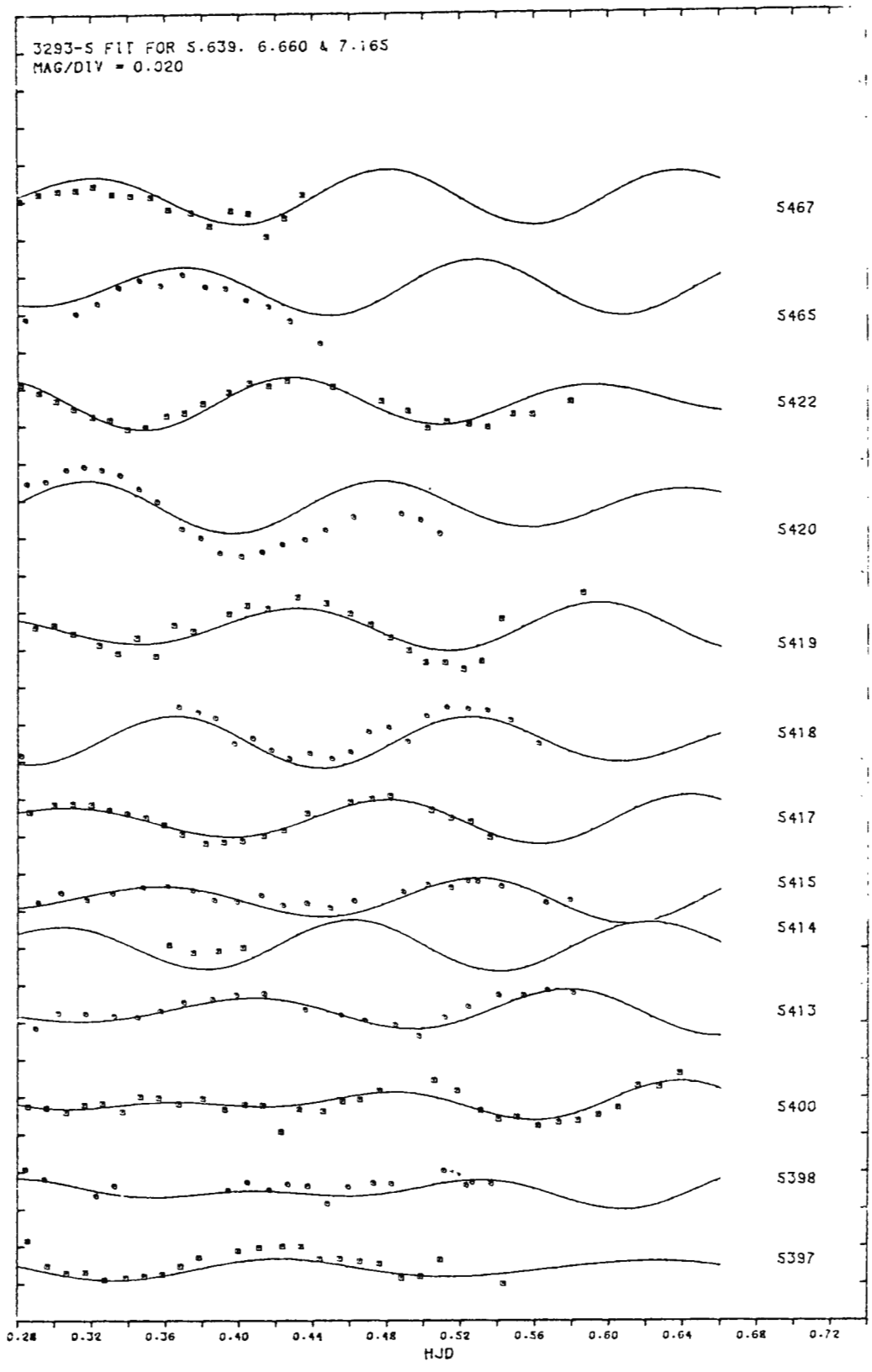

Figure 4.3: Fourier fit for 3293–5

4.4 THE STAR 3293–10

4.4.1 Periodograms

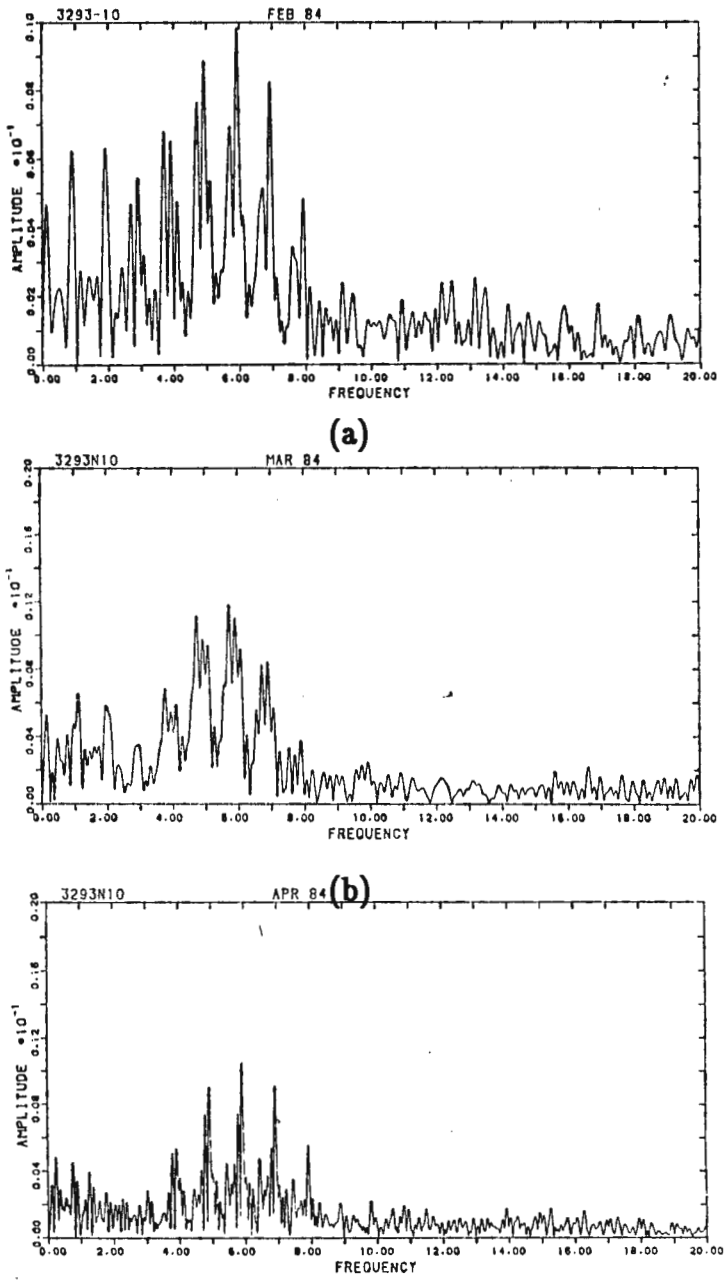

Figure 4.4 Periodograms of 3293–10

(a) 14–21 Feb 1984. (b) 13–20 Mar 1984. (c) 10–24 April 1984

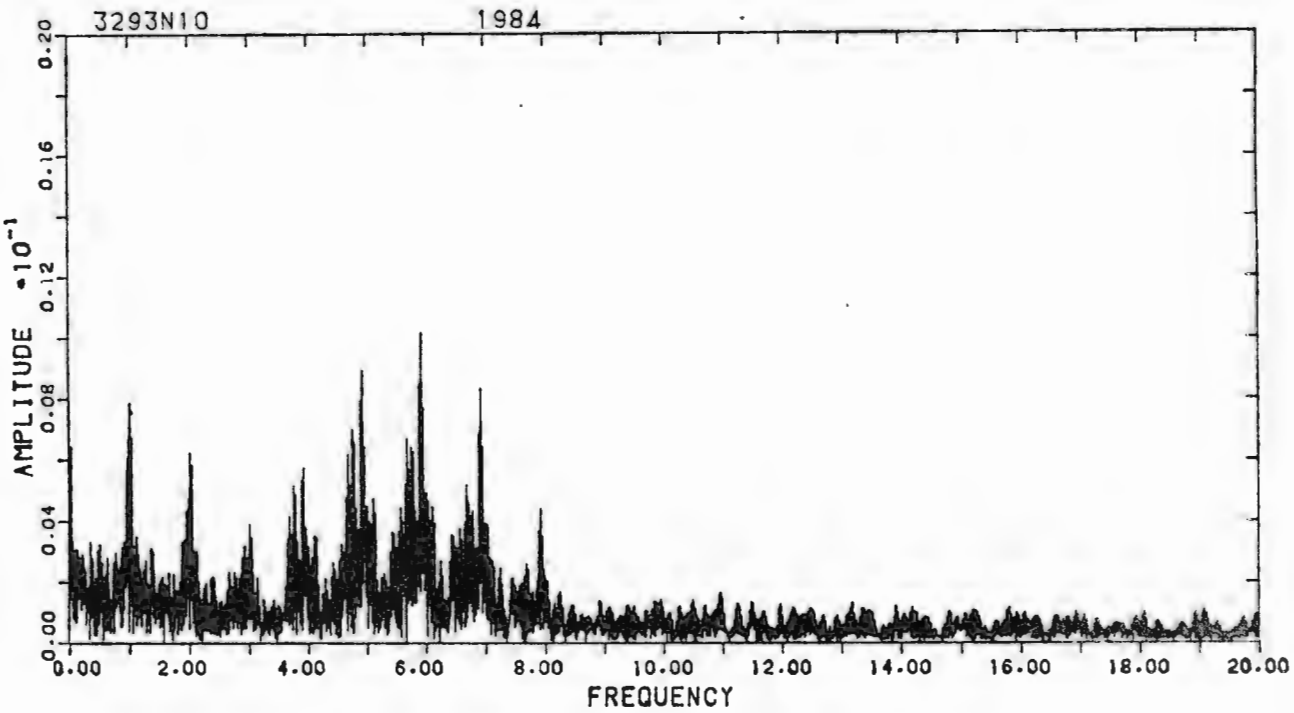

Figure 4.4 (d): Periodogram of 3293–10: Feb – Apr 1984

4.3.2 Pulsation frequencies identified

Table 4.2(a)

Pulsation frequencies of 3293–10

Frequency (cycles per day)	Amplitude (B magnitude)	Date
5.94	0.0100	14–21 Feb 1984
5.72	0.0078	
6.51	0.0037	
5.11	0.0029	
5.72	0.0121	13–20 Mar 1984
5.95	0.0097	
6.25	0.0042	
5.92	0.0107	10–24 Apr 1984
4.79	0.0047	
6.69	0.0036	
5.03	0.0033	
6.12	0.0032	
5.92	0.0103	Feb – Apr 1984
5.68	0.0071	
4.76	0.0043	
6.11	0.0034	
5.46	0.0027	

4.3.3 Fourier fit

Table 4.2 (b)
Fourier parameters for 3293–10

Frequency (cycles per day)	Amplitude (B magnitude)
5.92	0.0100
5.68	0.0061
4.76	0.0043
6.11	0.0034
5.46	0.0027

Standard error of a single observation:

$0^{m}.0079$

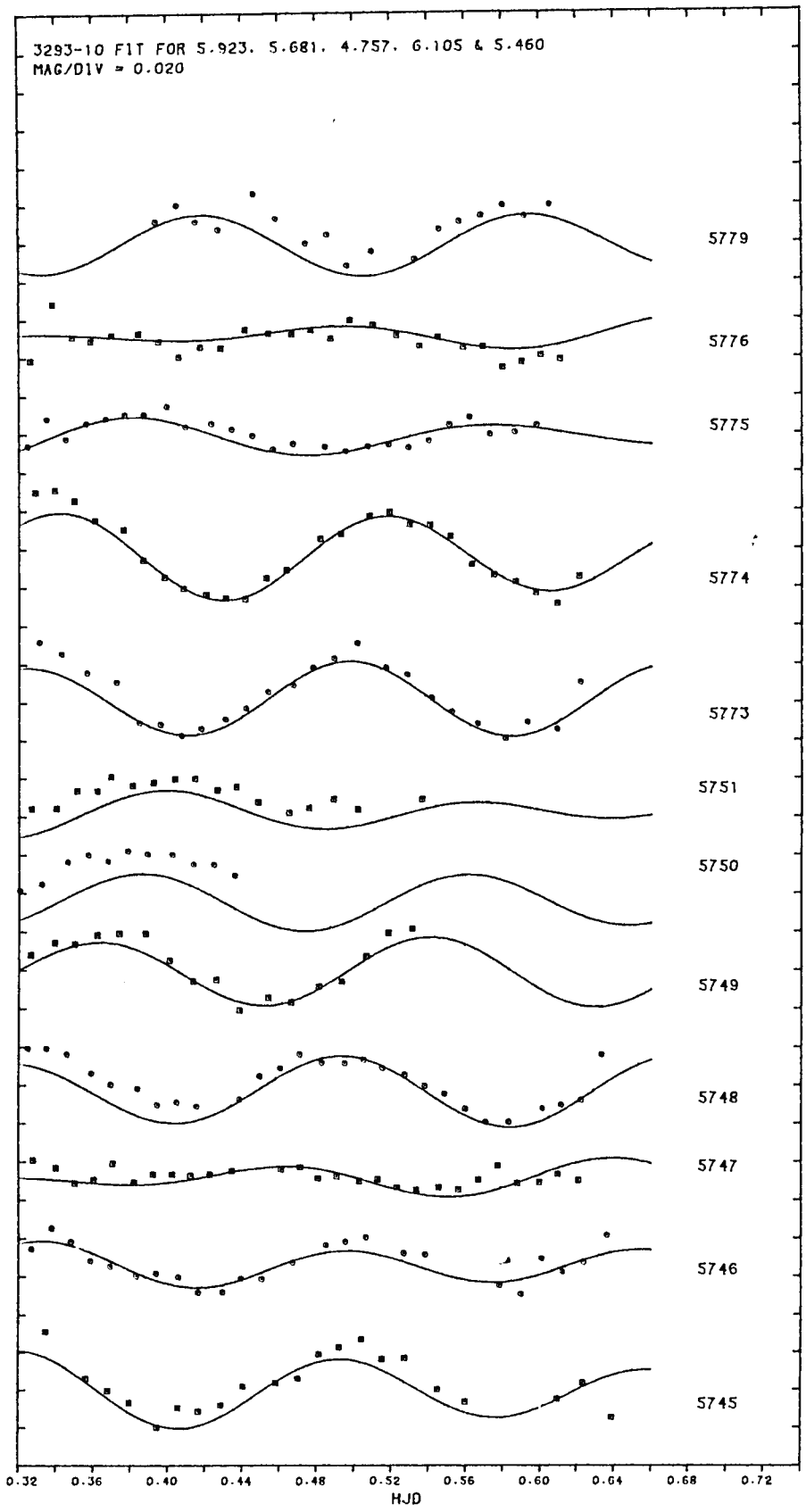

Figure 4.5: Fourier fit for 3293–10

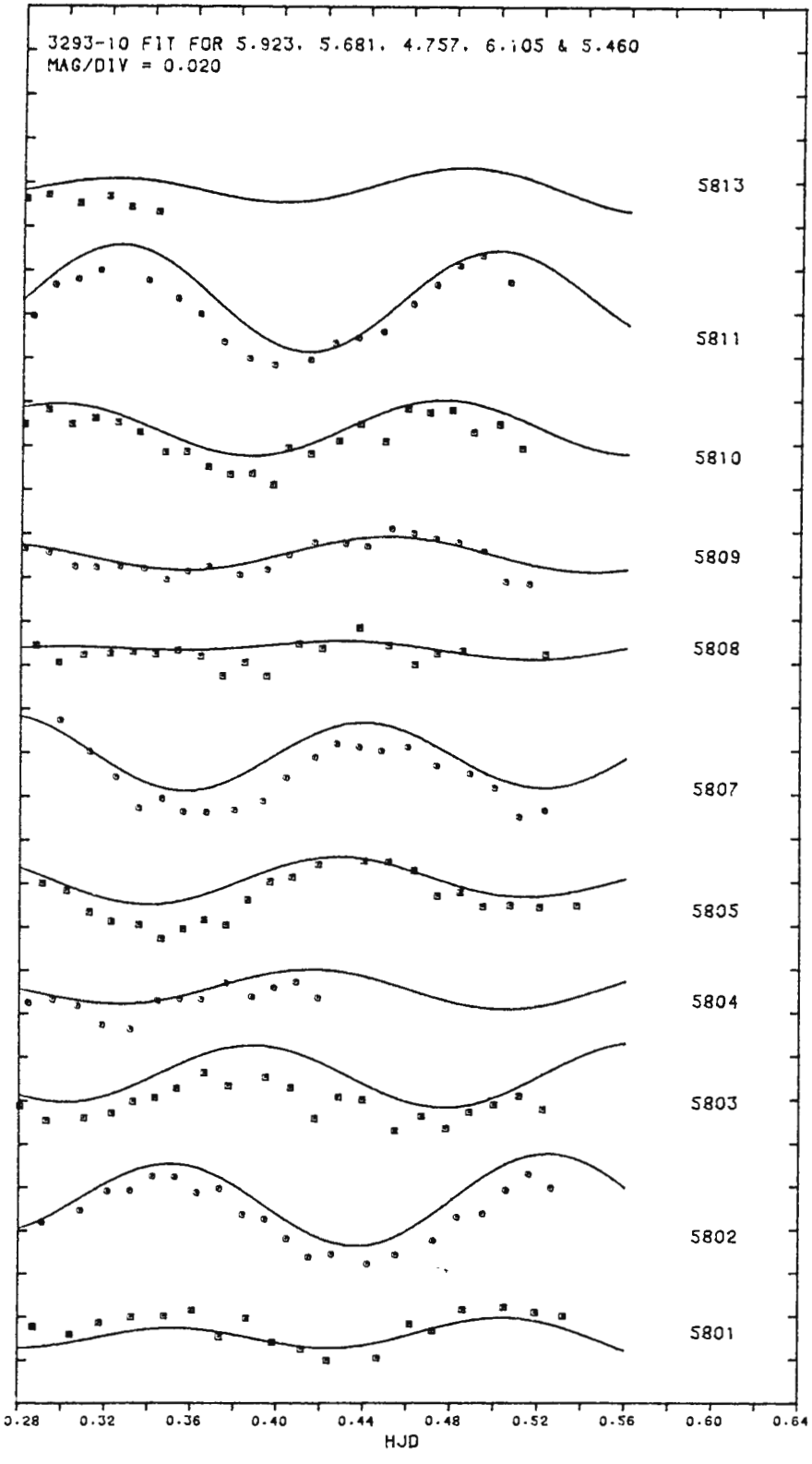

Figure 4.5 (continued):

4.5 THE STAR 3293–11

4.5.1 Periodograms

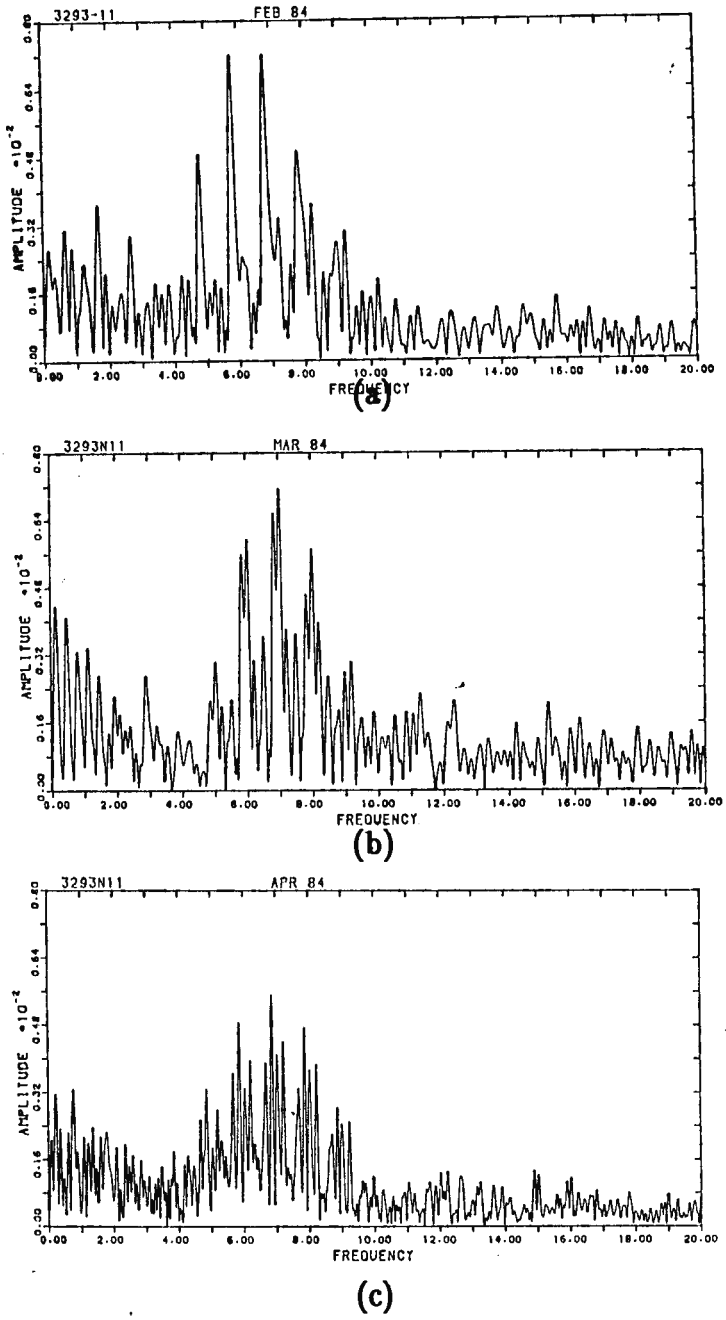

Figure 4.6 Periodograms of 3293–11

(a) 14–21 Feb 1984. (b) 13–20 Mar 1984. (c) 10–24 April 1984

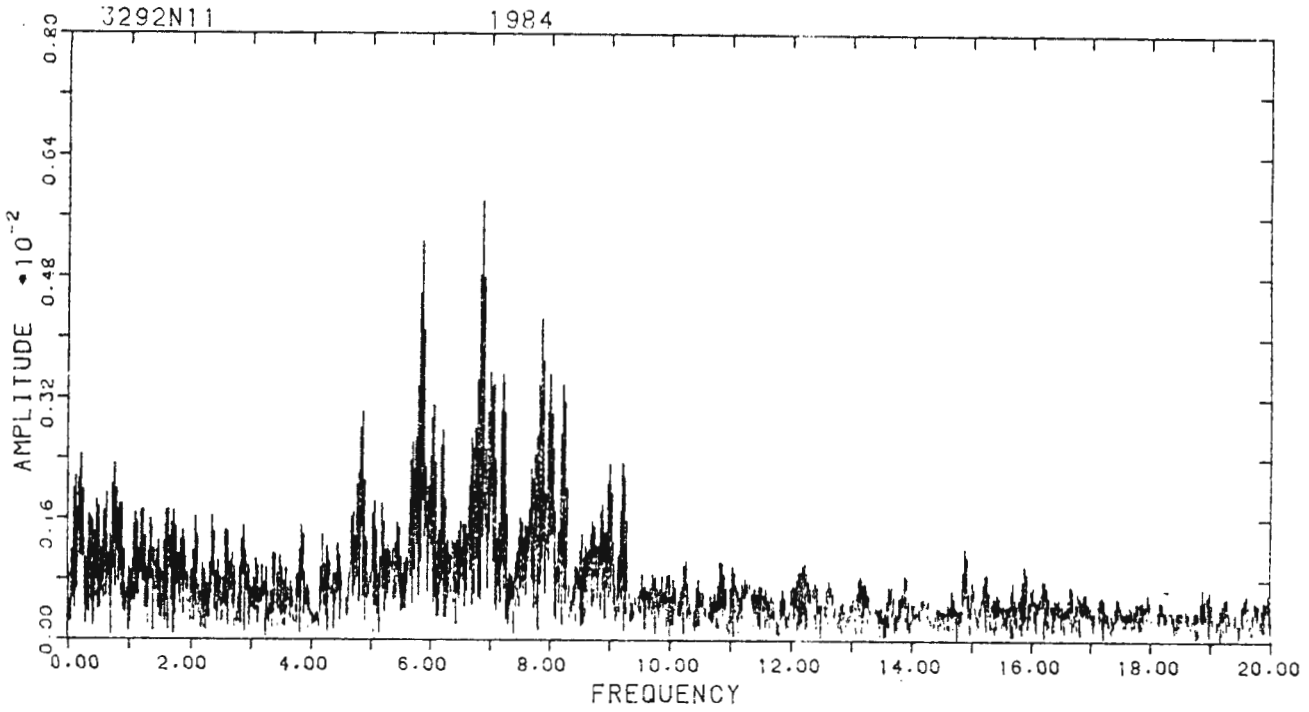

Figure 4.6 (d): Periodogram of 3293–11: Feb – Apr 1984

4.5.2 Pulsation frequencies identified

Table 4.3(a)

Pulsation frequencies of 3293–11

Frequency (cycles per day)	Amplitude (B magnitude)	Date
6.80	0.0072	14–21 Feb 1984
7.00	0.0038	
7.20	0.0035	
7.02	0.0071	13–20 Mar 1984
6.82	0.0038	
7.25	0.0023	
6.87	0.0057	10–24 Apr 1984
6.70	0.0045	
6.57	0.0038	
7.39	0.0023	
6.86	0.0059	Feb – Apr 1984
6.72	0.0039	
7.22	0.0031	
7.06	0.0029	
6.65	0.0022	

4.5.3 Fourier fit

Table 4.3 (b)
Fourier parameters for 3293–11

Frequency (cycles per day)	Amplitude (B magnitude)
6.86	0.0064
6.72	0.0040
7.22	0.0033
7.06	0.0029
6.65	0.0024

Standard error of a single observation:

$0^{m}.0045$

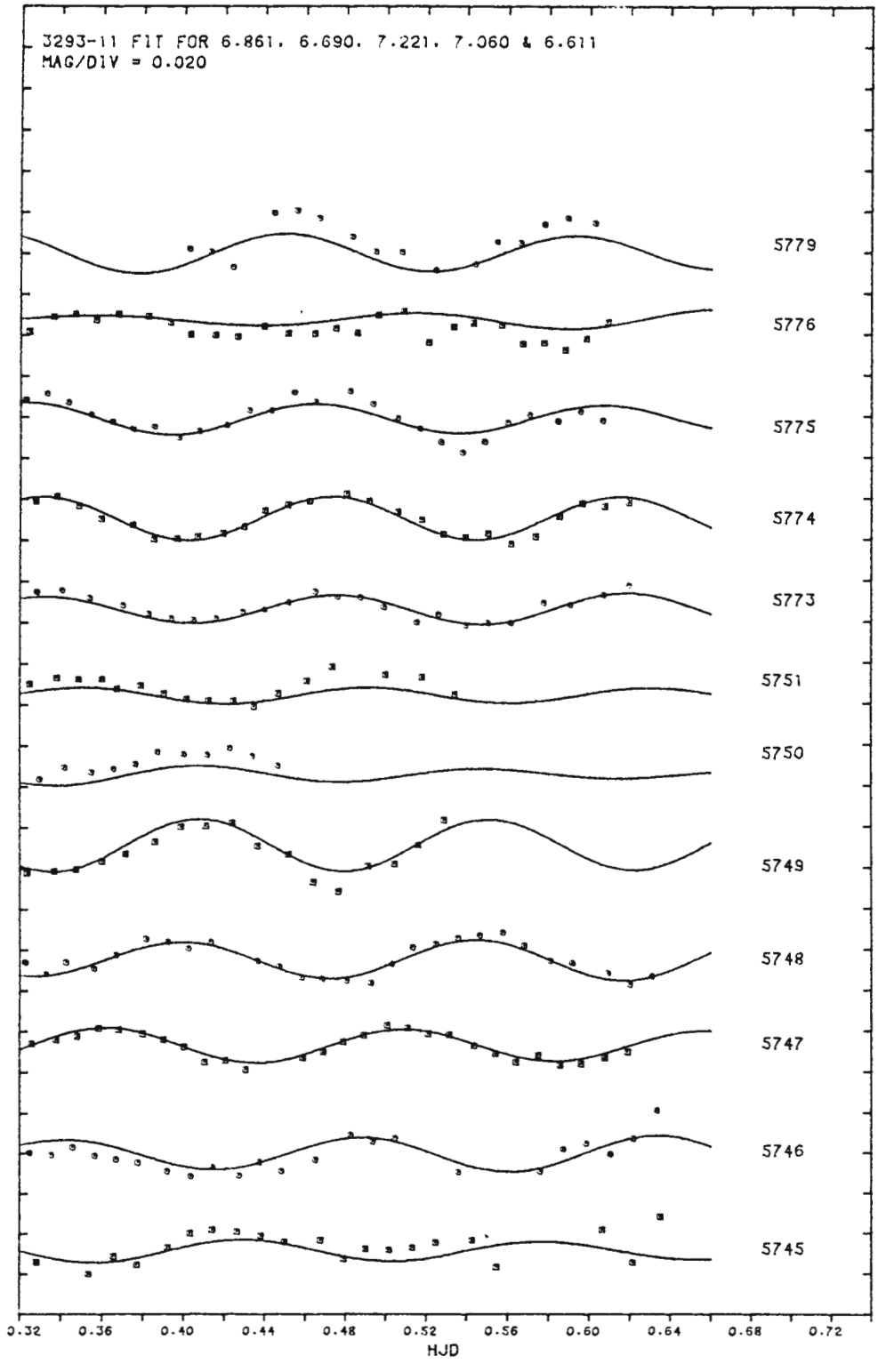

Figure 4.7: Fourier fit for 3293–11

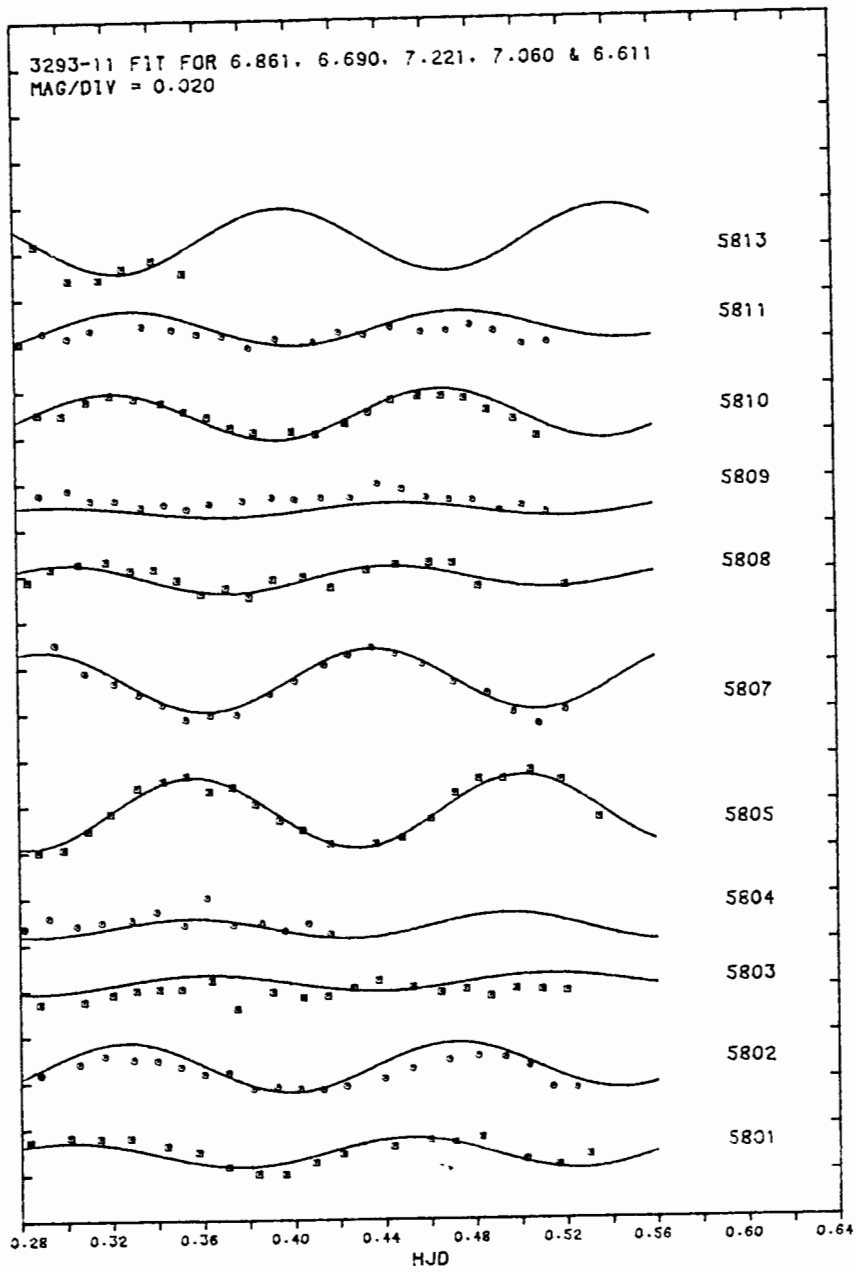

Figure 4.7 (continued):

4.6 THE STAR 3293–14

4.6.1 Periodograms

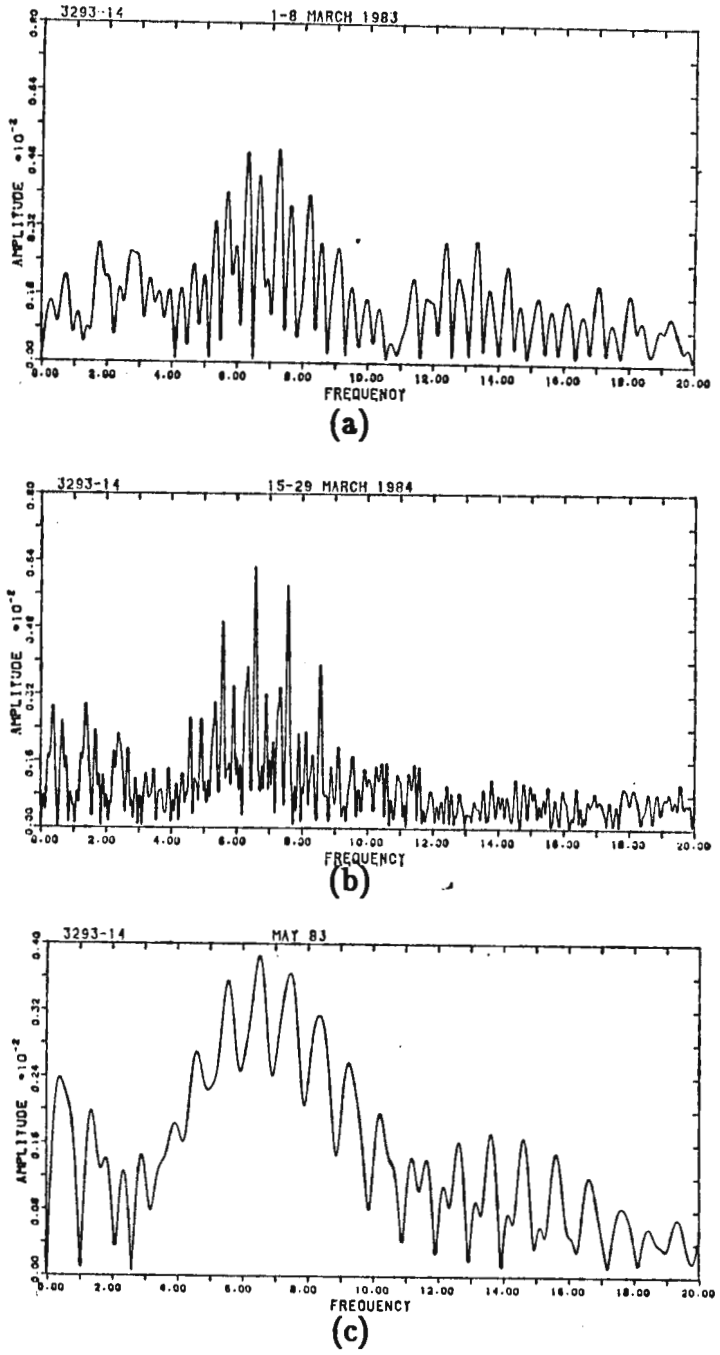

Figure 4.8 Periodograms of 3293–14

(a) 1–8 Mar 1983. (b) 15–29 Mar 1983. (c) 10–17 May 1983

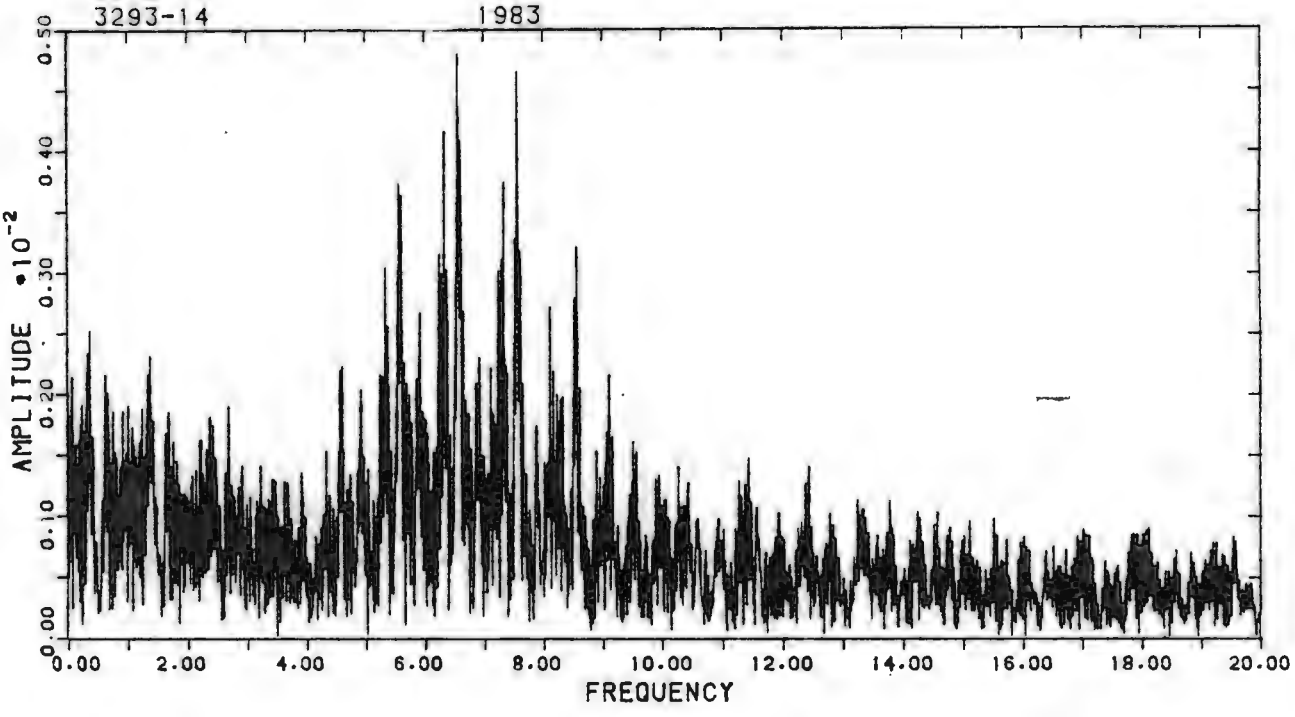

Figure 4.8 (d): Periodogram of 3293–14: Mar – May 1983

4.6.2 Pulsation frequencies identified

Table 4.4(a)

Pulsation frequencies of 3293–14

Frequency (cycles per day)	Amplitude (B magnitude)	Date
7.26	0.0051	1 – 8 Mar 1983
5.70	0.0031	
6.57	0.0063	15–29 Mar 1983
6.33	0.0037	
5.91	0.0022	
6.53	0.0039	10–17 May 1983
7.05	0.0037	
6.56	0.0048	March–May 1983
6.33	0.0038	
5.90	0.0028	

4.6.3 Fourier fit

Table 4.4 (b)
Fourier parameters for 3293–14

Frequency (cycles per day)	Amplitude (B magnitude)
6.56	0.0045
6.33	0.0040
5.90	0.0029

Standard error of a single observation:

$0^{m}.0048$

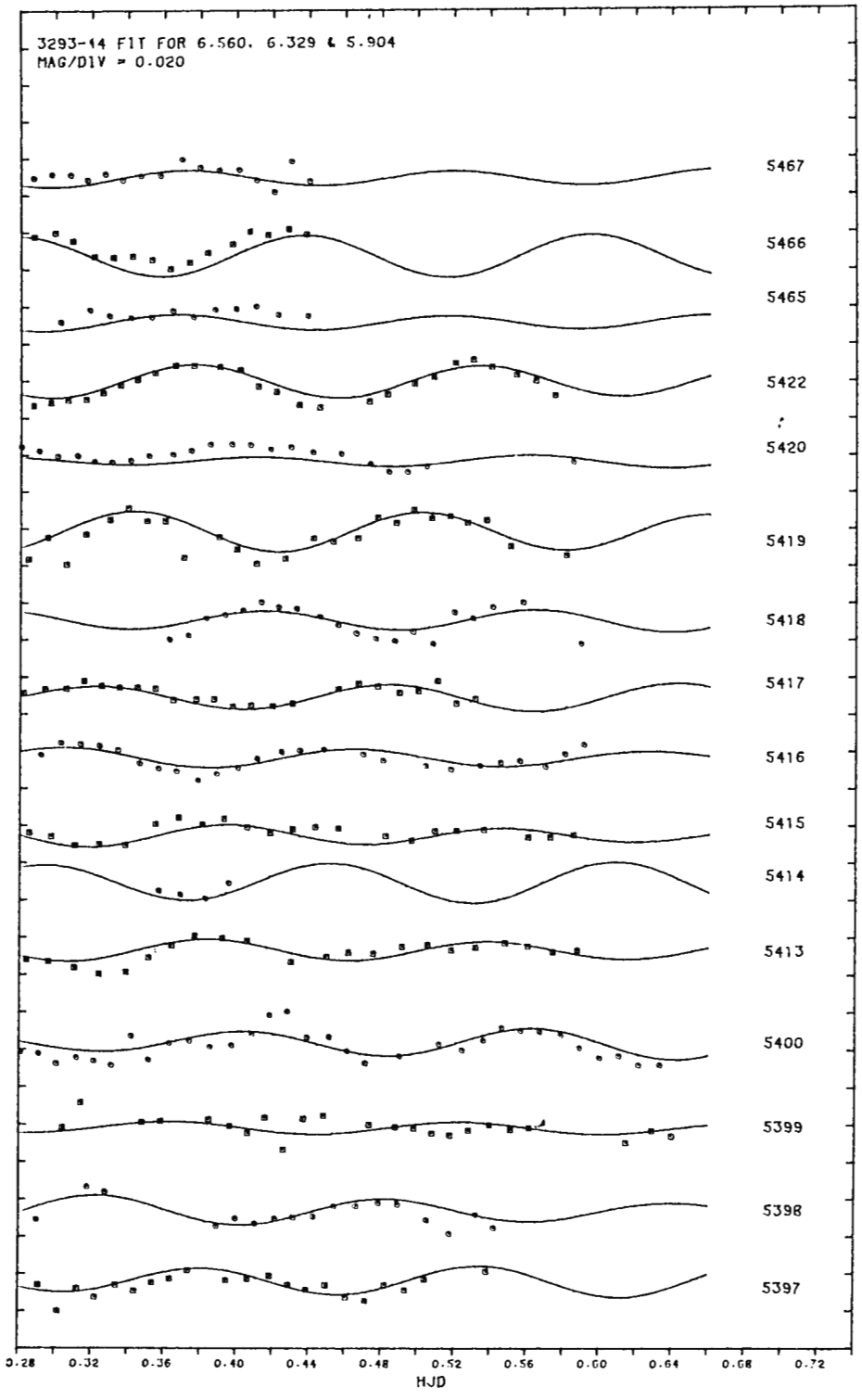

Figure 4.9: Fourier fit for 3293–14

4.7 THE STAR 3293–16

4.7.1 Periodograms

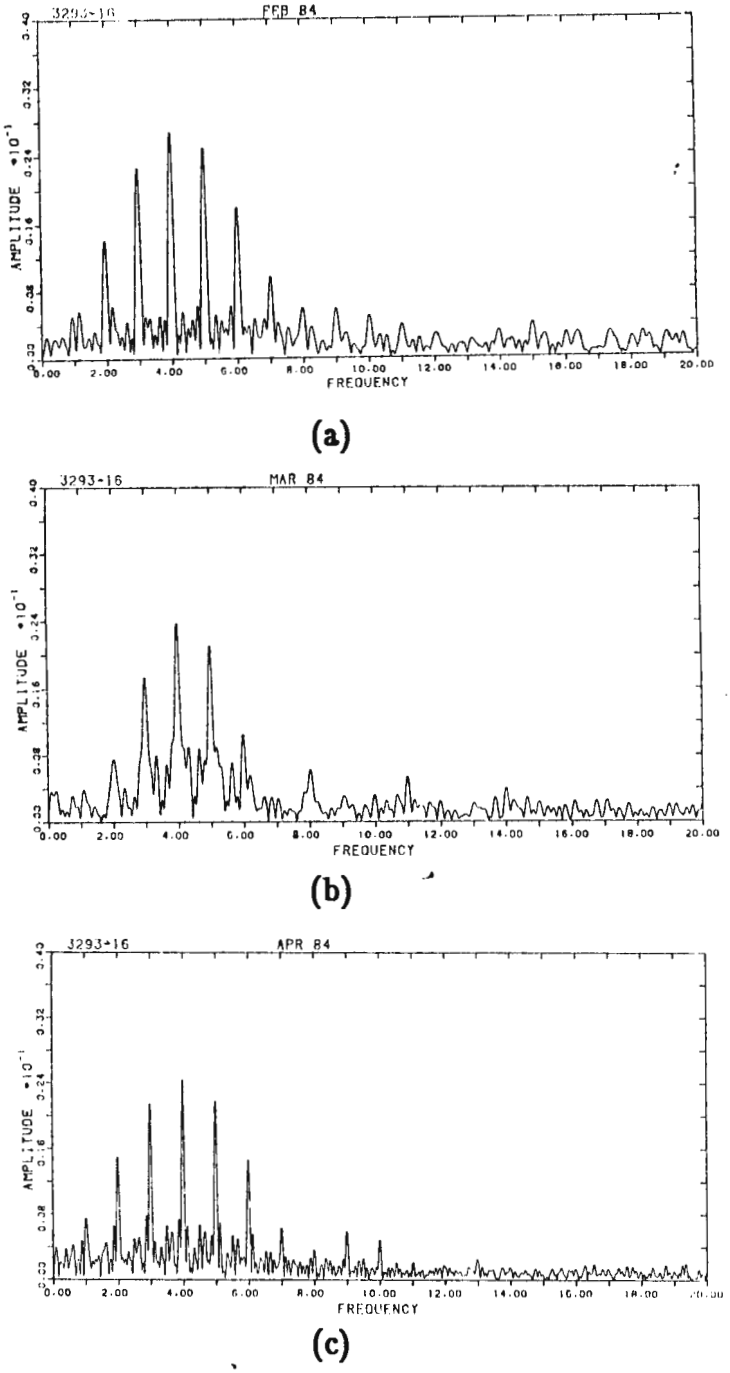

Figure 4.10 Periodograms of 3293–16

(a) 14–21 Feb 1984. (b) 13–20 Mar 1984. (c) 10–24 April 1984

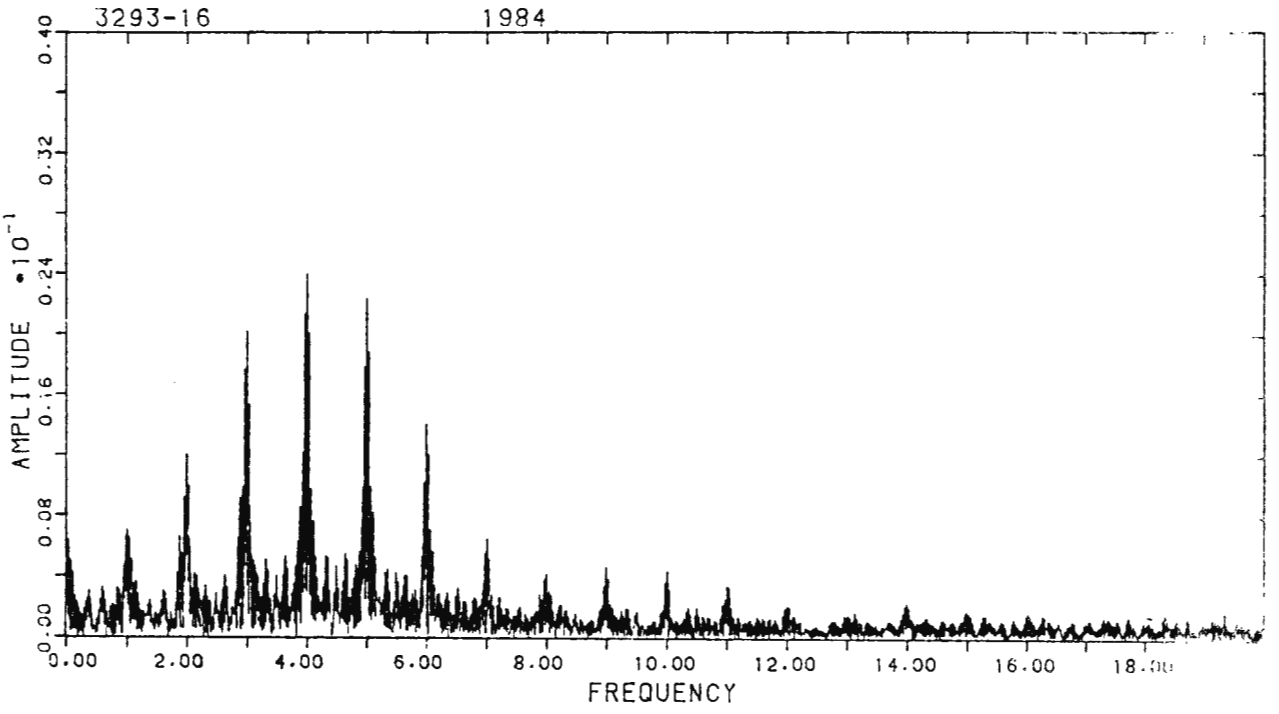

Figure 4.10 (d): Periodogram of 3293–16: Feb – Apr 1984

4.7.2 Pulsation frequencies identified

Table 4.5(a)

Pulsation frequencies of 3293–16

Frequency (cycles per day)	Amplitude (B magnitude)	Date
3.99	0.0291	14–21 Feb 1984
4.90	0.0029	
3.99	0.0251	13–20 Mar 1984
5.24	0.0026	
3.99	0.0261	10–24 Apr 1984
3.92	0.0022	
3.99	0.0268	Feb – Apr 1984
4.92	0.0021	

4.7.3 Fourier fit

Table 4.5 (b)
Fourier parameters for 3293–16

Frequency (cycles per day)	Amplitude (B magnitude)
3.99	0.0267
4.92	0.0023

Standard error of a single observation:

$0^{m}.0065$

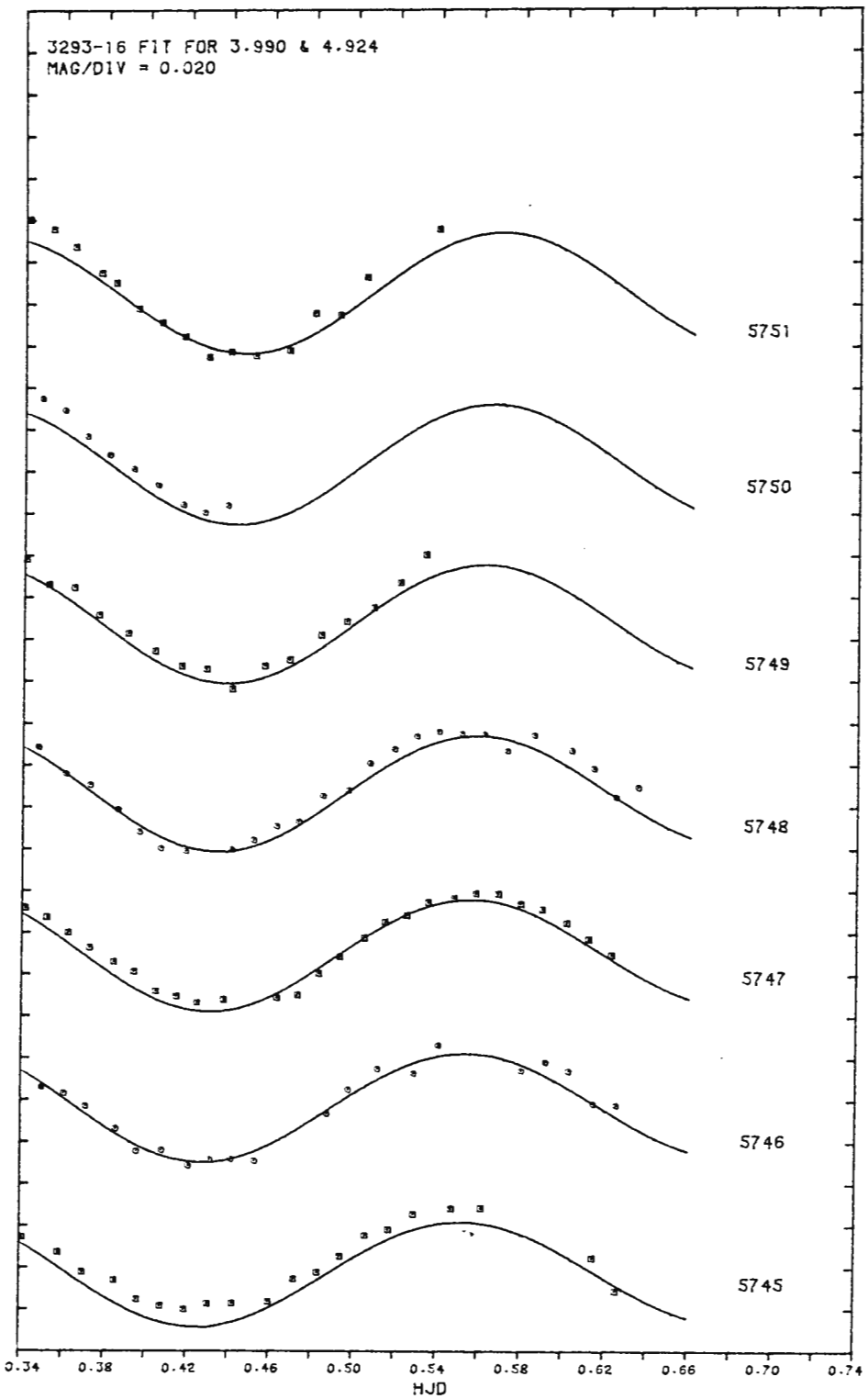

Figure 4.11: Fourier fit for 3293–16

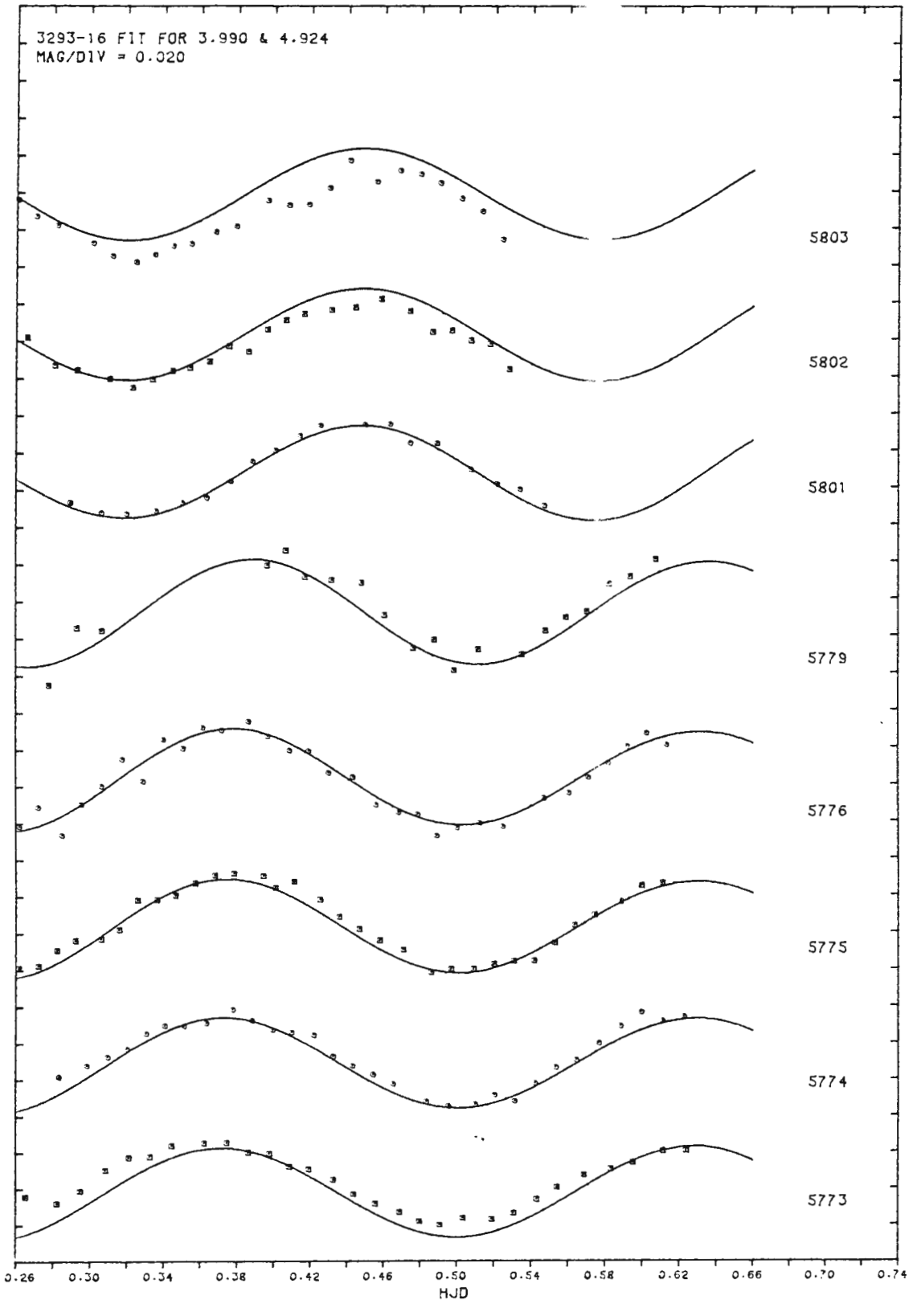

Figure 4.11 (continued):

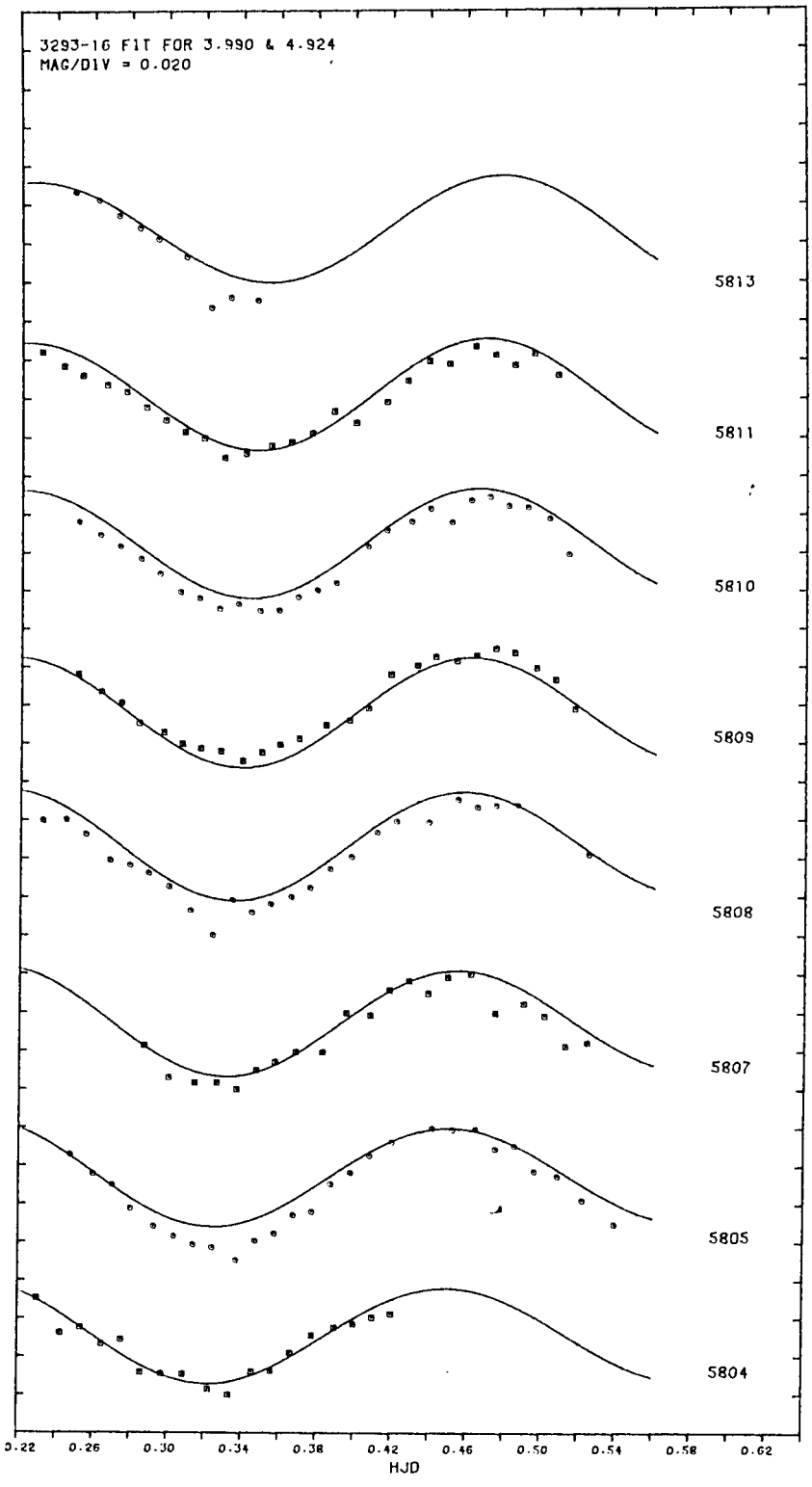

Figure 4.11 (continued)

4.8 THE STAR 3293–18

4.8.1 Periodograms

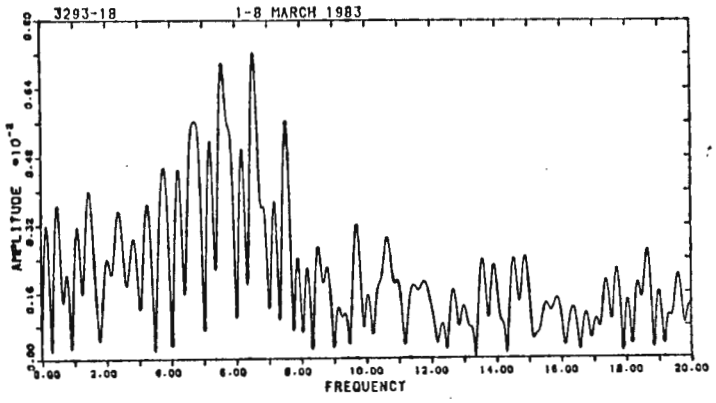

(a)

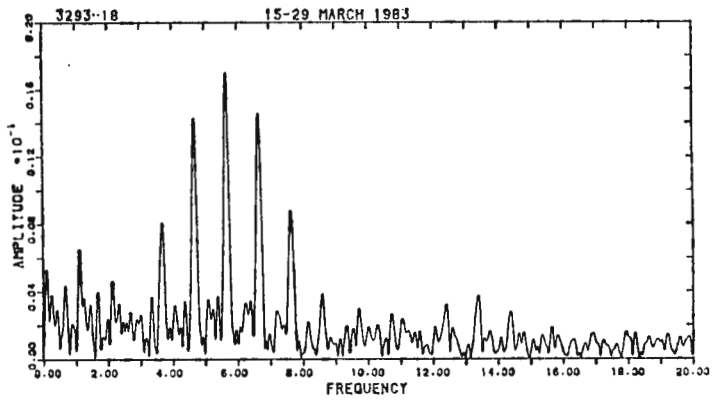

(b)

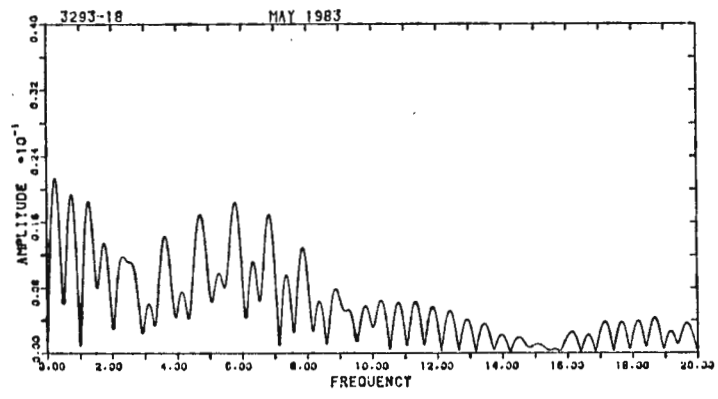

(c)

Figure 4.12 Periodograms of 3293–18

(a) 1–8 Mar 1983. (b) 15–29 Mar 1983. (c) 10–17 May 1983

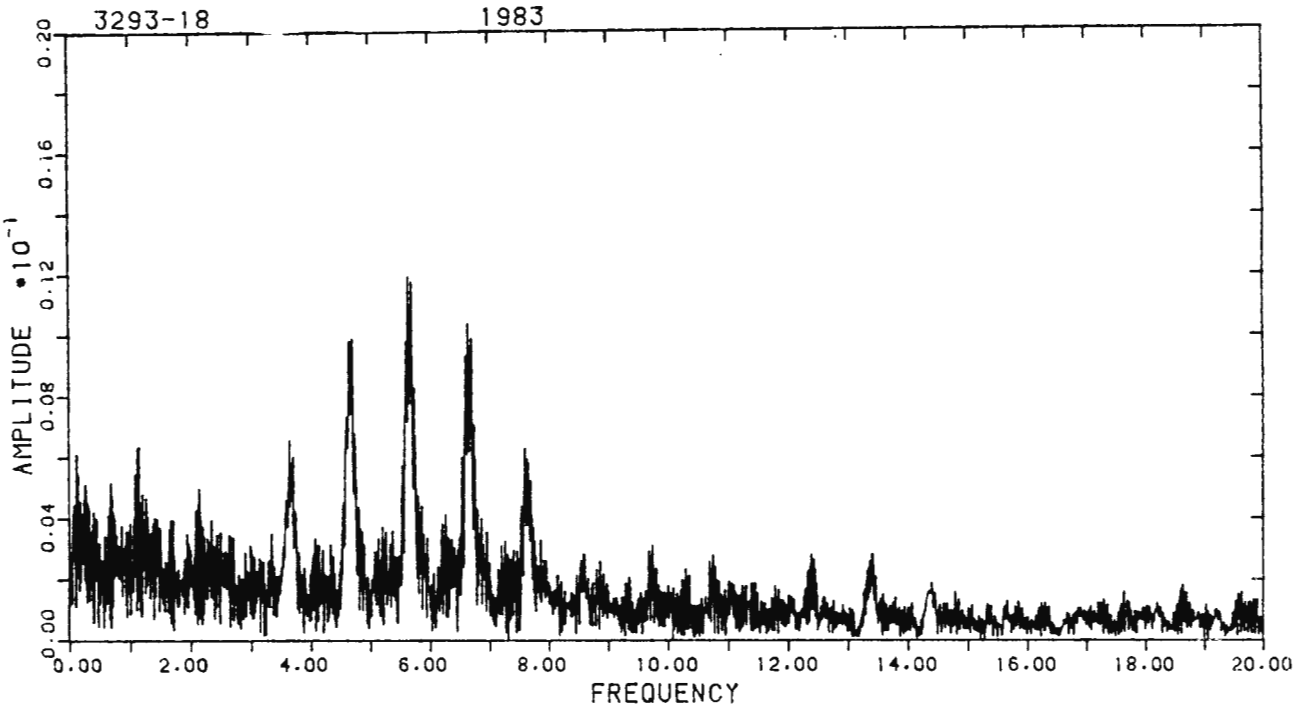

Figure 4.12 (d): Periodogram of 3293–18: March – May 1983

4.8.2 Pulsation frequencies identified

Table 4.6(a)

Pulsation frequencies of 3293–18

Frequency (cycles per day)	Amplitude (B magnitude)	Date
6.57	0.0077	1 – 8 Mar 1983
5.79	0.0058	
4.27	0.0037	
8.74	0.0023	
5.67	0.0168	15–29 Mar 1983
5.75	0.0070	
5.57	0.0062	
5.80	0.0181	10–17 May 1983
5.64	0.0118	March–May 1983
5.73	0.0094	
6.55	0.0047	
5.83	0.0040	

4.8.3 Fourier fit

Table 4.6 (b)
Fourier parameters for 3293–18

Frequency (cycles per day)	Amplitude (B magnitude)
5.64	0.0139
5.73	0.0104
6.55	0.0053
5.83	0.0042

Standard error of a single observation:

$0^{m}.0096$

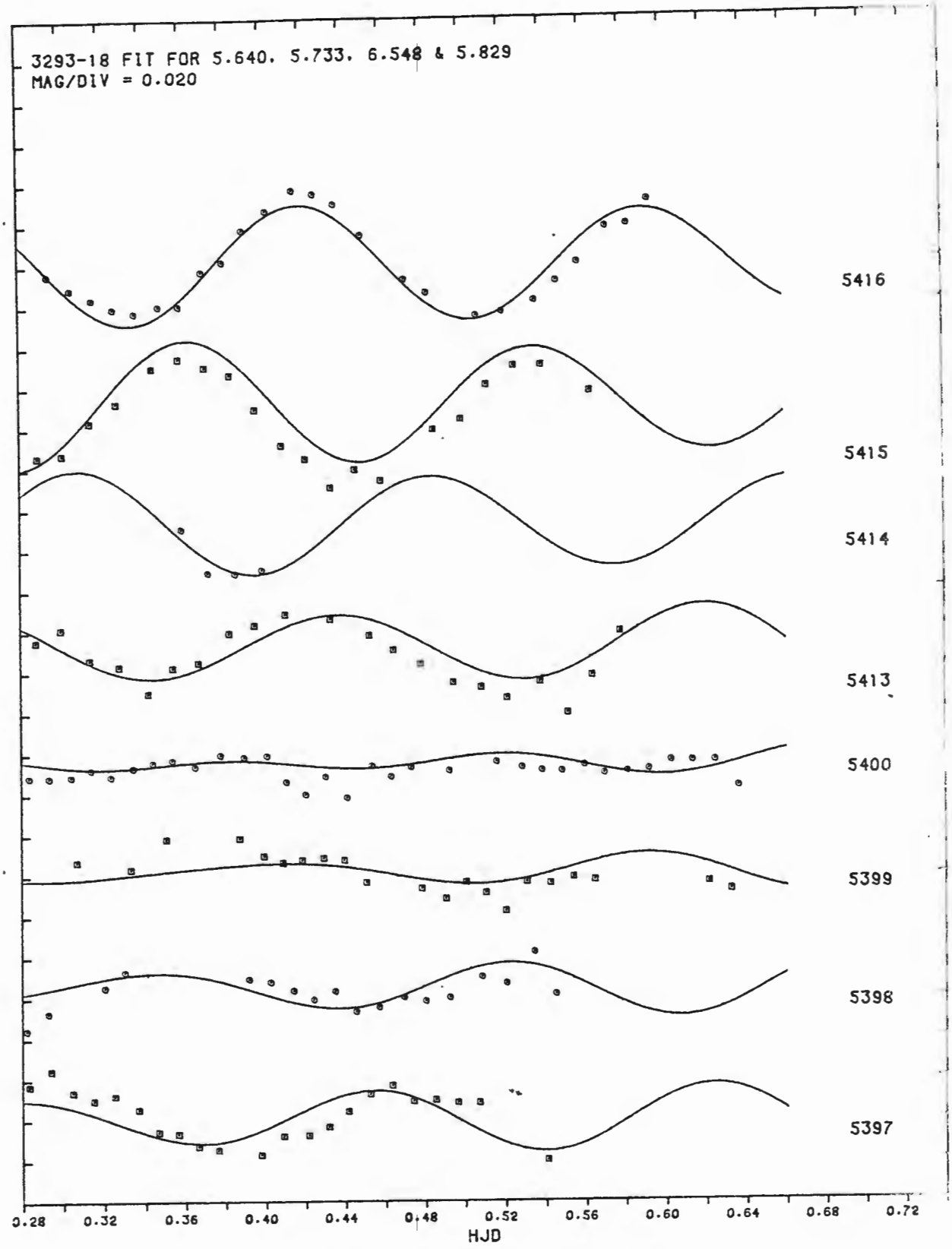

Figure 4.13: Fourier fit for 3293–18

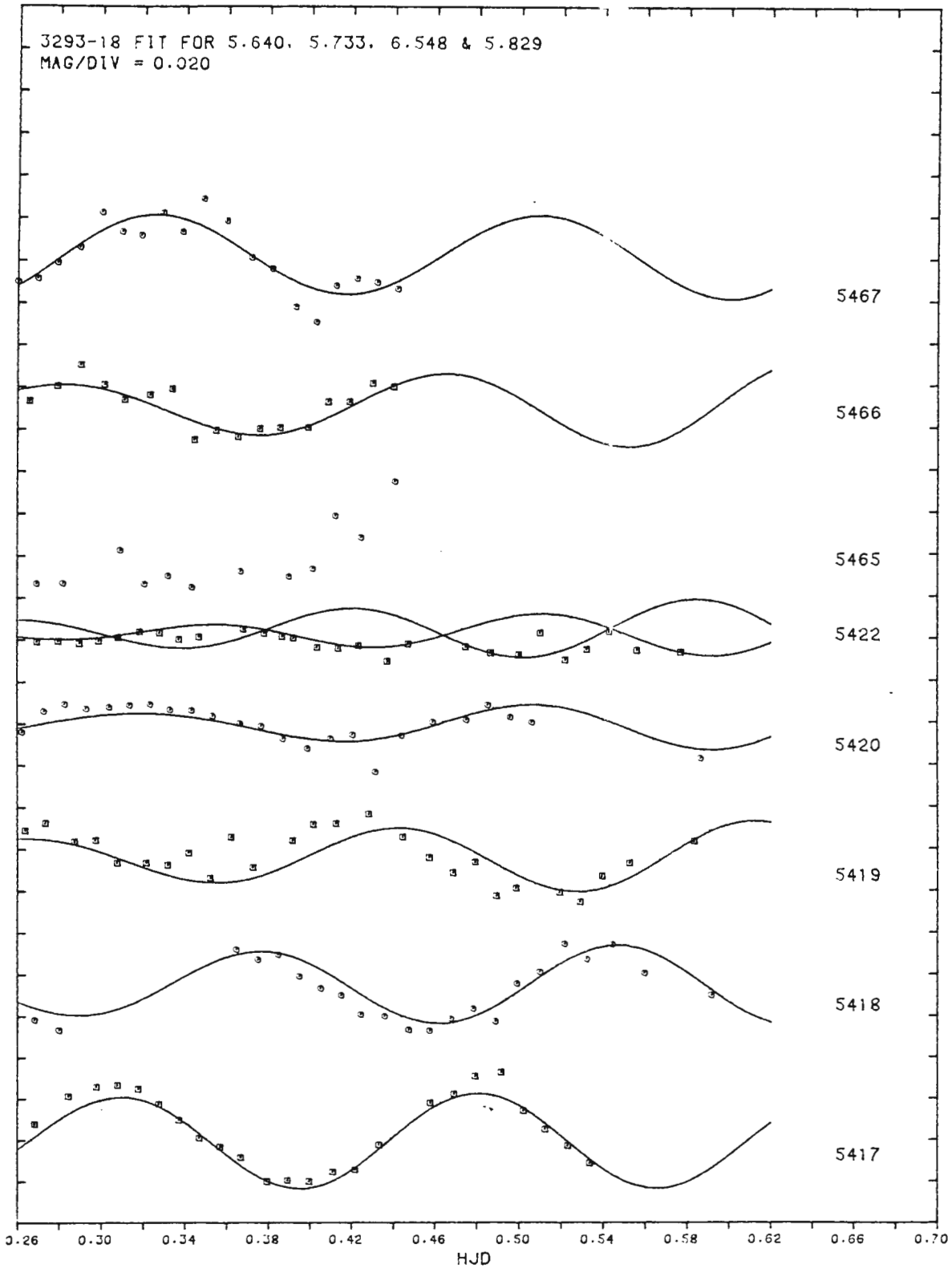

Figure 4.13 (continued):

4.9 THE STAR 3293–23

4.9.1 Periodograms

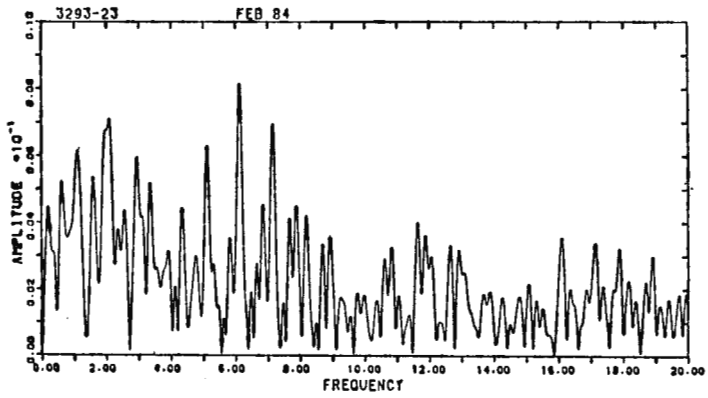

(a)

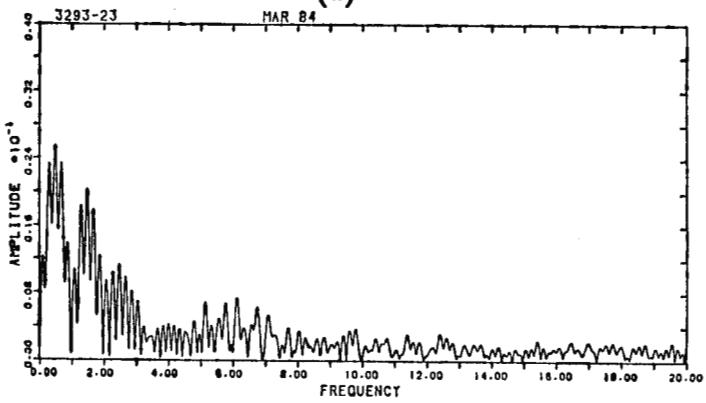

(b)

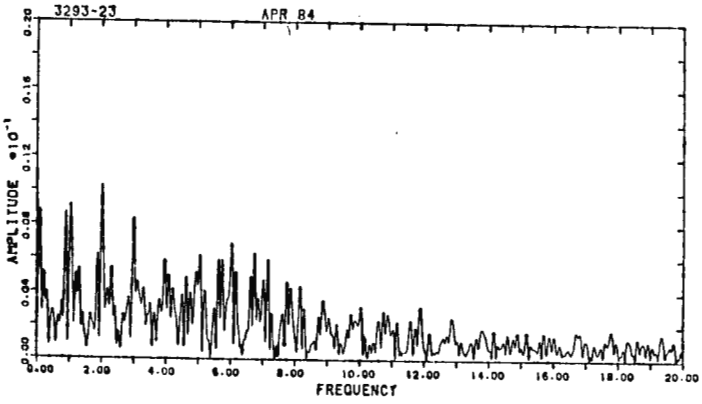

(c)

Figure 4.14 Periodograms of 3293–23

(a) 14–21 Feb 1984. (b) 13–20 Mar 1984. (c) 10–24 April 1984

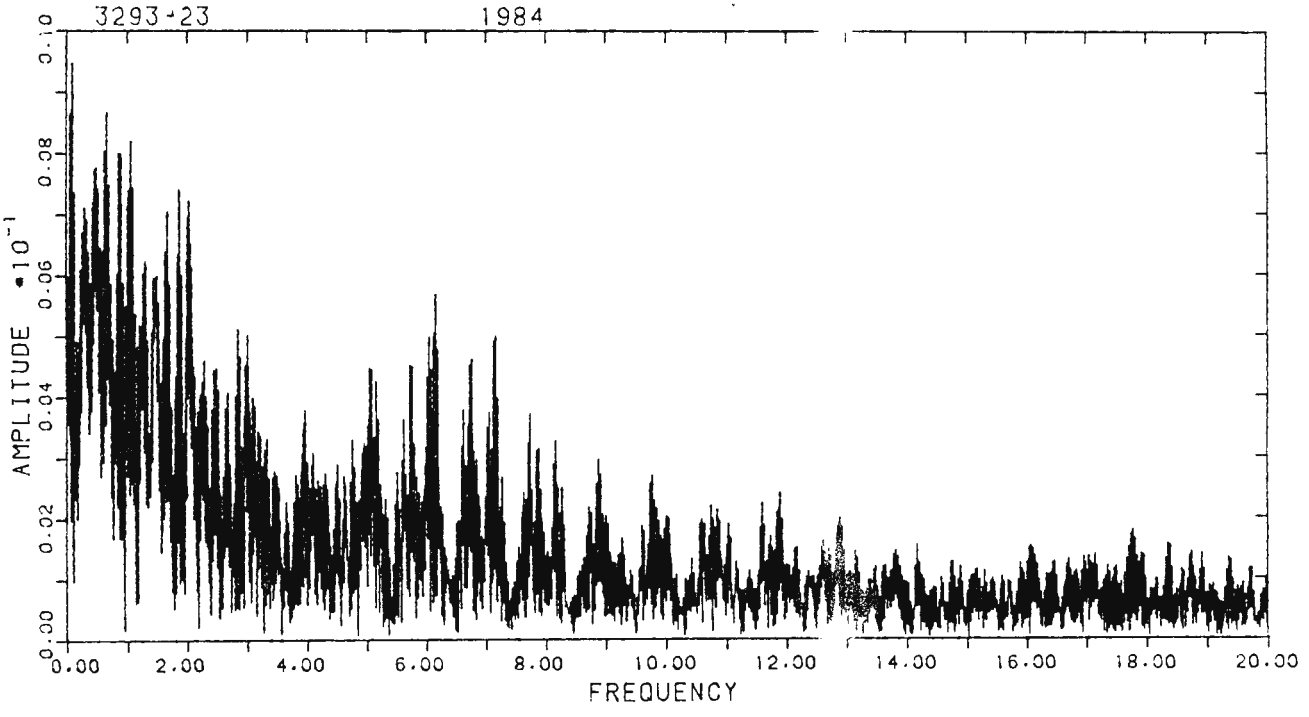

Figure 4.14 (d): Periodogram of 3293–23: Feb – Apr 1984

4.9.2 Pulsation frequencies identified

Table 4.7(a)

Pulsation frequencies of 3293–23

Frequency (cycles per day)	Amplitude (B magnitude)	Date
6.13	0.0086	14–21 Feb 1984
7.91	0.0047	
6.11	0.0079	13–20 Mar 1984
5.05	0.0048	10–24 Apr 1984
5.64	0.0047	
6.17	0.0052	Feb – Apr 1984
5.74	0.0042	
6.64	0.0030	

4.9.3 Fourier fit

Table 4.7 (b)
Fourier parameters for 3293–23

Frequency (cycles per day)	Amplitude (B magnitude)
6.17	0.0063
5.74	0.0043
6.64	0.0036

Standard error of a single observation (excluding nights 5774 & 5804):
$0^{m}.0100$

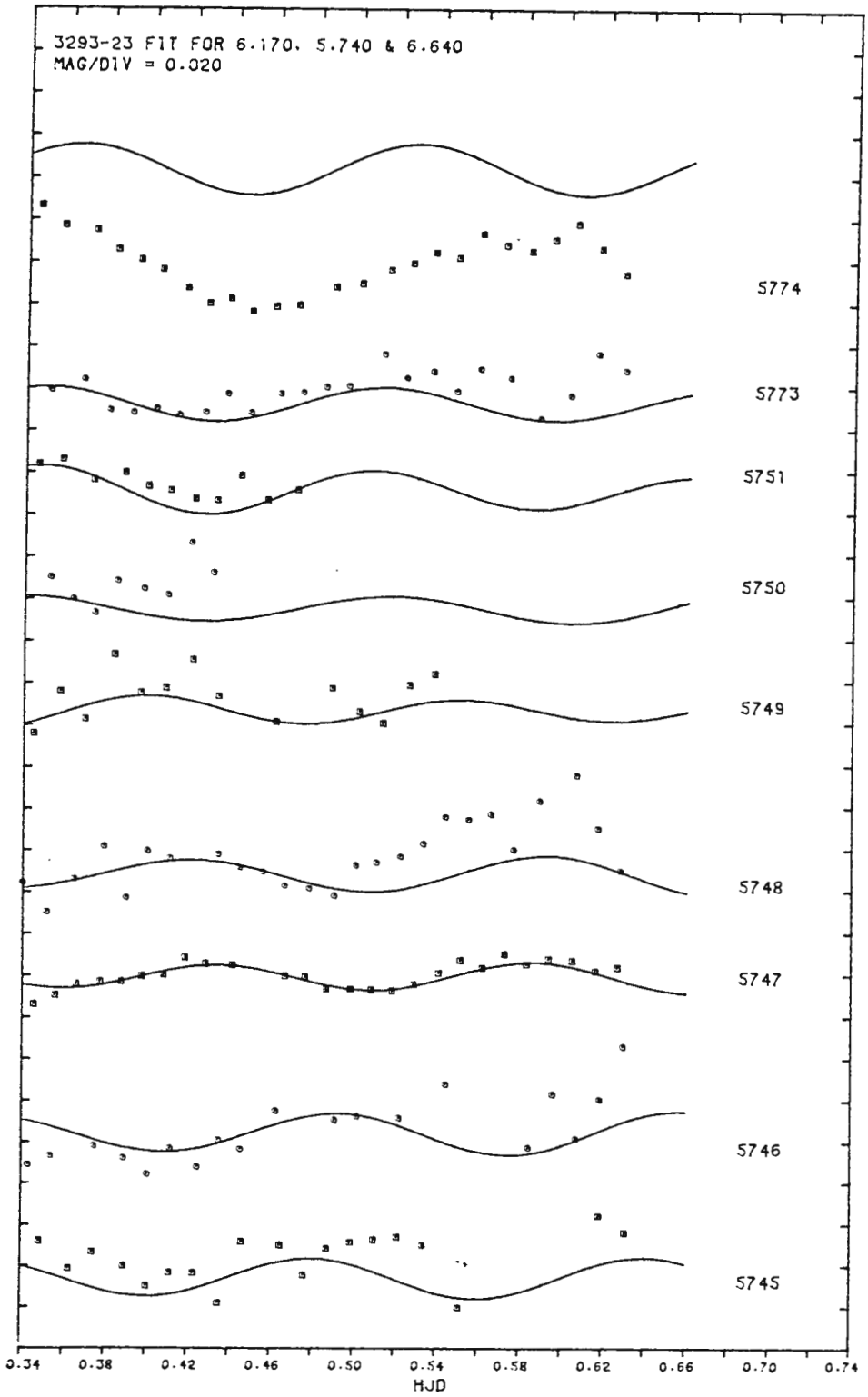

Figure 4.15: Fourier fit for 3293–23

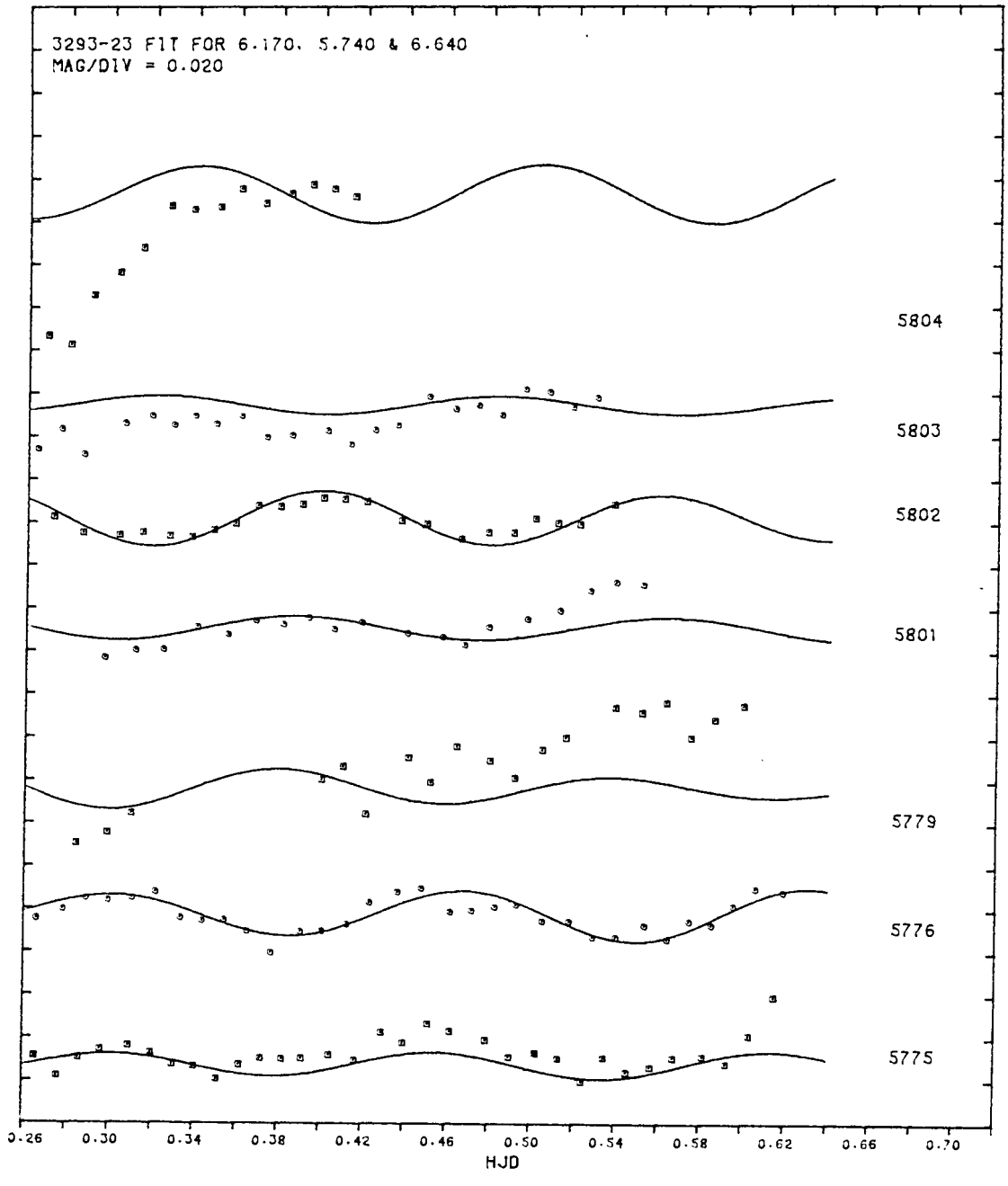

Figure 4.15 (continued):

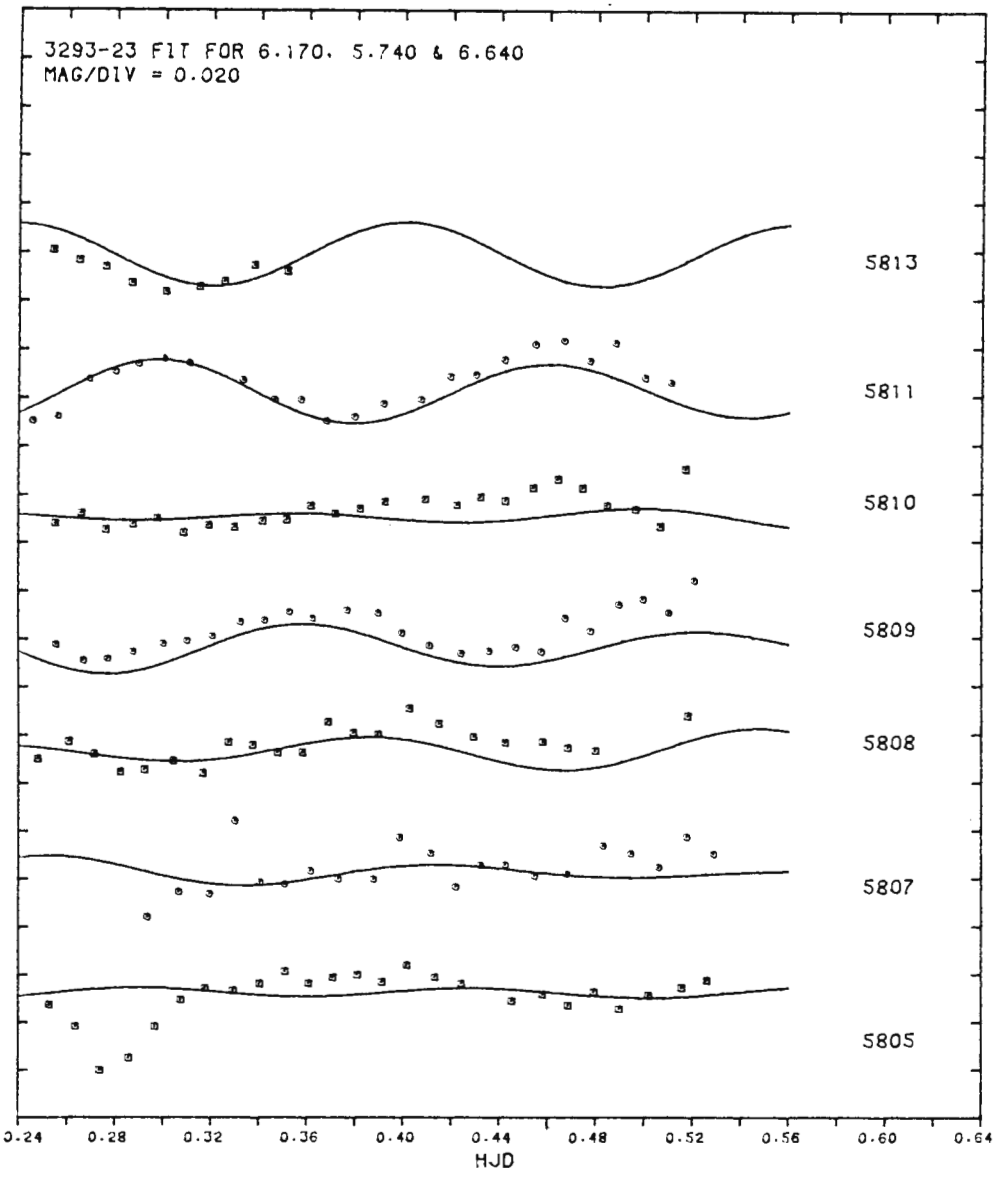

Figure 4.15 (continued):

4.10 THE STAR 3293–24

4.10.1 Periodograms

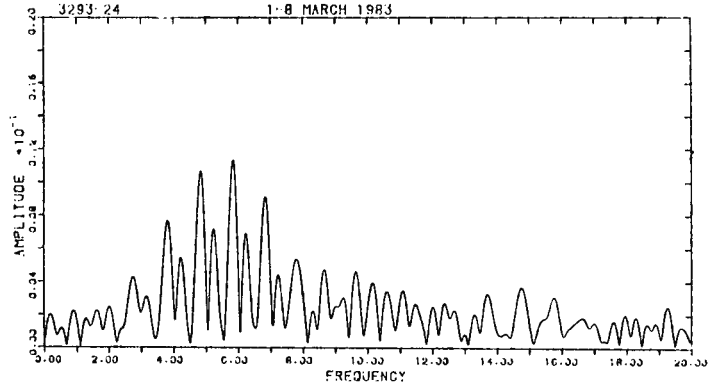

(a)

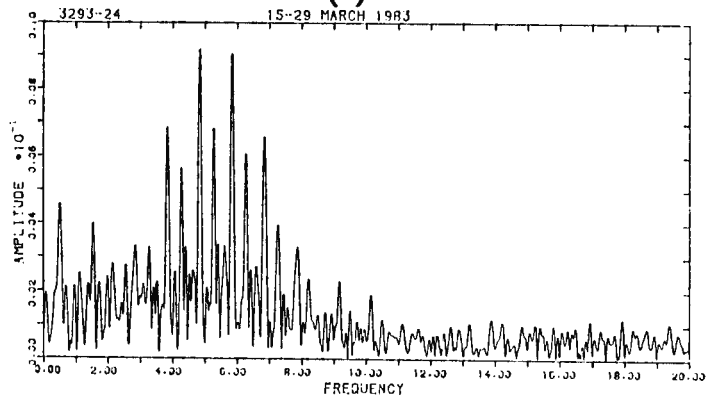

(b)

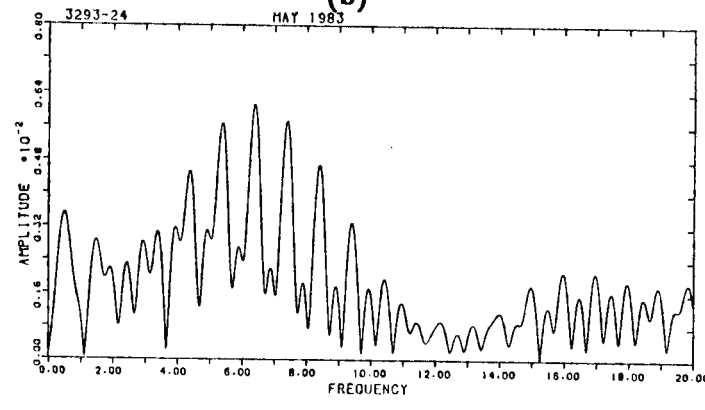

(c)

Figure 4.16 Periodograms of 3293–24

(a) 1–8 March 1983. (b) 15–29 Mar 1983. (c) 10–17 May 1983

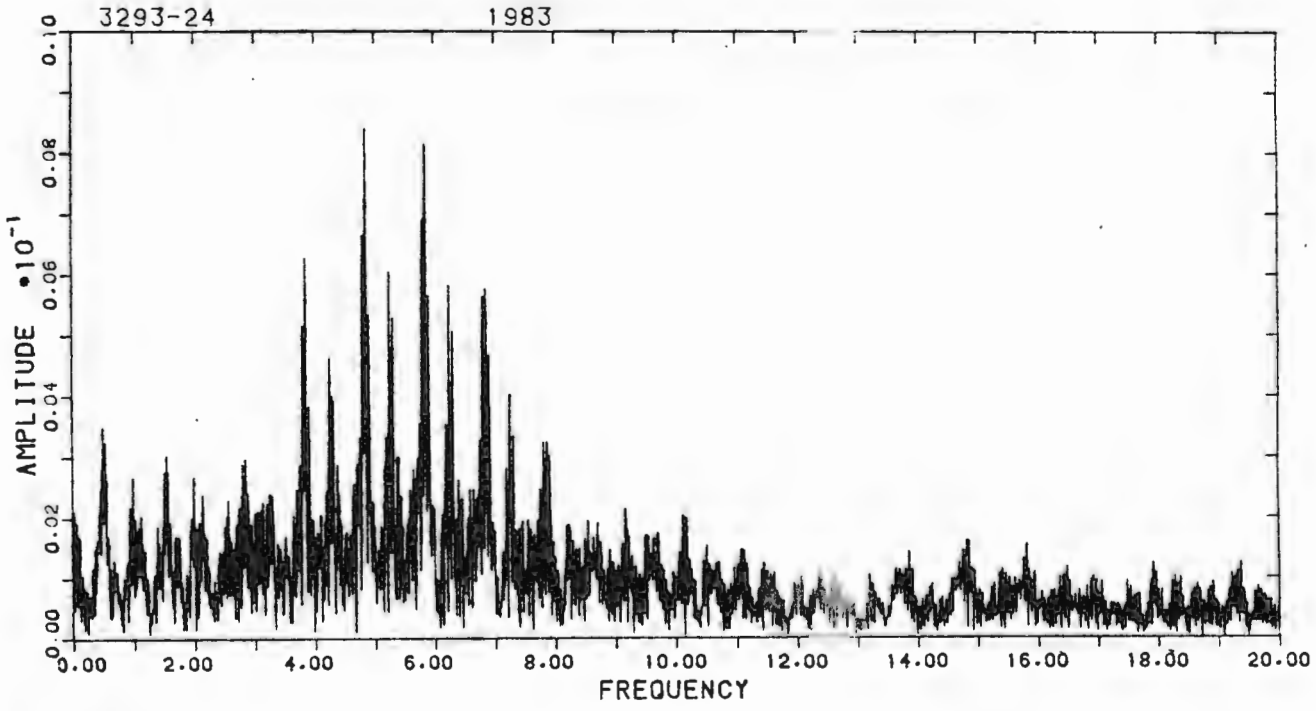

Figure 4.14 (d): Periodogram of 3293–24: March – May 1983

4.10.2 Pulsation frequencies identified

Table 4.8(a)

Pulsation frequencies of 3293–24

Frequency (cycles per day)	Amplitude (B magnitude)	Date
5.84	0.0122	1 – 8 Mar 1983
6.35	0.0053	
3.78	0.0040	
4.84	0.0091	15–29 Mar 1983
6.24	0.0054	
5.65	0.0029	
6.89	0.0030	
6.37	0.0063	10–17 May 1983
5.00	0.0039	
4.85	0.0085	March – May 1983
6.25	0.0057	
5.86	0.0038	
5.65	0.0032	

4.10.3 Fourier fit

Table 4.8 (b)
Fourier parameters for 3293–24

Frequency (cycles per day)	Amplitude (B magnitude)
4.85	0.0065
6.25	0.0062
5.86	0.0052
5.65	0.0034

Standard error of a single observation:

$0^{m}.0048$

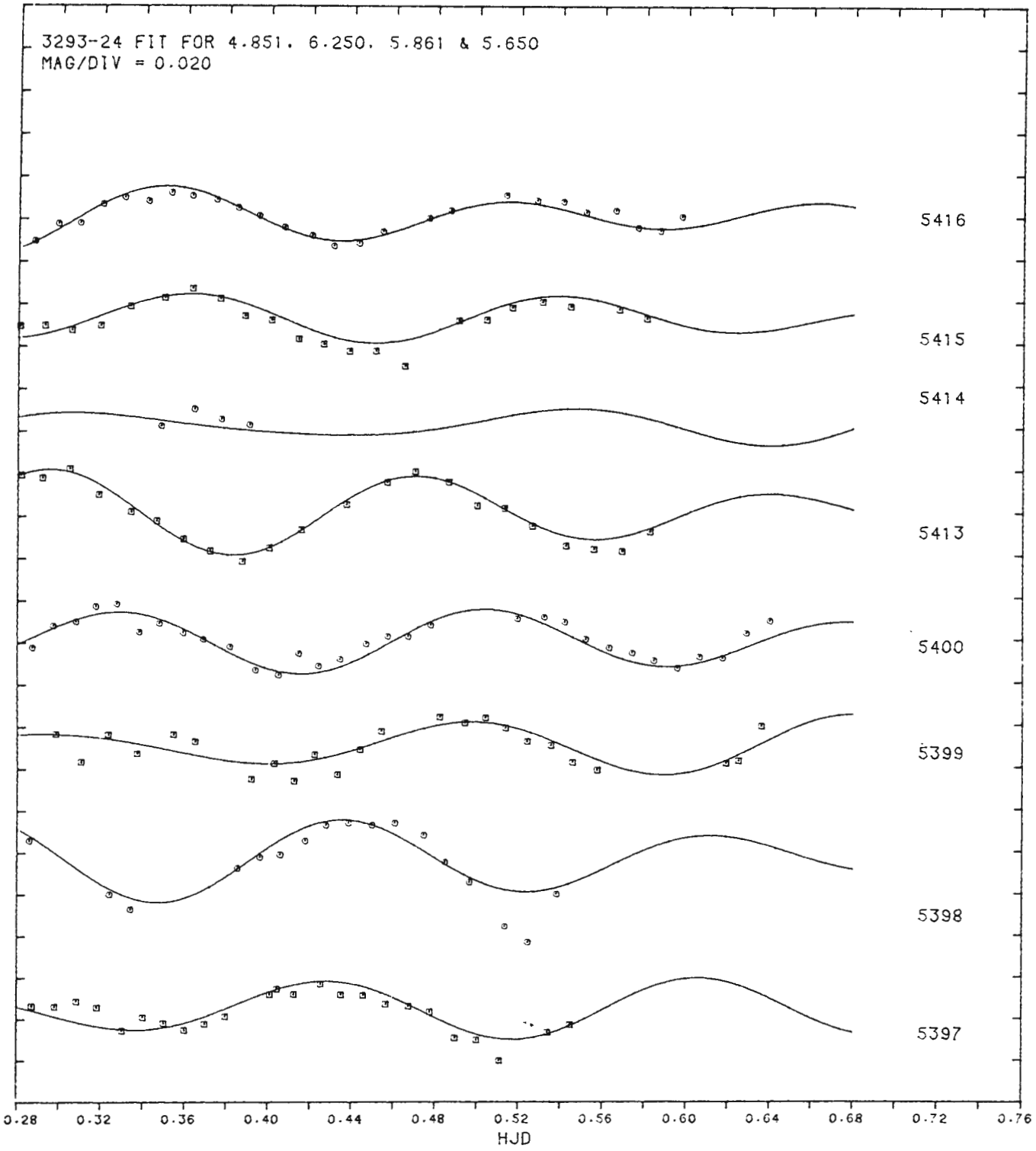

Figure 4.17: Fourier fit for 3293–24

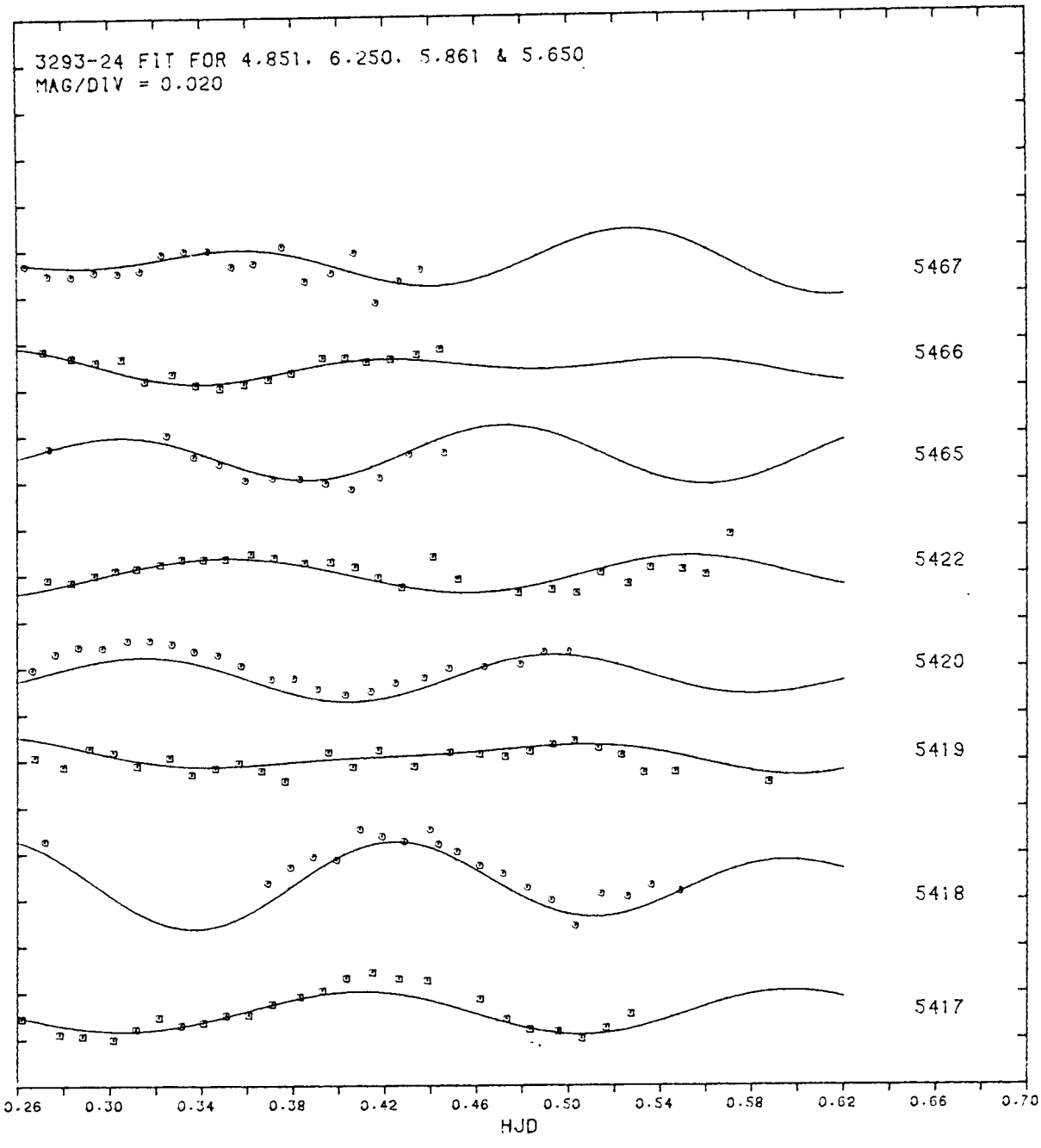

Figure 4.17 (continued):

4.11 THE STAR 3293–27

4.11.1 Periodograms

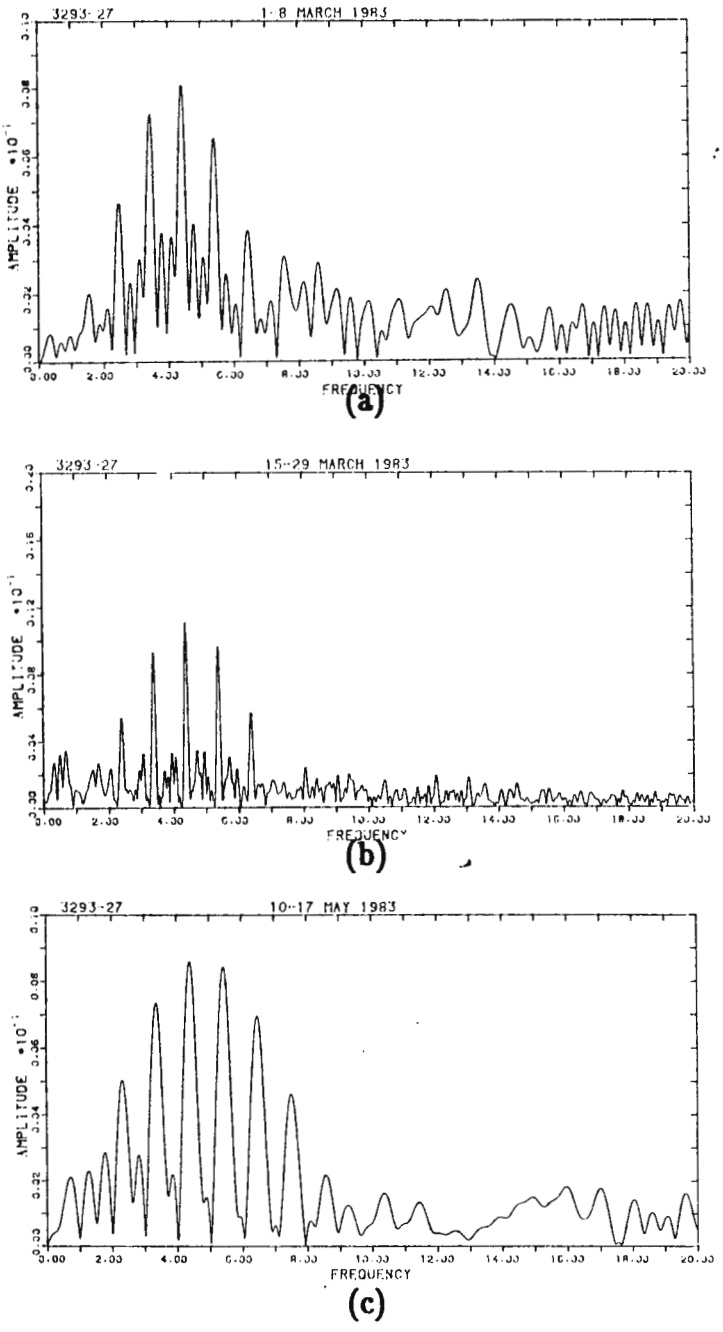

Figure 4.18 Periodograms of 3293–27

(a) 1–8 March 1983. (b) 15–29 Mar 1983. (c) 10–17 May 1983

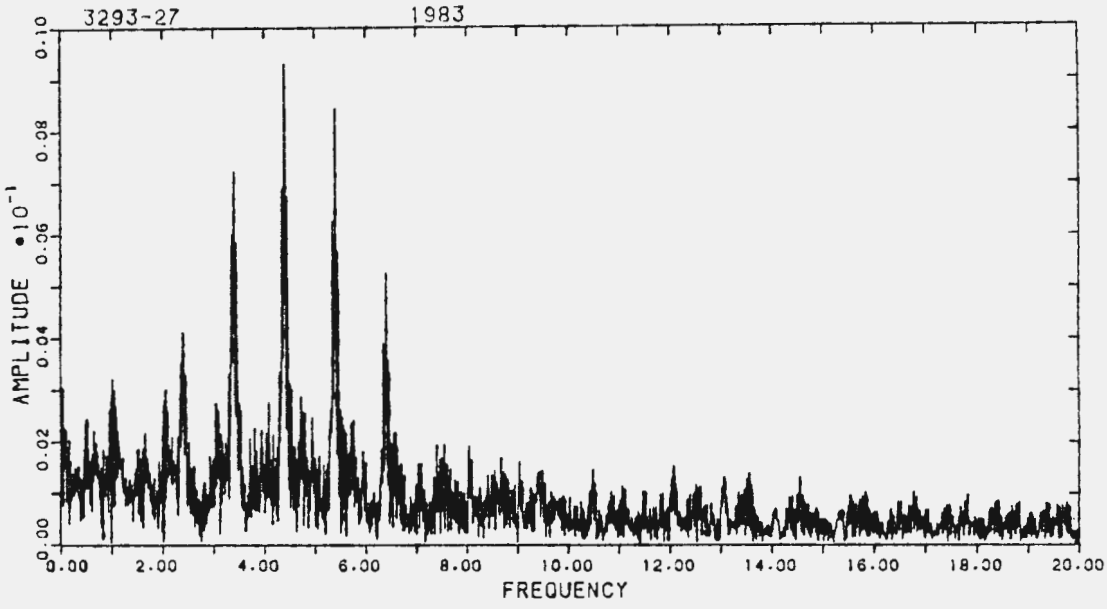

Figure 4.18 (d): Periodogram of 3293–27: March – May 1983

4.11.2 Pulsation frequencies identified

Table 4.9(a)

Pulsation frequencies of 3293–27

Frequency (cycles per day)	Amplitude (B magnitude)	Date
4.42	0.0089	1 – 8 Mar 1983
4.21	0.0021	
4.39	0.0113	15–29 Mar 1983
4.40	0.0086	10–17 May 1983
4.40	0.0100	March–May 1983
4.33	0.0024	

4.11.3 Fourier fit

Table 4.9 (b)
Fourier parameters for 3293–27

Frequency (cycles per day)	Amplitude (B magnitude)
4.40	0.0103
4.33	0.0022

Standard error of a single observation:

$0^{m}.0042$

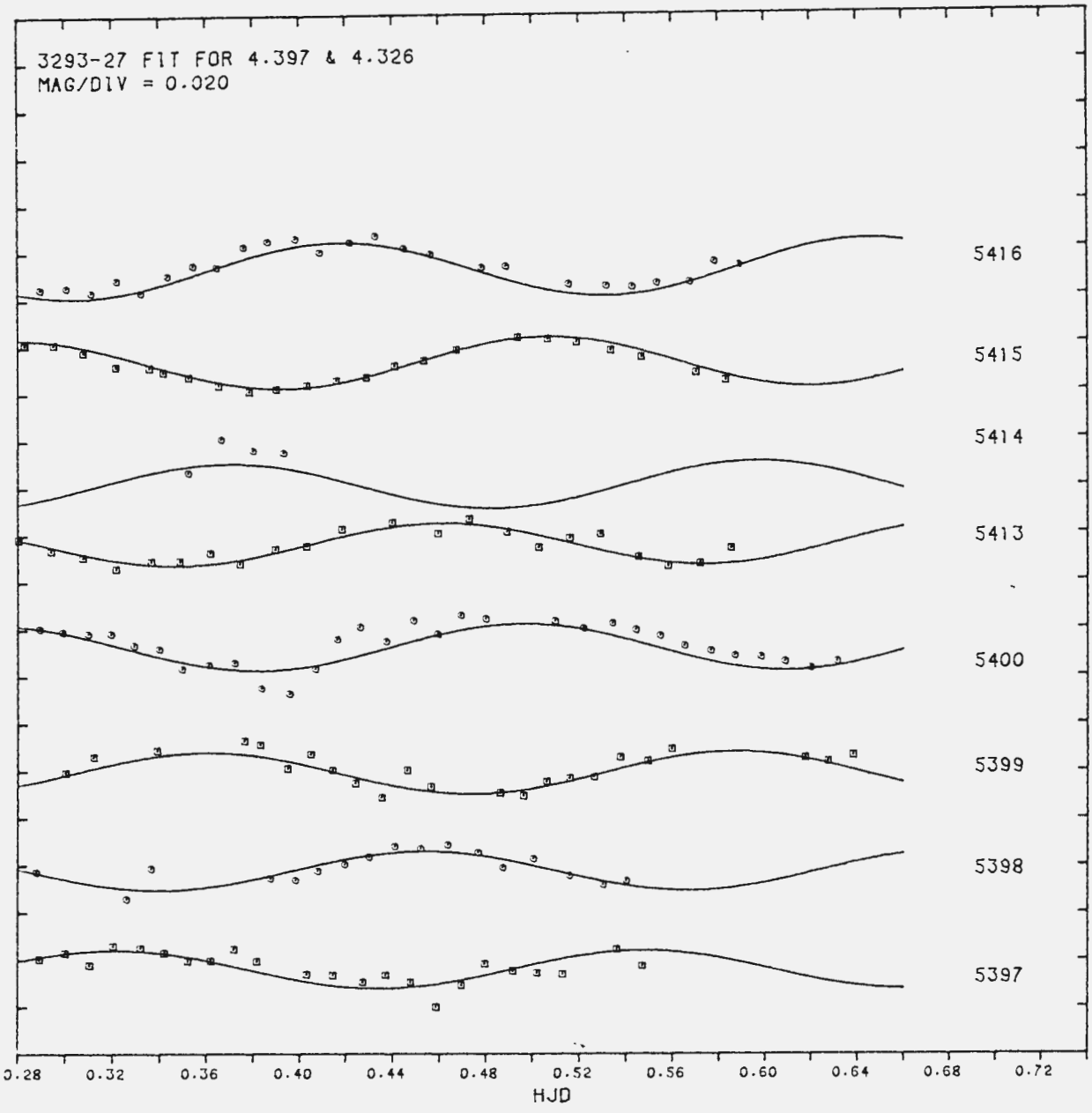

Figure 4.19: Fourier fit for 3293–27

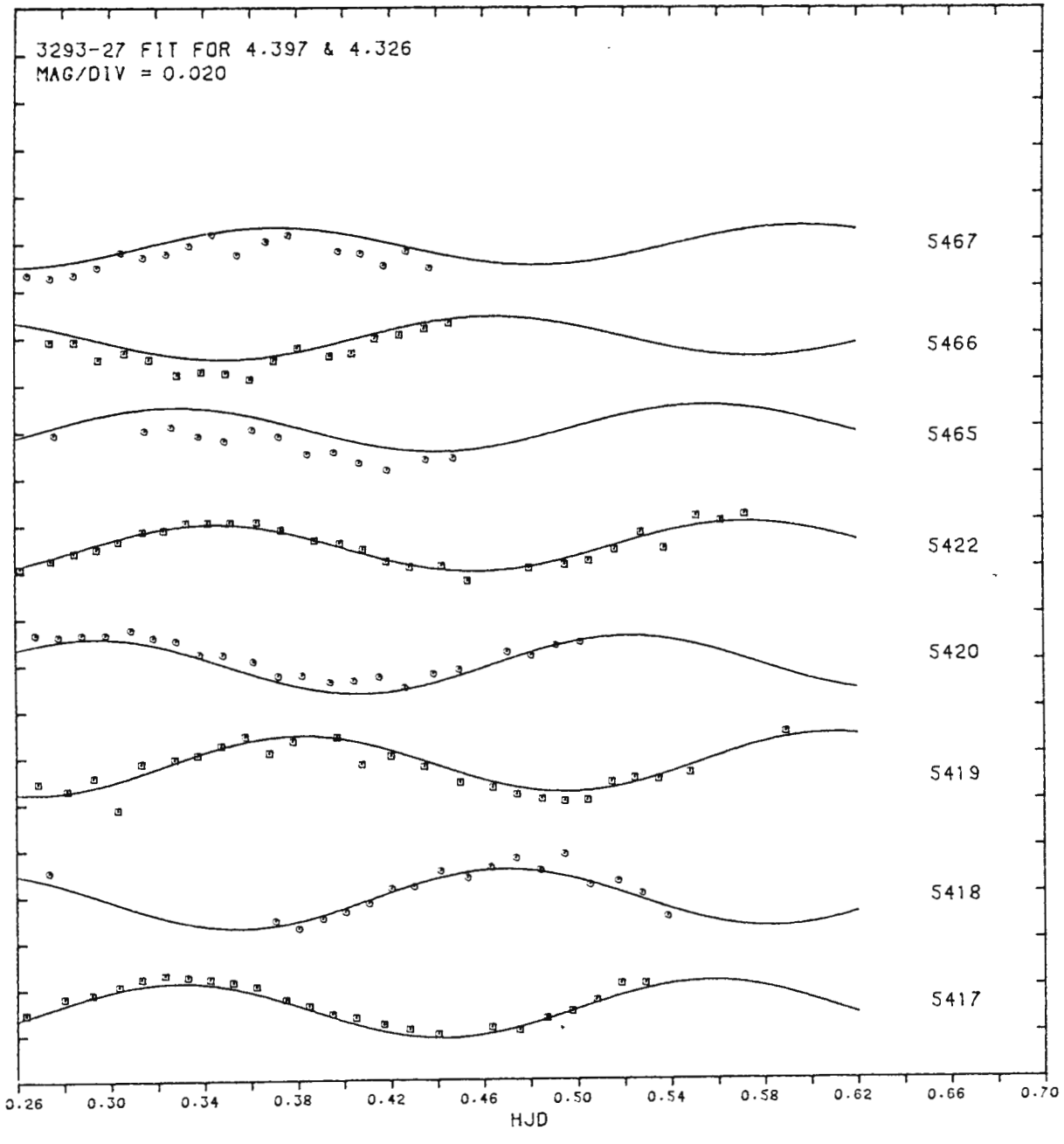

Figure 4.19 (continued):

4.12 THE STAR 3293–65

4.12.1 Periodograms

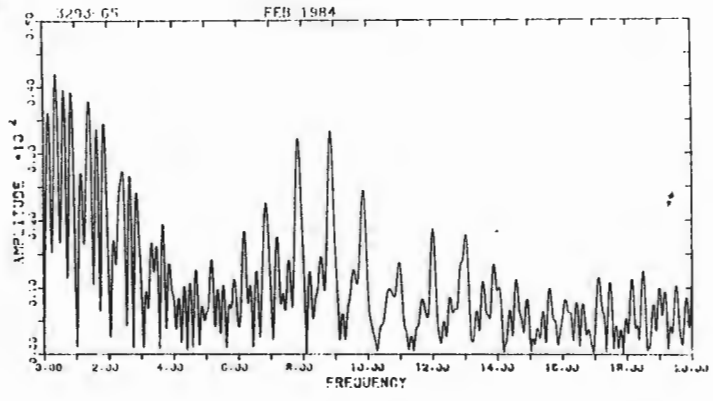

(a)

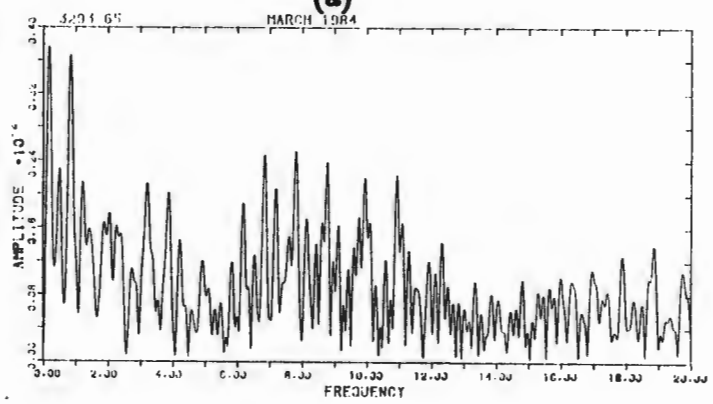

(b)

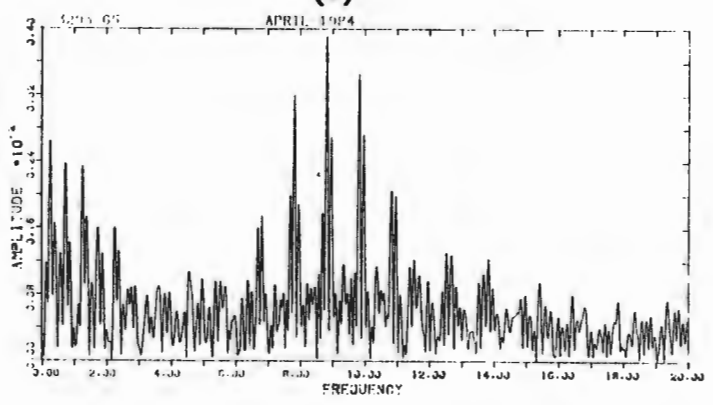

(c)

Figure 4.20 Periodograms of 3293–65

(a) 14–21 Feb 1984. (b) 13–20 Mar 1984. (c) 10–24 April 1984

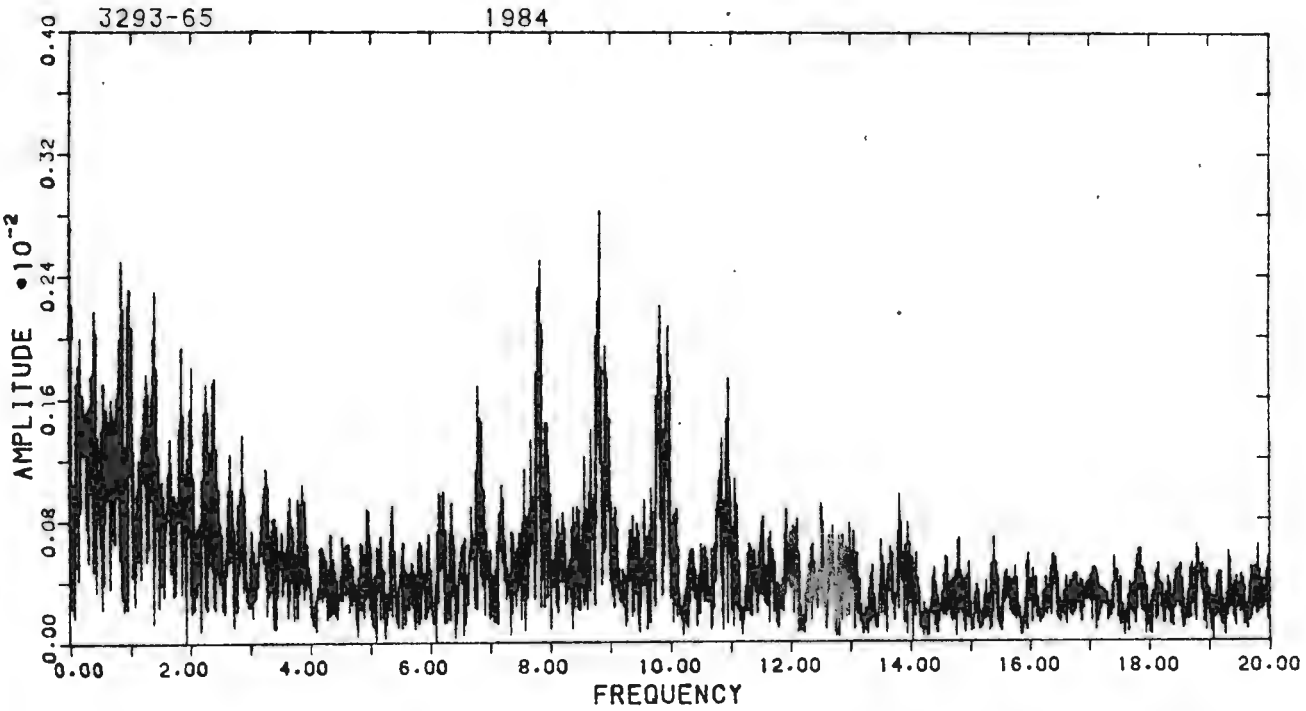

Figure 4.20 (d): Periodogram of 3293–65: Feb – Apr 1984

4.12.2 Pulsation frequencies identified

Table 4.10 (a)

Pulsation frequencies of 3293–65

Frequency (cycles per day)	Amplitude (B magnitude)	Date
8.85	0.0035	14–21 Feb 1984
8.77	0.0026	13–20 Mar 1984
8.82	0.0039	10–24 Apr 1984
9.98	0.0019	
8.81	0.0031	Feb – Apr 1984
9.97	0.0022	

4.12.3 Fourier fit

Table 4.10 (b)
Fourier parameters for 3293–65

Frequency (cycles per day)	Amplitude (B magnitude)
8.81	0.0030
9.97	0.0022

Standard error of a single observation:

$0^{m}.0048$

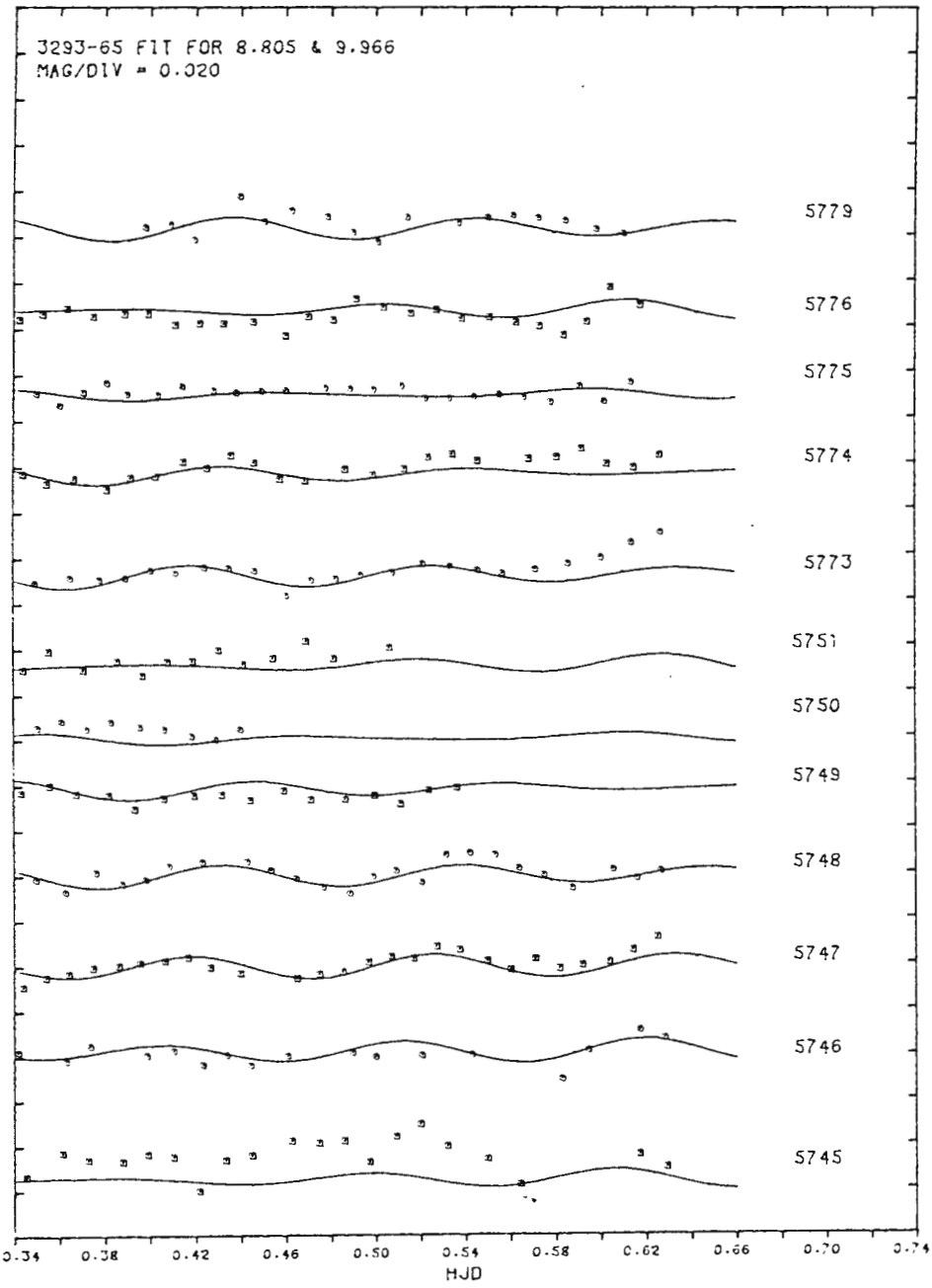

Figure 4.21: Fourier fit for 3293–65

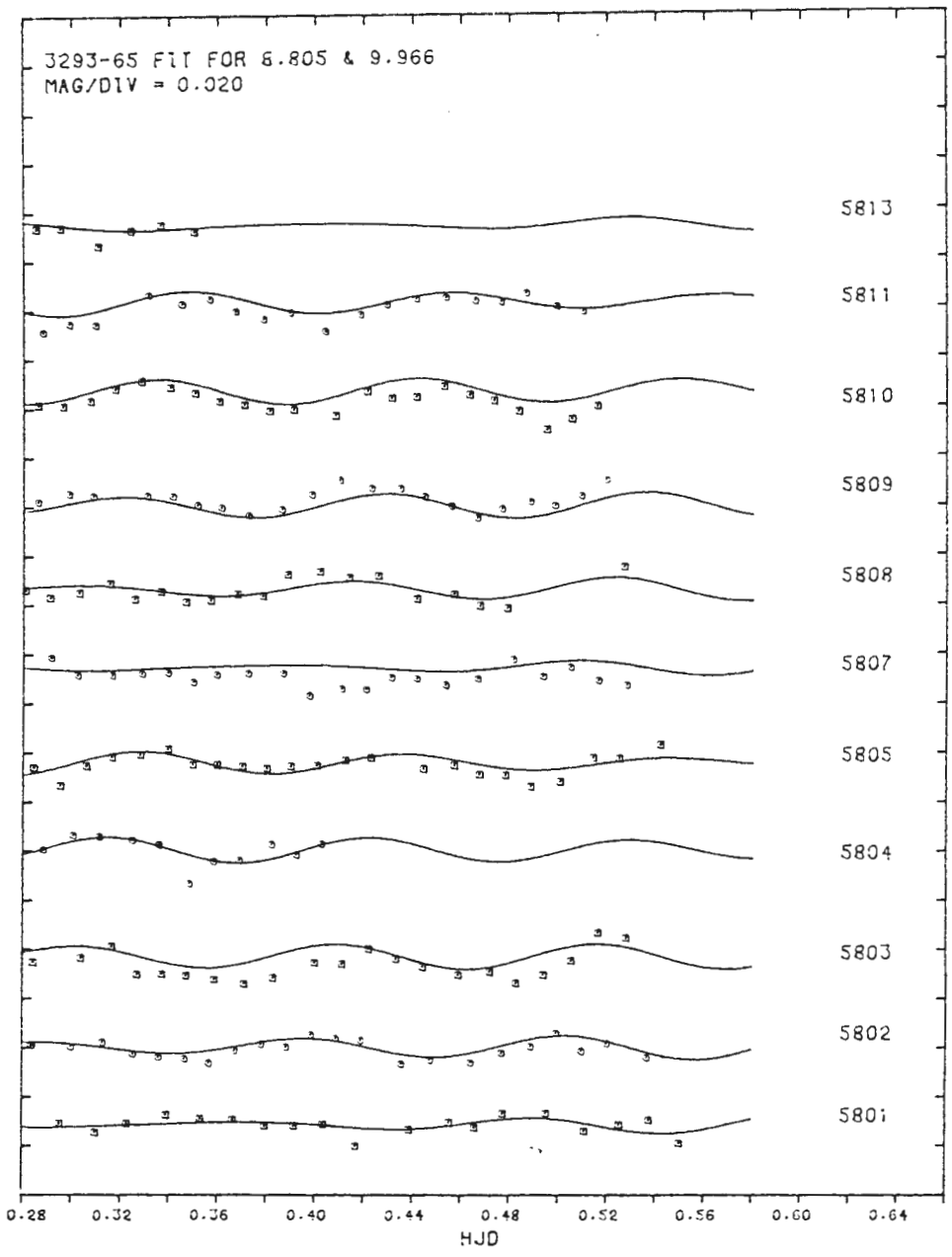

Figure 4.21 (continued):

CHAPTER 5
STELLAR PULSATION THEORY

5.1 INTRODUCTION

A brief introduction to stellar pulsation theory is presented in this chapter, to provide the necessary background to the further discussion of the results described in chapter 4. **Nonradial** stellar pulsation theory considers the periodic perturbation of a star in all three spatial dimensions, as opposed to merely one dimension in the case of purely radial pulsation. Books on pulsation theory (Cox and Giuli 1968, Unno et al. 1979 & 1989 and Cox 1980) give a thorough mathematical description of nonradial pulsation; only a brief summary appears in the following sections:

5.2 DIFFERENTIAL EQUATIONS

The pulsational behaviour of a star is governed by physical requirements expressed in the following four differential equations:

(Let ρ represent mass density, $\boldsymbol{v}$ velocity of a mass element, P pressure, ψ gravitational potential per unit mass, T temperature, S entropy per unit mass, ϵ rate of thermonuclear energy generation and $\boldsymbol{F}$ total heat flux, all at a position $\boldsymbol{r}$ in the star:)

(i) continuity equation (conservation of mass):

$$\frac{\partial \rho}{\partial t} + \nabla \cdot (\rho \boldsymbol{v}) = 0, \tag{5.1}$$

(ii) equation of linear momentum conservation (ignoring viscosity, large–scale magnetic fields and turbulence):

$$\rho \frac{dv}{dt} = -\nabla P - \rho \nabla \psi, \tag{5.2}$$

(iii) equation of energy conservation (under the same conditions as in (ii)):

$$T \frac{dS}{dt} = \epsilon - \frac{1}{\rho} \nabla \cdot \boldsymbol{F}, \tag{5.3}$$

(iv) Poisson's equation for the gravitational potential:

$$\nabla^2 \psi = 4\pi G \rho. \tag{5.4}$$

A pulsation of the star may be expressed as a perturbation of the variables appearing in these equations. When the perturbation is sufficiently small that second–order effects may be ignored (often expressed as the condition: $\Delta r/r \leq 0.1$), these differential equations may be linearized to express the behaviour of the perturbations. The perturbations are usually expressed as either Lagrangian or Eulerian variations. A lucid description of these two types of variation may be found in Tassoul(1978).

5.3 LINEARISATION

The **Lagrangian** variation of a variable quantity f (which describes the change in f of a **particular** mass element as it evolves in time) will be written as δf, while the **Eulerian** variation (which describes the change in f at a **fixed point** in the reference frame applied to the problem) will be written as f'.

The linearized versions of equations 10.1 – 10.4 are:

(i) $$\delta\rho + \rho \nabla \cdot (\delta \boldsymbol{r}) = 0, \tag{5.5}$$

(ii) $$\frac{d^2(\delta \boldsymbol{r})}{dt^2} = -\delta(\frac{1}{\rho}\nabla P) - \delta(\nabla\psi), \tag{5.6}$$

(iii) $$T\,\frac{d(\delta S)}{dt} = \delta(\epsilon - \frac{1}{\rho}\nabla\cdot \boldsymbol{F}), \tag{5.7}$$

(iv) $$\nabla^2\psi' = 4\pi G\rho'. \tag{5.8}$$

5.4 SEPARATION INTO SPACE AND TIME COORDINATES

If the pulsation is regarded as a harmonic oscillation, the time dependence of a variation δf may be separated out as follows:

$$\delta f = \delta f(\boldsymbol{r})e^{i\omega t}, \tag{5.9}$$

where ω represents the **frequency** of oscillation, of course. Usually, separation of the space dependence into a radial part and an angular part with the following form is assumed:

$$\delta f(\boldsymbol{r}) = \delta f(r)\mathrm{Y}_{\ell}^{m}(\theta,\phi) \tag{5.10}$$

(where $\mathrm{Y}_{\ell}^{m}(\theta,\phi)$ is a spherical harmonic).

When constitutive relations for P, S, ϵ and $\boldsymbol{F}$ (appropriate for the particular stellar model under consideration) are supplied, the linearized differential equations can be solved for appropriate boundary conditions. The spherical harmonic index ℓ takes on integer values 0, 1, 2, 3,..., of course, and an additional index, k, indicates the number of nodes in the **radial** part of the pulsational **displacement** eigenfunction (ie the Lagrangian

variation of position in the star). Put more simply, k specifies the overtone of the radial part of the pulsation; it is often called the order of the pulsation mode (as was done in chapter 1).

The system of equations will only satisfy the boundary conditions for the corresponding eigenvalues of ω^2. A different solution exists for each value of ℓ and each value of k. For a particular star (with a particular mass) each pair of values of k and ℓ will then correspond to its respective eigenvalue of ω^2. Therefore, the value of ω^2 in a real variable star is an indicator of the values of k and ℓ.

5.5 MODAL STRUCTURE OF EIGENSOLUTIONS

The eigenfrequencies for the pulsations, found by the method just outlined, fall into two groups; tending either to infinity or to zero as the number of radial nodes increases. Cowling (1941) distinguished between these two groups as "pressure modes" (p–modes for short) and "gravity modes" (g–modes) respectively, referring to the fact that in the pressure modes the pressure gradient resulting from a perturbation in the stellar fluid is the dominant agent restoring the fluid to its unperturbed state, while in the gravity modes the inequality in gravitational potential caused by perturbation is the dominant restoring agent. This is simply due to the difference in relative importance of changes in pressure and gravitational potential respectively, in the different regions of the star where p–modes and g–modes respectively are dominant. The frequency spectra of the p– and g–modes respectively are illustrated in Figure 5.1, which is taken from Cox (1980). The symbol n is substituted for k in the figure. Note that g–modes only occur with nonradial pulsation, while the p–modes are simply the "extension" of the radial modes to the nonradial situation.

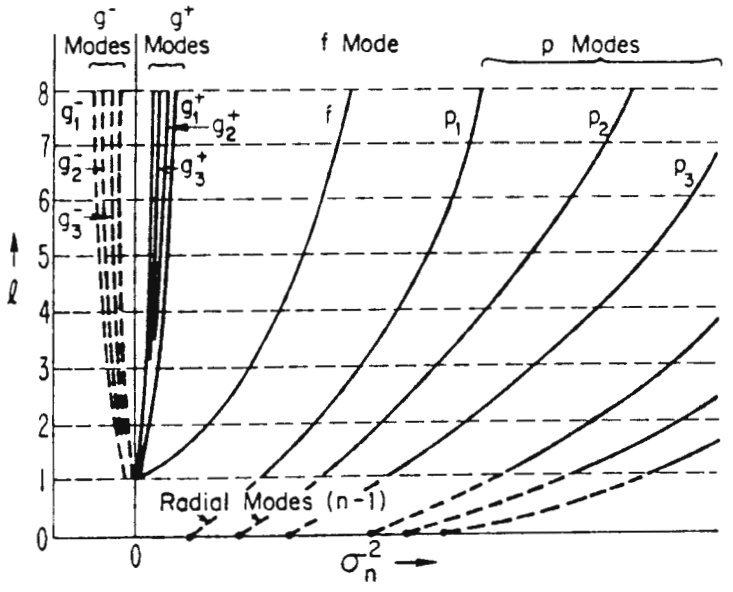

Figure 5.1. Theoretical behaviour of pulsation eigenfrequencies with order and overtone, for polytropes. (From Cox (1980)).

The **pressure** modes follow the behaviour of radial modes in having higher frequencies for successive overtones (p_1, p_2, p_3,...) for a fixed value of ℓ. For a given overtone, the frequencies also increase with increasing ℓ.

The g–modes are split into a group with $\omega^2 > 0$ (g^+–modes) and a group with $\omega^2 < 0$ (g^-–modes). The g^+–modes **decrease** in frequency with increasing **overtone**, but follow the p–modes in **increasing** in frequency as ℓ increases, for a given overtone. The g^-–modes are not physically real and are ignored in the further consideration of stellar pulsation in this thesis.

Pressure modes and gravity modes have a common fundamental mode, labeled the f mode. Modes designated by p_k or g_k are k–th overtone modes.

5.6 EFFECTS OF STELLAR ROTATION

The pulsations of stars are significantly affected by the fact that all real stars **rotate** about an axis. In a stationary (ie nonrotating) star, the nonradial pulsation modes are degenerate in frequency for the different values of the azimuthal spherical harmonic index m corresponding to each value of ℓ.

The effect of stellar rotation on the pulsational behaviour of stars includes the removal of this degeneracy in values of the pulsation eigenfrequency ω. Saio (1981) has derived a second–order expression for this effect in a uniformly rotating polytrope of index 3:

$$\omega = \omega_0 - (1 - C_1)m\Omega + C_2\Omega^2/\omega_0^2, \tag{5.11}$$

where ω = frequency of a particular mode in the rotating star,

ω_0 = frequency of this mode in a nonrotating star,

C_1 = a constant, the value of which depends on k and ℓ, as well as on the specific structure of the star,

Ω = angular rotation speed of the star, and

C_2 = a constant which depends on m, k and ℓ, as well as on the specific structure of the star.

The effect of **differential** rotation (ie where not all parts of the stellar surface are rotating at the same value of Ω), to first order in Ω, has been investigated by Hansen et al. (1977). They found that the distribution of angular momentum is closely approximated by the expression:

$$\Omega(\varpi) = \Omega_0(1 + \Omega_1\varpi + \Omega_2\varpi^2), \qquad (5.12)$$

where ϖ = the cylindrical radial coordinate (ie the perpendicular distance from the polar axis of the star),

Ω_0 = the angular rotation velocity at the stellar poles and

Ω_1 and Ω_2 are constants depending on the stellar model in use.

Hansen et al. explained that **axially** symmetric rotation, where the angular momentum is still dependent on both ϖ and the "vertical" cylindrical coordinate z (ie $\Omega = \Omega(\varpi,z)$), is rapidly changed to cylindrical symmetry ($\Omega = \Omega(\varpi)$) by the demand for stability in a star. According to these authors, the first–order frequency splitting in a **differentially** rotating star is given by

$$\omega = \omega_0 - m(1 - C_1 - C_3)\Omega_0, \qquad (5.13)$$

where C_3 = a constant incorporating the effect represented by Ω_1 and Ω_2,

and the other symbols have the meanings stated earlier. Of course, Ω_0 is simply the uniform surface angular rotation velocity when there is no differential rotation, in which case equation 5.13 reduces to the first–order form of equation 5.11. Hansen et al. have calculated the values of C_3 for models of massive zero–age main sequence stars including $10M_\odot$ and $20M_\odot$ models, for $\ell = 1$ and $\ell = 2$, and their results are reproduced in Table 5.1. The parameter β appearing in the table represents the ratio of equatorial surface angular velocity to polar (central) angular velocity. It is clear that the magnitude of the frequency splitting in a differentially rotating star is less than that in a uniformly rotating star (at least to first order in Ω), since the value of C_3 is positive.

For the β Cephei stars under discussion in this thesis, the first–order splitting for

differential rotation is about 65% of that for uniform rotation for $\ell = 1$, about 79% for $\ell = 2$ with $|m| = 1$ and about 68% for $\ell = 2$ with $|m| = 2$, according to Hansen et al.'s tables. An observed decrease in the observed pulsation period of a star with time may therefore be due to a change in the stellar rotation rate rather than due to evolutionary effects.

Since the degree of differential rotation present in early B stars is an unknown quantity at present, the analyses in the following chapters assume uniform rotation.

Table 5.1. Values of coefficients for differential rotation (from Hansen et al. 1977).

Results for Zero-Age Main Sequence

Model	Mode	ℓ = 2 P(hours)	C	$C_1(1)$	$C_1(2)$	ℓ = 1 P(hours)	C	$C_1(1)$
10 $M_\odot$ log T_{eff} = 4.422	p_2	1.21	0.067	0.265	0.391	1.34	0.075	0.333
log $L/L_\odot$ = 3.757	p_1	1.61	0.104	0.248	0.335	1.83	0.083	0.294
Ω_1 = -9.078(-13)	f	2.39	0.422	0.109	0.131	--	---	---
Ω_2 = -6.686(-23)	g_1	5.00	0.083	0.169	0.179	7.87	0.399	0.113
β = 0.342	g_2	7.57	0.092	0.198	0.207	--	---	---
20 $M_\odot$ log T_{eff} = 4.552	p_2	1.62	0.077	0.234	0.326	1.81	0.093	0.299
log $L/L_\odot$ = 4.637	p_1	2.18	0.113	0.218	0.300	2.51	0.124	0.250
Ω_1 = -4.034(-13)	f	3.34	0.446	0.095	0.133	--	---	---
Ω_2 = -3.129(-24)	g_1	8.47	0.058	0.179	0.190	13.52	0.374	0.126
β = 0.385	g_2	13.06	0.086	0.206	0.214	--	---	---
30 $M_\odot$ log T_{eff} = 4.645	p_2	2.12	0.090	0.229	0.315	2.40	0.110	0.291
log $L/L_\odot$ = 5.352	p_1	2.85	0.132	0.211	0.287	3.38	0.178	0.229
Ω_1 = -3.059(-13)	f	4.44	0.458	0.099	0.114	--	---	---
Ω_2 = -1.303(-24)	g_1	14.76	0.034	0.216	0.229	23.92	0.350	0.150
β = 0.405	g_2	23.08	0.092	0.234	0.234	--	---	---
50 $M_\odot$ log T_{eff} = 4.685	p_2	2.46	0.097	0.237	0.320	2.80	0.117	0.298
log $L/L_\odot$ = 5.706	p_1	3.31	0.143	0.217	0.290	3.98	0.209	0.227
Ω_1 = -3.130(-13)	f	5.15	0.461	0.107	0.122	--	---	---
Ω_2 = -7.349(-25)	g_1	20.67	0.026	0.249	0.264	33.82	0.342	0.174
β = 0.405	g_2	32.51	0.097	0.258	0.267	--	---	---
80 $M_\odot$ log T_{eff} = 4.707	p_2	2.73	0.102	0.242	0.325	3.11	0.121	0.304
log $L/L_\odot$ = 5.933	p_1	3.67	0.151	0.221	0.294	4.47	0.229	0.227
Ω_1 = -2.998(-13)	f	5.70	0.461	0.113	0.128	--	---	---
Ω_2 = -5.017(-25)	g_1	26.37	0.022	0.272	0.288	43.46	0.339	0.190
β = 0.400	g_2	41.59	0.099	0.276	0.284	--	---	---

Note that C in the table corresponds to C_1 in the text, and C_1 in the table corresponds to C_3 in the text.

CHAPTER 6

IDENTIFICATION OF PULSATION MODES OF β CEPHEI STARS IN NGC 3293

6.1 THE CASE FOR NONRADIAL PULSATIONS

The most reasonable explanation of the observed behaviour of β Cephei stars is that of stellar pulsation. The typical length of the periods with which they vary ($3 - 7$ hours) is too short to be caused by eclipses either of or by a companion star, and also too short to be due to changing surface characteristics as the star rotates, since typical rotation velocities correspond to rotation periods longer than a day. The almost perfect constancy of the periods also excludes atmospheric phenomena as the cause. Furthermore, the periods agree very well with theoretical predictions for the periods of certain pulsation modes, as will be seen in this chapter.

The frequent occurrence of closely spaced frequencies in these stars implies that most of their pulsations are nonradial (in other words, that mass elements in the star are displaced "horizontally" (changing their angular spherical coordinates) as well as "vertically" (changing their radial spherical coordinate), since the spacings of the observed frequencies are much smaller than the frequency spacing of successive overtones of purely radial pulsation, in the relevant frequency range. Nonradial pulsation modes populate a given frequency range much more densely than radial modes do, and can be matched to the frequency ranges which are observed. The specific identities of the modes observed in the β Cephei stars are still being debated, although many proposals have been made, as discussed in chapter 1.

6.2 COMPARISON OF NUMERICALLY CALCULATED PULSATION FREQUENCIES WITH OBSERVATIONS

The observationally determined pulsation frequencies for the β Cephei stars in NGC 3293, as discussed in chapter 4, are accurate to less than one part in four hundred, and the corresponding modes can be estimated by comparing the following observed quantities with their theoretically expected values:

(a) The **numerical value** of the frequencies;

(b) The degree of **rotational splitting** of frequencies.

6.2.1 Theoretical frequency values

The published literature displays a fair degree of divergence among the theoretical values of pulsation frequencies obtained by different authors. These authors made linear analyses of model stars (with appropriate masses and compositions for β Cephei stars) at the end of core hydrogen burning, which is the evolutionary stage at which most β Cephei stars seem to be found (see chapter 1). Table 6.1 summarises the nature of the analyses made by various authors.

The various papers quoted in Table 6.1 will henceforth be referred to by the abbreviations indicated in the table. In LA it is reported that nonadiabatic computations performed by the authors produced eigenfrequencies which were essentially the same as those found adiabatically. The same conclusion is made in SC, and Cox (1980) has stated that this is true for pulsating stars in general, as the pulsations are in fact nearly adiabatic throughout most of a star. Results obtained by adiabatic and nonadiabatic analyses respectively will hence be freely compared with each other.

TABLE 6.1

Analyses of β Cephei models

Authors	Analysis
Smeyers & Denis (SD) (1971)	Linear adiabatic oscillations of a homogeneous, compressible spheroid
Deupree (De) (1974)	Linear adiabatic oscillations of stellar models up to the end of core hydrogen burning
Lesh & Aizenman (LA) (1974)	Linear adiabatic oscillations of stellar models up to and beyond the end of core hydrogen burning
Osaki (Os) (1975)	Linear adiabatic oscillations of stellar models up to the end of core hydrogen burning
Stothers (St) (1976)	Linear nonadiabatic oscillations of stellar models up to the end of core hydrogen burning
Saio & Cox (SC) (1980)	Linear nonadiabatic oscillations of stellar models up to and beyond the end of core hydrogen burning
Saio (Sa) (1981)	Linear adiabatic oscillations of a polytrope of index 3 with $\gamma = 5/3$.

The eigenfrequency of a specific pulsation mode in a star is related to the stellar mass and radius by the familiar "pulsation equation":

$$P_e \sqrt{\bar{\rho}/\bar{\rho}_\odot} = Q \qquad (6.1)$$

where P_e = pulsation period,

$\bar{\rho}$ = mean stellar density,

$\bar{\rho}_\odot$ = mean solar density

and Q = the so–called **pulsation constant** for the pulsation mode.

The following alternative way of stating this relationship is in common use and will be used in the rest of this thesis:

$$\omega_{nd}^2 = \frac{\omega^2 R^3}{GM} \tag{6.2}$$

where ω_{nd} = the so–called **dimensionless frequency**,

ω = the observed pulsation frequency,

M and R = stellar mass and radius respectively

and G = Newton's gravitation constant.

The values of ω_{nd}^2 found by the authors in Table 6.1 are shown in Table 6.2. Stellar masses and radii as well as chemical compositions, as used in constructing the models, are also given. Values for the radii were not quoted in LA and St – the values (quoted in parentheses) in Table 6.2 were calculated from the luminosities and effective temperatures quoted in these two papers, using the Stefan–Boltzmann law in the following form:

$$L = 4\pi\sigma_s R^2 T_e^4 \tag{6.3}$$

where L = stellar luminosity,

σ_s = the Stefan–Boltzmann constant

and T_e = stellar effective temperature.

Since β Cephei variability occurs most frequently at the end of core hydrogen burning (at least this appears to be the case in NGC 3293), and the effective temperature of a star briefly rises immediately after this evolutionary stage, the results of the abovementioned authors were evaluated at the point of minimum effective temperature

in the initial evolution off the main sequence. This approach required interpolation between adjacent steps in the model calculations of De and Os.

The next two columns in Table 6.2 contain the values of the spherical harmonic index ℓ and the pulsation type, ie whether it is a p–mode or a g–mode, as well as the overtone (as a subscript). Gravity modes pulsating in the first overtone are represented as g_1, the fundamental nonradial mode as f and first and second overtone pressure modes as p_1 and p_2 respectively. The mass fractions of hydrogen left in the stellar core at this point in the model stars' evolution, X_c , appear in the next column. Interpolation was necessary in De and Os again. No values are quoted in LA.

The eigenfrequencies ω^2_{nd} appear in the eighth column. The values for SD, Os and St were taken directly from these papers, while the others were calculated from the respective values of frequency (or period), mass and radius. Values of both the periods and the eigenfrequencies are given in St, allowing a comparison between his quoted value and that calculated via equation 6.2. The calculated values turn out slightly lower than the published ones, possibly due to the fact that equation 6.3 is an approximation, so that the calculated values of R in Table 6.2 are slightly different from the true values. The **published** values of ω^2_{nd} in St appear in Table 6.2. Since the pulsation "constant" Q is widely used in the literature, its values (in the unit of a day) are included in the penultimate column, with the reference in the final column.

Comparison between results for different authors in Table 6.2 clearly shows a considerable spread in the eigenfrequencies found for any particular mode. Historically, the pressure modes have attracted greater attention than the gravity modes in the greater proportion of studies of β Cephei stars, and are therefore given preferential treatment in table 6.2.

Table 6.2

Details of models and eigenfrequencies published by various authors

$M/M_\odot$	$R/R_\odot$	X	Z	ℓ	mode	X_c	ω^2	Q	Ref
	not specified			1	g_1	–	–0.421	0.179	SD
	"			1	g_1	–	2.516	0.073	Sa
	"			1	p_1	–	4.754	0.053	SD
	"			1	p_1	–	11.40	0.034	Sa
	"			1	p_2	–	21.55	0.025	Sa
	"			2	g_1	–	–0.716	0.137	SD
20	(13.00)	0.739	0.021	2	g_1	–	3.01	0.067	LA
15	(10.40)	0.739	0.021	2	g_1	–	4.54	0.054	LA
	not specified			2	g_1	–	4.915	0.052	Sa
7	6.04	0.7	0.03	2	g_1	0.047	9.88	0.037	SC
10	(7.79)	0.739	0.021	2	g_1	–	10.88	0.035	LA
10	7.78	0.7	0.03	2	g_1	0.052	17.28	0.028	Os
10.9	(9.16)	0.73	0.02	2	g_1	0.064	19.7	0.026	St
15	(14.00)	0.73	0.02	2	g_1	0.064	23.8	0.024	St
	not specified			2	f	–	0.800	0.130	SD
	"			2	f	–	8.175	0.041	Sa
20	(13.00)	0.739	0.021	2	f	–	8.74	0.039	LA
15	(10.40)	0.739	0.021	2	f	–	9.91	0.037	LA
12	8.93	0.7	0.03	2	f	0.054	10.1	0.037	De
10	8.03	0.7	0.03	2	f	0.050	10.8	0.035	De
8	6.88	0.7	0.03	2	f	0.050	11.5	0.034	De
7	6.04	0.7	0.03	2	f	0.047	11.94	0.034	SC
10	(7.79)	0.739	0.021	2	f	–	14.41	0.031	LA
10	7.78	0.7	0.03	2	f	0.052	24.59	0.023	Os
15	(14.00)	0.73	0.02	2	f	0.064	29.3	0.021	St
10.9	(9.16)	0.73	0.02	2	f	0.064	29.7	0.021	St

(Table 6.2 continued:)

$M/M_\odot$	$R/R_\odot$	X	Z	ℓ	mode	X_c	ω^2	Q	Ref
	not specified			2	p_1	–	8.382	0.040	SD
	"			2	p_1	–	15.26	0.030	Sa
20	(13.00)	0.739	0.021	2	p_1	–	15.64	0.029	LA
12	8.93	0.7	0.03	2	p_1	0.054	15.8	0.029	De
10	8.03	0.7	0.03	2	p_1	0.050	15.8	0.029	De
20	13.06	0.7	0.03	2	p_1	0.025	16.52	0.029	SC
15	(10.40)	0.739	0.021	2	p_1	–	17.29	0.028	LA
8	6.88	0.7	0.03	2	p_1	0.050	17.4	0.028	De
7	6.04	0.7	0.03	2	p_1	0.047	18.09	0.027	SC
10	(7.79)	0.739	0.021	2	p_1	–	18.15	0.027	LA
10	7.78	0.7	0.03	2	p_1	0.052	28.26	0.022	Os
15	(14.00)	0.73	0.02	2	p_1	0.064	38.3	0.019	St
10.9	(9.16)	0.73	0.02	2	p_1	0.064	39.0	0.019	St
20	(13.00)	0.739	0.021	2	p_2	–	24.17	0.024	LA
20	13.06	0.7	0.03	2	p_2	0.025	26.60	0.023	SC
	not specified			2	p_2	–	26.72	0.022	Sa
15	(10.40)	0.739	0.021	2	p_2	–	27.23	0.022	LA
7	6.04	0.7	0.03	2	p_2	0.047	27.45	0.022	SC
10	(7.79)	0.739	0.021	2	p_2	–	27.73	0.022	LA
10	7.78	0.7	0.03	2	p_2	0.052	40.13	0.018	Os
10.9	(9.16)	0.73	0.02	2	p_2	0.064	42.0	0.018	St
15	(14.00)	0.73	0.02	2	p_2	0.064	50.6	0.016	St

Note that four groups, viz De, LA, SC and Sa agree reasonably in their results, while Os and St consistently find higher values of ω^2_{nd} (The results of SD can probably be discounted due to the differences between their model (see Table 6.1) and real stars). This systematic discrepancy is probably the result of confusion concerning mode identity, arising from the phenomenon of so–called **avoided crossings** in the frequency

spectrum. This problem of different mode assignments by different researchers was already pointed out by Osaki (1975). The phenomenon of avoided crossings is discussed in detail in Cox (1980) and in Unno et al. (1989), and has to do with the behaviour of the eigenfrequency spectrum for different nonradial modes. An example, for a few ($\ell = 2$) modes, appears in figure 6.1, taken from Dziembowski & Pamyatnykh (1993):

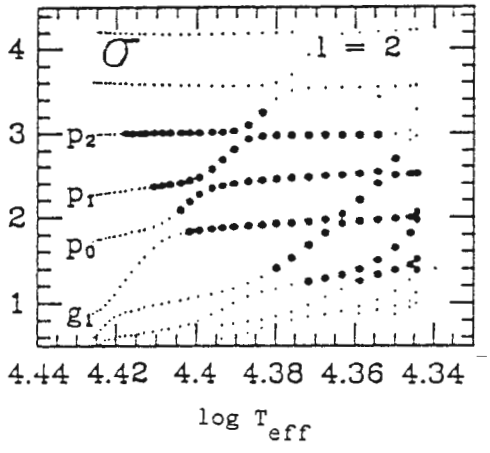

Figure 6.1: Dimensionless frequencies for modes with $\ell = 2$ in a model β Cephei star (from Dziembowski & Pamyatnykh (1993)

In the figure it can be clearly seen how the value of ω_{nd} (corresponding to $\sqrt{3}$ times the value of the parameter σ used in the figure) for, say, the p_1–mode, rises rapidly when log T_e drops below 4,4, "taking over" the value that corresponded to the p_2–mode at higher temperatures. In such a situation, some of the authors represented in Table 6.1 would identify the mode as a p_1–mode, while others would call it a p_2 –mode. For instance, the values of ω^2_{nd} for the p_2 mode in De, LA, SC and Sa are similar to the value for the p_1 mode obtained in Os, while the value for the p_3 mode in Sa is close to the values for the p_2 mode in Os and St. The reason for the values in St being even higher than those in Os are unclear. Judging from figure 6.2, again from Dziembowski & Pamyatnykh (1993), which shows practically identical eigenfrequencies for metallicities of Z = 0.02 and Z = 0.03 respectively, Stothers' results can probably not be ascribed to the lower metal content adopted in his models.

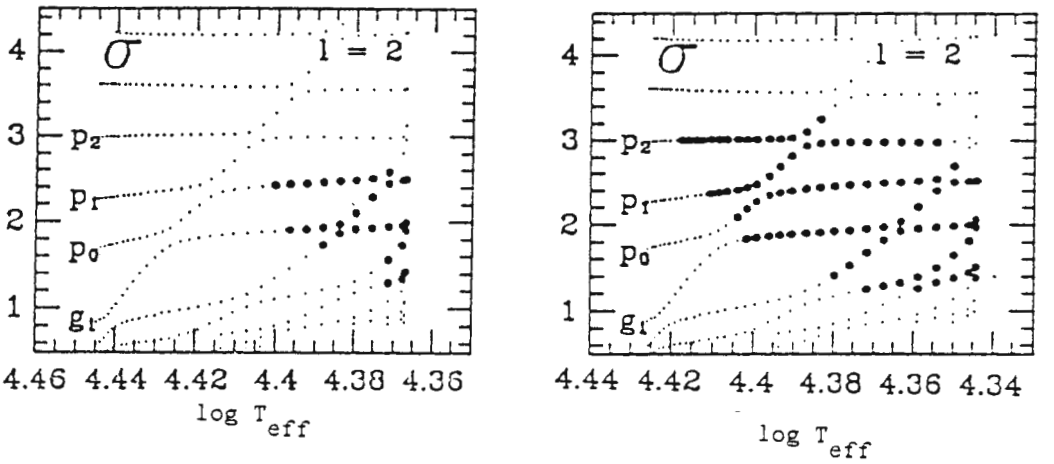

Figure 6.2: Dimensionless frequencies for modes with $\ell = 2$ for β Cephei star models with Z = 0.02 (left) and 0.03 (right) respectively (from Dziembowski & Pamyatnykh (1993)

6.2.2 Pulsation frequencies observed in NGC 3293

How do these theoretical results compare with the observations under discussion ?

Since the eigenfrequencies depend on stellar mass, radius and age, these properties have to be determined for the β Cephei stars in NGC 3293 before comparisons with the theoretical values can be made. Balona (1984) has derived an empirical–cum–theoretical calibration of stellar mass, effective temperature and bolometric correction for early–type stars, making use of Strömgren photometric parameters. Shobbrook (1983) has published Strömgren photometry and Johnson magnitudes of stars in NGC 3293, allowing a determination of masses and radii to be made for the stars under discussion. The mass calibration given by Balona has the following form:

$$logM = -1.7110 + 0.4225 logT_e + 0.2365 logL \qquad (6.4)$$

(where the mass M and the luminosity L are expressed in solar units),

while he has derived the following procedure to obtain $logT_e$ and $logL$:

(a) Given Strömgren parameters β and c_0,

set $[\beta] = log(\beta - 2.500)$,

and $[c] = log(c_0 + 0.200)$.

Then $$logT_e = 3.9036 - 0.4816[c] - 0.5290[\beta] - 0.1260[c]^2 + 0.0924[\beta][c] - 0.4013[\beta]^2, \quad (6.5)$$

while the bolometric correction

$$BC = 0.2900 + 2.8467[c] + 2.8334[\beta] + 0.6481[c]^2 - 0.2997[\beta][c] + 2.1487[\beta]^2. \quad (6.6)$$

(b) With the solar bolometric magnitude $M_{bol_\odot} = 4.75$, and taking a value of 12.15 for the distance modulus of NGC 3293 (Balona and Shobbrook 1984),

$$logL = -0.4(V_0 - 12.15 + BC - 4.75) \quad (6.7)$$

The luminosity is calculated using Shobbrook's Johnson V measurements, rather than his Strömgren β measurements, since the former are known to higher precision. The radius is trivially found from equation 6.3, once T_e and L are known. Application of these calibrations to the β Cephei stars in NGC 3293 produced the results shown in Table 6.3. Projected rotation velocities obtained by Balona (1975) appear in the final column, expressed in units of km/s.

Table 6.3

Observational and physical properties of β Cephei stars in NGC 3293

Star	β	c_0	M_V	$\log T_e$	BC	$\log \frac{L}{L_\odot}$	$M/M_\odot$	$R/R_\odot$	v
5	2.600	–0.014	–3.78	4.379	–2.332	4.345	14.62	8.52	122
	±0.010	±0.015	±0.06	±0.020	±0.098	±0.047	±0.48	±0.97	±30
10	2.605	0.009	–3.44	4.368	–2.261	4.180	13.27	7.53	125
	±0.011	±0.016	±0.07	±0.019	±0.092	±0.046	±0.40	±0.81	±30
11	2.611	0.012	–3.14	4.372	–2.290	4.072	12.57	6.51	42
	±0.012	±0.017	±0.07	±0.019	±0.090	±0.045	±0.38	±0.70	±30
14	2.597	–0.010	–3.45	4.384	–2.352	4.221	13.79	7.32	129
	±0.011	±0.016	±0.06	±0.020	±0.095	±0.046	±0.45	±0.82	±30
16	2.593	–0.008	–4.08	4.365	–2.237	4.427	15.14	10.15	50
	±0.005	±0.009	±0.06	±0.012	±0.060	±0.033	±0.32	±0.70	±30
18	2.609	0.016	–3.55	4.360	–2.214	4.205	13.35	8.05	4
	±0.011	±0.016	±0.06	±0.019	±0.095	±0.046	±0.44	±0.87	±30
23	2.605	–0.002	–3.80	4.369	–2.267	4.327	14.40	8.85	10
	±0.011	±0.015	±0.06	±0.020	±0.101	±0.048	±0.47	±1.00	±30
24	2.596	–0.034	–3.82	4.400	–2.438	4.403	15.46	8.40	194
	±0.011	±0.015	±0.06	±0.022	±0.105	±0.049	±0.54	±1.03	±30
27	2.604	0.018	–4.15	4.340	–2.100	4.400	14.57	11.01	203
	±0.005	±0.009	±0.06	±0.012	±0.059	±0.033	±0.31	±0.76	±30
65	2.599	0.038	–3.08	4.350	–2.163	3.997	11.81	6.62	–
	±0.012	±0.017	±0.07	±0.017	±0.085	±0.044	±0.36	±0.65	

The values of the pulsation frequencies found observationally and the masses and radii shown in Table 6.3 were used to calculate eigenfrequencies ω^2_{nd} for the variables. The results are shown in Table 6.4. The standard error in the values of ω^2_{nd} is approximately 1 for all the stars. The magnitude of this error is mainly due to the number of algebraic manipulations involved in obtaining the values of the temperature, luminosity, mass and radius for each star, which causes considerable error accumulation. The primary sources of error in the latter quantities are the photometric errors in the Stromgren parameters β and c_0 (ie *uvby*) and in the Johnson V magnitude.

The eigenfrequencies for a particular star will depend on its structure, which is a function of its mass, chemical composition and age. The open cluster NGC 3293 presumably formed from one distinct cloud or complex of gas and dust, during a distinct epoch between 10 and 20 million years ago. The β Cephei stars in the cluster can therefore be expected to be nearly identical in chemical composition and age, so that the stellar mass is the only remaining factor affecting the eigenfrequencies. The data in Table 6.4 are graphically represented in Figure 6.3, where each star's pulsation eigenfrequencies are shown as a function of its mass. The sets of eigenfrequencies clearly fall into two groups, indicated by the brackets. The largest group is centred on $\omega^2_{nd} = 15.1$ and the other group on $\omega^2_{nd} = 24.7$. Note that these values agree very well with the theoretical eigenfrequencies for quadrupole p_1– and p_2–modes respectively, as found by Sa, LA, De and SC.

Table 6.4

Eigenfrequencies for β Cephei stars in NGC 3293

Star	$M/M_\odot$	Frequency (cycles/day)	ω^2_{nd}
5	14.62 ± 0.48	5.64	18.09
		6.66	25.23
		7.17	29.20

(Table 6.4 continued:)

Star	$M/M_\odot$	Frequency (cycles/day)	ω^2_{nd}
10	13.27 ± 0.40	5.92	15.14
		5.68	13.93
		4.76	9.77
		6.11	16.09
		5.46	12.87
11	12.57 ± 0.38	6.86	13.85
		6.69	13.17
		7.22	15.34
		7.06	14.66
		6.61	12.86
14	13.79 ± 0.45	6.56	16.45
		6.33	15.31
		5.90	13.33
16	15.14 ± 0.32	3.99	14.75
		4.92	22.47
18	13.35 ± 0.44	5.66	16.77
		5.74	17.28
		6.58	22.73
		5.77	17.44
23	14.40 ± 0.47	6.17	24.57
		5.74	21.27
		6.64	28.46
24	15.46 ± 0.54	4.85	12.12
		6.25	20.11
		5.86	17.69
		5.65	16.44
27	14.57 ± 0.31	4.40	23.77
		4.33	23.01
65	11.81 ± 0.36	8.81	25.53
		9.97	32.71

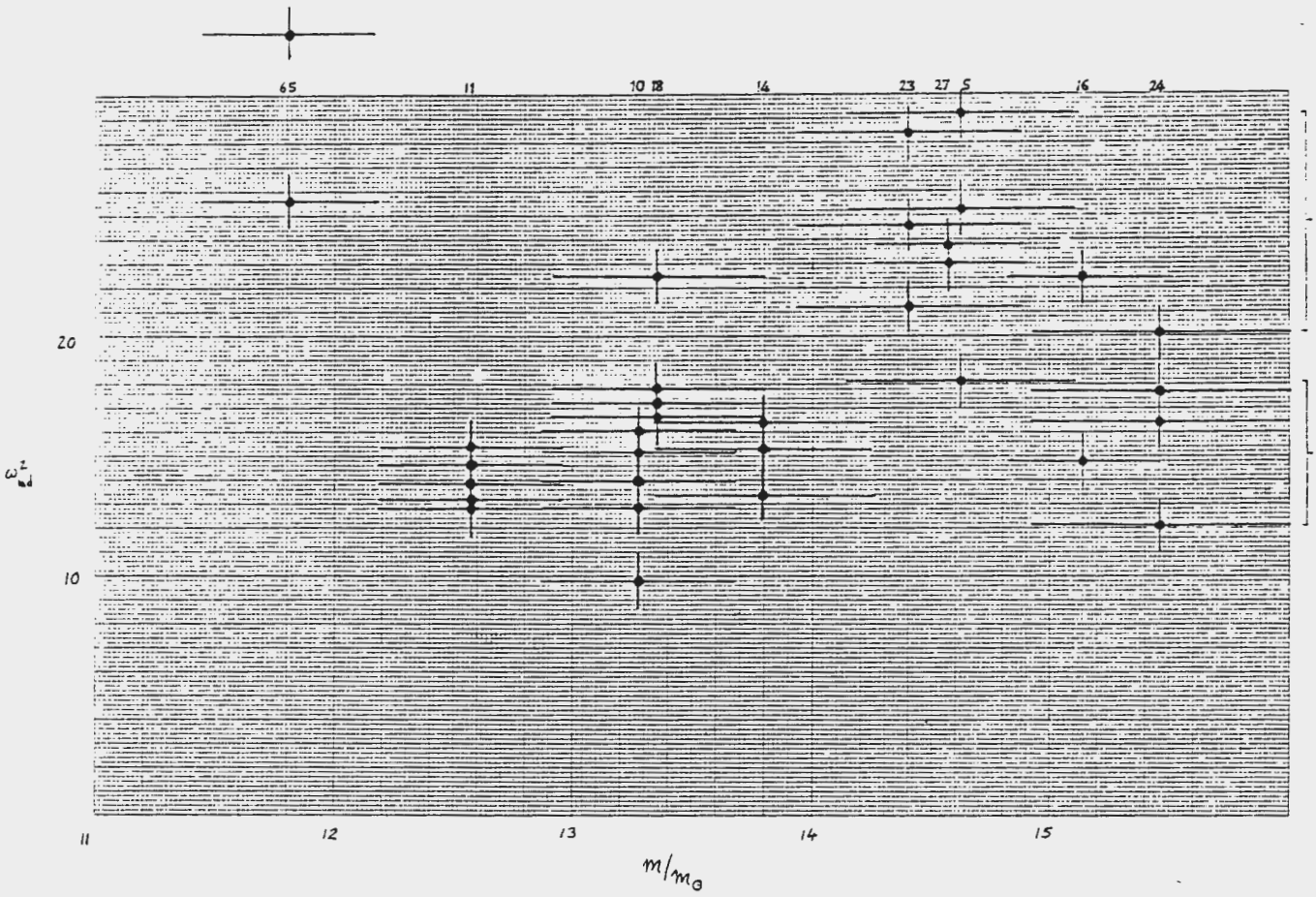

Figure 6.3

Dimensionless eigenfrequencies as a function of mass,

for β Cephei stars in NGC 3293

However, a few of the eigenfrequencies for the g_1 and f modes quoted in Table 6.2 also correspond to the regions enclosed by the brackets in Figure 6.3. These are the values quoted in Os and St, and the agreement with observational values follows from the abovementioned phenomenon of conflicting mode identifications. Note that Figure 6.3 shows no obvious trend in $\omega^2_{\rm nd}$ with increasing mass, except for a "bump" between 14 $M_\odot$ and 15 $M_\odot$.

If the mode identification of Os is correct, the two groups in Figure 6.3 correspond to g–modes and the f–mode respectively, while the values in St imply that higher overtone g–modes have been observed. The discussion of driving mechanisms in chapter 1 refers

to the fact that the relatively deep location of the driving region in the β Cephei stars is compatible with g–mode pulsation. Although the results for four groups of authors in Table 6.2 show close agreement in indicating that p–modes are operating in these stars, while only Os finds a g–mode in the range spanned by the lower bracket in Figure 6.3, Osaki's (1975) comments concerning avoided crossings, and the results shown in figure 6.1, imply that all these authors are dealing with the same modes, choosing different terminology with which to name them. The more popular terminology (eg p_1 instead of g) will be adopted here.

As discussed in the following section, many of the frequencies observed could be members of non–degenerate multiplets resulting from stellar rotation. These multiplets correspond to a single degree (ℓ) and overtone (k), but differ in the azimuthal spherical harmonic index m. The so–called **unperturbed** frequencies of the β Cephei stars in NGC 3293, which are a more accurate reflection of these stars' structure, are derived in the following section. In summary: the comparison of observed frequencies with theoretical analyses strongly supports the view that the β Cephei stars in NGC 3293 are pulsating in quadrupole pressure modes (altrnatively, g_1– and f–modes) of the first and second overtones, although it has not been determined that comparisons with theoretical values for dipole or octopole modes could not yield similar results.

6.3 ROTATIONAL SPLITTING OF EIGENFREQUENCIES

The effect of stellar rotation on the pulsation frequency spectrum was discussed in chapter 5. The following description of this effect to second order was given by Saio (1981):

$$\omega = \omega_0 - (1-C_1)m\Omega + C_2\omega_0(\Omega/\omega_0)^2 \qquad (6.8)$$

(symbols are explained in chapter 5)

The most extensive range of published values for C_1 and C_2 is also found in Saio (1981). The results obtained by Saio for his polytropic model, as far as the eigenfrequencies are concerned, agree very well with those for more realistic stellar models. Hence his values for C_1 and C_2 are used in the calculations to follow in this chapter.

The value of C_1 depends on the overtone k and on the spherical harmonic degree ℓ, whereas C_2 has a more complicated structure (the following expression from Saio (1981) has been generalised to include a binary star scenario):

$$C_2 = X_1 + m^2 Y_1 + Z + \left(1+\frac{3M_2}{2(M_1+M_2)}\right)(X_2+m^2 Y_2) \qquad (6.9)$$

where M_1 = mass of the primary star in a binary system,

M_2 = mass of a stellar companion,

X_1, X_2, Y_1, Y_2, Z = constants for given k and ℓ

and m = azimuthal spherical harmonic index.

With the exception of 3293–5, and perhaps 3293–23, no sign of a stellar companion was detected for any of the β Cephei stars in the cluster. In the absence of such a companion,

$$C_2 = (X_1+X_2+Z) + (Y_1+Y_2)m^2 \qquad (6.10)$$
$$= X + Ym^2, \text{ say.}$$

Comparison between the theoretical and observed splitting in the eigenfrequencies, due to rotation, was made by the following procedure:

(i) For each star, each of its observed frequencies was paired with every of the other, in turn.

(ii) All combinations of spherical harmonic indices ℓ and m for $\ell < 4$ were assigned to each pair, and the rotational velocities corresponding to the separation and the mode assignments were calculated. The unperturbed eigenfrequencies $(\omega^2_{nd})_0$ for each assignment (the frequencies which would be observed in the absence of stellar rotation) were calculated in the process. For each star, each set of mode assignments which were compatible with a unique rotational velocity was retained, with the requirement that the set had to account for all frequencies of the star. Higher order modes ($\ell \geq 4$) were not considered since it has been shown that these modes would have light amplitudes much lower than those observed in these stars (Dziembowski 1977). All calculations were based on equation 6.8 and the tables in Saio (1981). Linear interpolations in these tables were made according to the value of ω^2_{nd} corresponding to the unperturbed frequency for each mode assignment.

(iii) Balona (1975) obtained projected rotational velocities for all but one of these stars, and these were used to disqualify some of the assignments on the basis that the true rotation velocity had to exceed the projected one. Balona's quoted errors of approximately 30 km/s were taken into account.

(iv) The physical behaviour of the eigenfrequencies also allowed some disqualification of mode assignments, since the values for successive degrees ($\ell = 0, 1, 2,...$) and for successive overtones ($f, p_1, p_2,...$) are related to each other in certain ratios (eg see Saio 1981). The average ratios for radial and for nonradial quadrupole overtones found in six papers (De, LA, Os, SC, St and Davey 1973) are as follows (1H meaning radial first harmonic, and F radial fundamental mode):

$$1H:F \quad = \quad 1.36 \pm 0.04$$

$$p_1{:}f \quad = \quad 1.23 \pm 0.09 \quad (\ell = 2)$$
$$p_2{:}p_1 \quad = \quad 1.22 \pm 0.06 \quad (\ell = 2)$$

No mass dependence was detected in the published ratios. When the modes which Os and St identify as f and p_1 are regarded as p_1 and p_2 respectively (to bring them into line with the other authors) the average ratios show a slight change:

$$p_1{:}f \quad = \quad 1.25 \pm 0.09$$
$$p_2{:}p_1 \quad = \quad 1.20 \pm 0.06$$

Since the range in these ratios is quite large for nonradial modes, it was decided to use the minimum and maximum values quoted in the abovementioned papers (after adjusting those in Os and St as mentioned above) as guidelines for choosing physically meaningful mode assignments for the observed frequencies. Hence all mode assignments falling within the following limits were considered:

$$p_1{:}f \quad = \quad 1.08 - 1.34$$
$$p_2{:}p_1 \quad = \quad 1.11 - 1.27$$

(v) Velocities above 300 km/s were disregarded since this value is substantially higher than the typical rotational velocity for stars of spectral type B0 – B2, and the highest projected rotation velocity measured for the β Cephei stars in this cluster was 203 km/s.
(vi) Mode assignments which required an unperturbed eigenfrequency more than 22% above or 11% below those of Saio (1981) were discarded for the following reasons: In the first place, errors in the calculated values of the eigenfrequencies have values between 3% and 10%. Secondly, the range in $\omega^2_{\rm nd}$ for the quadrupole p_1 mode amounts to 19% for the group of authors mentioned in the previous section (see Table 6.2), relative to

Saio's value. The standard error of these four values as they stand is 5%. Since Saio's values are the lowest of the four, the errors are calculated as follows: the root of the sum of squares of 10%, 19% and 5% above Saio's values; and the root of the sum of squares of 10% and 5% below his values. Thus: errors of 22% above, and 11% below Saio's values are considered reasonable.

The results are shown in Table 6.5. The columns contain the identification number of the star, the pulsation frequency in cycles per day, mode identification (values of ℓ and m), type of pulsation (p_1, p_2, p_3 : pressure mode; f: fundamental mode; 1H : radial first harmonic mode), rotation velocity in km/s, and dimensionless frequency squared. For a set of two or more frequencies, the unperturbed value $(\omega^2_{nd})_0$ of the dimensionless frequency squared is given, indicated by the symbol ω^2 in the column heading. The following notes apply:

(i) In a star where the pulsation axis is inclined by 90° to the line of sight, light variations will not be observed for the $(\ell,m) = (1,0); (2,\pm1); (3,0); (3,\pm2)$ modes, due to the symmetry of these modes. This will disqualify some of the entries for 3293–5 and many of those for 3293–23 as well, if the latter is a binary.

(ii) The (ℓ=2) p_2–mode identification for the 6.58 cycle per day frequency in 3293–18 does not quite fall within the limits described under note (v) above, but this represents the closest identification.

(iii) No measured rotation velocity is available for 3293–65 and hence no lower limit has been placed on the values thereof for this star.

(iv) In principle, a set of four frequencies could represent pulsations in radial, dipole, quadrupole and octopole modes respectively. A list of such possible permutations has no bearing on rotational splitting of pulsation modes and Table 6.5 does not contain mode identifications for which more than one of the frequencies is not paired with another.

(v) The decrease in pulsation amplitude as the degree ℓ increases has been taken into account by requiring that the strongest (highest amplitude) frequency for a particular degree (eg $\ell = 1$) must have a higher amplitude than the strongest frequencies for higher orders (eg $\ell = 2, 3$).

(vi) No combination fulfilling the above–mentioned conditions could be found for 3293–27. The pair closest to fitting the conditions is shown in Table 6.5, parentheses applying if 3293–27 is an equal component binary, as suggested by Shobbrook (1985).

(vii) The last five pairs for 3293–65 have high values of $(\omega^2_{nd})_0$ which correspond to the values for p_3–modes as given by Saio (1981). These identifications have to be regarded as tentative, however, since no other comparison with theory could be made.

(viii) If 3293–23 is a member of an eclipsing binary, as suggested in chapter 4, with its rotation axis perpendicular to the orbital plane, its true rotation velocity v_e will be very close to the projected value as found in Balona (1975). Including the quoted error of 30 km/s, the upper limit for v_e is 40 km/s. None of the mode assignments for 3293–23 in Table 6.5 satisfies this limit, the closest velocity being 57 km/s.

Table 6.5

Mode identifications for stars in NGC 3293

St	Fr	Mo	T	v	ω^2	Fr	Mo	T	v	ω^2
5	7.17	3 -1	p_2	120	28.02	7.17	3 -1	p_2	120	28.02
	6.66	3 1				6.66	3 1			
	5.64	3 1,0	p_1		18.09	5.64	2 -2, -1	p_1		18.09
	7.17	3 -1	p_2	120	28.02					
	6.66	3 1				7.17	3 -1	p_2	120	28.02
	5.64	1 1	p_2		18.09	6.66	3 1			
						5.64	0	1H		18.09
	7.17	3 0	p_2	109	29.88					
	6.66	3 2				7.17	3 0	p_2	109	29.88
	5.64	3 1,0	p_1		18.09	6.66	3 2			
						5.64	2 -2, -1	p_1		18.09
	7.17	3 0	p_2	109	29.88					
	6.66	3 2				7.17	3 0	p_2	109	29.88
	5.64	1 1	p_2		18.09	6.66	3 2			
						5.64	0	1H		18.09
	7.17	3 1	p_2	100	31.69					
	6.66	3 3				7.17	3 1	p_2	100	31.69
	5.64	3 1,0	p_1		18.09	6.66	3 3			
						5.64	2 -2, -1	p_1		18.09
	7.17	3 1	p_2	100	31.69					
	6.66	3 3				7.17	2 -1	p_2	119	28.09
	5.64	1 1	p_2		18.09	6.66	2 1			
						5.64	2 -2, -1	p_1		18.09
	7.17	3 1	p_2	100	31.69					
	6.66	3 3				7.17	2 -1	p_2	119	28.09
	5.64	0	1H		18.09	6.66	2 1			
						5.64	0	1H		18.09
	7.17	2 -1	p_2	119	28.09					
	6.66	2 1				7.17	2 0	p_2	100	29.75
	5.64	1 1	p_2		18.09	6.66	2 2			
						5.64	1 1	p_2		18.09
	7.17	2 0	p_2	100	29.75					
	6.66	2 2				6.66	2 -1	p_2	145	24.07
	5.64	2 -2, -1	p_1		18.09	5.64	2 2			
						7.17	3 -1, 0,1,2	p_2		29.20
	7.17	2 0	p_2	100	29.75					
	6.66	2 2								
	5.64	0	1H		18.09					
10	5.92	2 0	p_1	104	15.36	6.11	3 -3	f	243	9.91
	5.68	2 1				5.68	3 -2			
	5.46	3 -2	f		10.93	5.46	3 1	p_1		17.48
	4.76	3 1				4.76	3 2			
	6.11	3 1, 2,3	p_1		16.09	5.92	2 0,1	p_1		15.14

(Table 6.5 continued)

St	Fr	Mo	T	v	ω^2	Fr	Mo	T	v	ω^2
10	6.11	3 -3	f	243	9.91	6.11	3 -3	f	243	9.91
	5.68	3 -2				5.68	3 -2			
	5.46	3 1	p_1		17.48	5.46	3 1	p_1		17.48
	4.76	3 2				4.76	3 2			
	5.92	1 1	p_2		15.14	5.92	0	1H		15.14
	6.11	3 1	p_1	163	19.02	6.11	3 1	p_1	163	19.02
	5.68	3 2				5.68	3 2			
	5.46	3 -2	f		9.99	5.46	3 -2	f		9.99
	4.76	3 0				4.76	3 0			
	5.92	2 0,1	p_1		15.14	5.92	0	1H		15.14
	6.11	2 -1	p_1	221	14.90	6.11	2 -1	p_1	221	14.90
	5.68	2 0				5.68	2 0			
	5.46	3 2	p_1		20.50	5.46	3 2	p_1		20.50
	4.76	3 3				4.76	3 3			
	5.92	1 1	p_2		15.14	5.92	0	1H		15.14
	6.11	2 0	p_1	169	16.83					
	5.68	2 1								
	5.46	3 -2	f		9.99					
	4.76	3 0								
	5.92	0	1H		15.14					
11	7.22	2 -1	p_1	69	14.78	7.06	1 -1	p_1	71	13.95
	7.06	2 0				6.86	1 0			
	6.69	2 2				6.61	1 1			
	6.86	1 0	p_1		13.94	7.22	2 -1	p_1		14.78
	6.61	1 1				6.69	2 2			
	7.22	2 -1	p_1	63	14.69	7.22	2 -1	p_1	66	14.78
	7.06	2 0				7.06	2 0			
	6.86	2 1				6.86	1 -1	p_1		13.25
	6.69	2 2				6.69	1 0			
	6.61	3 -3	f		12.86	6.61	3 -3	f		12.86
	7.22	2 0	p_1	63	15.44	7.22	2 1	p_1	54	16.09
	7.06	2 1				7.06	2 2			
	6.86	1 -1	p_1		13.25	6.86	1 0	p_1		13.91
	6.69	1 0				6.69	1 1			
	6.61	3 -3	f		12.86	6.61	3 -3	f		12.86
14	6.56	2 -1	p_1	107	15.54	6.33	3 1	p_1	158	17.90
	6.33	2 0				5.90	3 2			
	5.90	3 -3, -2	f		13.33	6.56	2 -1, 0	p_1		16.45
	6.33	3 1	p_1	158	17.90	6.33	3 1	p_1	158	17.90
	5.90	3 2				5.90	3 2			
	6.56	1 1	p_2		16.45	6.56	0	1H		16.45

(Table 6.5 continued)

St	Fr	Mo	T	v	ω^2	Fr	Mo	T	v	ω^2
14	6.33	3 2	p_1	145	19.82	6.33	3 2	p_1	145	19.82
	5.90	3 3				5.90	3 3			
	6.56	2 -1, 0	p_1		16.45	6.56	1 1	p_2		16.45
	6.33	3 2	p_1	145	19.82	6.33	2 0	p_1	170	15.89
	5.90	3 3				5.90	2 1			
	6.56	0	1H		16.45	6.56	1 1	p_2		16.45
	6.33	2 0	p_1	170	15.89	5.46	2 1	p_1	144	17.63
	5.90	2 1				5.90	2 2			
	6.56	0	1H		16.45	6.56	1 1	p_2		16.45
	6.33	2 1	p_1	144	17.63					
	5.90	2 2								
	6.56	0	1H		16.45					
16	4.92	3 -3	p_1	152	17.58	4.92	3 -3	p_1	113	18.47
	3.99	3 1				3.99	3 2			
	4.92	3 -3	p_1	90	17.58	4.92	3 -2	p_1	194	18.87
	3.99	3 3				3.99	3 1			
	4.92	3 -2	p_1	135	19.47	4.92	3 -2	p_1	104	19.96
	3.99	3 2				3.99	3 3			
	4.92	3 1	p_2	193	28.15	4.92	2 0	p_2	196	24.27
	3.99	3 3				3.99	2 2			
18	5.77	2 -2	p_1	16	17.11	5.77	2 -2	p_1	13	17.15
	5.74	2 -1				5.74	2 -1			
	5.66	2 1				5.66	2 2			
	6.58	2	p_2		22.73	6.58	2	p_2		22.73
	5.77	2 -1	p_1	16	17.32					
	5.74	2 0								
	5.66	2 2								
	6.58	2	p_2		22.73					
23	6.64	3 -1	p_2	260	28.15	6.64	3 0	p_2	207	31.08
	6.17	3 0				6.17	3 1			
	5.74	3 2,3	p_2		21.27	5.74	3 2,3	p_2		21.27
		-2	p_1				-3,-2	p_1		
	6.64	3 0	p_2	105	29.14	6.64	3 0	p_2	70	28.83
	6.17	3 2				6.17	3 3			
	5.74	3 -3, -2,-1	p_1		21.27	5.74	3 -3, -2,-1	p_1		21.27

(Table 6.5 continued)

St	Fr	Mo	T	v	ω^2	Fr	Mo	T	v	ω^2
23	6.64	3 1	p_2	179	34.26	6.64	3 1	p_2	97	30.90
	6.17	3 2				6.17	3 3			
	5.74	3 2,3	p_2		21.27	5.74	3 -3,	p_1		21.27
		-2,-1	p_1				-2,-1			
	6.64	2 -2	p_2	162	25.82	6.64	2 -2	p_2	83	26.42
	6.17	2 0				6.17	2 1			
	5.74	3 -2,-1	p_1		21.27	5.74	3 -3,	p_1		21.27
		3	p_2				-2,-1			
	6.64	2 -2	p_2	57	26.90	6.64	2 -1	p_2	115	27.39
	6.17	2 2				6.17	2 1			
	5.74	3 -3,	p_1		21.27	5.74	3 -2,	p_1		21.27
		-2,-1					-1			
	6.64	2 -1	p_2	72	27.61	6.64	2 0	p_2	97	29.02
	6.17	2 2				6.17	2 2			
	5.74	3 -3,	p_1		21.27	5.74	3 -3,	p_1		21.27
		-2,-1					-2,-1			
	6.17	3 -3	p_1	135	20.10	6.17	2 -1	p_2	281	24.62
	5.74	3 -1				5.74	2 0			
	6.64	3 0,	p_2		28.46	6.64	3 -1,	p_2		28.46
		1,2					0			
	6.17	2 -1	p_2	68	23.81	6.17	2 0	p_2	181	26.14
	5.74	2 2				5.74	2 1			
	6.64	3 0,	p_2		28.46	6.64	3 0,1	p_2		28.46
		1,2,3								
	6.17	2 0	p_2	92	25.00	6.17	2 1	p_2	148	28.59
	5.74	2 2				5.74	2 2			
	6.64	3 0,	p_2		28.46	6.64	3 0,	p_2		28.46
		1,2,3					1,2			
24	6.25	3 -1	p_1	201	18.81					
	5.86	3 0								
	5.65	2 -1	p_1		15.22					
	4.85	2 1								
27*	4.40	1 -1	p_2	222	23.18					
	4.33	1 0								
	(4.40	0	F		9.31)					
	(4.33	3 0,1	f		9.02)					
65	9.97	3 -3	p_2	118	28.26	9.97	3 -3	p_2	88	29.08
	8.81	3 1				8.81	3 2			

(Table 6.5 continued)

St	Fr	Mo	T	v	ω^2	Fr	Mo	T	v	ω^2
65	9.97 8.81	3 -3 3 3	p_2	70	29.64	9.97 8.81	3 -2 3 0	p_2	278	29.46
	9.97 8.81	3 -2 3 1	p_2	151	29.37	9.97 8.81	3 -2 3 2	p_2	105	29.98
	9.97 8.81	3 -2 3 3	p_2	81	30.44	9.97 8.81	3 -1 3 1	p_2	210	31.86
	9.97 8.81	3 -1 3 2	p_2	132	31.52	9.97 8.81	3 -1 3 3	p_2	96	31.63
	9.97 8.81	3 0 3 2	p_2	179	34.75	9.97 8.81	3 0 3 3	p_2	119	33.63
	9.97 8.81	3 1 3 2	p_3	281	45.65	9.97 8.81	3 2 3 3	p_3	241	50.77
	9.97 8.81	2 1 2 2	p_3	232	42.36	9.97 8.81	1 -1 1 1	p_3	201	33.79
	9.97 8.81	1 0 1 1	p_3	214	34.81					

*The value of ω_0^2 for star 27 is slightly outside the limits described in the text but this identification comes closest to the limits imposed.

The unperturbed frequencies determined by the above procedure are shown in Figure 6.4, on the same basis as Figure 6.3. The triangles in figure 6.4 represent different possibilities for 3293–27; the lower mass corresponding to its being a binary. The median values of ω^2_{nd} for the two groups of frequencies are higher than in Figure 6.3: ω^2_{nd} = 16.2 and 27.4 respectively, although the borders of these groups are ambiguous and the higher frequencies found in 3293–65 are not indicated. Upper and lower limits of the theoretical values of two of the quadrupole modes (see Table 6.2) are indicated by the lines crossing the diagram. The dashed lines correspond to the g_1–mode and the dotted lines to the p_1–mode. The variation of ω^2_{nd} with mass indicated by some authors is shown as a linear interpolation. The values which Saio (1981) found for a polytrope ar

indicated by open circles on the right–hand margin. The digits indicate degree (ℓ) and overtone (k). The stellar eigenfrequencies lie remarkably close to the locations of nonradial quadrupole modes predicted by theory. Unfortunately the published data for theoretical analyses of dipole modes are too sparse to make a valid comparison with theory.

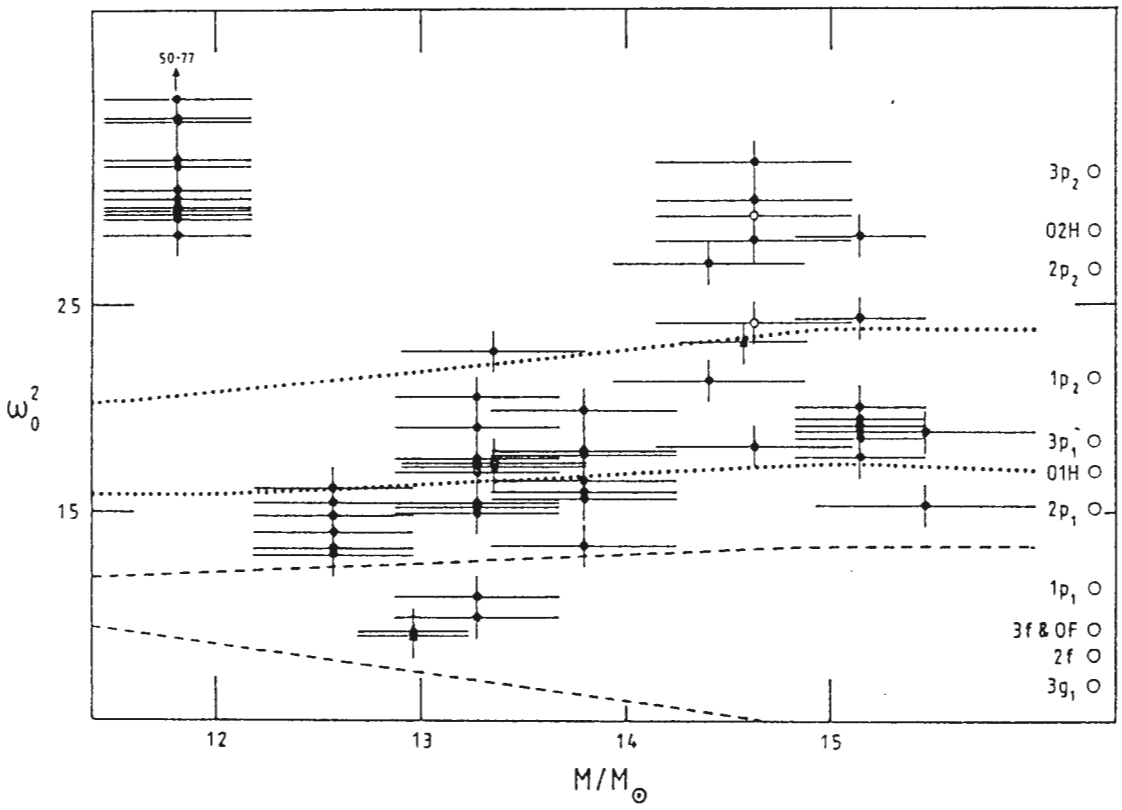

Figure 6.4

Unperturbed dimensionless eigenfrequencies for

β Cephei stars in NGC 3293

The range of frequencies spanned in both groups in figure 6.4 is of the same order as that in Figure 6.3, and no convincing mass dependence (besides the 14–15 $M_\odot$ bump) in $(\omega^2_{nd})_0$ is seen here either. One trend which is apparent in both diagrams, however, is the change in frequency distribution as the mass increases. Stars 3293–11, 3293–10, 3293–18 and 3293–14, all in the lower 60 % of the mass range, have no frequencies

among the higher group, while 3293–65, by far the least massive of the sample, has no frequency in the lower group. A similar trend (admittedly very slight) is seen in Shobbrook's (1985) results for 42 β Cephei stars; his numerical data are graphically expressed in Figure 6.5. The lower densities and greater radii of the more massive stars may allow these stars to excite a second radial mode, while the less massive stars (possibly being too compact) fail to do so. However, this would not account for the high frequencies found for 3293–65 (which is the least massive of these stars). Sterken & Jerzykiewicz (1990) reported that this star has a peculiar β index, and its calculated mass may therefore be in error.

The large number of mode identifications in Table 6.5 can be seen as valid ways of arranging degrees (ℓ = 0, 1, 2, 3) and overtones (f, p_1 or 1H, p_2, p_3) among the observed frequencies of β Cephei stars in NGC 3293. Differential rotation would alter the results significantly; the results of Hansen et al. (1977) for dipole and quadrupole modes in models approximating β Cephei stars imply that a given frequency splitting would require a substantially lower equatorial rotation velocity than in the case of uniform rotation. The distribution of degrees (ℓ) and overtones (k) among the mode combinations in Table 6.5 is shown in figure 6.6. The (2ℓ+1)–fold multiplicity of rotationally split modes was used to weigh the distribution, a weight of 1/7 being allocated to a (ℓ=3) mode, 1/5 to a (ℓ=2) mode, and so on. Dashes apply if 3293–27 is indeed a binary, and dots if 3293–23 is a binary. The distribution resulting from a direct comparison between the observed frequencies listed in table 6.4 and Saio's theoretical eigenfrequencies appears in figure 6.7. The dashes apply if 3293–27 is a binary. First–overtone pulsation is clearly dominant in both figures 6.7 and 6.8, followed by second–overtone pulsation, while a radial mode may possibly be present in about half of these stars. Comparison of these two figures shows that the main effect of taking rotational splitting into account is the suppression of the probable number of

dipole modes and the increase of the probable number of of octopole modes present in these stars. Only star 3293–27 does not have either a quadrupole or an octopole mode (or both) as one of its possibilities, while only this star and 3293–65 do not include a first overtone mode among their possibilities.

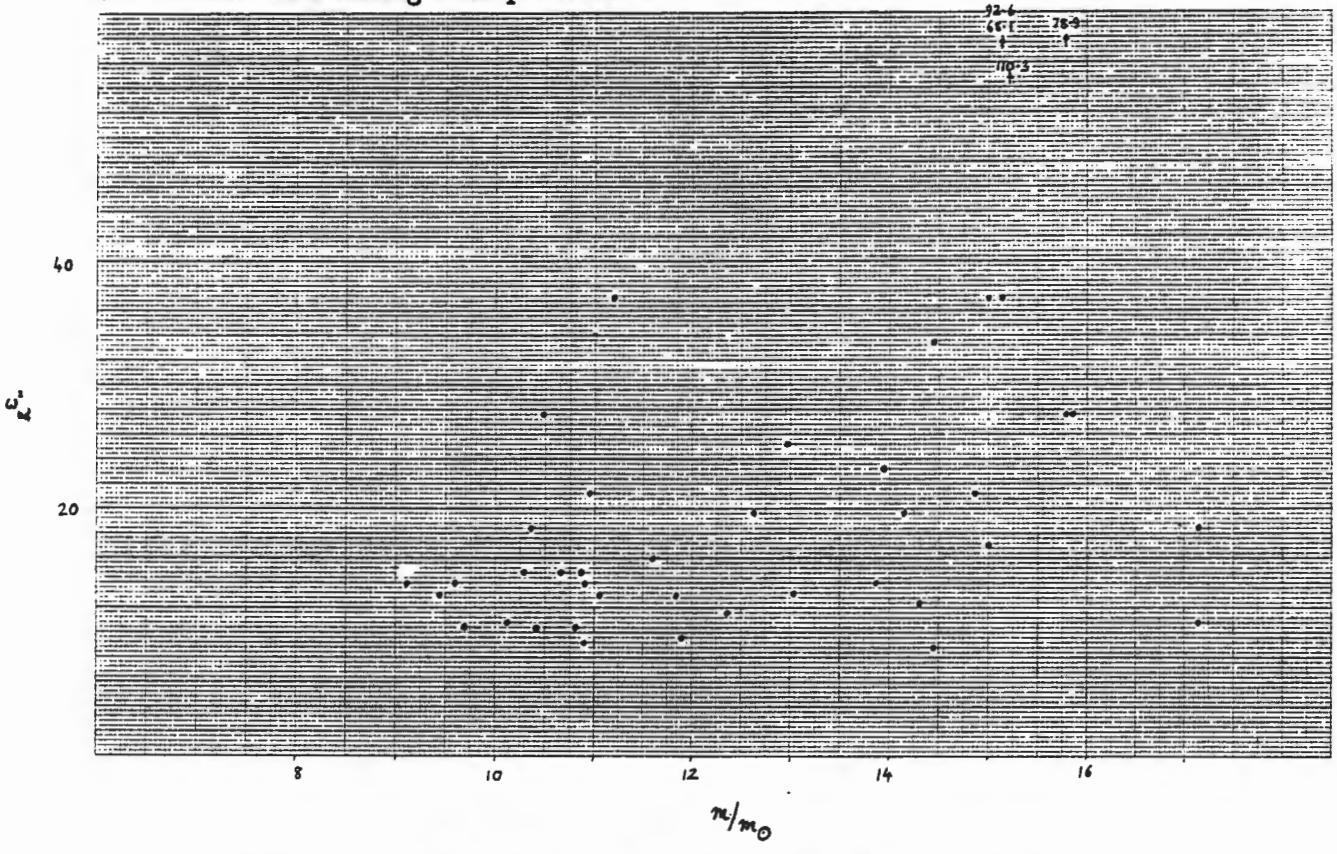

Figure 6.5. Dimensionless eigenfrequencies of 42 β Cephei stars, based on data in Shobbrook (1985)

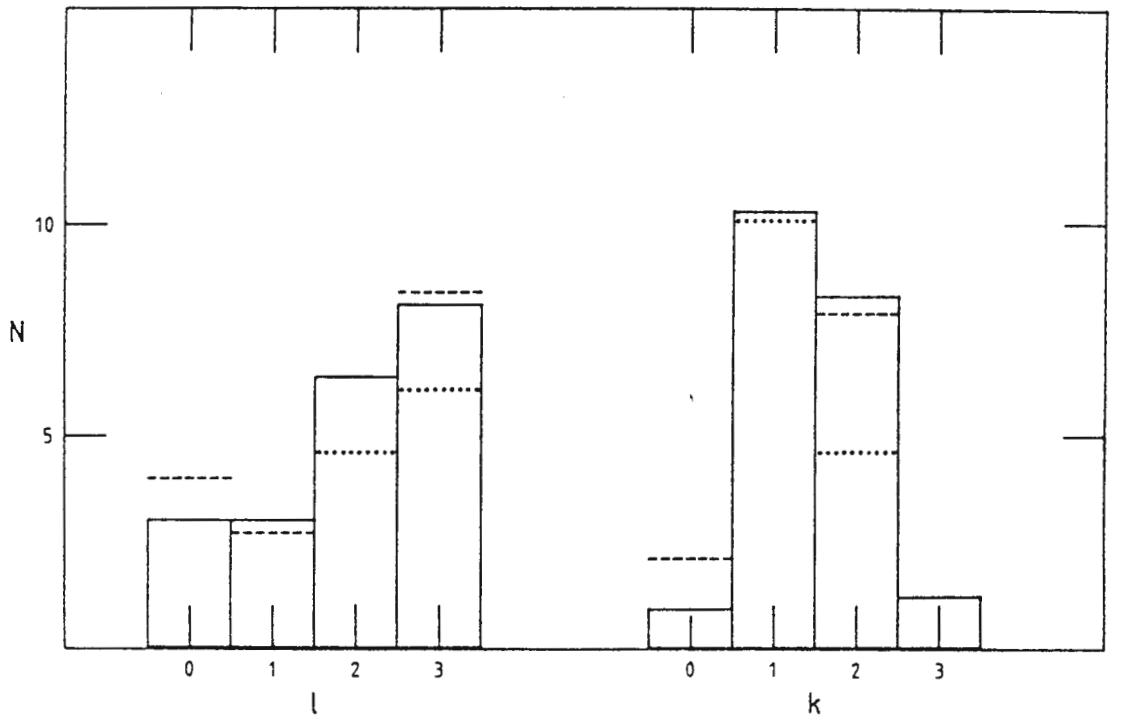

Figure 6.6. Distribution of possible degrees and overtones of pulsation modes in β Cephei stars in NGC 3293, with rotational splitting taken into account

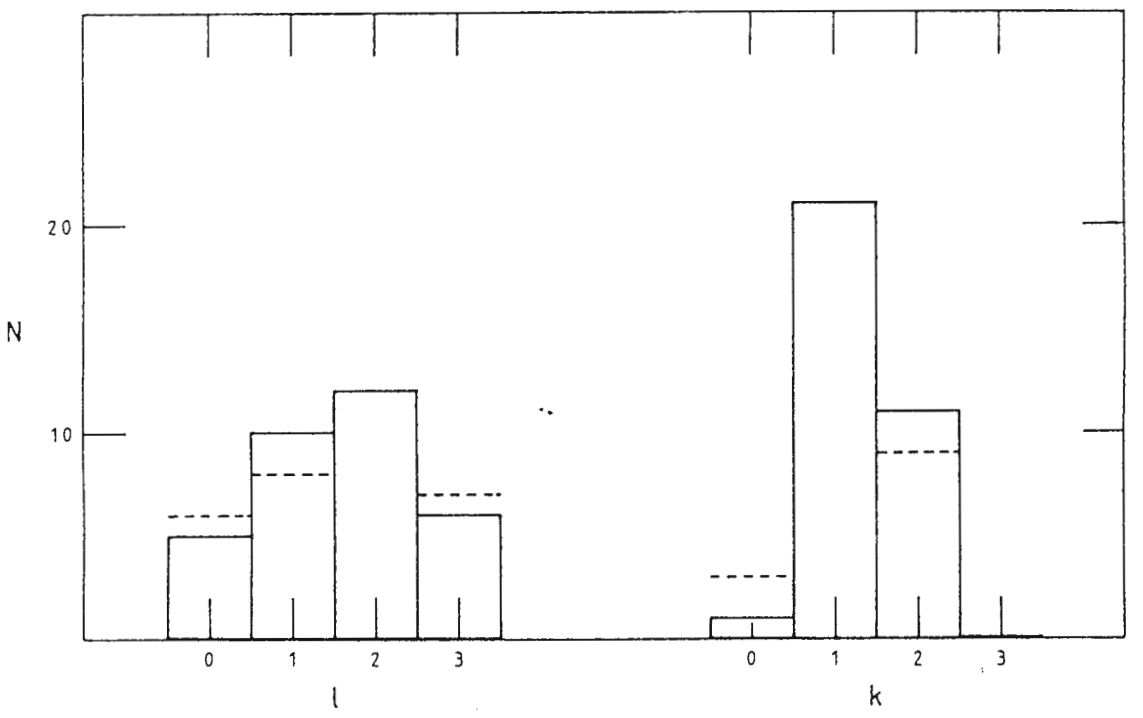

Figure 6.7. Distribution of possible degrees and overtones of pulsation modes in β Cephei stars in NGC 3293, without rotational splitting

The view that individual β Cephei stars may pulsate in only one overtone (Shobbrook 1985) is not proven for NGC 3293, but for each of the ten stars here there is a possible mode identification in Table 6.5 for which this is true.

Only for the stars for which no more than two pulsation frequencies were found, could a single value of the degree and of the overtone account for all the frequencies, although one of the mode assignments for 3293–11 ($\ell = 2, m = -1, 0, 1, 2$; $\ell = 3$) and one of the mode assignments for 3293–18 ($\ell = 2, m = -2, -1, 0$; $\ell = 3$) come quite close to attaining this ideal. It is clear, however, that more stringent physical limits on the degree, overtone and azimuthal index (m) of pulsation modes need to be determined before the number of possible mode assignments compatible with the observations presented here can be reduced.

Summarizing the results described in this section, it appears that β Cephei stars in NGC 3293 prefer quadrupole and octopole pulsation modes above radial and dipole modes (although the latter do occur) and that pulsation in the first overtone is highly preferred, with second overtone pulsation a distant second. Fundamental modes do occur, albeit in small numbers.

CHAPTER 7

CALCULATING GEOMETRICAL EFFECTS ON OBSERVATIONAL CHARACTERISTICS OF RAPIDLY ROTATING BETA CEPHEI STARS

7.1 INTRODUCTION

The previous chapters were mainly concerned with the analysis of the periods observed in the light output of the β Cephei stars in NGC 3293, leading eventually to a reasonable conclusion about the active **modes** of pulsation in these stars. However, the results of the last chapter fail to achieve the sharp distinction between alternative modes that one would have desired, inviting the question: could alternative methods of mode identification produce more precise results ?

The remaining mode identification methods, viz analysis of amplitude ratios and line profiles respectively, require spectroscopic observation of stars. Since only photometry was obtained for the β Cephei stars in this study, these methods can not at this stage be applied to these stars specifically. However, an important aspect of stellar behaviour has as yet not received detailed attention in the application of these methods in general, and is consequently taken up in the following chapters. The specific point of interest is the effect of the **geometric** consequences of **stellar rotation** on the observable amplitude ratios and spectral line profiles of rotating stars.

This issue has specific importance for the study of β Cephei stars, since many B stars are rapid rotators, making it necessary to estimate what effects rotation could have on our

analyses of the pulsations of these stars. As a start, the current published work on this topic is considered:

A large proportion of the published papers on stellar rotation are concerned with the effect of rotation on the stability and on the frequency spectra of stellar pulsations. A few of these analyses were discussed in chapter 6. Much of the remaining literature on stellar rotation deals with the physical structure of rotating stars. More will be said about this topic at the end of this chapter. Some of the remaining points are now mentioned very briefly.

About 30 years ago, Roxburgh et al. (1965) found the following relations for the luminosity L and radius R of a star in rapid uniform rotation:

$$L = L_0(1 - 0.247\alpha^2); \tag{7.1}$$

$$R_p = R_{0_p}(1 - 0.1087\alpha^2), \tag{7.2}$$

where $\alpha^2 = \Omega^2/\Omega_b^2$,

$\Omega_b^2 = GM/R_{e,b}^3$ (the subscript b refers to the breakup velocity)

R_p = polar radius,

R_e = equatorial radius,

Ω = angular velocity,

G represents the gravitational constant,

M represents the stellar mass

and the subscript 0 refers to the equilibrium state (no rotation)

A few years later, Hardorp & Strittmatter (1968a), employing theoretical calculations following the technique of Collins (1963), also studied the effect of rapid rotation on the

observed radiation of stars. They showed that a rotating star appears **brighter** than it would in a non–rotating state, when viewed at small inclination angles (ie approximately pole–on), and **fainter** than in a non–rotating state when viewed at large inclination angles (approximately equator–on). The difference between pole–on and equator–on views can be almost one magnitude in the B wavelength band. Also, at a given colour (or spectral type), a rotating star always appears brighter than its spherical counterpart would. In a companion paper, Hardorp & Strittmatter (1968b) investigated the effect of rapid rotation on stellar **absorption lines**. They argued that the neglect of the rotational distortion of the stellar surface can lead to severe underestimates of the true equatorial rotation velocities when these are obtained from observed spectral line widths. Their results suggested that the observed upper limit of approximately 450 km/s quoted for early B stars is up to 150 km/s lower than the true value, which implies that rotation velocities right up to break–up values are actually observed in B stars. Even worse, different spectral lines observed in the same star were predicted to produce different amounts of rotational broadening.

These matters were discussed more extensively in a review paper by Strittmatter (1969).

Osaki (1971), in a study of spectral line profiles, found that line widths were significantly affected by the ratio of a star's **pulsation amplitude** to its **equatorial rotation velocity**, supporting Hardorp & Strittmatter's conclusion that actual rotation velocities determined for β Cephei stars could be subject to underestimation.

In a detailed study of the O9.5 main sequence star ζ Oph, Vogt & Penrod (1983) concluded that high–degree ($\ell = 8; m = -8$) nonradial pulsations were present in this star. They detected "moving" bumps on a severely rotationally broadened spectral line with sizes as small as 0.005 of the continuum radiation level. The speed with which

these bumps appeared to traverse the line profiles was approximately 35% in excess of the stellar equatorial rotation velocity. Vogt & Penrod pointed out that rapid rotation may actually enhance the spectroscopic visibility of higher–degree nonradial pulsation modes, by "resolving" the spatial structure of the stellar disk along a line profile.

Finally, the graphs in Deupree (1990) clearly illustrate how the central density of a star increases with rotation velocity, while the central temperature and the total luminosity of the star drop to lower values as rotation velocity increases.

I now proceed to derive equations expressing, in fine detail, the effects of the geometrical distortion of a rapidly rotating star on the observed brightness and on the observed spectral lines (and, therefore, radial velocity) of such a star:

For a star which is rotating **uniformly**, with the axis of rotation determining the z–axis of the spherical coordinate system to be used, the Stokes derivative d/dt appearing in equations (5.1) to (5.8) becomes:

$$\frac{d}{dt} \quad (= \frac{\partial}{\partial t} + \mathbf{v}\cdot\nabla) \quad = \frac{\partial}{\partial t} + \Omega\frac{\partial}{\partial \phi} \qquad (7.3)$$

(where Ω is the rotation frequency).

A model describing such a rotating, pulsating star has been studied in detail by Carroll (1981), following an initial study of its vibrational properties by Hansen, Cox and Carroll (1978). A prominent feature of their approach is so–called "second linearisation", where, under the assumption of slow rotation (ie $|\Omega|/|\omega| \leq 0.1$, where ω now signifies the pulsation frequency), each of the stellar variables y_i (by now converted to dimensionless form) is written as the sum of the variation in the case of no rotation, y_{i0}, and a rotational correction, $\overline{y}_i$. After obtaining expressions for the variation in

radial coordinate, δr, by this procedure, the time derivative is taken to find the velocity of a mass element at any point on the star. These velocity components, as calculated by Carroll(1981), were:

$$\begin{aligned} v_r = -N_{\ell m}\{ & |\xi_r|(\kappa_0 + m\Omega C_i)P_\ell^m \cos(\omega_r t + m\phi + \chi_r) \\ & + |\xi_r|(\omega_{0r} + m\Omega C_r)P_\ell^m \sin(\omega_r t + m\phi + \chi_r) \\ & + |\bar{\xi}_r|\kappa_0 P_\ell^m \cos(\omega_r t + m\phi + \chi_r') \\ & + |\bar{\xi}_r|\omega_{0r} P_\ell^m \sin(\omega_r t + m\phi + \chi_r') \\ & - |\xi_h| m\Omega P_\ell^m \sin(\omega_r t + m\phi + \chi_h)\}; \end{aligned} \tag{7.4}$$

$$\begin{aligned} v_\theta = -N_{\ell m}\{ & |\xi_h|(\kappa_0 - m\Omega C_i)\frac{dP_\ell^m}{d\theta} \cos(\omega_r t + m\phi + \chi_h) \\ & + |\xi_h|[(\omega_{0r} - m\Omega C_r)\frac{dP_\ell^m}{d\theta} + m\Omega\frac{\cos\theta}{\sin\theta}P_\ell^m] \sin(\omega_r t + m\phi + \chi_h) \\ & + |\bar{\xi}_h|\kappa_0\frac{dP_\ell^m}{d\theta} \cos(\omega_r t + m\phi + \chi_h') \\ & + |\bar{\xi}_h|\omega_{0r}\frac{dP_\ell^m}{d\theta} \sin(\omega_r t + m\phi + \chi_h')\}; \end{aligned} \tag{7.5}$$

$$\begin{aligned} v_\phi = \Omega r\sin\theta - N_{\ell m}\{ & |\xi_r|\Omega\sin\theta P_\ell^m \cos(\omega_r t + m\phi + \chi_r) \\ & + |\xi_h|[(\omega_{0r} - m\Omega C_r)\frac{m}{\sin\theta}P_\ell^m + \Omega\cos\theta\frac{dP_\ell^m}{d\theta}] \cos(\omega_r t + m\phi + \chi_h) \\ & - |\xi_h|(\kappa_0 - m\Omega C_i)\frac{m}{\sin\theta}P_\ell^m \sin(\omega_r t + m\phi + \chi_h) \\ & + |\bar{\xi}_h|\omega_{0r}\frac{m}{\sin\theta}P_\ell^m \cos(\omega_r t + m\phi + \chi_h') \\ & - |\bar{\xi}_h|\kappa_0\frac{m}{\sin\theta}P_\ell^m \sin(\omega_r t + m\phi + \chi_h')\} \end{aligned} \tag{7.6}$$

(where $N_{\ell m} = \sqrt{\frac{2\ell+1(\ell-m)!}{4\pi(\ell+m)!}}(-1)^m$, $|\xi_r|$ is the complex amplitude of the **radial** pulsational displacement and $|\xi_h|$ the complex amplitude of the so–called **horizontal** (ie normal to the radius vector) pulsational displacement, both in the

nonrotating case. The symbols $\bar{\xi}_r$ and $\bar{\xi}_h$ represent the rotational corrections to be added to ξ_r and ξ_h respectively. The complex pulsation frequency (as an eigenvalue of the set of differential equations) is written as $\omega = \omega_r + i\kappa$ (for $\Omega = 0$, the notation is $\omega_0 = \omega_{0r} + i\kappa_0$), $C = C_r + iC_i$ is the so–called 'work integral', and χ_r, χ_r', χ_h and χ_h' represent the **phase** of ξ_r, $\bar{\xi}_r$, ξ_h and $\bar{\xi}_h$ respectively. The associated Legendre function $P_\ell^m(cos\theta)$ is written simply as P_ℓ^m).

The effect of rotation is thus clearly separated.

As with most other investigations of this kind, the distortion of the **geometry** of the star due to rotation is ignored by Carroll in the work referred to above, since this distortion is a second–order effect (put differently, the centrifugal forces which are associated with the distortion are proportional to the **square** of the rotation speed). The primary purpose of the current and following chapters is to investigate under which conditions this approximation is no longer justified.

An important approximation is made in this investigation: Due to the mathematical complexity of solving equations (5.5) to (5.8) for a **nonspherical** star, pulsation eigenfunctions accounting for the effect of rotation to **second** order in Ω have not been obtained to date. Therefore, the analysis which follows is of a hybrid nature, imposing the **first**–order pulsation eigenfunctions of Carroll (1981) on to a **second**–order stellar geometry. Obviously, this casts doubt on the reliability of the results obtained. However, the general trends effected by rotational distortion, as observed in the results, may still hold even when (eventually) second–order eigenfunctions are applied in a similar analysis. At the least, this constitutes an attempt to identify these trends despite the present ignorance of the exact form of the second–order eigenfunctions. As a blind attempt at rectifying this somewhat stretched approximation, the effect of adding

an ad–hoc second–order term to the eigenfunctions will also be investigated.

Observationally, stellar pulsation is investigated by means of stellar spectra and light curves. The theoretical description of rotating, pulsating stars discussed above now has to be expressed in **observational** terms, ie in terms of light curves and spectra.

7.2 THE LIGHT CURVE OF A RAPIDLY ROTATING β CEPHEI STAR

Firstly, we consider the light curve: The luminous power L_0 emitted at a wavelength λ by a region on a stellar surface is given by the following equation:

$$L_0 = F_\lambda \times (d\boldsymbol{A} \cdot \hat{n}), \tag{7.7}$$

where F_λ represents the radiative flux through this region at the wavelength λ,
$d\boldsymbol{A}$ represents the surface area vector of the region, and
$\hat{n}$ represents the unit vector normal to this region on the surface.

The amount L of this power detected by an observer is given by:

$$L = F_\lambda \times h \times (d\boldsymbol{A} \cdot \hat{z}), \tag{7.8}$$

where h represents the limb–darkening function at the position of the surface element (at the wavelength λ) and
$\hat{z}$ represents the unit vector pointing towards the observer.

Rotation and pulsation of a star will each effect changes in the values of various measurable quantities of the star. These changes will now be discussed in turn:

1. **Radius**: The surface of a uniformly rotating star is distorted in accordance with the Clairaut–Legendre expansion (see chapter 5 of Tassoul(1978)):

$$R = R_0(1 - \sum_{n=1}^{\infty} \epsilon_{2n}(R_0)P_{2n}(cos\theta)) \qquad (7.9)$$

where $P_{2n}(cos\theta)$ represents a Legendre polynomial.

Tassoul (1978) implies that terms with n > 1 can be neglected if the distortion is small. It will be shown later that this assumption is accommodated by a value < 0.1 for ϵ_2 even for rotation speeds as high as 400 km/s. If I make the **assumption** that the next relevant coefficient, ϵ_4, will be of the order $(\epsilon_2)^2$, then my results will be affected by less than 1% in accuracy by retaining only the first term in the series. Renaming ϵ_2 as ϵ_r, the following expression for the rotational distortion of the stellar radius will then be used in what follows:

$$\delta R^{\rm rot} (= R - R_0) = -\epsilon_r R_0 P_2^0(cos\theta) \qquad (7.10)$$

The distortion of the radius due to the **pulsation** of a star is simply given by the radial component of the pulsational displacement. As indicated in section 5.4, the pulsational displacement eigenfunctions for a perfectly spherical star are described by the standard spherical harmonic functions. In a particular star, the polar coordinate axis is accordingly defined by the pulsations. A **rotating** star is not a perfect sphere, however, and will have different pulsational displacement eigenfunctions. To be completely consistent, this deviation of the stellar shape from a perfect sphere has to be taken into account in the process of deriving and solving the pulsation equations. This exercise has not been undertaken in any published work to date, due to its mathematical

intractibility. It is hoped that any effect which the geometrical distortion of the star may prove to have on the existing pulsation eigenfunctions (as obtained for **spherical** stars) will apply at least qualitatively to the true eigenfunctions for rotationally distorted stars as well. However, some attempt at accounting for this alteration in the pulsation eigenfunctions will be made: Following Hansen et al.(1978), the first–order effect of rotation on the pulsation eigenfunctions is explicitly expressed by writing the pulsational displacement as the sum of the displacement obtaining in a nonrotating star and a **correction factor** which accounts for the effect of rotation:

$$\delta R^{\rm pul} = [\xi_{\rm r} cos(m\phi+\omega t+\chi_{\rm r}) + \xi'_{\rm r} cos(m\phi+\omega t+\chi'_{\rm r})] N_{\ell m} P_\ell^m(cos\theta) \tag{7.11}$$

where $\xi_{\rm r}$ represents the displacement amplitude,

m the azimuthal spherical harmonic index,

ϕ the azimuthal angular coordinate,

ω the pulsation frequency (corrected for rotation as in equation 5.11),

t the time coordinate,

$\chi_{\rm r}$ the phase of the displacement,

$\xi'_{\rm r}$ and $\chi'_{\rm r}$ the rotational corrections to $\xi_{\rm r}$ and $\chi_{\rm r}$,

$N_{\ell m}$ the spherical harmonic normalisation factor: $\sqrt{\frac{(2\ell+1)(\ell-m)!}{4\pi(\ell-m)!}}(-1)^m$

and P_ℓ^m the associated Legendre function $P_\ell^m(cos\theta)$.

2. **Surface area**: The distortion of the stellar radius causes distortion of the **area** of any element on the stellar surface. Following Buta and Smith(1979), the surface area of an element defined by a displacement $d\theta$ in the θ coordinate and a displacement $d\phi$ in the ϕ coordinate is given by the following:

$$dA = \left[\frac{\partial \boldsymbol{R}}{\partial \theta} \times \frac{\partial \boldsymbol{R}}{\partial \phi}\right] d\theta d\phi \tag{7.12}$$

where $\partial\theta$ and $\partial\phi$ refer to the angular dimensions of the surface element, and the derivatives are taken at the position of the element.

For a rotating and pulsating star the surface area of the element becomes:

$$dA+\delta dA = \left[\frac{\partial \boldsymbol{R}}{\partial \theta} \times \frac{\partial \boldsymbol{R}}{\partial \phi}\right] d\theta d\phi$$

$$= \frac{\partial}{\partial\theta}[(R_0+\delta R^{\rm rot}+\delta R^{\rm pul})\hat{r}] \times \frac{\partial}{\partial\phi}[(R_0+\delta R^{\rm rot}+\delta R^{\rm pul})\hat{r}] \; d\theta d\phi$$

$$= \left\{\left[\frac{\partial}{\partial\theta}(\delta R^{\rm rot}+\delta R^{\rm pul})\right]\hat{r} + (R_0+\delta R^{\rm rot}+\delta R^{\rm pul})\hat{\theta}\right\}$$

$$\times \left\{\left[\frac{\partial}{\partial\phi}(\delta R^{\rm rot}+\delta R^{\rm pul})\right]\hat{r} + (R_0+\delta R^{\rm rot}+\delta R^{\rm pul})sin\theta\,\hat{\phi}\right\} \; d\theta d\phi$$

$$= [(R_0+\delta R^{\rm rot}+\delta R^{\rm pul})(R_0+\delta R^{\rm rot}+\delta R^{\rm pul})sin\theta\,\hat{r}$$

$$- (R_0+\delta R^{\rm rot}+\delta R^{\rm pul})\frac{\partial}{\partial\theta}(\delta R^{\rm rot}+\delta R^{\rm pul})sin\theta\,\hat{\theta}$$

$$- (R_0+\delta R^{\rm rot}+\delta R^{\rm pul})\frac{\partial}{\partial\phi}(\delta R^{\rm rot}+\delta R^{\rm pul})\,\hat{\phi}] \; d\theta d\phi \tag{7.13}$$

where $\hat{r}$, $\hat{\theta}$ and $\hat{\phi}$ represent the respective unit vectors of the coordinate system defined by the pulsations.

Substituting the expressions for $\delta R^{\rm rot}$ and $\delta R^{\rm pul}$ given above, the following equation is

obtained:

$$\frac{\delta(dA)}{d\theta d\phi} = \Big\{2R_0[-\epsilon_r R_0 P_2^0 + (\xi_r cos(m\phi+\omega t+\chi_r)$$

$$+\xi'_r cos(m\phi+\omega t+\chi'_r))N_{\ell m}P_\ell^m(cos\theta)] + R_0^2\epsilon_r^2(P_2^0(cos\theta))^2$$

$$+ [\xi_r^2 cos(2m\phi+2\omega t+2\chi_r)+(\xi'_r)^2 cos(2m\phi+2\omega t+2\chi'_r)$$

$$+2\xi_r\xi'_r cos(2m\phi+2\omega t+\chi_r+\chi'_r)]N_{\ell m}^2(P_\ell^m(cos\theta))^2$$

$$- 2R_0\epsilon_r[\xi_r cos(m\phi+\omega t+\chi_r)+\xi'_r cos(m\phi+\omega t+\chi'_r)]$$

$$\times P_2^0(cos\theta)N_{\ell m}P_\ell^m(cos\theta)\Big\}\, sin\theta\,\hat{r}$$

$$-\Big\{(R_0-\epsilon_r R_0 P_2^0(cos\theta))\times[(\xi_r cos(m\phi+\omega t+\chi_r)$$

$$+\xi'_r cos(m\phi+\omega t+\chi'_r))N_{\ell m}\frac{d}{d\theta}P_\ell^m(cos\theta) - \epsilon_r R_0\frac{d}{d\theta}P_2^0(cos\theta)]$$

$$+ [(\xi_r cos(m\phi+\omega t+\chi_r)+\xi'_r cos(m\phi+\omega t+\chi'_r))N_{\ell m}\frac{d}{d\theta}P_\ell^m(cos\theta) - \epsilon_r R_0\frac{d}{d\theta}P_2^0]$$

$$\times(\xi_r cos(m\phi+\omega t+\chi_r)+\xi'_r cos(m\phi+\omega t+\chi'_r))N_{\ell m}P_\ell^m(cos\theta)\Big\}\, sin\theta\,\hat{\theta}$$

$$-\Big\{-R_0(\xi_r sin(m\phi+\omega t+\chi_r)+\xi'_r sin(m\phi+\omega t+\chi'_r))mN_{\ell m}P_\ell^m(cos\theta)$$

$$+ R_0 \epsilon_r P_2^0(\cos\theta)(\xi_r \sin(m\phi+\omega t+\chi_r)+\xi'_r \sin(m\phi+\omega t+\chi'_r))mN_{\ell m}P_\ell^m(\cos\theta)$$

$$-(\xi_r \cos(m\phi+\omega t+\chi_r)+\xi'_r \cos(m\phi+\omega t+\chi'_r))N_{\ell m}P_\ell^m(\cos\theta)$$

$$\times(\xi_r \sin(m\phi+\omega t+\chi_r)+\xi'_r \sin(m\phi+\omega t+\chi'_r))mN_{\ell m}P_\ell^m(\cos\theta)\Big\}\,\hat{\phi} \tag{7.14}$$

3. **Radiative flux**: Still following Buta and Smith(1979), the effect of the rotation and pulsation of a star on its radiative flux is derived. In the Cowling approximation, a change in radius of the star causes a change in pressure of the form:

$$\frac{\delta P}{P} = \left[\frac{\ell(\ell+1)}{\omega_{nd}^2} - 4 - \omega_{nd}^2\right]\frac{\delta R}{R} \tag{7.15}$$

$$= f_p(\ell,\omega_{nd}^2)\frac{\delta R}{R}, \text{ say.}$$

Using the adiabatic relation:

$$\frac{\delta T}{T} = \frac{\Gamma_2 - 1}{\Gamma_2}\frac{\delta P}{P}, \tag{7.16}$$

it follows that

$$\frac{\delta T}{T} = \frac{\Gamma_2 - 1}{\Gamma_2} f_p(\ell,\omega_{nd}^2)\frac{\delta R}{R} \tag{7.17}$$

$$= f_t(\ell,\omega_{nd}^2)\frac{\delta R}{R}, \text{ say.}$$

In the blackbody approximation, a temperature change effects the following change in the radiative flux at the wavelength λ:

$$\frac{\delta F_\lambda}{F_\lambda} = \frac{xe^x}{e^x-1}\frac{\delta T}{T} \text{ (where } x = \frac{hc}{\lambda kT}\text{)}, \tag{7.18}$$

finally giving the following relation between a change in the radius and the corresponding change in the flux:

$$\frac{\delta F_\lambda}{F_\lambda} = \frac{xe^x}{e^x-1} f_t(\ell,\omega^2_{nd})\frac{\delta R}{R} = f_\lambda(\ell,\omega^2_{nd},T)\frac{\delta R}{R}, \text{ say,} \tag{7.19}$$

and, written out explicitly:

$$\delta F_\lambda = F_\lambda f_\lambda(\ell,\omega^2_{nd},T)[(\epsilon cos(m\phi+\omega t+\chi_r)+\epsilon' cos(m\phi+\omega t+\chi'_r))$$

$$\times N_{\ell m} P^m_\ell(cos\theta)-\epsilon_r P^0_2(cos\theta)] , \tag{7.20}$$

where $\epsilon = \frac{\xi_r}{R}$ and $\epsilon' = \frac{\xi'_r}{R}$, and a typical value for f_λ, calculated for $T = 21100$ K, $\ell = 2$, $\omega^2_{nd} = 17.9$ and $\lambda = 420$ nm (these choices are explained later), is:

$$f_{420}\,(2,17.9,21100) = -17.5.$$

Von Zeipel's law of gravity darkening (see chapter 7 of Tassoul(1978)) states that, under the assumption of radiative equilibrium, the emitted flux at the surface of a uniformly rotating star varies as the effective surface gravity, which means that this flux may also be written as:

$$F = F_0(1 - \epsilon_f P_2^0(cos\vartheta)). \tag{7.21}$$

Comparing with equation (7.20), the factor ϵ_f is identified as:

$$\epsilon_f = f_\lambda(\ell, \omega_{nd}^2, T)\epsilon_r.$$

4. Limb darkening

The form of the equations presented so far refers to a spherical coordinate system centred in the star, with the z–axis of the system coinciding with the rotation and pulsation axes of the star. A practical reference frame from the observer's point of view is one which is also centred in the star, but with the z–axis pointing towards the observer. Coordinates in this frame will be represented by r, ϑ and φ in this chapter. The **normalised** limb–darkening law for a perfectly spherical star is customarily written as follows:

$$h(cos\vartheta) = \frac{6}{(3-u)}(1 - u + ucos\vartheta) \tag{7.22}$$

(where u is chosen as appropriate for the type of star under investigation).

The $cos\vartheta$ factor is simply the form of the scalar vector product $\hat{n}\cdot\hat{z}$ (with $\hat{n}$ and $\hat{z}$ defined at the start of section 7.2), for a spherical star. For the purposes of computation, a value of u appropriate for the β Cephei stars was chosen, using the tables in Al–Naimiy(1978). The effective temperatures of these stars fall in the range 21000 to 26000 K, while log(surface gravity) falls in the range 1.5 to 1.9 (3.5 to 3.9 when g is expressed in cgs units), indicating a value of u slightly below 0.4 for observations in the Johnson B band.

Still following Buta and Smith(1979), the total limb–darkening function, including the

distortion of the stellar surface, will be given by:

$$h+\delta h = \frac{6}{(3-u)}(1-u+u(\hat{n}+\delta\hat{n})\cdot\hat{z}) = \frac{6}{(3-u)}(1-u+u\left[\frac{dA+\delta dA}{|dA+\delta dA|}\right]\cdot\hat{z}. \tag{7.23}$$

Looking back at equation (7.14), it is obvious that the term $|dA+\delta dA| = ((dA+\delta dA)\cdot(dA+\delta dA))^{1/2}$ contains many products of ϵ, ϵ' and ϵ_r. This expression is represented to an accuracy of better than 99 % (as may be seen by working through many pages of algebra, which are not reproduced here) by omitting all terms containing ϵ^2, $(\epsilon')^2$, $\epsilon\epsilon'$, $\epsilon_r^2\epsilon$, $\epsilon_r^2\epsilon'$ or ϵ_r^3 (provided that $\epsilon \leq 0.005$, $\epsilon' \leq 0.005$ and $\epsilon_r \leq 0.1$ – these limits will be justified later). The following expression then remains:

$$|dA+\delta dA|^2 = R_0^4\Big\{\Big[1+\epsilon_r(-4P_0^2) + \epsilon_r^2(6P_0^2 + (P_0^{2\prime})^2)$$

$$+(\epsilon cos(m\phi+\omega t+\chi_r)+\epsilon' cos(m\phi+\omega t+\chi_r'))4N_{\ell m}P_\ell^m$$

$$+\epsilon_r(\epsilon cos(m\phi+\omega t+\chi_r)+\epsilon' cos(m\phi+\omega t+\chi_r'))(-12P_0^2N_{\ell m}P_\ell^m - 2P_0^{2\prime}N_{\ell m}P_\ell^{m\prime})\Big]sin^2\theta$$

$$-m^2(\epsilon^2 cos(2m\phi+2\omega t+2\chi_r)+(\epsilon')^2 cos(2m\phi+2\omega t+2\chi_r')$$

$$+2\epsilon\epsilon' cos(2m\phi+2\omega t+\chi_r+\chi_r'))N_{\ell m}^2(P_\ell^m)^2\Big\}(d\theta d\phi)^2. \tag{7.24}$$

(where $P_\ell^{m\prime} = \frac{d}{d\theta}P_\ell^m(cos\theta)$). The expression $\frac{1}{|dA+\delta dA|}$ may be written in the form of a binomial expansion. To retain an accuracy of higher than 99 %, the first four terms of the expansion are needed (again obvious after many pages of algebra). When written out fully, these terms will contain many expressions of exceedingly small numerical value. Writing down only those terms necessary to represent at least 99 % of the total

numerical value,

$$\frac{1}{|dA+\delta dA|} = \frac{1}{R^2 sin\theta d\theta d\phi}\Big\{1+2\epsilon_r P_0^2+\epsilon_r^2(3(P_0^2)^2-0{,}5(P_0^{2'})^2)$$

$$+\epsilon_r^3(2(P_2^0)^3-3P_0^2(P_0^{2'})^2)-76{,}5\epsilon_r^4(P_0^2)^4+135\epsilon_r^5(P_0^2)^5$$

$$-2N_{\ell m}P_\ell^m(\epsilon cos(\omega_r t+m\phi+\chi_r)+\epsilon' cos(\omega_r t+m\phi+\chi_r'))$$

$$+\epsilon_r N_{\ell m}(-6P_0^2P_\ell^m(\epsilon cos(\omega_r t+m\phi+\chi_r)+\epsilon' cos(\omega_r t+m\phi+\chi_r))$$

$$+(P_0^2)'(P_\ell^m)'(\epsilon cos(\omega_r t+m\phi+\chi_r)+\epsilon' cos(\omega_r t+m\phi+\chi_r))$$

$$+360\epsilon_r^3 N_{\ell m}(P_0^2)^3P_\ell^m(\epsilon cos(\omega_r t+m\phi+\chi_r)+\epsilon' cos(\omega_r t+m\phi+\chi_r))$$

$$-\frac{m^2}{sin^2\theta}N_{\ell m}^2(P_\ell^m)^2(\epsilon^2 cos(2m\phi+2\omega t+2\chi_r)+(\epsilon')^2 cos(2m\phi+2\omega t+2\chi_r')$$

$$+2\epsilon\epsilon' cos(2m\phi+2\omega t+\chi_r+\chi_r'))\Big\}. \qquad (7.25)$$

The scalar product $(dA+\delta dA)\cdot\hat{z}$ is of the following form:

$$(dA+\delta dA)\cdot\hat{z} = R^2 sin\theta d\theta d\phi\Big\{[(1+2N_{\ell m}P_\ell^m(\epsilon cos(\omega_r t+m\phi+\chi_r)+\epsilon' cos(\omega_r t+m\phi+\chi_r')))$$

$$\times(1-2\epsilon_r P_0^2)+\epsilon_r^2(P_0^2)^2]\,\hat{z}_r$$

$$+[\epsilon_r P_0^{2'}-N_{\ell m}P_\ell^{m'}(\epsilon cos(\omega_r t+m\phi+\chi_r)+\epsilon' cos(\omega_r t+m\phi+\chi_r'))-\epsilon_r^2 P_0^2 P_0^{2'}$$

$$+ \epsilon_r N_{\ell m}(P_0^2 P_\ell^{m'}(\epsilon cos(\omega_r t+m\phi+\chi_r)+\epsilon' cos(\omega_r t+m\phi+\chi_r'))$$

$$+ P_0^{2'} P_\ell^m(\epsilon cos(\omega_r t+m\phi+\chi_r)+\epsilon' cos(\omega_r t+m\phi+\chi_r')))]\ \hat{z}_\theta$$

$$+ m[N_{\ell m} P_\ell^m(\epsilon sin(\omega_r t+m\phi+\chi_r)+\epsilon' sin(\omega_r t+m\phi+\chi_r'))(1-\epsilon_r P_0^2)$$

$$+ N_{\ell m}^2(P_\ell^m)^2(\epsilon^2 sin(2m\phi+2\omega t+2\chi_r)+(\epsilon')^2 sin(2m\phi+2\omega t+2\chi_r')$$

$$+2\epsilon\epsilon' sin(2m\phi+2\omega t+\chi_r+\chi_r'))sin(m\phi)cos(m\phi)]\ \hat{z}_\phi\Big\}. \qquad (7.26)$$

The components of $\hat{z}$ in the stellar coordinate system are:

$$\begin{aligned} \hat{z}_r &= sin(i)sin\theta sin\phi - cos(i)cos\theta \\ \hat{z}_\theta &= sin(i)cos\theta sin\phi + cos(i)sin\theta \\ \hat{z}_\phi &= sin(i)cos\phi \end{aligned} \qquad (7.27)$$

where i is the angle of inclination between the positive polar axis (θ=0) of the star and the line of sight from the observer towards the star.

The terms appearing in equation 7.8 have now all been derived for a rotationally distorted, monoperiodic β Cephei star. Once the variation in luminosity of the star has been obtained, the variation in magnitude (ie the light curve) is obtained from the simple relation:

$$m - m_0 = -1.08574\ ln(L/L_0) \qquad (7.28)$$

The radial velocity of such a star will now be addressed.

7.3 THE RADIAL VELOCITY OF A RAPIDLY ROTATING β CEPHEI STAR

The Lagrangian variation (see chapter 5) in the velocity of a particular stellar surface element, due to pulsation of the star, is described by:

$$\delta v = \frac{\partial \xi}{\partial t} + v \cdot \nabla \xi$$

$$= \frac{\partial \xi}{\partial t} + \Omega r sin\theta \, \hat{\phi} \cdot \nabla \xi. \qquad (7.29)$$

Assuming the harmonic time variation described in equation 5.9, and a spherical harmonic function associated with the pulsation displacement vector ξ, as in equation 5.10, equation 7.29 reduces to:

$$\delta v = i(\omega + m\Omega)\xi - \xi_\phi \Omega sin\theta \, \hat{r} - \xi_\phi \Omega cos\theta \, \hat{\theta}$$
$$+ (\xi_r \Omega sin\theta + \xi_\theta \Omega cos\theta) \, \hat{\phi}. \qquad (7.30)$$

Since the Eulerian variation $v' = \delta v - \xi \cdot \nabla v$ (see Tassoul (1978), p 118, or Cox (1980), p 53), it can be expressed as:

$$v' = i(\omega + m\Omega)\xi + \Omega(-\xi_\phi sin\theta \, \hat{r} - \xi_\phi cos\theta \, \hat{\theta}) \qquad (7.31)$$

The frequency ω of an oscillation in a rotating star is approximated by the expression in equation 5.11:

$$\omega = \omega_0 - (1 - C_1)m\Omega + C_2\Omega^2/\omega_0^2, \qquad (7.32)$$

while the displacement eigenfunction ξ may be written as the sum:

$$\xi = \xi_0 + \xi_1,$$

where ξ_0 = the eigenfunction that would obtain if the star was not rotating,
and ξ_1 = the rotational correction to ξ_0, as described by Carroll (1981).

The components of ξ_0 may be written as:

$$\xi_{0_r} = \epsilon R_0 N_{\ell m} P_\ell^m exp(i(m\phi+\omega t+\chi_r)),$$

$$\xi_{0\theta} = \epsilon_h R_0 N_{\ell m} P_\ell^{m'} exp(i(m\phi+\omega t+\chi_h)), \text{ and}$$

$$\xi_{0\phi} = \epsilon_h R_0 (\frac{im}{sin\theta}) N_{\ell m} P_\ell^m exp(i(m\phi+\omega t+\chi_h)), \qquad (7.33)$$

where ϵ_h = the horizontal (or nonradial) displacement amplitude
(to be discussed later),
and the other terms are defined above. The components of ξ_1 have been derived by Carroll (1981) and Saio (1981):

$$\xi_{1_r} = \epsilon' R_0 N_{\ell m} P_\ell^m exp(i(m\phi+\omega t+\chi_r')),$$

$$\xi_{1\theta} = [\epsilon_h' exp(i\chi_h') R_0 - \frac{2m\Omega}{\omega_0} C_1 \epsilon_h exp(i\chi_h) R_0] N_{\ell m} P_\ell^{m'} exp(i(m\phi+\omega t))$$
$$+ \frac{2m\Omega}{\omega_0} \frac{cos\theta}{sin\theta} \epsilon_h R_0 N_{\ell m} P_\ell^m exp(i(m\phi+\omega t+\chi_h)), \text{ and}$$

$$\xi_{1\phi} = [\epsilon_h' exp(i\chi_h') R_0 - \frac{2m\Omega}{\omega_0} C_1 \epsilon_h exp(i\chi_h) R_0] (\frac{im}{sin\theta}) N_{\ell m} P_\ell^m exp(i(m\phi+\omega t))$$
$$+ \frac{2i\Omega}{\omega_0} (\epsilon R_0 sin\theta N_{\ell m} P_\ell^m exp(i(m\phi+\omega t+\chi_r)) + \epsilon_h R_0 cos\theta N_{\ell m} P_\ell^{m'} exp(i(m\phi+\omega t+\chi_h)).$$

(7.34)

The total velocity of an element on the stellar surface, due to the rotation as well as the

pulsation of the star, is given by:

$$\boldsymbol{v} = \Omega r sin\theta\ \hat{\phi} + \boldsymbol{v}'. \tag{7.35}$$

Substituting equations 7.31 to 7.34 in 7.35, and keeping only the real parts, produces the following expressions for the components of surface velocity in the (r,θ,ϕ) system:

$$\begin{aligned}
v_r = R_0 N_{\ell m}[&(-\omega - m\Omega)P_\ell^m(\epsilon sin(m\phi+\omega t+\chi_r)+\epsilon' sin(m\phi+\omega t+\chi_r'))\\
&+ m\Omega P_\ell^m(\epsilon_h sin(m\phi+\omega t+\chi_h)+\epsilon_h' sin(m\phi+\omega t+\chi_h'))\\
-\frac{m^2\Omega^2}{\omega_0} C_1 P_\ell^m \epsilon_h sin(m\phi+\omega t+\chi_h) &- 2\frac{\Omega^2}{\omega_0} sin\theta(sin\theta P_\ell^m \epsilon sin(m\phi+\omega t+\chi_r)\\
&+ cos\theta P_\ell^{m'} \epsilon_h sin(m\phi+\omega t+\chi_h))],
\end{aligned}$$

$$\begin{aligned}
v_\theta = R_0 N_{\ell m}\Big\{&(-\omega - m\Omega)[P_\ell^{m'}(\epsilon_h sin(m\phi+\omega t+\chi_h)+\epsilon_h' sin(m\phi+\omega t+\chi_h'))\\
&- 2\frac{\Omega}{\omega_0} C_1 P_\ell^{m'} \epsilon_h sin(m\phi+\omega t+\chi_h) + \frac{2m\Omega}{\omega_0}\frac{cos\theta}{sin\theta} P_\ell^m \epsilon_h sin(m\phi+\omega t+\chi_h)]\\
&+ m\Omega\frac{cos\theta}{sin\theta}[P_\ell^m(\epsilon_h sin(m\phi+\omega t+\chi_h)+\epsilon_h' sin(m\phi+\omega t+\chi_h))\\
&- 2m\frac{\Omega C_1}{\omega_0} P_\ell^m \epsilon_h sin(m\phi+\omega t+\chi_h)]\\
+ 2\frac{\Omega^2}{\omega_0} cos\theta[sin\theta P_\ell^m \epsilon sin(m\phi+\omega t+\chi_r) &+ cos\theta P_\ell^{m'} \epsilon_h sin(m\phi+\omega t+\chi_h)]\Big\}, \text{ and}
\end{aligned}$$

$$\begin{aligned}
v_\phi = R_0(-\omega - m\Omega)N_{\ell m}[&\frac{m}{sin\theta}(P_\ell^m(\epsilon_h cos(m\phi+\omega t+\chi_h)+\epsilon_h' cos(m\phi+\omega t+\chi_h'))\\
&- 2\frac{m\Omega C_1}{\omega_0} P_\ell^m \epsilon_h cos(m\phi+\omega t+\chi_h)) + \frac{2\Omega}{\omega_0}(sin\theta P_\ell^m \epsilon cos(m\phi+\omega t+\chi_r)\\
&+ cos\theta P_\ell^{m'} \epsilon_h cos(m\phi+\omega t+\chi_h))] + R_0\Omega sin\theta,
\end{aligned} \tag{7.36}$$

expressions containing Ω to second order, instead of the expressions of Carroll in equations 7.4 to 7.6, which only contain Ω to first order.

The **radial** velocity (in the direction of the observer) of a particular surface element is the scalar product of $\boldsymbol{v}$ with $\hat{z}$:

$$v_{\rm rad} = v_{\rm r}\hat{z}_{\rm r} + v_\theta\hat{z}_\theta + v_\phi\hat{z}_\phi \qquad (7.37)$$

To find the radial velocity for the star as a whole, the radial velocity for each element is weighted by the **luminosity** $L_{\rm el}(\theta,\phi)$ of the element, as a proportion of the total luminosity L of the star. This average radial velocity $\bar{v}_{\rm rad}$ found by adding the weighted velocities for all the visible elements together is also known as the **centroid** of the resulting velocity distribution:

$$\bar{v}_{\rm rad} = \sum_{\theta,\phi} \left(v_{\rm rad}(\theta,\phi) \frac{L_{\rm el}(\theta,\phi)}{L} \right) \qquad (7.38)$$

A "raw" (ie unbroadened) spectral line profile for the star may be constructed at any phase in its pulsation cycle by simply binning together the luminosities of surface elements according to radial velocity, obtaining what is essentially a graph of luminosity as a function of radial velocity. This procedure will be discussed in more depth in chapter 9.

7.4 TRANSFORMING TO THE OBSERVER'S COORDINATES

Expressions for the magnitude and the radial velocity of a rapidly rotating, monoperiodic nonradially pulsating star were derived in the previous two sections. Since the numerical calculation of these quantities is more easily done in terms of the **observer's** coordinate system (defined at the start of point 4 under section 7.2), all quantities should be expressed in this system. The transformations of expressions from the stellar coordinate system (r,θ,ϕ) to the observer's system (r,ϑ,φ) are now derived:

The observer's z axis is chosen such that the positive axis points from the stellar centre directly towards the observer. The observer's x axis is chosen to fall inside the plane defined by the z axes of the stellar and observer's coordinate systems. The Eulerian angles for the transformation between these two systems (see eg Goldstein 1950) then have the following values:

$$\begin{aligned} \phi &= 0, \\ \theta &= 180^{\circ} - i, \\ \psi &= 0. \end{aligned} \tag{7.39}$$

(The definition of i appears immediately after equation 7.27). Using the transformation matrices described by Goldstein (1950), the relations in equation 7.27 can easily be derived. The trigonometric quantities appearing in various equations in this chapter transform as follows (the reader is reminded that θ and ϕ refer to the stellar system and ϑ and φ refer to the observer's system):

$$cos\theta = -sin(i)\ sin\vartheta\ sin\varphi - cos(i)\ cos\vartheta, \tag{7.40}$$

$$\begin{aligned} sin\theta = (&sin^2\vartheta\ cos^2\varphi + cos^2(i)\ sin^2\vartheta\ sin^2\varphi + sin^2(i)\ cos^2\vartheta \\ &- 2\ sin(i)\ cos(i)\ cos\vartheta\ sin\vartheta\ sin\varphi)^{1/2}, \end{aligned} \tag{7.41}$$

$$sin\phi = \frac{-\ cos(i)\ sin\vartheta\ sin\varphi\ +\ sin(i)\ cos\vartheta}{sin\theta}, \tag{7.42}$$

$$cos\phi = \frac{sin\vartheta\ cos\varphi}{sin\theta}. \tag{7.43}$$

The transformation of associated Legendre functions from the stellar to the observer's system is more complicated. A standard reference in the literature concerning this

transformation is that of Jeffreys (1965). The results in this reference have to be treated with caution, however, since different definitions of the associated Legendre function appear in the literature, and the results of Jeffreys apply to one specific such definition. Jeffreys used

$$P_\ell^m(x) = \frac{(\ell-m)!}{2^\ell(\ell!)^2}(1-x^2)^{m/2}\,\frac{d^{\ell+m}}{dx^{\ell+m}}(x^2-1)^\ell, \tag{7.44}$$

while the definition which is used in this thesis is the standard (Courant & Hilbert (1953), Margenau & Murphy (1956), Spiegel (1968) and Arfken (1985), to mention a few) one:

$$P_\ell^m(x) = \frac{1}{2^\ell(\ell!)}(1-x^2)^{m/2}\,\frac{d^{\ell+m}}{dx^{\ell+m}}(x^2-1)^\ell. \tag{7.45}$$

Working through the derivations in Jeffreys (1965) revealed a few misprints in the paper. The most significant is that appearing in equation (5) of section 4 of the paper, an equation which has been quoted in the literature in various instances. In this equation, the power of (–1) is indicated as $(\ell-m-r)$, while analysis shows that this should be $(\ell-s-r)$. Application of Jeffreys' method to equation 8.45 instead of 8.44 produces the following transformation equation for the associated Legendre functions:

$$P_\ell^m(\cos\theta)e^{im\phi} = (\ell+m)!\sum_{k=-\ell}^{\ell}[a_{\ell mk}(i)\,(\ell-k)!\,P_\ell^k(\cos\vartheta)e^{ik\varphi}], \tag{7.46}$$

where

$$a_{\ell mk}(i) = \sum_{r=r_1}^{r_2}\left\{(-1)^{\ell-k-r}\frac{[\cos(i'/2)]^{2r+m+k}[\sin(i'/2)]^{2\ell-2r-m-k}}{r!\,(\ell-m-r)!\,(\ell-k-r)!\,(m+k+r)!}\right\},$$

(7.47)

7.5 INPUT PARAMETERS FOR CALCULATION

The final ingredients required to proceed with calculating the observational characteristics of model β Cephei stars are the values of various physical parameters. These are now discussed in turn.

The basic stellar parameters of radius, mass and temperature were chosen to give a reasonable representation of a β Cephei star. Convenient values could be chosen for the mass and radius:

$$R = 5 \times 10^6 \text{ km } (= 7.184\ R_\odot), \text{ and}$$

$$M = 10 M_\odot,$$

but the value of the effective temperature then had to be carefully matched to the first two values above, to ensure consistency with a reasonable β Cephei star model. Tables of mass, radius and temperature for $10M_\odot$ stellar models close to the end of core–hydrogen burning were published by Davey (1973), Deupree (1974) and Osaki (1975). Averaging of their results (including interpolation where necessary) for the evolutionary stage where the $10M_\odot$ model had the radius of 7.184 $R_\odot$ mentioned above, produced the following numbers (rounded off) for the core hydrogen content X_c, the central density ρ_c and the effective temperature T_e:

$$X_c = 0.18,$$

$$\rho_c = 10.2 \text{ g/(cm)}^3,$$

$$T_e = 21100 \text{ K}.$$

A representative value (considering the results presented in chapter 4) for the unperturbed pulsation frequency is

$$\omega_0 = 6 \text{ cycles per day}.$$

$$\omega_0 = 6 \text{ cycles per day.}$$

As mentioned earlier in this chapter, the effective frequency reflecting the influence of rotation is

$$\omega = \omega_0 - (1 - C_1)\mathrm{m}\Omega + C_2\Omega^2/\omega_0^2,$$

where the values of C_1 and C_2 are obtained from Saio (1981). As far as the pulsation amplitude is concerned, the results in chapter 4 indicate that individual modes have light amplitudes roughly of the order of 0.01 magnitudes in B. The following (radial) amplitude used in the calculations produced light curves of similar amplitudes:

$$\epsilon\ (=\Delta R/R_0) = 0.005.$$

This value is supported by Peters et al. (1987), who deduced values of 0.004 and 0.007 for the real β Cephei stars γ Peg and δ Cet respectively. According to Buta & Smith (1979), the value $\epsilon = 0.005$ corresponds to an amplitude in radial velocity variation of

$$\Delta v_{\mathrm{rad}} = 10.9 \text{ km/s}.$$

The value of the horizontal displacement amplitude was calculated from the relation in Dziembowski (1977):

$$\epsilon_{\mathrm{h}} = \frac{GM}{\omega_0^2 R_0^3}\,\epsilon = 0.0558\epsilon$$

for the choices made above. The rotational corrections to these two amplitudes, introduced by Carroll (1981), are:

$$\epsilon' = (0.2)\frac{2m\Omega}{\omega_0}\,\epsilon \text{ and}$$

$$\epsilon'_{\mathrm{h}} = (0.2)\frac{2m\Omega}{\omega_0}\,\epsilon_{\mathrm{h}}.$$

The phases of these variations, relative to an arbitrary starting phase of, say, the radial unperturbed variation, are indicated by the symbols χ_{r}, χ_{h}, χ'_{r} and χ'_{h} respectively. A study of Carroll's (1981) results shows that, for a model β Cephei star pulsating in a

less. It therefore appears prudent to set all these phases to the same simple value at the start of the calculation:

$$\chi_r = 0,$$
$$\chi_h = 0,$$
$$\chi_r' = 0,$$
$$\chi_h' = 0.$$

As discussed on page 138, the second–order effect of rotational distortion was crudely imposed as an ad–hoc term. Using Carroll's form of thr first–order correction term as a guideline, the second–order terms were simply chosen as:

$$\epsilon'' = (0.4)m\,(\Omega^2/\omega_0^2)\,\epsilon$$

and

$$\epsilon_h'' = (0.4)m\,(\Omega^2/\omega_0^2)\,\epsilon_h.$$

As was the case for the first–order correction, a phase difference of zero was assumed for these terms relative to the zero–th order terms.

The thermodynamic parameter Γ is set to the generally accepted value for the type of stellar model applicable to the β Cephei stars:

$$\Gamma = 5/3,$$

while, as mentioned earlier, the limb–darkening coefficient has the value

$$u = 0.4.$$

The value of –17.5 for the parameter f_λ in equation 7.19 was derived for adiabatic conditions. Provision was made for the nonadiabaticity of the observed photospheres by varying the value of f_λ between –5 and –30 and investigating the effect on the calculated results for light and velocity variations.

Since the Johnson B filter shows its transmission peak at 420 nm, this value is assigned to the λ appearing in the flux variation derivation:

$$\lambda = 420 \text{ nm},$$

while the dimensionless frequency squared also appearing in this derivation follows from values already determined above:

$$\omega_{nd}^2 = \frac{\omega_0^2 R_0^3}{GM} = 17.9.$$

The values of the coefficient ϵ_r introduced in equation 8.10 are now considered. James (1964) published tables of equatorial to polar radii for rotating polytropes, which may be used to estimate ϵ_r. According to Clement (1965), the polytropes most closely approximating β Cephei stars have a polytropic index of 3 or slightly higher. James' results for a polytrope of index $n = 3$ are of the same order of magnitude than those calculated by Clement (1989), specifically for a $15M_\odot$, rotating stellar model, and identical to the results of Hachisu (1986), also for a polytrope with $n = 3$ (but using a different method of calculation). Since the tables published by James are much more detailed for the range of speeds under consideration here, they were used to calculate values of ϵ_r corresponding to the choices of equatorial rotation speed v_e. Using James' terminology,

$$\epsilon_r = 1 - \frac{\xi_p}{\xi_e},$$

where the values of ξ_p and ξ_e are obtained from the tables published by James (1964), interpolating where necessary. The values of these coefficients depend on the angular rotation velocity and the central density of the model. The following table was obtained by following this method:

Table 7.1

Rotational distortion parameter

v_e(km/s)	ϵ_r
0	0
40	0.00064
80	0.00254
120	0.00571
160	0.01048
200	0.01598
240	0.02325
280	0.03202
320	0.04241
360	0.05460
400	0.06889

An algorithm for the calculation of Johnson B light curves and radial velocity (centroid) curves of rapidly rotating stars, pulsating in one nonradial mode, can now be compiled from the various elements discussed in this chapter. Such an algorithm appears in appendix 3. The results obtained by applying this algorithm appear in the following two chapters.

CHAPTER 8

RELATIVE AMPLITUDES OF MAGNITUDE AND RADIAL VELOCITY VARIATIONS

The algorithm described in the previous chapter was used to obtain light curves, radial velocity curves and spectral line profiles for a rotating model β Cephei star. The relative amplitudes of light curves and radial velocity curves are discussed in this chapter.

Balona & Stobie (1979a), following Dziembowski (1977), derived first–order relationships for the radial velocity variation of the stellar disk of a nonradially pulsating, but otherwise undistorted star, as well as its magnitude variation. They concluded that the **ratio** of these two variations' respective amplitudes is independent of the angle of inclination of the pulsation axis to the observer's line of sight (i). For odd values of the degree ℓ of a pulsation mode, they found that the projected area variation was zero, independent of i. Their relationships could be used (at least for even ℓ) to infer the value of ℓ from the observed magnitude and colour variations and a knowledge of the stellar radius. In a subsequent paper, Balona & Stobie (1979b) pointed out that identification of the azimuthal pulsation index m required additional observations, viz of spectral line profiles or frequency splittings. They concluded that ℓ was identifiable from the relative **phase** of light and radial velocity observations.

Neither colour measurements nor spectroscopic measurements were obtained in this

study of β Cephei stars in NGC 3293. In what follows, only the relative amplitudes of magnitude and radial velocity variations are considered. The relative amplitudes of the Johnson B magnitude variation and the radial velocity (centroid) variation, for the β Cephei star model described in the previous chapter, are shown in the following figures. In each figure, the top panel shows the results taking the rotational distortion of the star into account, while the bottom panel shows the results when the star is assumed to remain spherical despite its rotation. Results are shown for modes with $\ell = 0$, 1, 2, 3 and 4, with $m = 0$ and $m = -\ell$ respectively. The motivation for these choices of m is discussed in chapter 9. When $m = -\ell$, the variation in radial velocity and the variation in magnitude both approach zero as the inclination angle (i) approaches zero. Therefore, the ratio of amplitudes becomes a meaningless concept at $i = 0$, and no curve for this value of i appears in the graphs where $m = -\ell$. For the same reason, when $m = 0$, the amplitude ratios become meaningless as i approaches 90°. No ($i = 90^{\circ}$) curves appear in the graphs where $m = 0$. The effect of rotational distortion is clearly discernible in figures 8.1 to 8.9. Figure 8.10 contains all the previous results (with distortion taken into account), combined into one graph. The small digits appearing in the graph indicate the pulsation mode. The table on the following page matches digits to modes.

Mode identification by this method appears impossible, at least when the relative amplitude is lower than about 150 km/s per magnitude. Above this value a reasonable estimate may be made, at least for rotation velocities below about 250 km/s. It also has to be borne in mind that only nine different modes appear on this graph, and inclusion of further possibilities will probably increase the complexity of this graph.

digit	(ℓ,m)
0	0, 0
1	1, 0
2	1,–1
3	2, 0
4	2,–2
5	3, 0
6	3,–3
7	4, 0
8	4,–4

As mentioned in chapter 7, the flux variation coefficient f_λ (see equation 7.19) and the pulsation eigenfunction (see section 7.5) took various forms during the calculation of light and velocity variations of the stellar model. The effect of changes to the eigenfunction is shown in figures 8.11 to 8.14. One example of a sectoral mode, with $(\ell,m) = (2,-2)$, and one example of an axisymmetric mode, with $(\ell,m) = (2,0)$, are shown. In these figures, the bottom panels indicate the amplitude ratios obtained with the first–order rotationally corrected eigenfunctions of Carroll (1981), described in section 7.5. The top panels in figures 8.11 and 8.13 indicate the ratios obtained with an uncorrected eigenfunction (ie the eigenfunction normally applicable to a nonrotating star), while the top panels in figures 8.12 and 8.14 indicate the ratios obtained with the ad–hoc second–order term (see section 7.5) added to the first–order correction. Inspection reveals that the rotational corrections to the eigenfunctions do not affect the results at all. At least as far as the amplitude ratios are concerned, the fact that use is made of eigenfunctions which are not strictly correct appears to be unimportant.

The coefficient f_λ was assigned various ad–hoc values for comparison with the results obtained with adiabatic value of –17.5 (see section 7.5 again). Figures 8.15 to 8.22 illustrate the dramatic effect which the choice of f_λ has on the calculated amplitude ratios. The top panels in figures 8.15 to 8.18 show the ratios obtained for the axisymmetric $(\ell,m) = (2,0)$ mode with $f_\lambda = -5, -10, -20$ and -30 respectively, while the bottom panel in each of these figures shows the results obtained with the adaibatic value of –17.5. Figures 8.19 to 8.22 repeat this sequence for the sectoral $(\ell,m) = (2,-2)$ mode. It is clear that the use of amplitude ratios for the purpose of mode identification is dependent on a reliable estimate of the flux variation coefficient f_λ.

Provided, then, that the value of f_λ may be estimated, the graphs shown in figures 8.1 to 8.9 may be used to determine either the equatorial rotation velocity or the angle of inclination of a star, if the mode has already been identified and the complementary parameter (inclination angle and rotation velocity, respectively) is also known.

These results may be compared to the value of

$$\Delta v_{rad}/\Delta m_v \simeq 500 \text{ km/s/mag}$$

(where m_v represents visual magnitude) found by Jerzykiewicz (1978) for the β Cephei star 12 Lac. Lesh & Aizenman (1978) compiled light (visual magnitude) and radial velocity amplitudes for 21 β Cephei stars. Their quoted values yield ratios from 110 km/s/mag to 2500 km/s/mag, with an average around 700 km/s/mag. The radiation spectrum of β Cephei stars implies that these ratios would be smaller when m_B instead of m_v was used, of course. The work of Stamford and Watson in this regard was discussed in chapter 1.

Investigation of figures 8.1 to 8.9 prompts the following observations:

1. Balona & Stobie's conclusion that the amplitude ratios of light and radial velocity variation are independent of i is borne out almost perfectly by the graphs for $m = -\ell$. However, the $(m = 0)$ graphs show a small amount of variation with i.

2. Jerzykiewicz (1978) quoted a value of 500 km/s/mag for $\Delta v_{rad}/\Delta m_V$ in 12 Lac and concluded that a $(\ell = 3)$ mode was most probably operating in this star. Inspection of the results in Heynderickx (1991) indicate that the ratio $\Delta m_B/\Delta m_V$ could be as high as 1.4, which in this particular case would predict a $\Delta v_{rad}/\Delta m_B$ (not m_V) ratio of about 350 km/s/mag. This value is best accommodated by the graphs for $(\ell,m) = (3,0)$ (especially in view of the low *vsini* value of between 30 and 40 km/s found for this star), in agreement with Jerzykiewicz's own conclusions.

3. The most striking effect of taking the rotational distortion into account, is the "spreading out" of the curves for the different inclination angles. This phenomenon implies that the diagnostic utility of these curves is greater than would have been suspected if the distortion had been ignored. Naturally, this is especially true at the higher velocities.

The final conclusion to be made from these results is that this method of mode identification, or parameter determination, will probably only prove effective when used in conjunction with other methods, especially line profile analysis, which is the focus of the next chapter.

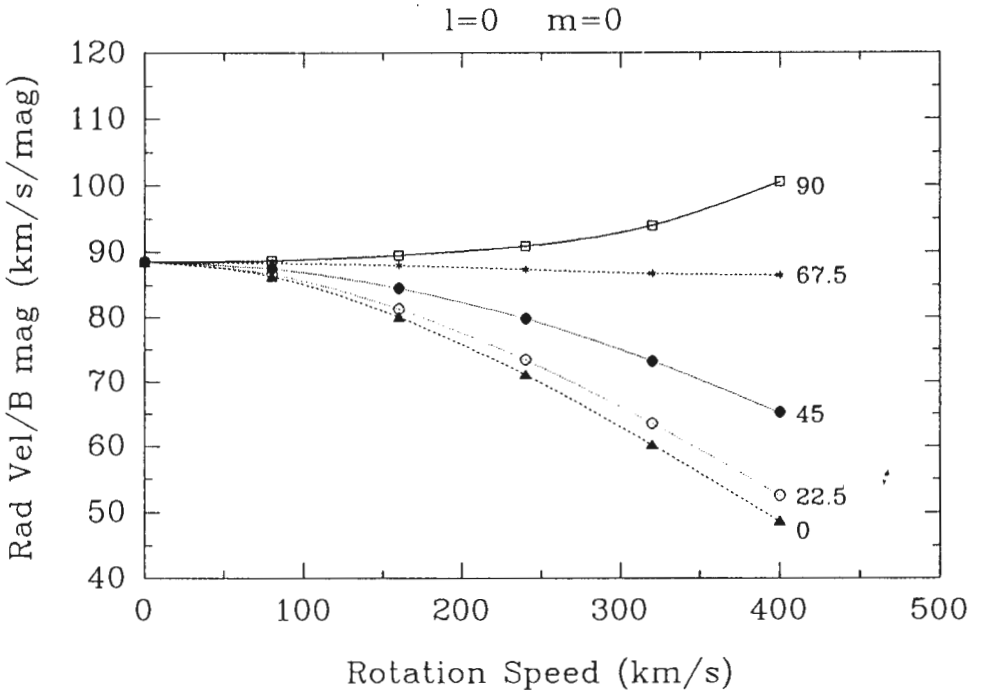
l=0 m=0
Rad Vel/B mag (km/s/mag)
Rotation Speed (km/s)
120
110
100
90
80
70
60
50
40
0
100
200
300
400
500
90
67.5
45
22.5
0

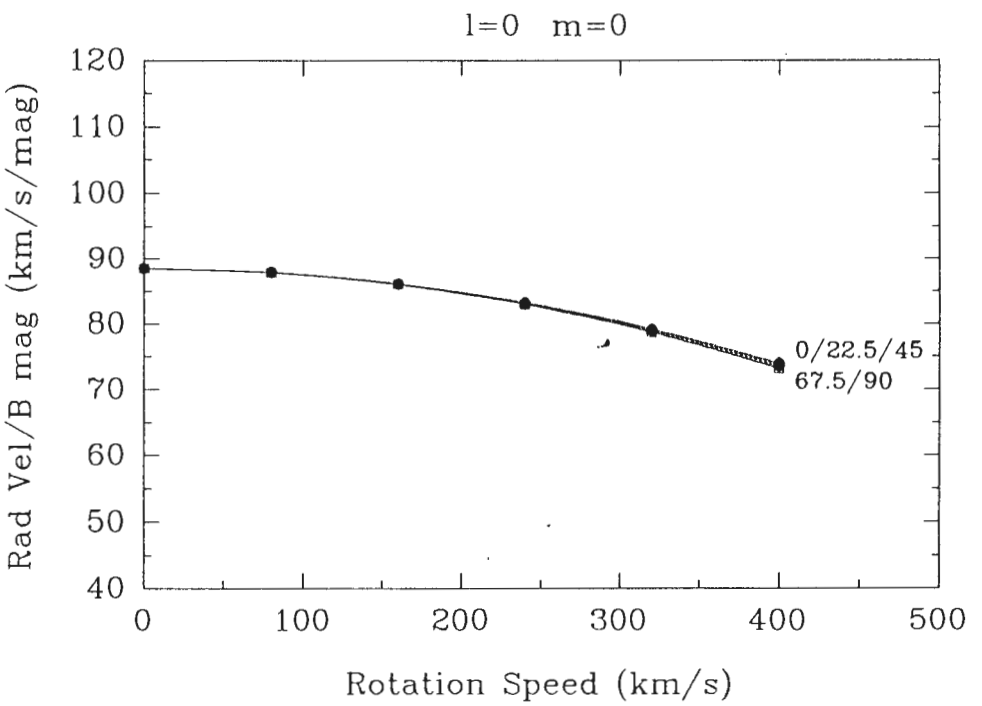
l=0 m=0
Rad Vel/B mag (km/s/mag)
Rotation Speed (km/s)
120
110
100
90
80
70
60
50
40
0
100
200
300
400
500
0/22.5/45
67.5/90

Figure 8.1

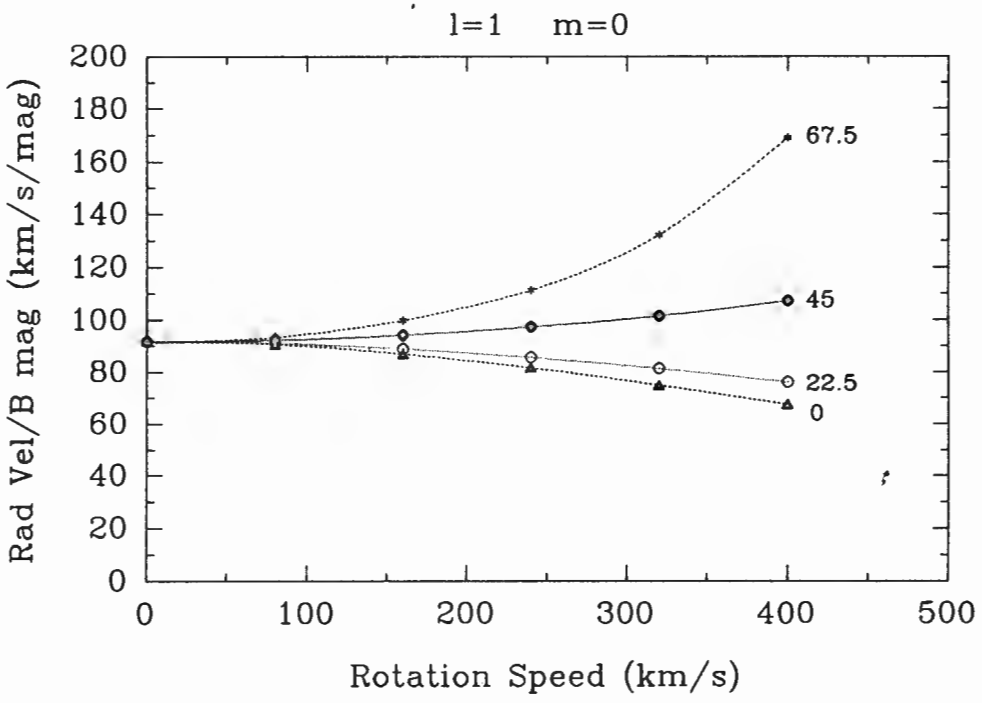
l=1 m=0
Rad Vel/B mag (km/s/mag)
Rotation Speed (km/s)
67.5
45
22.5
0
0
20
40
60
80
100
120
140
160
180
200
0
100
200
300
400
500

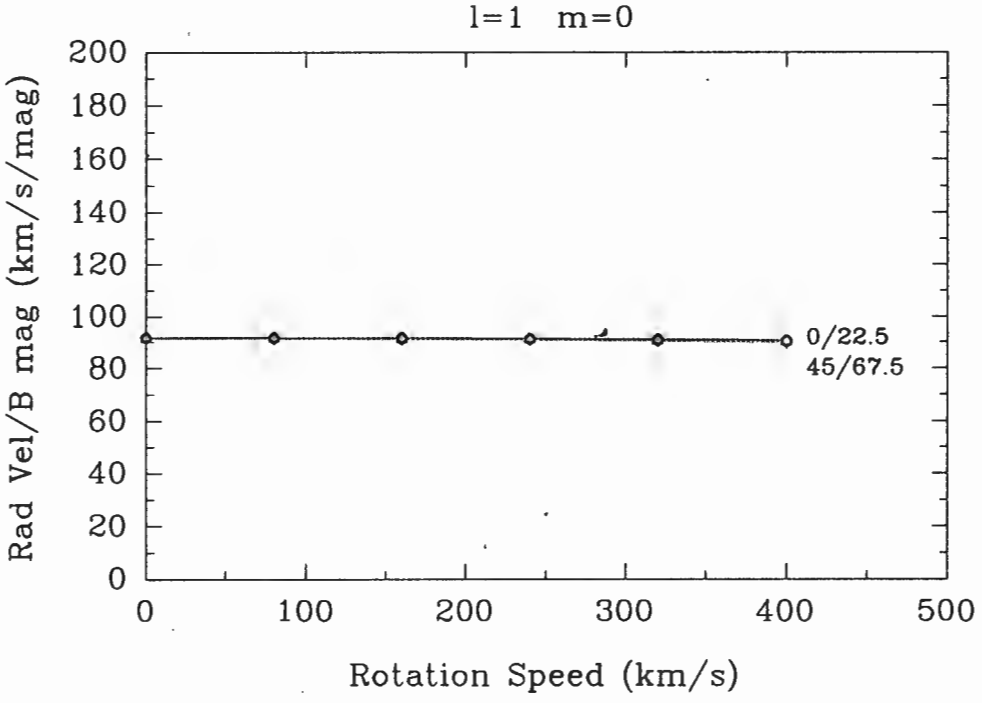
l=1 m=0
Rad Vel/B mag (km/s/mag)
Rotation Speed (km/s)
0/22.5
45/67.5
0
20
40
60
80
100
120
140
160
180
200
0
100
200
300
400
500

Figure 8.2

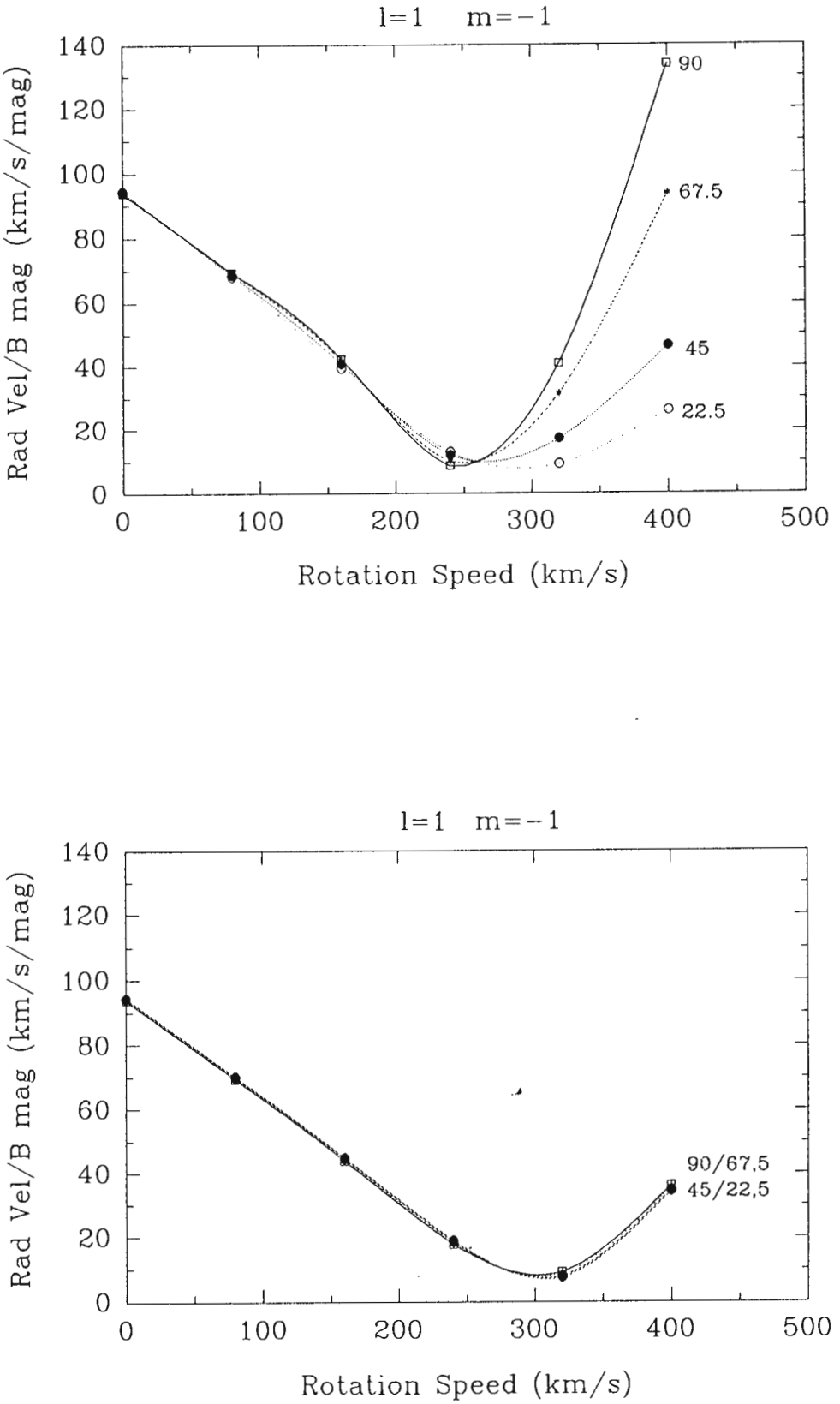
l=1 m=-1
Rad Vel/B mag (km/s/mag)
Rotation Speed (km/s)
90
67.5
45
22.5
0
20
40
60
80
100
120
140
0
100
200
300
400
500
l=1 m=-1
Rad Vel/B mag (km/s/mag)
Rotation Speed (km/s)
90/67.5
45/22.5

Figure 8.3

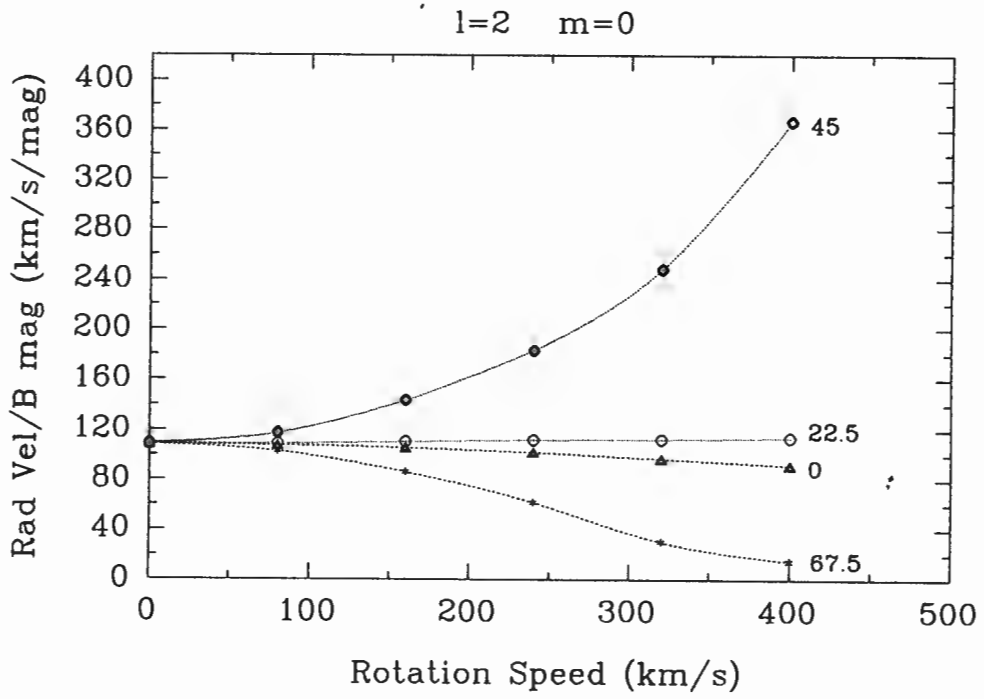
l=2 m=0
Rad Vel/B mag (km/s/mag)
400
360
320
280
240
200
160
120
80
40
0
0
100
200
300
400
500
Rotation Speed (km/s)
45
22.5
0
67.5

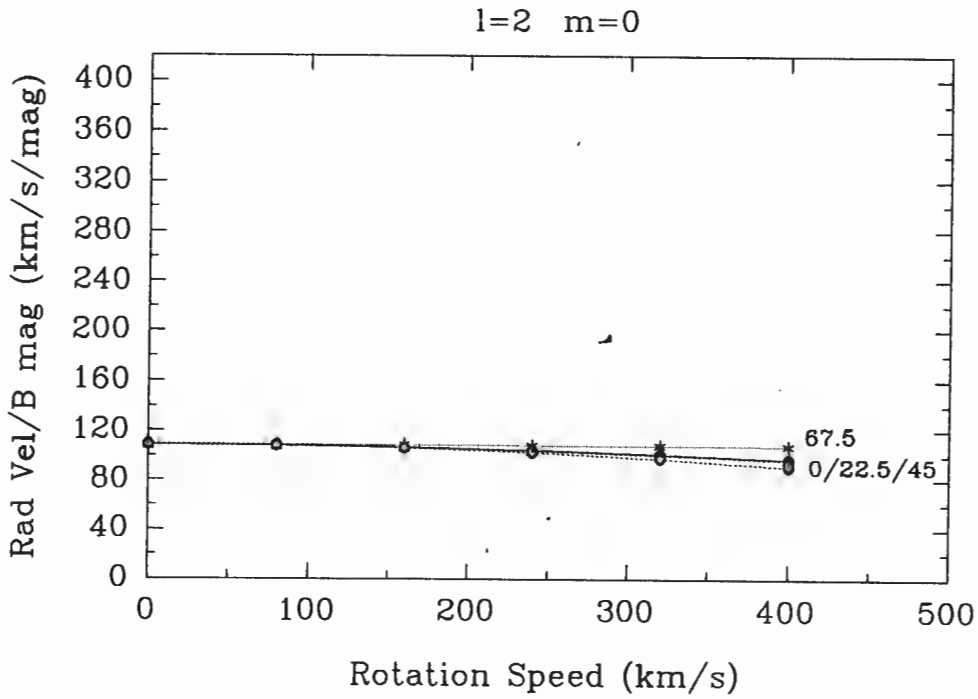
l=2 m=0
Rad Vel/B mag (km/s/mag)
400
360
320
280
240
200
160
120
80
40
0
0
100
200
300
400
500
Rotation Speed (km/s)
67.5
0/22.5/45

Figure 8.4

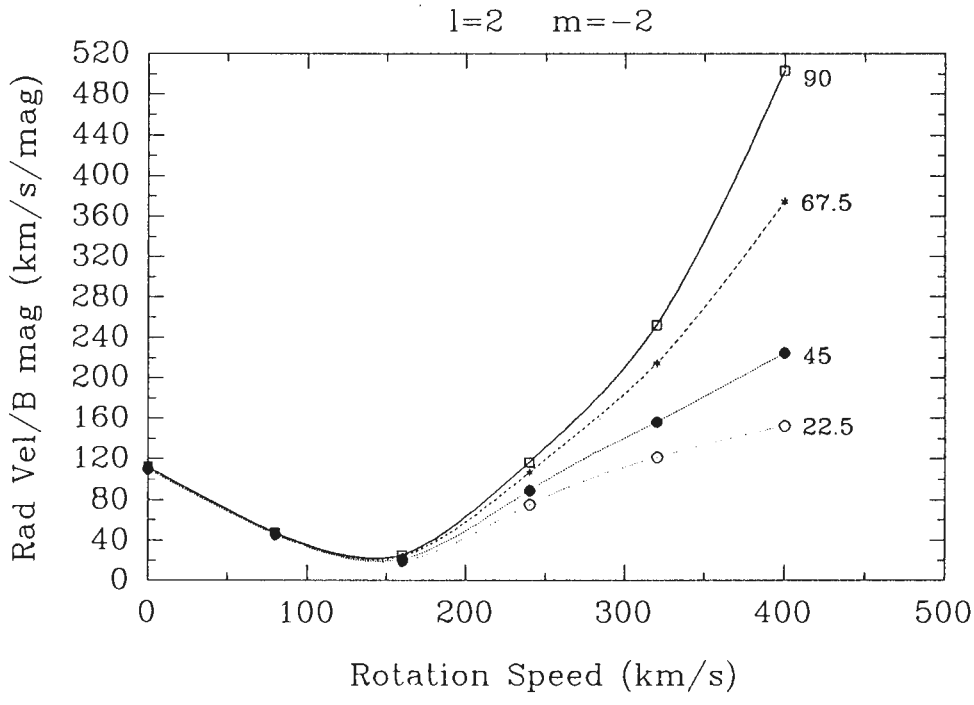
l=2 m=−2
Rad Vel/B mag (km/s/mag)
Rotation Speed (km/s)
90
67.5
45
22.5
0
40
80
120
160
200
240
280
320
360
400
440
480
520
0
100
200
300
400
500

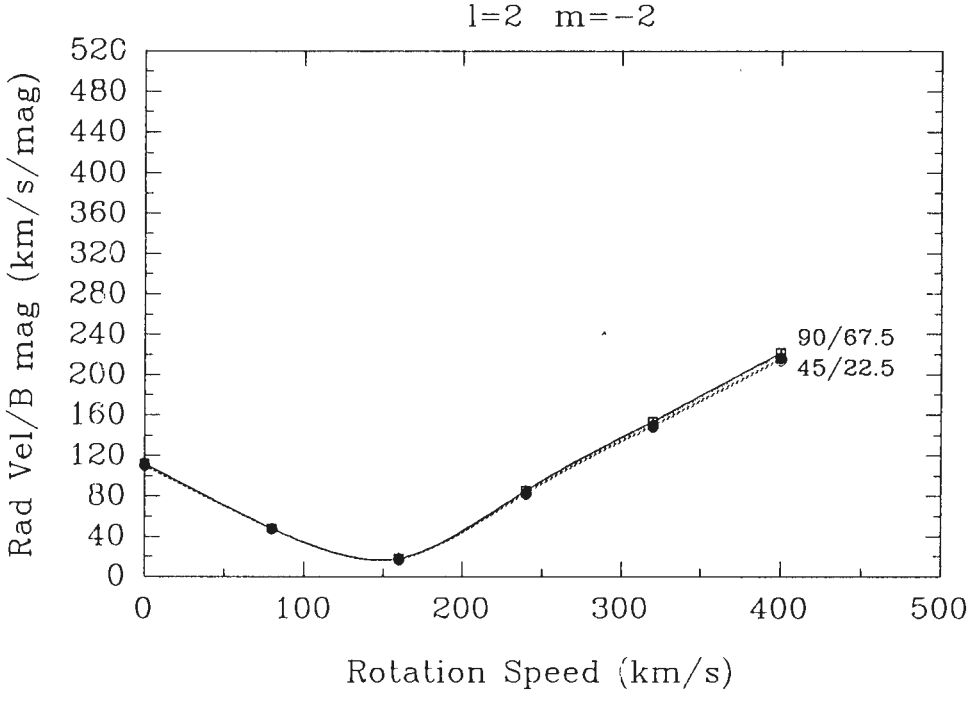
l=2 m=−2
Rad Vel/B mag (km/s/mag)
Rotation Speed (km/s)
90/67.5
45/22.5
0
40
80
120
160
200
240
280
320
360
400
440
480
520
0
100
200
300
400
500

Figure 8.5

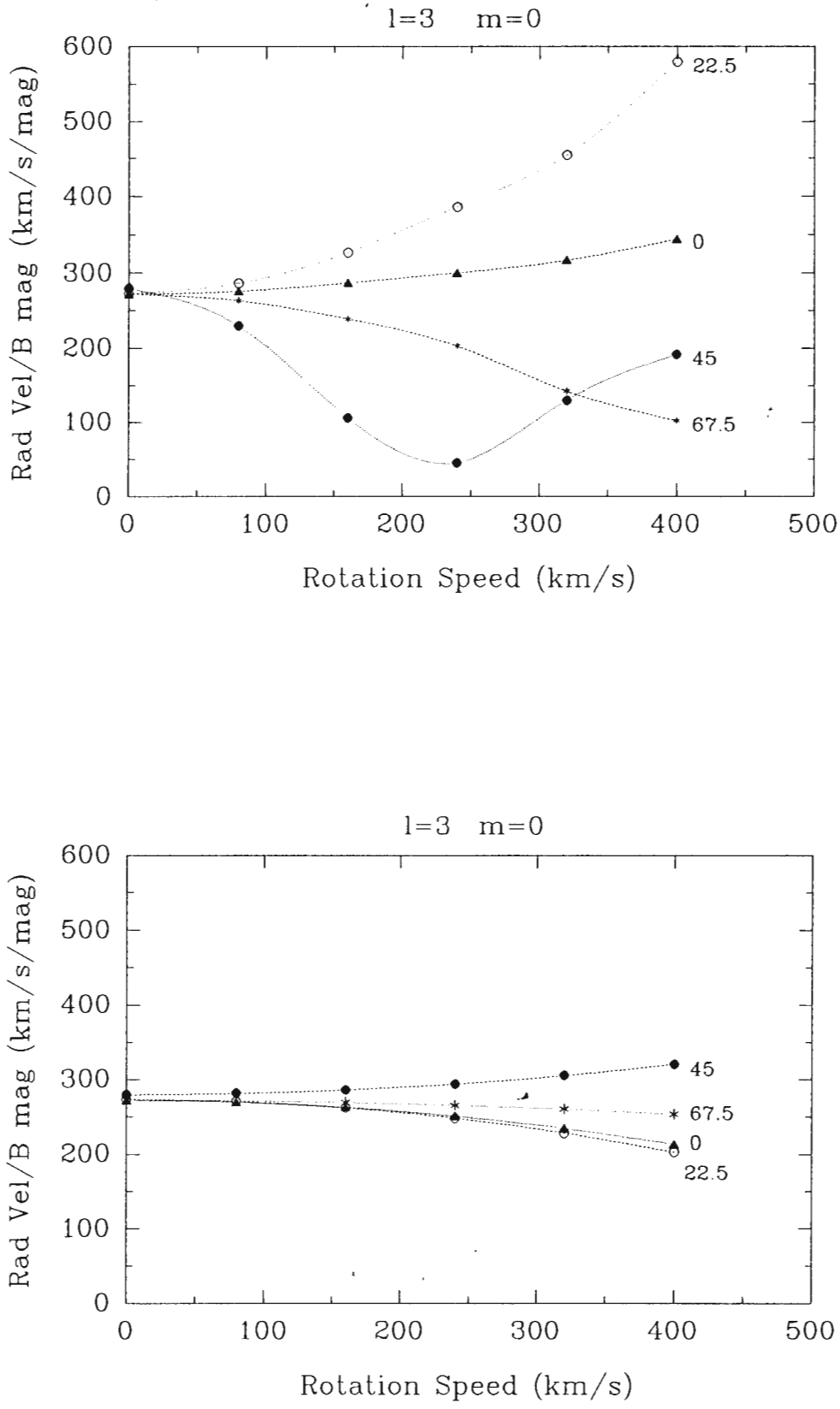
l=3 m=0
Rad Vel/B mag (km/s/mag)
Rotation Speed (km/s)
22.5
0
45
67.5
0
100
200
300
400
500
600
l=3 m=0
Rad Vel/B mag (km/s/mag)
Rotation Speed (km/s)
45
67.5
0
22.5

Figure 8.6

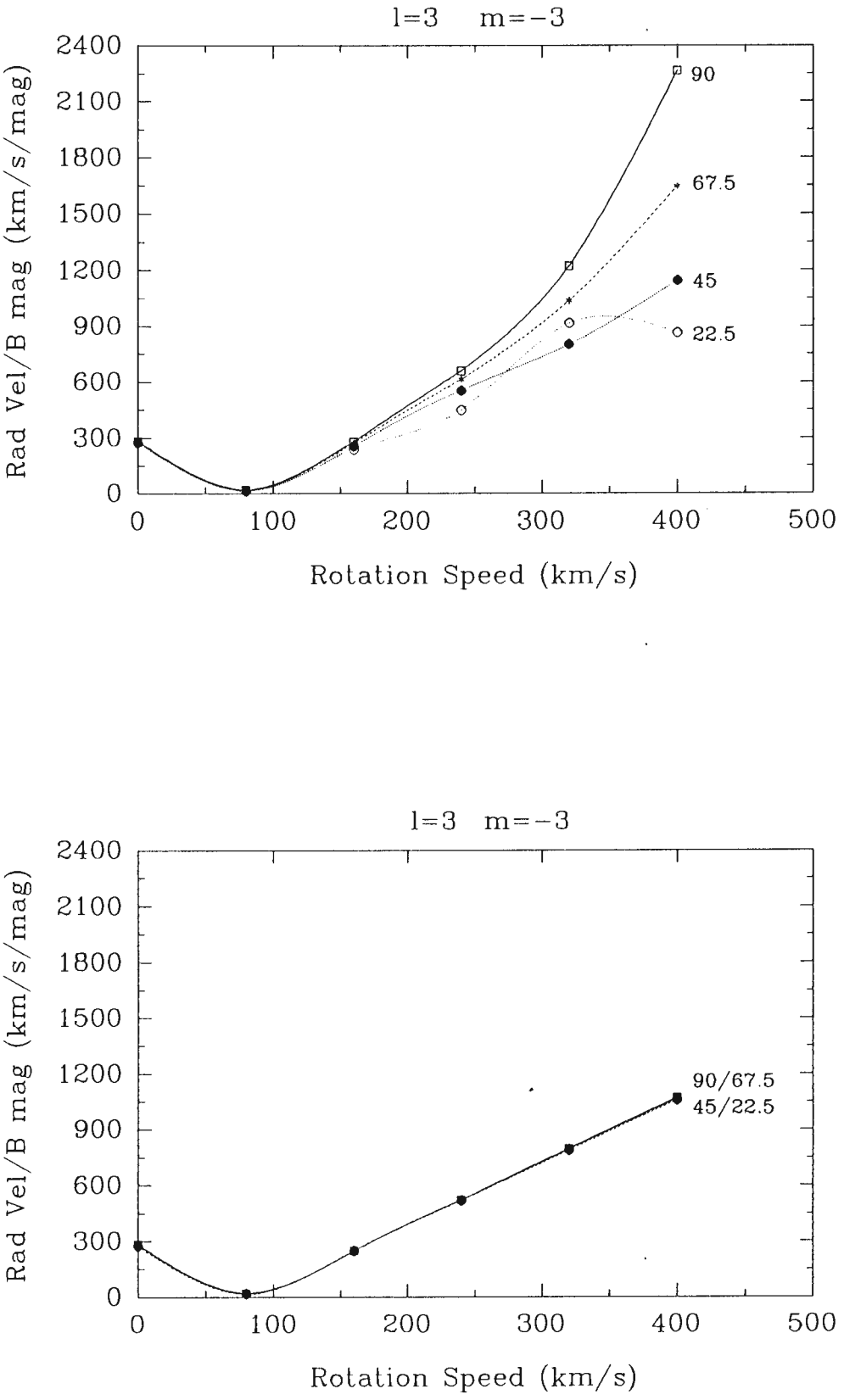
l=3 m=-3
Rad Vel/B mag (km/s/mag)
Rotation Speed (km/s)
90
67.5
45
22.5
90/67.5
45/22.5
0
300
600
900
1200
1500
1800
2100
2400
0
100
200
300
400
500

Figure 8.7

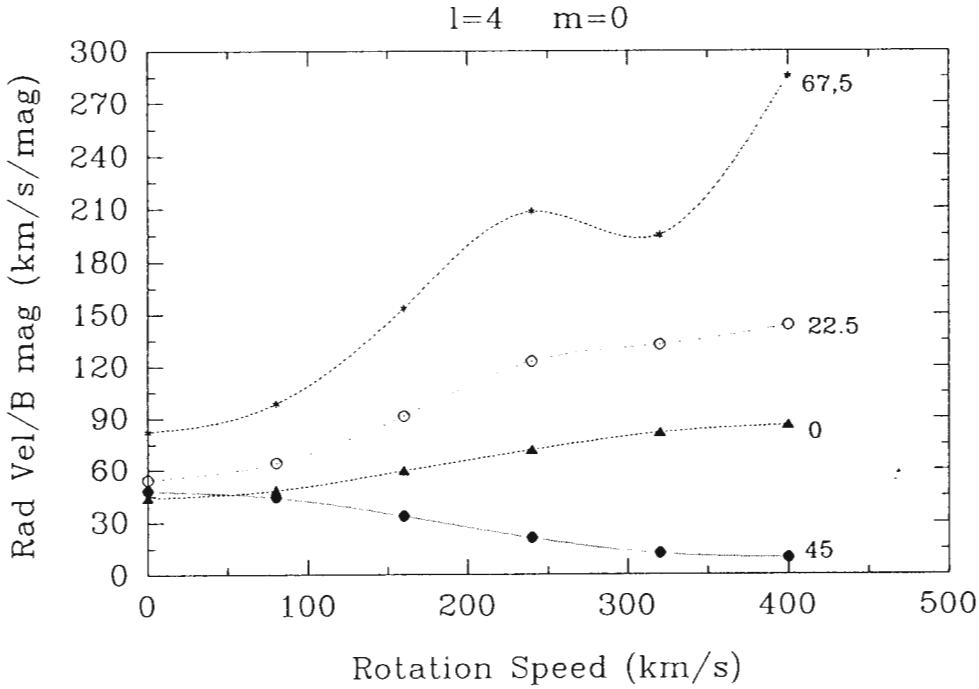
l=4 m=0
Rad Vel/B mag (km/s/mag)
Rotation Speed (km/s)
67,5
22.5
0
45
0
30
60
90
120
150
180
210
240
270
300
0
100
200
300
400
500

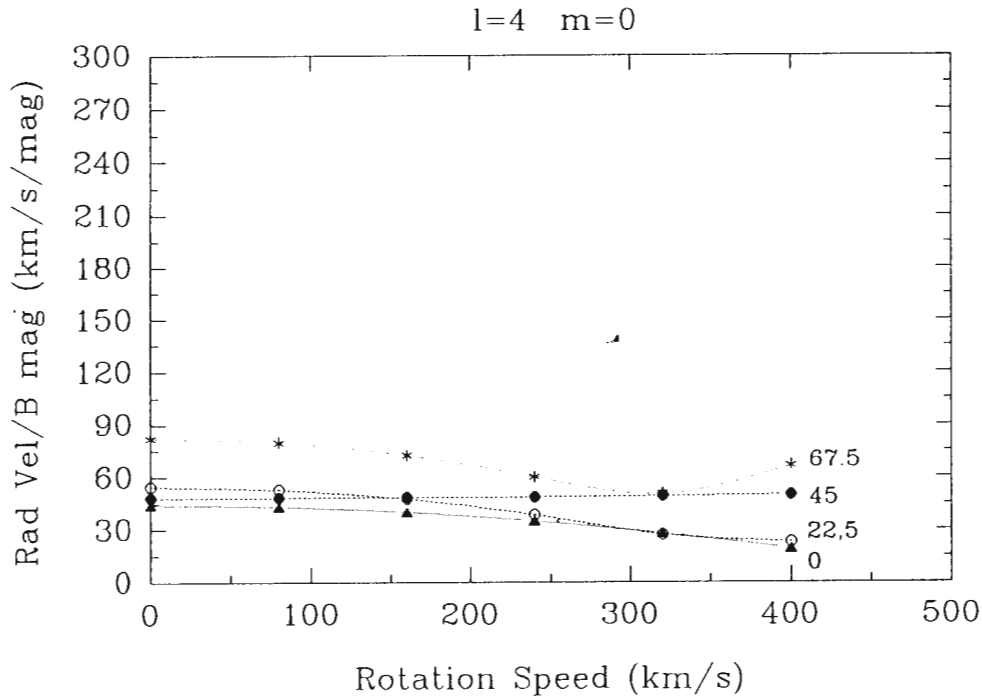
l=4 m=0
Rad Vel/B mag (km/s/mag)
Rotation Speed (km/s)
67.5
45
22,5
0
0
30
60
90
120
150
180
210
240
270
300
0
100
200
300
400
500

Figure 8.8

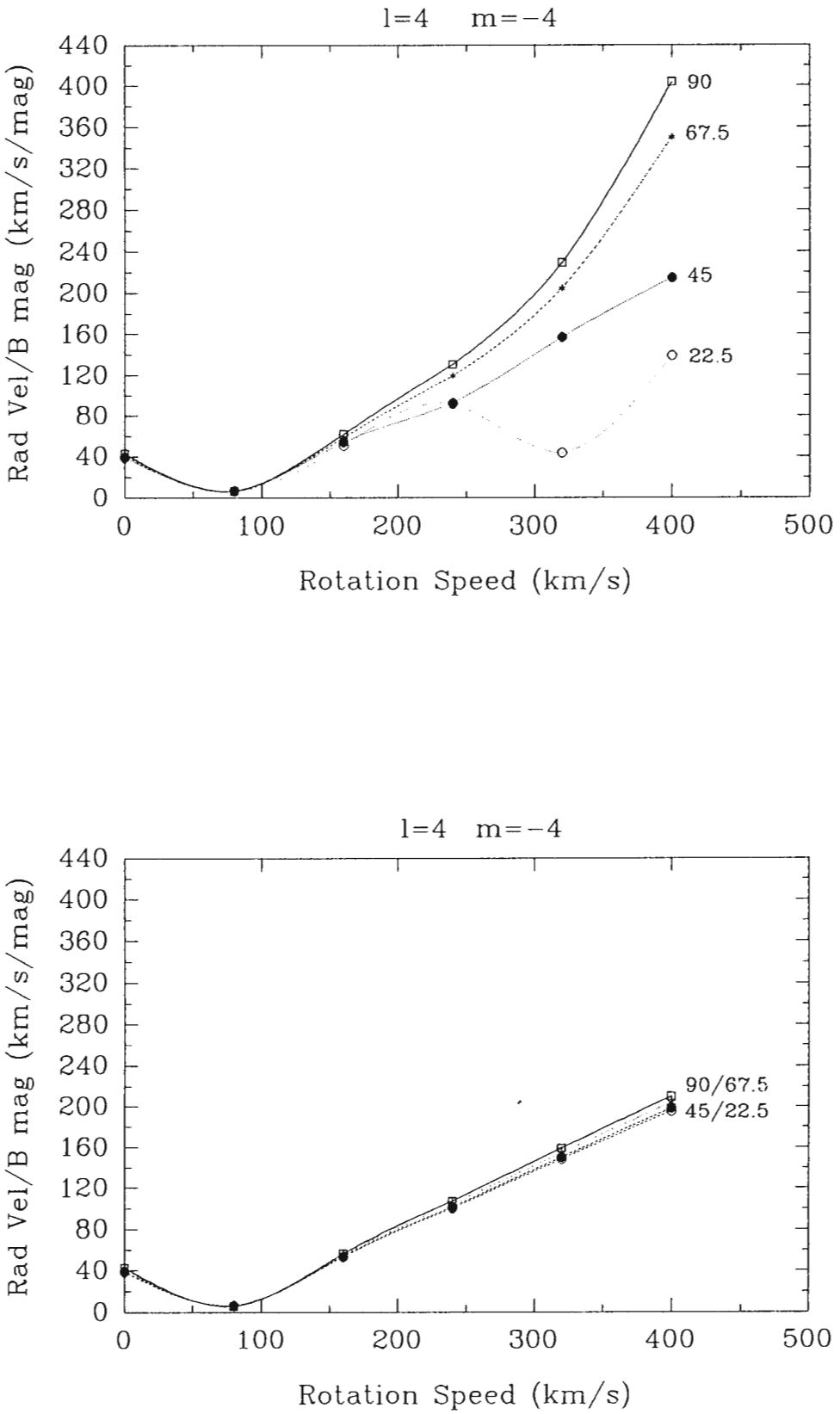
l=4 m=-4
Rad Vel/B mag (km/s/mag)
Rotation Speed (km/s)
90
67.5
45
22.5
0
40
80
120
160
200
240
280
320
360
400
440
0
100
200
300
400
500
l=4 m=-4
Rad Vel/B mag (km/s/mag)
Rotation Speed (km/s)
90/67.5
45/22.5

Figure 8.9

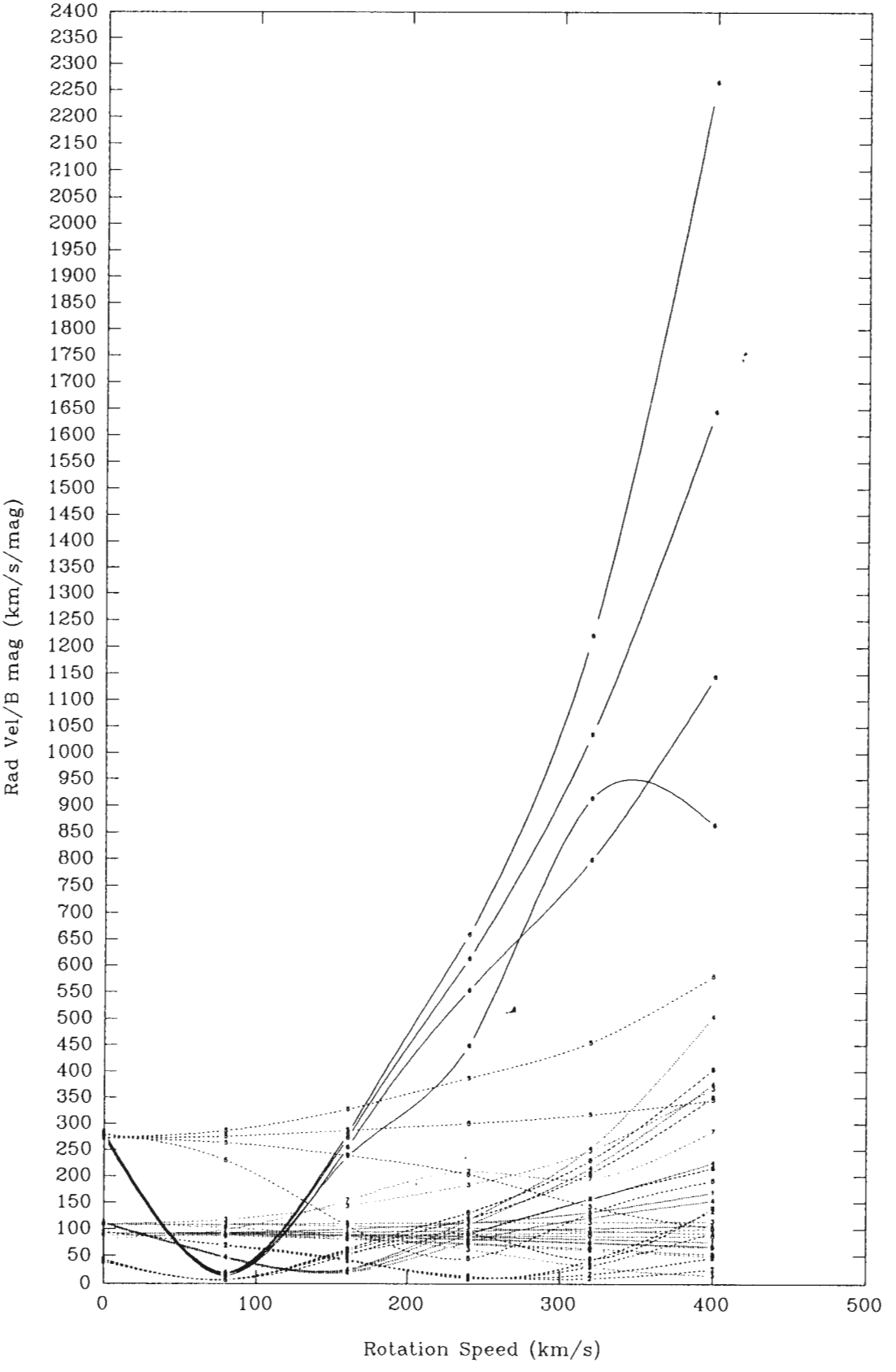
Rad Vel/B mag (km/s/mag)
2400
2350
2300
2250
2200
2150
2100
2050
2000
1950
1900
1850
1800
1750
1700
1650
1600
1550
1500
1450
1400
1350
1300
1250
1200
1150
1100
1050
1000
950
900
850
800
750
700
650
600
550
500
450
400
350
300
250
200
150
100
50
0
0
100
200
300
400
500
Rotation Speed (km/s)

Figure 8.10

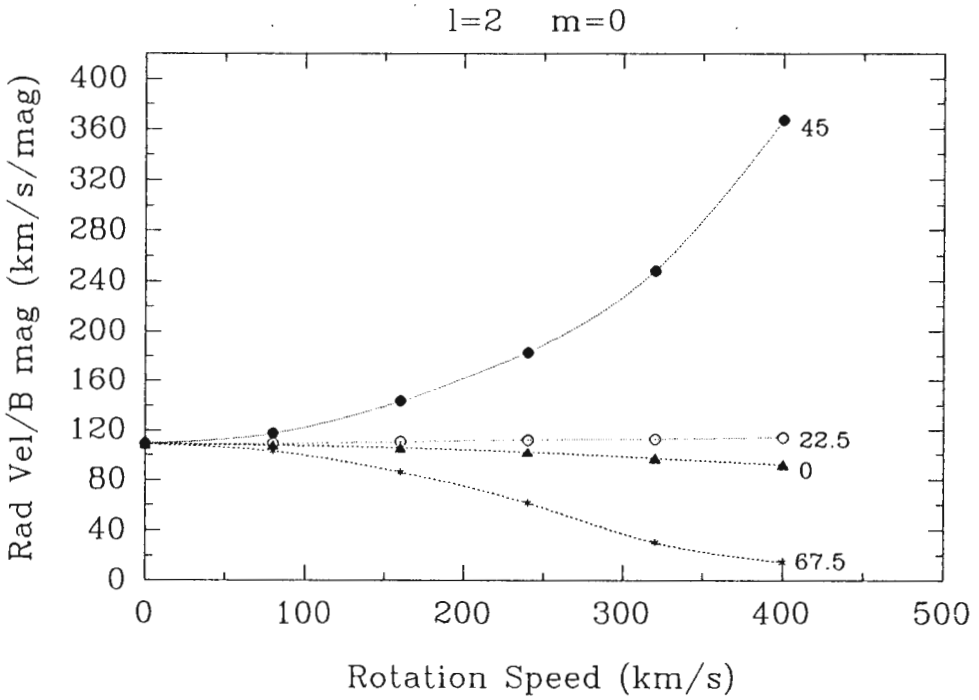
l=2 m=0
Rad Vel/B mag (km/s/mag)
Rotation Speed (km/s)
45
22.5
0
67.5

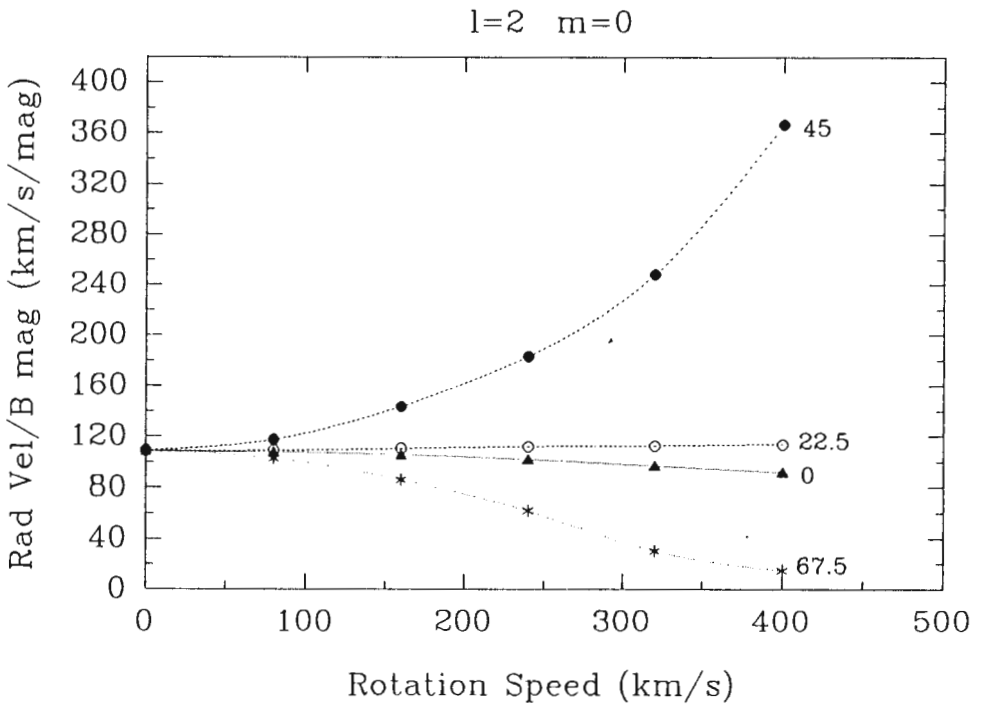
l=2 m=0
Rad Vel/B mag (km/s/mag)
Rotation Speed (km/s)
45
22.5
0
67.5

Figure 8.11

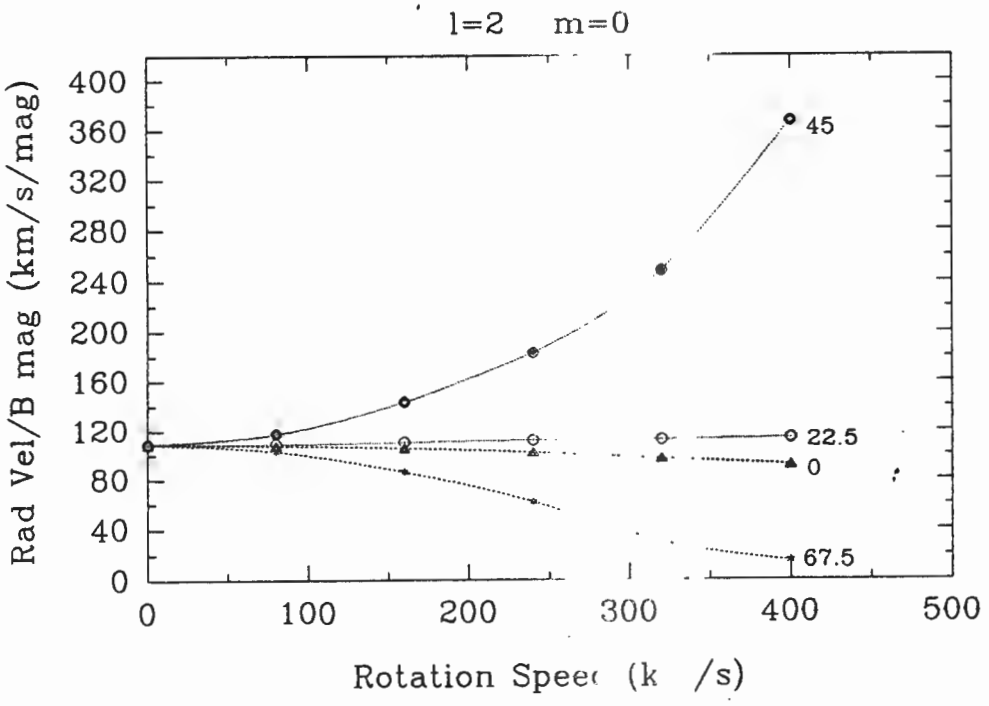
l=2 m=0
Rad Vel/B mag (km/s/mag)
400
360
320
280
240
200
160
120
80
40
0
0
100
200
300
400
500
45
22.5
0
67.5
Rotation Spee (k /s)

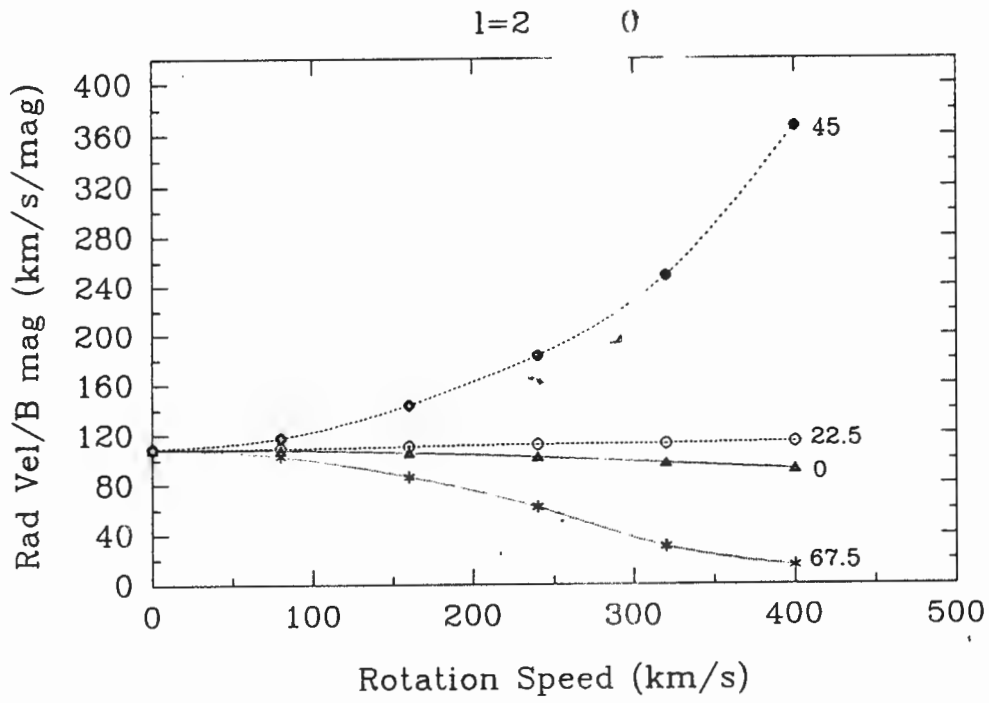
l=2 0
Rad Vel/B mag (km/s/mag)
400
360
320
280
240
200
160
120
80
40
0
0
100
200
300
400
500
45
22.5
0
67.5
Rotation Speed (km/s)

Figure 8.12

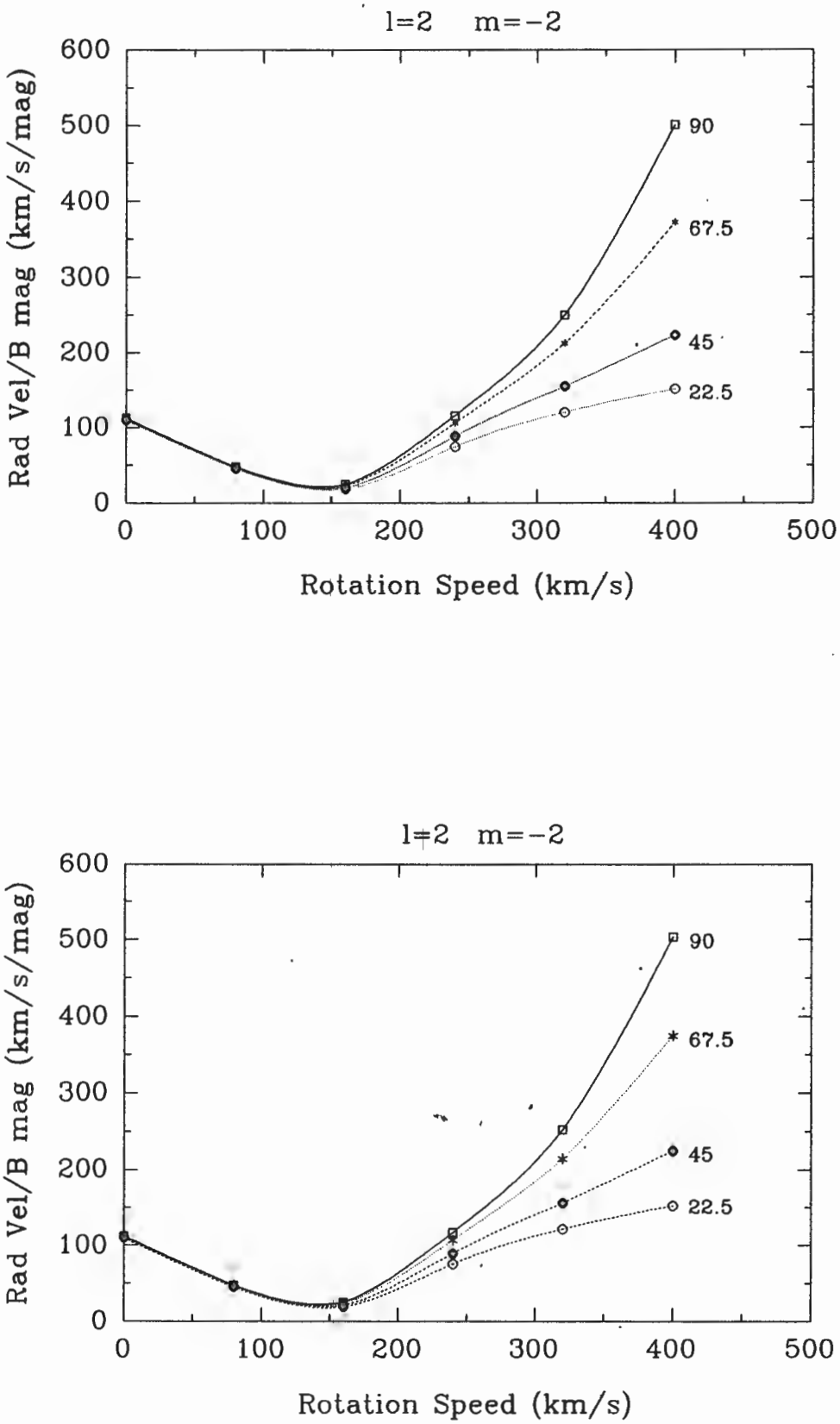
l=2 m=-2
Rad Vel/B mag (km/s/mag)
Rotation Speed (km/s)
90
67.5
45
22.5
0
100
200
300
400
500
600
l=2 m=-2
Rad Vel/B mag (km/s/mag)
Rotation Speed (km/s)
90
67.5
45
22.5

Figure 8.13

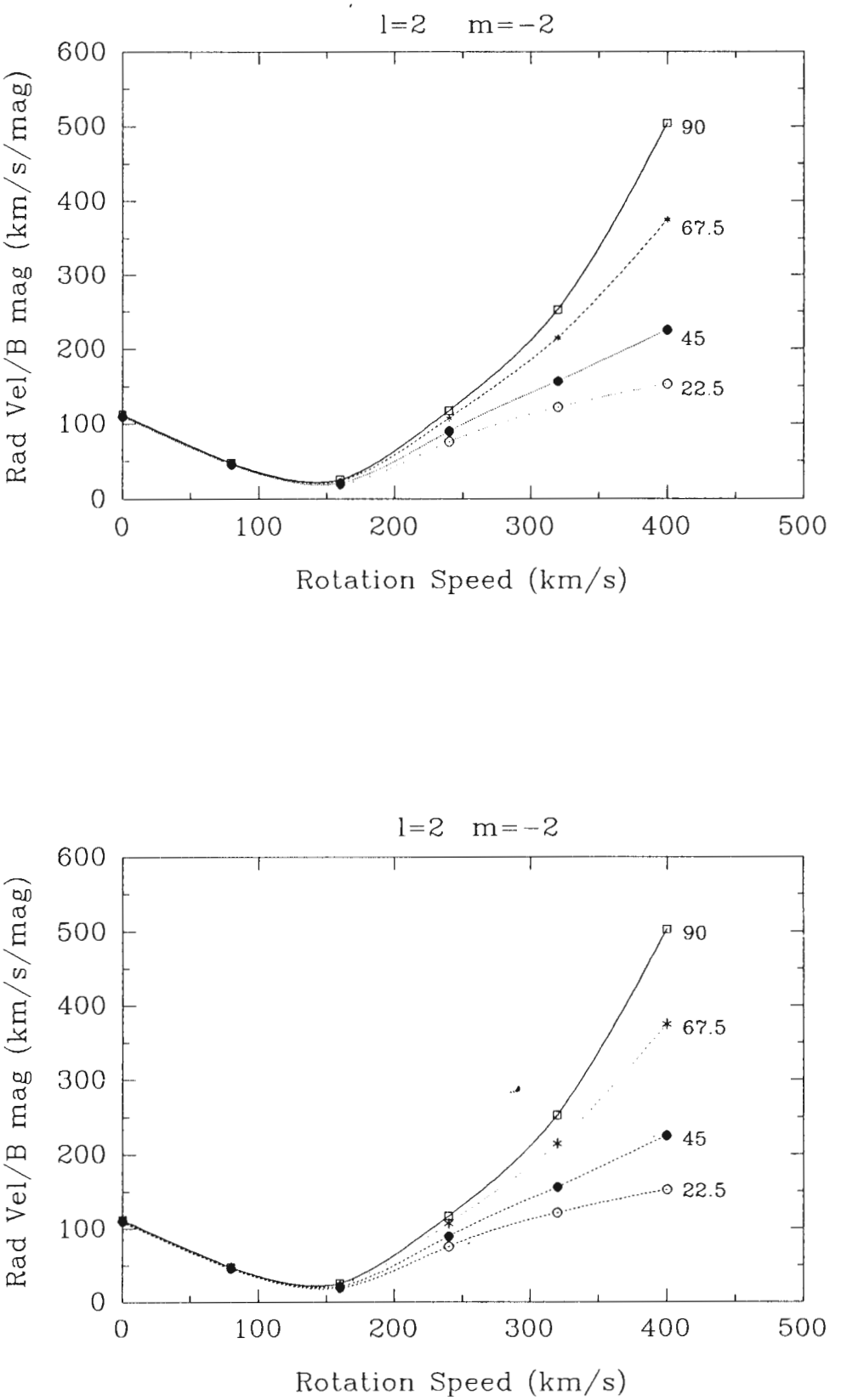
l=2 m=-2
Rad Vel/B mag (km/s/mag)
Rotation Speed (km/s)
90
67.5
45
22.5
0
100
200
300
400
500
600

Figure 8.14

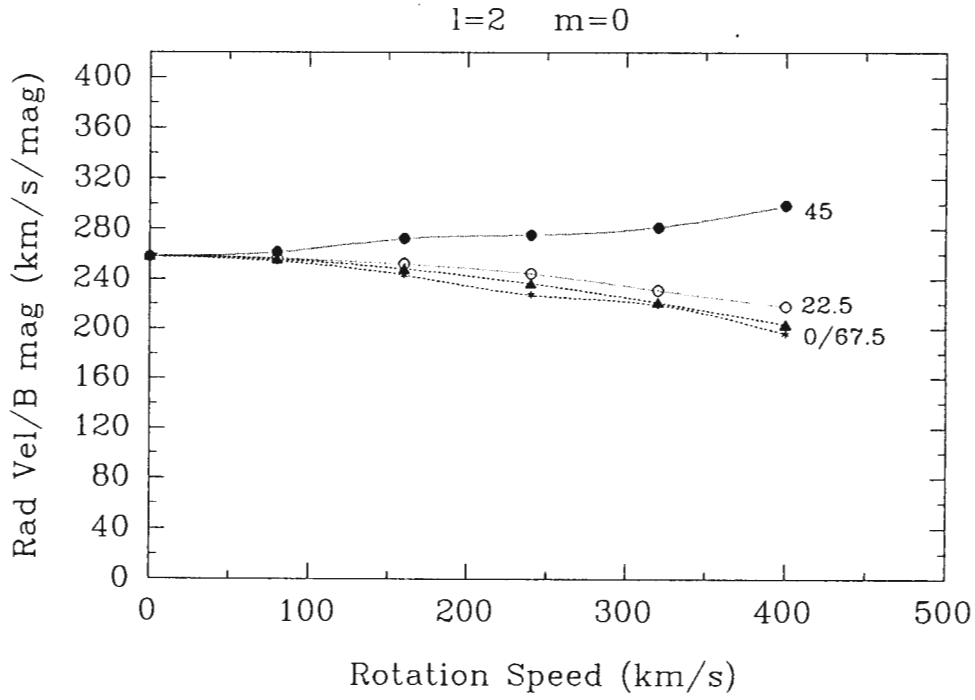
l=2 m=0
Rad Vel/B mag (km/s/mag)
Rotation Speed (km/s)
45
22.5
0/67.5

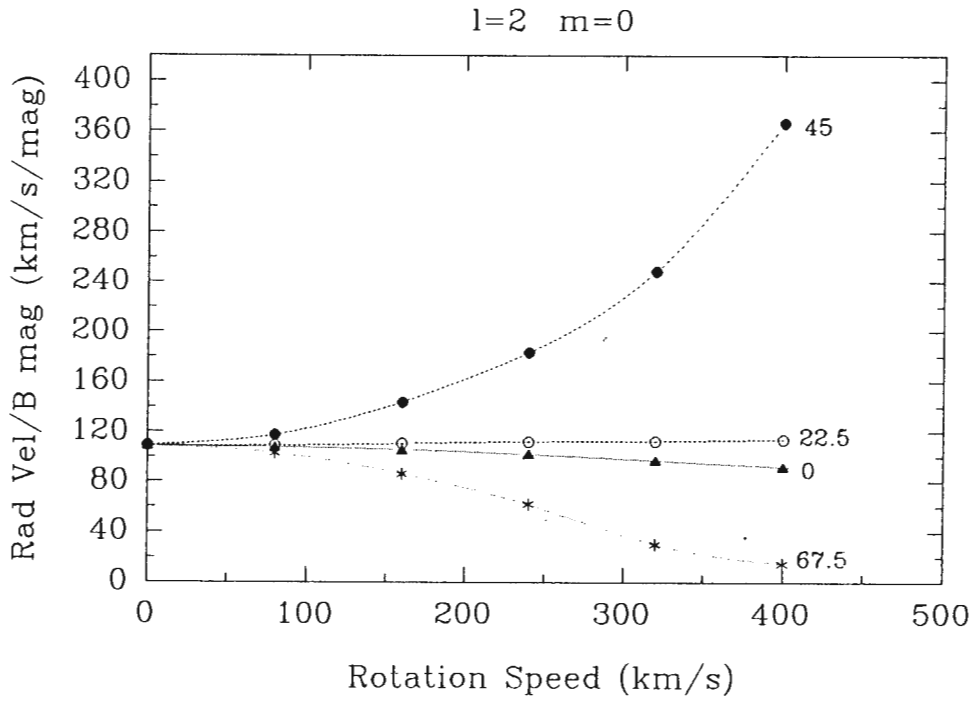
l=2 m=0
Rad Vel/B mag (km/s/mag)
Rotation Speed (km/s)
45
22.5
0
67.5

Figure 8.15

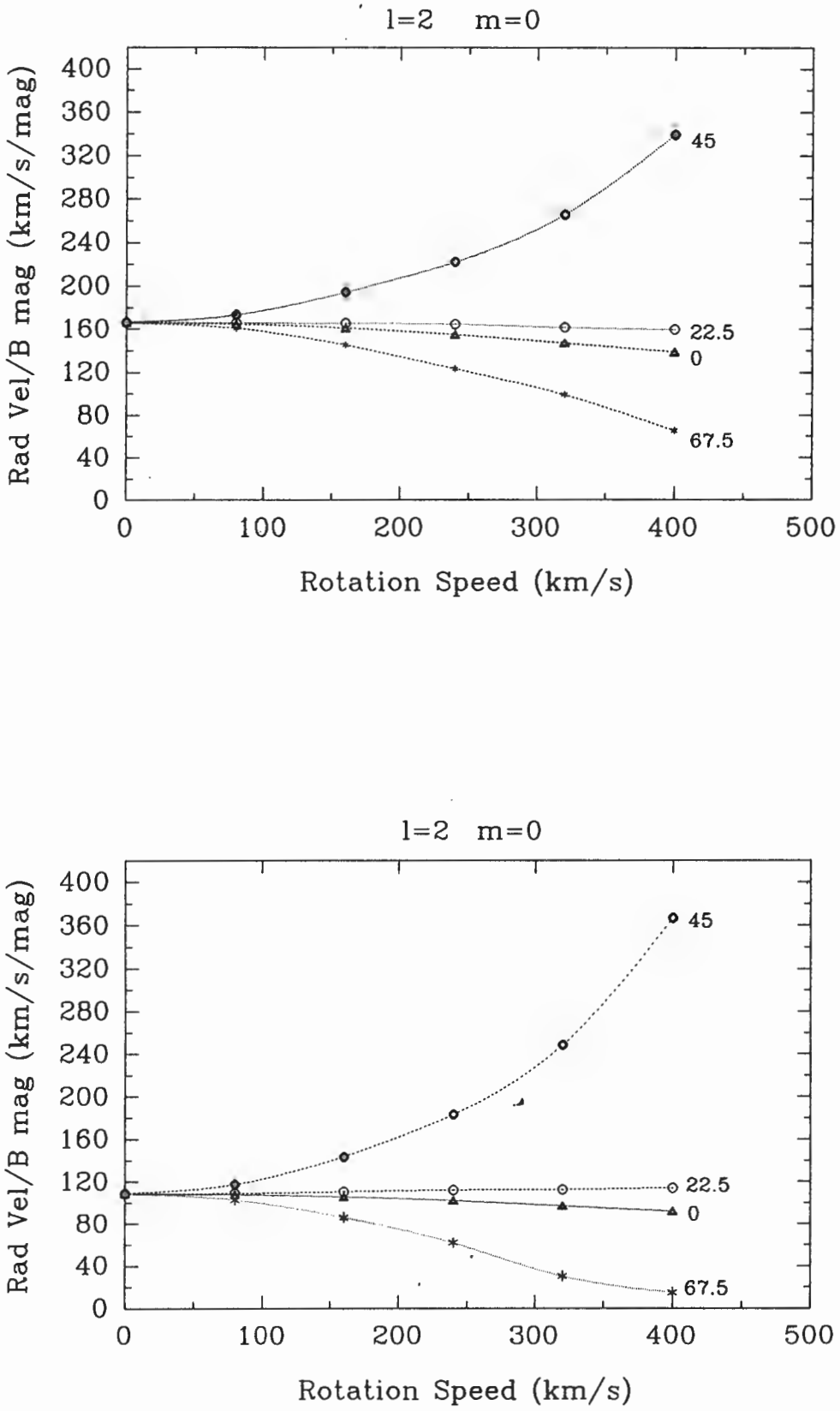
l=2 m=0
Rad Vel/B mag (km/s/mag)
Rotation Speed (km/s)
45
22.5
0
67.5
0
40
80
120
160
200
240
280
320
360
400
0
100
200
300
400
500

Figure 8.16

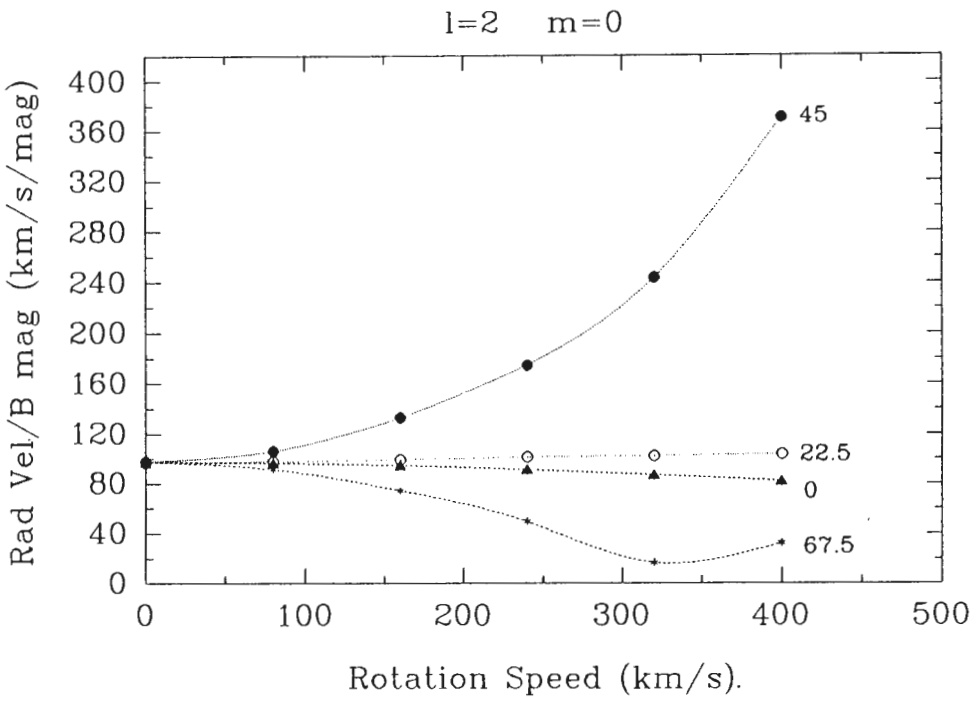
l=2 m=0
Rad Vel/B mag (km/s/mag)
400
360
320
280
240
200
160
120
80
40
0
0
100
200
300
400
500
Rotation Speed (km/s).
45
22.5
0
67.5

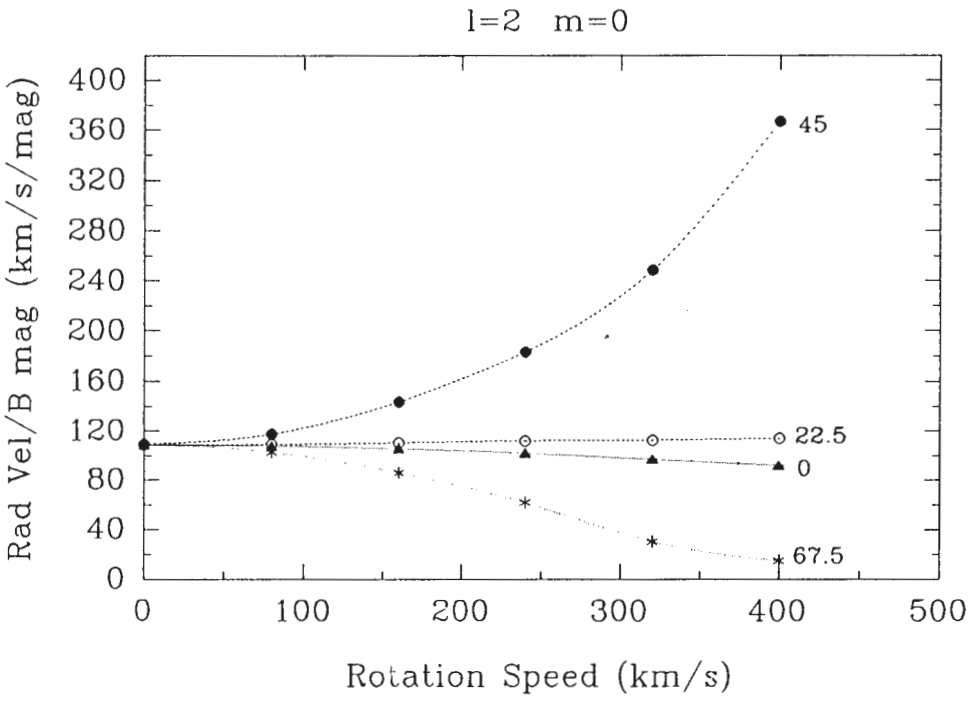
l=2 m=0
Rad Vel/B mag (km/s/mag)
400
360
320
280
240
200
160
120
80
40
0
0
100
200
300
400
500
Rotation Speed (km/s)
45
22.5
0
67.5

Figure 8.17

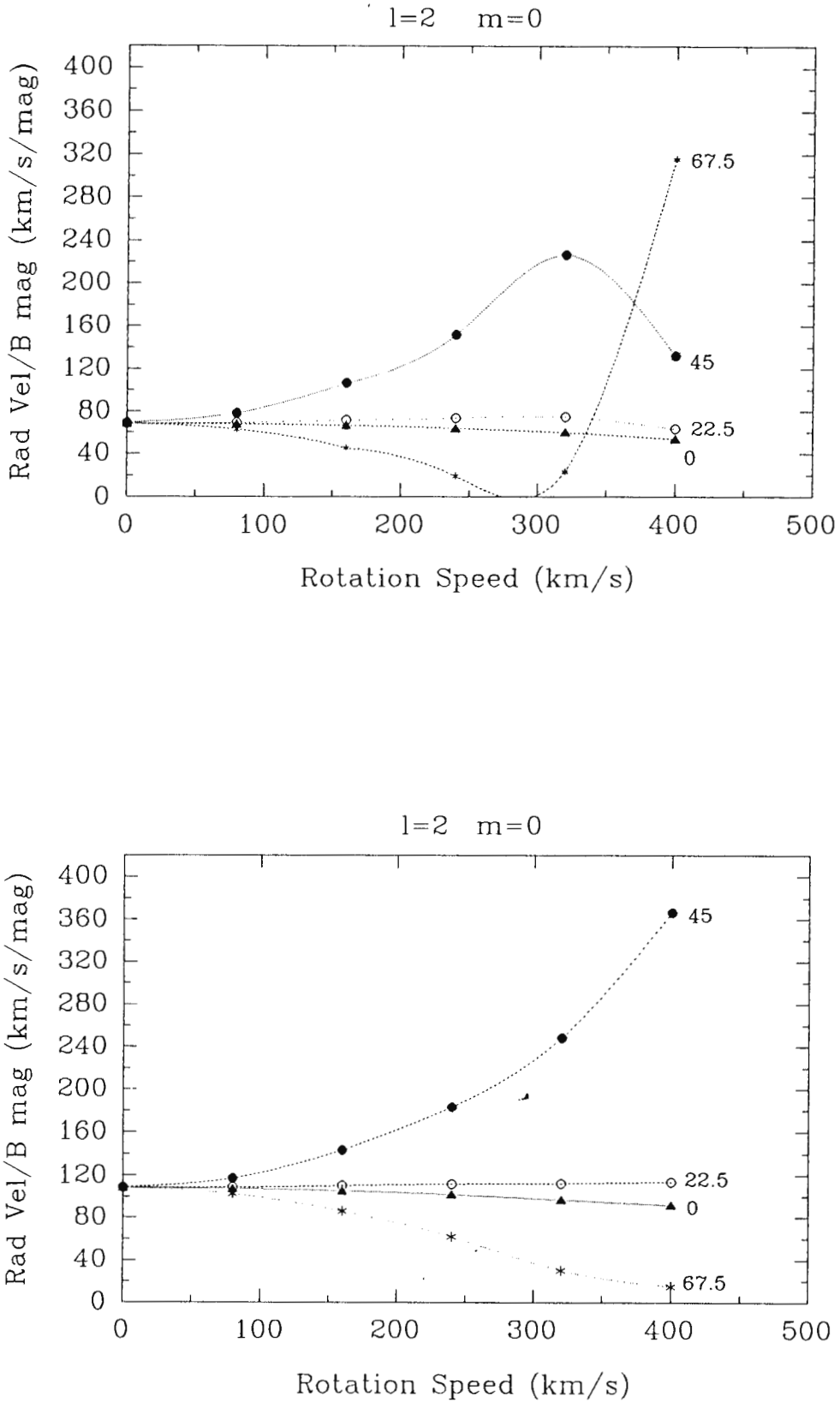
l=2 m=0
Rad Vel/B mag (km/s/mag)
Rotation Speed (km/s)
0
40
80
120
160
200
240
280
320
360
400
0
100
200
300
400
500
67.5
45
22.5
0
l=2 m=0
Rad Vel/B mag (km/s/mag)
Rotation Speed (km/s)
45
22.5
0
67.5

Figure 8.18

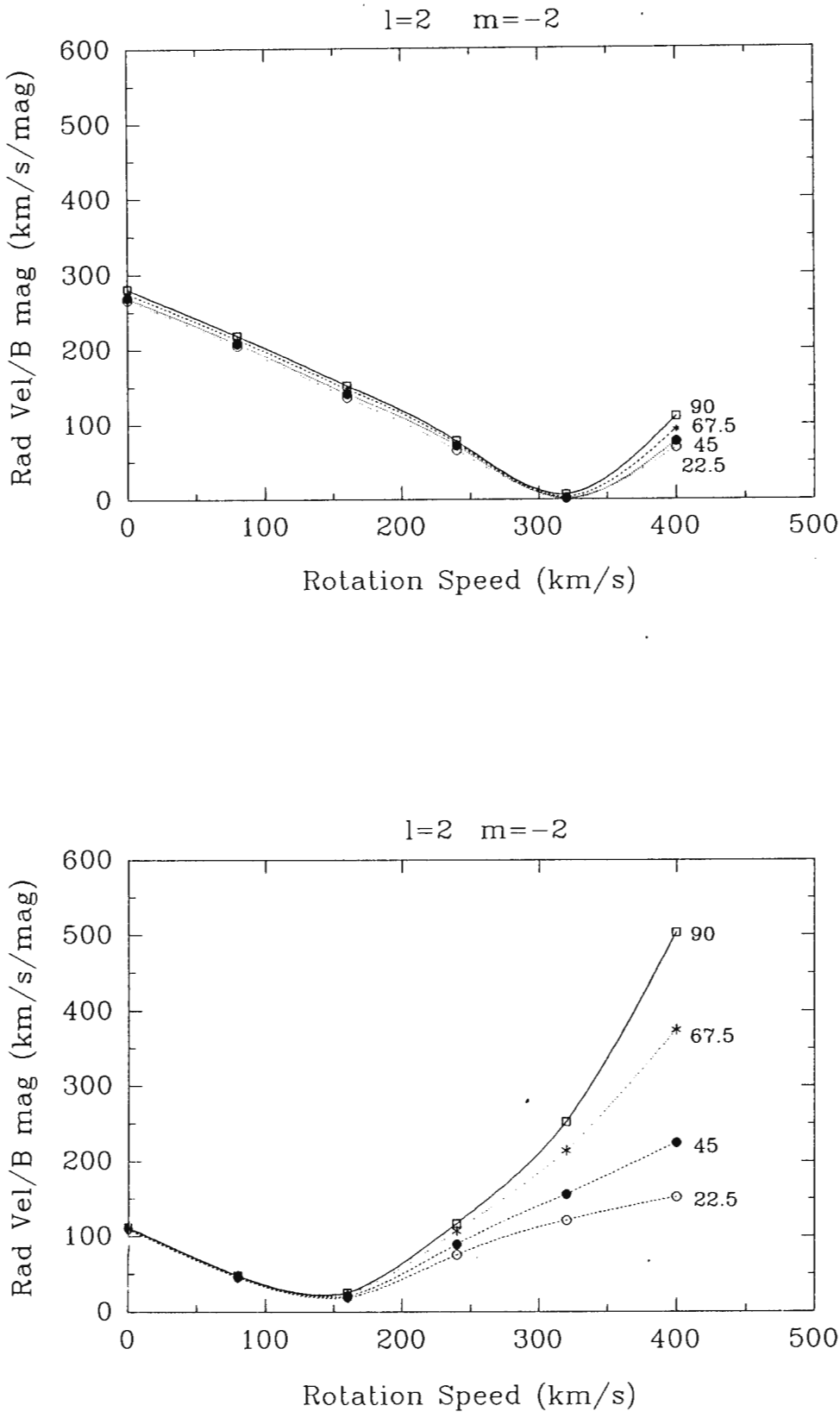
l=2 m=-2
Rad Vel/B mag (km/s/mag)
Rotation Speed (km/s)
0
100
200
300
400
500
600
90
67.5
45
22.5
l=2 m=-2
Rad Vel/B mag (km/s/mag)
Rotation Speed (km/s)
90
67.5
45
22.5

Figure 8.19

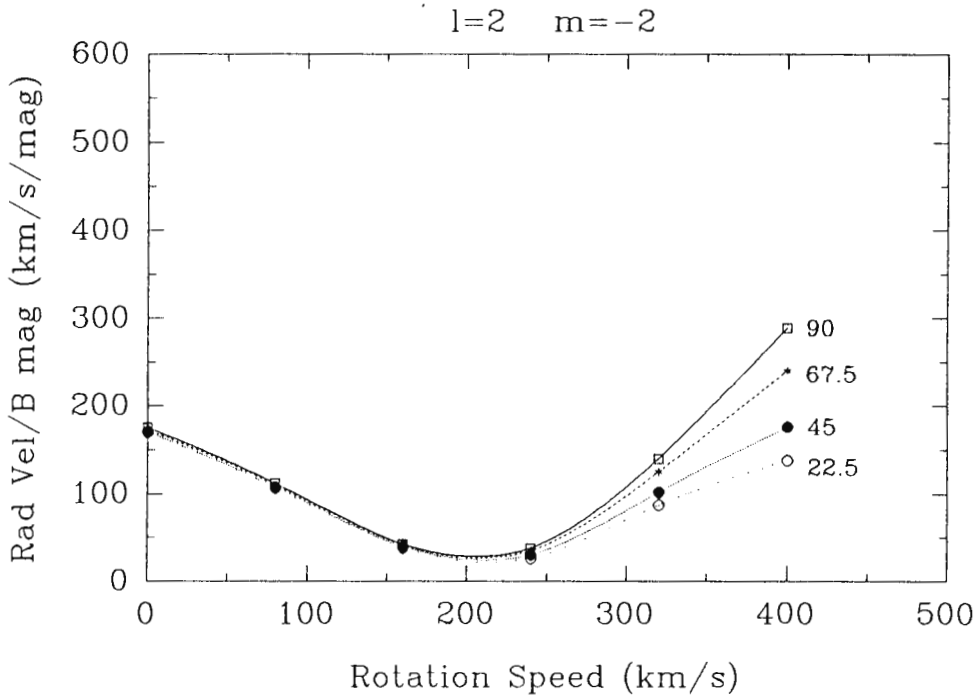
l=2 m=-2
Rad Vel/B mag (km/s/mag)
Rotation Speed (km/s)
0
100
200
300
400
500
600
90
67.5
45
22.5

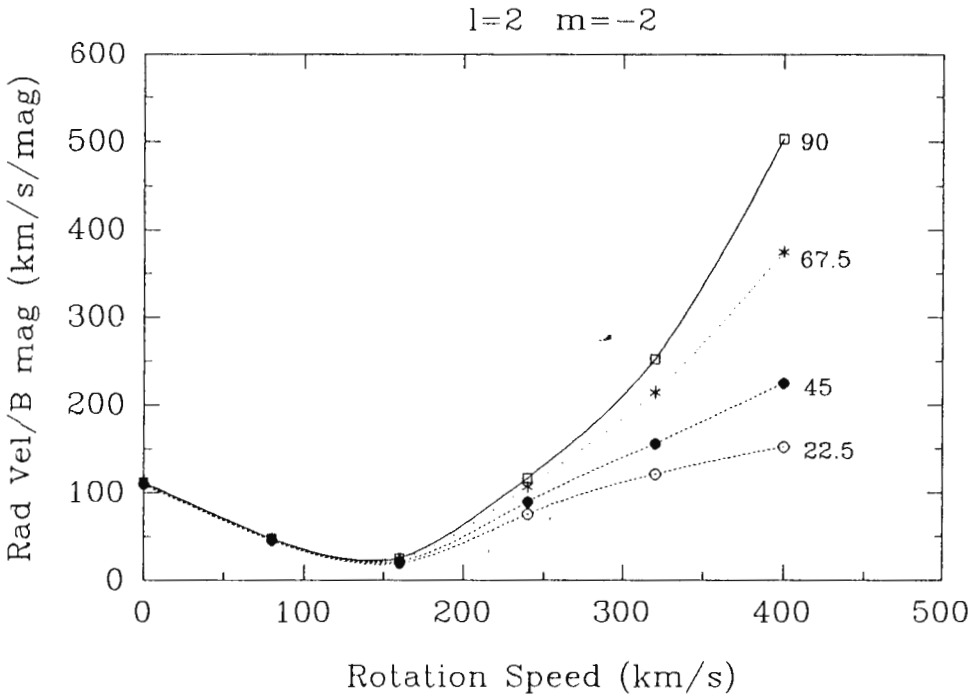
l=2 m=-2
Rad Vel/B mag (km/s/mag)
Rotation Speed (km/s)
0
100
200
300
400
500
600
90
67.5
45
22.5

Figure 8.20

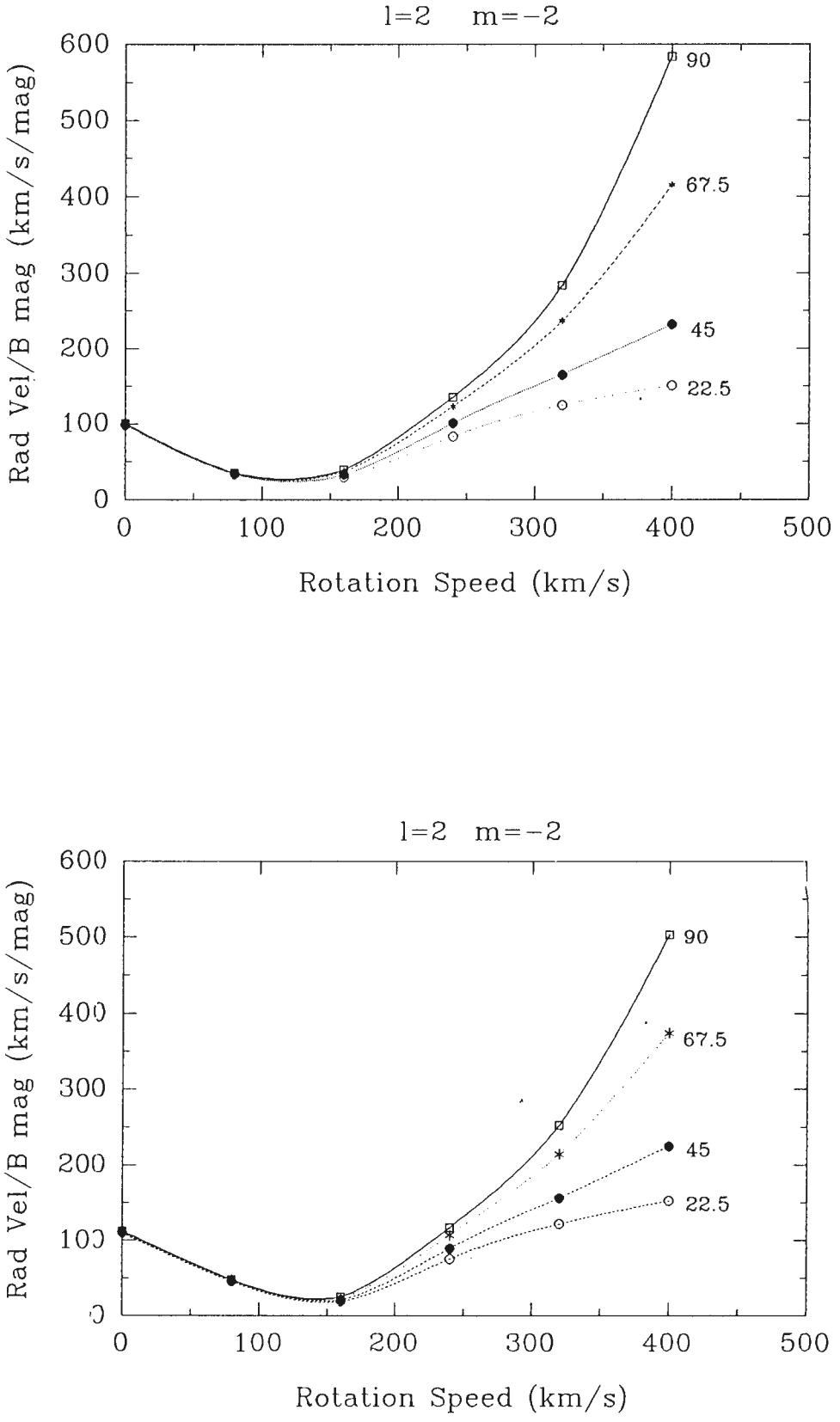
l=2 m=-2
Rad Vel/B mag (km/s/mag)
Rotation Speed (km/s)
90
67.5
45
22.5
0
100
200
300
400
500
600

Figure 8.21

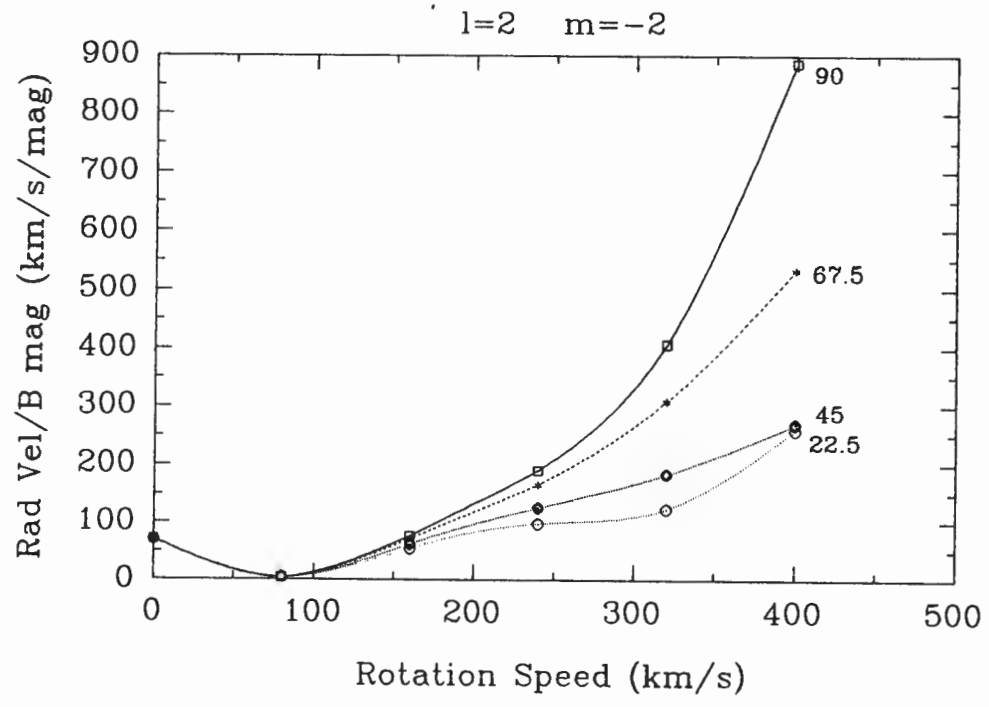
l=2 m=-2
Rad Vel/B mag (km/s/mag)
900
800
700
600
500
400
300
200
100
0
0
100
200
300
400
500
Rotation Speed (km/s)
90
67.5
45
22.5

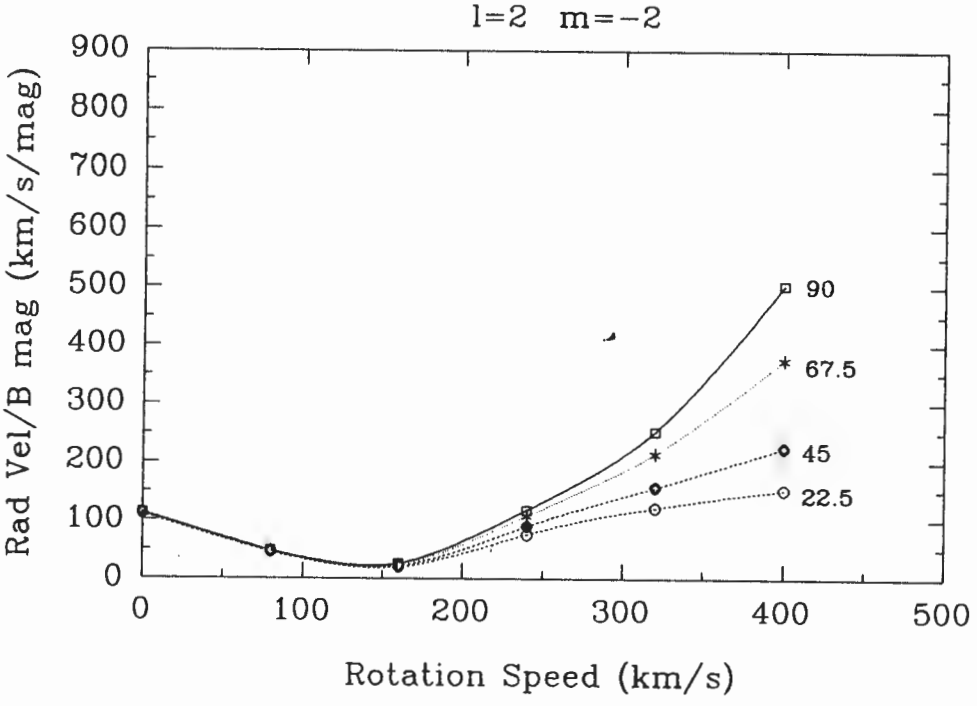
l=2 m=-2
Rad Vel/B mag (km/s/mag)
900
800
700
600
500
400
300
200
100
0
0
100
200
300
400
500
Rotation Speed (km/s)
90
67.5
45
22.5

Figure 8.22

CHAPTER 9

SPECTRAL LINE PROFILES

The final tool for mode identification, viz the study of spectral line profiles, is considered in this chapter. The chapter is introduced by a review of previous work.

9.1 INTRODUCTION

Osaki (1971) observed that, with some exceptions, retrograde quadrupole modes (ie modes with $(\ell,m) = (2,+2)$) were incompatible with observations of β Cephei stars. Further conclusions of Osaki were that antisymmetric modes (ie where $|m| = \ell-1$) were most favourably viewed from an inclination angle i of 45°, and that the symmetry of the $(\ell,m) = (2,-2)$ mode increased its probability of being excited above that of the (2,–1) mode. Stamford & Watson (1977), reviewing previous work on spectral line profiles by various authors, indicated that the $(\ell,m) = (2,-2)$ mode corresponded to the line broadening and "doubling" observed in β Cephei stars.

Buta & Smith (1979) found that the line profile variations in the mid–B star 53 Per were best explained by modes with $m = -\ell$ and $m = -(\ell-1)$, while Walker et al. (1979) found that line profile variations caused by nonradial pulsation are also detectable in rapidly rotating stars in the form of "bumps" moving "through" the line profiles. Vogt & Penrod (1983) studied this "bump" phenomenon extensively in their analysis of the O9.5 star ζ Oph (referred to already in chapter 7), and motivated their calculation of profile variations for modes with $m = -\ell$ by the fact that this choice produced the

largest possible line profile variation for the minimum radial velocity variation.

Smith (1981) emphasized Stamford & Watson's amplitude ratio method (see chapter 1) as well as spectral line profile analysis as the most pertinent methods of mode identification, claiming that nonadiabatic effects in the envelopes of β Cephei stars precluded mode identification by means of either photometric data or line profiles **alone**. Smith further argued that observations of real stars indicated a preference for modes with $m = -\ell$ to become excited.

Mode identification through line profile analysis has almost exclusively been done by a trial–and–error procedure, comparing calculations to observations until a match is found. A more objective approach was introduced by Balona (1986a, 1986b, 1987), obviating the need for matching computed profiles to observed ones. The method requires the calculation of the **moments** of a line profile, as follows:

$$\text{the n}^{\text{th}} \text{ moment } \mathrm{M_n} = \int_{-\infty}^{\infty} x^n f(x) g(x)\, dx \qquad (9.1)$$

where $g(x)$ describes the intrinsic profile and $f(x)$ the projection towards the observer of the velocity field due to pulsation and rotation. In this scheme, the zeroth moment represents the equivalent width of the line, the first moment the radial velocity and the second moment the line broadening. The ratios among the amplitudes of these moments differ for different values of ℓ, m, and i, allowing identification of these parameters by analysis of observed line profiles. Comparison of the **ratios** among each other would allow mode identification in multiperiodic stars as well.

Balona claimed that his method would be most efficient for determining sectoral modes (ie where $|m| = \ell$), and least efficient for axisymmetric modes ($m = 0$), while it was best suited to modes with $\ell < 5$. He also suggested that the **centroid** of a line profile

was the only appropriate determinant of radial velocity for nonradial pulsation modes, since measurement of other features of a line might lead to fictitious conclusions.

In the second paper of the series, Balona considered the case of what he termed **moderate rotation**, which implied that terms containing the pulsation velocity v_p in a form higher than the first power could be neglected. He developed a least–squares algorithm to match observed Fourier amplitudes to theoretical amplitudes of line profile moments, with the mode identification following from the choice of ℓ, m and i which minimized the variance between the observed and theoretical amplitudes. Balona concluded that further progress required greater clarity on the effect of moderate to rapid rotation on the pulsation eigenfunctions.

The effect of temperature variations in a rapidly rotating pulsating star on the star's observed line profiles was investigated in the final paper (Balona (1987)). Aerts et al. (1992) applied the method developed in Balona's trilogy of papers to a real β Cephei star, δ Ceti. They found the method capable of producing an unambiguous identification of this star as a radial pulsator.

Gies & Kullavanijaya (1988) presented a method consisting of taking the Fourier transform of line–profile variations at specific wavelengths, and plotting the complex phase of the power spectrum at each signal frequency versus line position, to determine the value of m. Kambe et al. (1990) carefully investigated the efficiency of line profile analysis, applied specifically to ζ Oph. They followed the abovementioned procedure of Gies & Kullavanijaya, modified by employing the so–called Akaike Information Criterion to determine the **number** of pulsation modes responsible for the observed line profile variations.

Fullerton (1991) discussed line profile variablity in general in O stars, based on a detailed study of $\simeq$ 30 bright O stars with projected rotation velocities from 50 km/s to 400 km/s. He was able to identify **variations** with amplitudes as small as 0.002 of the local continuum level. The observed variations consisted of so–called "bumps", "moving through" the profiles, apparently from the blue wing to the red wing (ie the same direction as the stellar rotation) in most cases. The bumps appeared to move more rapidly in the spectra of the more rapidly rotating stars. The observations also showed subtle variations in line depth and symmetry, as well as shifts in line position.

The results reviewed above clearly demonstrate the wealth of detail being uncovered in the field of line profile analysis at present, and the strong rationale for choosing to focus the calculations discussed in chapters 8 and 9 on the prograde sectoral modes (ie modes with $m = -\ell$). The axial symmetry of the modes with $m = 0$ prompted the calculation of results for these modes as well.

Line profiles were constructed in the following manner:

9.2 CALCULATING RAW PROFILES

Profiles were sampled at five phases of the pulsation cycle of the monoperiodic model star described in chapter 7. Note that the profiles were calculated for a velocity distribution described by equation 7.36, which contains both first and second–order effects of rotation. Following the usage in many sources in the literature, a complete cycle of the star's variation was equated to 90° in phase. The computations were performed such that the star's magnitude then reaches its maximum when the phase $\phi = 0^\circ$ and 90°, and its minimum when $\phi = 45^\circ$. The radial velocity curve is 22.5° (a quarter period) out of phase with the magnitude variation. The line profiles were

computed at intervals of 21°, specifically at 21°, 42°, 63°, 84° and 105° (which is identical to 15°). As fractions of a full period, these phases correspond to the values ϕ = 0.2333; 0.4667; 0.7; 0.9333 and 0.1667 respectively. By taking profiles at these phases instead of the perfect fractions 0.25; 0.5; 0.75 and 1, the calculated profiles correspond more closely to the typical forms one would expect to obtain in a random observation, since the forms of the profile at the "turning points" in the cycle are unique, and could be difficult to relate to profiles obtained at other phases.

For a particular phase, the maximum and minimum of the radial velocities (see equations 7.36 and 7.37) obtained for all 62500 surface elements facing the observer were determined, and this range in velocity was then divided into 90 bins. The luminosity (as a fraction of the total luminoity) calculated for each surface element was then accumulated in the bin corresponding to its radial velocity, producing a total profile for the entire visible hemisphere of the star. Care was taken to neither exclude the edges of the bins, nor duplicate them in the counting process. The profile was then inverted to correspond to an absorption profile.

9.3 BROADENING THE PROFILES

Real profiles will include the effects of broadening by other physical processes in the star, which were taken into account as follows:

The major broadening agent is the thermal motion of the surface material. This effect is calculated following the discussion in Böhm–Vitense (1989):

The line depth R_{λ} at wavelength λ is defined as :

$$R_{\lambda} = 1 - {}^{F\lambda}/_{F_c}, \qquad (9.1)$$

where F denotes flux and c refers to the continuum. The thermal broadening is described by the Maxwell distribution:

$$exp(-(v/\gamma_0)^2), \tag{9.2}$$

where v represents the radial velocity and

$$\gamma_0 = \sqrt{(\frac{2RT}{\mu})}, \tag{9.3}$$

where R = the gas constant = 8.31 J K^{-1} mol^{-1},

T = the stellar effective temperature

and μ = the atomic mass.

Lesh & Aizenman (1978) claimed that absorption lines of silicon were most frequently used in line profile studies. Taking the corresponding value of 28 for μ, and setting T = 21100 K, we find:

$$\gamma_0 = 3.54 \text{ km/s}.$$

The line depth R_λ due only to thermal broadening is then proportional to the expression in equation 9.2, with the proportionality constant such that the equivalent width of the line is preserved.

For each of the 90 bins comprising each calculated "raw" profile, the luminosity represented in that bin was redistributed according to the Maxwellian distribution in equation 9.2, with v now the radial velocity relative to the bin velocity. Since

$$\int_{-\infty}^{\infty} exp(-x^2/\gamma^2)dx = \gamma\sqrt{\pi}, \tag{9.4}$$

the equivalent width of each bin was preserved by factoring in a normalisation constant of $1/(\gamma\sqrt{\pi})$. The full broadening algorithm appears in Appendix 3. The calculations were performed with γ rounded to 4 km/s.

9.4 RESULTS

The complete set of broadened profiles for modes with ℓ from 0 to 4, and m = 0 and $-\ell$, appears in appendix 2. The salient features of these profiles are now discussed.

The line profiles are arranged according to pulsation mode and rotation velocity. For a particular choice of ℓ, m and v_{rot}, a page contains five panels of profiles for values of i = 0°, 22.5°, 45°, 67.5° and 90° respectively. Within each panel, line profiles for phases at 21°, 42°, 63°, 84° and 105° (ie 15°) respectively are shown. In most cases, a clearer picture of line profile variaition with phase was obtained by displaying only a few of these phases. The phases which are being displayed are indicated by the corresponding numbers next to the profiles. When no numbers are indicated, all the phases are being displayed. This is usually done when there is no change in the appearance of the line profile with a change in phase, so that only one unchanging profile is obtained. In the cases where a limited number of phases are displayed, the line profiles for the absent phases may be accepted to have shapes "interpolated" between those which are displayed. In all cases where line profiles take on unexpected shapes, they are displayed.

The captions applied to each of the panels should be interpreted as follows: The captions at the top of a panel indicate, in turn, the equatorial rotation velocity, mode parameters ℓ and m, and the inclination angle i. The axis on the left of a panel indicates the depth of the line relative to the local continuum, while the axis at the bottom af a panel indicates the Doppler–shifted wavelength of the entire range of a line profile, relative to its stationary value, expressed in terms of velocity. The number of surface elements differentiated on the observed stellar hemisphere for numerical integration is indicated by "el", in units of 100. So, "el = 625" means that 62500 surface elements were used. The number of bins used to construct the line profile from the

results of the numerical integration of the stellar surface is also indicated.

9.4.1 The effect of rotational distortion

Firstly, I show a series of comparisons between profiles for stellar models which have been appropriately distorted by rotation, and profiles for models which have been assumed to remain spherical, for increasing rotation velocities. Figures 9.1 to 9.5 respectively correspond to velocities of 400, 320, 240, 160 and 80 km/s, with the figure on the left (part (a)) in each case showing the profiles for the spherical model, and the figure on the right (part(b)) the profiles for the appropriately distorted model. The profiles for $(\ell,m) = (3,0)$ are shown, since this particular choice contains readily visible asymmetries in the profiles for various phases and inclination angles, demonstrating the effect of rotation to great effect. If one considers the most extreme case, in figure 9.1, there is an obvious difference between the linewidth at half maximum of the two profiles. The undistorted star's profile is $20 - 25$ % broader than the corrected profile.

The importance of using appropriate pulsation eigenfunctions should be addressed before making further conclusions. Figures 9.16 and 9.17 show line profiles for the axisymmetric $(\ell,m) = (4,0)$ mode, using the zeroth order (ie no correction for rotation) eigenfunction and the second order (including the ad–hoc second order correction described in section 7.5 in addition to the first order rotatioinal correction of Carroll (1981)) eigenfunctions respectively. Figures 9.18 and 9.19 repeat this sequence for the sectoral $(\ell,m) = (4,-4)$ mode. In all four of these figures, the profiles are shown for a rotation velocity of 400 km/s, to allow the influence of rotational corrections to the eigenfunctions to be displayed to maximum effect. As was found for the amplitude ratios discussed in chapter 8, the line profiles appear unaffected by the choice of rotational correction to the eigenfunctions. The only discernible effect is seen in the ($i =$

0) panels for the $(\ell,m) = (4,-4)$ mode, where the minimum of the profiles obtained with the second order eigenfunction is about 3% deeper than the minimum of the profiles obtained with the zeroth order eigenfunction. There is no difference between the profiles obtained with the first order and second order eigenfunctions respectively. These results suggest that the profiles calculated according to the procedure outlined in chapter 7 may be accepted without concern for the fine details of rotational effects on the pulsation eigenfunctions used in these calculations.

Returning to the observation immediately preceding the last paragraph, it follows that equatorial rotation velocities estimated on the basis of spherical stars will be significantly in error, specifically by implying rotation speeds which are smaller than in reality. The size of this discrepancy could well account for the recorded gap (see section 7.1) between the highest measured rotation speeds for B stars, around 450 km/s, and the break–up velocity of around 600 km/s. Going on to figures 9.2 to 9.5, this effect becomes less noticeable, of course, and at speeds below 250 km/s it is no longer discernible. It can therefore categorically be stated that rotational distortion needs to be properly taken into account when estimating stellar rotation velocities, at least when these velocities exceed 250 km/s.

9.4.2 The effect of the flux variation coefficient f_λ

Following the results described in chapter 8, the effect of the value of the flux variation coefficient on the calculated line profiles also needs to be investigated. Figures 9.20 and 9.21 show line profiles obtained for the axisymmetric $(\ell,m) = (3,0)$ mode with $f_\lambda = -5$ and -30 respectively, while figures 9.22 and 9.23 show the corresponding profiles for the sectoral $(\ell,m) = (3,-3)$ mode. Comparison with the profiles obtained with the adiabatic value of $f_\lambda = -17.5$, appearing in Appendix 2, reveals no differences between these

profiles. This suggests that the line profiles collected in Appendix 2 may be interpreted and used without concern for the effect of a nonadiabatic photosphere on the flux variation coefficient.

9.4.3 Mode identification

A study of the profiles in Appendix 2 clearly indicates the strength of line profiles as instruments of pulsation mode identification. Asymmetries and spikes in the profiles take on various forms and appear in various intensities, and even the relative change in a profile with phase could serve as an instrument of mode identification. An obvious extension of these results, for which there is no more space available in this thesis, would be the compilation of a complete "atlas" of line profiles for, say, all modes from $\ell = 0$ to $\ell = 8$, with finer gradations of rotation velocity, phase and inclination angle as well.

The profiles catalogued in this thesis may in many cases also serve to identify rotation velocities and inclination angles, especially when the latter have low values. Certain common trends among different modes are clearly visible. The clearest trends are illustrated in figures 9.6 to 9.15. Firstly, a sequence of modes with $m = 0$ is presented. The modes for $\ell = 0$ to $\ell = 4$ are shown for the rotation velocity of 80 km/s, where there is still enough of the pulsation's effect visible in the profile shapes (at higher velocities this tends to be swamped by the rotational broadening). The growth of line asymmetry is clearly discernible as one moves from $\ell = 0$ to $\ell = 4$. This sequence is followed by one for the modes with $m = -\ell$, from $\ell = 1$ to $\ell = 4$. The major feature in this sequence is the growth of the "spike" in the $i = 0^{\circ}$ profile. This spike also grows with rotation velocity, as is evidenced by figure 9.15, which shows the $(\ell,m) = (4,-4)$ spike for a rotation velocity of 400 km/s.

Further permutations among the profiles may be discerned by studying appendix 2. The main conclusion to be drawn from the content of this chapter is the clear effect that rotational distortion has on the form of spectral line profiles, and, therefore, the care that needs to be taken when interpreting stellar spectral line profiles to obtain information about particular stars.

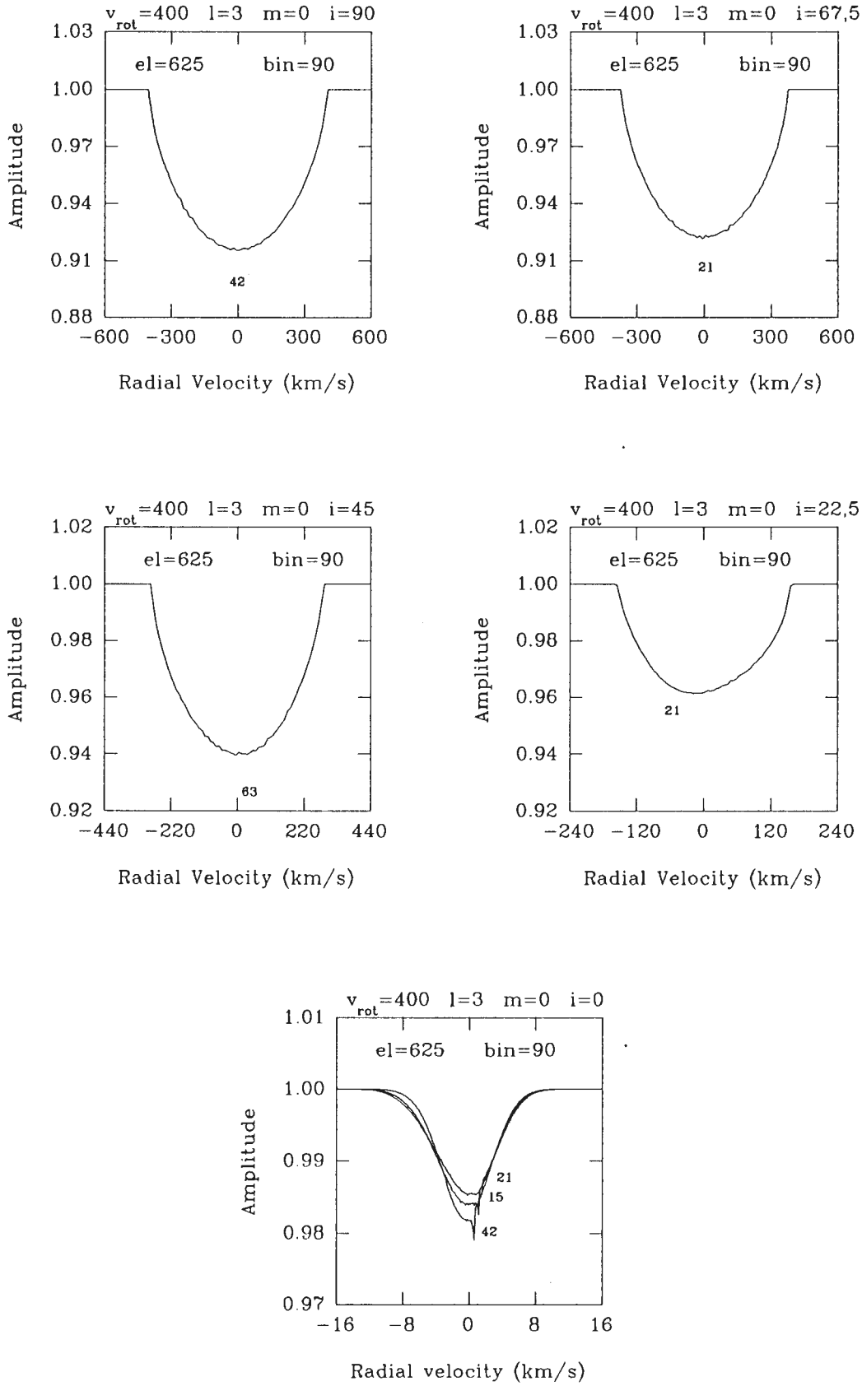
v rot =400 l=3 m=0 i=90
el=625 bin=90
Amplitude
1.03
1.00
0.97
0.94
0.91
0.88
42
−600 −300 0 300 600
Radial Velocity (km/s)
v rot =400 l=3 m=0 i=67,5
el=625 bin=90
Amplitude
1.03
1.00
0.97
0.94
0.91
0.88
21
−600 −300 0 300 600
Radial Velocity (km/s)
v rot =400 l=3 m=0 i=45
el=625 bin=90
Amplitude
1.02
1.00
0.98
0.96
0.94
0.92
63
−440 −220 0 220 440
Radial Velocity (km/s)
v rot =400 l=3 m=0 i=22,5
el=625 bin=90
Amplitude
1.02
1.00
0.98
0.96
0.94
0.92
21
−240 −120 0 120 240
Radial Velocity (km/s)
v rot =400 l=3 m=0 i=0
el=625 bin=90
Amplitude
1.01
1.00
0.99
0.98
0.97
21
15
42
−16 −8 0 8 16
Radial velocity (km/s)

Figure 9.1 (a)

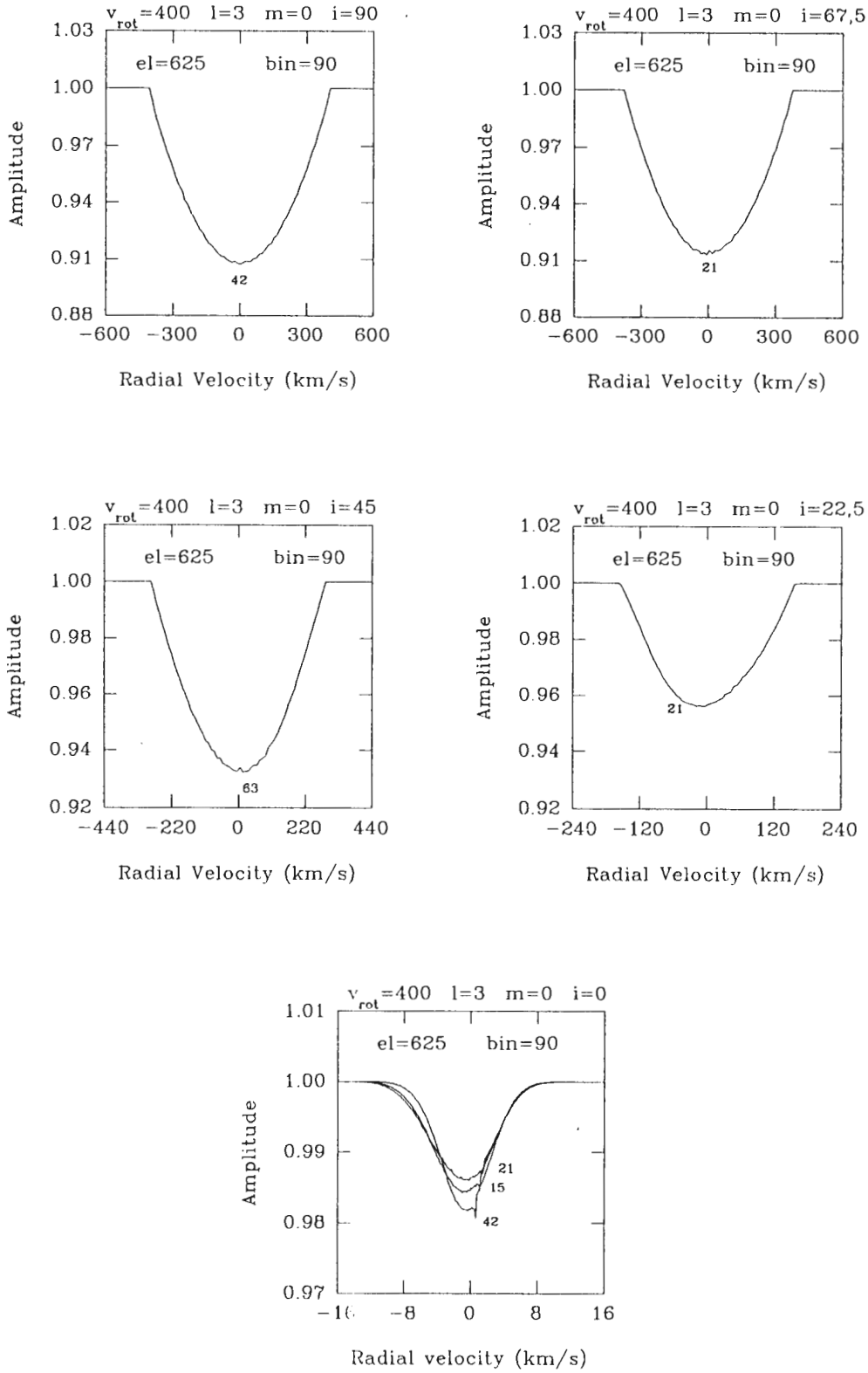
v rot =400 l=3 m=0 i=90
el=625 bin=90
Amplitude
1.03
1.00
0.97
0.94
0.91
0.88
42
−600 −300 0 300 600
Radial Velocity (km/s)
v rot =400 l=3 m=0 i=67,5
el=625 bin=90
Amplitude
1.03
1.00
0.97
0.94
0.91
0.88
21
−600 −300 0 300 600
Radial Velocity (km/s)
v rot =400 l=3 m=0 i=45
el=625 bin=90
Amplitude
1.02
1.00
0.98
0.96
0.94
0.92
63
−440 −220 0 220 440
Radial Velocity (km/s)
v rot =400 l=3 m=0 i=22,5
el=625 bin=90
Amplitude
1.02
1.00
0.98
0.96
0.94
0.92
21
−240 −120 0 120 240
Radial Velocity (km/s)
v rot =400 l=3 m=0 i=0
el=625 bin=90
Amplitude
1.01
1.00
0.99
0.98
0.97
21
15
42
−8 0 8 16
Radial velocity (km/s)

Figure 9.1 (b)

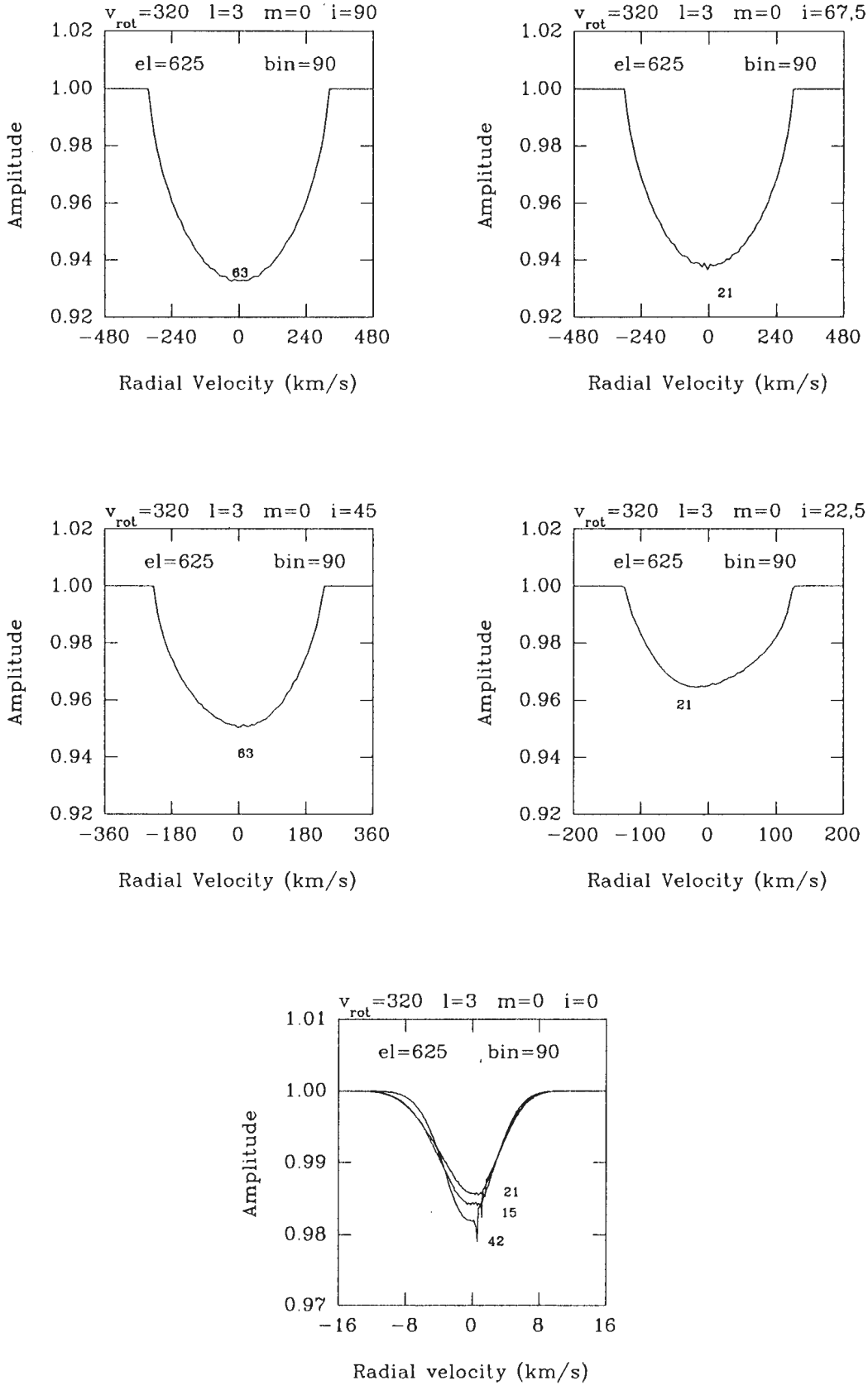
v_rot=320 l=3 m=0 i=90
el=625 bin=90
63
Amplitude
Radial Velocity (km/s)
v_rot=320 l=3 m=0 i=67,5
el=625 bin=90
21
Amplitude
Radial Velocity (km/s)
v_rot=320 l=3 m=0 i=45
el=625 bin=90
63
Amplitude
Radial Velocity (km/s)
v_rot=320 l=3 m=0 i=22,5
el=625 bin=90
21
Amplitude
Radial Velocity (km/s)
v_rot=320 l=3 m=0 i=0
el=625 bin=90
21
15
42
Amplitude
Radial velocity (km/s)

Figure 9.2 (a)

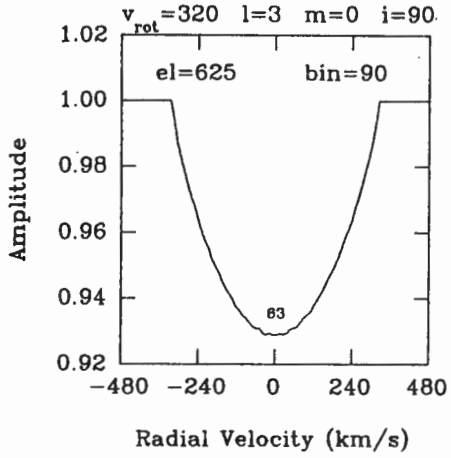
v_rot=320 l=3 m=0 i=90
el=625 bin=90
63
Amplitude
Radial Velocity (km/s)

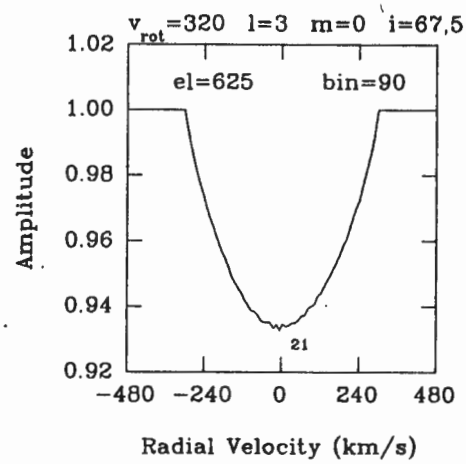
v_rot=320 l=3 m=0 i=67,5
el=625 bin=90
21
Amplitude
Radial Velocity (km/s)

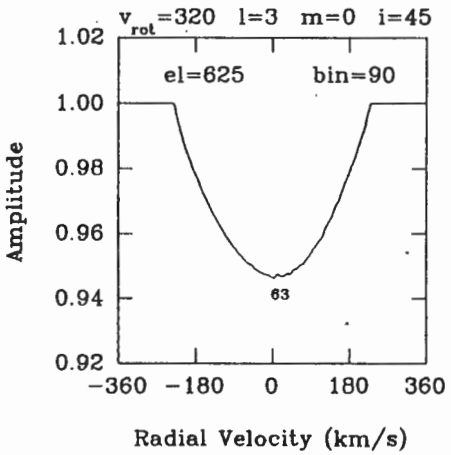
v_rot=320 l=3 m=0 i=45
el=625 bin=90
63
Amplitude
Radial Velocity (km/s)

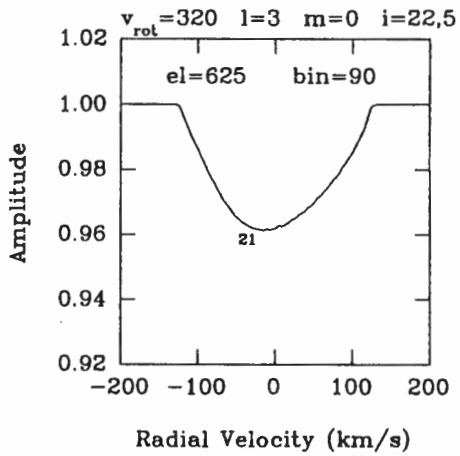
v_rot=320 l=3 m=0 i=22,5
el=625 bin=90
21
Amplitude
Radial Velocity (km/s)

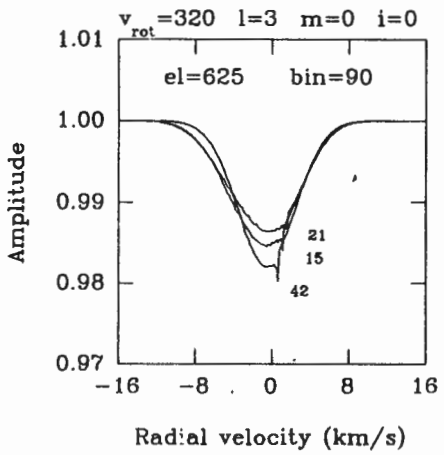
v_rot=320 l=3 m=0 i=0
el=625 bin=90
21
15
42
Amplitude
Radial velocity (km/s)

Figure 9.2 (b)

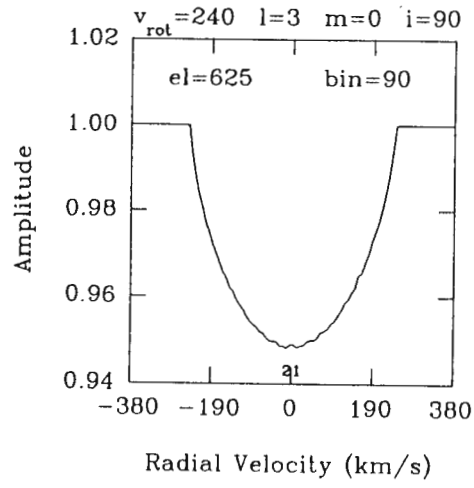
v rot =240 l=3 m=0 i=90
el=625 bin=90
21
Amplitude
1.02
1.00
0.98
0.96
0.94
−380 −190 0 190 380
Radial Velocity (km/s)

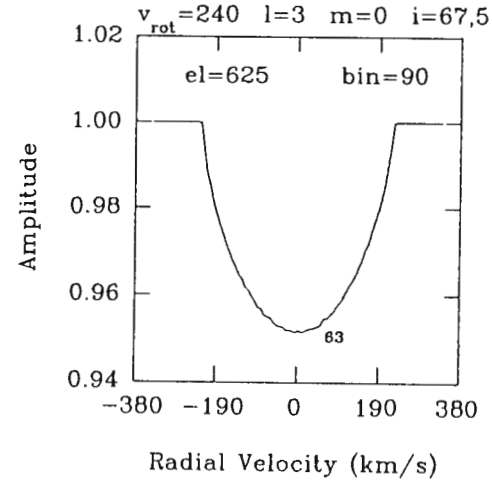
v rot =240 l=3 m=0 i=67,5
el=625 bin=90
63
Amplitude
1.02
1.00
0.98
0.96
0.94
−380 −190 0 190 380
Radial Velocity (km/s)

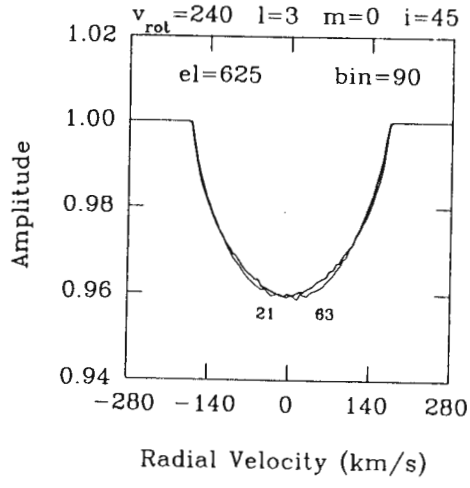
v rot =240 l=3 m=0 i=45
el=625 bin=90
21 63
Amplitude
1.02
1.00
0.98
0.96
0.94
−280 −140 0 140 280
Radial Velocity (km/s)

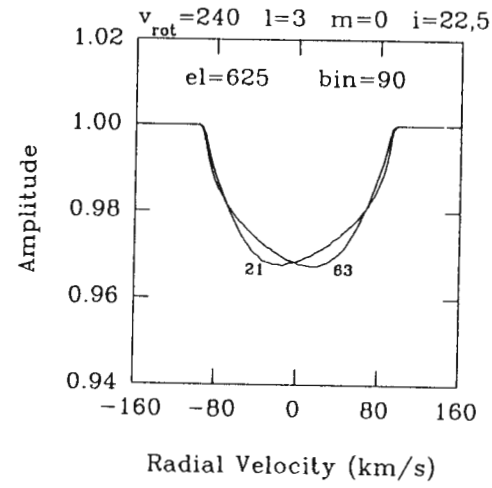
v rot =240 l=3 m=0 i=22,5
el=625 bin=90
21 63
Amplitude
1.02
1.00
0.98
0.96
0.94
−160 −80 0 80 160
Radial Velocity (km/s)

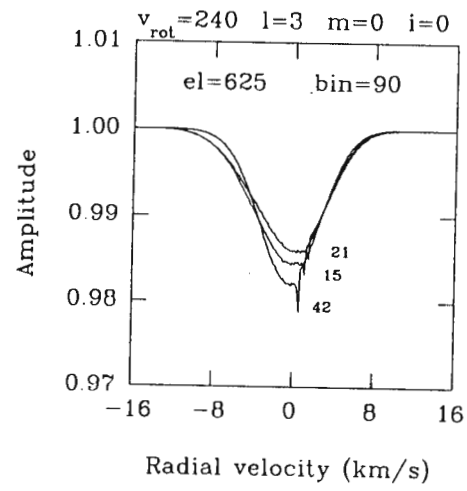
v rot =240 l=3 m=0 i=0
el=625 bin=90
21
15
42
Amplitude
1.01
1.00
0.99
0.98
0.97
−16 −8 0 8 16
Radial velocity (km/s)

Figure 9.3 (a)

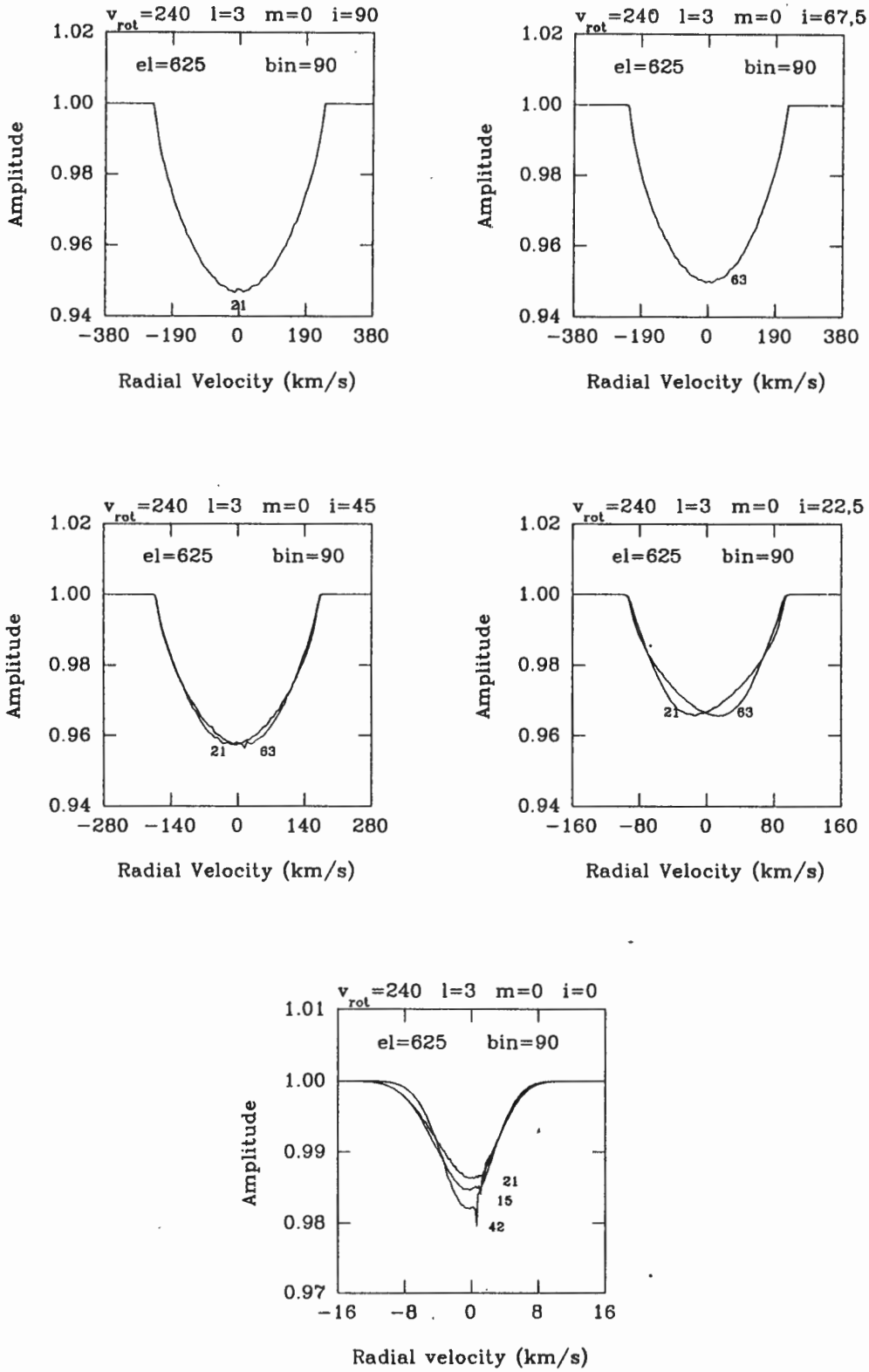
v_rot=240 l=3 m=0 i=90
el=625 bin=90
21
Amplitude
Radial Velocity (km/s)
v_rot=240 l=3 m=0 i=67,5
el=625 bin=90
63
Amplitude
Radial Velocity (km/s)
v_rot=240 l=3 m=0 i=45
el=625 bin=90
21 63
Amplitude
Radial Velocity (km/s)
v_rot=240 l=3 m=0 i=22,5
el=625 bin=90
21 63
Amplitude
Radial Velocity (km/s)
v_rot=240 l=3 m=0 i=0
el=625 bin=90
21
15
42
Amplitude
Radial velocity (km/s)

Figure 9.3 (b)

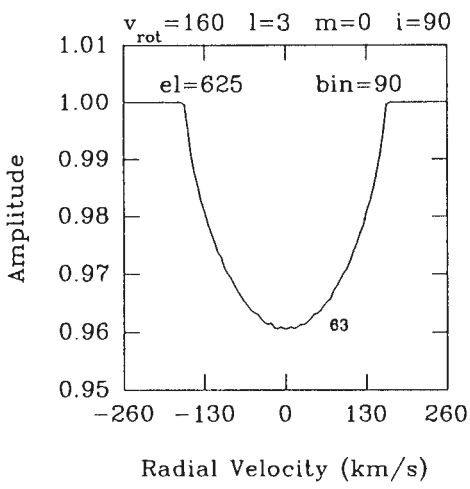
v rot =160 l=3 m=0 i=90
el=625 bin=90
63
Amplitude
1.01
1.00
0.99
0.98
0.97
0.96
0.95
−260 −130 0 130 260
Radial Velocity (km/s)

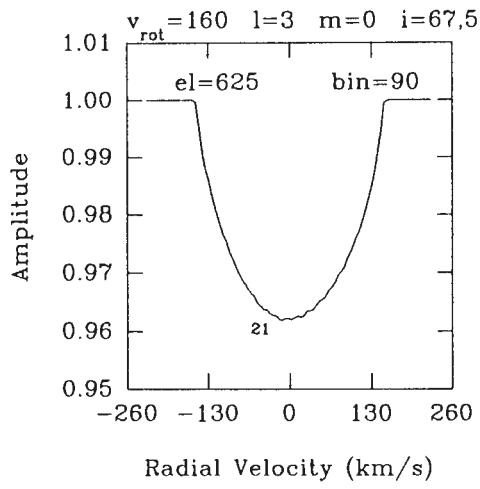
v rot =160 l=3 m=0 i=67,5
el=625 bin=90
21
Amplitude
1.01
1.00
0.99
0.98
0.97
0.96
0.95
−260 −130 0 130 260
Radial Velocity (km/s)

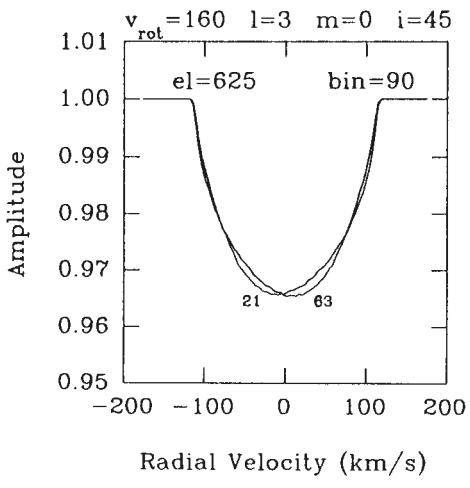
v rot =160 l=3 m=0 i=45
el=625 bin=90
21 63
Amplitude
1.01
1.00
0.99
0.98
0.97
0.96
0.95
−200 −100 0 100 200
Radial Velocity (km/s)

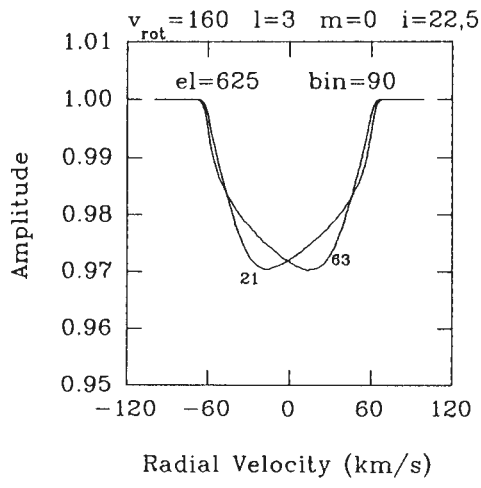
v rot =160 l=3 m=0 i=22,5
el=625 bin=90
21 63
Amplitude
1.01
1.00
0.99
0.98
0.97
0.96
0.95
−120 −60 0 60 120
Radial Velocity (km/s)

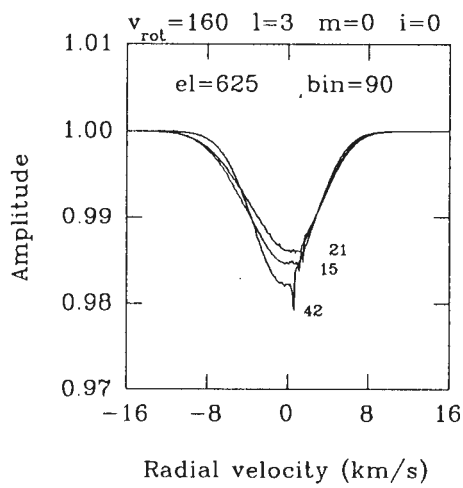
v rot =160 l=3 m=0 i=0
el=625 bin=90
21
15
42
Amplitude
1.01
1.00
0.99
0.98
0.97
−16 −8 0 8 16
Radial velocity (km/s)

Figure 9.4 (a)

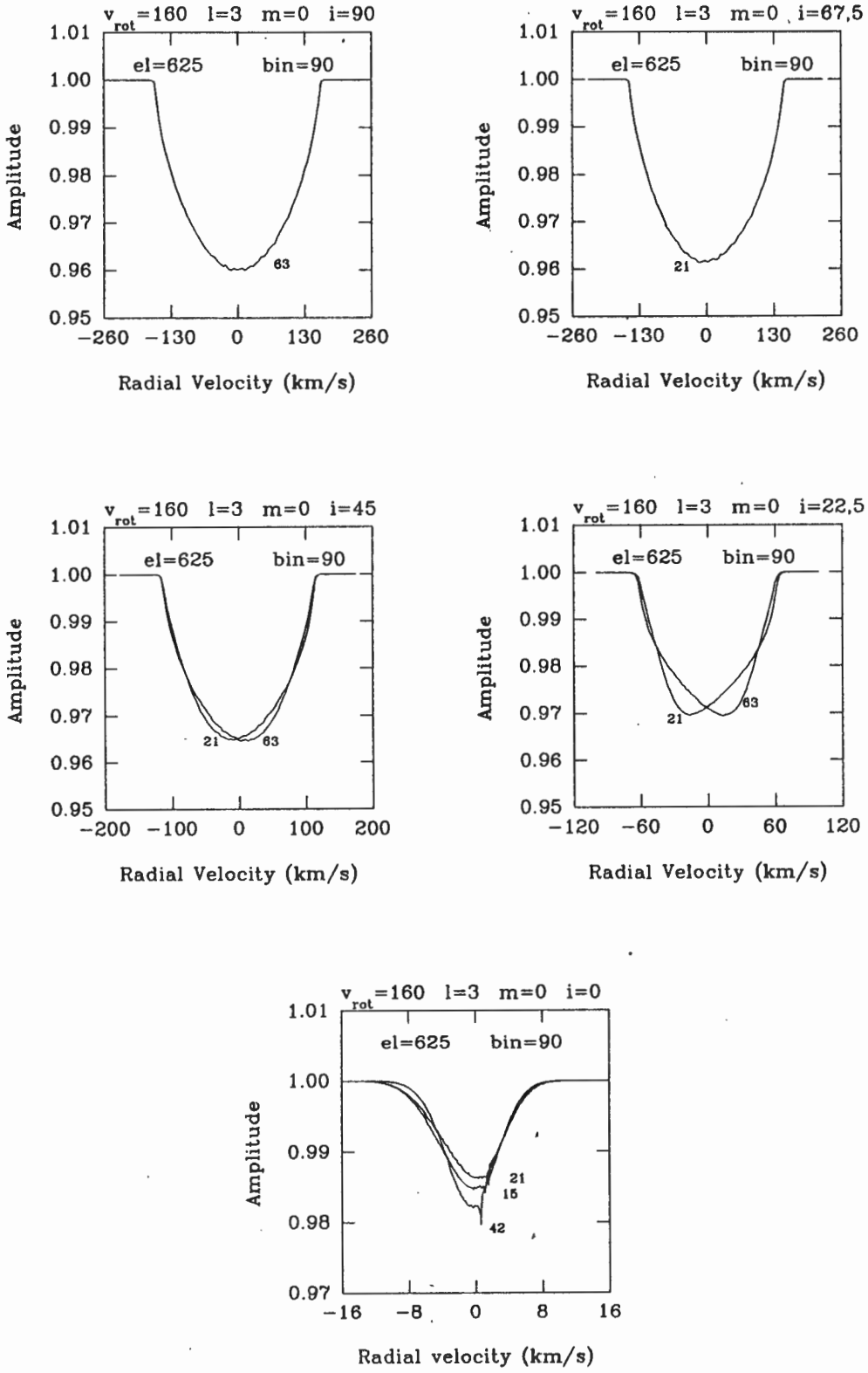
v_rot=160 l=3 m=0 i=90
el=625 bin=90
63
v_rot=160 l=3 m=0 i=67,5
el=625 bin=90
21
v_rot=160 l=3 m=0 i=45
el=625 bin=90
21
63
v_rot=160 l=3 m=0 i=22,5
el=625 bin=90
21
63
v_rot=160 l=3 m=0 i=0
el=625 bin=90
21
15
42
Amplitude
Radial Velocity (km/s)
Radial velocity (km/s)

Figure 9.4 (b)

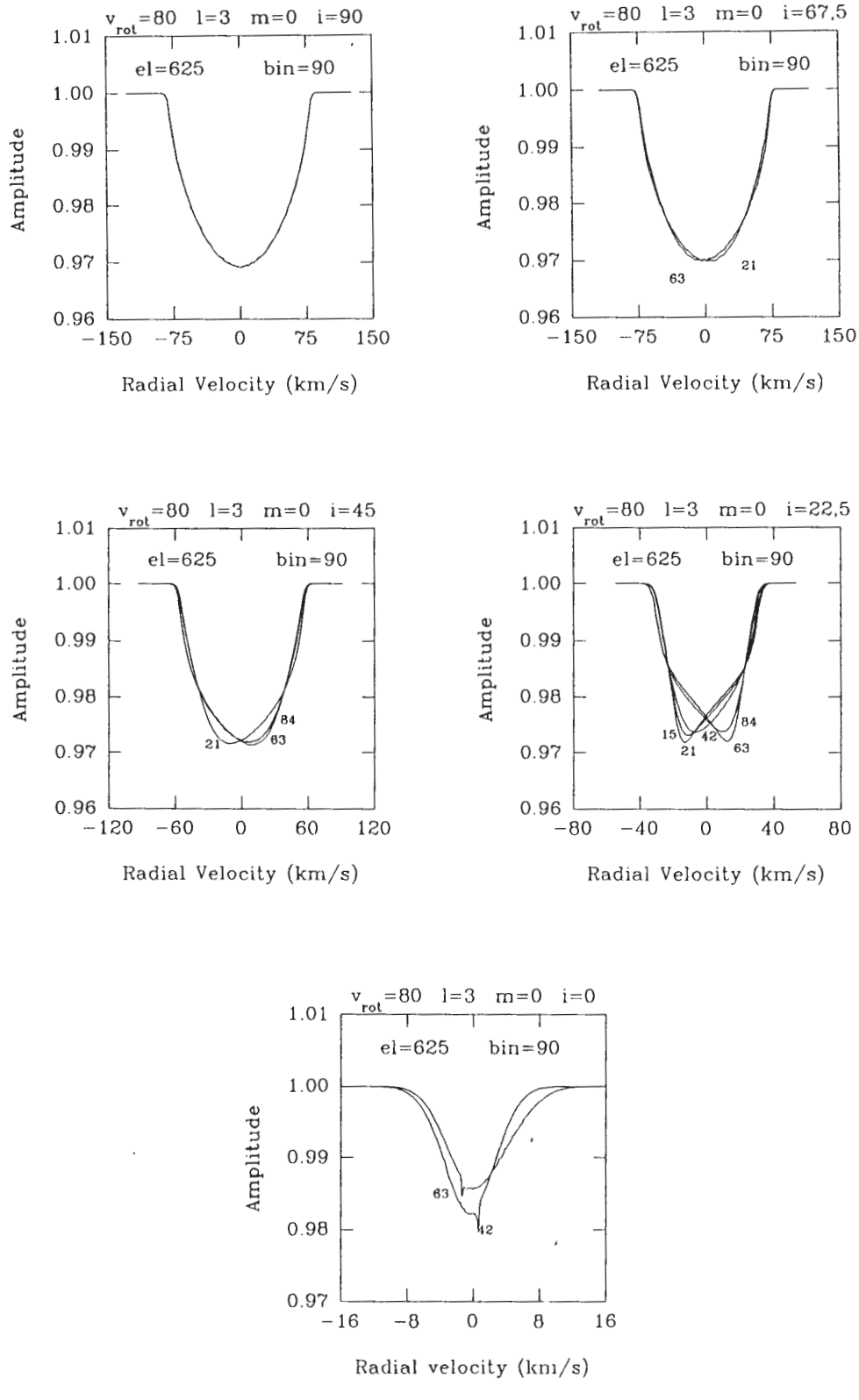
v rot =80 l=3 m=0 i=90
el=625 bin=90
Amplitude
Radial Velocity (km/s)
v rot =80 l=3 m=0 i=67,5
el=625 bin=90
63
21
Amplitude
Radial Velocity (km/s)
v rot =80 l=3 m=0 i=45
el=625 bin=90
84
21
63
Amplitude
Radial Velocity (km/s)
v rot =80 l=3 m=0 i=22,5
el=625 bin=90
84
15
42
21
63
Amplitude
Radial Velocity (km/s)
v rot =80 l=3 m=0 i=0
el=625 bin=90
63
42
Amplitude
Radial velocity (km/s)

Figure 9.5 (a)

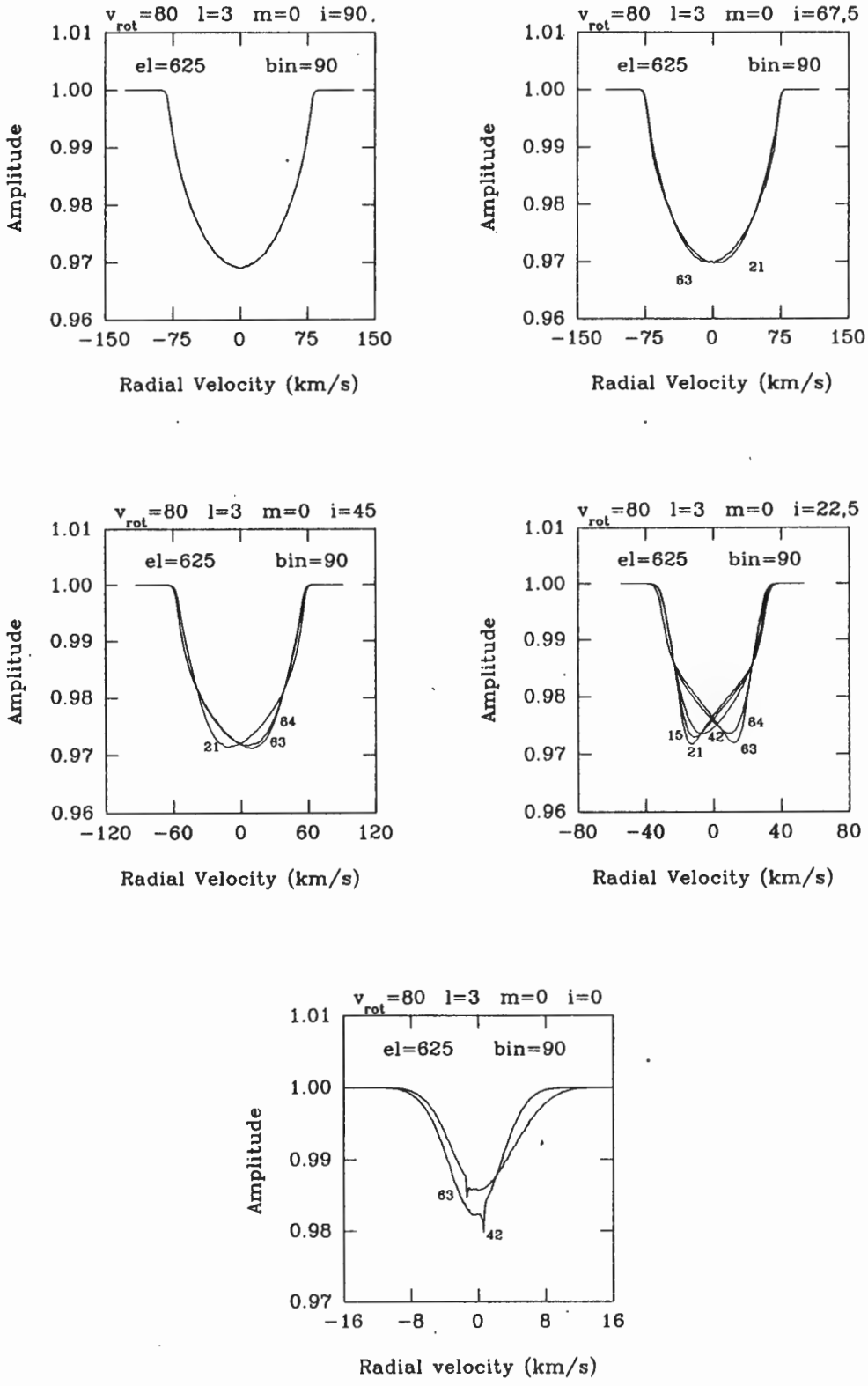
v_rot=80 l=3 m=0 i=90.
el=625 bin=90
Amplitude
Radial Velocity (km/s)
v_rot=80 l=3 m=0 i=67,5
el=625 bin=90
63
21
Amplitude
Radial Velocity (km/s)
v_rot=80 l=3 m=0 i=45
el=625 bin=90
64
21
63
Amplitude
Radial Velocity (km/s)
v_rot=80 l=3 m=0 i=22,5
el=625 bin=90
15
42
64
21
63
Amplitude
Radial Velocity (km/s)
v_rot=80 l=3 m=0 i=0
el=625 bin=90
63
42
Amplitude
Radial velocity (km/s)

Figure 9.5 (b)

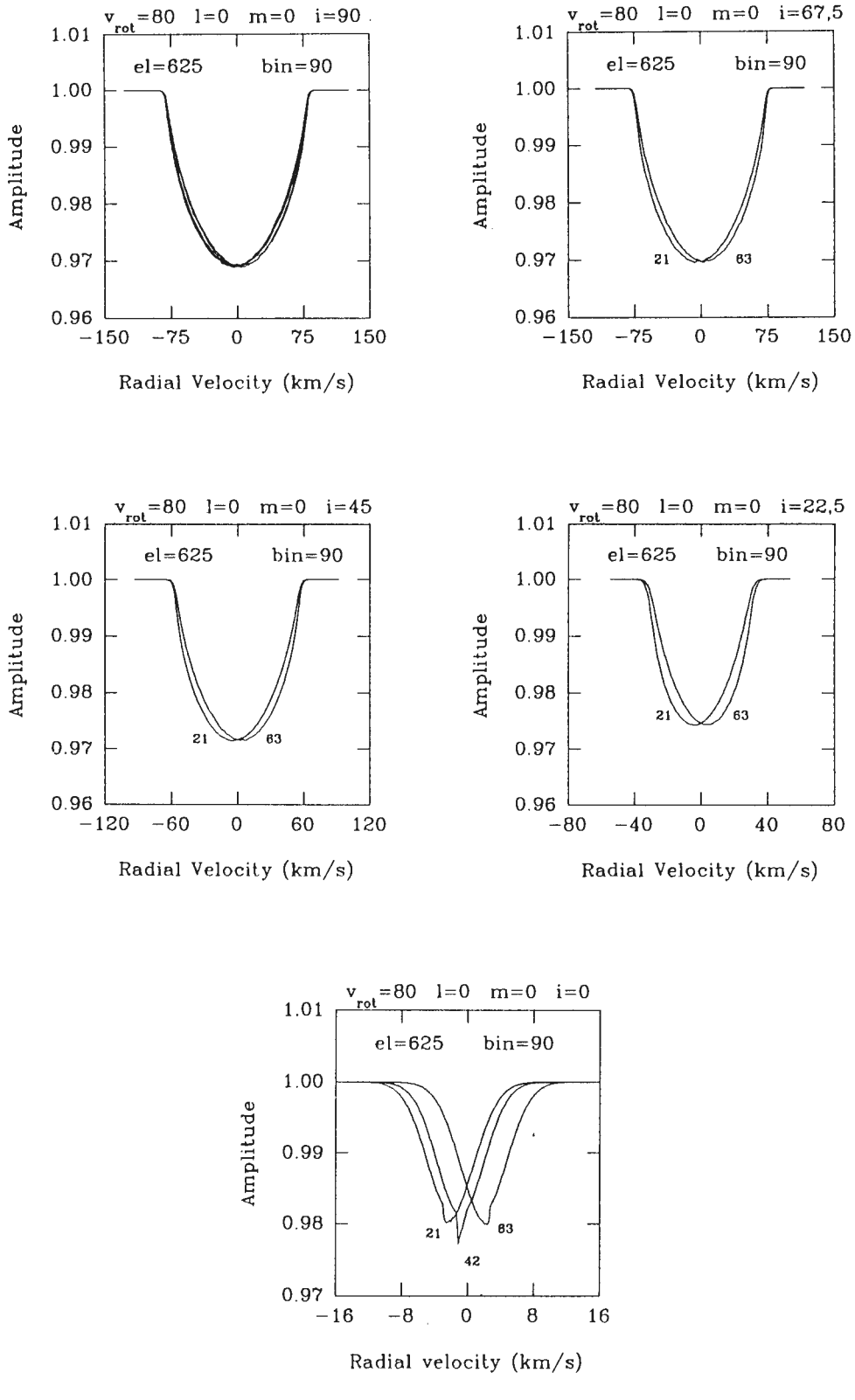
v rot =80 l=0 m=0 i=90
el=625 bin=90
v rot =80 l=0 m=0 i=67,5
el=625 bin=90
21
63
v rot =80 l=0 m=0 i=45
el=625 bin=90
21
63
v rot =80 l=0 m=0 i=22,5
el=625 bin=90
21
63
v rot =80 l=0 m=0 i=0
el=625 bin=90
21
63
42
Amplitude
Radial Velocity (km/s)
Radial velocity (km/s)

Figure 9.6

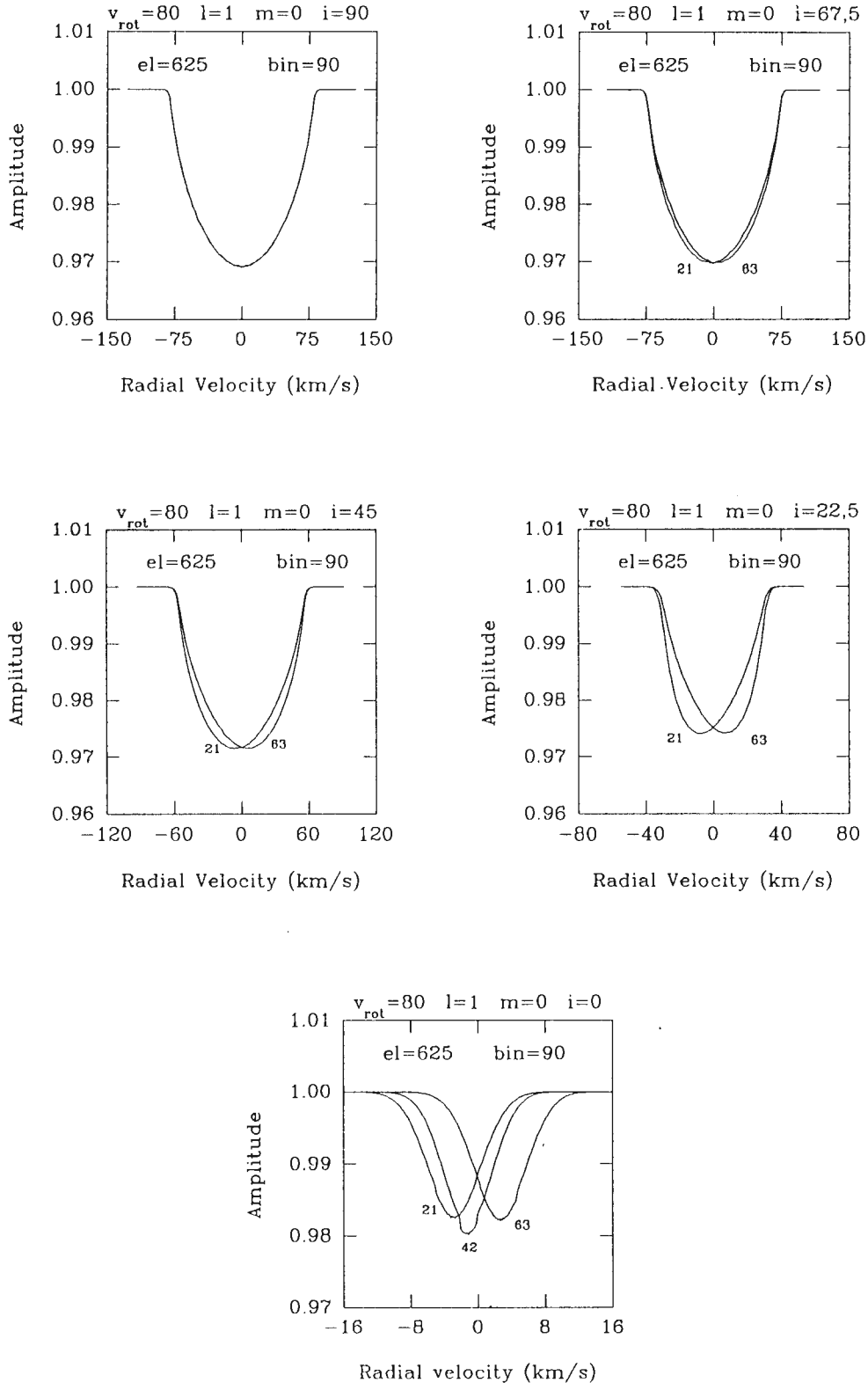
v rot =80 l=1 m=0 i=90
el=625 bin=90
Amplitude
Radial Velocity (km/s)
v rot =80 l=1 m=0 i=67,5
21
63
v rot =80 l=1 m=0 i=45
v rot =80 l=1 m=0 i=22,5
v rot =80 l=1 m=0 i=0
42

Figure 9.7

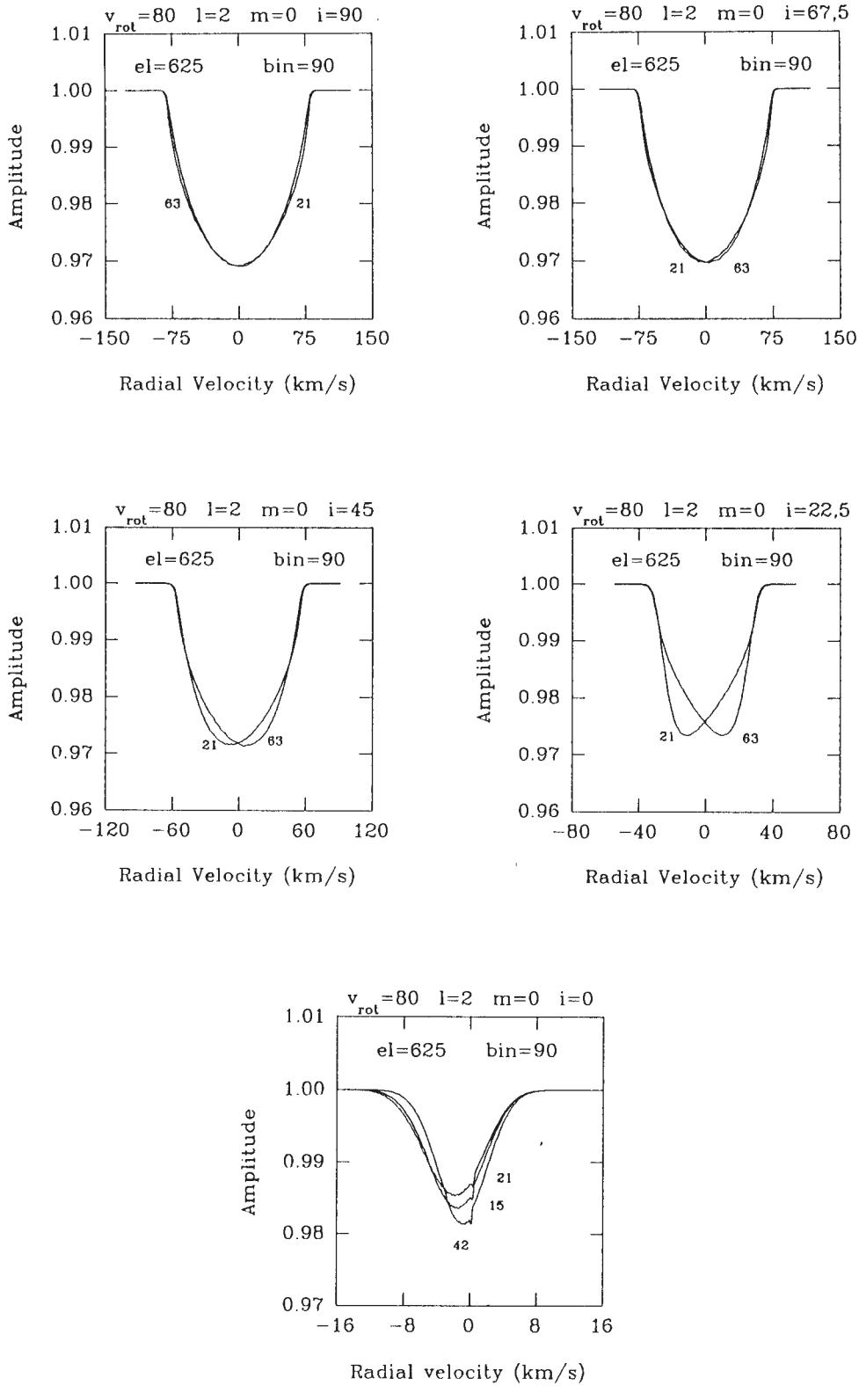
v_rot=80 l=2 m=0 i=90
el=625 bin=90
63
21
v_rot=80 l=2 m=0 i=67,5
el=625 bin=90
21
63
v_rot=80 l=2 m=0 i=45
el=625 bin=90
21
63
v_rot=80 l=2 m=0 i=22,5
el=625 bin=90
21
63
v_rot=80 l=2 m=0 i=0
el=625 bin=90
21
15
42
Amplitude
1.01
1.00
0.99
0.98
0.97
0.96
−150 −75 0 75 150
−120 −60 0 60 120
−80 −40 0 40 80
−16 −8 0 8 16
Radial Velocity (km/s)
Radial velocity (km/s)

Figure 9.8

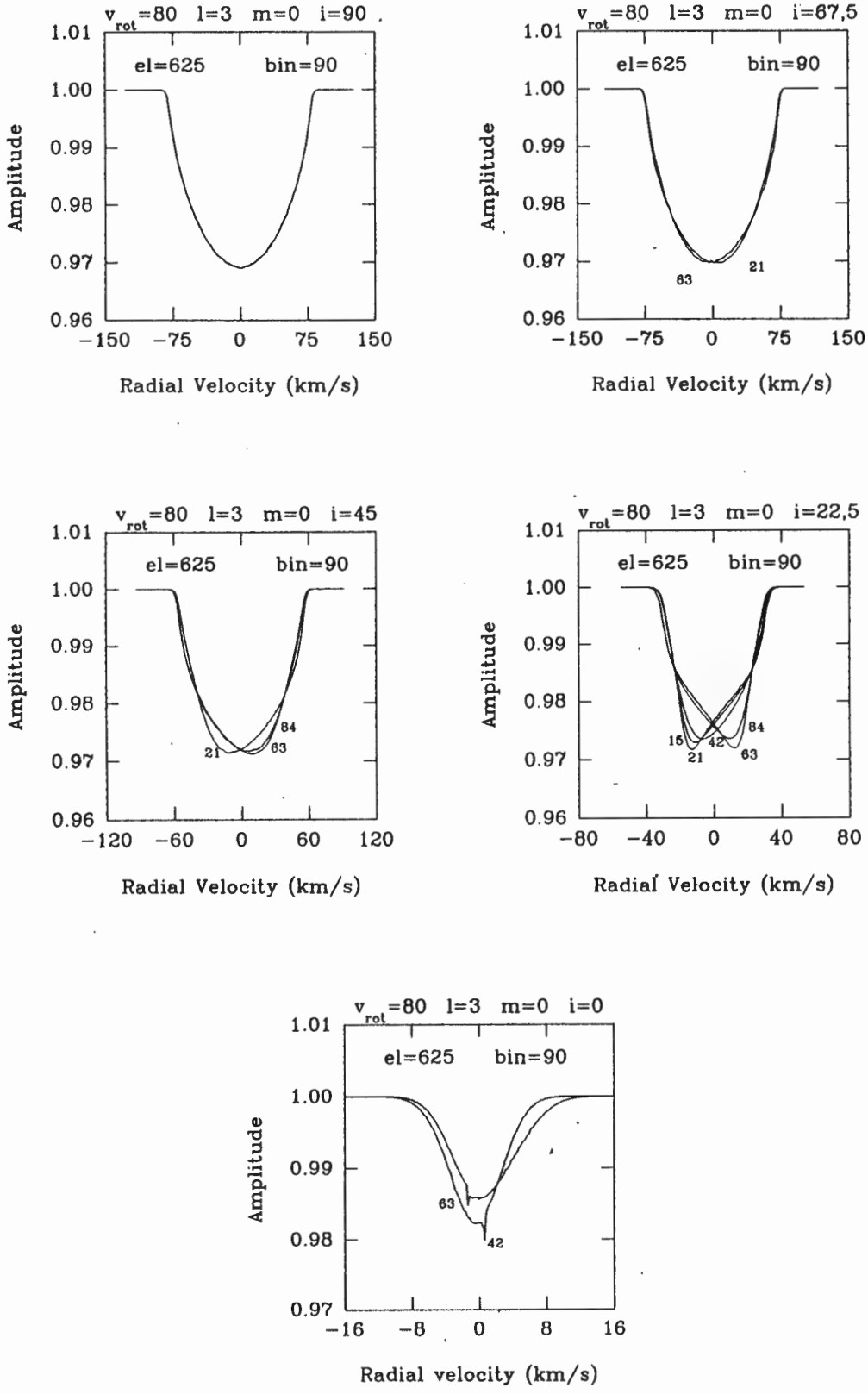
v rot =80 l=3 m=0 i=90
el=625 bin=90
Amplitude
Radial Velocity (km/s)
v rot =80 l=3 m=0 i=67,5
el=625 bin=90
63
21
Amplitude
Radial Velocity (km/s)
v rot =80 l=3 m=0 i=45
el=625 bin=90
84
21
63
Amplitude
Radial Velocity (km/s)
v rot =80 l=3 m=0 i=22,5
el=625 bin=90
84
15
42
21
63
Amplitude
Radial Velocity (km/s)
v rot =80 l=3 m=0 i=0
el=625 bin=90
63
42
Amplitude
Radial velocity (km/s)

Figure 9.9

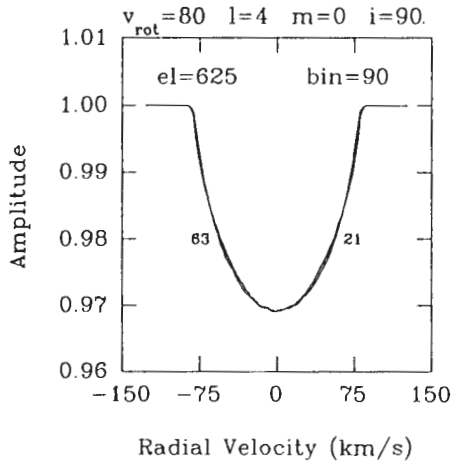
v rot =80 l=4 m=0 i=90.
el=625 bin=90
63
21
Amplitude
1.01
1.00
0.99
0.98
0.97
0.96
−150 −75 0 75 150
Radial Velocity (km/s)

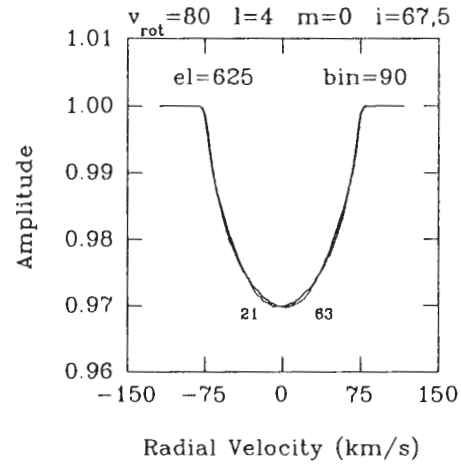
v rot =80 l=4 m=0 i=67,5
el=625 bin=90
21
63
Amplitude
1.01
1.00
0.99
0.98
0.97
0.96
−150 −75 0 75 150
Radial Velocity (km/s)

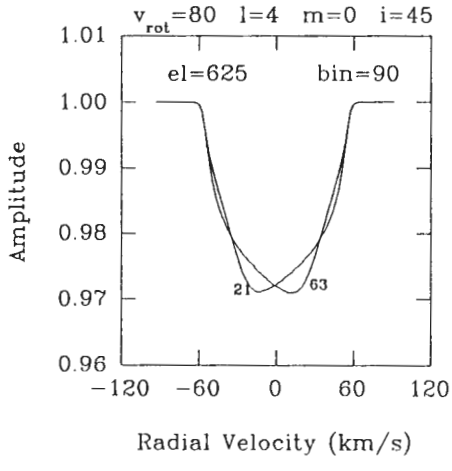
v rot =80 l=4 m=0 i=45
el=625 bin=90
21
63
Amplitude
1.01
1.00
0.99
0.98
0.97
0.96
−120 −60 0 60 120
Radial Velocity (km/s)

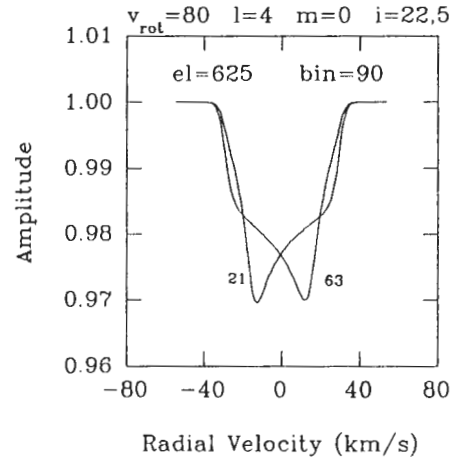
v rot =80 l=4 m=0 i=22,5
el=625 bin=90
21
63
Amplitude
1.01
1.00
0.99
0.98
0.97
0.96
−80 −40 0 40 80
Radial Velocity (km/s)

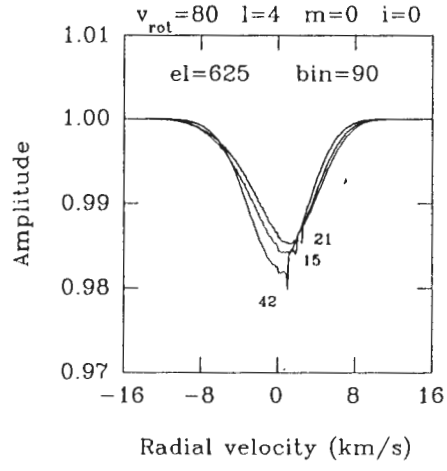
v rot =80 l=4 m=0 i=0
el=625 bin=90
21
15
42
Amplitude
1.01
1.00
0.99
0.98
0.97
−16 −8 0 8 16
Radial velocity (km/s)

Figure 9.10

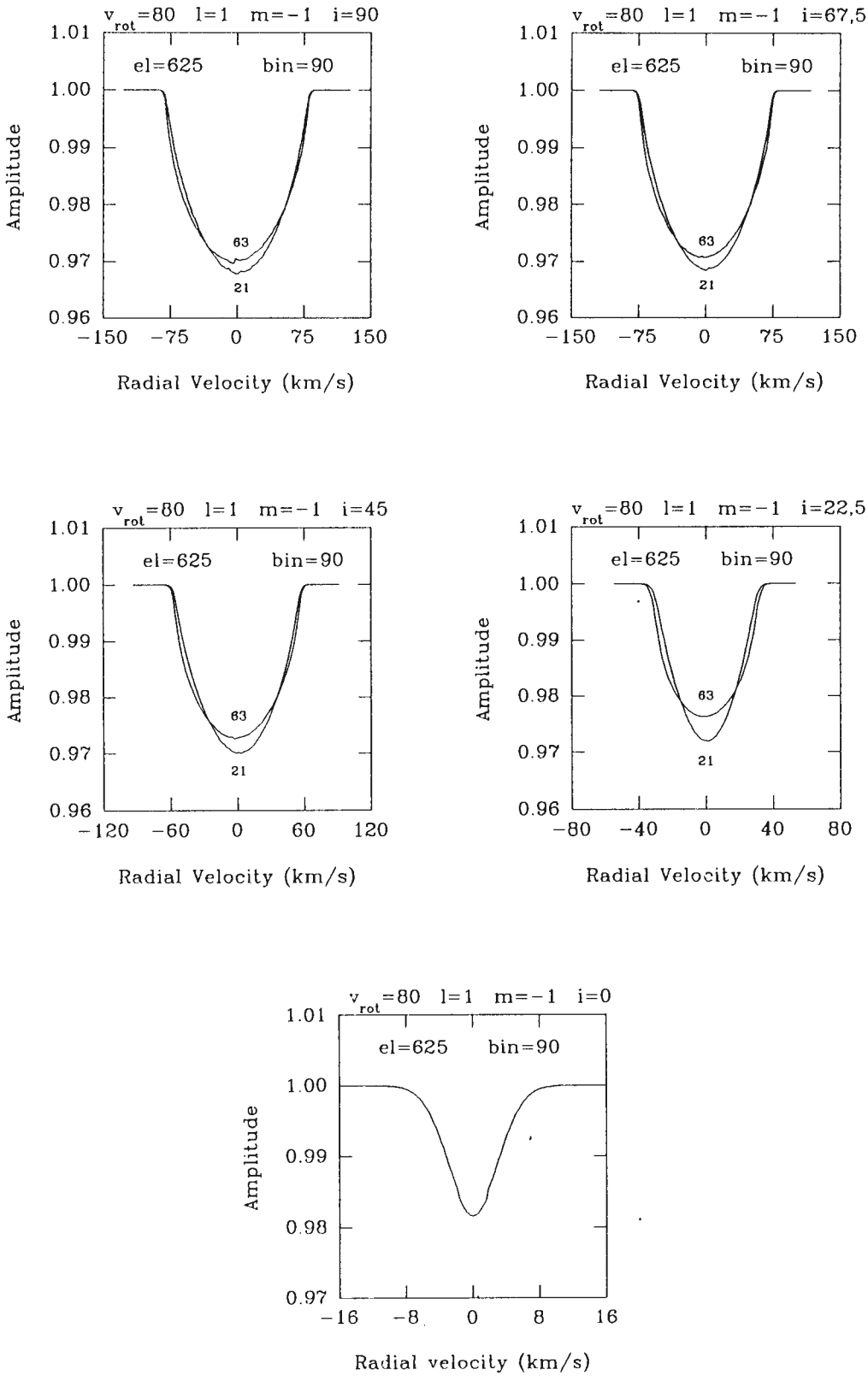
v rot =80 l=1 m=-1 i=90
el=625 bin=90
63
21
Amplitude
Radial Velocity (km/s)
v rot =80 l=1 m=-1 i=67,5
el=625 bin=90
63
21
Amplitude
Radial Velocity (km/s)
v rot =80 l=1 m=-1 i=45
el=625 bin=90
63
21
Amplitude
Radial Velocity (km/s)
v rot =80 l=1 m=-1 i=22,5
el=625 bin=90
63
21
Amplitude
Radial Velocity (km/s)
v rot =80 l=1 m=-1 i=0
el=625 bin=90
Amplitude
Radial velocity (km/s)

Figure 9.11

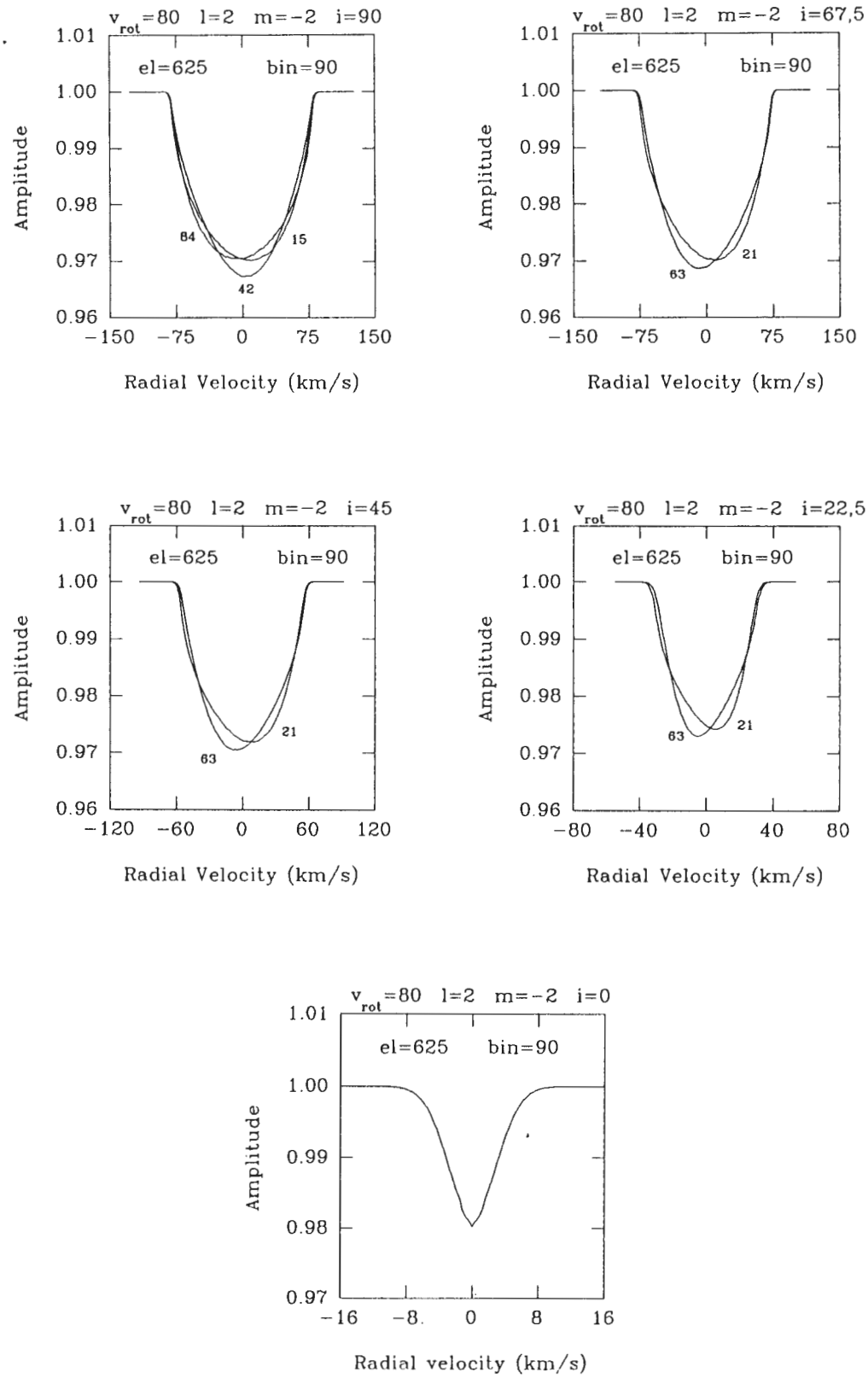
v_rot=80 l=2 m=-2 i=90
el=625 bin=90
84
15
42
v_rot=80 l=2 m=-2 i=67,5
el=625 bin=90
21
63
v_rot=80 l=2 m=-2 i=45
el=625 bin=90
21
63
v_rot=80 l=2 m=-2 i=22,5
el=625 bin=90
21
63
v_rot=80 l=2 m=-2 i=0
el=625 bin=90
Amplitude
Radial Velocity (km/s)
Radial velocity (km/s)

Figure 9.12

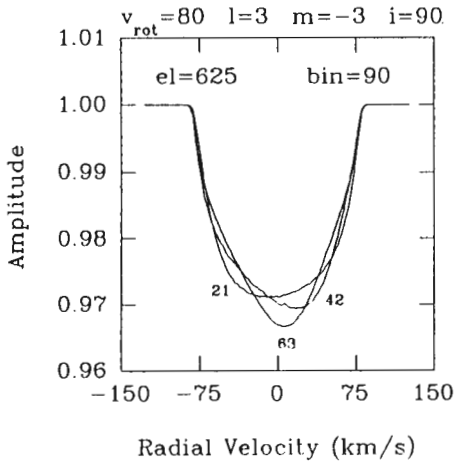
v rot =80 l=3 m=-3 i=90
el=625 bin=90
21
42
63
Amplitude
1.01
1.00
0.99
0.98
0.97
0.96
-150 -75 0 75 150
Radial Velocity (km/s)

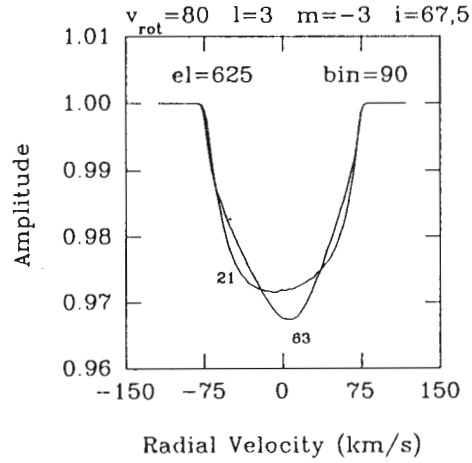
v rot =80 l=3 m=-3 i=67,5
el=625 bin=90
21
63
Amplitude
1.01
1.00
0.99
0.98
0.97
0.96
-150 -75 0 75 150
Radial Velocity (km/s)

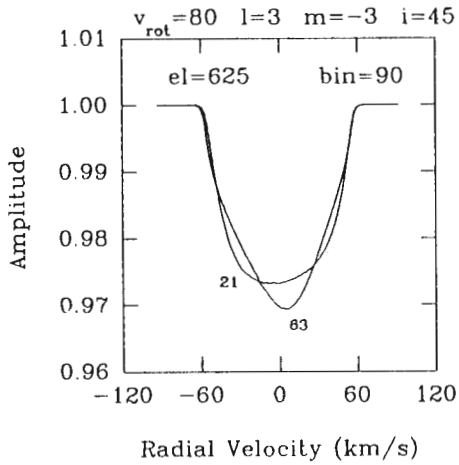
v rot =80 l=3 m=-3 i=45
el=625 bin=90
21
63
Amplitude
1.01
1.00
0.99
0.98
0.97
0.96
-120 -60 0 60 120
Radial Velocity (km/s)

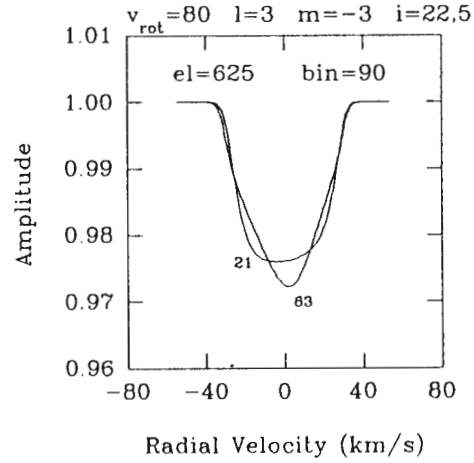
v rot =80 l=3 m=-3 i=22,5
el=625 bin=90
21
63
Amplitude
1.01
1.00
0.99
0.98
0.97
0.96
-80 -40 0 40 80
Radial Velocity (km/s)

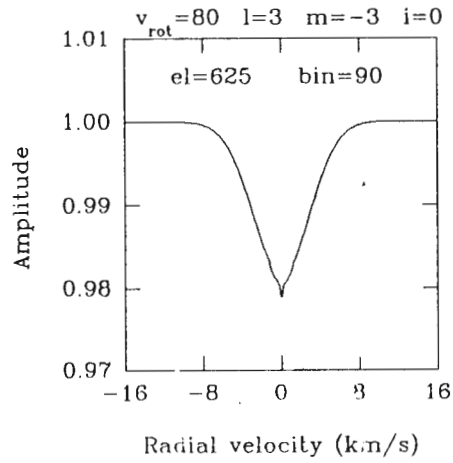
v rot =80 l=3 m=-3 i=0
el=625 bin=90
Amplitude
1.01
1.00
0.99
0.98
0.97
-16 -8 0 8 16
Radial velocity (km/s)

Figure 9.13

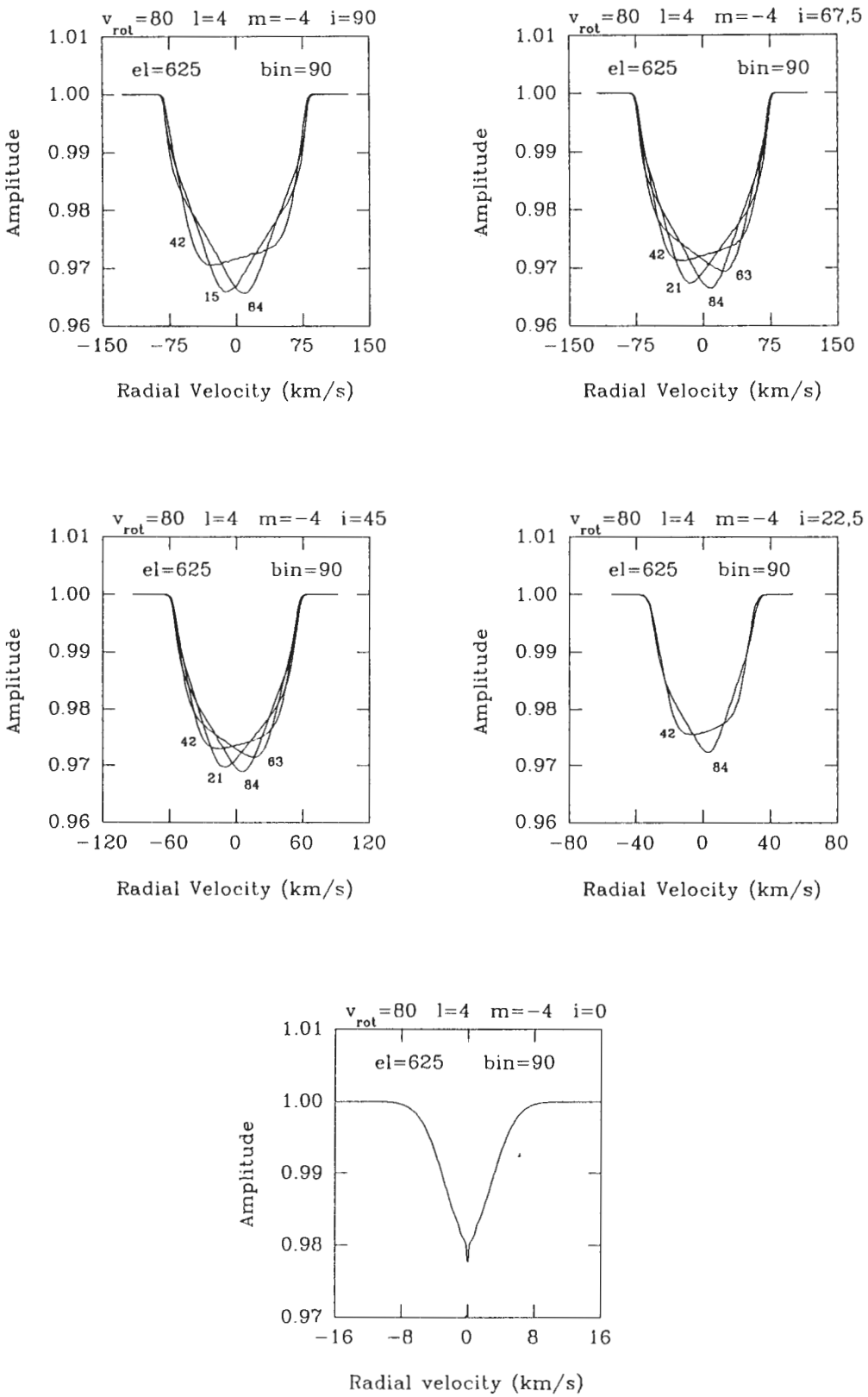
v rot =80 l=4 m=-4 i=90
el=625 bin=90
Amplitude
Radial Velocity (km/s)
v rot =80 l=4 m=-4 i=67,5
el=625 bin=90
Amplitude
Radial Velocity (km/s)
v rot =80 l=4 m=-4 i=45
el=625 bin=90
Amplitude
Radial Velocity (km/s)
v rot =80 l=4 m=-4 i=22,5
el=625 bin=90
Amplitude
Radial Velocity (km/s)
v rot =80 l=4 m=-4 i=0
el=625 bin=90
Amplitude
Radial velocity (km/s)

Figure 9.14

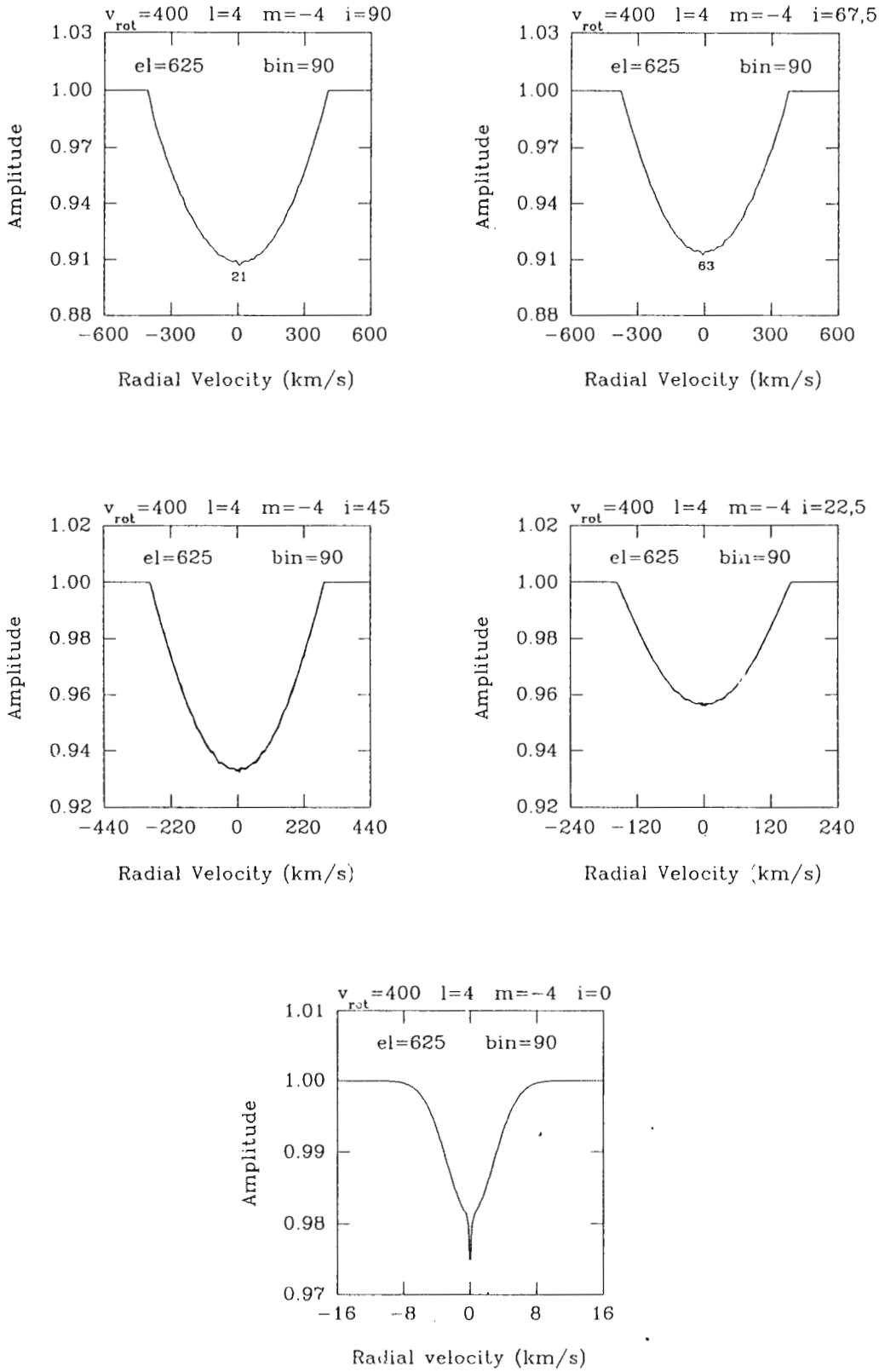
v rot =400 l=4 m=−4 i=90
el=625 bin=90
21
Amplitude
Radial Velocity (km/s)
v rot =400 l=4 m=−4 i=67,5
el=625 bin=90
63
Amplitude
Radial Velocity (km/s)
v rot =400 l=4 m=−4 i=45
el=625 bin=90
Amplitude
Radial Velocity (km/s)
v rot =400 l=4 m=−4 i=22,5
el=625 bin=90
Amplitude
Radial Velocity (km/s)
v rot =400 l=4 m=−4 i=0
el=625 bin=90
Amplitude
Radial velocity (km/s)

Figure 9.15

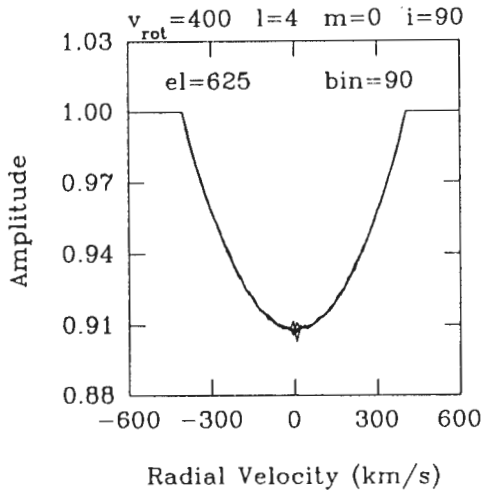
v rot =400 l=4 m=0 i=90
el=625 bin=90
Amplitude
1.03
1.00
0.97
0.94
0.91
0.88
−600 −300 0 300 600
Radial Velocity (km/s)

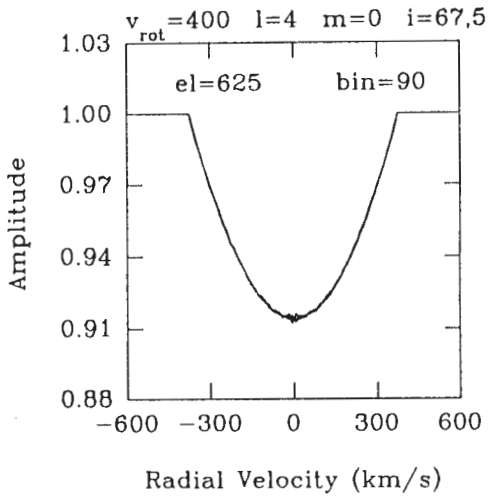
v rot =400 l=4 m=0 i=67,5
el=625 bin=90
Amplitude
1.03
1.00
0.97
0.94
0.91
0.88
−600 −300 0 300 600
Radial Velocity (km/s)

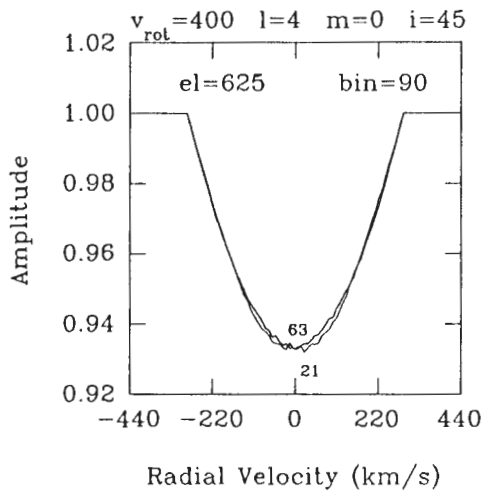
v rot =400 l=4 m=0 i=45
el=625 bin=90
Amplitude
1.02
1.00
0.98
0.96
0.94
0.92
63
21
−440 −220 0 220 440
Radial Velocity (km/s)

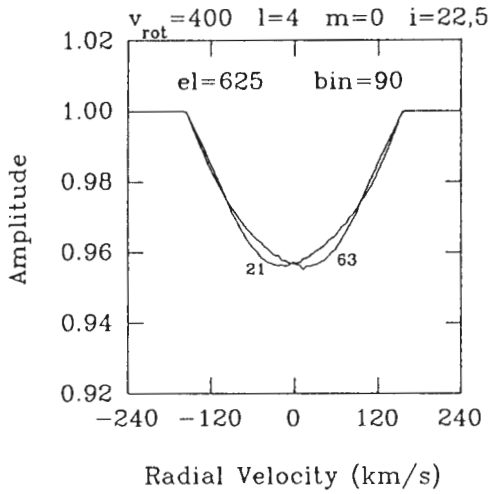
v rot =400 l=4 m=0 i=22,5
el=625 bin=90
Amplitude
1.02
1.00
0.98
0.96
0.94
0.92
21
63
−240 −120 0 120 240
Radial Velocity (km/s)

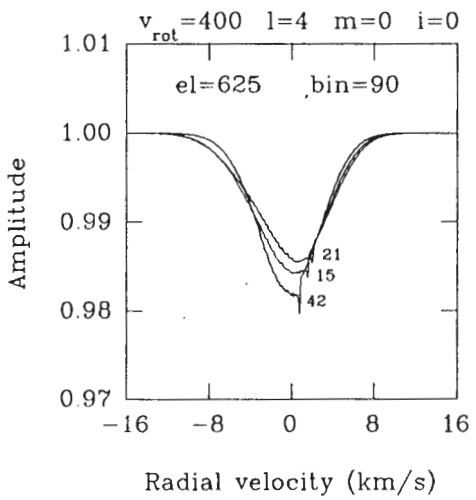
v rot =400 l=4 m=0 i=0
el=625 bin=90
Amplitude
1.01
1.00
0.99
0.98
0.97
21
15
42
−16 −8 0 8 16
Radial velocity (km/s)

Figure 9.16

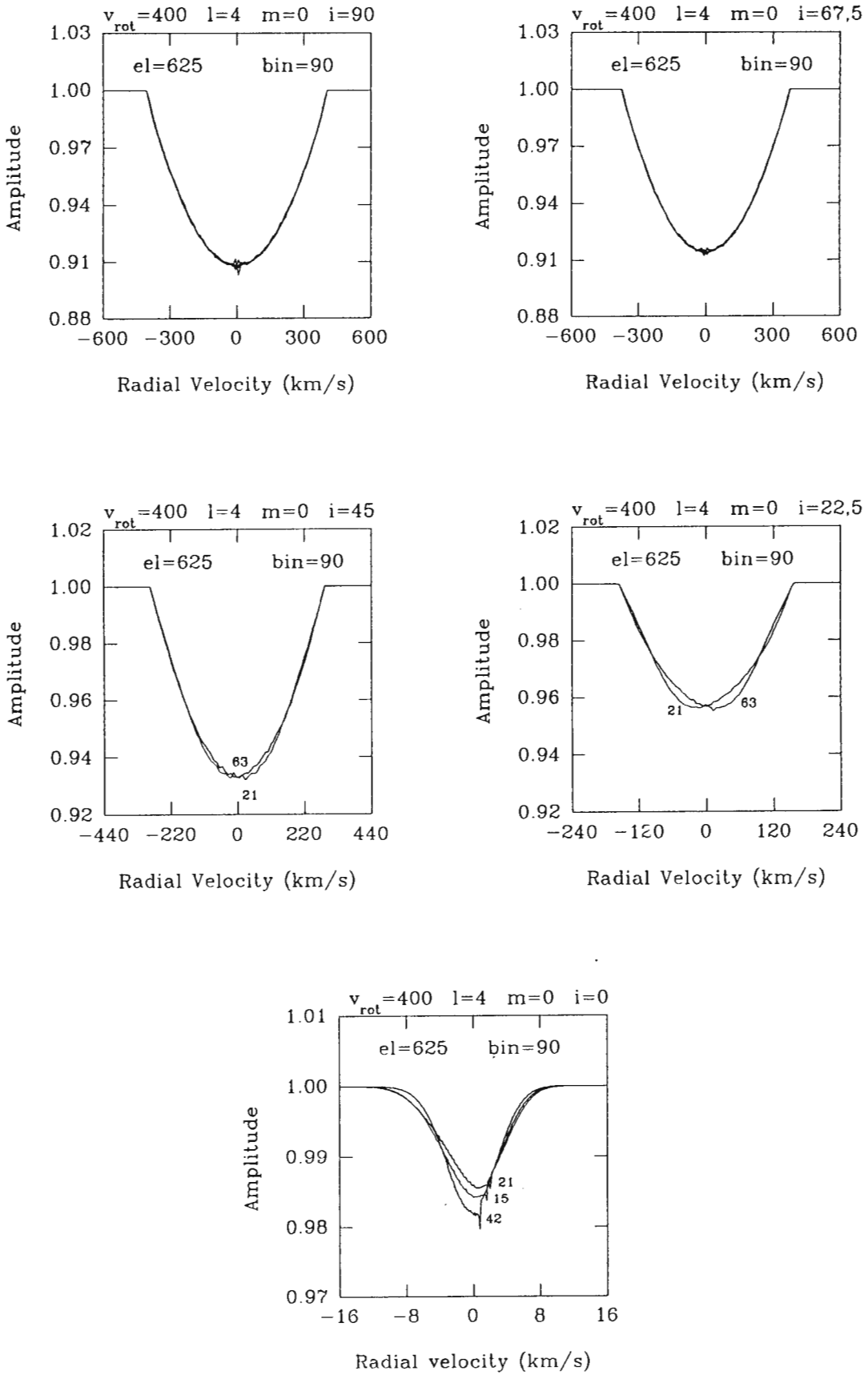
v_rot=400 l=4 m=0 i=90
el=625 bin=90
Amplitude
Radial Velocity (km/s)
v_rot=400 l=4 m=0 i=67,5
el=625 bin=90
Amplitude
Radial Velocity (km/s)
v_rot=400 l=4 m=0 i=45
el=625 bin=90
63
21
Amplitude
Radial Velocity (km/s)
v_rot=400 l=4 m=0 i=22,5
el=625 bin=90
21
63
Amplitude
Radial Velocity (km/s)
v_rot=400 l=4 m=0 i=0
el=625 bin=90
21
15
42
Amplitude
Radial velocity (km/s)

Figure 9.17

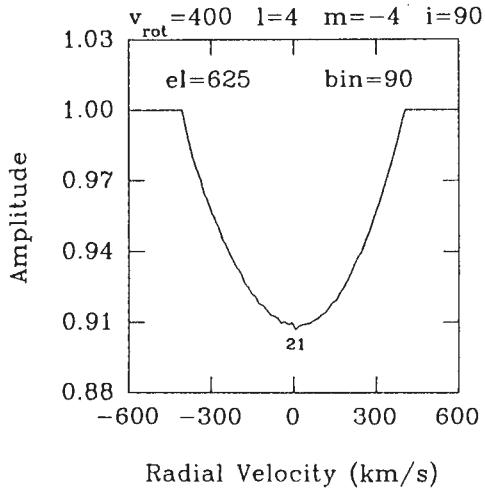
v rot =400 l=4 m=−4 i=90
el=625 bin=90
21
Amplitude
1.03
1.00
0.97
0.94
0.91
0.88
−600 −300 0 300 600
Radial Velocity (km/s)

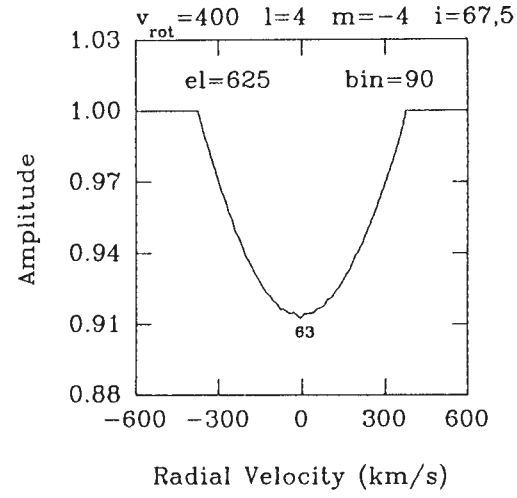
v rot =400 l=4 m=−4 i=67,5
el=625 bin=90
63
Amplitude
1.03
1.00
0.97
0.94
0.91
0.88
−600 −300 0 300 600
Radial Velocity (km/s)

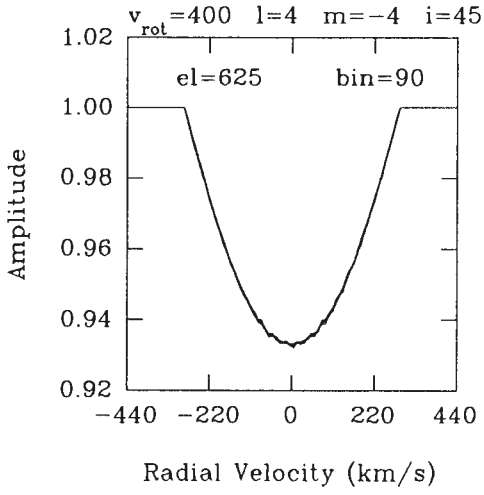
v rot =400 l=4 m=−4 i=45
el=625 bin=90
Amplitude
1.02
1.00
0.98
0.96
0.94
0.92
−440 −220 0 220 440
Radial Velocity (km/s)

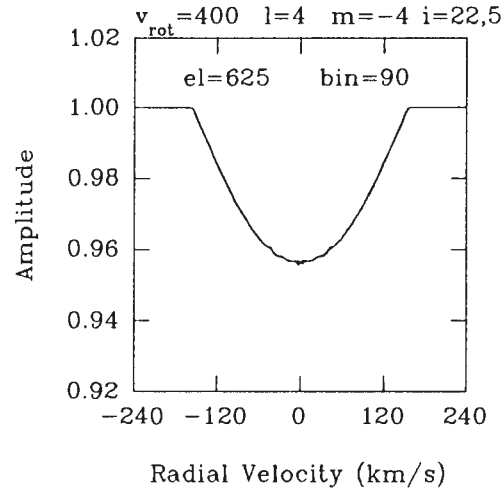
v rot =400 l=4 m=−4 i=22,5
el=625 bin=90
Amplitude
1.02
1.00
0.98
0.96
0.94
0.92
−240 −120 0 120 240
Radial Velocity (km/s)

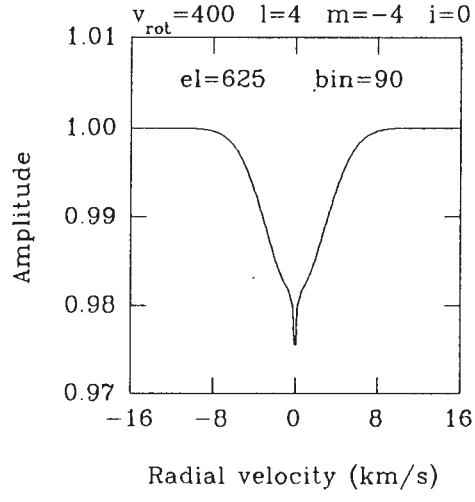
v rot =400 l=4 m=−4 i=0
el=625 bin=90
Amplitude
1.01
1.00
0.99
0.98
0.97
−16 −8 0 8 16
Radial velocity (km/s)

Figure 9.18

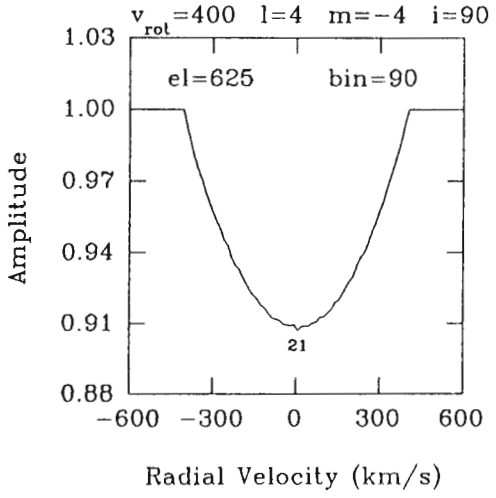
v rot =400 l=4 m=−4 i=90
el=625 bin=90
21
Amplitude
Radial Velocity (km/s)

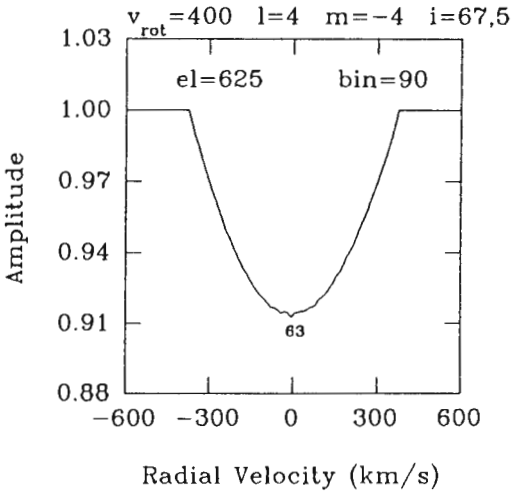
v rot =400 l=4 m=−4 i=67,5
el=625 bin=90
63
Amplitude
Radial Velocity (km/s)

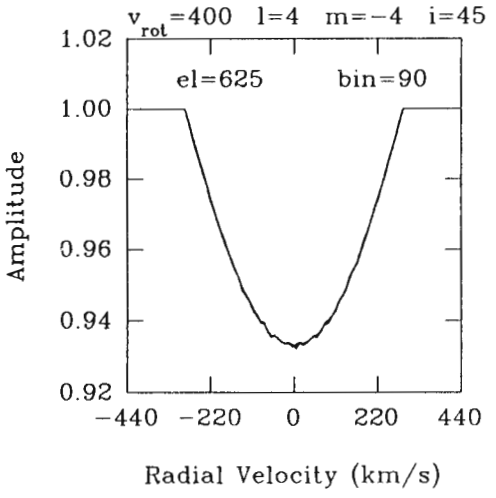
v rot =400 l=4 m=−4 i=45
el=625 bin=90
Amplitude
Radial Velocity (km/s)

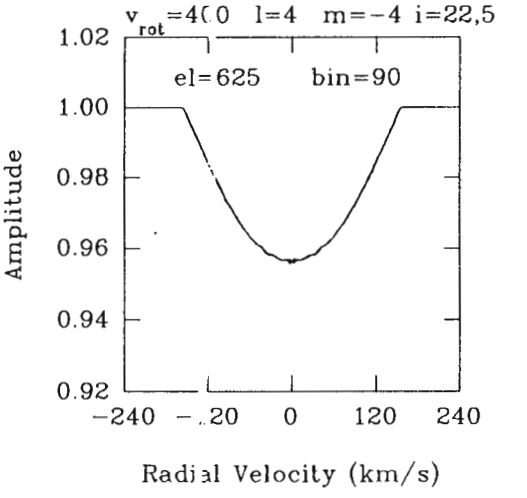
v rot =400 l=4 m=−4 i=22,5
el=625 bin=90
Amplitude
Radial Velocity (km/s)

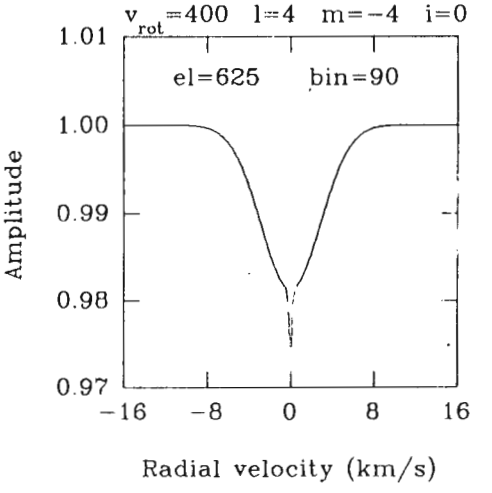
v rot =400 l=4 m=−4 i=0
el=625 bin=90
Amplitude
Radial velocity (km/s)

Figure 9.19

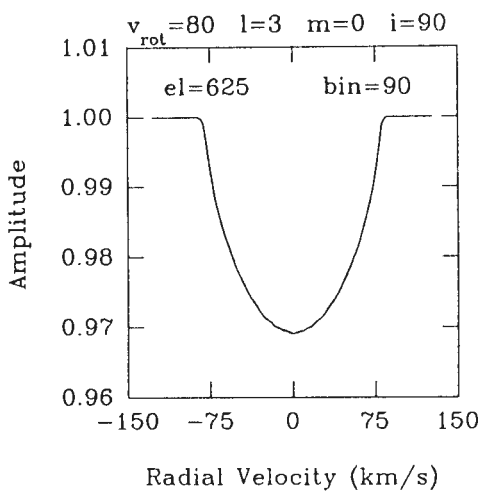
v rot =80 l=3 m=0 i=90
el=625 bin=90
Amplitude
1.01
1.00
0.99
0.98
0.97
0.96
−150 −75 0 75 150
Radial Velocity (km/s)

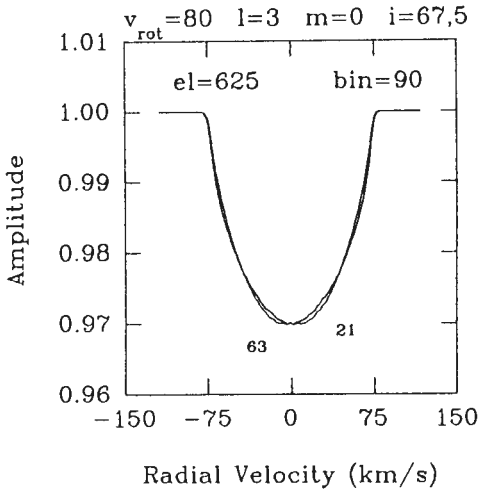
v rot =80 l=3 m=0 i=67,5
el=625 bin=90
Amplitude
1.01
1.00
0.99
0.98
0.97
0.96
63
21
−150 −75 0 75 150
Radial Velocity (km/s)

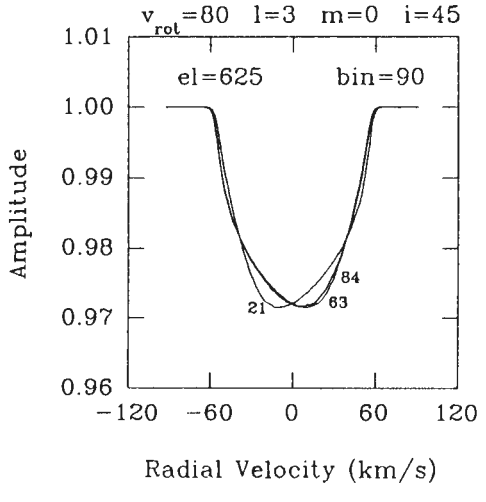
v rot =80 l=3 m=0 i=45
el=625 bin=90
Amplitude
1.01
1.00
0.99
0.98
0.97
0.96
84
21
63
−120 −60 0 60 120
Radial Velocity (km/s)

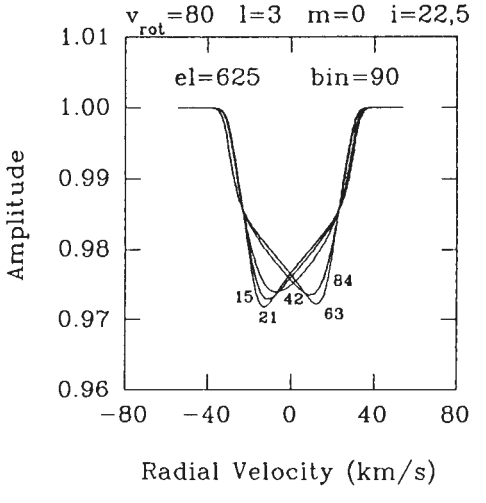
v rot =80 l=3 m=0 i=22,5
el=625 bin=90
Amplitude
1.01
1.00
0.99
0.98
0.97
0.96
15
42
84
21
63
−80 −40 0 40 80
Radial Velocity (km/s)

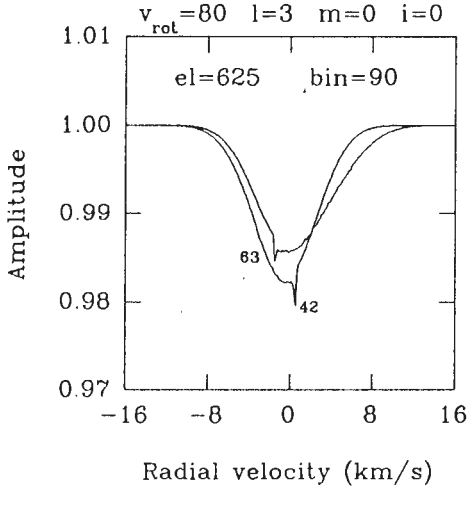
v rot =80 l=3 m=0 i=0
el=625 bin=90
Amplitude
1.01
1.00
0.99
0.98
0.97
63
42
−16 −8 0 8 16
Radial velocity (km/s)

Figure 9.20

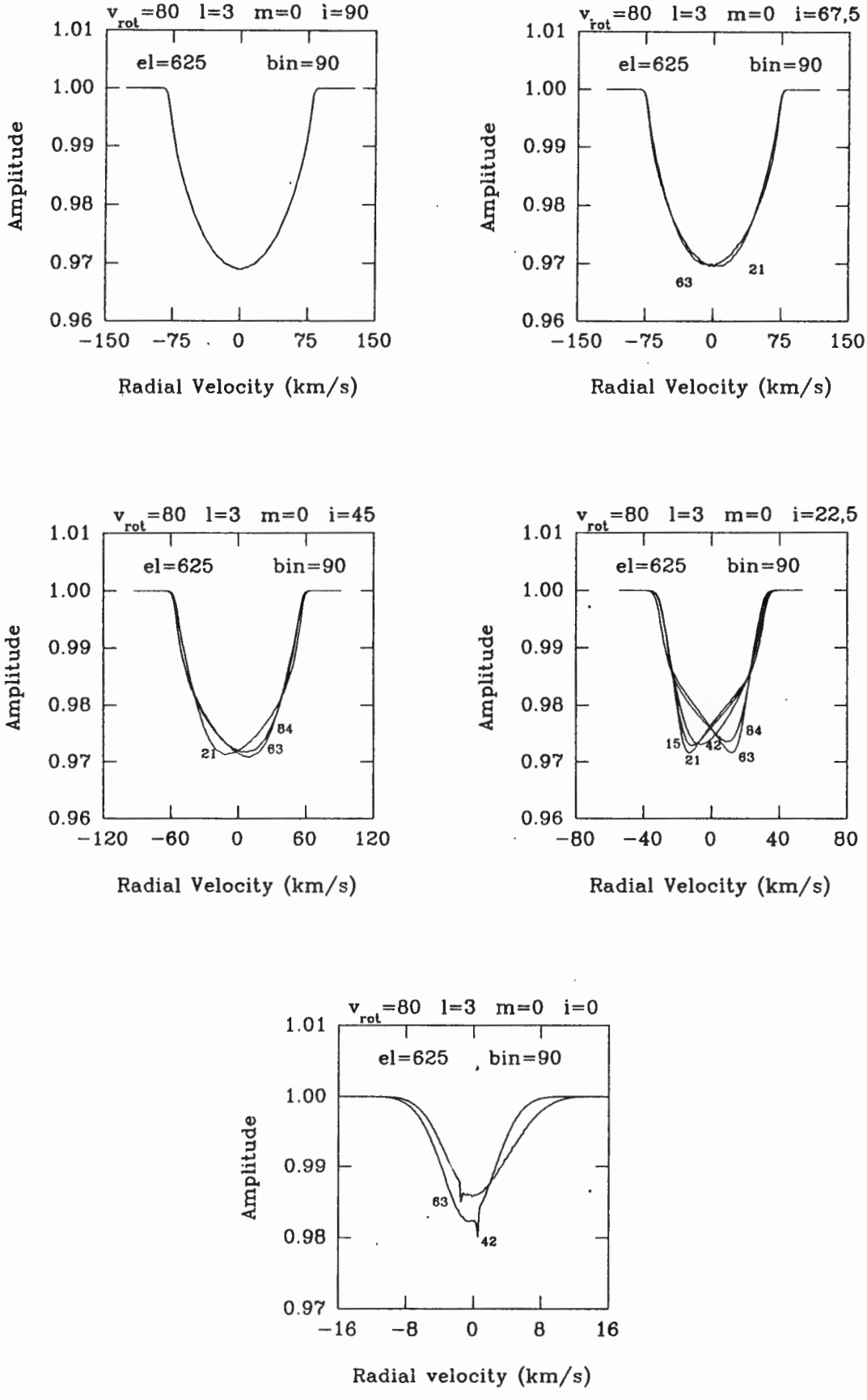
v_rot=80 l=3 m=0 i=90
el=625 bin=90
Amplitude
Radial Velocity (km/s)
v_rot=80 l=3 m=0 i=67,5
el=625 bin=90
63
21
Amplitude
Radial Velocity (km/s)
v_rot=80 l=3 m=0 i=45
el=625 bin=90
84
21
63
Amplitude
Radial Velocity (km/s)
v_rot=80 l=3 m=0 i=22,5
el=625 bin=90
15
42
84
21
63
Amplitude
Radial Velocity (km/s)
v_rot=80 l=3 m=0 i=0
el=625 bin=90
63
42
Amplitude
Radial velocity (km/s)

Figure 9.21

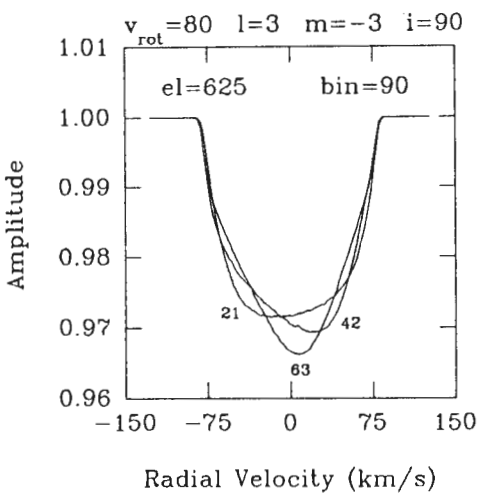
v rot =80 l=3 m=-3 i=90
el=625 bin=90
Amplitude
1.01
1.00
0.99
0.98
0.97
0.96
21
42
63
−150 −75 0 75 150
Radial Velocity (km/s)

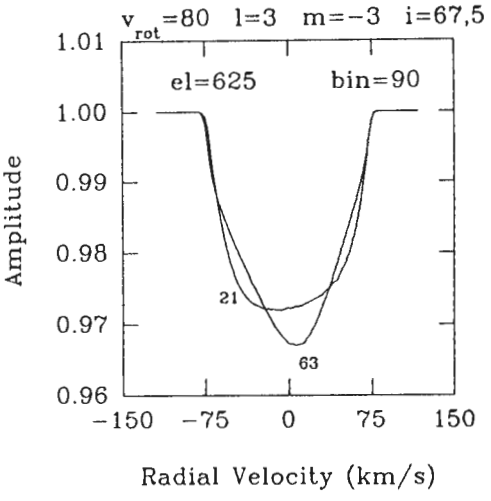
v rot =80 l=3 m=-3 i=67,5
el=625 bin=90
Amplitude
1.01
1.00
0.99
0.98
0.97
0.96
21
63
−150 −75 0 75 150
Radial Velocity (km/s)

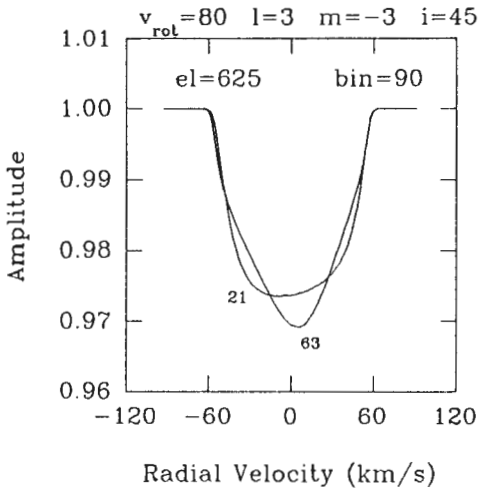
v rot =80 l=3 m=-3 i=45
el=625 bin=90
Amplitude
1.01
1.00
0.99
0.98
0.97
0.96
21
63
−120 −60 0 60 120
Radial Velocity (km/s)

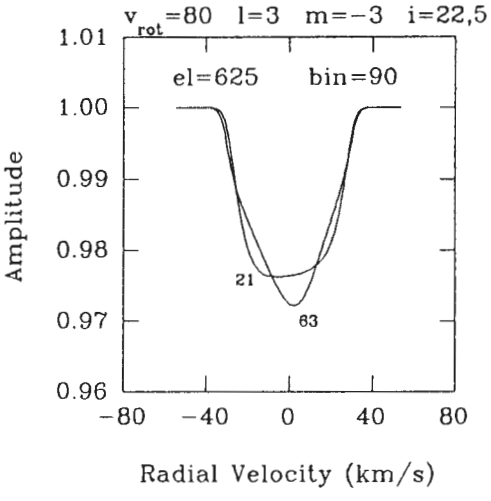
v rot =80 l=3 m=-3 i=22,5
el=625 bin=90
Amplitude
1.01
1.00
0.99
0.98
0.97
0.96
21
63
−80 −40 0 40 80
Radial Velocity (km/s)

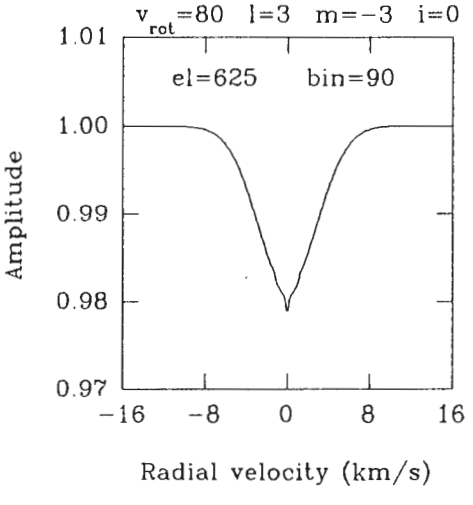
v rot =80 l=3 m=-3 i=0
el=625 bin=90
Amplitude
1.01
1.00
0.99
0.98
0.97
−16 −8 0 8 16
Radial velocity (km/s)

Figure 9.22

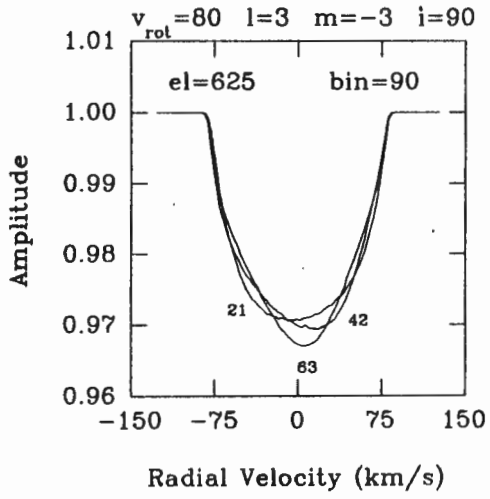
v_rot=80 l=3 m=-3 i=90
el=625 bin=90
21
42
63
Amplitude
Radial Velocity (km/s)

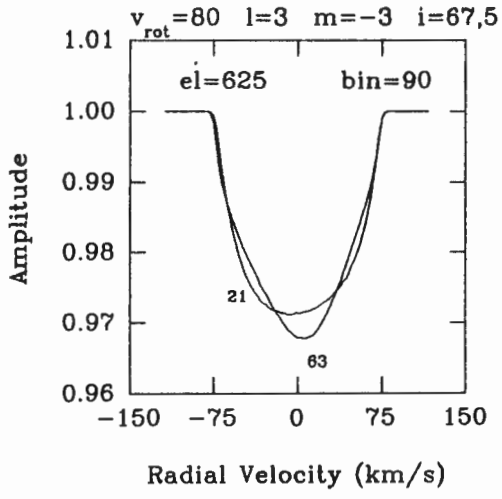
v_rot=80 l=3 m=-3 i=67,5
el=625 bin=90
21
63
Amplitude
Radial Velocity (km/s)

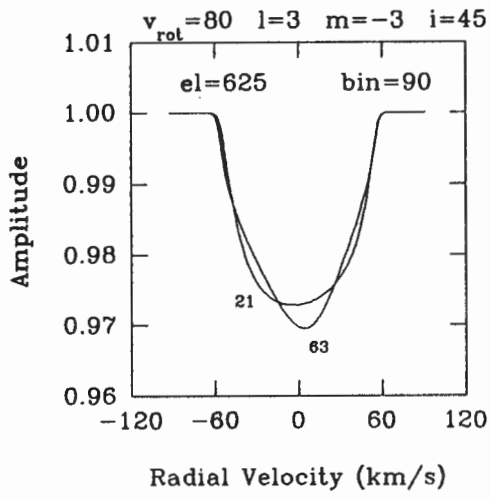
v_rot=80 l=3 m=-3 i=45
el=625 bin=90
21
63
Amplitude
Radial Velocity (km/s)

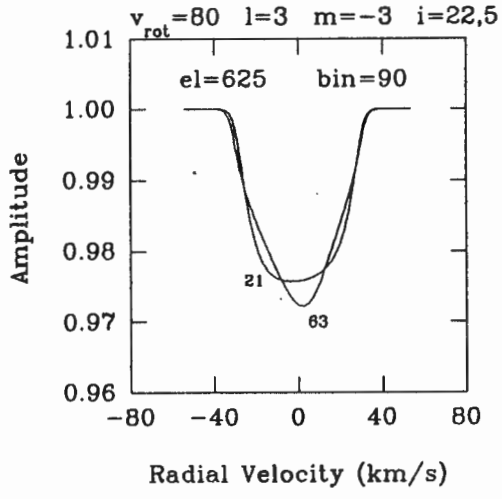
v_rot=80 l=3 m=-3 i=22,5
el=625 bin=90
21
63
Amplitude
Radial Velocity (km/s)

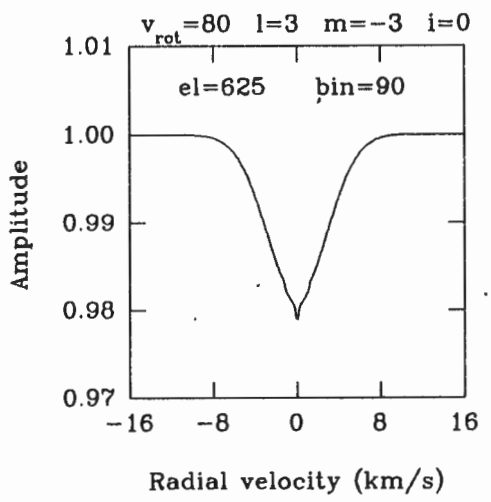
v_rot=80 l=3 m=-3 i=0
el=625 bin=90
Amplitude
Radial velocity (km/s)

Figure 9.23

CHAPTER 10

THE ECLIPSING BINARY SYSTEM CONTAINING 3293–5

As mentioned in chapter 3, one of the β Cephei stars found in NGC 3293 is also a member of an eclipsing binary system. The only other β Cephei star known to be part of such a system is 16 Lac (Jerzykiewicz et al. 1978), but it has a shallower primary eclipse than 3293–5 and does not show a secondary eclipse. After discovery of the binary nature of 3293–5, it was monitored whenever possible to obtain its binary light curve. These observations (with 3293–20 as the adopted standard – see chapter 2) were continued up to April 1984 and are tabulated in Table 10.2, at the end of this chapter.

The least–squares fit of the pulsation frequencies (see chapter 4) is superimposed on the observed light curves of 3293–5 in Figure 10.1. The fit was calculated without taking data during eclipse phase into account (to prevent distortion of the results), so that the fit on nights 5399, 5416 and other nights when eclipses were observed, shows where the light level would have been had the β Cephei star been unobscured. Data for nights on which only a few observations were obtained are not included in Figure 10.1. The Heliocentric Julian Date relative to the epoch 2440000 is indicated at the right of each curve and the time of day along the bottom of the diagram. The divisions on the vertical axis are 0.02 mag. apart. Note the eclipses on nights 5399, 5416, 5466, 5749 and 5774 (primary eclipse) and on night 5803 (secondary eclipse). The frequencies are out of phase for the last four light curves, due to the gap of more than nine months (representing over a thousand pulsation cycles) separating the bulk of the data from these last four nights, keeping in mind that the frequencies were determined from the

former nights.

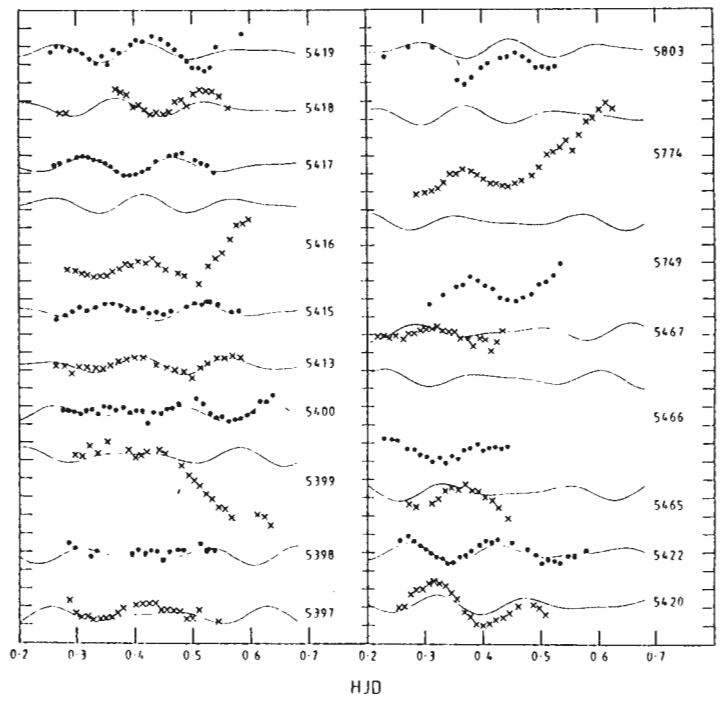

Figure 10.1. Magnitude variations of 3293–5, with Fourier fits from chapter 4 superimposed

The pulsations of the β Cephei star in the binary system are clearly visible during both primary and secondary eclipse, indicating that the companion star is the smaller of the two. The constant mean magnitude of the light curve maintained for at least a few hours on nights 5416, 5466 and 5749 indicates that the eclipse is total. A search for the orbital period was made by applying a phase dispersion minimization technique to the data, since the non–sinusoidal nature of the binary light curve is not suited to the periodogram analysis used to determine the pulsation frequencies (see chapter 4).

Phase dispersion minimization consists of dividing the phase diagram for a given period into bins and calculating the scatter of points in each bin. The most probable period

found by this method was 8.323 ± 0.001 days. IM Coulson and JW Menzies at the South African Astronomical Observatory have written a computer program based on the equations in Irwin (1962) for obtaining basic elements of eclipsing binary systems. The program requires starting values of the ratios of radii and luminosities of the components as part of an iterative procedure. These starting values were derived as follows:

Since the secondary is both the fainter and smaller of the two stars, and the cluster is very young (10–20 million years), the secondary almost certainly has a lower surface temperature than the primary. In that case, primary minimum is due to a transit of the secondary across the face of the primary. From the secondary minimum we know that the light loss due to occultation of the secondary is 0.018 mag. Hence the luminosity ratio $L_s / L_p = 0.0167$, or, using the Stefan–Boltzmann law (see equation 6.3):

$$\frac{R_s^2 \; T_s^4}{R_p^2 \; T_p^4} = 0.0167, \qquad (10.1)$$

where R and T represent the stellar radius and effective temperature respectively, and the subscripts s and p refer to the secondary and the primary star respectively. As argued above, $T_s < T_p$, so that equation 10.1 implies that

$$R_s/R_p < 0.129. \qquad (10.2)$$

Limb darkening coefficients of 0.35 for the primary and 0.40 for the secondary, corresponding to their estimated spectral types, were adopted for use in the program.

A phase diagram of the best fit to the data, prewhitened by the β Cephei pulsations, and adopting the period mentioned above, appears in Figure 10.2. Despite the prewhitening,

a considerable degree of scatter still remains. The scatter at primary light minimum is centred about a depth of 0.081 mag. If the same amount of scatter is presumed at secondary minimum, the depth thereof is 0.018 mag. The appearance of secondary minimum at phase 0.5 indicates a very low eccentricity of orbit.

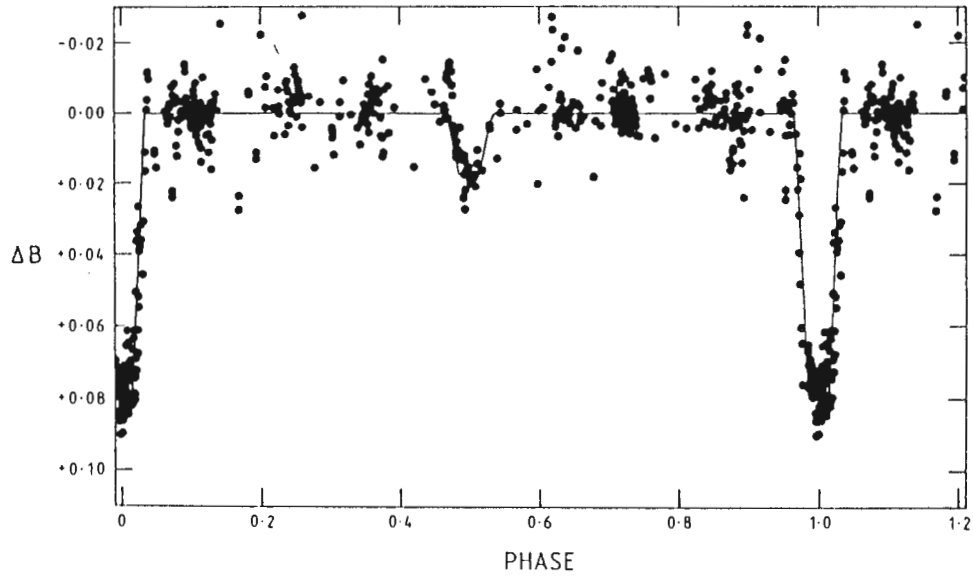

Figure 10.2. The eclipsing light curve for the binary star 3293–5

The binary elements corresponding to the fit in Figure 10.2 are listed in Table 10.1.

Table 10.1

Binary elements of 3293–5

Period	8.323 ± 0.001 days
Depth of primary eclipse	0.081 ± 0.005 mag
Depth of secondary eclipse	0.018 ± 0.005 mag
Epoch of primary eclipse	HJD 2445391.43 ± 0.02
Inclination of the orbit	$86^{\circ} \pm 1^{\circ}$
(Radius of secondary)/(separation)	0.055 ± 0.002
Ratio of radii	0.320 ± 0.005
Magnitude difference	4.5 ± 0.2 mag

The two stars are separated by almost six times the radius of the primary, which precludes tidal distortion of the stars, according to Kopal (1959).

The absolute magnitude $M_V = -3.78$ of 3293–5 and the abovementioned luminosity ratio put the absolute magnitude of the secondary at +0.69. The youth of NGC 3293 requires that the secondary is still on the main sequence, where its magnitude corresponds to spectral type B8, in agreement with the radius of $2.7R_\odot$ deduced from Tables 6.3 and 10.1.

The rotation velocity of 3293–5 quoted by Balona (1975) corresponds to a rotation period of 3.2 days, which differs substantially from the orbital period. The system is sufficiently detached that there is no problem in accommodating this. For a star viewed equator–on, the observed luminosity for certain pulsation modes remains constant throughout the pulsation cycle, due to the particular symmetry of these modes. For $\ell < 4$, these modes are the following:

$$\ell = 1 : \; m = 0$$
$$\ell = 2 : \; m = 1$$
$$\ell = 3 : \; m = 0,2$$

These modes can therefore be discarded from the identifications for 3293–5 in Table 6.5. This has a negligible effect on the histograms in Figures 6.6 and 6.7.

Spectroscopic observation of this system may lead to a direct determination of the masses and radii of the components and hence a more precise comparison with models of β Cephei stars and their pulsation frequencies. The physical quantities of 3293–5 appearing in Table 6.3 have been corrected for the effect of its companion.

Summarizing the results of this chapter:

(a) The star 3293–5 is an eclipsing binary.

(b) The companion is smaller than the β Cephei star.

(c) The eclipse is total.

(d) The orbit is circular.

(e) The system is detached by about six times the primary's radius.

(f) The components are a B1 giant (Feast 1958) and a B8 dwarf.

Table 10.2

Johnson B magnitudes of 3293–5 relative to 3293–20

The Heliocentric Julian Date is measured relative to JD2445000.0000

HJD	ΔB	HJD	ΔB	HJD	ΔB	HJD	ΔB
397.2853	0.924	400.3365	0.943	415.4487	0.945	418.4265	0.949
.2962	0.938	.3461	0.934	.4618	0.941	.4378	0.946
.3064	0.942	.3561	0.935	.4885	0.936	.4496	0.949
.3165	0.941	.3670	0.938	.5019	0.933	.4596	0.945
.3269	0.945	.3798	0.935	.5145	0.934	.4696	0.935
.3385	0.944	.3919	0.941	.5233	0.931	.4803	0.932
.3484	0.944	.4027	0.939	.5287	0.931	.4907	0.940
.3582	0.943	.4125	0.939	.5417	0.934	.5011	0.926
.3680	0.938	.4224	0.953	.5656	0.942	.5121	0.922
.3779	0.933	.4323	0.941	.5784	0.941	.5235	0.922
.3993	0.930	.4451	0.942	416.2819	1.015	.5339	0.923
.4107	0.928	.4557	0.937	.2963	1.016	.5464	0.929
.4233	0.927	.4652	0.936	.3073	1.019	.5615	0.941
.4334	0.928	.4757	0.931	.3179	1.021	419.2553	0.941
.4434	0.934	.5056	0.926	.3283	1.023	.2656	0.935
.4543	0.934	.5179	0.931	.3399	1.022	.2761	0.935
.4654	0.935	.5306	0.942	.3507	1.022	.2893	0.940
.4759	0.937	.5404	0.946	.3606	1.017	.2995	0.939
.4877	0.945	.5501	0.945	.3722	1.014	.3097	0.943
.4982	0.944	.5615	0.950	.3825	1.009	.3236	0.949
.5089	0.935	.5727	0.948	.3927	1.011	.3338	0.953
.5429	0.948	.5829	0.947	.4046	1.006	.3439	0.945
398.2841	0.929	.5939	0.944	.4161	1.008	.3541	0.955
.2945	0.934	.6048	0.940	.4287	1.003	.3641	0.938
.3222	0.943	.6155	0.928	.4393	1.009	.3744	0.942
.3322	0.938	.6270	0.929	.4524	1.015	.3937	0.932
.3938	0.940	.6381	0.922	.4744	1.019	.4037	0.928
.4041	0.936	413.2624	0.941	.4848	1.022	.4146	0.930
.4160	0.940	.2767	0.942	.5098	1.030	.4308	0.923
.4260	0.937	.2897	0.950	.5261	1.011	.4463	0.927
.4369	0.938	.3019	0.942	.5387	1.002	.4594	0.932
.4475	0.947	.3164	0.943	.5495	0.996	.4706	0.938
.4588	0.938	.3318	0.944	.5638	0.981	.4812	0.945
.4725	0.936	.3444	0.944	.5744	0.965	.4913	0.952
.4823	0.936	.3570	0.941	.5851	0.963	.5005	0.959
.5109	0.929	.3697	0.936	.5954	0.958	.5111	0.959
.5227	0.937	.3850	0.935	417.2602	0.941	.5210	0.962
.5261	0.935	.3981	0.932	.2700	0.939	.5309	0.958
.5364	0.936	.4132	0.932	.2863	0.935	.5415	0.935
399.2966	0.940	.4355	0.940	.2997	0.932	.5854	0.921
.3087	0.941	.4548	0.943	.3095	0.931	420.2543	0.944
.3216	0.929	.4679	0.946	.3194	0.932	.2642	0.943
.3355	0.938	.4841	0.948	.3292	0.934	.2747	0.930
.3529	0.925	.4973	0.954	.3388	0.936	.2846	0.925
.3892	0.934	.5111	0.944	.3487	0.938	.2948	0.924
.4010	0.943	.5239	0.939	.3586	0.942	.3059	0.918
.4107	0.940	.5403	0.933	.3685	0.947	.3153	0.916
.4204	0.937	.5537	0.933	.3811	0.952	.3250	0.918
.4423	0.934	.5666	0.930	.3911	0.951	.3348	0.921
.4525	0.938	.5803	0.931	.4014	0.951	.3450	0.928
.4803	0.952	414.3617	0.936	.4127	0.948	.3550	0.935
.4926	0.962	.3747	0.940	.4236	0.945	.3682	0.949
.5026	0.968	.3883	0.939	.4364	0.936	.3784	0.954
.5124	0.974	.4018	0.937	.4597	0.930	.3888	0.962
.5227	0.983	415.2631	0.951	.4713	0.928	.4006	0.964
.5331	0.989	.2783	0.946	.4813	0.927	.4117	0.962
.5442	0.998	.2908	0.942	.5039	0.934	.4226	0.958
.5559	0.999	.3032	0.937	.5144	0.939	.4349	0.955
.5666	1.008	.3169	0.941	.5249	0.941	.4458	0.950
.6112	1.005	.3309	0.937	.5355	0.949	.4612	0.943
.6234	1.008	.3473	0.934	418.2701	0.948	.4871	0.941
.6344	1.017	.3607	0.933	.2818	0.947	.4976	0.945
400.2757	0.938	.3742	0.936	.3667	0.921	.5080	0.952
.2855	0.940	.3858	0.941	.3769	0.924	422.2575	0.928
.2955	0.941	.3983	0.942	.3865	0.927	.2713	0.924
.3061	0.943	.4115	0.938	.3969	0.941	.2816	0.929
.3158	0.939	.4232	0.944	.4069	0.938	.2914	0.934
.3257	0.938	.4363	0.943	.4169	0.944	.3006	0.938

Table 10.2 (continued):

HJD	ΔB	HJD	ΔB	HJD	ΔB	HJD	ΔB
422.3099	0.942	467.3308	0.939	741.4261	0.951	775.2555	0.952
.3200	0.947	.3408	0.940	743.3843	0.935	.4765	0.909
.3295	0.948	.3515	0.941	745.3191	0.948	776.2561	0.948
.3389	0.953	.3613	0.948	746.3084	0.946	.4587	0.918
.3484	0.952	.3735	0.950	.3090	0.946	.6162	0.966
.3598	0.946	.3834	0.957	.4586	0.930	777.3088	0.943
.3696	0.944	.3950	0.948	.4592	0.930	.4237	0.920
.3797	0.939	.4046	0.950	.6404	0.961	779.2639	0.963
.3938	0.933	.4143	0.962	747.3221	0.946	.2957	0.942
.4051	0.929	.4242	0.952	.4954	0.937	.4353	0.931
.4153	0.930	.4338	0.940	.6289	0.943	.5965	0.926
.4253	0.927	522.2431	0.940	748.3081	0.940	801.2930	0.938
.4501	0.930	.2454	0.942	.4752	0.910	802.2570	0.925
.4764	0.938	524.2076	0.962	.6376	0.937	.4619	0.956
.4909	0.944	.2103	0.960	749.3078	1.034	.5346	0.933
.5016	0.953	.2143	0.945	.3316	1.024	803.2307	0.950
.5120	0.949	.2465	0.942	.3543	1.015	.2730	0.939
.5239	0.951	525.2077	0.962	.3661	1.013	.3146	0.939
.5339	0.952	.2114	0.963	.3779	1.004	.3572	0.975
.5476	0.946	.2545	0.947	.3919	1.008	.3699	0.979
.5580	0.946	526.2109	0.955	.4048	1.013	.3817	0.973
.5787	0.939	.2148	0.957	.4177	1.017	.3987	0.962
460.2531	0.939	527.2120	0.939	.4301	1.027	.4100	0.957
463.2600	0.942	.2146	0.935	.4426	1.030	.4321	0.951
465.2717	0.955	532.1987	0.926	.4577	1.031	.4432	0.950
.2841	0.958	533.2292	0.936	.4699	1.027	.4579	0.945
.3112	0.955	679.5623	0.917	.4849	1.022	.4707	0.950
.3227	0.950	.5648	0.921	.4973	1.012	.4819	0.954
.3343	0.941	681.5742	0.940	.5101	1.009	.4928	0.961
.3455	0.937	.5748	0.944	.5227	1.002	.5042	0.960
.3569	0.940	682.5333	0.952	.5351	0.989	.5153	0.962
.3688	0.934	683.5599	0.936	750.3017	0.929	.5264	0.960
.3810	0.941	684.5701	0.953	751.3123	0.921	804.2326	0.932
.3921	0.942	686.4483	0.929	.4584	0.930	.2995	0.941
.4033	0.948	687.4638	0.939	773.2557	0.954	.3806	0.931
.4154	0.951	.4668	0.933	.2563	0.954	.4579	0.947
.4268	0.959	.5867	0.947	.4583	0.918	.5226	0.913
.4433	0.971	688.4614	0.944	.5981	0.928	805.2500	0.925
466.2287	1.008	.4628	0.952	774.2855	1.029	.3264	0.953
.2431	1.009	.5630	0.922	.3002	1.027	.4107	0.931
.2527	1.010	691.4651	0.957	.3117	1.024	.4990	0.939
.2692	1.019	.4656	0.958	.3224	1.022	806.2264	0.953
.2818	1.020	692.4720	0.965	.3327	1.015	807.3707	0.943
.2920	1.025	.4726	0.961	.3431	1.006	.4645	1.011
.3031	1.027	.5862	0.935	.3537	1.006	.4771	1.011
.3130	1.033	.5867	0.934	.3658	1.001	.4923	1.009
.3252	1.029	693.5875	0.946	.3800	1.003	.5035	1.005
.3356	1.034	.5881	0.947	.3908	1.007	.5150	1.008
.3462	1.026	.5927	0.949	.4017	1.011	.5267	1.008
.3568	1.030	695.4616	0.939	.4137	1.016	808.2355	0.925
.3674	1.020	.4623	0.941	.4243	1.016	.3140	0.949
.3775	1.018	.5899	0.942	.4349	1.019	.3998	0.930
.3908	1.014	.5905	0.940	.4452	1.020	.4774	0.952
.4009	1.020	706.4389	0.933	.4566	1.016	809.2528	0.924
.4104	1.018	.4395	0.929	.4670	1.013	.3293	0.923
.4208	1.017	708.4251	0.938	.4857	1.008	.4085	0.947
.4319	1.018	.5809	0.934	.4979	0.999	.4867	0.934
.4422	1.016	.5814	0.932	.5123	0.984	810.2527	0.936
467.2177	0.946	709.4327	0.936	.5228	0.981	.3387	0.935
.2284	0.945	.4333	0.942	.5337	0.976	.4197	0.950
.2383	0.948	.5863	0.946	.5447	0.969	.4936	0.940
.2491	0.945	.5869	0.941	.5560	0.980	811.2333	0.924
.2618	0.949	718.5827	0.952	.5672	0.963	.3429	0.949
.2713	0.943	719.5354	0.964	.5797	0.948	.4018	0.936
.2810	0.943	720.5317	0.952	.5908	0.944	.4519	0.938
.2914	0.939	722.4096	0.946	.6018	0.934	.4970	0.949
.3018	0.938	723.5654	0.953	.6137	0.928	813.2513	0.943
.3114	0.937	739.4348	0.935	.6252	0.934	.3345	0.931
.3207	0.935	740.4265	0.957	775.2549	0.948		

CHAPTER 11

SUMMARY AND DISCUSSION

The main results described in the previous chapters were the following:

(a) All ten β Cephei stars in NGC 3293 are multiperiodic. Forty per cent (3293–10, 3293–11, 3293–18 and 3293–24) show four or more periods, thirty per cent (3293–5, 3293–14 and 3293–23) show three and thirty per cent (3293–16, 3293–27 and 3293–65) show two periods. This is contrary to the general belief for β Cephei stars as a whole, where only 50 per cent are thought to be multiperiodic. More precise observations of the classical β Cephei stars, coupled with Fourier analysis techniques, may reveal other pulsation frequencies than those already identified.

(b) Although the Fourier analysis applied to the ten stars in this study apparently revealed the pulsation **frequencies** accurately, the pulsation **amplitudes** determined by this analysis do not match the observations for 3293–10, 3293–16 and 3293–65 on a number of occasions. This is especially true of 3293–10. This star possibly undergoes irregular fluctuations in its pulsation amplitude. Furthermore, 3293–18 shows indications of irregular fluctuations in its pulsation **frequencies**.

(c) Star 3293–5 was identified as an eclipsing binary, while 3293–23 showed strong signs of being one as well. Shobbrook (1985) has stated that 3293–27 could be an almost equal component binary – if so, the mode assignment best describing the observed pulsation frequencies of this star would change. Statistically, two more of the ten stars

studied could be expected to be binaries (since approximately 50 % of all known stars are) – if this is so, and the components are roughly equal, the distribution of possible pulsation modes and overtones would be different to that found here, with a shift towards lower overtones. Shobbrook (1985) found no other candidates for significantly similar component binaries among nine (3293–65 was not considered) of these ten stars, however.

(d) The **dominant** frequencies in 3293–10 and 3293–11 respectively clearly changed within a matter of weeks, although the frequencies themselves did not change.

(e) The eigenfrequencies found for these stars fall into two groups, corresponding to the theoretical eigenfrequencies of model β Cephei stars for the ($\ell = 2$) p_1 and p_2 modes. The more massive 50 % of the stars have frequencies corresponding to both p_1 and p_2 modes, while the less massive stars show only p_1 modes, with one exception. (The apparently least massive star shows only a higher overtone mode. However, there is evidence that this star is peculiar). For an envelope mechanism, this overtone distribution implies that the more massive stars, being less condensed, can be excited in the second overtone while the less massive stars fail to do so, possibly being too compact. The results therefore agree very well with what is expected for quadrupole first and second overtone pressure modes, although the case is not closed.

(f) Rotational splitting of pulsation frequencies appears in most, if not all of the stars. Subject to the qualifications mentioned in chapter 6, application of the theory of rotational frequency splitting indicates that quadrupole and octopole modes are the most common in the ten stars studied here. First overtone pulsation is much more common than any other overtone, while second overtone pulsation also occurs to a significant degree. No mass dependence in the degree ℓ is evident from the results of the

rotational splitting study, but a trend may be present for the overtone. Second overtone pulsation was only seen in the mode assignments of the stars at the higher end of the mass spectrum (excepting 3293–65), while fundamental mode pulsation occured in the mode assignments of stars in the middle range in mass. These conclusions correspond with those in the previous paragraph. This does not mean that quadrupole and octopole modes are **exclusively** present. Results for 3293–27 are best accommodated by other degrees ℓ of the pulsation. Neither is first overtone pulsation exclusively present, 3293–65 and 3293–27 being the exceptions in this case.

(g) It is possible to accomodate the results for all ten stars within the hypothesis that each star is pulsating in only one overtone, although this need not be the same overtone for all of the stars.

(h) The degree to which differential rotation is present in these stars will determine to what extent the results of section 6.3 are correct. The same program which was used to calculate which modes correspond to the observed rotational splitting can be used with adjusted values for the theoretical magnitude of the splitting if the extent of differential rotation could be established.

(i) Pulsation mode identification by comparison of amplitudes of light and velocity variation (A_v and A_B respectively) appears to be impossible when $A_v / A_B < 150$ km/s/mag, due to the lack of differentiation between ratios for different modes. Above this value, some success may be achieved for rotation velocities below 250 km/s. However, the ratios may be usefully applied to determine rotation velocities or inclination angles when the mode has already been identified.

(j) The effect of rotational distortion definitely needs to be taken into account, at least

to first order, if accurate determinations are to be made by the amplitude ratio method, and the diagnostic utility of this method is greater than would have appeared to be the case if the rotational distortion was ignored.

(k) Spectral line profiles calculated for models which do not take rotational distortion into account can be at least 25% broader than the corresponding profiles for appropriately distorted models. It is obviously essential that this distortion is taken into account when any quantitative conclusions are to be made from the analysis of such profiles, at least when rotation velocities exceed 250 km/s. The magnitude of this effect indicates that there are observed B stars rotating at their break–up velocities of approximately 600 km/s.

(l) Line profiles show the potential to be very useful instruments for mode identification. Further development of this method is required (see (p) below). Alternatively, profiles could also be used to determine rotation velocities and/or inclination angles of pulsating stars.

(m) The relationship between the changes in flux and the changes in radius at the stellar surface, due to pulsation and rotation, has a significant effect on the ratios between the observed variations in light and velocity. A good estimate of this relationship is necessary if quantitative conclusions are to be made on the basis of these ratios.

Suggestions for advancing the work discussed in the previous chapters include the following:

(n) Spectroscopic observations of the ten β Cephei stars in NGC 3293 could allow for the true pulsation modes of these stars to be pinned down more precisely, by comparing

observations with the predicted results discussed in chapters 8 and 9.

(o) In view of the large number of β Cephei stars pulsating in more than one mode, the light curves, velocity curves and line profiles of multimode β Cephei models should also be investigated.

(p) The theoretical analysis developed in chapter 7 could be extended to other classes of pulsating stars, eg δ Scuti stars and variable white dwarfs.

(q) The utility of spectral line profiles as mode identifiers should be investigated by designing a structured system of profile parametrization, where quantitative values are attached to aspects such as form and degree of asymmetry, relative position of profiles as a function of phase, individual features such as bumps and spikes, etc.

REFERENCES

Aerts C., De Pauw M., Waelkens C., 1992, Astron. Astrophys., 266, 294

Aerts C., Waelkens C., 1993, Astron. Astrophys., 273, 135

Al–Naimiy H.M., 1978, Astrophys. Space Sci., 53, 181

Alfaro E.J., Delgado A.J., García–Pelayo J.M., Garrido R., Sáez M., 1985, Astron. Astrophys. Suppl. Ser., 59, 441

Ando H., 1981, Mon. Not. R. Astr. Soc., 197, 1139

Arfken G., 1985, '*Mathematical Methods for Physicists*', Academic Press, London, 3 ed

Balona L.A., 1975, Mem. R. Astr. Soc., 78, 51

Balona L.A., 1977, Mem. R. Astr. Soc., 84, 101

Balona L.A., 1983, Mon. Not. R. Astr. Soc., 203, 1041

Balona L.A., 1984, Mon. Not. R. Astr. Soc., 211, 973

Balona L.A., 1986a, Mon. Not. R. Astr. Soc., 219, 111

Balona L.A., 1986b, Mon. Not. R. Astr. Soc., 220, 647

Balona L.A., 1987, Mon. Not. R. Astr. Soc., 224, 41

Balona L.A., 1992, Mon. Not. R. Astr. Soc., 256, 425

Balona L.A., 1993, Mon. Not. R. Astr. Soc., 260, 795

Balona L.A., Engelbrecht C.A., 1981, '*Workshop on Pulsating B Stars*', eds. '*Groupe Etoiles Variables de l'Observatoire de Nice*' and Sterken C., Nice Observatory, p 195

Balona L.A., Engelbrecht C.A., 1983, Mon. Not. R. Astr. Soc., 202, 293

Balona L.A., Engelbrecht C.A., 1985, Mon. Not. R. Astr. Soc., 212, 889

Balona L.A., Feast, M.W., 1975, Mon. Not. R. Astr. Soc. 172, 191

Balona L.A., Menzies J.W., Whitelock P.A.W., 1979, '*SAAO People's Photometer Manual*', S.A. Astronomical Observatory, p 34

Balona L.A., Rozowsky J., 1991, Mon. Not. R. Astr. Soc., 251, 66P

Balona L.A., Shobbrook R.R., 1984, Mon. Not. R. Astr. Soc., 211, 375

Balona L.A., Stobie R.S., 1979a, Mon. Not. R. Astr. Soc., 187, 217

Balona L.A., Stobie R.S., 1979b, Mon. Not. R. Astr. Soc., 189, 649

Balona L.A., Stobie, R.S., 1980, Space Sci. Rev. 27, 371

Böhm–Vitense E., 1989, '*Introduction to Stellar Astrophysics*', Cambridge University Press, Cambridge, vol 2

Borisova I., Chelebiev E., Kowatschev B., 1991, '*ESO Workshop on Rapid Variability of*

OB–Stars: Nature and Diagnostic Value', ed. Baade D., European Southern Observatory, p 49
Buta R.J., Smith M.A., 1979, Ap. J., 232, 213

Campbell W.W., 1908, Lick Observatory Bull., 5, 62
Campos A.J., Smith M.A., 1980, Ap. J., 238, 250
Carroll B.W., 1981, Ph.D. thesis, University of Colorado at Boulder
Chapellier E., 1985, Astron. Astrophys., 147, 135
Chapellier E., Valtier J.C., 1992, Astron. Astrophys., 257, 587
Clement M.J., 1965, Ap. J., 141, 1443
Clement M.J., 1989, Ap. J., 339, 1022
Collins G.W., 1963, Ap. J., 138, 1134
Courant R., Hilbert D., 1953, '*Methods of Mathematical Physics*', Interscience Publishers, New York, vol 1
Cowling T.G., 1941, Mon. Not. R. Astr. Soc. 101, 367
Cox A.N., 1981, '*Workshop on Pulsating B Stars*', eds. '*Groupe Etoiles Variables de l'Observatoire de Nice*' and Sterken C., Nice Observatory, p
Cox A.N., 1987, '*Stellar Pulsation*', Proc. J.P. Cox Mem. Conf., Springer, Berlin, p 36
Cox A.N., Morgan S.M., 1990, '*Proc. Conf. Confrontation between Stellar Pulsation and Evolution*', eds. Cacciari C., Clementini G., Astron. Soc. Pacific, p 293
Cox A.N., Morgan S.M., Rogers F.J., Iglesias C.A., 1992, Ap. J., 393, 272
Cox J.P., 1980, '*Theory of Stellar Pulsation*', Princeton University Press.
Cox J.P., Giuli R.T., 1968, '*Principles of Stellar Structure*', Gordon and Breach, New York.
Cugier H., 1993, Acta Astron., 43, 27

Davey W.R., 1973, Ap. J., 179, 235
Deeming T.J., 1975, Astrophys. Space Sci., 36, 137
Delgado A.J., Alfaro E.J., 1990, Astrophys. Space Sci., 169, 117
Delgado A.J., Alfaro E.J., García–Pelayo J.M., Garrido R., Vidal S., 1984, Astron. Astrophys. Suppl. Ser., 58, 447
Delgado A.J., Alfaro E.J., García–Pelayo J.M., Garrido R., 1992, Astron. J., 103, 891
Deupree R.G., 1974, Ap. J., 190, 631
Deupree R.G., 1990, Ap. J., 357, 175
Dziembowski W., 1977, Acta Astron., 27, 203
Dziembowski W., Pamyatnykh A.A., 1993, Mon. Not. R. Astr. Soc., 262, 204

Feast M.W., 1958, Mon. Not. R. Astr. Soc., 118, 618
Frost E.B., 1902, Ap. J., 15, 340
Fullerton A.W., 1991, '*ESO Workshop on Rapid Variability of OB–Stars: Nature and Diagnostic Value*', ed. Baade D., European Southern Observatory, p 3

Gautschy A., Saio H., 1993, Mon. Not. R. Astr. Soc., 262, 213
Gies D.R., Kullavanijaya A., 1988, Ap. J., 326, 813
Goldstein H., 1950, '*Classical Mechanics*', Addison–Wesley, Reading, p 107

Hachisu I., 1986, Ap. J. Suppl. Ser., 61, 479
Hansen C.J., Cox J.P., van Horn H.M., 1977, Ap. J., 217, 151
Hansen C.J., Cox J.P., Carroll B.W., 1978, Ap. J., 226, 210
Hardorp J., Strittmatter P.A., 1968a, Ap. J. 151, 1057
Hardorp J., Strittmatter P.A., 1968b, Ap. J. 153, 465
Henroteau F., 1918, Lick Obs. Bull. 9, 173
Heynderickx D., 1991, Ph.D. thesis, Katholieke Universiteit Leuven
Hill G., 1967, Ap. J. Suppl. Ser., 14, 263

Iglesias C.A., Rogers F.J., Wilson B.G., 1987, Ap. J., 322, L45
Iglesias C.A., Rogers F.J., Wilson B.G., 1990, Ap. J., 360, 221
Iglesias C.A., Rogers F.J., Wilson B.G., 1992, Ap. J., 397, 717
Irwin J.B., 1962, '*Astronomical Techniques*', ed. Hiltner W.A., University of Chicago Press, p 584

Jakate S.M., 1978, Astron. J., 83, 1179
James R.A., 1964, Ap. J., 140, 552
Jeffreys B., 1965, Geophys. J., 10, 141
Jerzykiewicz M., 1978, Acta Astron., 28, 465
Jerzykiewicz M., 1993, Astron. Astrophys. Suppl. Ser., 97, 421
Jerzykiewicz M., Jarzebowski T., Le Contel J–M., Musielok B., 1978, Inf. Bull. Var. Stars, 1508
Jerzykiewicz M., Sterken C., 1977, Acta Astron., 27, 365
Jones D.H.P., Shobbrook R.R., 1974, Mon. Not. R. Astr. Soc., 166, 649

Kambe E., Ando H., Hirata R., 1990, Publ. Astron. Soc. Japan, 42, 687
Kambe E., Osaki Y., 1988, Publ. Astron. Soc. Japan, 40, 313

Kiriakidis M., El Eid M.F., Glatzel W., 1992, Mon. Not. R. Astr. Soc., 255, 1P
Kopal Z., 1959, '*Close Binary Systems*', John Wiley and Sons
Kubiak M., 1978, Acta Astron., 28, 153

Ledoux P., 1951, Ap. J., 114, 373
Ledoux P., Walraven T., 1958, '*Handbuch der Physik*', ed. Fluegge S., Springer, Berlin, Vol 51
Lee U., Osaki Y., 1982, Publ. Astron. Soc. Japan, 34, 39
Lee U., Jeffery C.S., Saio H., 1992, Mon. Not. R. Astr. Soc., 254, 185
Lee U., Saio H., 1990, Ap. J., 349, 570
Lesh J.R., 1981, '*Workshop on Pulsating B Stars*', eds '*Groupe Etoiles Variables de l'Observatoire de Nice*' and Sterken C., Nice Observatory, p 301
Lesh J.R., Aizenman M.L., 1974, Astron. Astrophys., 34, 203
Lesh J.R., Aizenman M.L., 1978, Ann. Rev. Astron. Astrophys., 16, 215

Margenau H., Murphy G.M., 1956, '*The Mathematics of Physics and Chemistry*', D. van Nostrand, Princeton, 2 ed.
Meyer W.F., 1934, Publ. Astron. Soc. Pacific, 46, 202
Moskalik P., Dziembowski W.A., 1992, Astron. Astrophys., 256, L5

Osaki Y., 1971, Publ. Astron. Soc. Japan, 23, 485
Osaki Y., 1974, Ap. J., 189, 469
Osaki Y., 1975, Publ. Astron. Soc. Japan, 27, 237
Osaki Y., 1982, '*Pulsations in Classical and Cataclysmic Variable Stars*', ed. Cox J.P., Joint Institute for Laboratory Astrophysics, Colorado, p 303
Percy J.R., 1970, Ap. J., 159, 177
Percy J.R., 1971, Astron. J., 76, 1105
Percy, J.R., 1981. '*Workshop on Pulsating B Stars*', eds. '*Groupe Etoiles Variables de l'Observatoire de Nice*' and Sterken C., Nice Observatory, p 119
Percy J.R., 1981, *op. cit.*, p 351
Percy J.R., Lane M.C., 1977, Astron. J., 82, 353
Percy J.R., Madore K., 1972, Astron. J., 77, 381
Peters G.J., Ogawa H.S., Judge K.S., Judge D.L., 1987, Ap. J., 314, 261

Roxburgh I.W., Griffith J.S., Sweet P.A., 1965, Z. Astrophys., 61, 203

Saio H., 1981, Ap. J., 244, 299
Saio H., Cox J.P., 1980, Ap. J., 236, 549
Scargle J.D., 1982, Ap. J., 263, 835
Selga M., 1916, Revista de la Soc. Astron. de España y América, 6, 41
Shibahashi H., Osaki Y., 1976, Publ. Astron Soc. Japan, 28, 199
Shobbrook R.R., 1979, Mon. Not. R. Astr. Soc., 189, 571
Shobbrook R.R., 1983, Mon. Not. R. Astr. Soc., 205, 1215
Shobbrook R.R., 1985, Mon. Not. R. Astr. Soc., 214, 33
Simon N.R., 1982, Ap. J., 260, L87
Slipher V.M., 1904, Ap. J., 20, 146
Smeyers P., Denis J., 1971, Astron. Astrophys., 14, 311
Smith M.A., 1981, '*Workshop on Pulsating B Stars*', eds. '*Groupe Etoiles Variables de l'Observatoire de Nice*' and Sterken C., Nice Observatory, p 317
Spiegel M.R., 1968, '*Mathematical Handbook*', McGraw–Hill, New York
Stamford P.A., Watson R.D., 1977, Mon. Not. R. Astr. Soc., 180, 551
Stamford, P.A. and Watson, R.D., 1979. '*Changing Trends in Variable Star Research*', eds. Bateson F.M., Smak J., Urch I.H., University of Waikato, Hamilton, p 504
Stebbins J., Kron G.E., 1954, Ap. J., 120, 189
Stellingwerf R.F., 1978, Astron. J., 83, 1184
Stellingwerf R.F., 1979, Ap. J., 227, 935
Sterken C., Jerzykiewicz M., 1988, Mon. Not. R. Astr. Soc., 235, 565
Sterken C., Jerzykiewicz M., 1991, '*ESO Workshop on Rapid Variability of OB–Stars: Nature and Diagnostic Value*', ed. Baade D., European Southern Observatory, p 105
Stothers R., 1976, Ap. J., 210, 434
Strittmatter P.A., 1969, Ann. Rev. Astron. Astrophys., 7, 665
Struve O., 1955, Publ. Astron. Soc. Pacific, 67, 135

Tassoul J–L., 1978, '*Theory of Rotating Stars*', Princeton University Press, Princeton
Turner D.G., Grieve G.R., Herbst W., Harris W.E., 1980, Astron. J., 85, 1193

Unno W., Osaki Y., Ando H., Shibahashi H., 1979, '*Nonradial Oscillations of Stars*', University of Tokyo Press.
Unno W., Osaki Y., Ando H., Saio H., Shibahashi H., 1989, '*Nonradial Oscillations of Stars*', University of Tokyo Press, 2 ed.

Van Hoof A., Struve O., 1953, Publ. Astron. Soc. Pacific, 65, 158
Vogt S.S., Penrod G.D., 1983, Ap. J., 275, 661

Waelkens C., Cuypers J., 1985, Astron. Astrophys., 152, 15
Waelkens C., Van den Abeele K., Van Winckel H., 1991, Astron. Astrophys., 251, 69
Walker G.A.H., Yang S., Fahlman G.G., 1979, Ap. J., 233, 199
Watson R.D., 1988, Astrophys. Space Sci., 140, 255
Young R.K., 1918, Dominion Astrophys. Obs. Publ., 1, 105

APPENDIX 1

This appendix contains the light curves of the β Cephei stars in NGC 3293, obtained as described in chapters 2 and 3. The curves are shown as they appear after being corrected for changes in atmospheric extinction during observation.

The fractional Julian Date is shown along the horizontal axis, while the Johnson B magnitude is indicated along the vertical axis. The divisions on this axis are 0.02 magnitudes apart. The Heliocentric Julian Dates of observation, relative to the epoch 2440000, appear on the right of the curves, while the name of the star appears in the top left corner.

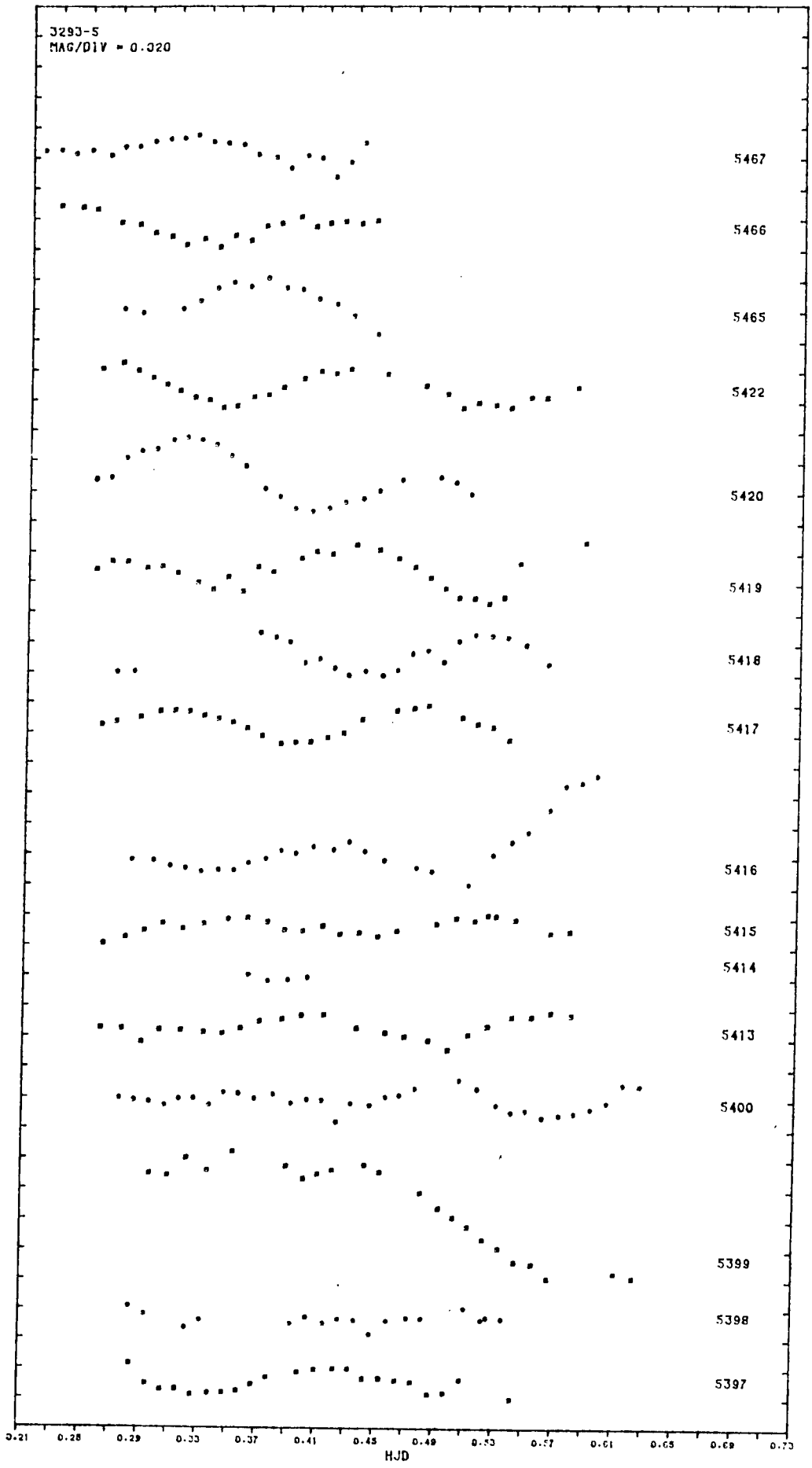
3293-5
MAG/DIV = 0.020
5467
5466
5465
5422
5420
5419
5418
5417
5416
5415
5414
5413
5400
5399
5398
5397
0.21
0.25
0.29
0.33
0.37
0.41
0.45
0.49
0.53
0.57
0.61
0.65
0.69
0.73
HJD

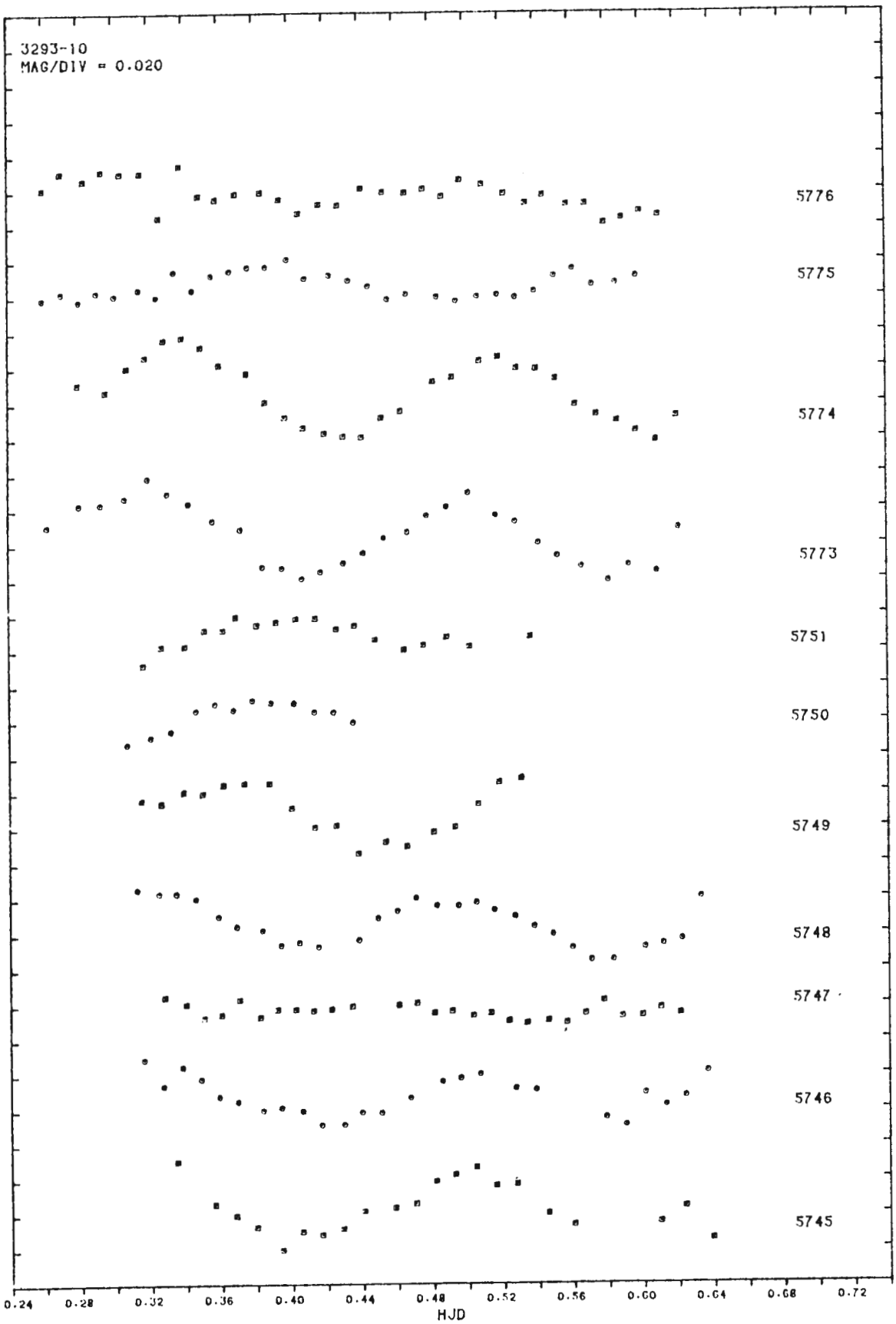
3293-10
MAG/DIV = 0.020
5776
5775
5774
5773
5751
5750
5749
5748
5747
5746
5745
0.24
0.28
0.32
0.36
0.40
0.44
0.48
0.52
0.56
0.60
0.64
0.68
0.72
HJD

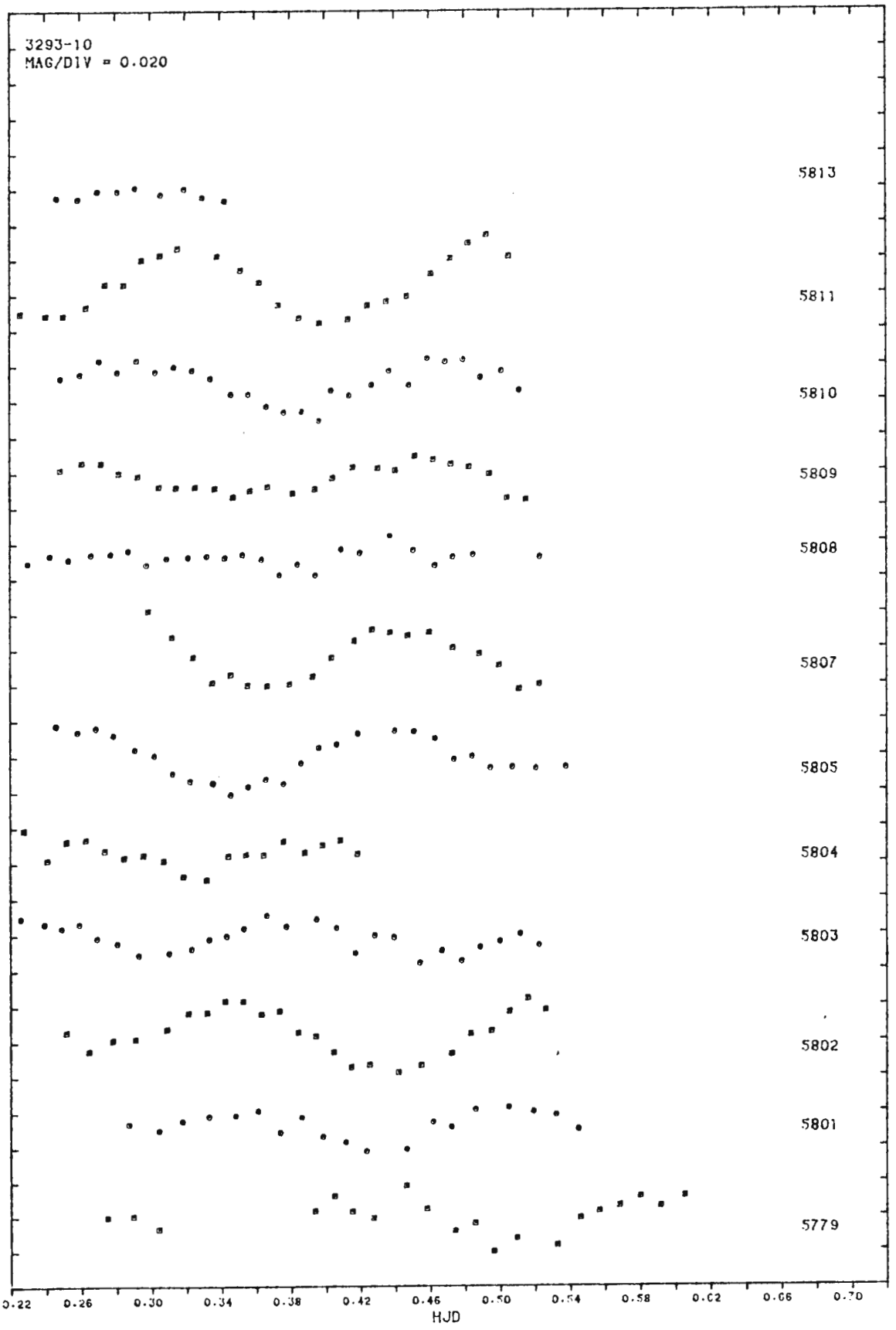
3293-10
MAG/DIV = 0.020
5813
5811
5810
5809
5808
5807
5805
5804
5803
5802
5801
5779
0.22
0.26
0.30
0.34
0.38
0.42
0.46
0.50
0.54
0.58
0.62
0.66
0.70
HJD

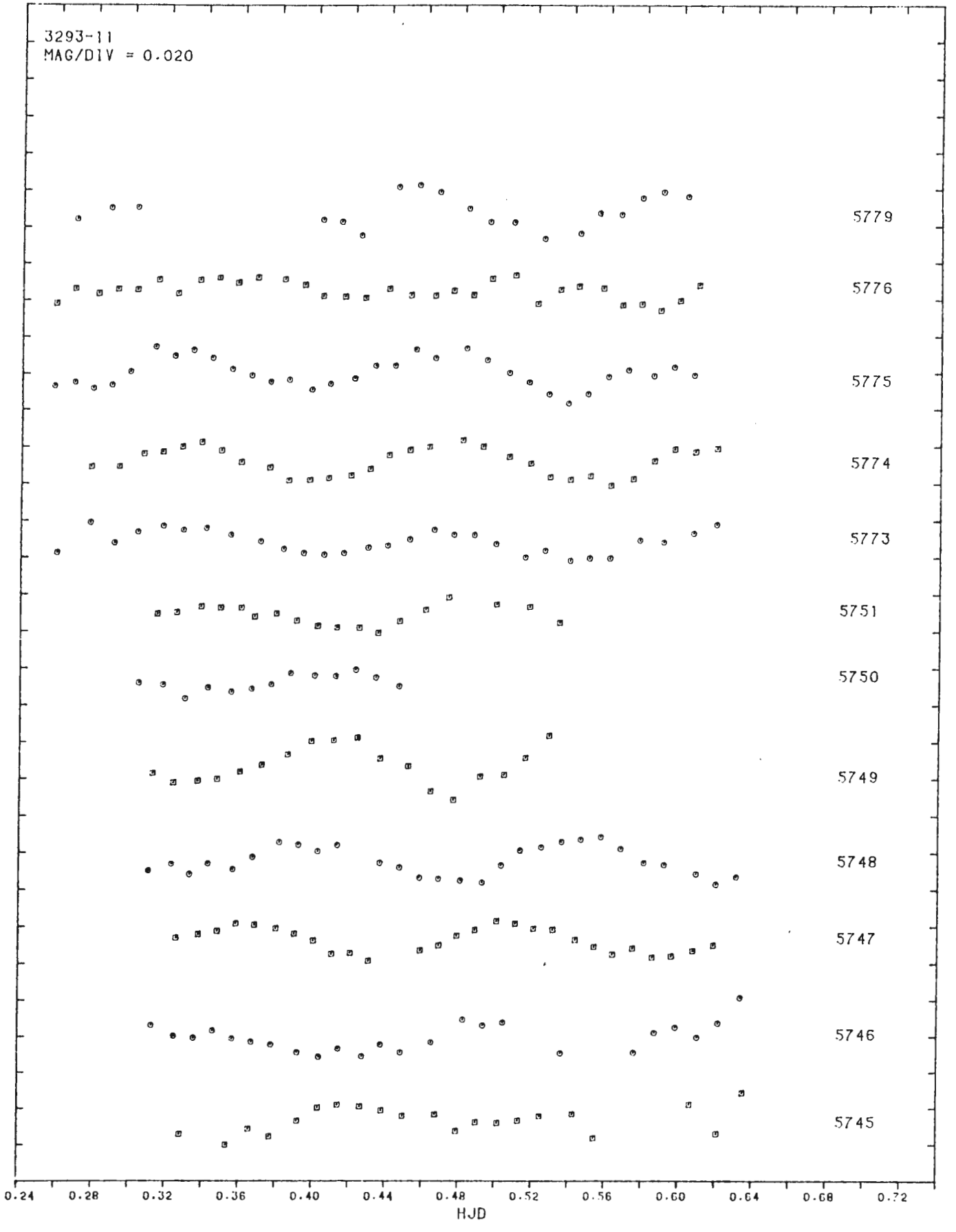
3293-11
MAG/DIV = 0.020
5779
5776
5775
5774
5773
5751
5750
5749
5748
5747
5746
5745
0.24
0.28
0.32
0.36
0.40
0.44
0.48
0.52
0.56
0.60
0.64
0.68
0.72
HJD

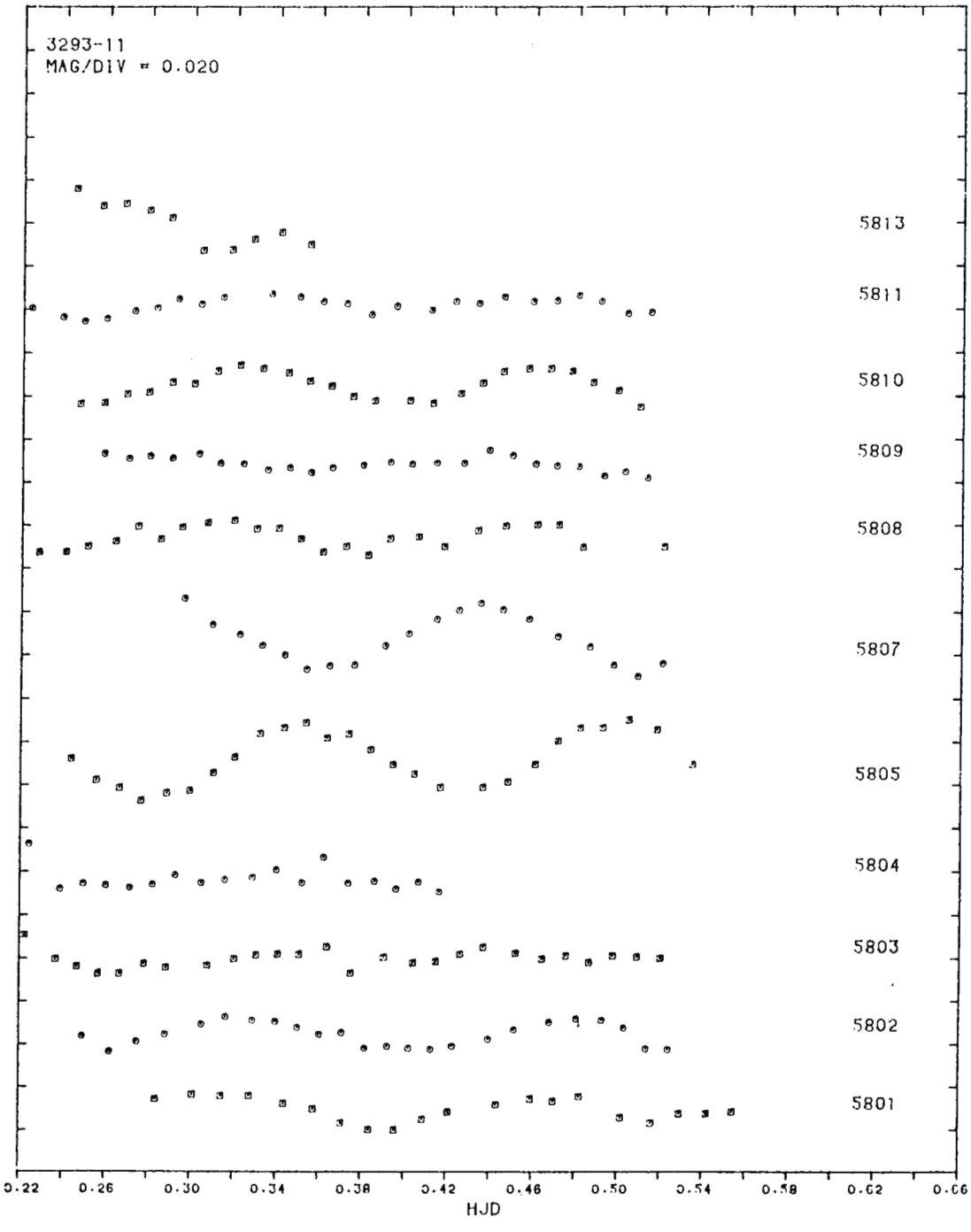
3293-11
MAG/DIV = 0.020
5813
5811
5810
5809
5808
5807
5805
5804
5803
5802
5801
0.22
0.26
0.30
0.34
0.38
0.42
0.46
0.50
0.54
0.58
0.62
0.66
HJD

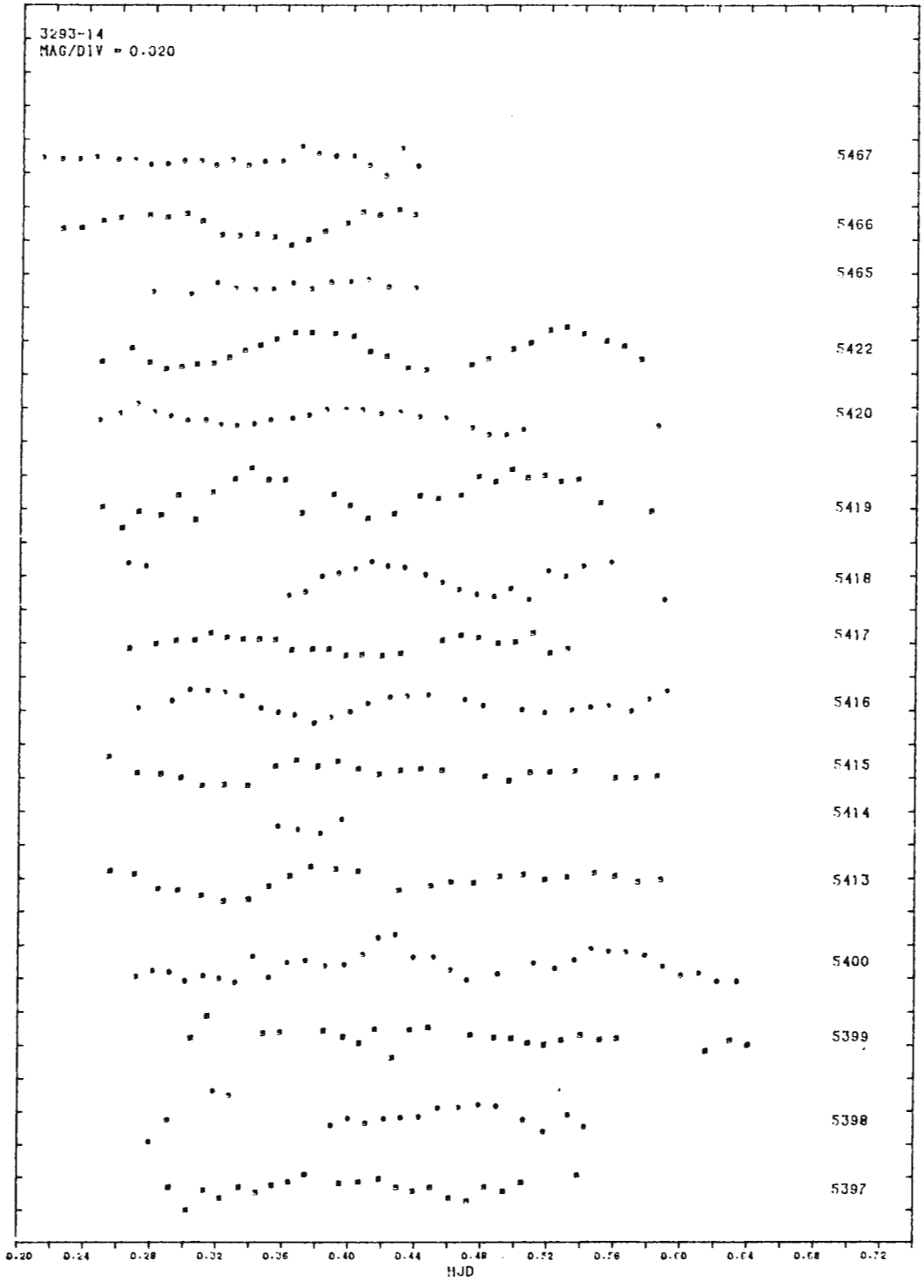
3293-14
MAG/DIV = 0.020
5467
5466
5465
5422
5420
5419
5418
5417
5416
5415
5414
5413
5400
5399
5398
5397
0.20
0.24
0.28
0.32
0.36
0.40
0.44
0.48
0.52
0.56
0.60
0.64
0.68
0.72
HJD

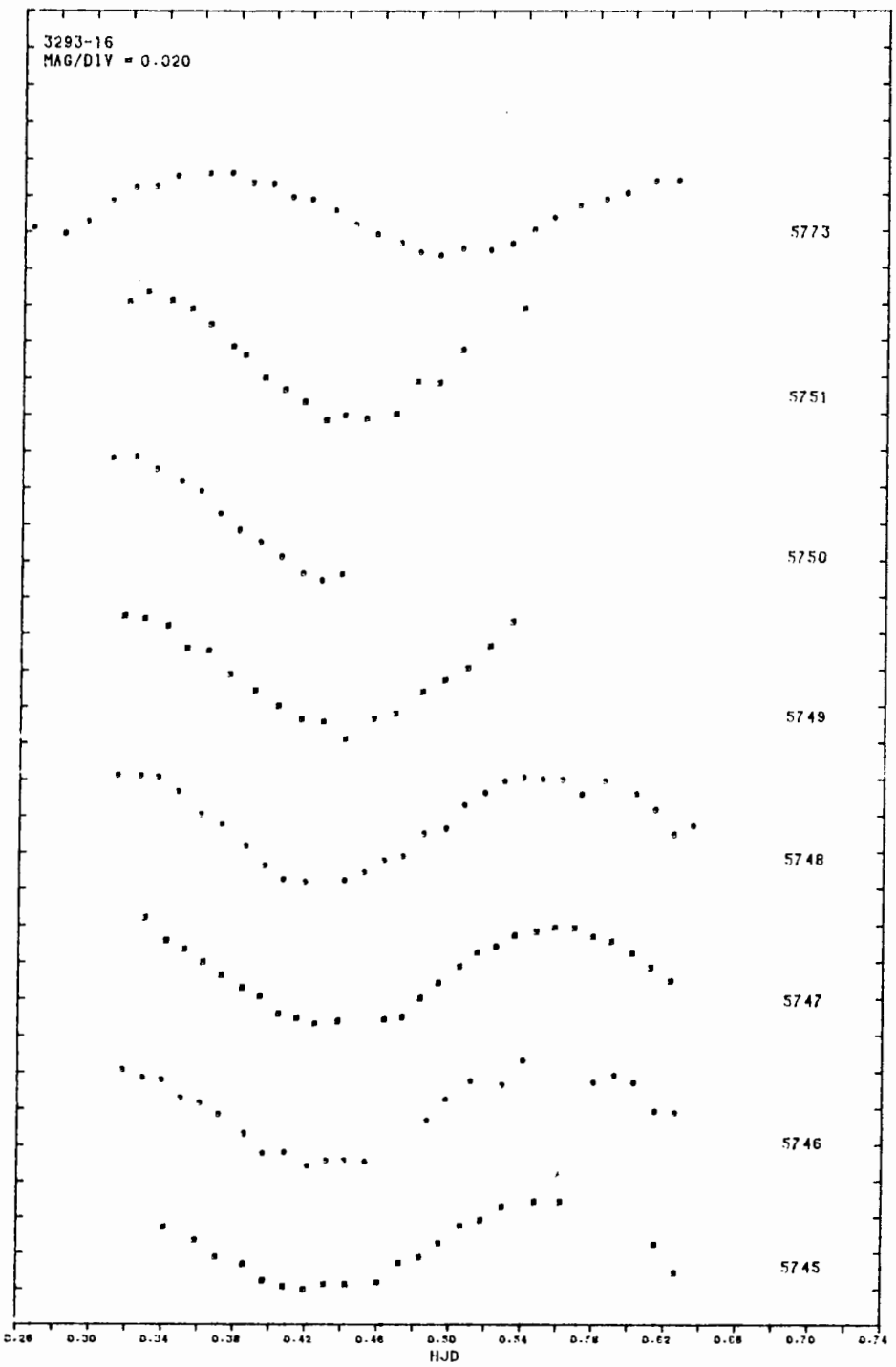
3293-16
MAG/DIV = 0.020
5773
5751
5750
5749
5748
5747
5746
5745
0.26
0.30
0.34
0.38
0.42
0.46
0.50
0.54
0.58
0.62
0.66
0.70
0.74
HJD

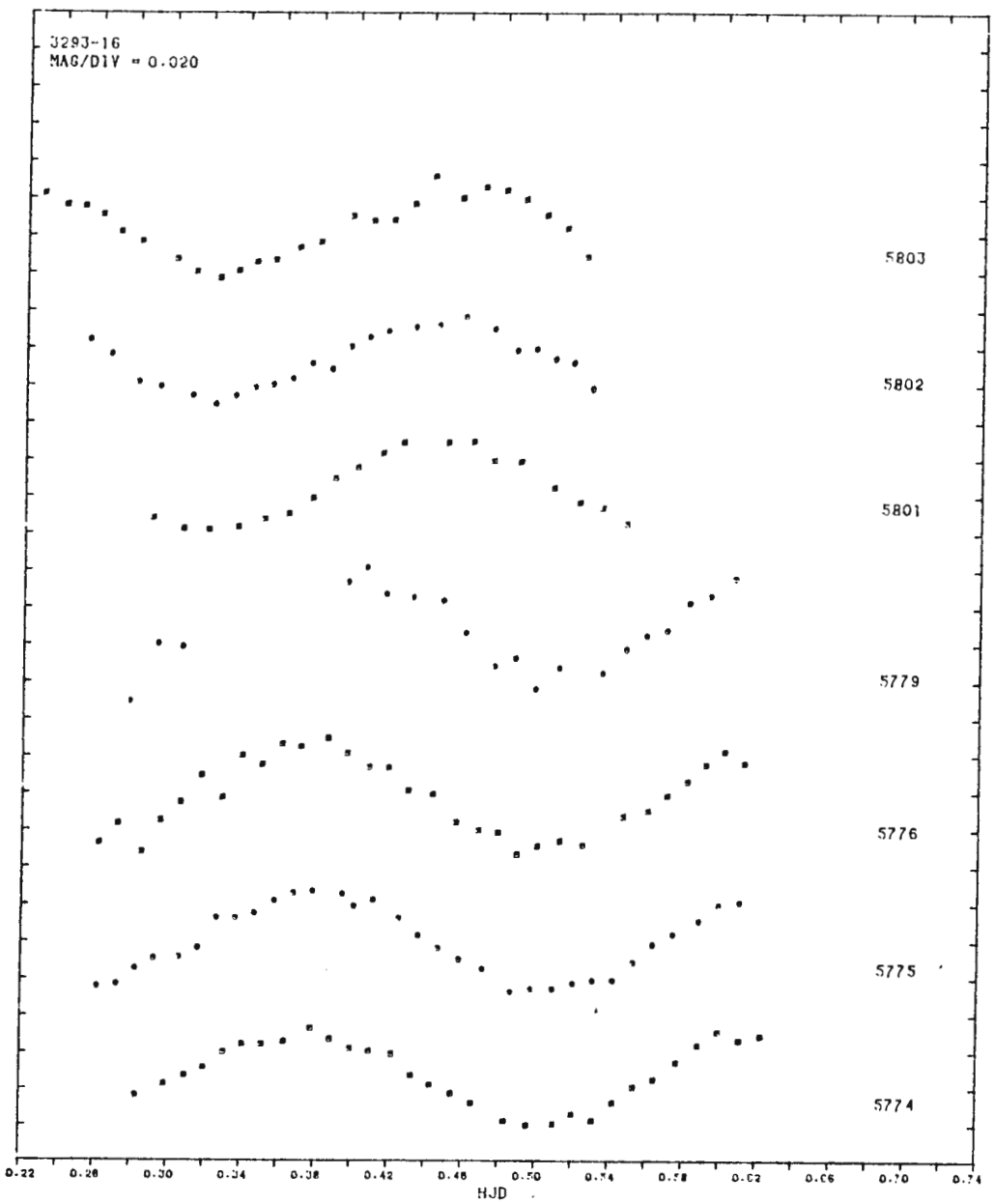
3293-16
MAG/DIV = 0.020
5803
5802
5801
5779
5776
5775
5774
0.22
0.26
0.30
0.34
0.38
0.42
0.46
0.50
0.54
0.58
0.62
0.66
0.70
0.74
HJD

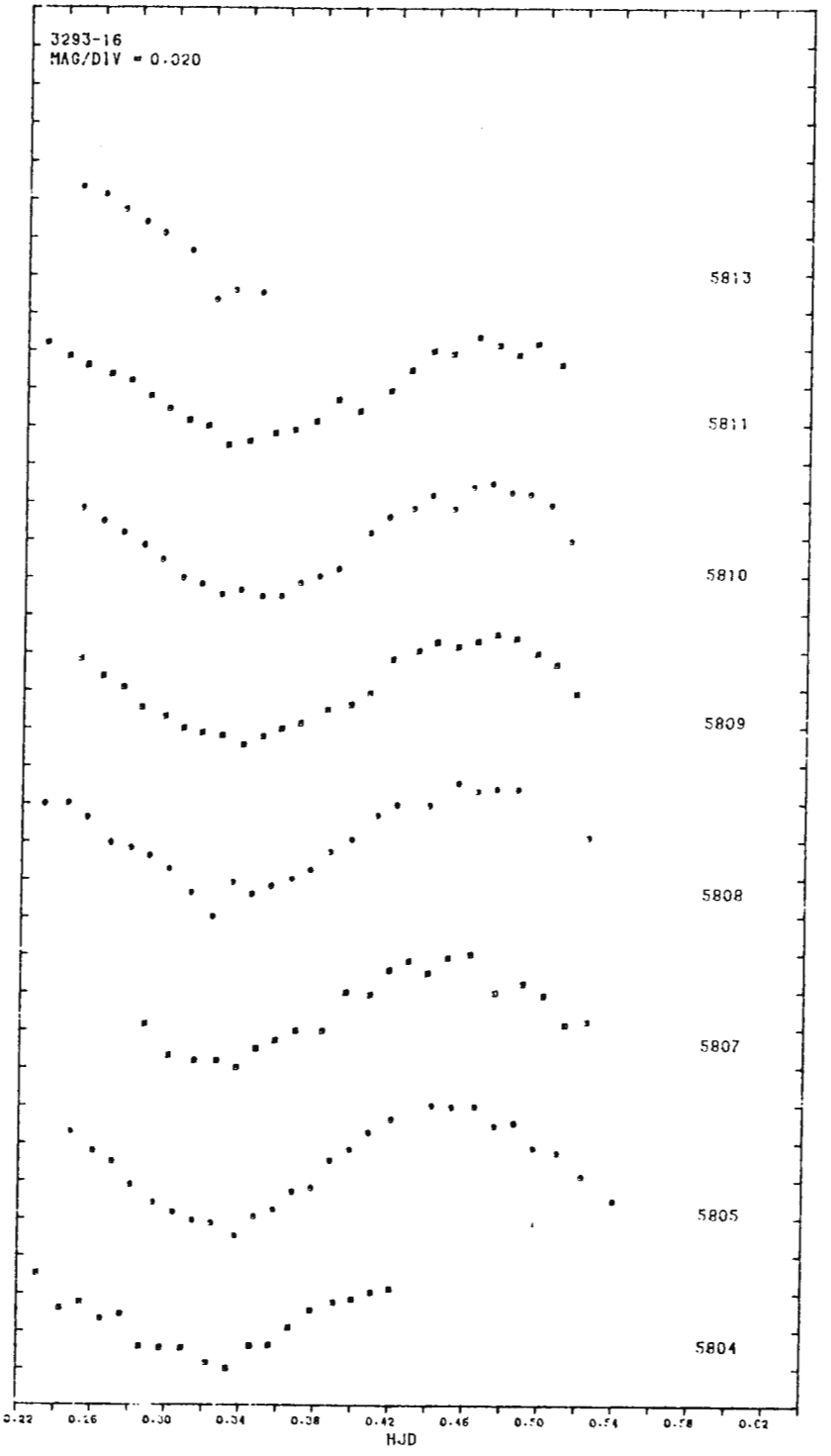
3293-16
MAG/DIV = 0.020
5813
5811
5810
5809
5808
5807
5805
5804
HJD

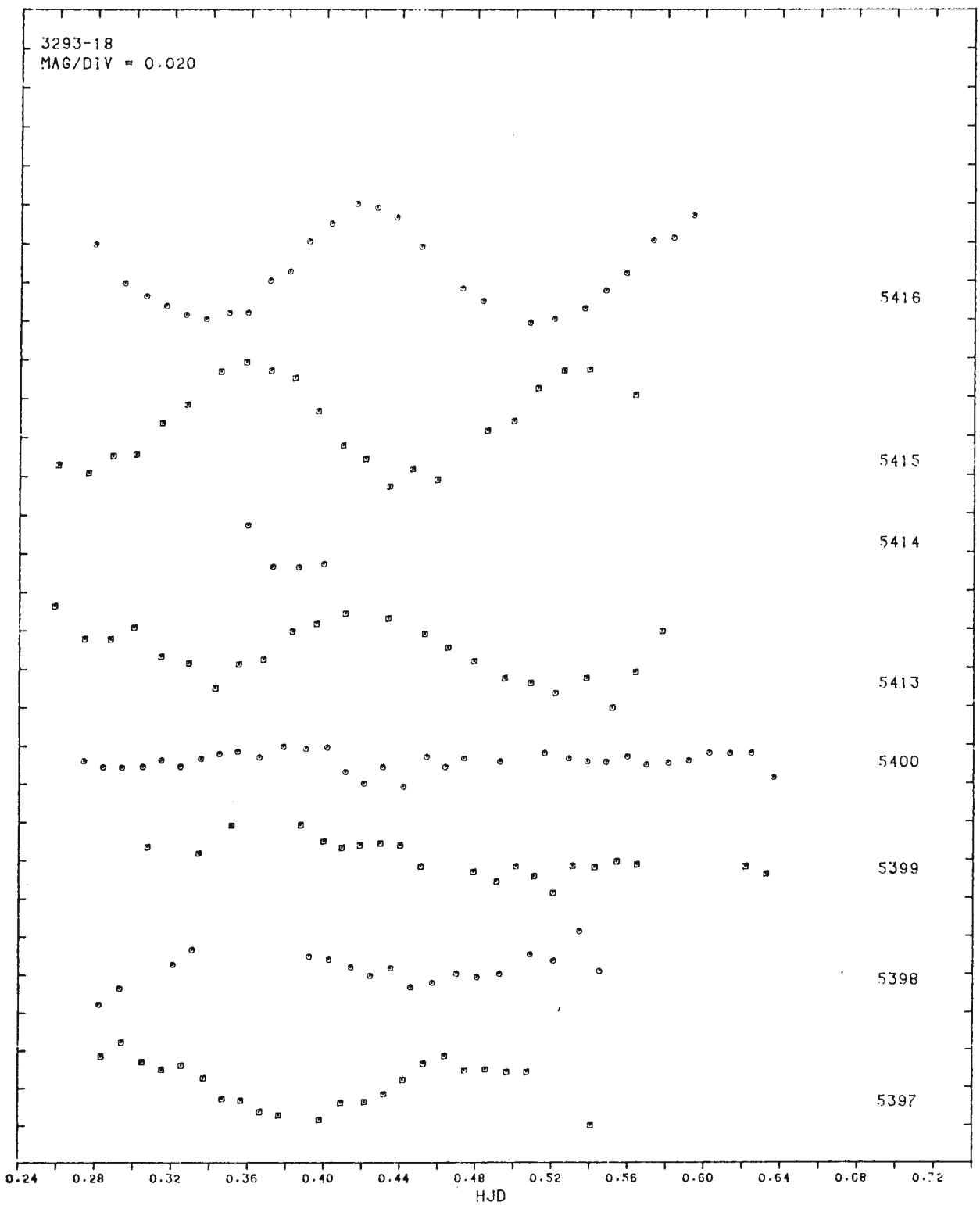
3293-18
MAG/DIV = 0.020
5416
5415
5414
5413
5400
5399
5398
5397
0.24
0.28
0.32
0.36
0.40
0.44
0.48
0.52
0.56
0.60
0.64
0.68
0.72
HJD

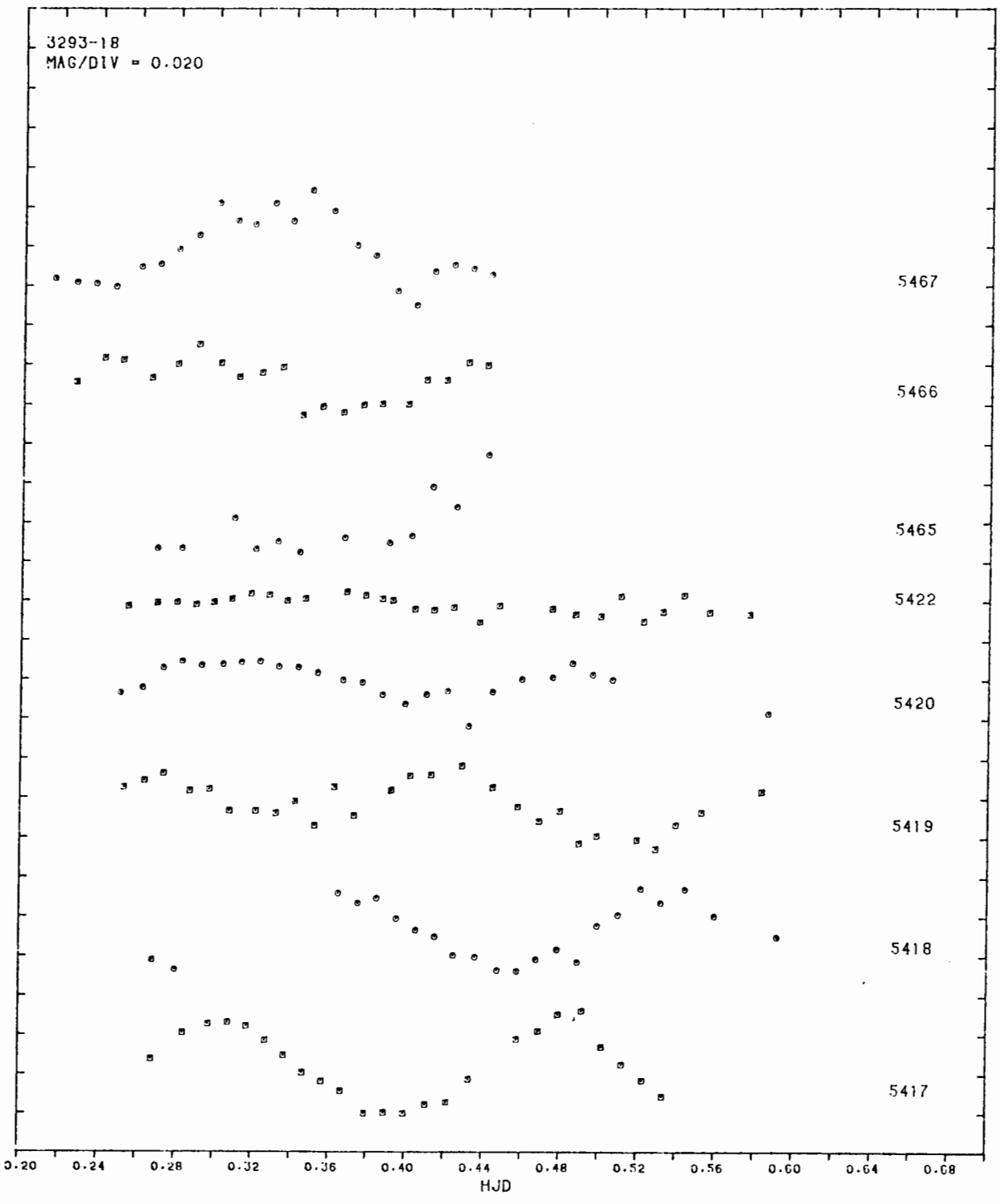
3293-18
MAG/DIV = 0.020
5467
5466
5465
5422
5420
5419
5418
5417
0.20
0.24
0.28
0.32
0.36
0.40
0.44
0.48
0.52
0.56
0.60
0.64
0.68
HJD

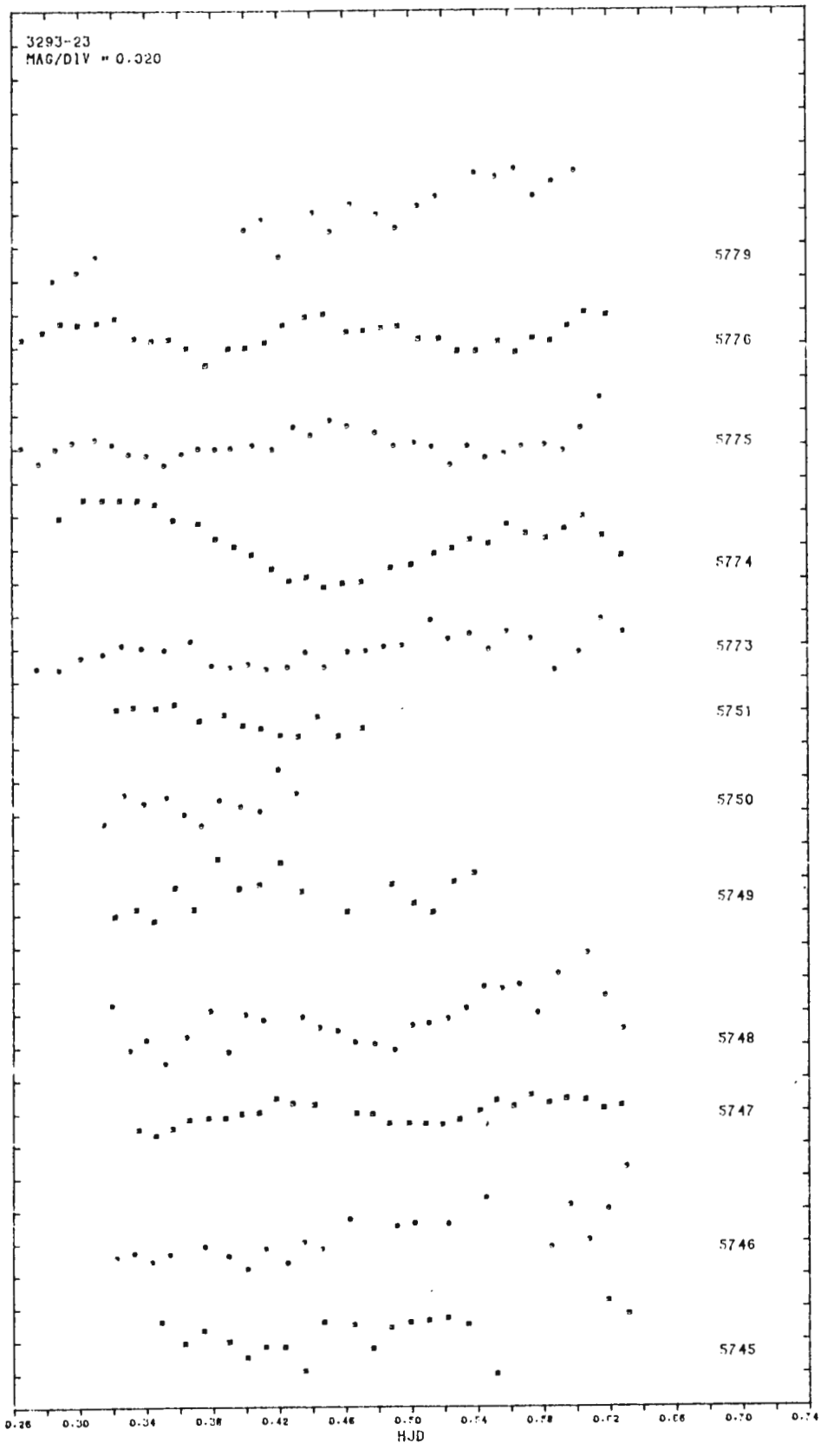
3293-23
MAG/DIV = 0.020
5779
5776
5775
5774
5773
5751
5750
5749
5748
5747
5746
5745
0.26
0.30
0.34
0.38
0.42
0.46
0.50
0.54
0.58
0.62
0.66
0.70
0.74
HJD

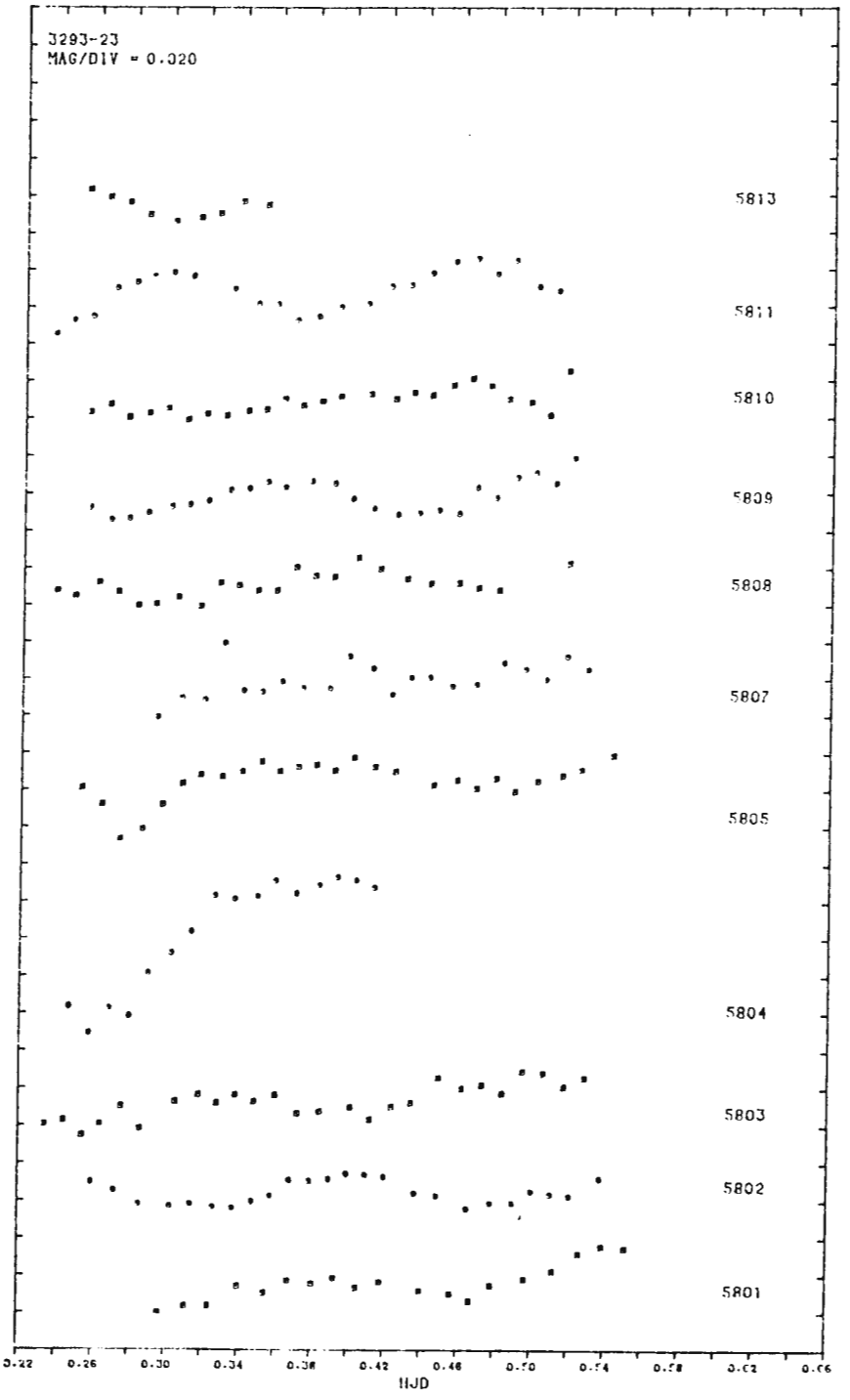
3293-23
MAG/DIV = 0.020
5813
5811
5810
5809
5808
5807
5805
5804
5803
5802
5801
0.22
0.26
0.30
0.34
0.38
0.42
0.46
0.50
0.54
0.58
0.62
0.66
HJD

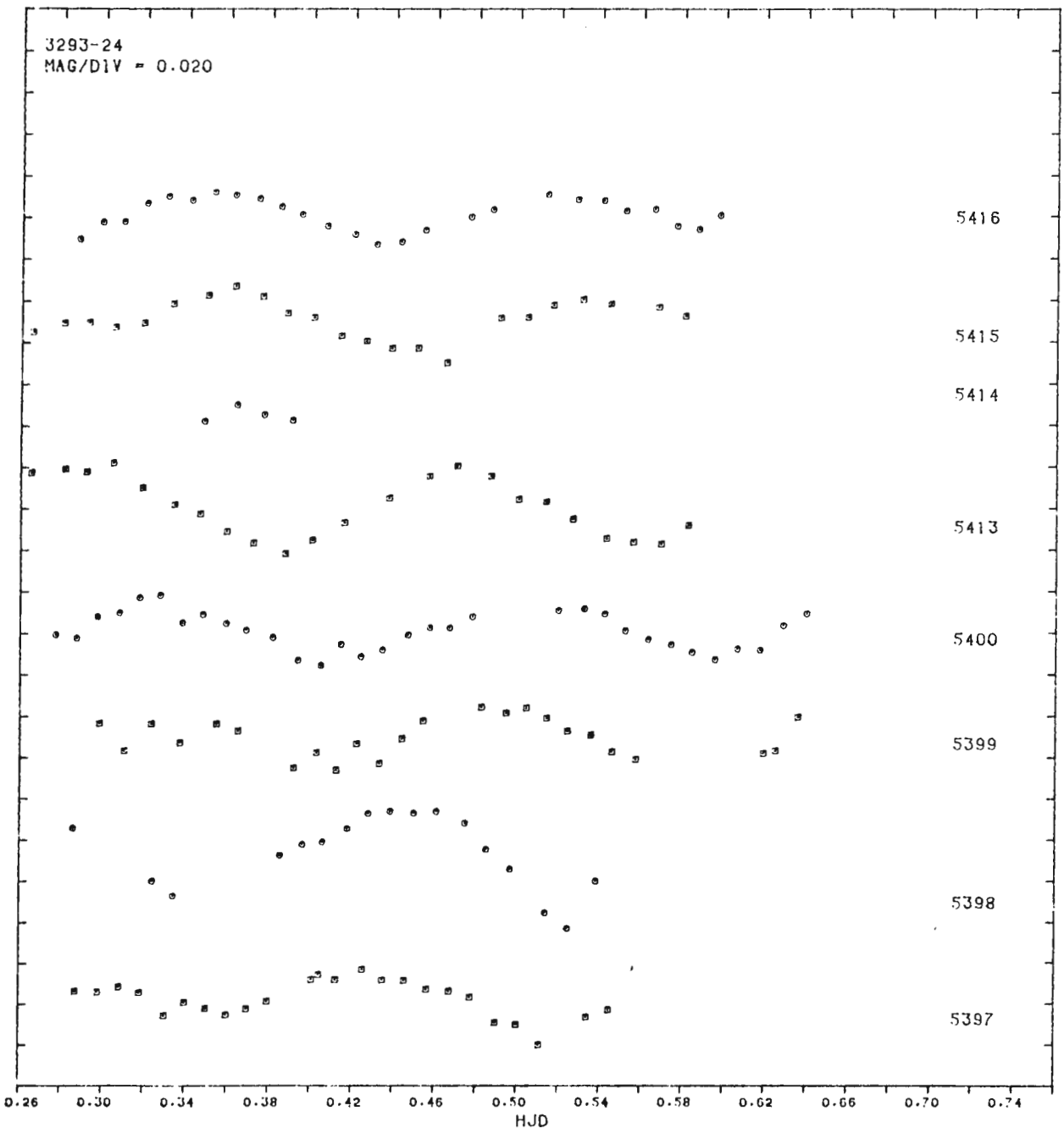
3293-24
MAG/DIV = 0.020
5416
5415
5414
5413
5400
5399
5398
5397
0.26
0.30
0.34
0.38
0.42
0.46
0.50
0.54
0.58
0.62
0.66
0.70
0.74
HJD

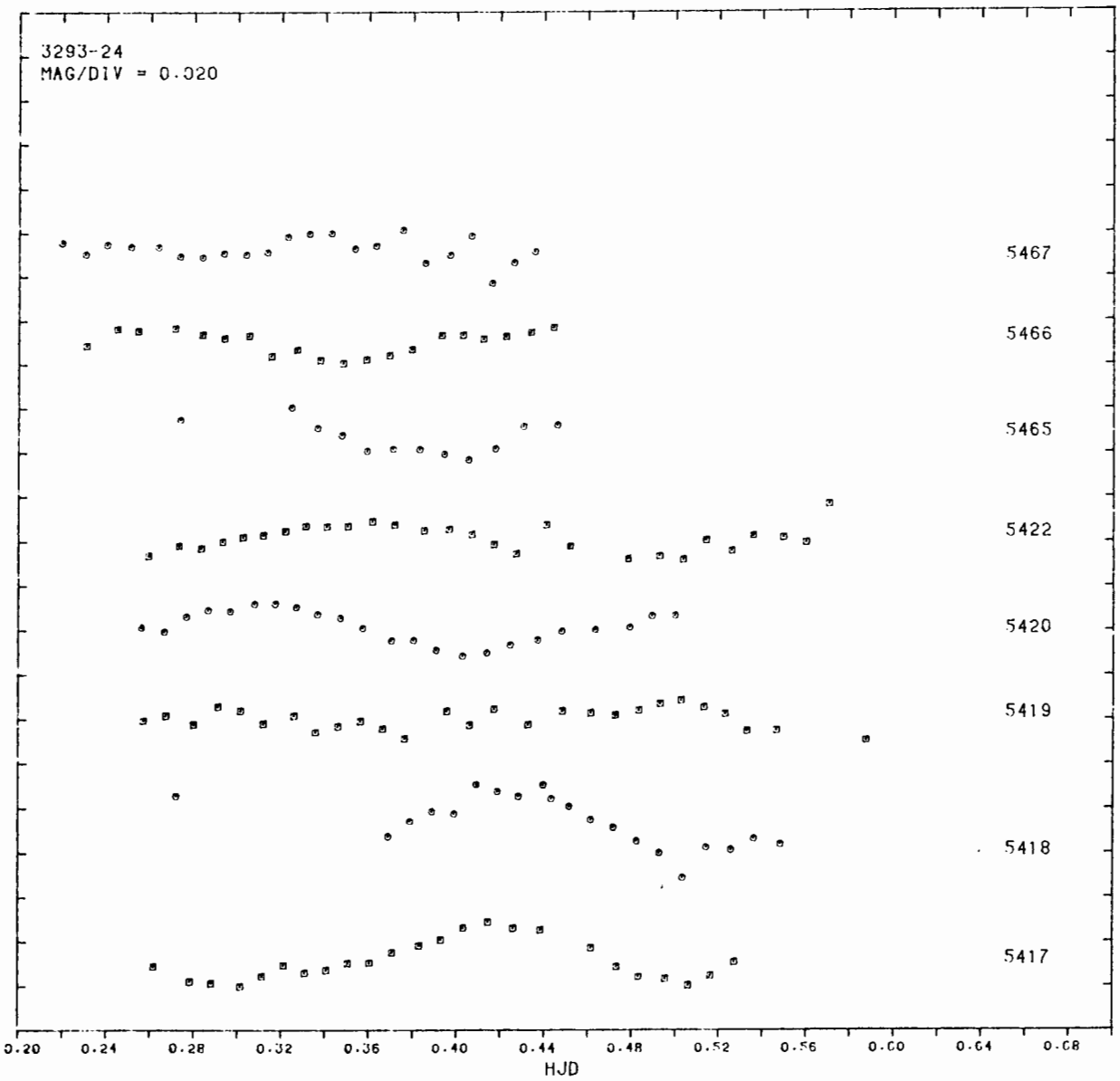
3293-24
MAG/DIV = 0.020
5467
5466
5465
5422
5420
5419
5418
5417
0.20
0.24
0.28
0.32
0.36
0.40
0.44
0.48
0.52
0.56
0.60
0.64
0.68
HJD

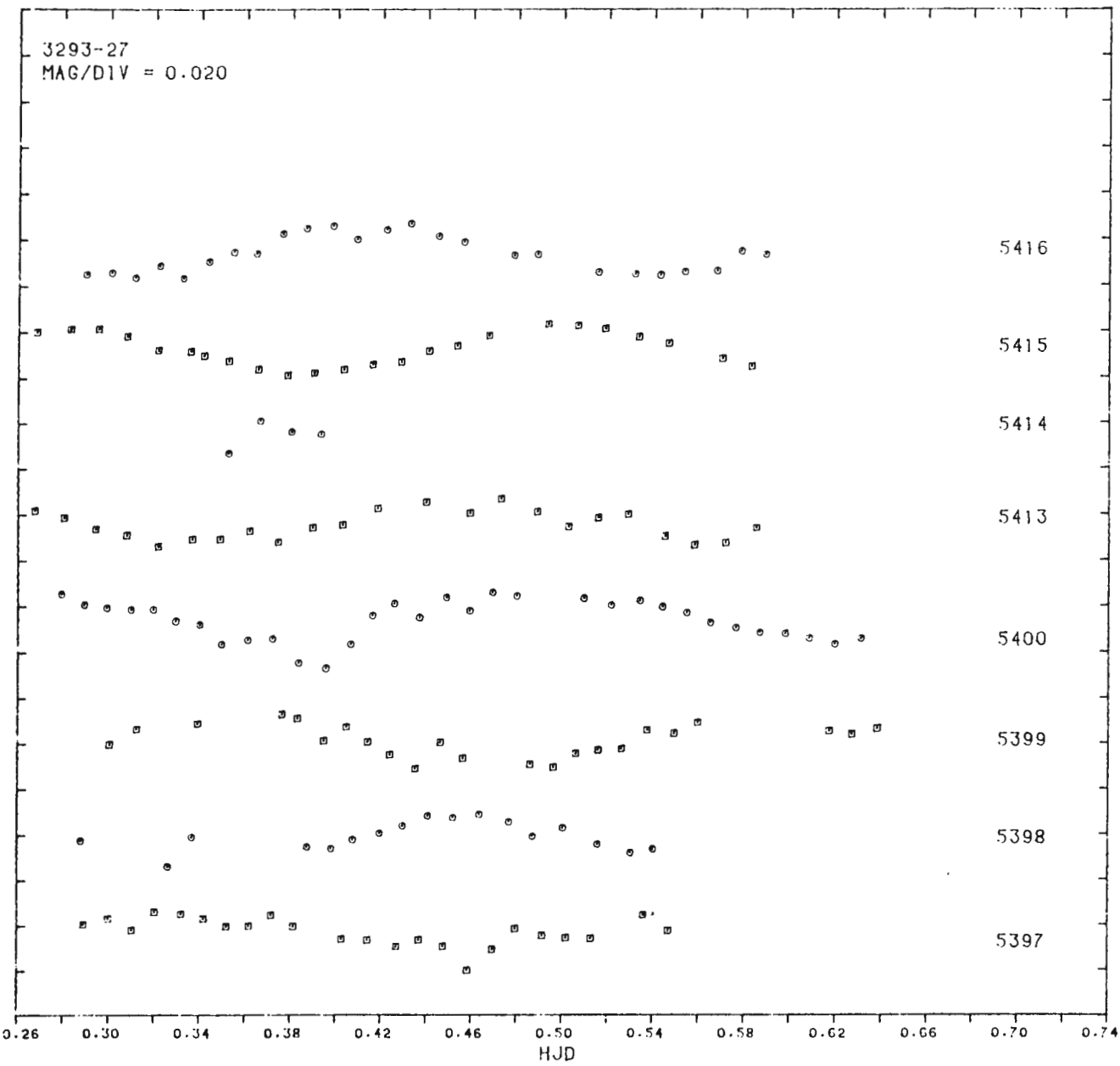
3293-27
MAG/DIV = 0.020
5416
5415
5414
5413
5400
5399
5398
5397
0.26
0.30
0.34
0.38
0.42
0.46
0.50
0.54
0.58
0.62
0.66
0.70
0.74
HJD

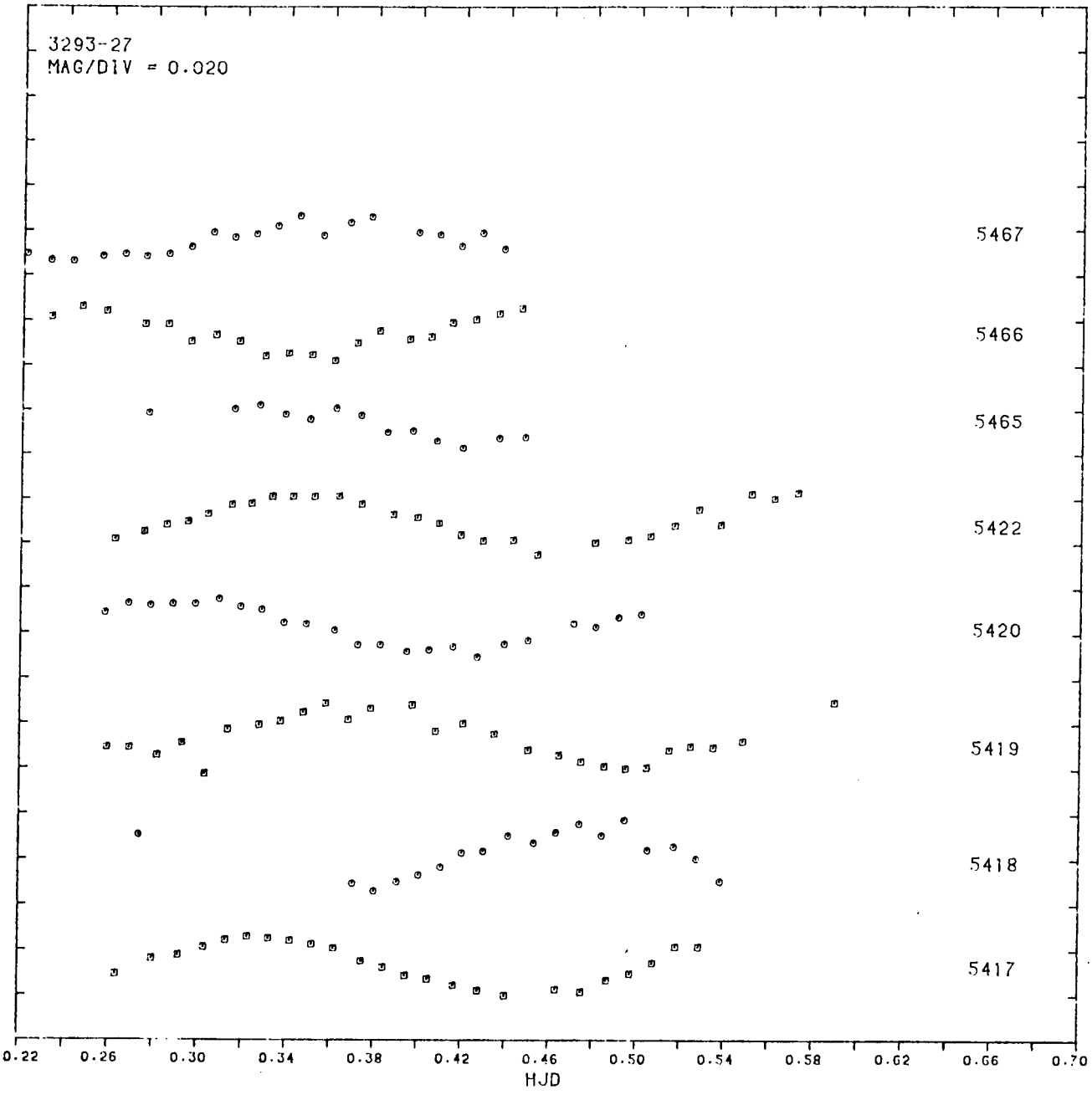
3293-27
MAG/DIV = 0.020
5467
5466
5465
5422
5420
5419
5418
5417
0.22
0.26
0.30
0.34
0.38
0.42
0.46
0.50
0.54
0.58
0.62
0.66
0.70
HJD

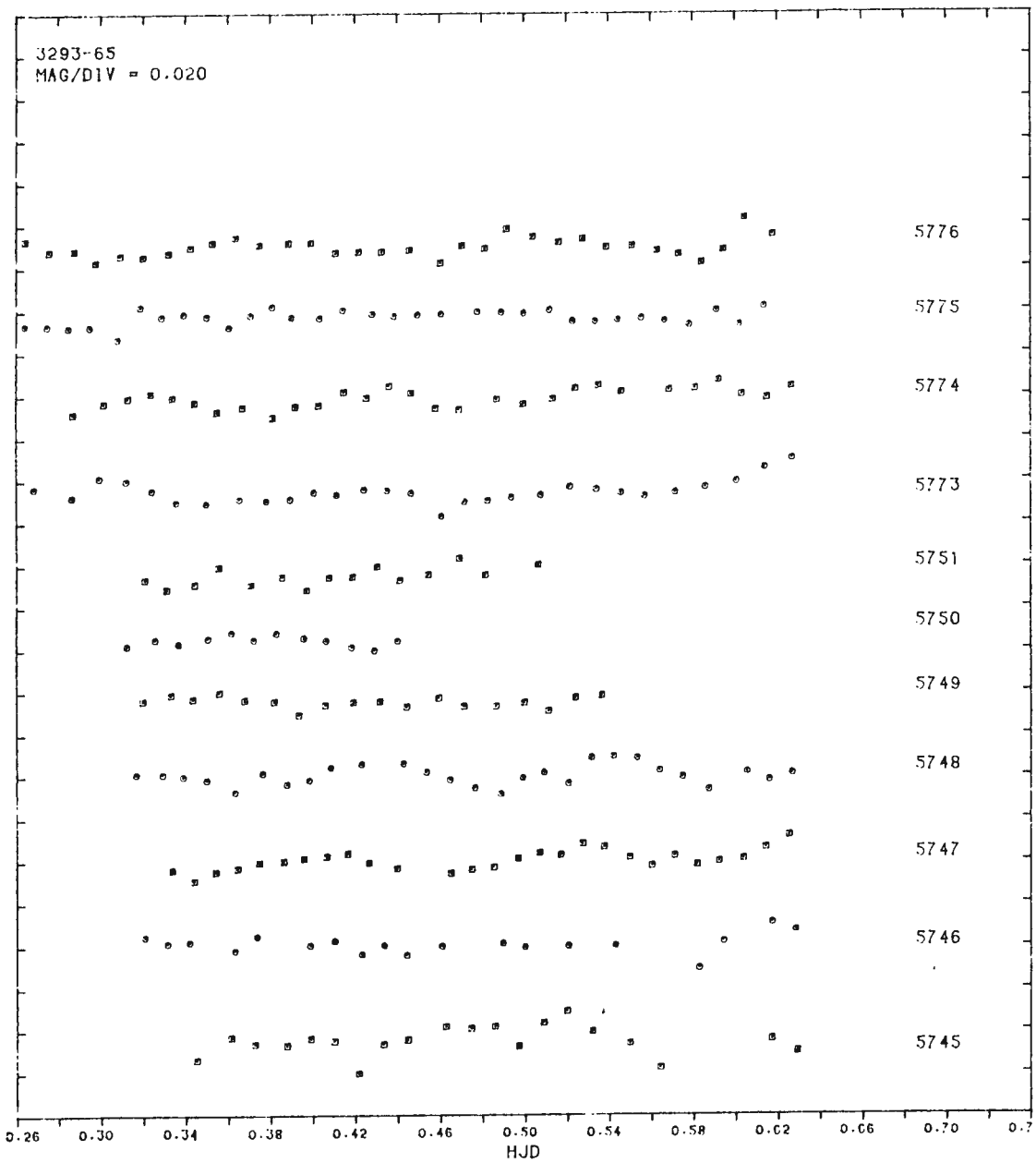
3293-65
MAG/DIV = 0.020
5776
5775
5774
5773
5751
5750
5749
5748
5747
5746
5745
0.26
0.30
0.34
0.38
0.42
0.46
0.50
0.54
0.58
0.62
0.66
0.70
0.74
HJD

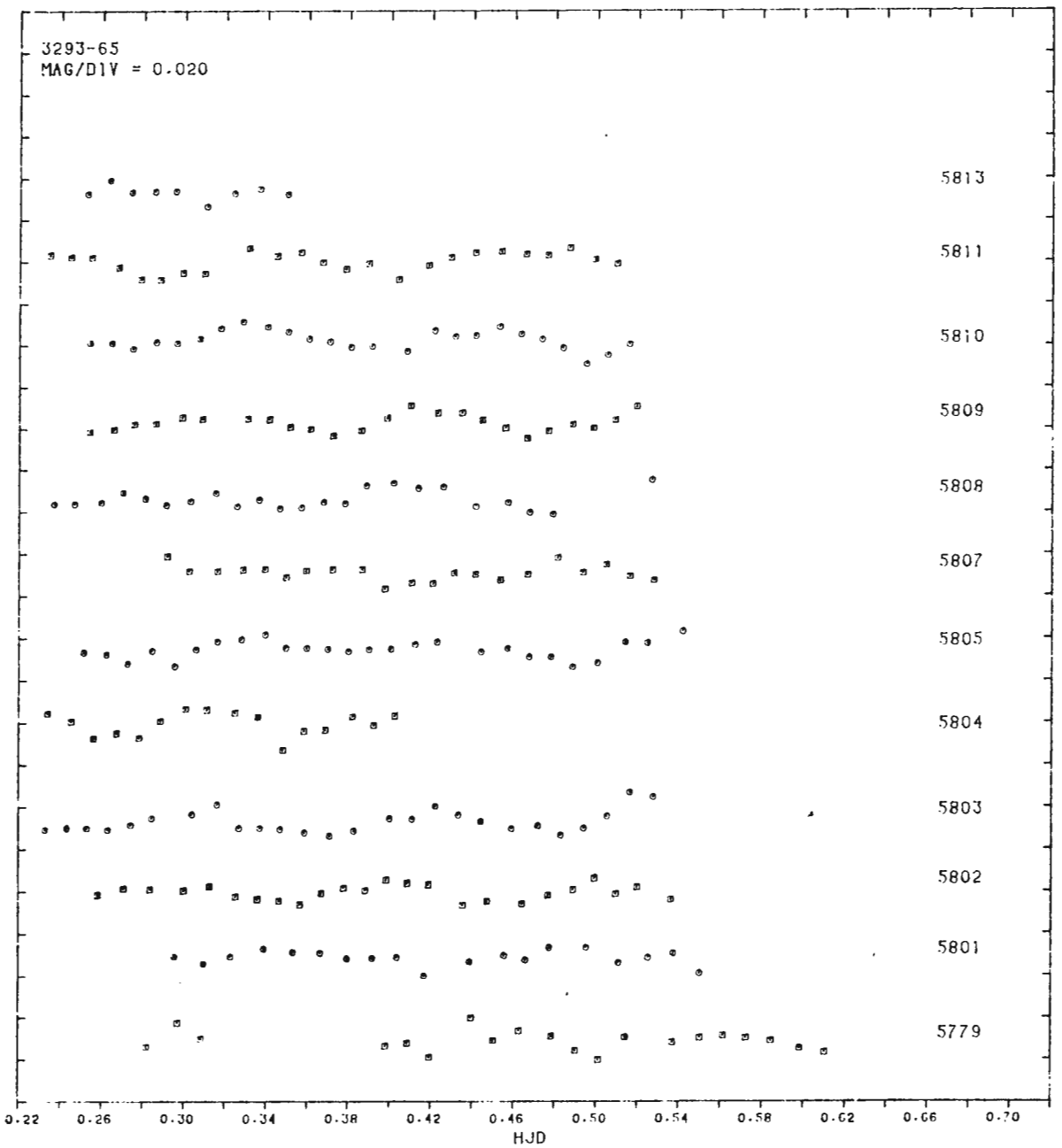
3293-65
MAG/DIV = 0.020
5813
5811
5810
5809
5808
5807
5805
5804
5803
5802
5801
5779
0.22
0.26
0.30
0.34
0.38
0.42
0.46
0.50
0.54
0.58
0.62
0.66
0.70
HJD

APPENDIX 2

This appendix contains the thermally broadened spectral line profiles calculated as described in chapters 7 and 9. The labelling of the plots containing the profiles is explained in section 9.4 of the main body of the thesis. The profiles shown here are arranged for increasing values of the degree ℓ and the azimuthal index m of the particular modes to which the profiles refer. The following values of these parameters are included: $\ell = 0$, 1, 2, 3 and 4; $m = 0, -\ell$.

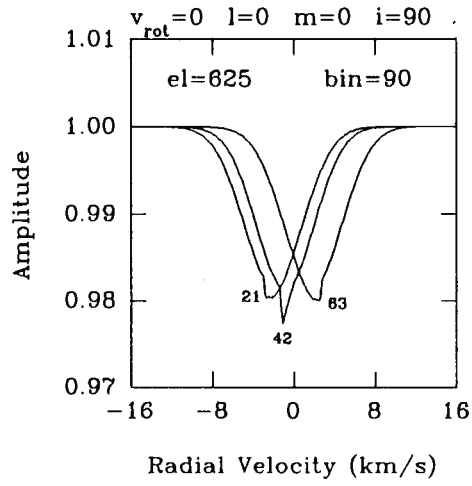
v_rot=0 l=0 m=0 i=90
el=625 bin=90
1.01
1.00
0.99
0.98
0.97
Amplitude
21
42
63
−16 −8 0 8 16
Radial Velocity (km/s)

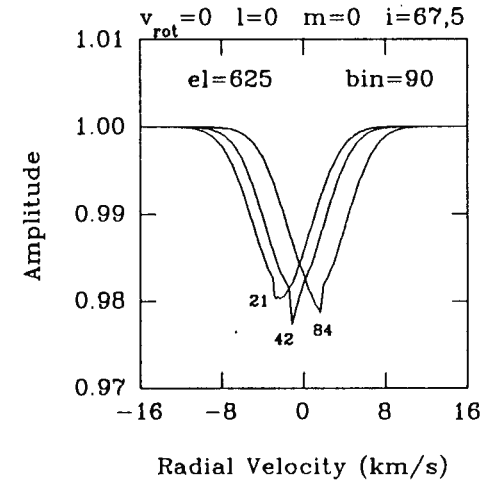
v_rot=0 l=0 m=0 i=67,5
el=625 bin=90
1.01
1.00
0.99
0.98
0.97
Amplitude
21
42
84
−16 −8 0 8 16
Radial Velocity (km/s)

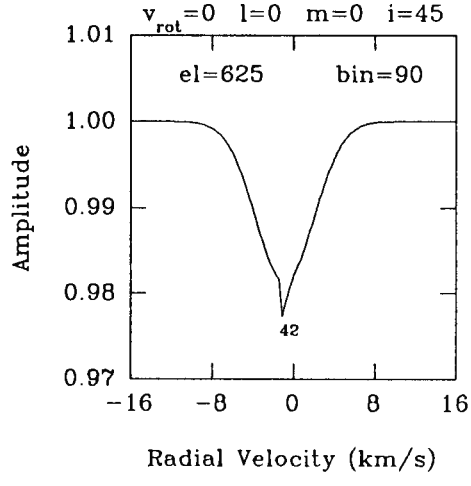
v_rot=0 l=0 m=0 i=45
el=625 bin=90
1.01
1.00
0.99
0.98
0.97
Amplitude
42
−16 −8 0 8 16
Radial Velocity (km/s)

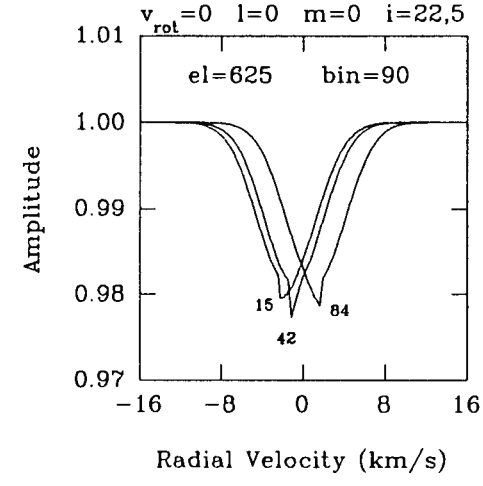
v_rot=0 l=0 m=0 i=22,5
el=625 bin=90
1.01
1.00
0.99
0.98
0.97
Amplitude
15
42
84
−16 −8 0 8 16
Radial Velocity (km/s)

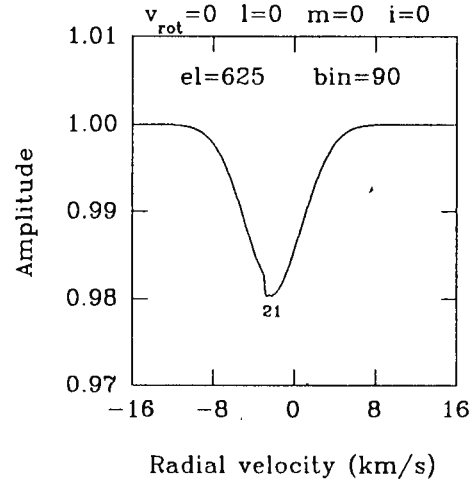
v_rot=0 l=0 m=0 i=0
el=625 bin=90
1.01
1.00
0.99
0.98
0.97
Amplitude
21
−16 −8 0 8 16
Radial velocity (km/s)

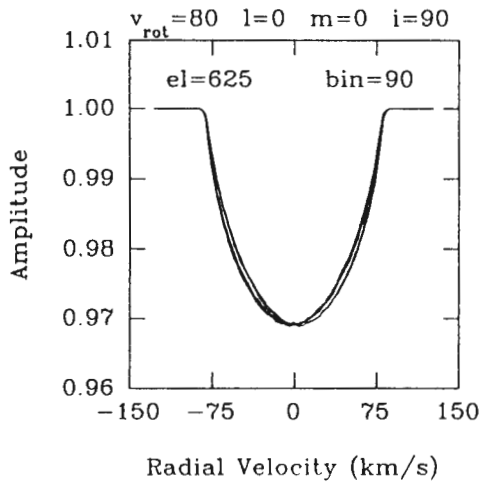
v rot =80 l=0 m=0 i=90
el=625 bin=90
Amplitude
1.01
1.00
0.99
0.98
0.97
0.96
−150 −75 0 75 150
Radial Velocity (km/s)

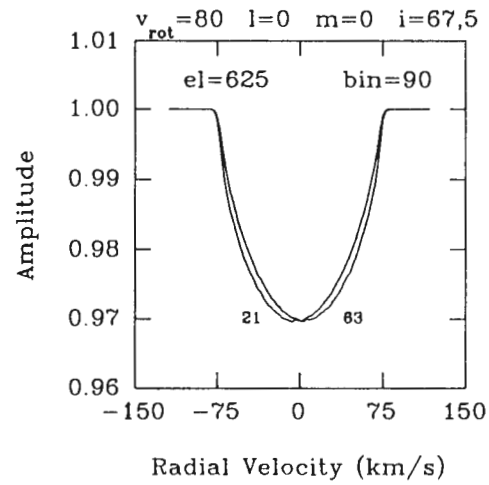
v rot =80 l=0 m=0 i=67,5
el=625 bin=90
21
63
Amplitude
1.01
1.00
0.99
0.98
0.97
0.96
−150 −75 0 75 150
Radial Velocity (km/s)

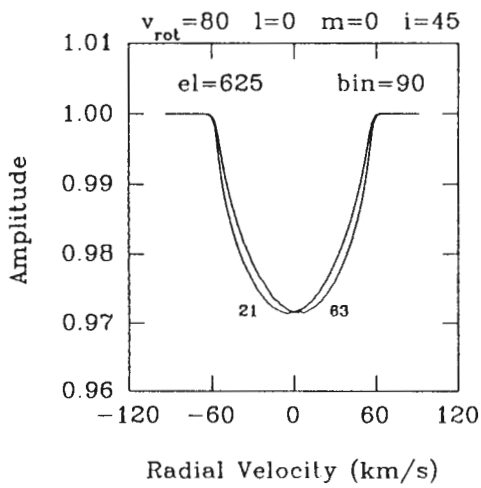
v rot =80 l=0 m=0 i=45
el=625 bin=90
21
63
Amplitude
1.01
1.00
0.99
0.98
0.97
0.96
−120 −60 0 60 120
Radial Velocity (km/s)

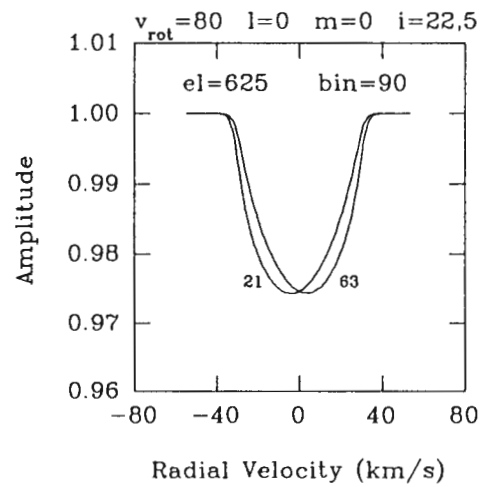
v rot =80 l=0 m=0 i=22,5
el=625 bin=90
21
63
Amplitude
1.01
1.00
0.99
0.98
0.97
0.96
−80 −40 0 40 80
Radial Velocity (km/s)

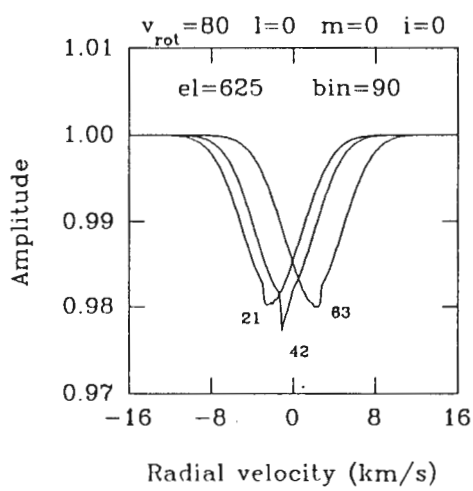
v rot =80 l=0 m=0 i=0
el=625 bin=90
21
42
63
Amplitude
1.01
1.00
0.99
0.98
0.97
−16 −8 0 8 16
Radial velocity (km/s)

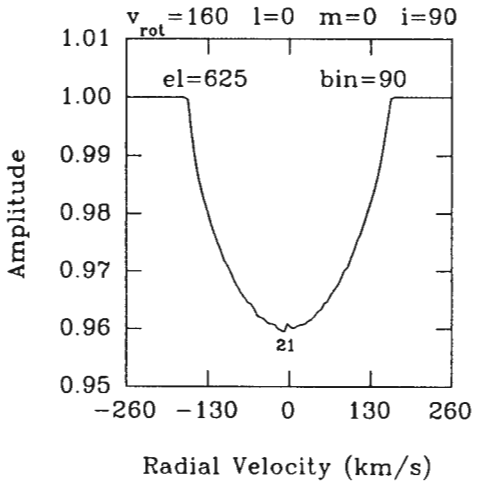
v rot =160 l=0 m=0 i=90
el=625 bin=90
Amplitude
1.01
1.00
0.99
0.98
0.97
0.96
0.95
21
−260 −130 0 130 260
Radial Velocity (km/s)

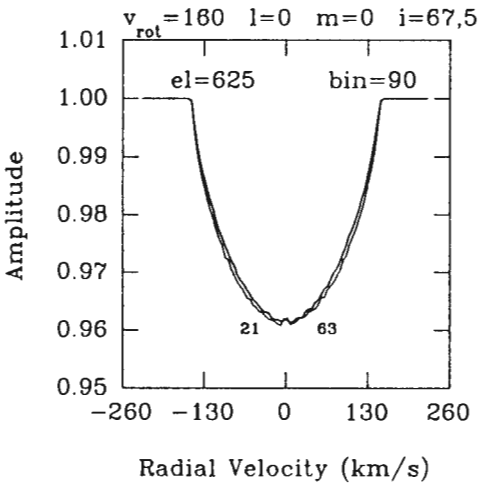
v rot =160 l=0 m=0 i=67,5
el=625 bin=90
Amplitude
1.01
1.00
0.99
0.98
0.97
0.96
0.95
21
63
−260 −130 0 130 260
Radial Velocity (km/s)

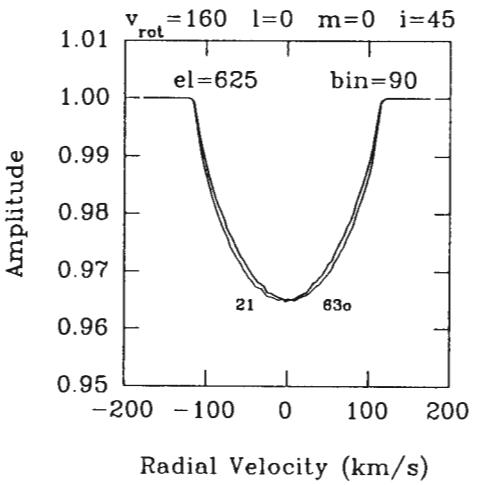
v rot =160 l=0 m=0 i=45
el=625 bin=90
Amplitude
1.01
1.00
0.99
0.98
0.97
0.96
0.95
21
63o
−200 −100 0 100 200
Radial Velocity (km/s)

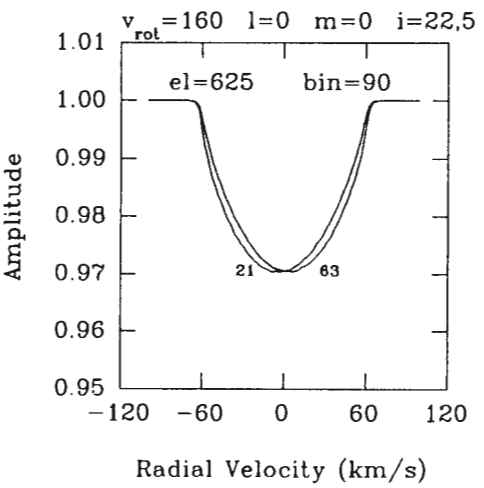
v rot =160 l=0 m=0 i=22,5
el=625 bin=90
Amplitude
1.01
1.00
0.99
0.98
0.97
0.96
0.95
21
63
−120 −60 0 60 120
Radial Velocity (km/s)

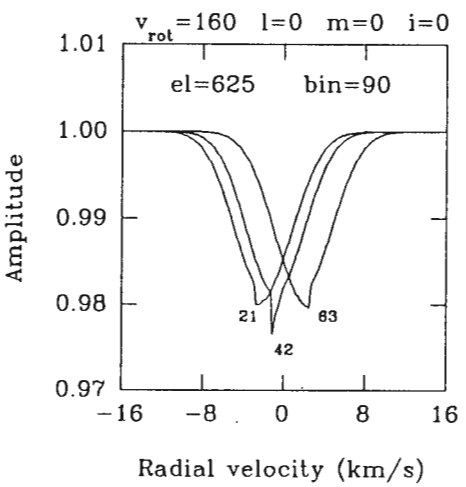
v rot =160 l=0 m=0 i=0
el=625 bin=90
Amplitude
1.01
1.00
0.99
0.98
0.97
21
63
42
−16 −8 0 8 16
Radial velocity (km/s)

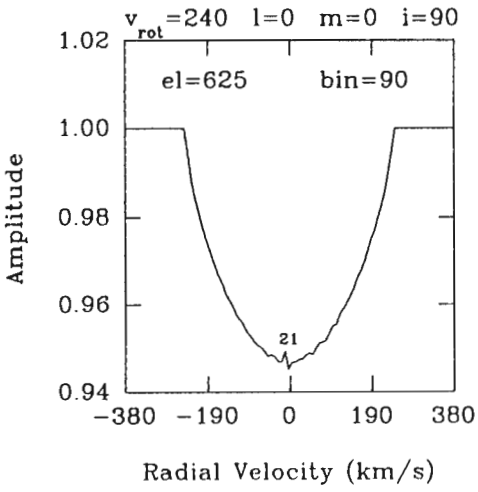
v rot =240 l=0 m=0 i=90
el=625 bin=90
Amplitude
1.02
1.00
0.98
0.96
0.94
21
−380 −190 0 190 380
Radial Velocity (km/s)

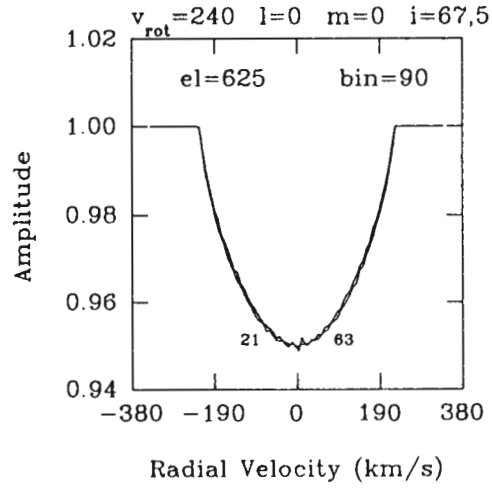
v rot =240 l=0 m=0 i=67,5
el=625 bin=90
Amplitude
1.02
1.00
0.98
0.96
0.94
21
63
−380 −190 0 190 380
Radial Velocity (km/s)

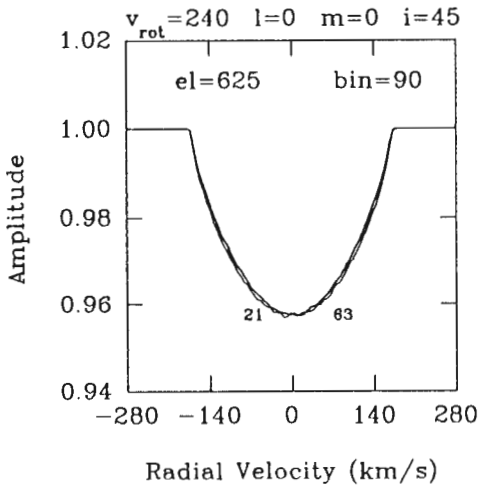
v rot =240 l=0 m=0 i=45
el=625 bin=90
Amplitude
1.02
1.00
0.98
0.96
0.94
21
63
−280 −140 0 140 280
Radial Velocity (km/s)

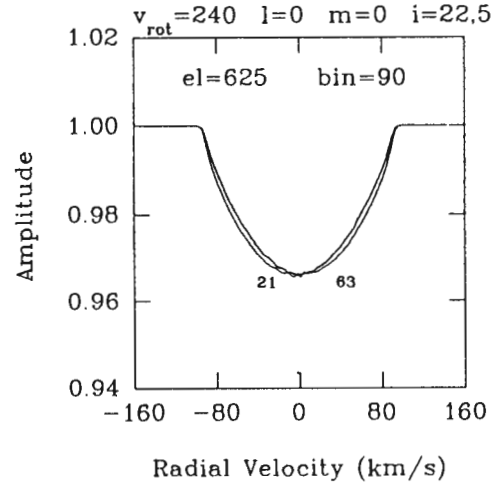
v rot =240 l=0 m=0 i=22,5
el=625 bin=90
Amplitude
1.02
1.00
0.98
0.96
0.94
21
63
−160 −80 0 80 160
Radial Velocity (km/s)

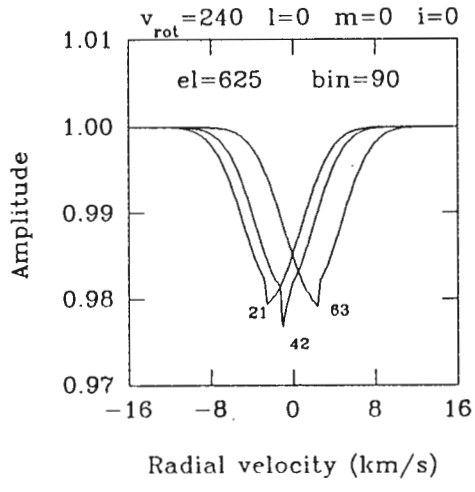
v rot =240 l=0 m=0 i=0
el=625 bin=90
Amplitude
1.01
1.00
0.99
0.98
0.97
21
42
63
−16 −8 0 8 16
Radial velocity (km/s)

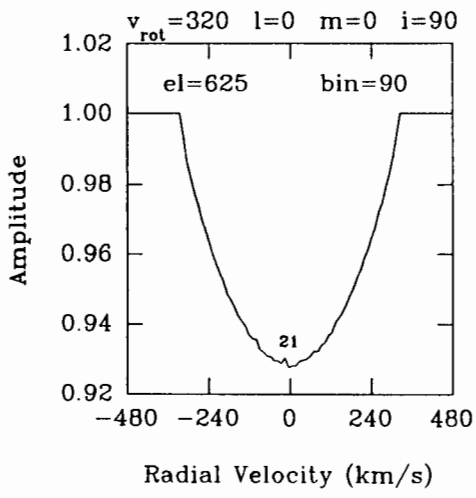
v rot =320 l=0 m=0 i=90
el=625 bin=90
Amplitude
1.02
1.00
0.98
0.96
0.94
0.92
21
−480 −240 0 240 480
Radial Velocity (km/s)

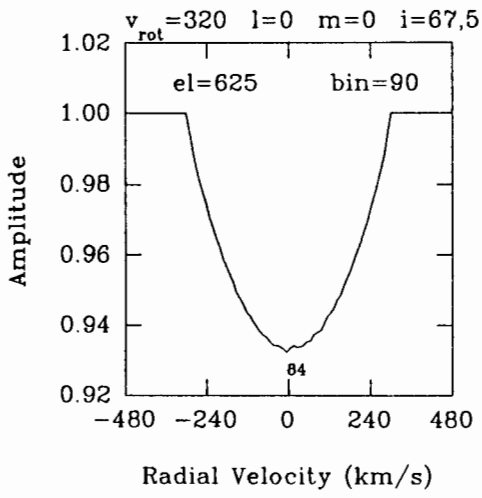
v rot =320 l=0 m=0 i=67,5
el=625 bin=90
Amplitude
1.02
1.00
0.98
0.96
0.94
0.92
84
−480 −240 0 240 480
Radial Velocity (km/s)

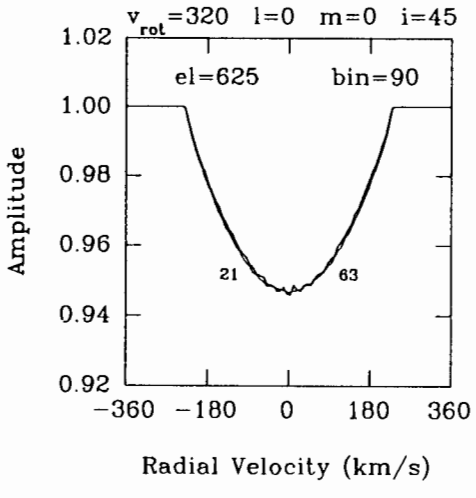
v rot =320 l=0 m=0 i=45
el=625 bin=90
Amplitude
1.02
1.00
0.98
0.96
0.94
0.92
21
63
−360 −180 0 180 360
Radial Velocity (km/s)

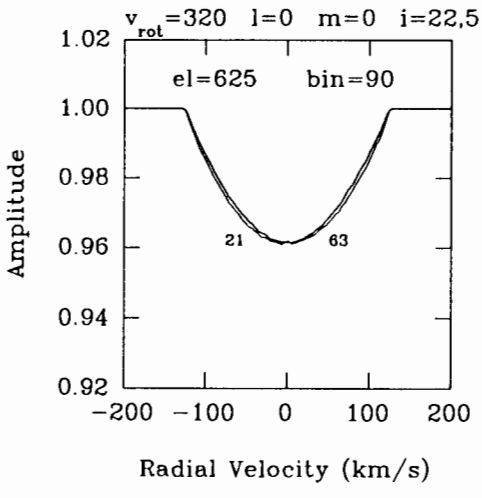
v rot =320 l=0 m=0 i=22,5
el=625 bin=90
Amplitude
1.02
1.00
0.98
0.96
0.94
0.92
21
63
−200 −100 0 100 200
Radial Velocity (km/s)

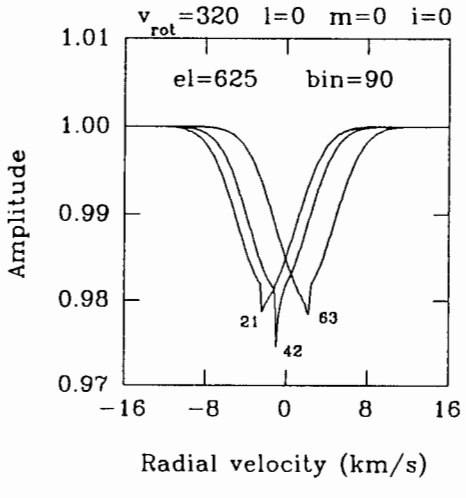
v rot =320 l=0 m=0 i=0
el=625 bin=90
Amplitude
1.01
1.00
0.99
0.98
0.97
21
63
42
−16 −8 0 8 16
Radial velocity (km/s)

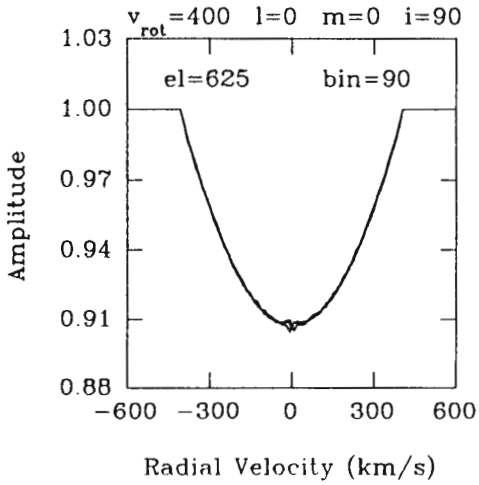
v rot =400 l=0 m=0 i=90
el=625 bin=90
Amplitude
1.03
1.00
0.97
0.94
0.91
0.88
−600 −300 0 300 600
Radial Velocity (km/s)

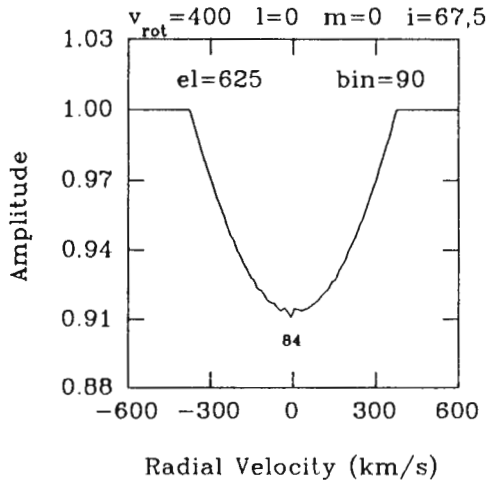
v rot =400 l=0 m=0 i=67,5
el=625 bin=90
Amplitude
1.03
1.00
0.97
0.94
0.91
0.88
84
−600 −300 0 300 600
Radial Velocity (km/s)

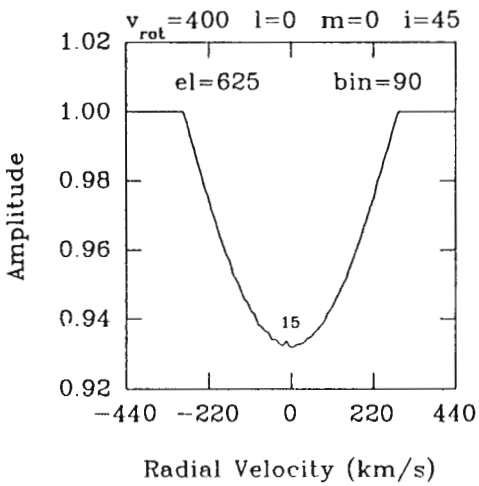
v rot =400 l=0 m=0 i=45
el=625 bin=90
Amplitude
1.02
1.00
0.98
0.96
0.94
0.92
15
−440 −220 0 220 440
Radial Velocity (km/s)

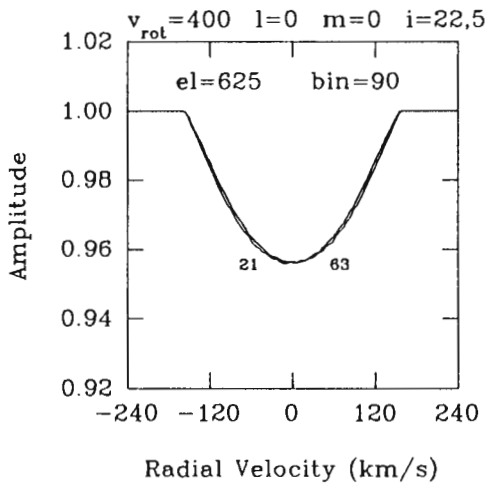
v rot =400 l=0 m=0 i=22,5
el=625 bin=90
Amplitude
1.02
1.00
0.98
0.96
0.94
0.92
21
63
−240 −120 0 120 240
Radial Velocity (km/s)

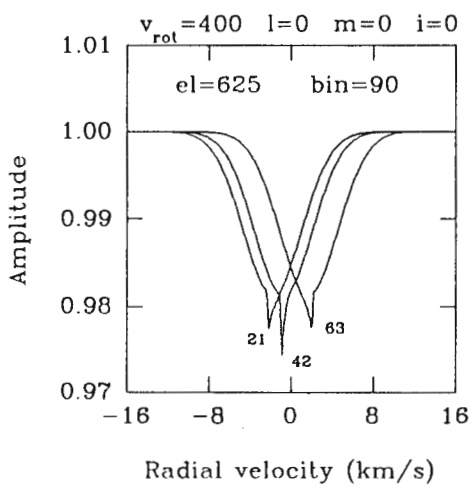
v rot =400 l=0 m=0 i=0
el=625 bin=90
Amplitude
1.01
1.00
0.99
0.98
0.97
21
42
63
−16 −8 0 8 16
Radial velocity (km/s)

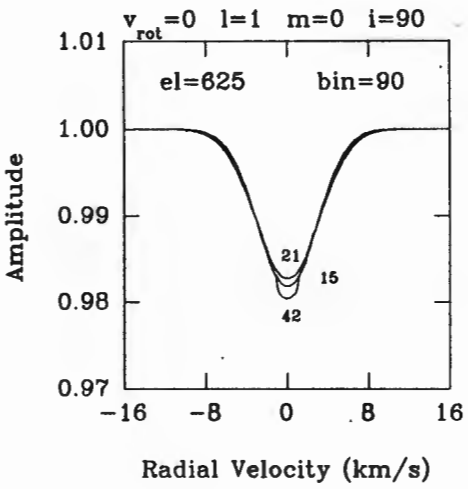
v_rot=0 l=1 m=0 i=90
el=625 bin=90
1.01
1.00
0.99
0.98
0.97
Amplitude
21
15
42
−16 −8 0 8 16
Radial Velocity (km/s)

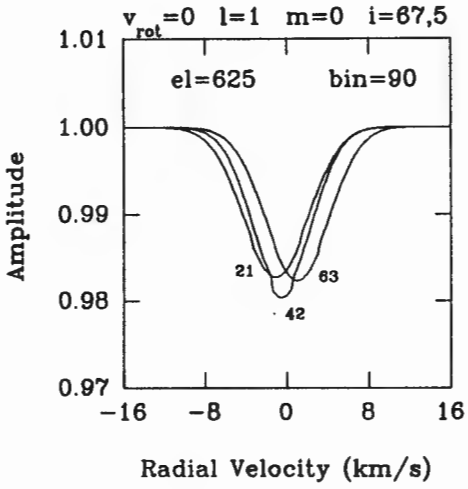
v_rot=0 l=1 m=0 i=67,5
el=625 bin=90
1.01
1.00
0.99
0.98
0.97
Amplitude
21
63
42
−16 −8 0 8 16
Radial Velocity (km/s)

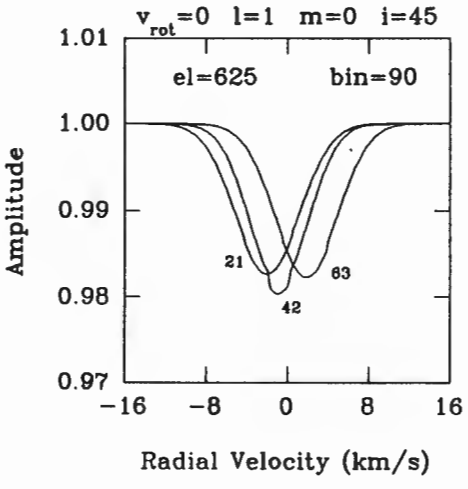
v_rot=0 l=1 m=0 i=45
el=625 bin=90
1.01
1.00
0.99
0.98
0.97
Amplitude
21
63
42
−16 −8 0 8 16
Radial Velocity (km/s)

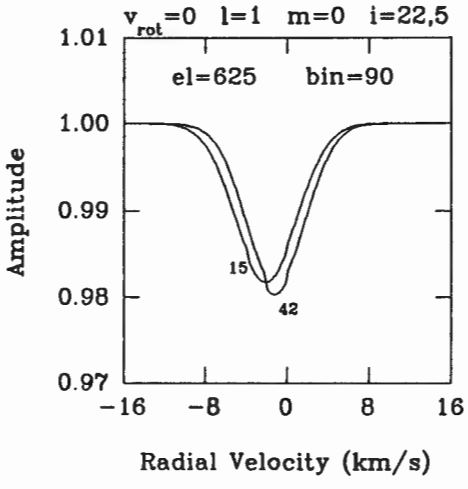
v_rot=0 l=1 m=0 i=22,5
el=625 bin=90
1.01
1.00
0.99
0.98
0.97
Amplitude
15
42
−16 −8 0 8 16
Radial Velocity (km/s)

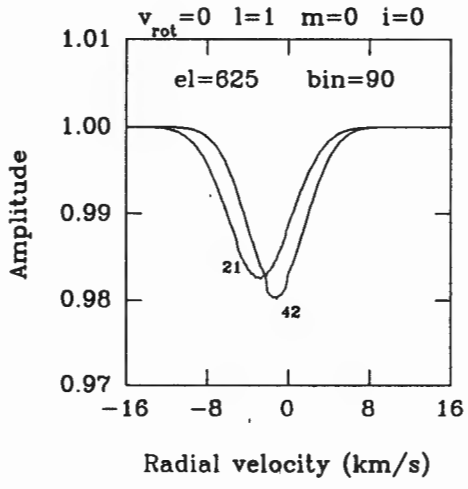
v_rot=0 l=1 m=0 i=0
el=625 bin=90
1.01
1.00
0.99
0.98
0.97
Amplitude
21
42
−16 −8 0 8 16
Radial velocity (km/s)

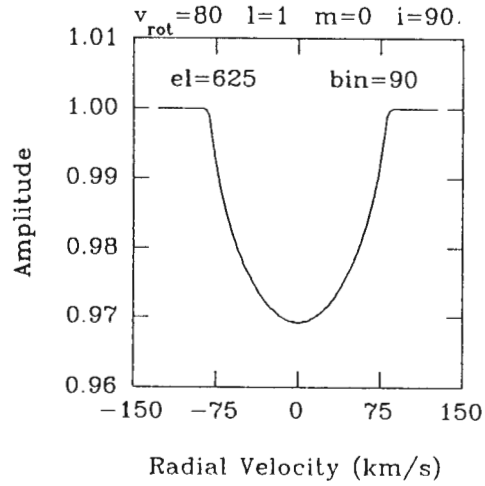
v rot =80 l=1 m=0 i=90.
el=625 bin=90
Amplitude
1.01
1.00
0.99
0.98
0.97
0.96
−150 −75 0 75 150
Radial Velocity (km/s)

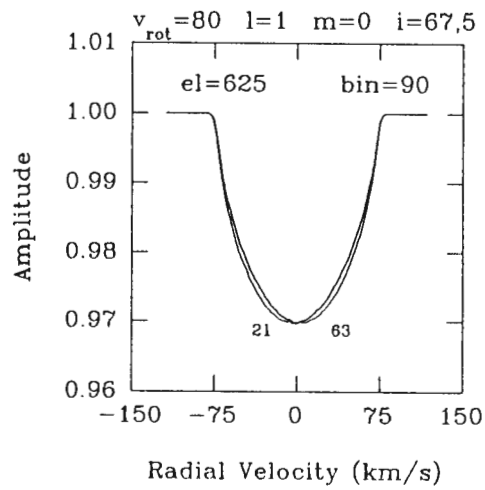
v rot =80 l=1 m=0 i=67,5
el=625 bin=90
21
63
Amplitude
1.01
1.00
0.99
0.98
0.97
0.96
−150 −75 0 75 150
Radial Velocity (km/s)

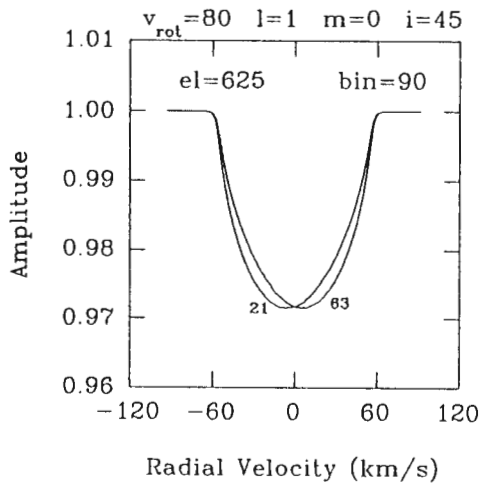
v rot =80 l=1 m=0 i=45
el=625 bin=90
21
63
Amplitude
1.01
1.00
0.99
0.98
0.97
0.96
−120 −60 0 60 120
Radial Velocity (km/s)

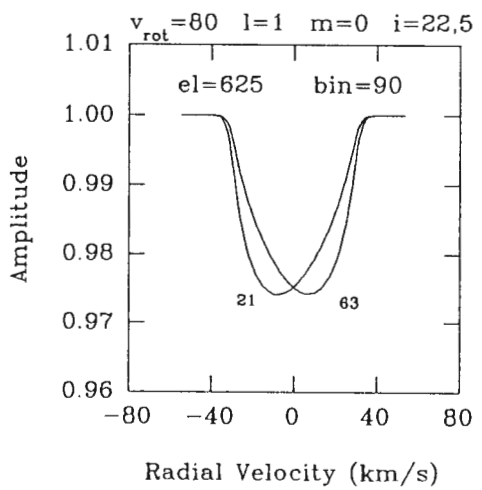
v rot =80 l=1 m=0 i=22,5
el=625 bin=90
21
63
Amplitude
1.01
1.00
0.99
0.98
0.97
0.96
−80 −40 0 40 80
Radial Velocity (km/s)

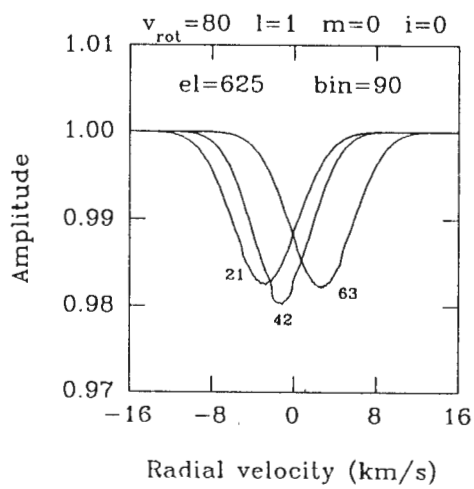
v rot =80 l=1 m=0 i=0
el=625 bin=90
21
42
63
Amplitude
1.01
1.00
0.99
0.98
0.97
−16 −8 0 8 16
Radial velocity (km/s)

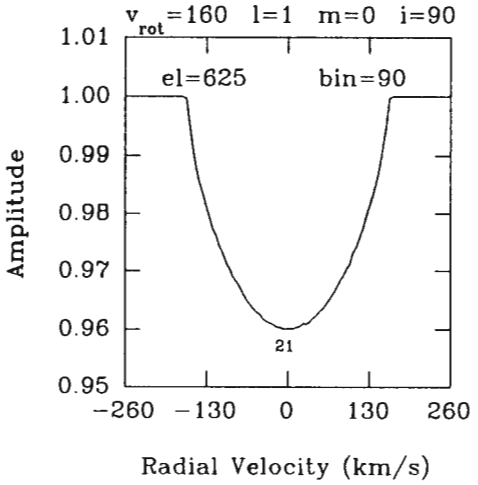
v rot =160 l=1 m=0 i=90
el=625 bin=90
21
Amplitude
1.01
1.00
0.99
0.98
0.97
0.96
0.95
−260 −130 0 130 260
Radial Velocity (km/s)

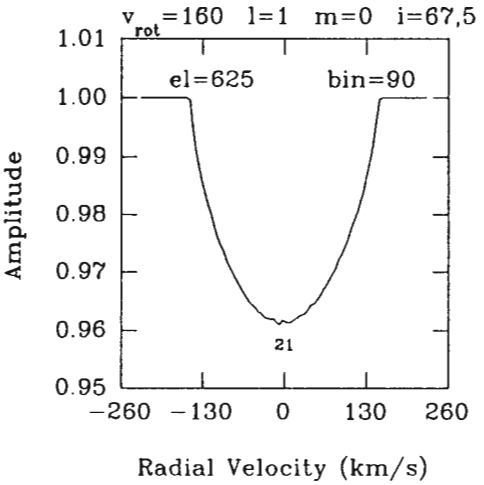
v rot =160 l=1 m=0 i=67,5
el=625 bin=90
21
Amplitude
1.01
1.00
0.99
0.98
0.97
0.96
0.95
−260 −130 0 130 260
Radial Velocity (km/s)

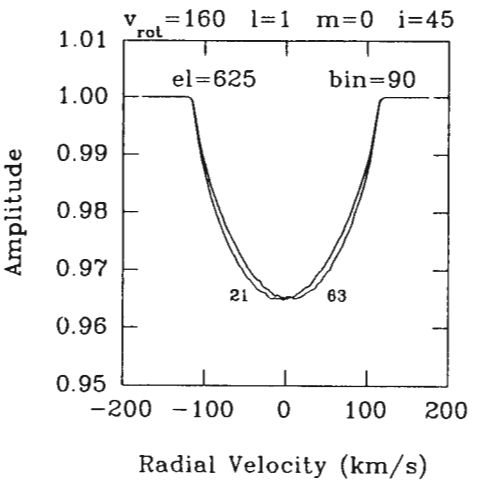
v rot =160 l=1 m=0 i=45
el=625 bin=90
21
63
Amplitude
1.01
1.00
0.99
0.98
0.97
0.96
0.95
−200 −100 0 100 200
Radial Velocity (km/s)

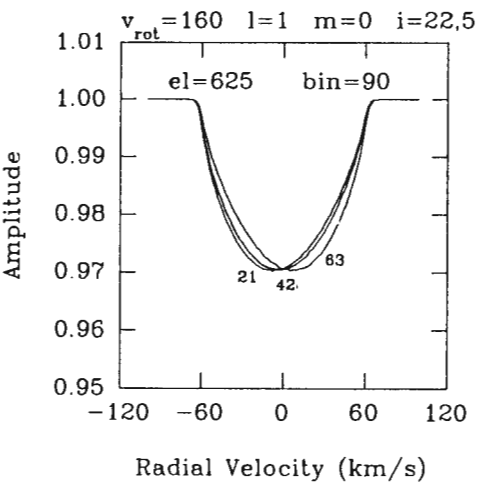
v rot =160 l=1 m=0 i=22,5
el=625 bin=90
21
42
63
Amplitude
1.01
1.00
0.99
0.98
0.97
0.96
0.95
−120 −60 0 60 120
Radial Velocity (km/s)

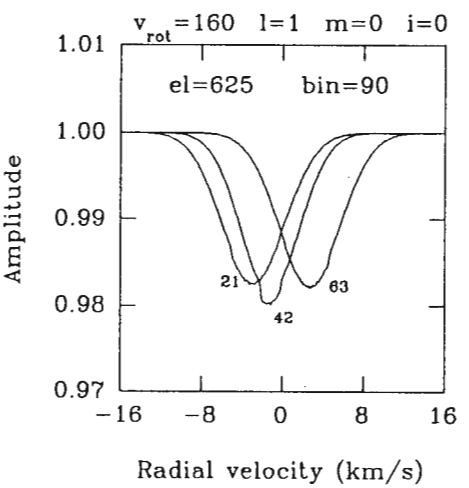
v rot =160 l=1 m=0 i=0
el=625 bin=90
21
42
63
Amplitude
1.01
1.00
0.99
0.98
0.97
−16 −8 0 8 16
Radial velocity (km/s)

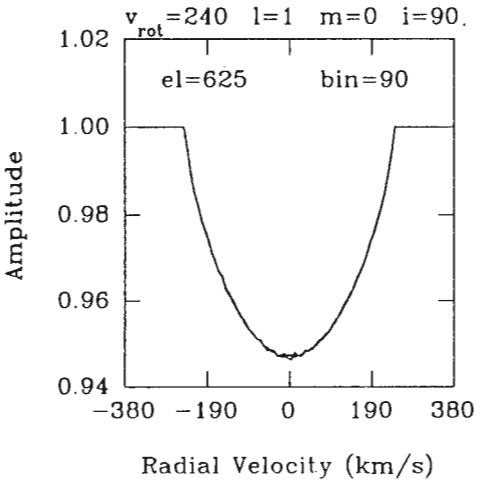
v rot =240 l=1 m=0 i=90.
el=625 bin=90
Amplitude
1.02
1.00
0.98
0.96
0.94
−380 −190 0 190 380
Radial Velocity (km/s)

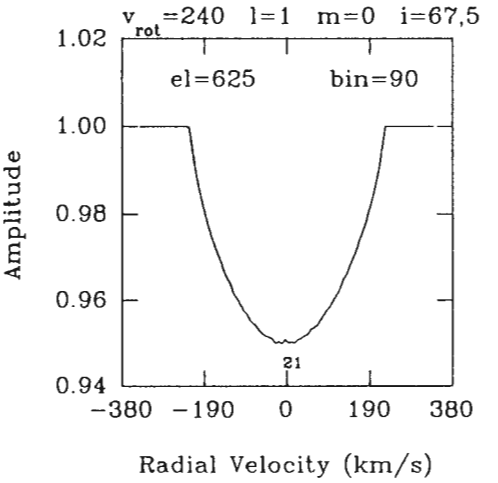
v rot =240 l=1 m=0 i=67,5
el=625 bin=90
Amplitude
1.02
1.00
0.98
0.96
0.94
21
−380 −190 0 190 380
Radial Velocity (km/s)

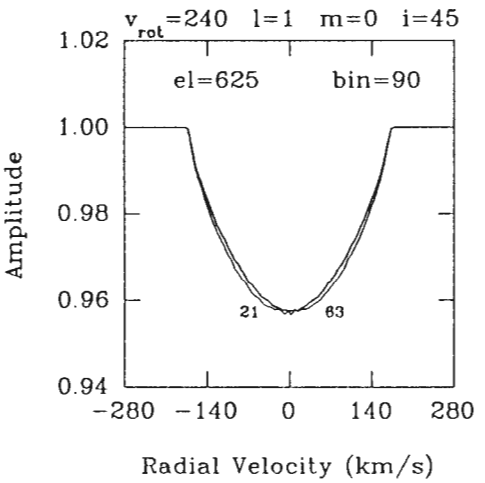
v rot =240 l=1 m=0 i=45
el=625 bin=90
Amplitude
1.02
1.00
0.98
0.96
0.94
21
63
−280 −140 0 140 280
Radial Velocity (km/s)

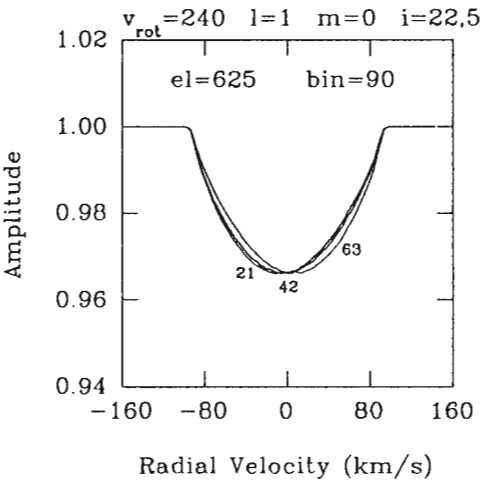
v rot =240 l=1 m=0 i=22,5
el=625 bin=90
Amplitude
1.02
1.00
0.98
0.96
0.94
21
42
63
−160 −80 0 80 160
Radial Velocity (km/s)

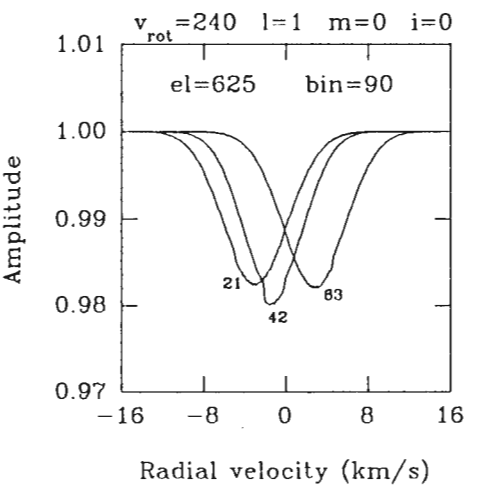
v rot =240 l=1 m=0 i=0
el=625 bin=90
Amplitude
1.01
1.00
0.99
0.98
0.97
21
42
63
−16 −8 0 8 16
Radial velocity (km/s)

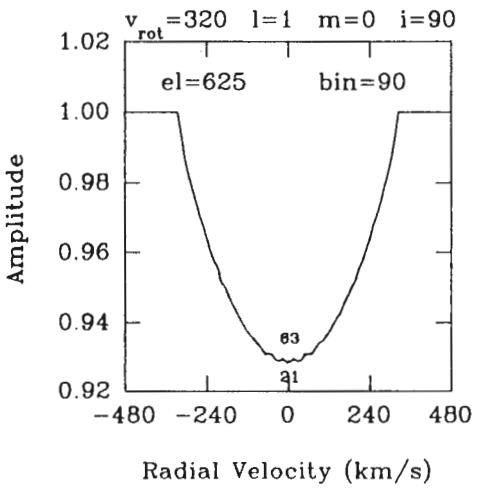
v rot =320 l=1 m=0 i=90
el=625 bin=90
Amplitude
1.02
1.00
0.98
0.96
0.94
0.92
63
21
−480 −240 0 240 480
Radial Velocity (km/s)

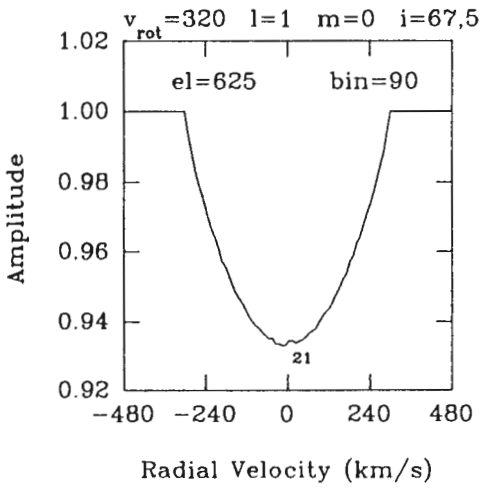
v rot =320 l=1 m=0 i=67,5
el=625 bin=90
Amplitude
1.02
1.00
0.98
0.96
0.94
0.92
21
−480 −240 0 240 480
Radial Velocity (km/s)

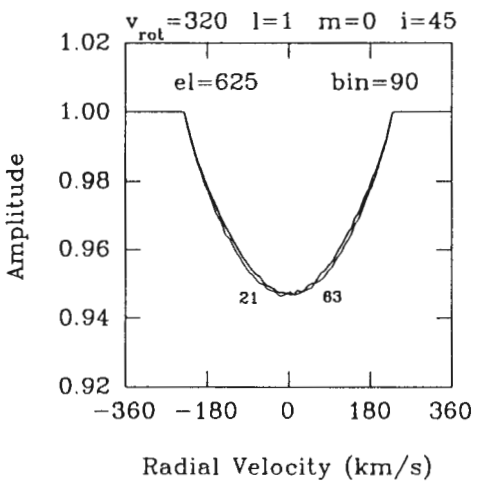
v rot =320 l=1 m=0 i=45
el=625 bin=90
Amplitude
1.02
1.00
0.98
0.96
0.94
0.92
21
63
−360 −180 0 180 360
Radial Velocity (km/s)

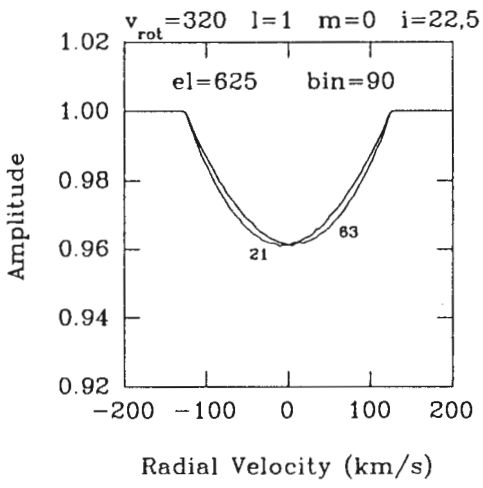
v rot =320 l=1 m=0 i=22,5
el=625 bin=90
Amplitude
1.02
1.00
0.98
0.96
0.94
0.92
21
63
−200 −100 0 100 200
Radial Velocity (km/s)

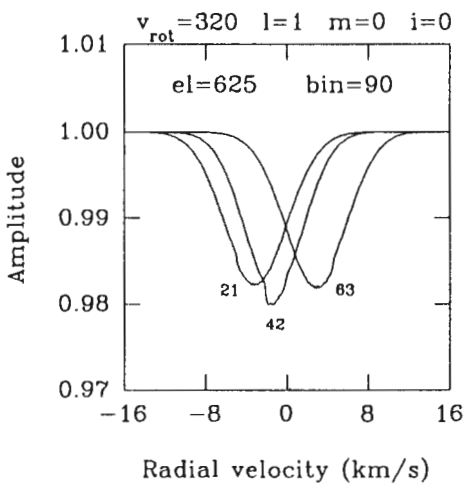
v rot =320 l=1 m=0 i=0
el=625 bin=90
Amplitude
1.01
1.00
0.99
0.98
0.97
21
42
63
−16 −8 0 8 16
Radial velocity (km/s)

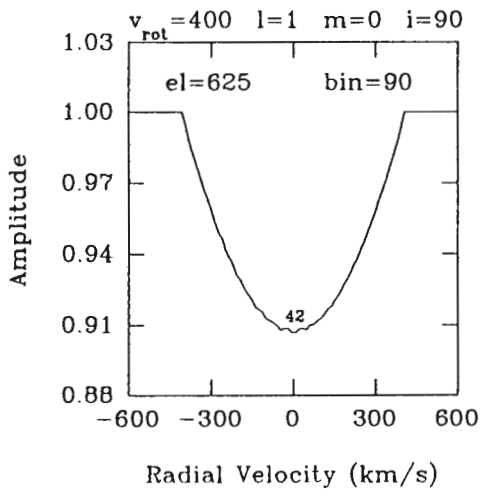
v rot =400 l=1 m=0 i=90
el=625 bin=90
1.03
1.00
0.97
0.94
0.91
0.88
42
−600 −300 0 300 600
Amplitude
Radial Velocity (km/s)

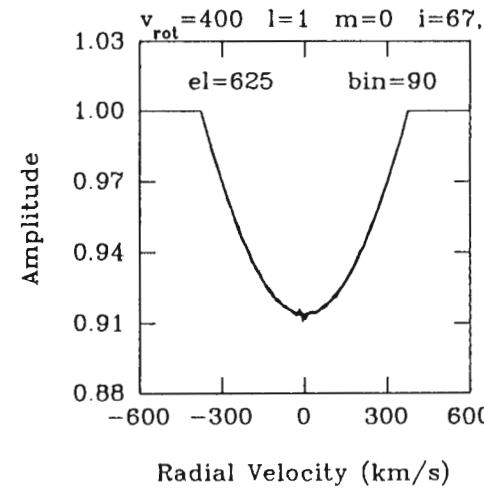
v rot =400 l=1 m=0 i=67,5
el=625 bin=90
1.03
1.00
0.97
0.94
0.91
0.88
−600 −300 0 300 600
Amplitude
Radial Velocity (km/s)

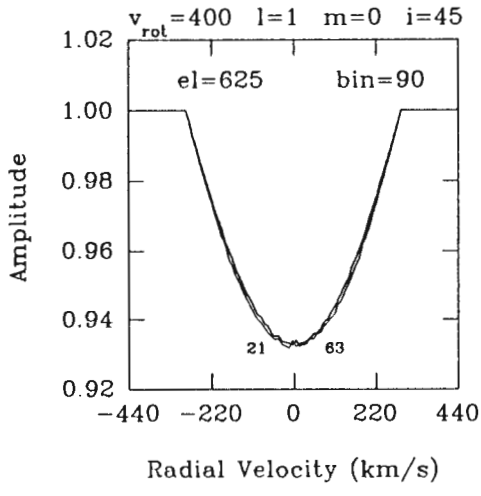
v rot =400 l=1 m=0 i=45
el=625 bin=90
1.02
1.00
0.98
0.96
0.94
0.92
21
63
−440 −220 0 220 440
Amplitude
Radial Velocity (km/s)

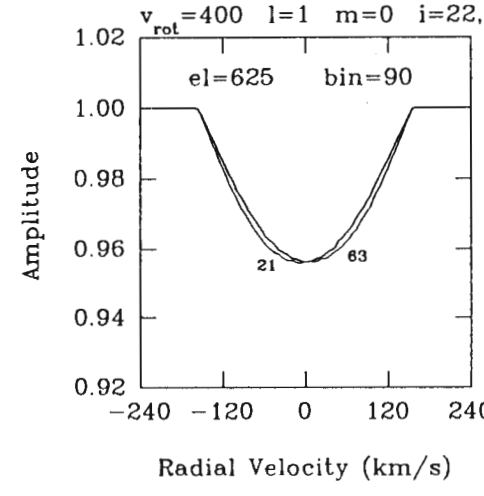
v rot =400 l=1 m=0 i=22,5
el=625 bin=90
1.02
1.00
0.98
0.96
0.94
0.92
21
63
−240 −120 0 120 240
Amplitude
Radial Velocity (km/s)

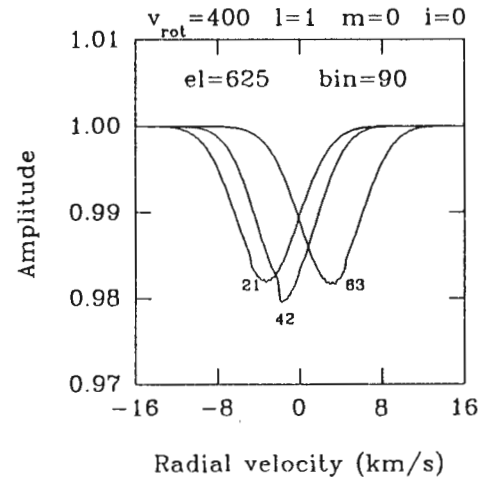
v rot =400 l=1 m=0 i=0
el=625 bin=90
1.01
1.00
0.99
0.98
0.97
21
42
63
−16 −8 0 8 16
Amplitude
Radial velocity (km/s)

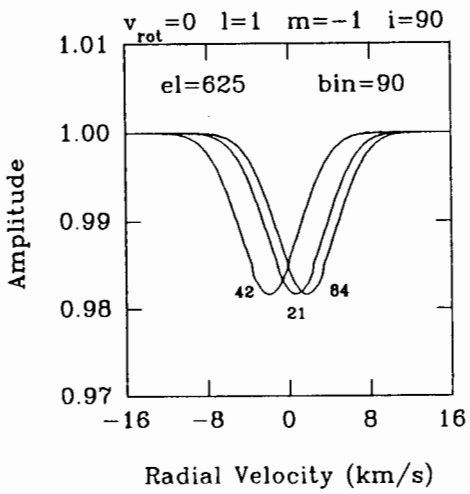
v rot =0 l=1 m=−1 i=90
el=625 bin=90
1.01
1.00
0.99
0.98
0.97
Amplitude
42
84
21
−16 −8 0 8 16
Radial Velocity (km/s)

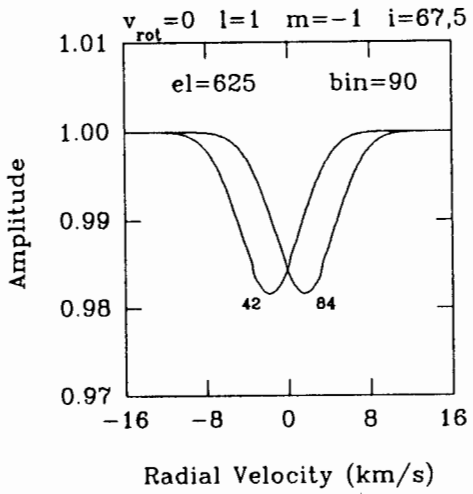
v rot =0 l=1 m=−1 i=67,5
el=625 bin=90
1.01
1.00
0.99
0.98
0.97
Amplitude
42
84
−16 −8 0 8 16
Radial Velocity (km/s)

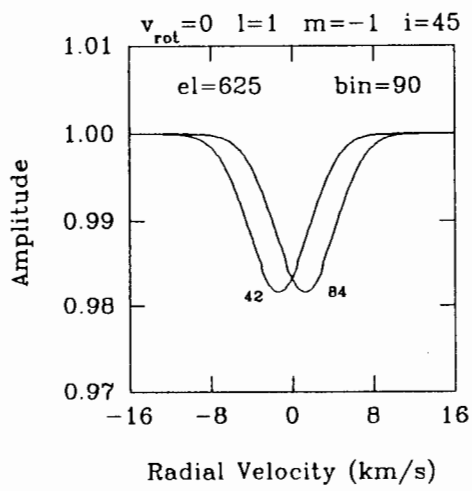
v rot =0 l=1 m=−1 i=45
el=625 bin=90
1.01
1.00
0.99
0.98
0.97
Amplitude
42
84
−16 −8 0 8 16
Radial Velocity (km/s)

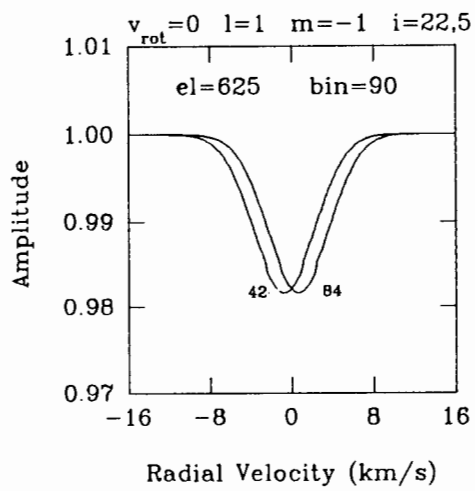
v rot =0 l=1 m=−1 i=22,5
el=625 bin=90
1.01
1.00
0.99
0.98
0.97
Amplitude
42
84
−16 −8 0 8 16
Radial Velocity (km/s)

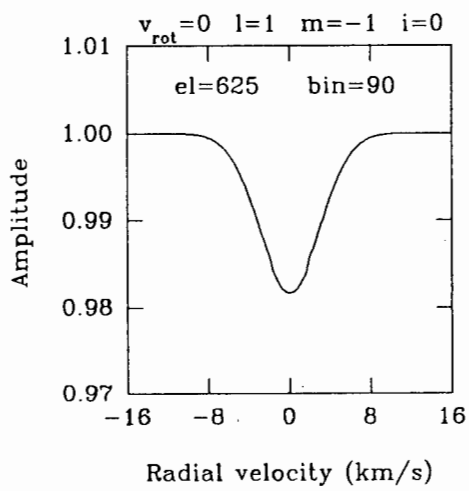
v rot =0 l=1 m=−1 i=0
el=625 bin=90
1.01
1.00
0.99
0.98
0.97
Amplitude
−16 −8 0 8 16
Radial velocity (km/s)

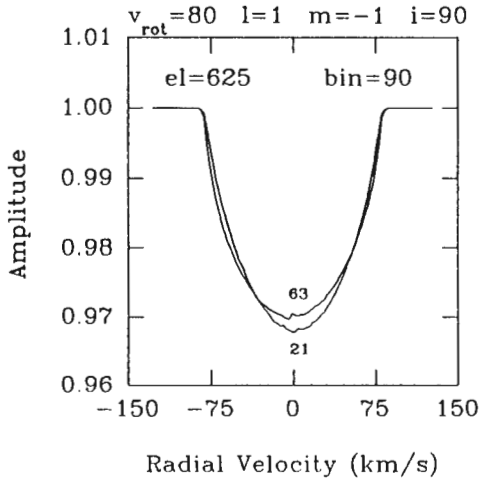
v rot =80 l=1 m=-1 i=90
el=625 bin=90
63
21
Amplitude
1.01
1.00
0.99
0.98
0.97
0.96
-150 -75 0 75 150
Radial Velocity (km/s)

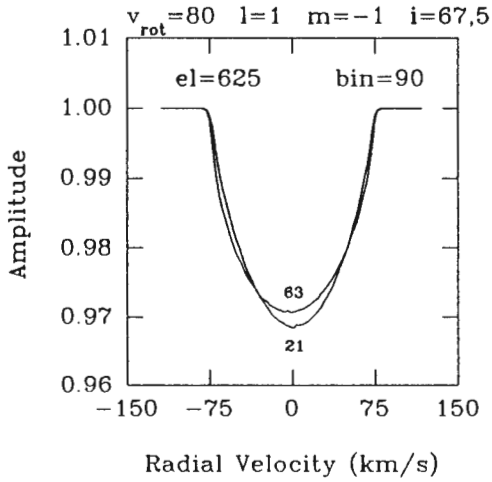
v rot =80 l=1 m=-1 i=67,5
el=625 bin=90
63
21
Amplitude
1.01
1.00
0.99
0.98
0.97
0.96
-150 -75 0 75 150
Radial Velocity (km/s)

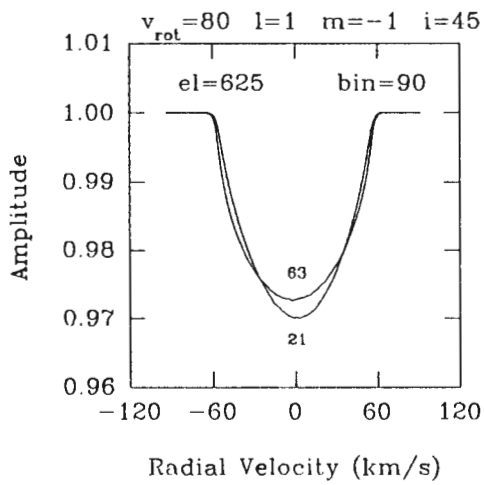
v rot =80 l=1 m=-1 i=45
el=625 bin=90
63
21
Amplitude
1.01
1.00
0.99
0.98
0.97
0.96
-120 -60 0 60 120
Radial Velocity (km/s)

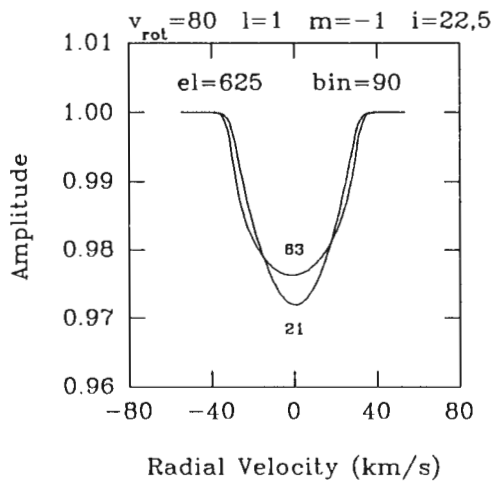
v rot =80 l=1 m=-1 i=22,5
el=625 bin=90
63
21
Amplitude
1.01
1.00
0.99
0.98
0.97
0.96
-80 -40 0 40 80
Radial Velocity (km/s)

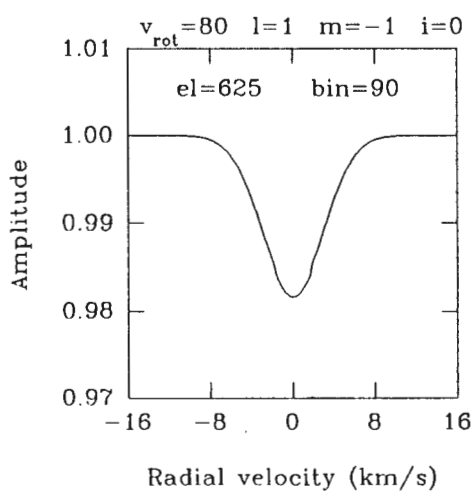
v rot =80 l=1 m=-1 i=0
el=625 bin=90
Amplitude
1.01
1.00
0.99
0.98
0.97
-16 -8 0 8 16
Radial velocity (km/s)

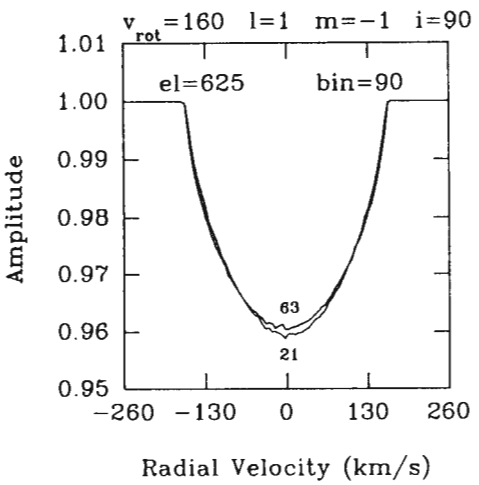
v rot =160 l=1 m=−1 i=90
el=625 bin=90
Amplitude
1.01
1.00
0.99
0.98
0.97
0.96
0.95
63
21
−260 −130 0 130 260
Radial Velocity (km/s)

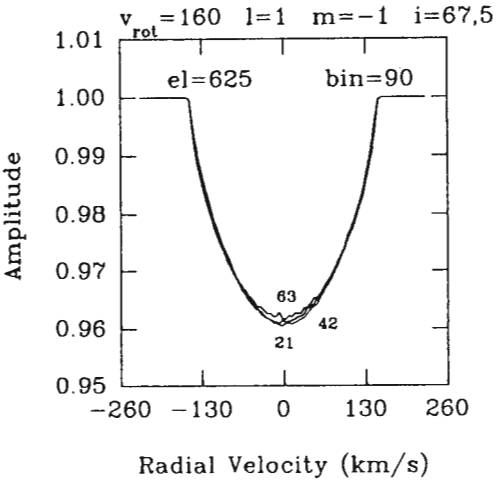
v rot =160 l=1 m=−1 i=67,5
el=625 bin=90
Amplitude
1.01
1.00
0.99
0.98
0.97
0.96
0.95
63
42
21
−260 −130 0 130 260
Radial Velocity (km/s)

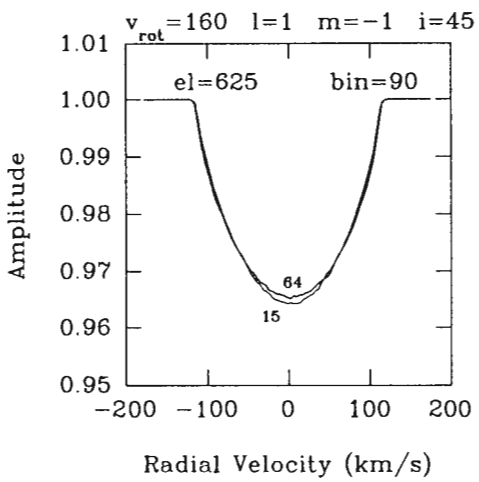
v rot =160 l=1 m=−1 i=45
el=625 bin=90
Amplitude
1.01
1.00
0.99
0.98
0.97
0.96
0.95
64
15
−200 −100 0 100 200
Radial Velocity (km/s)

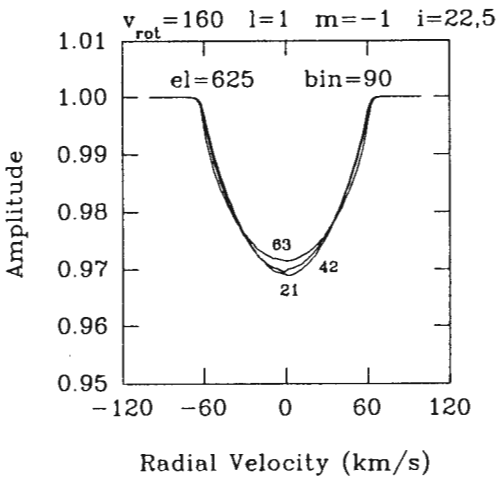
v rot =160 l=1 m=−1 i=22,5
el=625 bin=90
Amplitude
1.01
1.00
0.99
0.98
0.97
0.96
0.95
63
42
21
−120 −60 0 60 120
Radial Velocity (km/s)

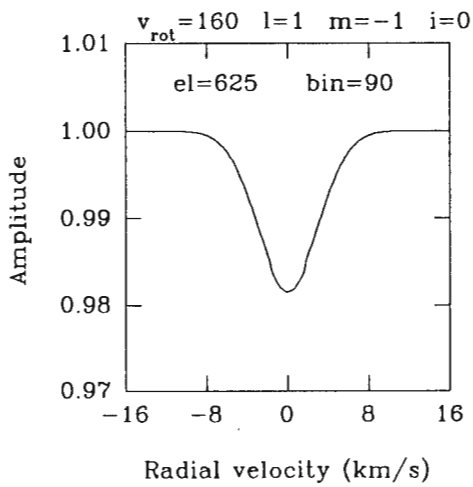
v rot =160 l=1 m=−1 i=0
el=625 bin=90
Amplitude
1.01
1.00
0.99
0.98
0.97
−16 −8 0 8 16
Radial velocity (km/s)

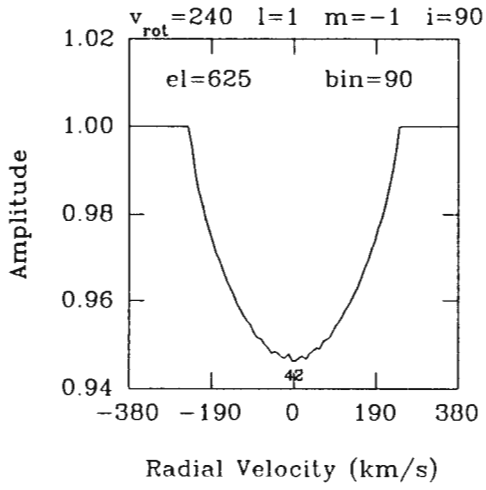
v rot =240 l=1 m=−1 i=90
el=625 bin=90
1.02
1.00
0.98
0.96
0.94
Amplitude
42
−380 −190 0 190 380
Radial Velocity (km/s)

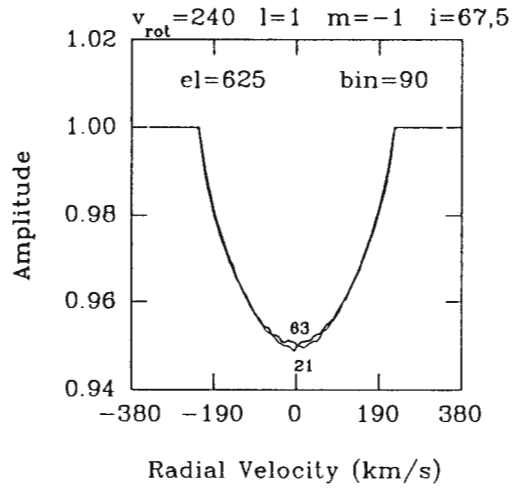
v rot =240 l=1 m=−1 i=67,5
el=625 bin=90
1.02
1.00
0.98
0.96
0.94
Amplitude
63
21
−380 −190 0 190 380
Radial Velocity (km/s)

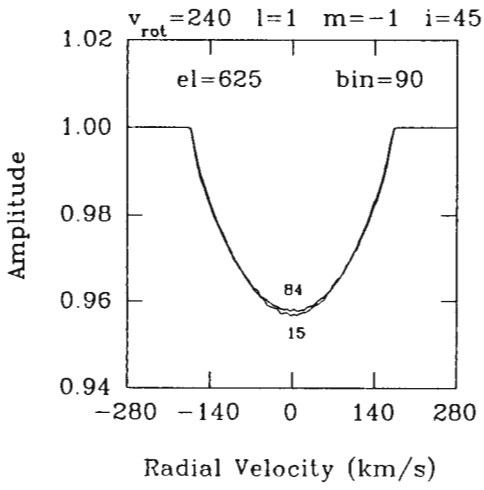
v rot =240 l=1 m=−1 i=45
el=625 bin=90
1.02
1.00
0.98
0.96
0.94
Amplitude
84
15
−280 −140 0 140 280
Radial Velocity (km/s)

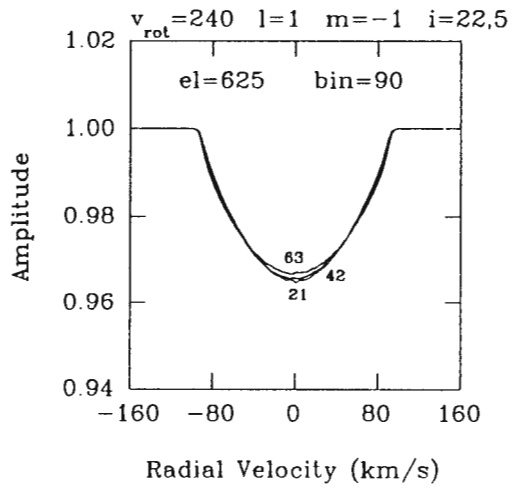
v rot =240 l=1 m=−1 i=22,5
el=625 bin=90
1.02
1.00
0.98
0.96
0.94
Amplitude
63
42
21
−160 −80 0 80 160
Radial Velocity (km/s)

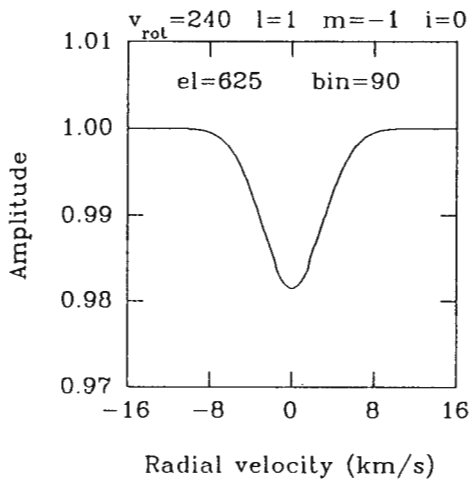
v rot =240 l=1 m=−1 i=0
el=625 bin=90
1.01
1.00
0.99
0.98
0.97
Amplitude
−16 −8 0 8 16
Radial velocity (km/s)

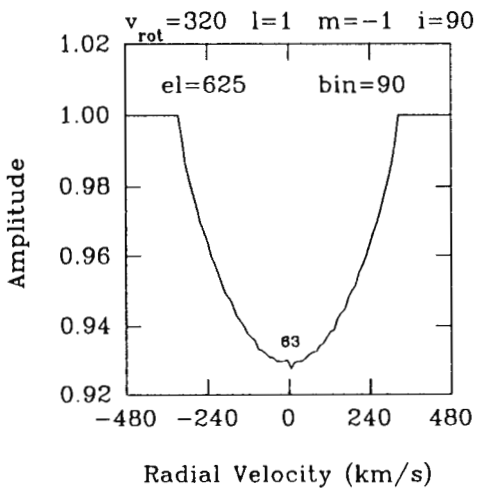
v rot =320 l=1 m=−1 i=90
el=625 bin=90
63
1.02
1.00
0.98
0.96
0.94
0.92
−480 −240 0 240 480
Amplitude
Radial Velocity (km/s)

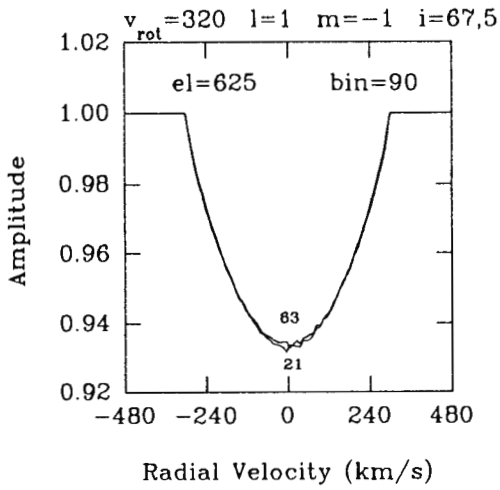
v rot =320 l=1 m=−1 i=67,5
el=625 bin=90
63
21
1.02
1.00
0.98
0.96
0.94
0.92
−480 −240 0 240 480
Amplitude
Radial Velocity (km/s)

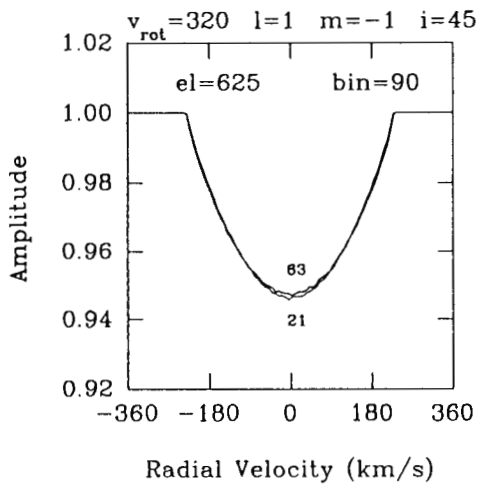
v rot =320 l=1 m=−1 i=45
el=625 bin=90
63
21
1.02
1.00
0.98
0.96
0.94
0.92
−360 −180 0 180 360
Amplitude
Radial Velocity (km/s)

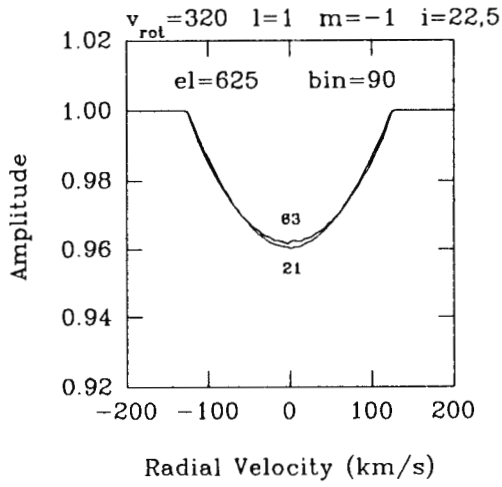
v rot =320 l=1 m=−1 i=22,5
el=625 bin=90
63
21
1.02
1.00
0.98
0.96
0.94
0.92
−200 −100 0 100 200
Amplitude
Radial Velocity (km/s)

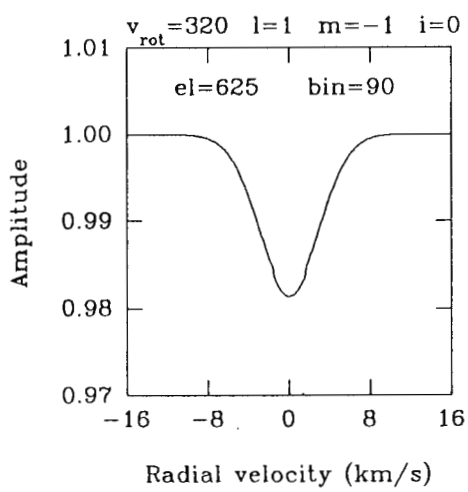
v rot =320 l=1 m=−1 i=0
el=625 bin=90
1.01
1.00
0.99
0.98
0.97
−16 −8 0 8 16
Amplitude
Radial velocity (km/s)

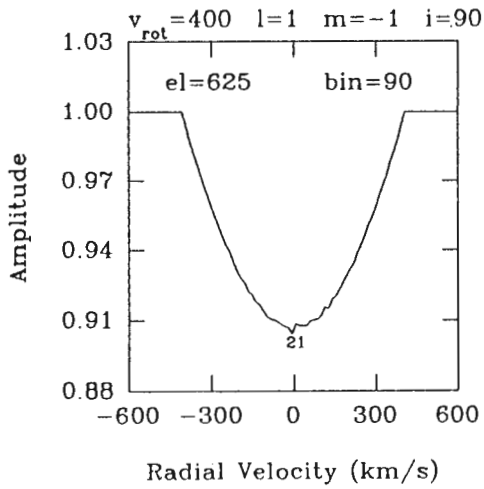
v rot =400 l=1 m=-1 i=90
el=625 bin=90
Amplitude
1.03
1.00
0.97
0.94
0.91
0.88
21
-600 -300 0 300 600
Radial Velocity (km/s)

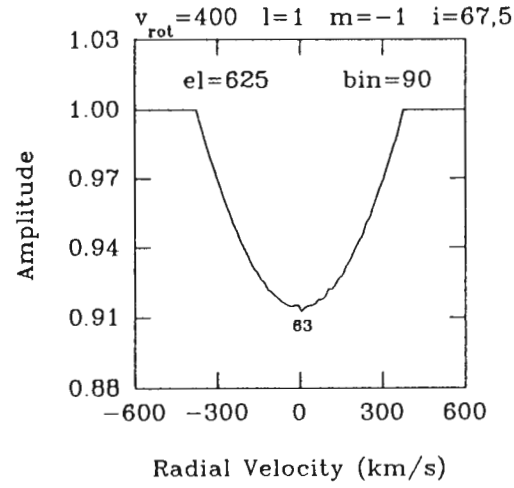
v rot =400 l=1 m=-1 i=67,5
el=625 bin=90
Amplitude
1.03
1.00
0.97
0.94
0.91
0.88
63
-600 -300 0 300 600
Radial Velocity (km/s)

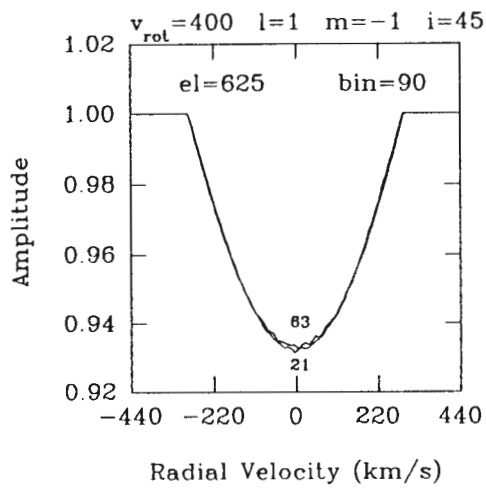
v rot =400 l=1 m=-1 i=45
el=625 bin=90
Amplitude
1.02
1.00
0.98
0.96
0.94
0.92
63
21
-440 -220 0 220 440
Radial Velocity (km/s)

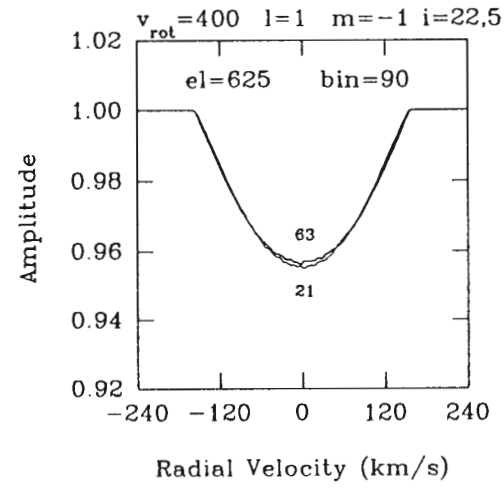
v rot =400 l=1 m=-1 i=22,5
el=625 bin=90
Amplitude
1.02
1.00
0.98
0.96
0.94
0.92
63
21
-240 -120 0 120 240
Radial Velocity (km/s)

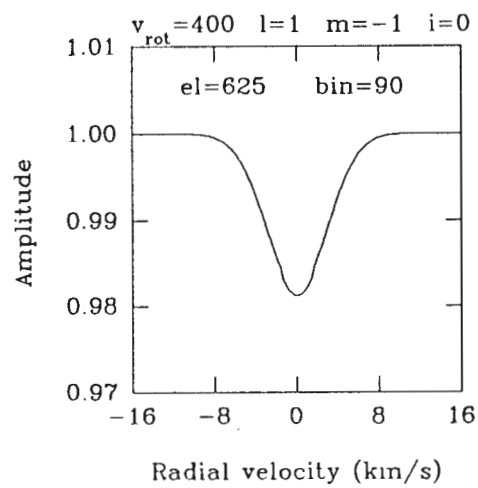
v rot =400 l=1 m=-1 i=0
el=625 bin=90
Amplitude
1.01
1.00
0.99
0.98
0.97
-16 -8 0 8 16
Radial velocity (km/s)

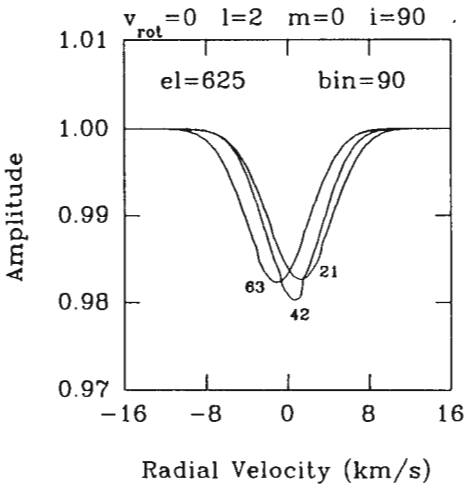
v rot =0 l=2 m=0 i=90
el=625 bin=90
1.01
1.00
0.99
0.98
0.97
Amplitude
63
21
42
−16 −8 0 8 16
Radial Velocity (km/s)

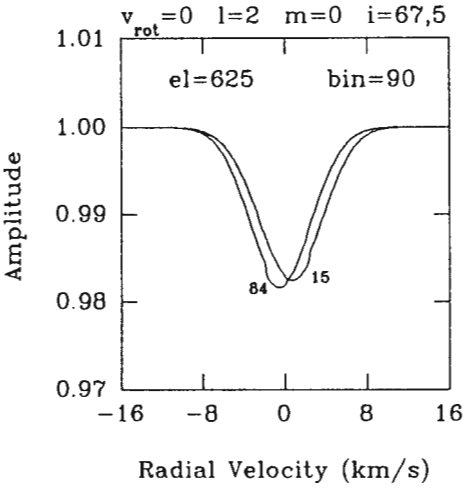
v rot =0 l=2 m=0 i=67,5
el=625 bin=90
1.01
1.00
0.99
0.98
0.97
Amplitude
84
15
−16 −8 0 8 16
Radial Velocity (km/s)

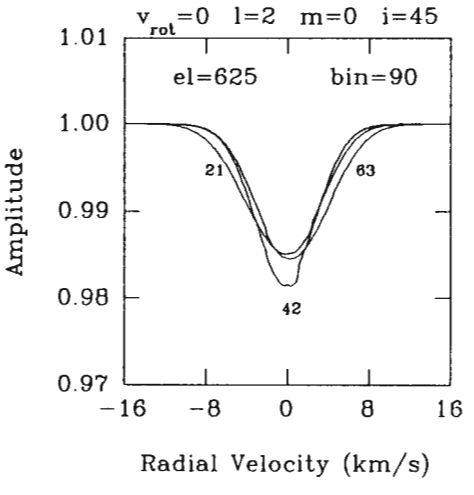
v rot =0 l=2 m=0 i=45
el=625 bin=90
1.01
1.00
0.99
0.98
0.97
Amplitude
21
63
42
−16 −8 0 8 16
Radial Velocity (km/s)

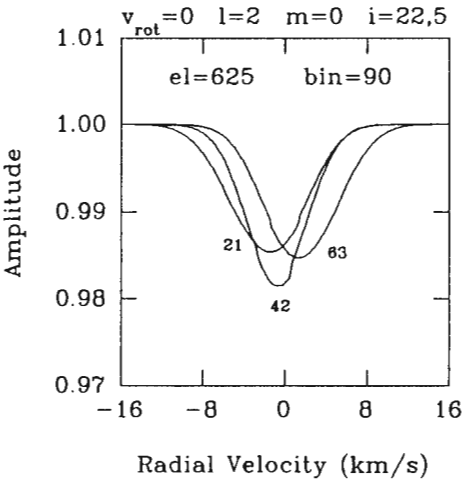
v rot =0 l=2 m=0 i=22,5
el=625 bin=90
1.01
1.00
0.99
0.98
0.97
Amplitude
21
63
42
−16 −8 0 8 16
Radial Velocity (km/s)

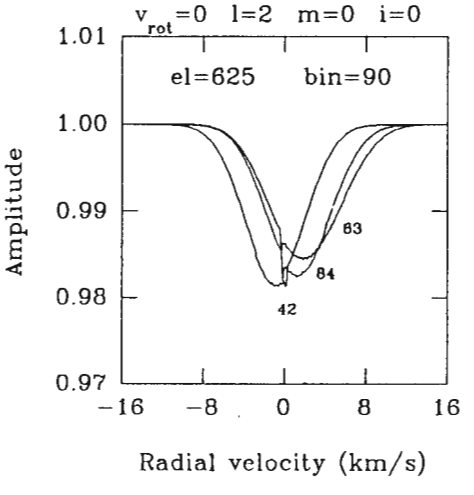
v rot =0 l=2 m=0 i=0
el=625 bin=90
1.01
1.00
0.99
0.98
0.97
Amplitude
63
84
42
−16 −8 0 8 16
Radial velocity (km/s)

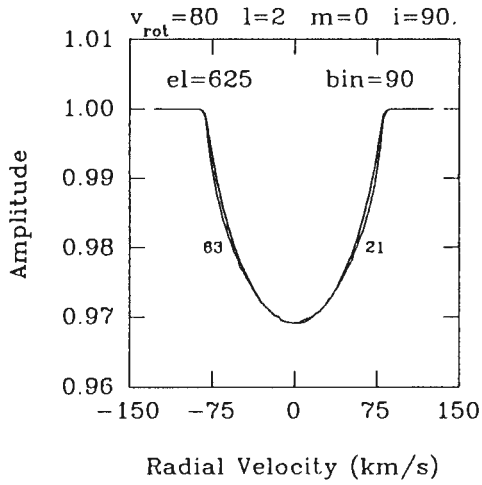
v rot =80 l=2 m=0 i=90.
el=625 bin=90
63
21
Amplitude
1.01
1.00
0.99
0.98
0.97
0.96
−150 −75 0 75 150
Radial Velocity (km/s)

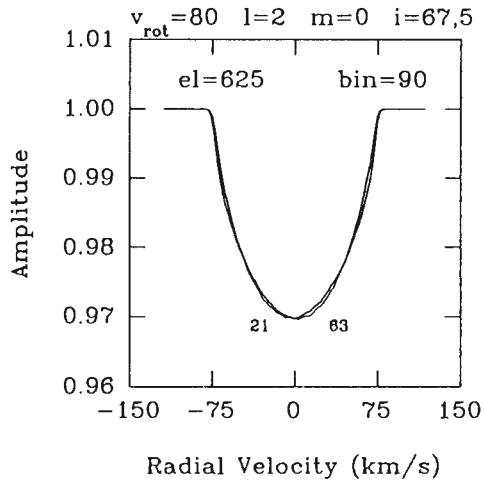
v rot =80 l=2 m=0 i=67,5
el=625 bin=90
21
63
Amplitude
1.01
1.00
0.99
0.98
0.97
0.96
−150 −75 0 75 150
Radial Velocity (km/s)

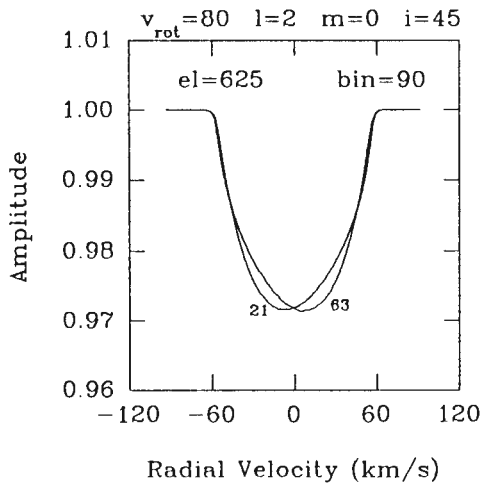
v rot =80 l=2 m=0 i=45
el=625 bin=90
21
63
Amplitude
1.01
1.00
0.99
0.98
0.97
0.96
−120 −60 0 60 120
Radial Velocity (km/s)

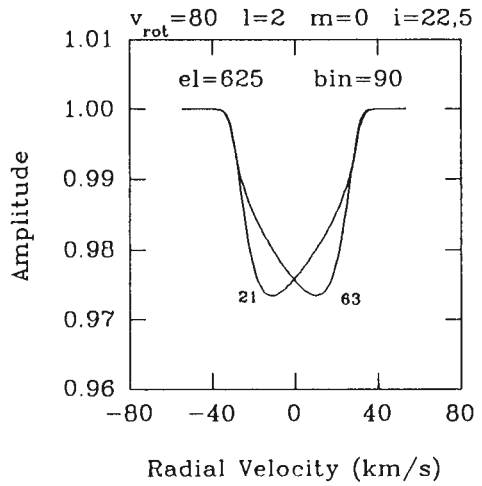
v rot =80 l=2 m=0 i=22,5
el=625 bin=90
21
63
Amplitude
1.01
1.00
0.99
0.98
0.97
0.96
−80 −40 0 40 80
Radial Velocity (km/s)

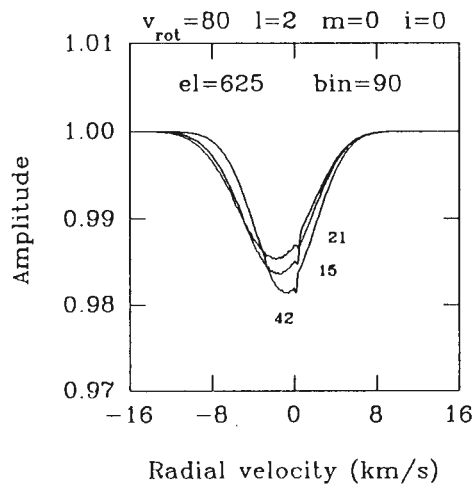
v rot =80 l=2 m=0 i=0
el=625 bin=90
21
15
42
Amplitude
1.01
1.00
0.99
0.98
0.97
−16 −8 0 8 16
Radial velocity (km/s)

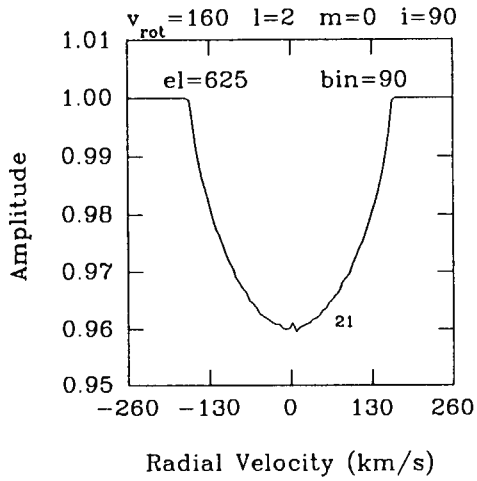
v rot =160 l=2 m=0 i=90
el=625 bin=90
21
Amplitude
1.01
1.00
0.99
0.98
0.97
0.96
0.95
−260 −130 0 130 260
Radial Velocity (km/s)

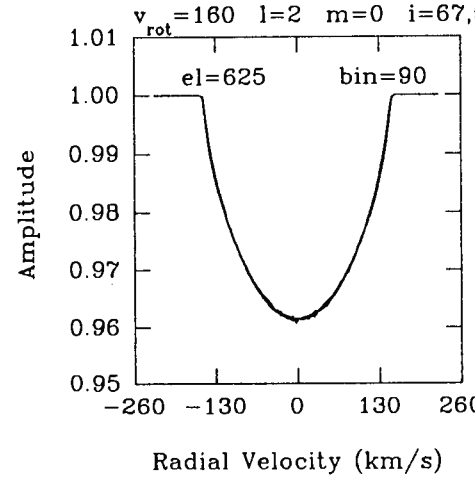
v rot =160 l=2 m=0 i=67,5
el=625 bin=90
Amplitude
1.01
1.00
0.99
0.98
0.97
0.96
0.95
−260 −130 0 130 260
Radial Velocity (km/s)

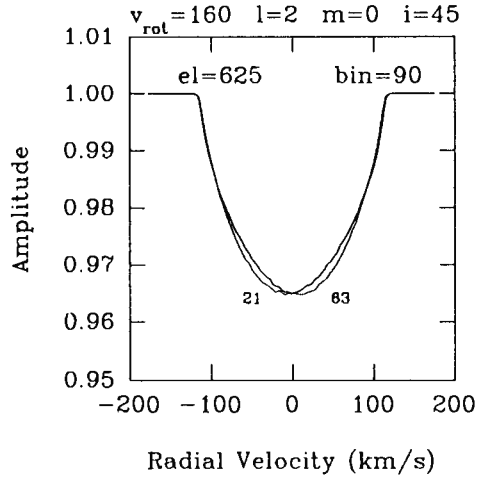
v rot =160 l=2 m=0 i=45
el=625 bin=90
21
63
Amplitude
1.01
1.00
0.99
0.98
0.97
0.96
0.95
−200 −100 0 100 200
Radial Velocity (km/s)

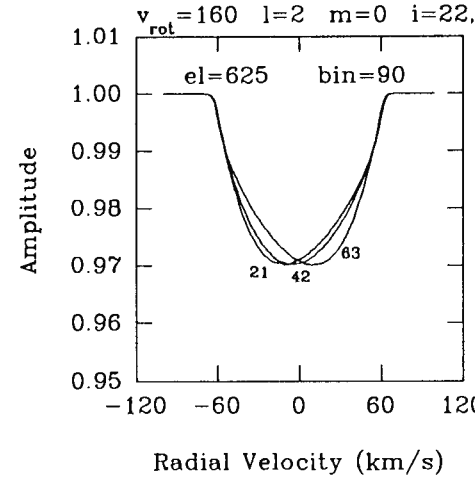
v rot =160 l=2 m=0 i=22,5
el=625 bin=90
21
42
63
Amplitude
1.01
1.00
0.99
0.98
0.97
0.96
0.95
−120 −60 0 60 120
Radial Velocity (km/s)

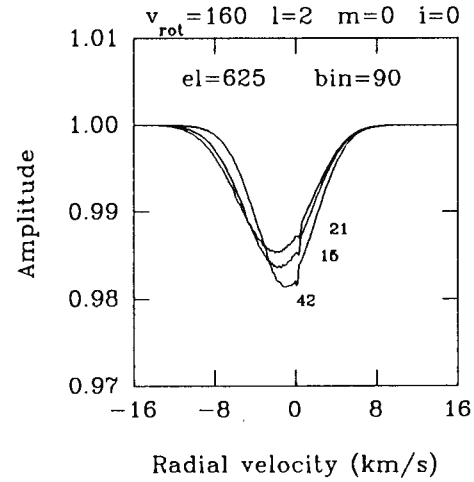
v rot =160 l=2 m=0 i=0
el=625 bin=90
21
16
42
Amplitude
1.01
1.00
0.99
0.98
0.97
−16 −8 0 8 16
Radial velocity (km/s)

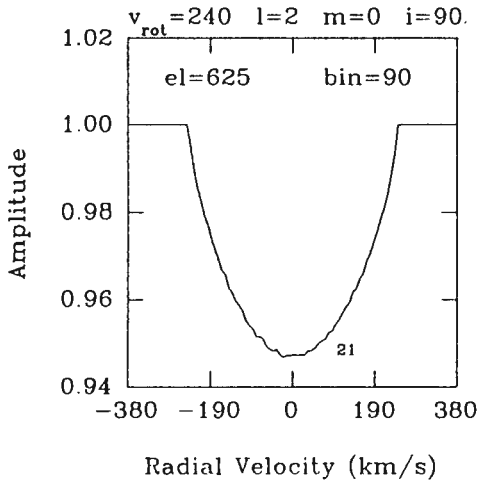
v rot =240 l=2 m=0 i=90.
el=625 bin=90
21
Amplitude
1.02
1.00
0.98
0.96
0.94
−380 −190 0 190 380
Radial Velocity (km/s)

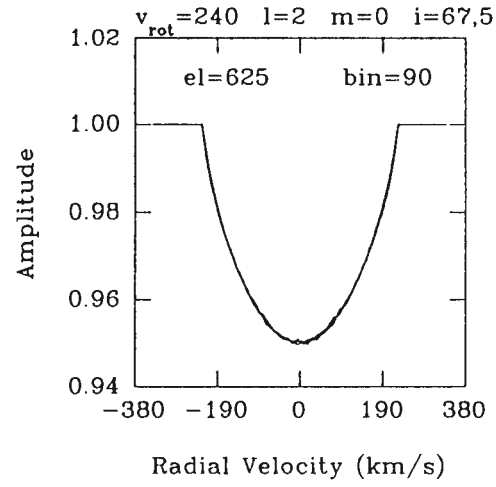
v rot =240 l=2 m=0 i=67,5
el=625 bin=90
Amplitude
1.02
1.00
0.98
0.96
0.94
−380 −190 0 190 380
Radial Velocity (km/s)

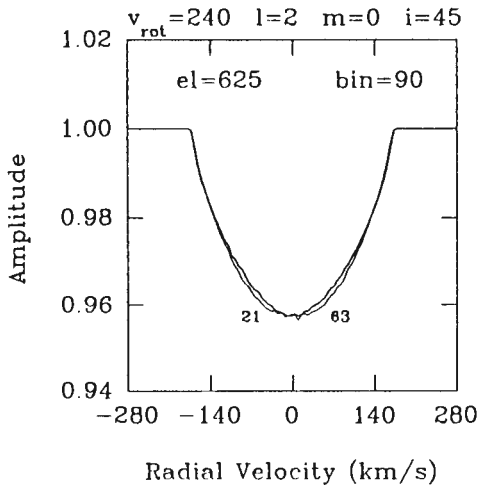
v rot =240 l=2 m=0 i=45
el=625 bin=90
21
63
Amplitude
1.02
1.00
0.98
0.96
0.94
−280 −140 0 140 280
Radial Velocity (km/s)

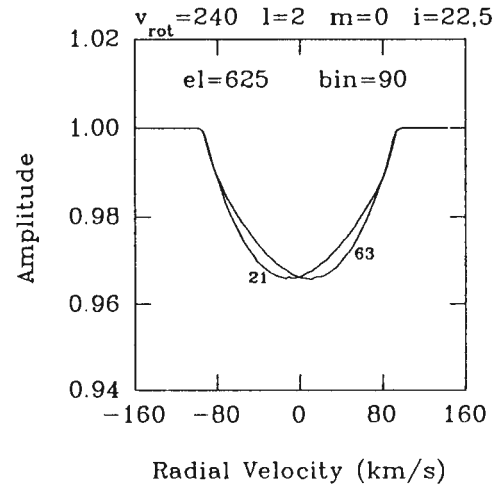
v rot =240 l=2 m=0 i=22,5
el=625 bin=90
21
63
Amplitude
1.02
1.00
0.98
0.96
0.94
−160 −80 0 80 160
Radial Velocity (km/s)

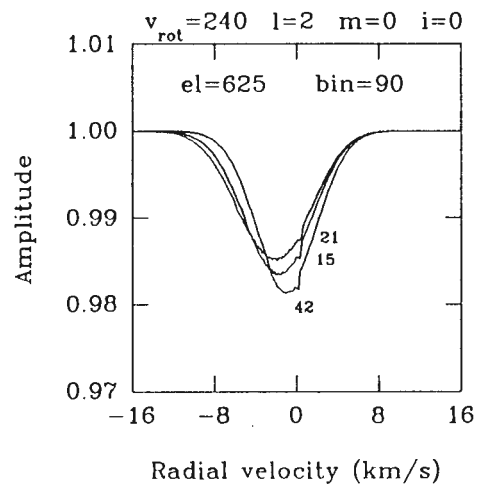
v rot =240 l=2 m=0 i=0
el=625 bin=90
21
15
42
Amplitude
1.01
1.00
0.99
0.98
0.97
−16 −8 0 8 16
Radial velocity (km/s)

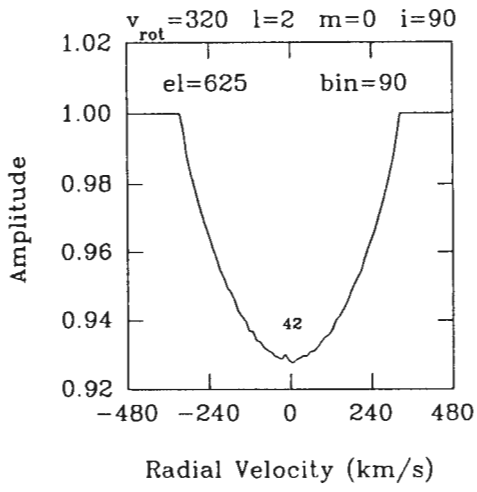
v rot =320 l=2 m=0 i=90
el=625 bin=90
Amplitude
1.02
1.00
0.98
0.96
0.94
0.92
42
−480 −240 0 240 480
Radial Velocity (km/s)

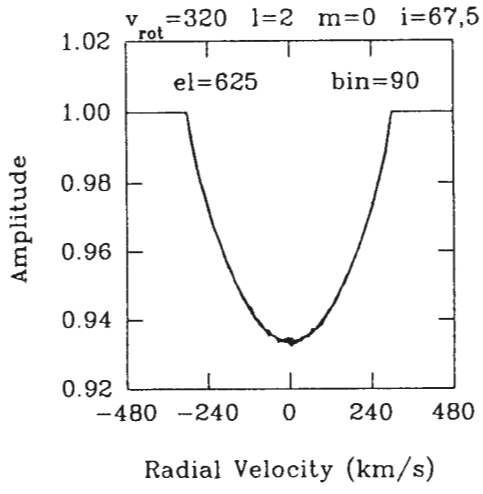
v rot =320 l=2 m=0 i=67,5
el=625 bin=90
Amplitude
1.02
1.00
0.98
0.96
0.94
0.92
−480 −240 0 240 480
Radial Velocity (km/s)

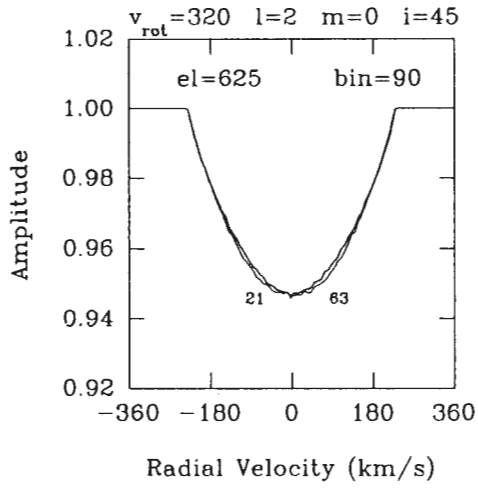
v rot =320 l=2 m=0 i=45
el=625 bin=90
Amplitude
1.02
1.00
0.98
0.96
0.94
0.92
21
63
−360 −180 0 180 360
Radial Velocity (km/s)

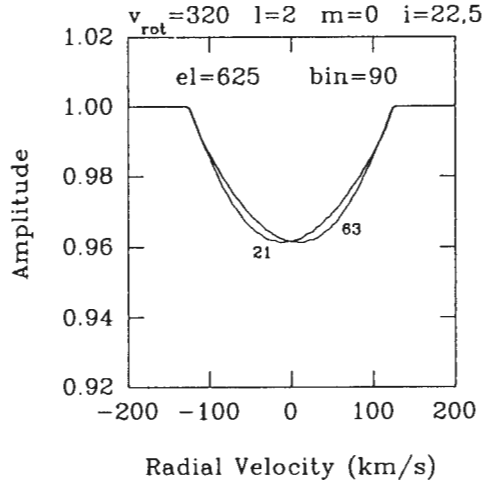
v rot =320 l=2 m=0 i=22,5
el=625 bin=90
Amplitude
1.02
1.00
0.98
0.96
0.94
0.92
21
63
−200 −100 0 100 200
Radial Velocity (km/s)

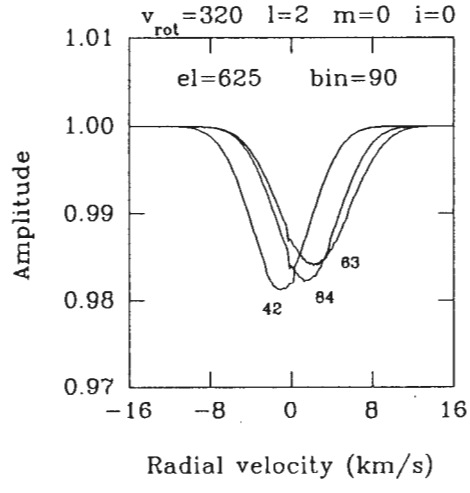
v rot =320 l=2 m=0 i=0
el=625 bin=90
Amplitude
1.01
1.00
0.99
0.98
0.97
42
84
63
−16 −8 0 8 16
Radial velocity (km/s)

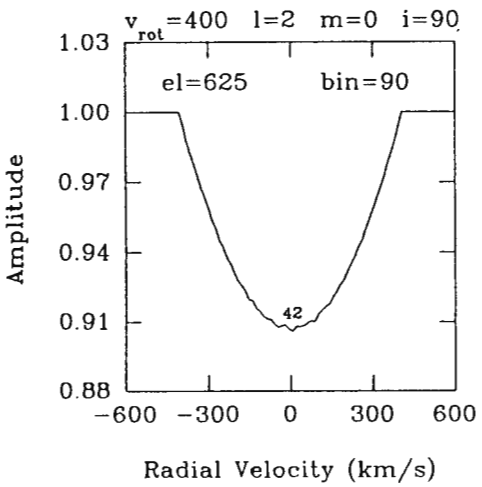
v rot =400 l=2 m=0 i=90
el=625 bin=90
42
Amplitude
1.03
1.00
0.97
0.94
0.91
0.88
−600 −300 0 300 600
Radial Velocity (km/s)

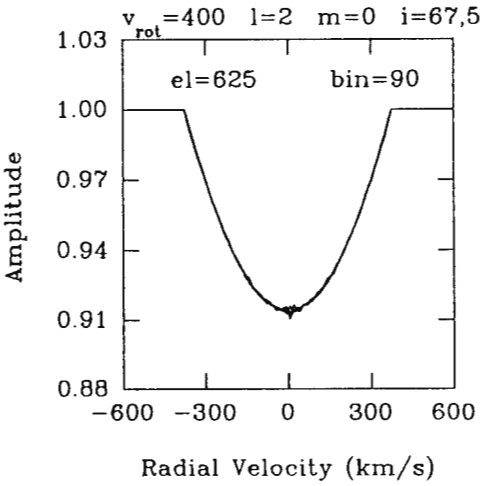
v rot =400 l=2 m=0 i=67,5
el=625 bin=90
Amplitude
1.03
1.00
0.97
0.94
0.91
0.88
−600 −300 0 300 600
Radial Velocity (km/s)

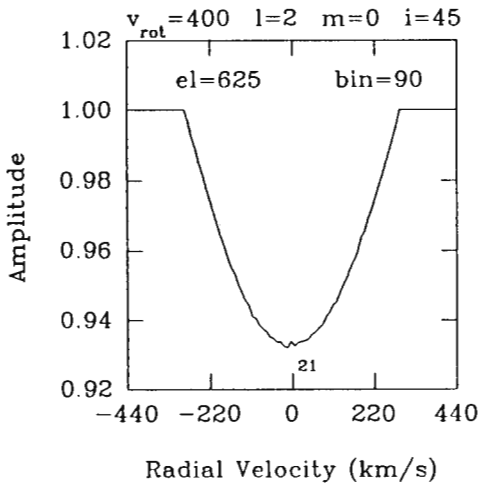
v rot =400 l=2 m=0 i=45
el=625 bin=90
21
Amplitude
1.02
1.00
0.98
0.96
0.94
0.92
−440 −220 0 220 440
Radial Velocity (km/s)

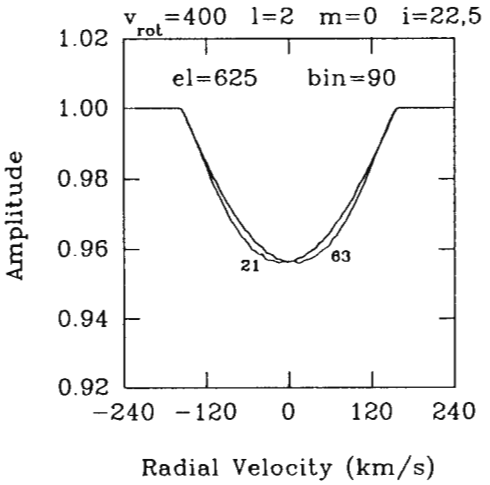
v rot =400 l=2 m=0 i=22,5
el=625 bin=90
21
63
Amplitude
1.02
1.00
0.98
0.96
0.94
0.92
−240 −120 0 120 240
Radial Velocity (km/s)

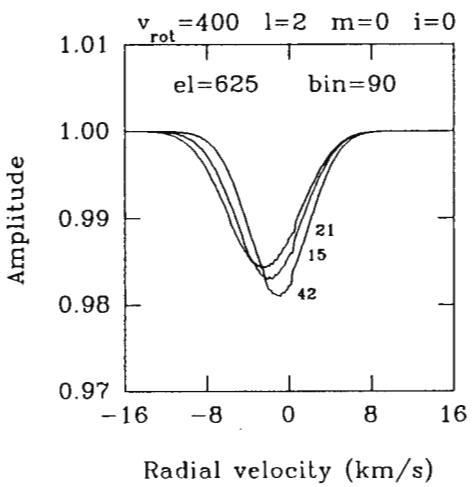
v rot =400 l=2 m=0 i=0
el=625 bin=90
21
15
42
Amplitude
1.01
1.00
0.99
0.98
0.97
−16 −8 0 8 16
Radial velocity (km/s)

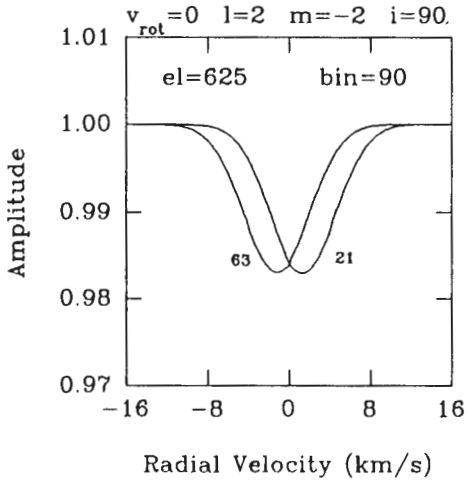
v rot =0 l=2 m=−2 i=90.
el=625 bin=90
63
21
Amplitude
1.01
1.00
0.99
0.98
0.97
−16 −8 0 8 16
Radial Velocity (km/s)

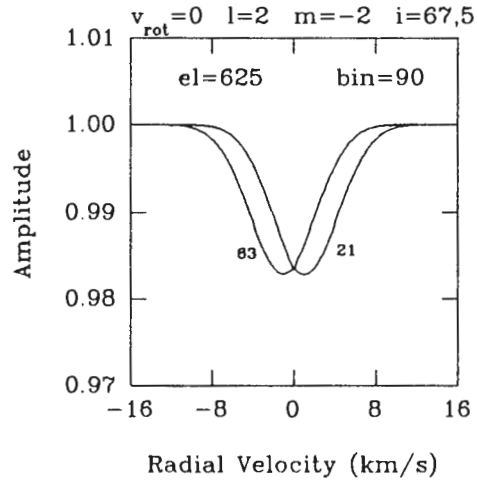
v rot =0 l=2 m=−2 i=67,5
el=625 bin=90
63
21
Amplitude
1.01
1.00
0.99
0.98
0.97
−16 −8 0 8 16
Radial Velocity (km/s)

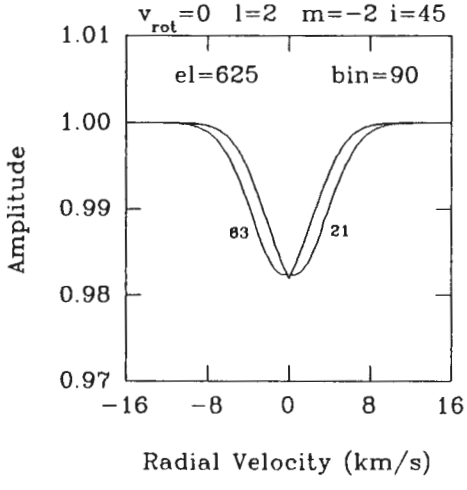
v rot =0 l=2 m=−2 i=45
el=625 bin=90
63
21
Amplitude
1.01
1.00
0.99
0.98
0.97
−16 −8 0 8 16
Radial Velocity (km/s)

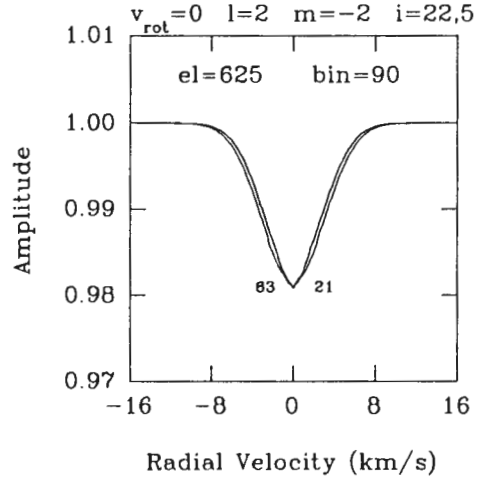
v rot =0 l=2 m=−2 i=22,5
el=625 bin=90
63
21
Amplitude
1.01
1.00
0.99
0.98
0.97
−16 −8 0 8 16
Radial Velocity (km/s)

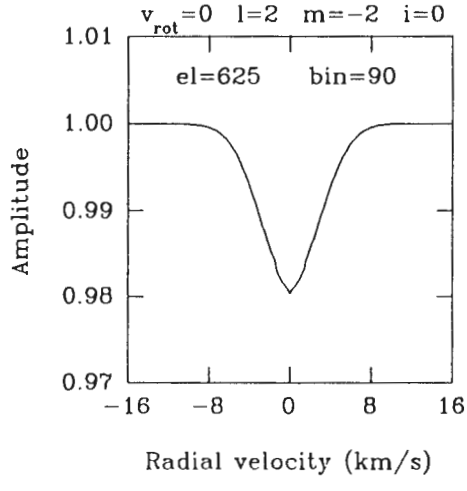
v rot =0 l=2 m=−2 i=0
el=625 bin=90
Amplitude
1.01
1.00
0.99
0.98
0.97
−16 −8 0 8 16
Radial velocity (km/s)

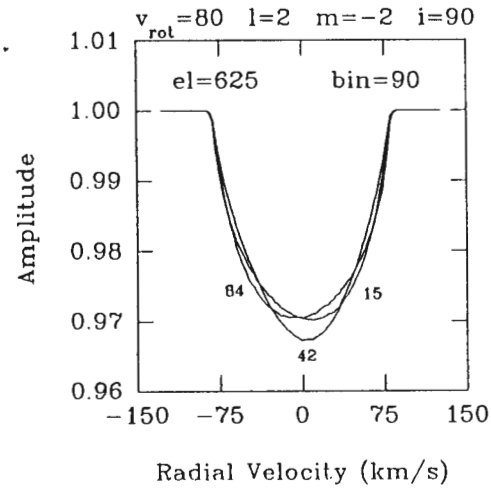
v rot =80 l=2 m=-2 i=90
el=625 bin=90
Amplitude
1.01
1.00
0.99
0.98
0.97
0.96
64
15
42
-150 -75 0 75 150
Radial Velocity (km/s)

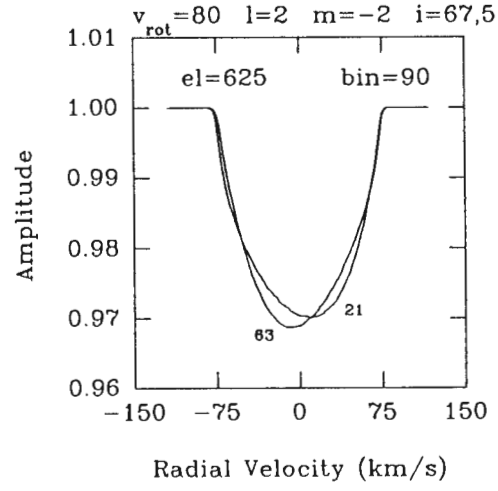
v rot =80 l=2 m=-2 i=67,5
el=625 bin=90
Amplitude
1.01
1.00
0.99
0.98
0.97
0.96
21
63
-150 -75 0 75 150
Radial Velocity (km/s)

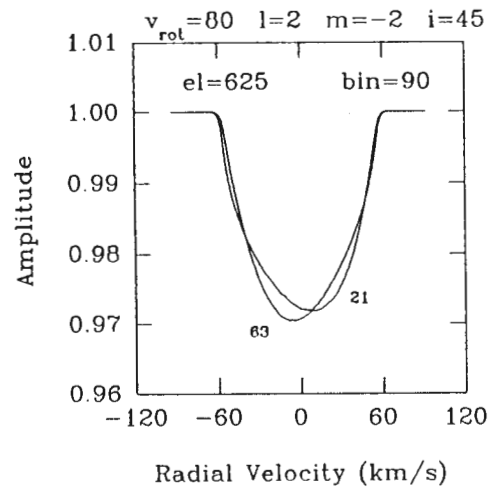
v rot =80 l=2 m=-2 i=45
el=625 bin=90
Amplitude
1.01
1.00
0.99
0.98
0.97
0.96
21
63
-120 -60 0 60 120
Radial Velocity (km/s)

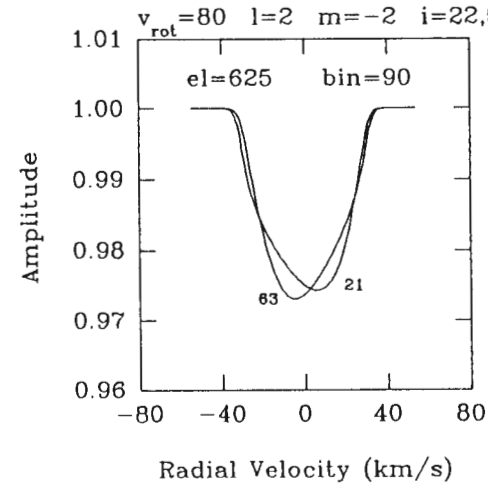
v rot =80 l=2 m=-2 i=22,5
el=625 bin=90
Amplitude
1.01
1.00
0.99
0.98
0.97
0.96
21
63
-80 -40 0 40 80
Radial Velocity (km/s)

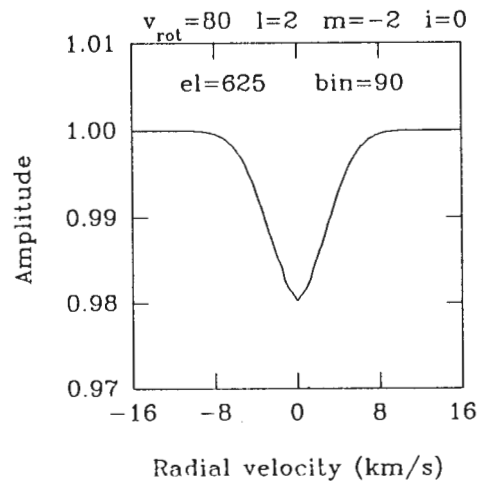
v rot =80 l=2 m=-2 i=0
el=625 bin=90
Amplitude
1.01
1.00
0.99
0.98
0.97
-16 -8 0 8 16
Radial velocity (km/s)

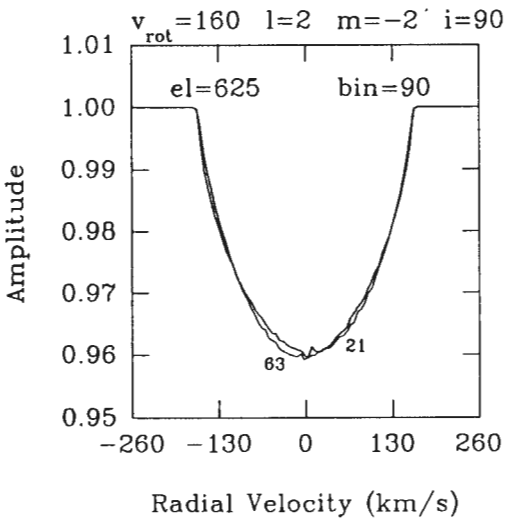
v rot =160 l=2 m=−2 i=90
el=625 bin=90
Amplitude
1.01
1.00
0.99
0.98
0.97
0.96
0.95
63
21
−260 −130 0 130 260
Radial Velocity (km/s)

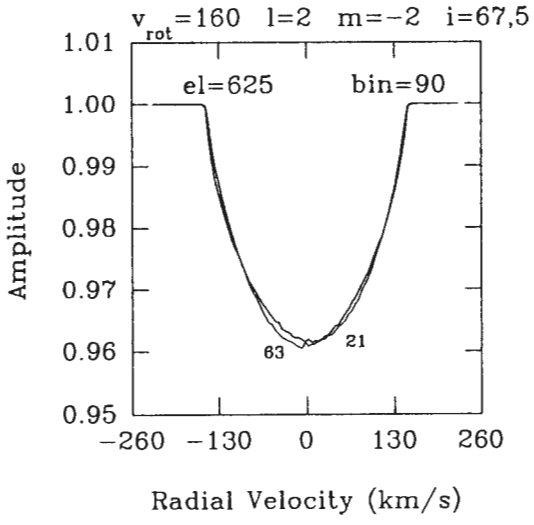
v rot =160 l=2 m=−2 i=67,5
el=625 bin=90
Amplitude
1.01
1.00
0.99
0.98
0.97
0.96
0.95
63
21
−260 −130 0 130 260
Radial Velocity (km/s)

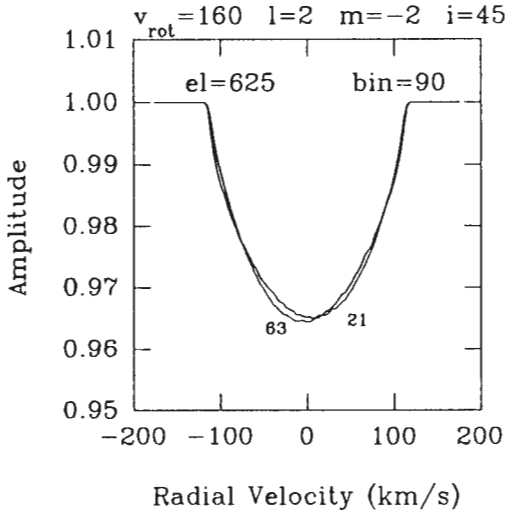
v rot =160 l=2 m=−2 i=45
el=625 bin=90
Amplitude
1.01
1.00
0.99
0.98
0.97
0.96
0.95
63
21
−200 −100 0 100 200
Radial Velocity (km/s)

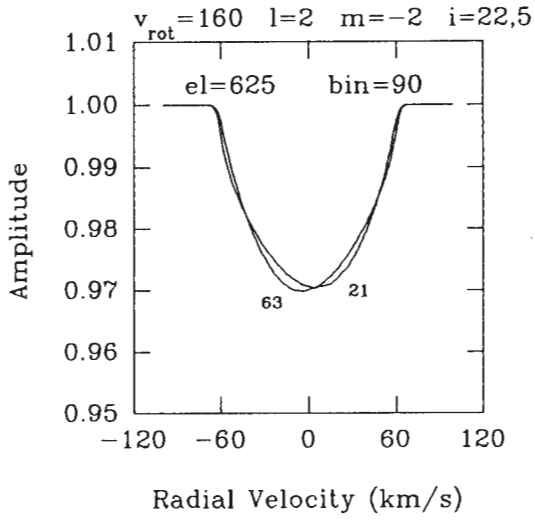
v rot =160 l=2 m=−2 i=22,5
el=625 bin=90
Amplitude
1.01
1.00
0.99
0.98
0.97
0.96
0.95
63
21
−120 −60 0 60 120
Radial Velocity (km/s)

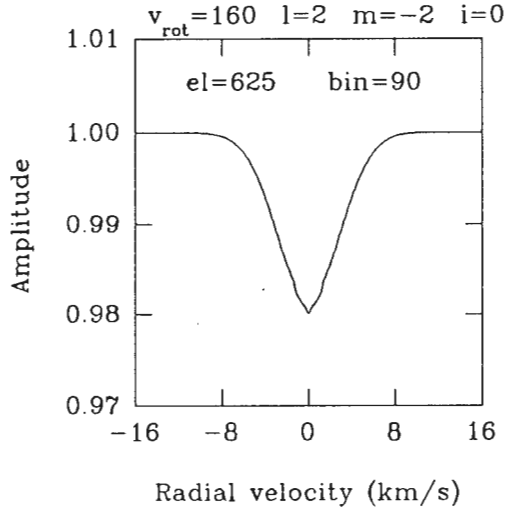
v rot =160 l=2 m=−2 i=0
el=625 bin=90
Amplitude
1.01
1.00
0.99
0.98
0.97
−16 −8 0 8 16
Radial velocity (km/s)

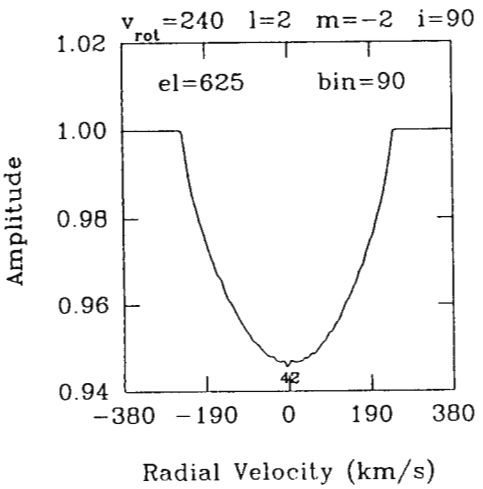
v rot =240 l=2 m=-2 i=90
el=625 bin=90
Amplitude
1.02
1.00
0.98
0.96
0.94
42
-380 -190 0 190 380
Radial Velocity (km/s)

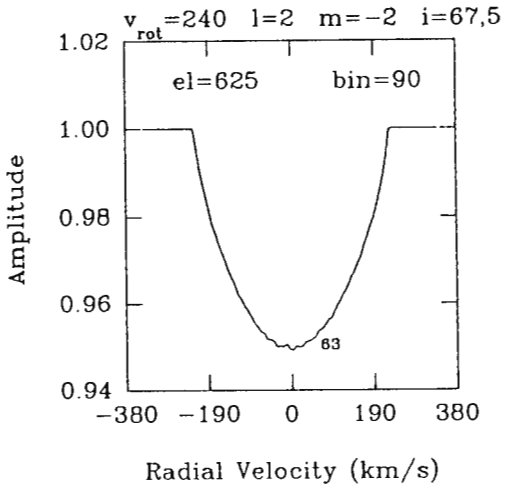
v rot =240 l=2 m=-2 i=67,5
el=625 bin=90
Amplitude
1.02
1.00
0.98
0.96
0.94
63
-380 -190 0 190 380
Radial Velocity (km/s)

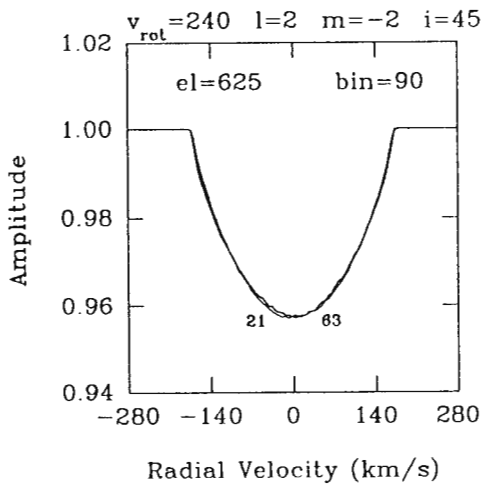
v rot =240 l=2 m=-2 i=45
el=625 bin=90
Amplitude
1.02
1.00
0.98
0.96
0.94
21
63
-280 -140 0 140 280
Radial Velocity (km/s)

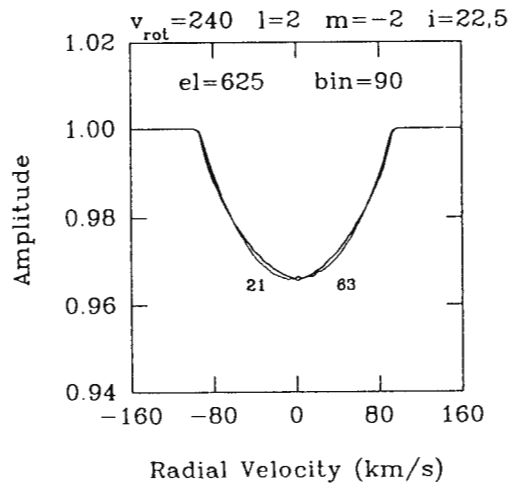
v rot =240 l=2 m=-2 i=22,5
el=625 bin=90
Amplitude
1.02
1.00
0.98
0.96
0.94
21
63
-160 -80 0 80 160
Radial Velocity (km/s)

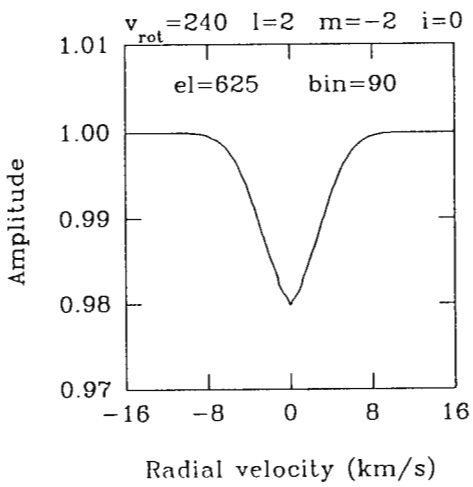
v rot =240 l=2 m=-2 i=0
el=625 bin=90
Amplitude
1.01
1.00
0.99
0.98
0.97
-16 -8 0 8 16
Radial velocity (km/s)

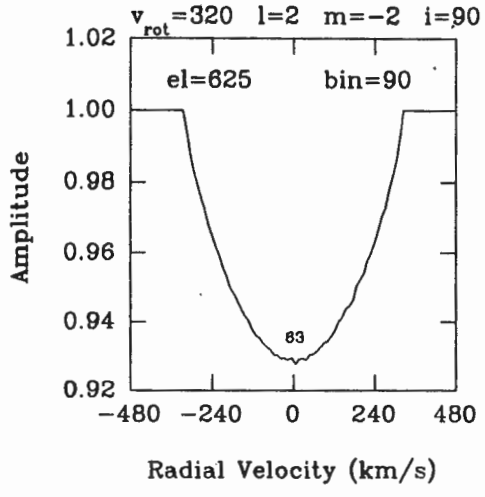
v_rot=320 l=2 m=-2 i=90
el=625 bin=90
63
Amplitude
Radial Velocity (km/s)

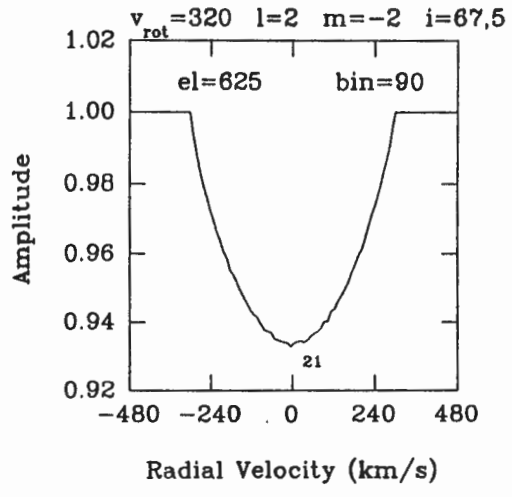
v_rot=320 l=2 m=-2 i=67,5
el=625 bin=90
21
Amplitude
Radial Velocity (km/s)

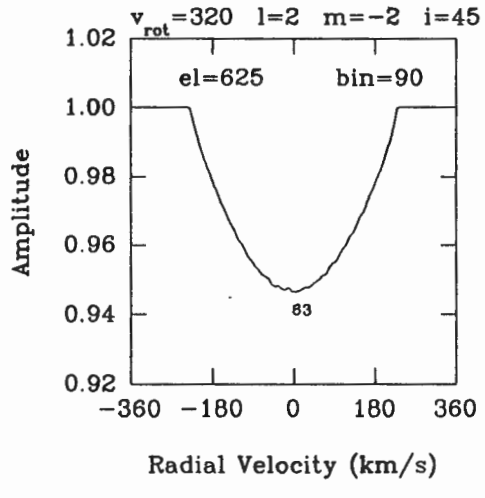
v_rot=320 l=2 m=-2 i=45
el=625 bin=90
63
Amplitude
Radial Velocity (km/s)

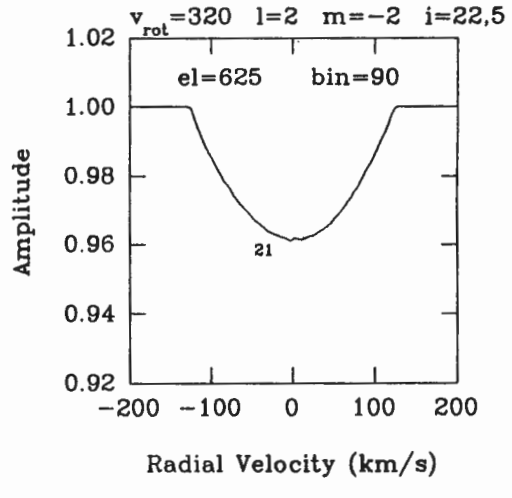
v_rot=320 l=2 m=-2 i=22,5
el=625 bin=90
21
Amplitude
Radial Velocity (km/s)

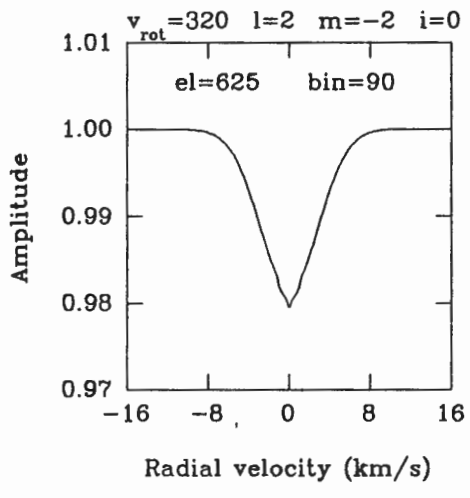
v_rot=320 l=2 m=-2 i=0
el=625 bin=90
Amplitude
Radial velocity (km/s)

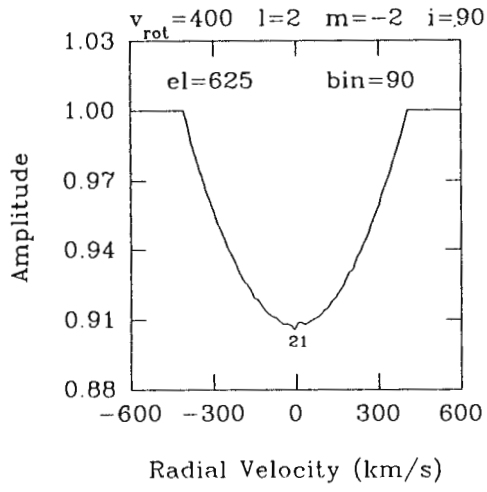
v rot =400 l=2 m=-2 i=90
el=625 bin=90
1.03
1.00
0.97
0.94
0.91
0.88
21
-600 -300 0 300 600
Amplitude
Radial Velocity (km/s)

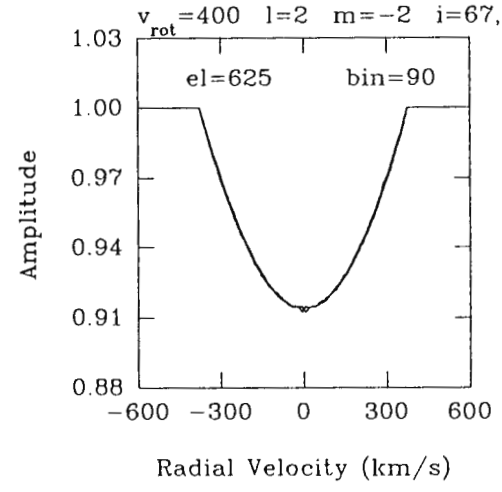
v rot =400 l=2 m=-2 i=67,5
el=625 bin=90
1.03
1.00
0.97
0.94
0.91
0.88
-600 -300 0 300 600
Amplitude
Radial Velocity (km/s)

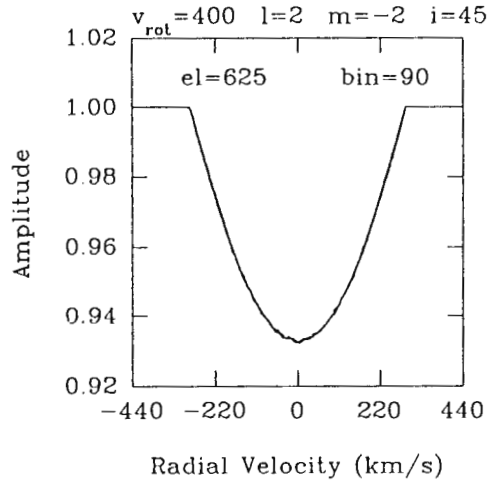
v rot =400 l=2 m=-2 i=45
el=625 bin=90
1.02
1.00
0.98
0.96
0.94
0.92
-440 -220 0 220 440
Amplitude
Radial Velocity (km/s)

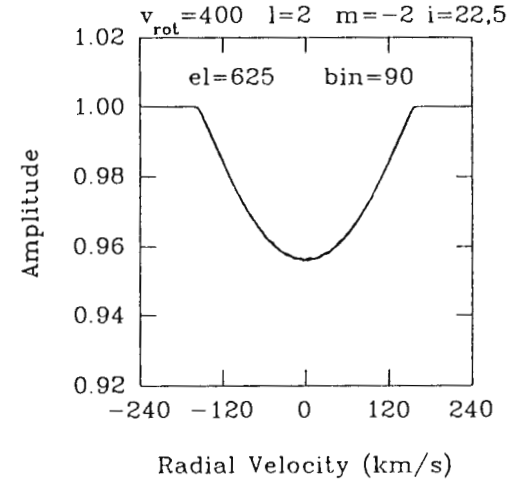
v rot =400 l=2 m=-2 i=22,5
el=625 bin=90
1.02
1.00
0.98
0.96
0.94
0.92
-240 -120 0 120 240
Amplitude
Radial Velocity (km/s)

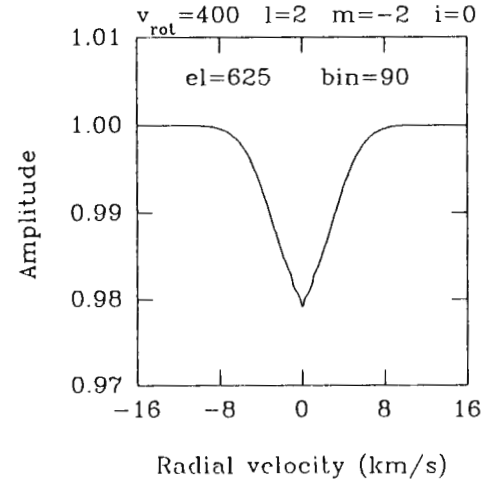
v rot =400 l=2 m=-2 i=0
el=625 bin=90
1.01
1.00
0.99
0.98
0.97
-16 -8 0 8 16
Amplitude
Radial velocity (km/s)

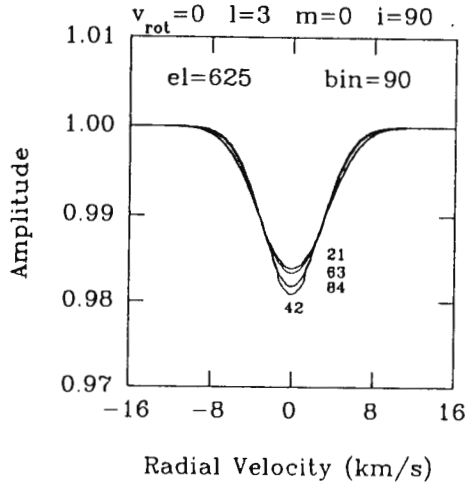
v_{rot}=0 l=3 m=0 i=90
el=625 bin=90
1.01
1.00
0.99
0.98
0.97
Amplitude
21
63
84
42
−16 −8 0 8 16
Radial Velocity (km/s)

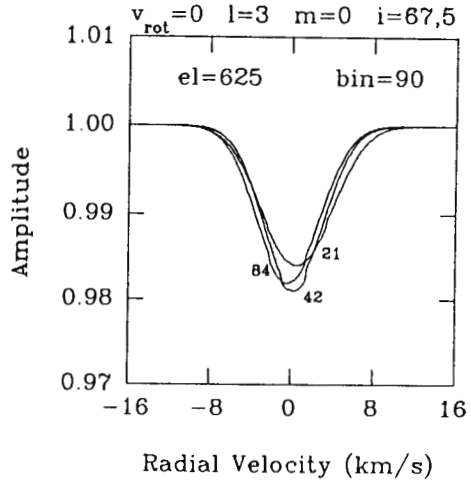
v_{rot}=0 l=3 m=0 i=67,5
el=625 bin=90
1.01
1.00
0.99
0.98
0.97
Amplitude
84
21
42
−16 −8 0 8 16
Radial Velocity (km/s)

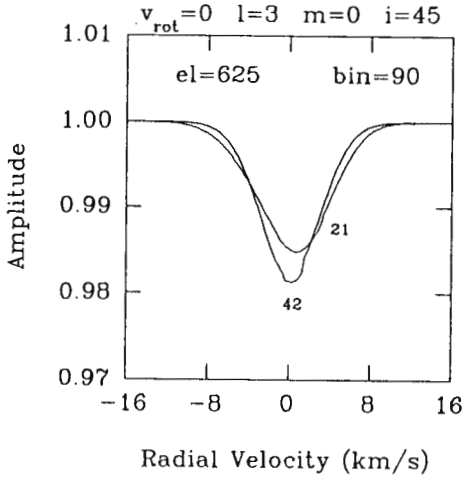
v_{rot}=0 l=3 m=0 i=45
el=625 bin=90
1.01
1.00
0.99
0.98
0.97
Amplitude
21
42
−16 −8 0 8 16
Radial Velocity (km/s)

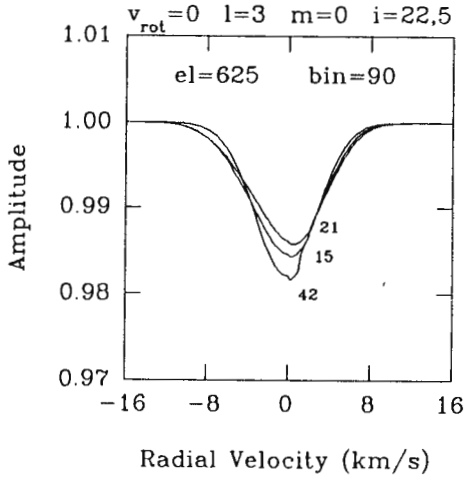
v_{rot}=0 l=3 m=0 i=22,5
el=625 bin=90
1.01
1.00
0.99
0.98
0.97
Amplitude
21
15
42
−16 −8 0 8 16
Radial Velocity (km/s)

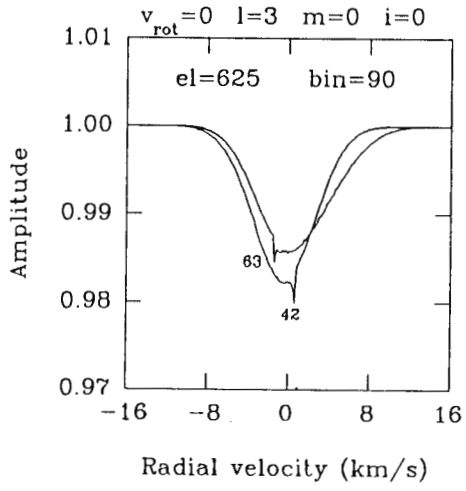
v_{rot}=0 l=3 m=0 i=0
el=625 bin=90
1.01
1.00
0.99
0.98
0.97
Amplitude
63
42
−16 −8 0 8 16
Radial velocity (km/s)

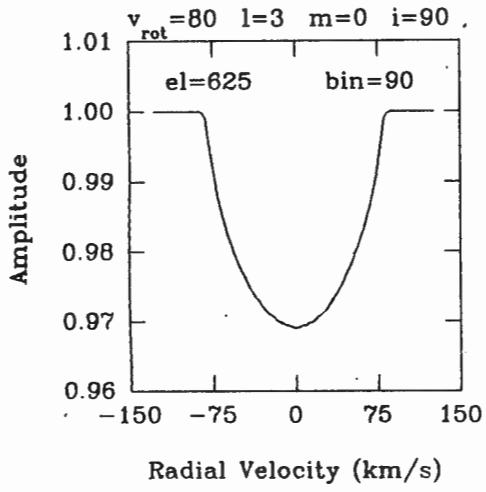
v rot =80 l=3 m=0 i=90
el=625 bin=90
Amplitude
1.01
1.00
0.99
0.98
0.97
0.96
−150 −75 0 75 150
Radial Velocity (km/s)

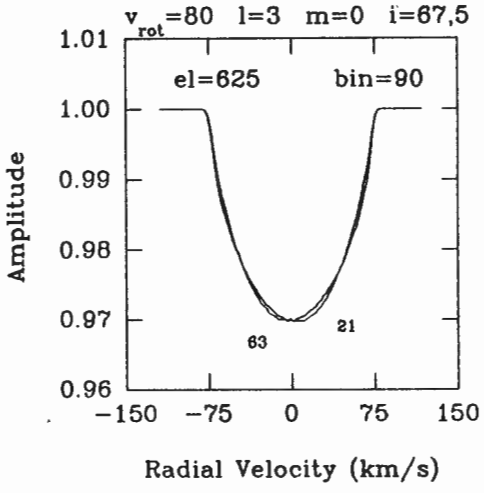
v rot =80 l=3 m=0 i=67,5
el=625 bin=90
Amplitude
1.01
1.00
0.99
0.98
0.97
0.96
63
21
−150 −75 0 75 150
Radial Velocity (km/s)

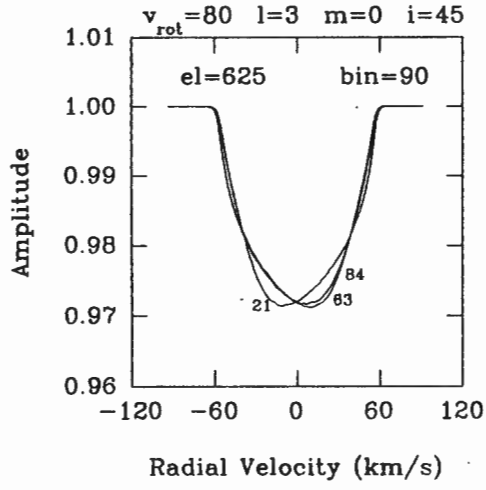
v rot =80 l=3 m=0 i=45
el=625 bin=90
Amplitude
1.01
1.00
0.99
0.98
0.97
0.96
84
21
63
−120 −60 0 60 120
Radial Velocity (km/s)

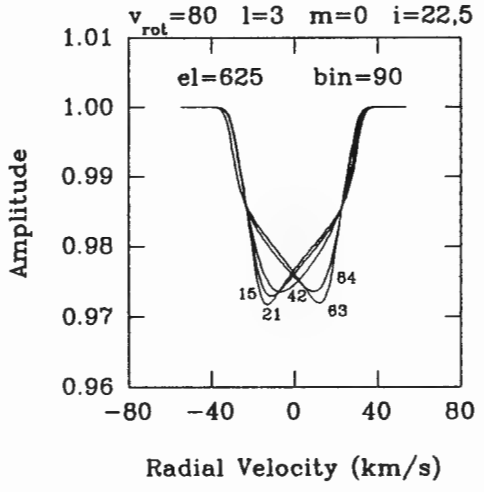
v rot =80 l=3 m=0 i=22,5
el=625 bin=90
Amplitude
1.01
1.00
0.99
0.98
0.97
0.96
15
42
64
21
63
−80 −40 0 40 80
Radial Velocity (km/s)

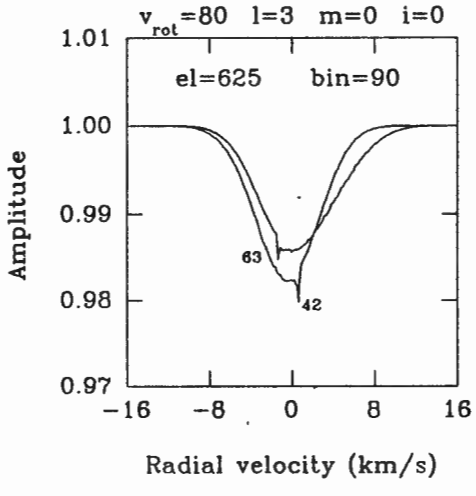
v rot =80 l=3 m=0 i=0
el=625 bin=90
Amplitude
1.01
1.00
0.99
0.98
0.97
63
42
−16 −8 0 8 16
Radial velocity (km/s)

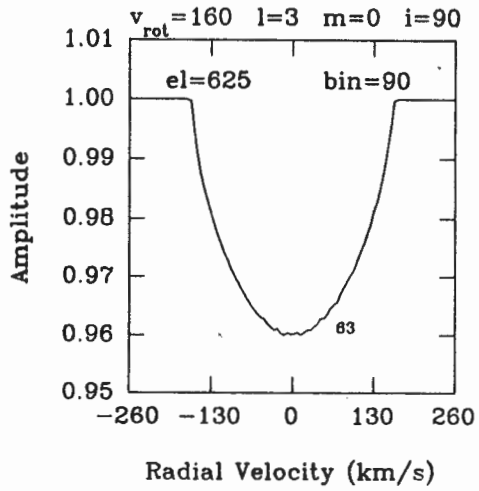
v_{rot}=160 l=3 m=0 i=90
el=625 bin=90
63
Amplitude
1.01
1.00
0.99
0.98
0.97
0.96
0.95
−260 −130 0 130 260
Radial Velocity (km/s)

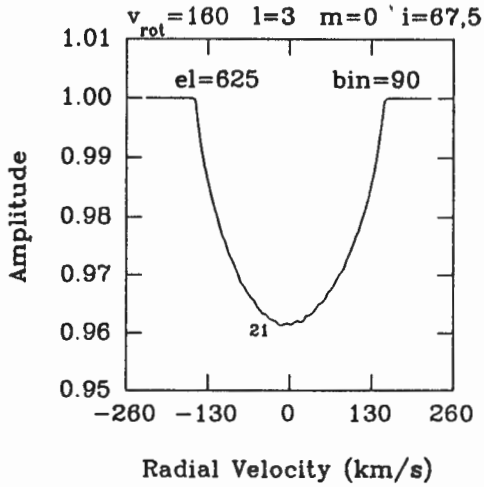
v_{rot}=160 l=3 m=0 i=67,5
el=625 bin=90
21
Amplitude
1.01
1.00
0.99
0.98
0.97
0.96
0.95
−260 −130 0 130 260
Radial Velocity (km/s)

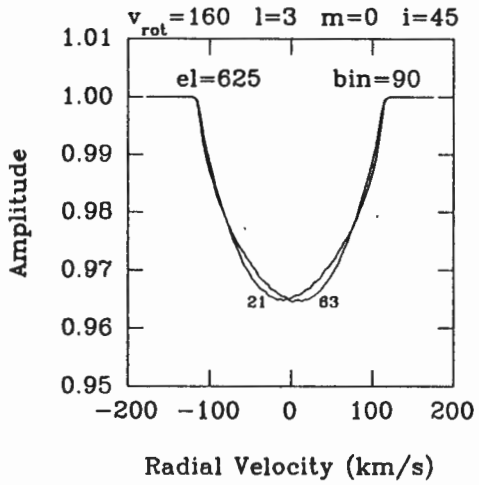
v_{rot}=160 l=3 m=0 i=45
el=625 bin=90
21 63
Amplitude
1.01
1.00
0.99
0.98
0.97
0.96
0.95
−200 −100 0 100 200
Radial Velocity (km/s)

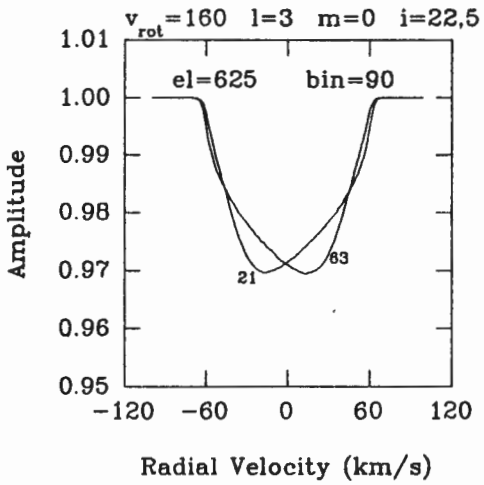
v_{rot}=160 l=3 m=0 i=22,5
el=625 bin=90
21 63
Amplitude
1.01
1.00
0.99
0.98
0.97
0.96
0.95
−120 −60 0 60 120
Radial Velocity (km/s)

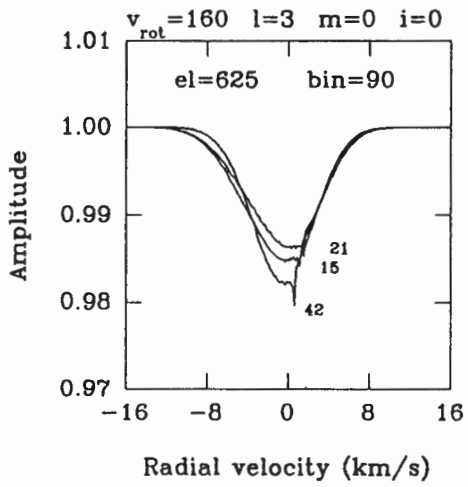
v_{rot}=160 l=3 m=0 i=0
el=625 bin=90
21
15
42
Amplitude
1.01
1.00
0.99
0.98
0.97
−16 −8 0 8 16
Radial velocity (km/s)

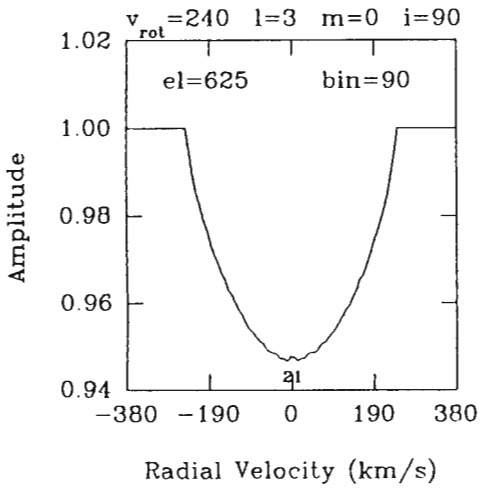
v rot =240 l=3 m=0 i=90
el=625 bin=90
21
Amplitude
1.02
1.00
0.98
0.96
0.94
−380 −190 0 190 380
Radial Velocity (km/s)

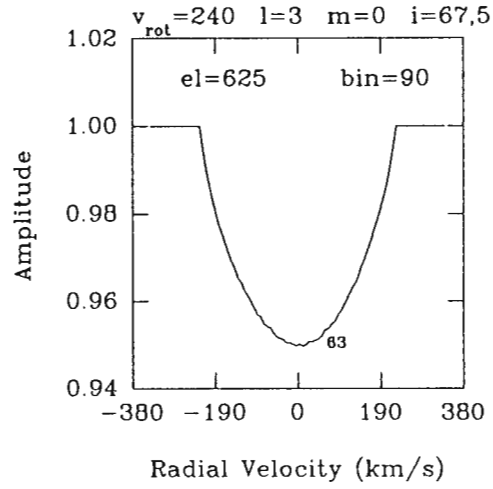
v rot =240 l=3 m=0 i=67,5
el=625 bin=90
63
Amplitude
1.02
1.00
0.98
0.96
0.94
−380 −190 0 190 380
Radial Velocity (km/s)

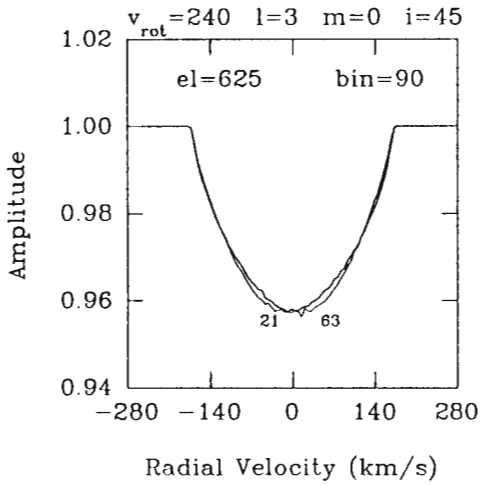
v rot =240 l=3 m=0 i=45
el=625 bin=90
21
63
Amplitude
1.02
1.00
0.98
0.96
0.94
−280 −140 0 140 280
Radial Velocity (km/s)

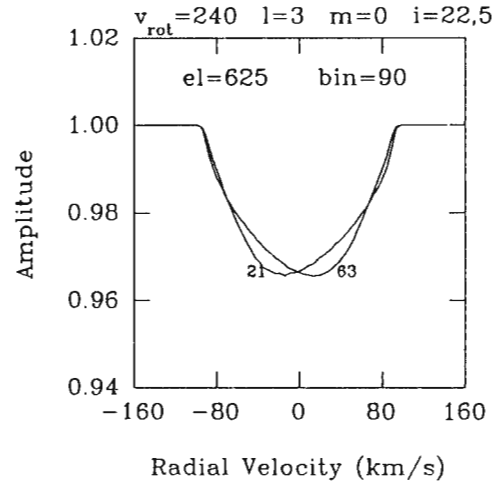
v rot =240 l=3 m=0 i=22,5
el=625 bin=90
21
63
Amplitude
1.02
1.00
0.98
0.96
0.94
−160 −80 0 80 160
Radial Velocity (km/s)

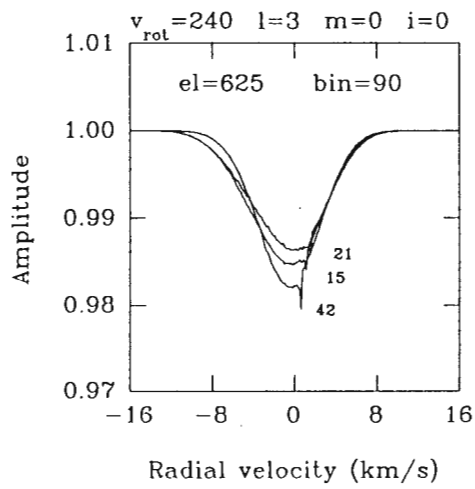
v rot =240 l=3 m=0 i=0
el=625 bin=90
21
15
42
Amplitude
1.01
1.00
0.99
0.98
0.97
−16 −8 0 8 16
Radial velocity (km/s)

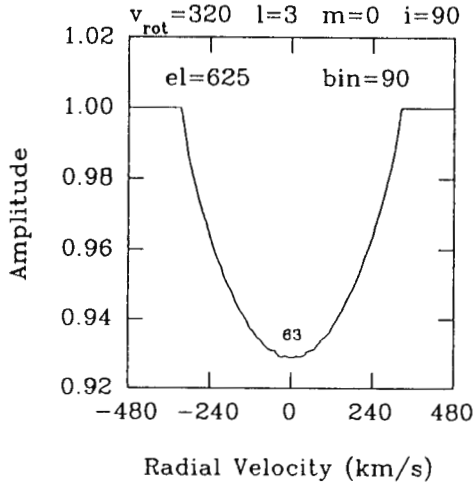
v_{rot}=320 l=3 m=0 i=90
el=625 bin=90
Amplitude
1.02
1.00
0.98
0.96
0.94
0.92
63
−480 −240 0 240 480
Radial Velocity (km/s)

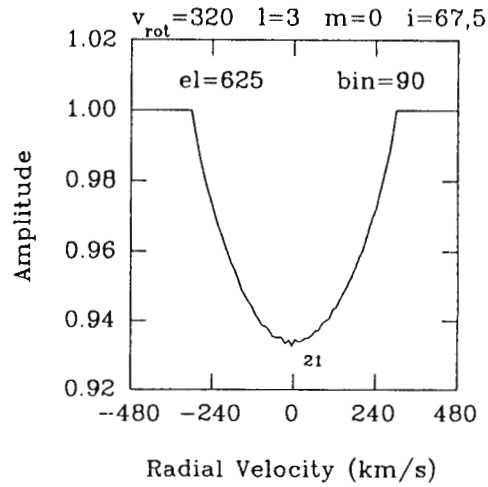
v_{rot}=320 l=3 m=0 i=67,5
el=625 bin=90
Amplitude
1.02
1.00
0.98
0.96
0.94
0.92
21
−480 −240 0 240 480
Radial Velocity (km/s)

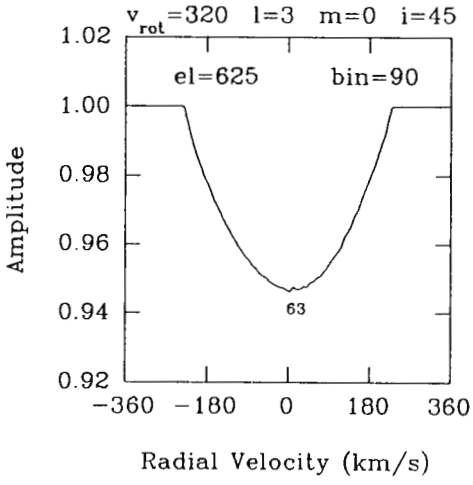
v_{rot}=320 l=3 m=0 i=45
el=625 bin=90
Amplitude
1.02
1.00
0.98
0.96
0.94
0.92
63
−360 −180 0 180 360
Radial Velocity (km/s)

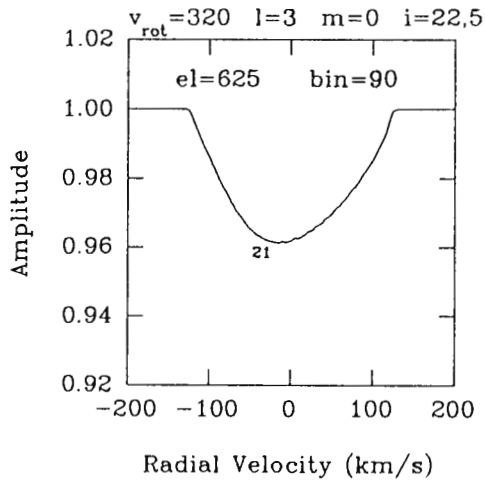
v_{rot}=320 l=3 m=0 i=22,5
el=625 bin=90
Amplitude
1.02
1.00
0.98
0.96
0.94
0.92
21
−200 −100 0 100 200
Radial Velocity (km/s)

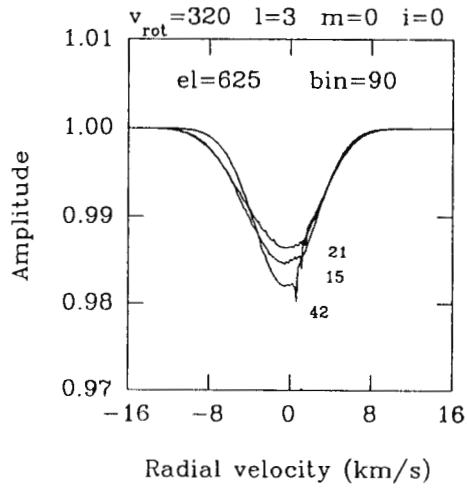
v_{rot}=320 l=3 m=0 i=0
el=625 bin=90
Amplitude
1.01
1.00
0.99
0.98
0.97
21
15
42
−16 −8 0 8 16
Radial velocity (km/s)

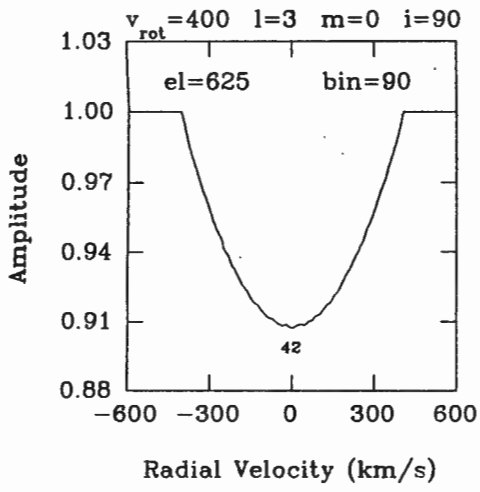
v_rot=400 l=3 m=0 i=90
el=625 bin=90
Amplitude
1.03
1.00
0.97
0.94
0.91
0.88
42
−600 −300 0 300 600
Radial Velocity (km/s)

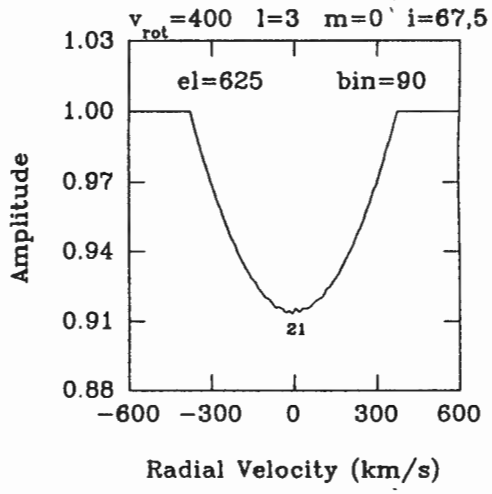
v_rot=400 l=3 m=0 i=67,5
el=625 bin=90
Amplitude
1.03
1.00
0.97
0.94
0.91
0.88
21
−600 −300 0 300 600
Radial Velocity (km/s)

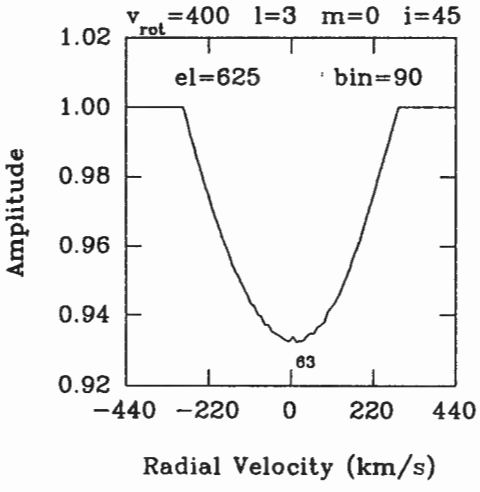
v_rot=400 l=3 m=0 i=45
el=625 bin=90
Amplitude
1.02
1.00
0.98
0.96
0.94
0.92
63
−440 −220 0 220 440
Radial Velocity (km/s)

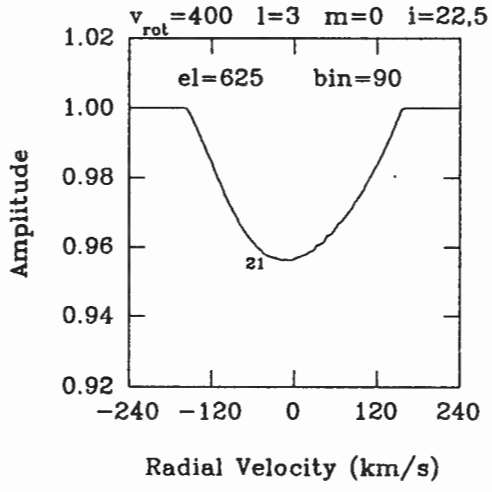
v_rot=400 l=3 m=0 i=22,5
el=625 bin=90
Amplitude
1.02
1.00
0.98
0.96
0.94
0.92
21
−240 −120 0 120 240
Radial Velocity (km/s)

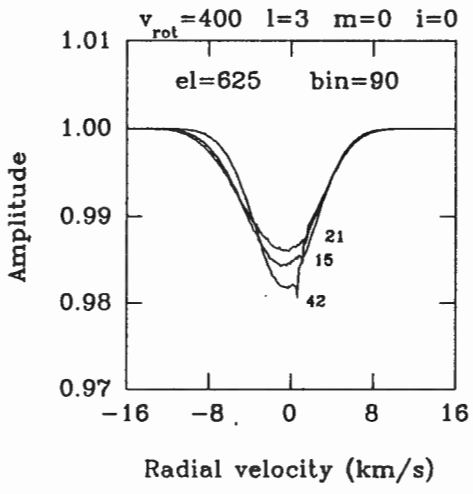
v_rot=400 l=3 m=0 i=0
el=625 bin=90
Amplitude
1.01
1.00
0.99
0.98
0.97
21
15
42
−16 −8 0 8 16
Radial velocity (km/s)

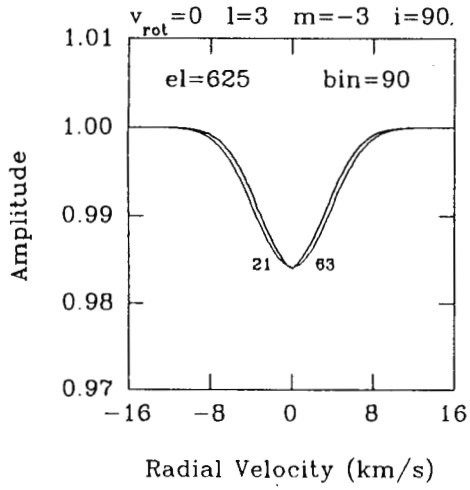
v_rot=0 l=3 m=-3 i=90.
el=625 bin=90
21
63
1.01
1.00
0.99
0.98
0.97
Amplitude
−16 −8 0 8 16
Radial Velocity (km/s)

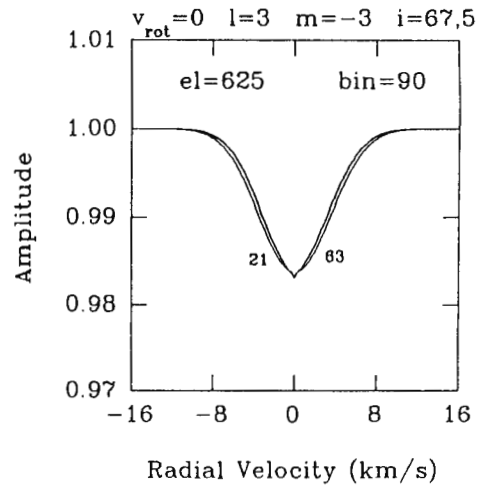
v_rot=0 l=3 m=-3 i=67,5
el=625 bin=90
21
63
1.01
1.00
0.99
0.98
0.97
Amplitude
−16 −8 0 8 16
Radial Velocity (km/s)

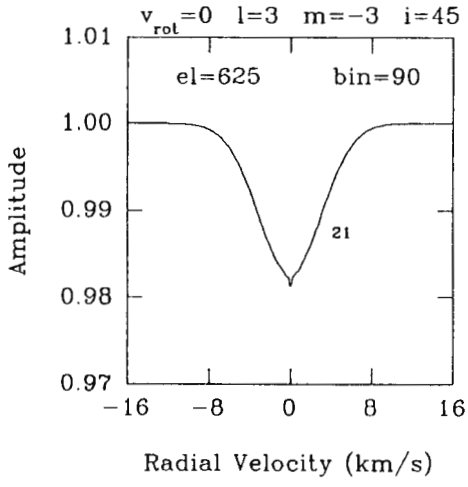
v_rot=0 l=3 m=-3 i=45
el=625 bin=90
21
1.01
1.00
0.99
0.98
0.97
Amplitude
−16 −8 0 8 16
Radial Velocity (km/s)

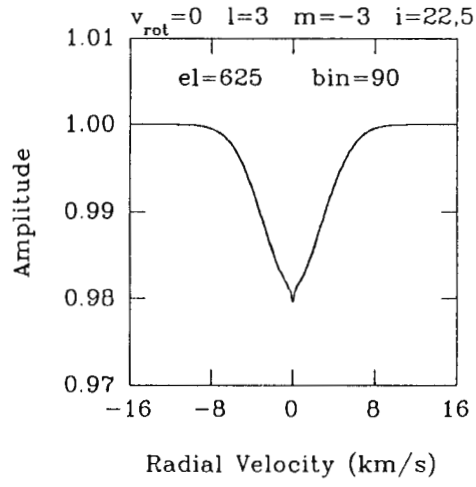
v_rot=0 l=3 m=-3 i=22,5
el=625 bin=90
1.01
1.00
0.99
0.98
0.97
Amplitude
−16 −8 0 8 16
Radial Velocity (km/s)

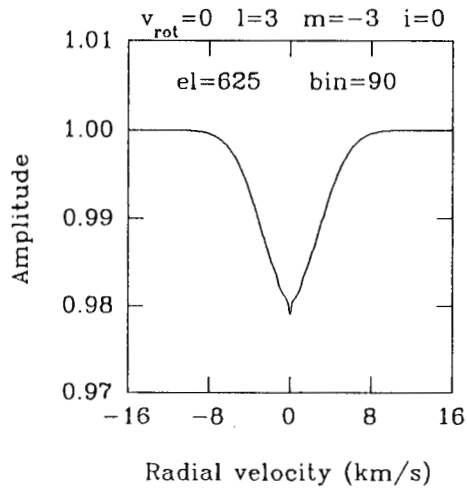
v_rot=0 l=3 m=-3 i=0
el=625 bin=90
1.01
1.00
0.99
0.98
0.97
Amplitude
−16 −8 0 8 16
Radial velocity (km/s)

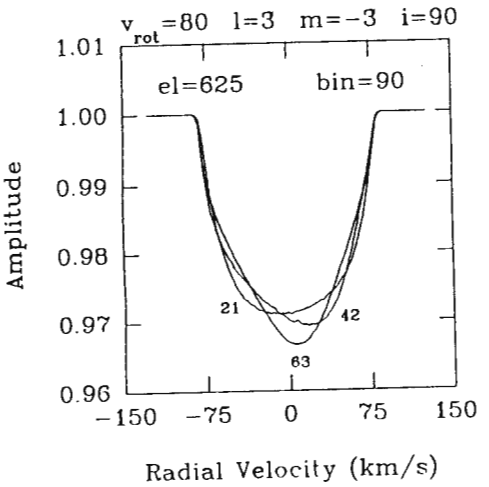
v rot =80 l=3 m=-3 i=90
el=625 bin=90
21
42
63
Amplitude
1.01
1.00
0.99
0.98
0.97
0.96
-150 -75 0 75 150
Radial Velocity (km/s)

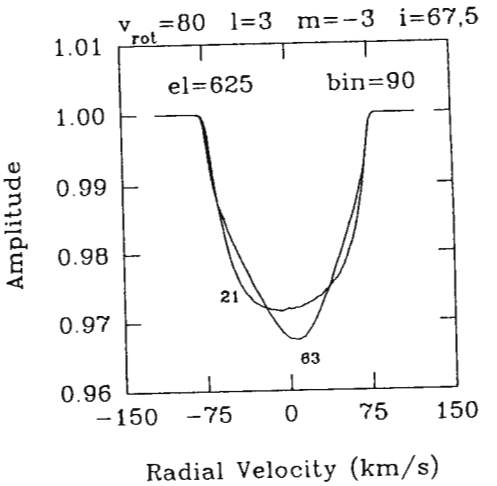
v rot =80 l=3 m=-3 i=67,5
el=625 bin=90
21
63
Amplitude
1.01
1.00
0.99
0.98
0.97
0.96
-150 -75 0 75 150
Radial Velocity (km/s)

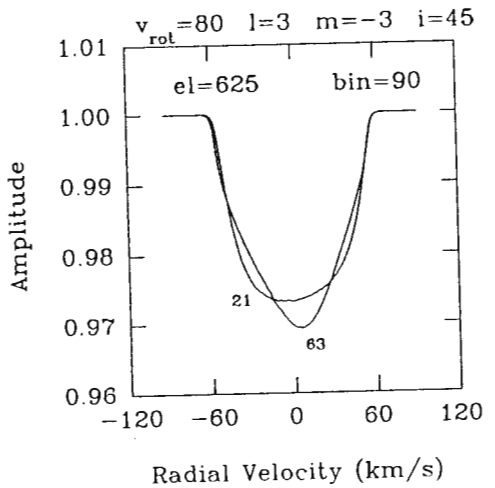
v rot =80 l=3 m=-3 i=45
el=625 bin=90
21
63
Amplitude
1.01
1.00
0.99
0.98
0.97
0.96
-120 -60 0 60 120
Radial Velocity (km/s)

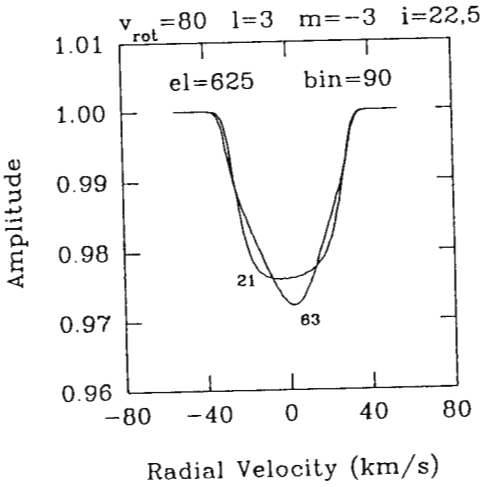
v rot =80 l=3 m=-3 i=22,5
el=625 bin=90
21
63
Amplitude
1.01
1.00
0.99
0.98
0.97
0.96
-80 -40 0 40 80
Radial Velocity (km/s)

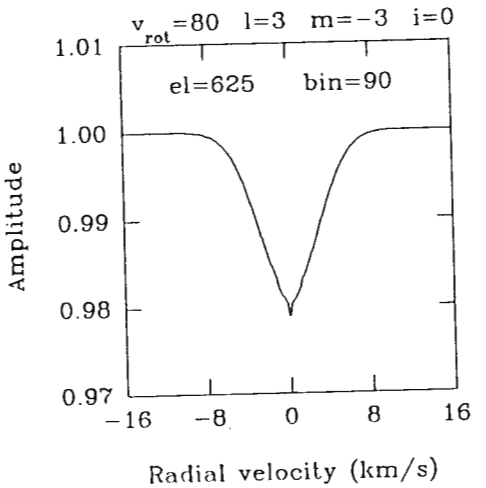
v rot =80 l=3 m=-3 i=0
el=625 bin=90
Amplitude
1.01
1.00
0.99
0.98
0.97
-16 -8 0 8 16
Radial velocity (km/s)

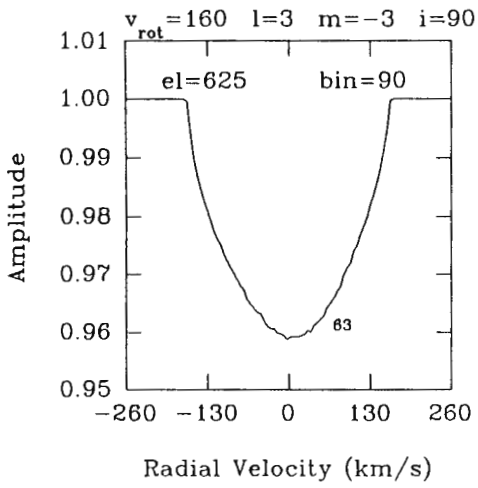
v rot =160 l=3 m=−3 i=90
el=625 bin=90
63
Amplitude
1.01
1.00
0.99
0.98
0.97
0.96
0.95
−260 −130 0 130 260
Radial Velocity (km/s)

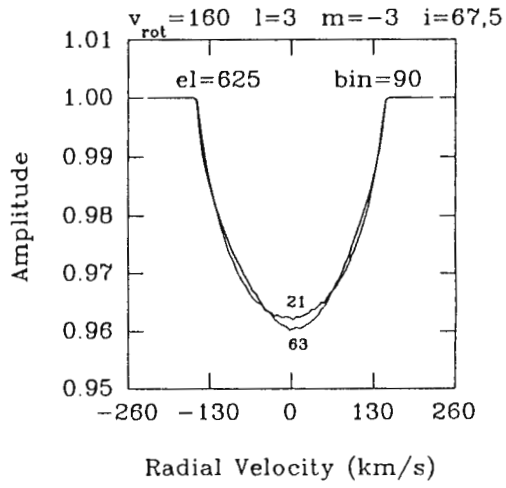
v rot =160 l=3 m=−3 i=67,5
el=625 bin=90
21
63
Amplitude
1.01
1.00
0.99
0.98
0.97
0.96
0.95
−260 −130 0 130 260
Radial Velocity (km/s)

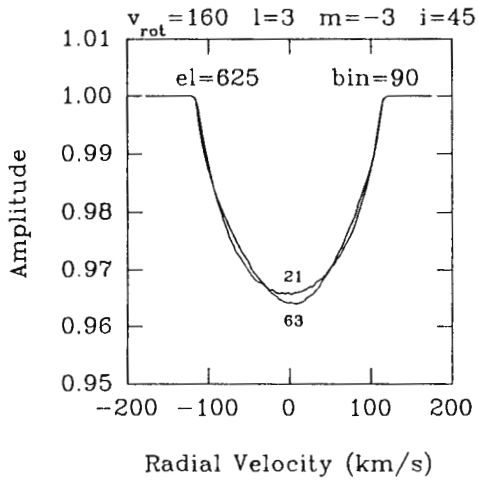
v rot =160 l=3 m=−3 i=45
el=625 bin=90
21
63
Amplitude
1.01
1.00
0.99
0.98
0.97
0.96
0.95
−200 −100 0 100 200
Radial Velocity (km/s)

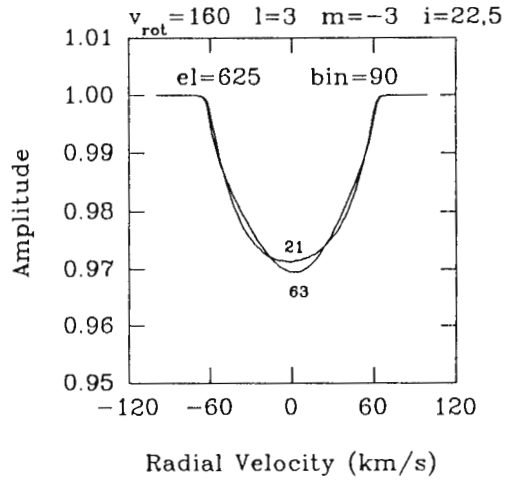
v rot =160 l=3 m=−3 i=22,5
el=625 bin=90
21
63
Amplitude
1.01
1.00
0.99
0.98
0.97
0.96
0.95
−120 −60 0 60 120
Radial Velocity (km/s)

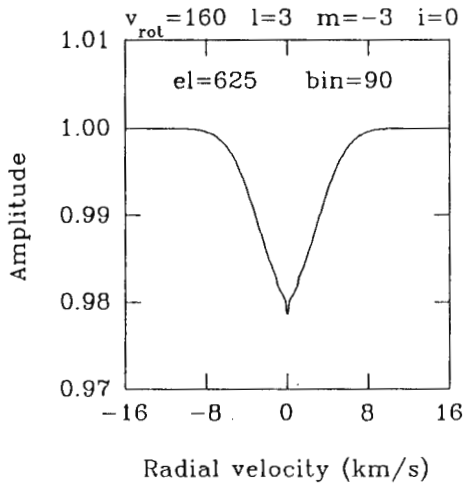
v rot =160 l=3 m=−3 i=0
el=625 bin=90
Amplitude
1.01
1.00
0.99
0.98
0.97
−16 −8 0 8 16
Radial velocity (km/s)

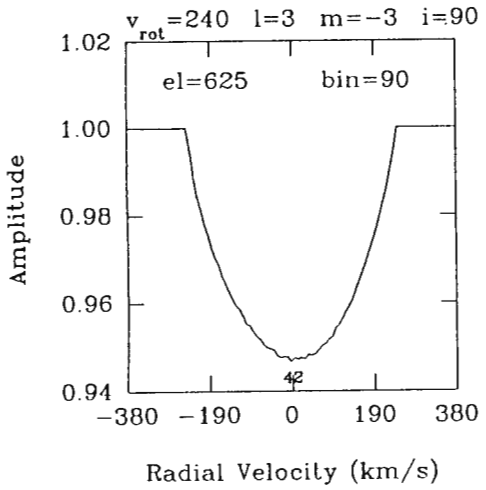
v rot =240 l=3 m=−3 i=90
el=625 bin=90
1.02
1.00
0.98
0.96
0.94
Amplitude
42
−380 −190 0 190 380
Radial Velocity (km/s)

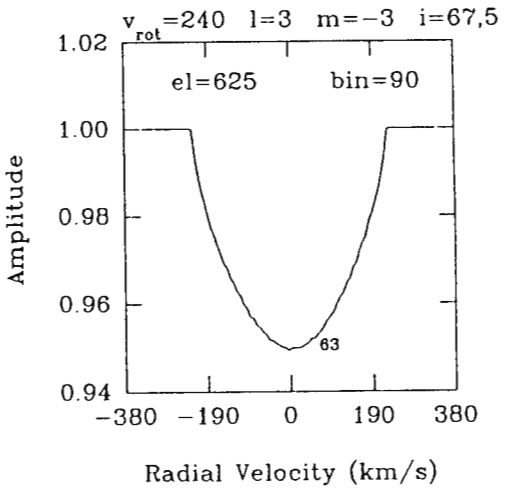
v rot =240 l=3 m=−3 i=67,5
el=625 bin=90
1.02
1.00
0.98
0.96
0.94
Amplitude
63
−380 −190 0 190 380
Radial Velocity (km/s)

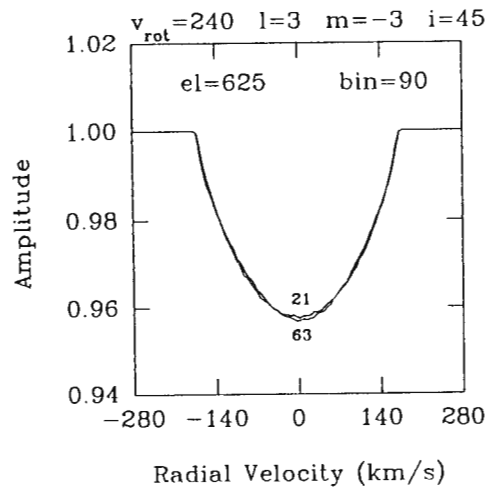
v rot =240 l=3 m=−3 i=45
el=625 bin=90
1.02
1.00
0.98
0.96
0.94
Amplitude
21
63
−280 −140 0 140 280
Radial Velocity (km/s)

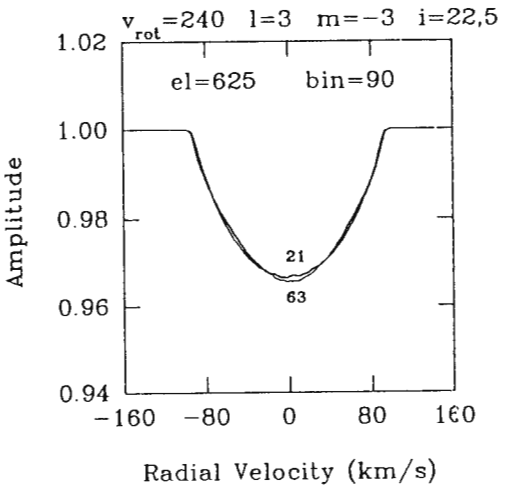
v rot =240 l=3 m=−3 i=22,5
el=625 bin=90
1.02
1.00
0.98
0.96
0.94
Amplitude
21
63
−160 −80 0 80 160
Radial Velocity (km/s)

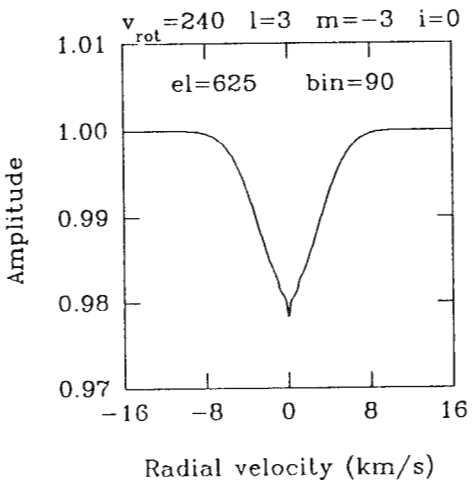
v rot =240 l=3 m=−3 i=0
el=625 bin=90
1.01
1.00
0.99
0.98
0.97
Amplitude
−16 −8 0 8 16
Radial velocity (km/s)

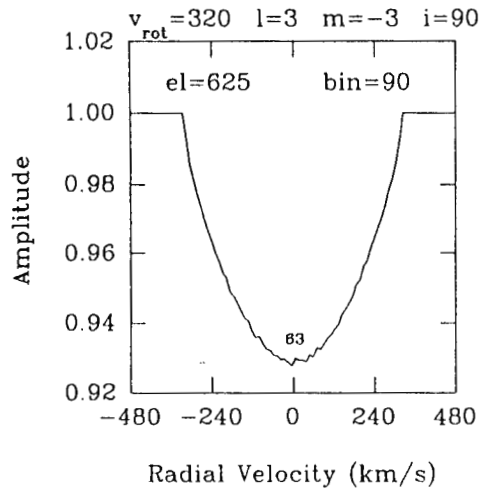
v rot =320 l=3 m=-3 i=90
el=625 bin=90
63
Amplitude
1.02
1.00
0.98
0.96
0.94
0.92
-480 -240 0 240 480
Radial Velocity (km/s)

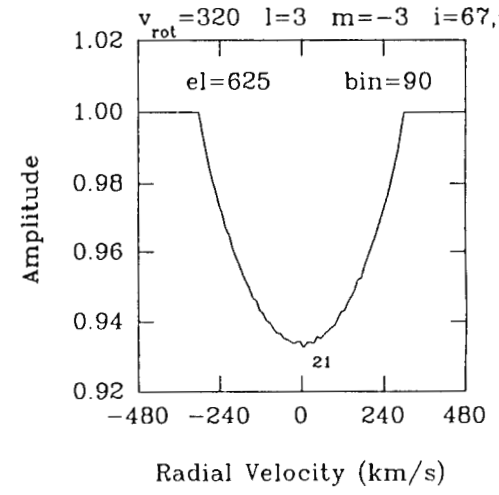
v rot =320 l=3 m=-3 i=67,5
el=625 bin=90
21
Amplitude
1.02
1.00
0.98
0.96
0.94
0.92
-480 -240 0 240 480
Radial Velocity (km/s)

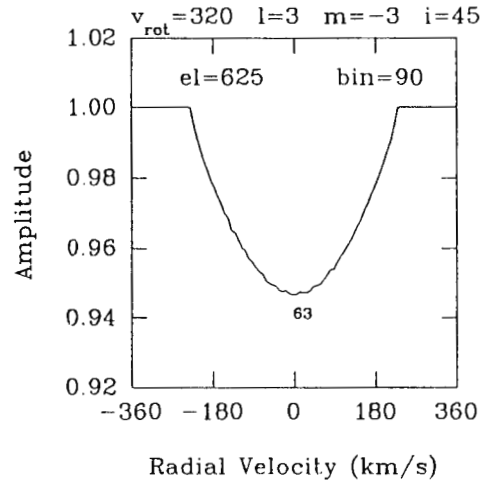
v rot =320 l=3 m=-3 i=45
el=625 bin=90
63
Amplitude
1.02
1.00
0.98
0.96
0.94
0.92
-360 -180 0 180 360
Radial Velocity (km/s)

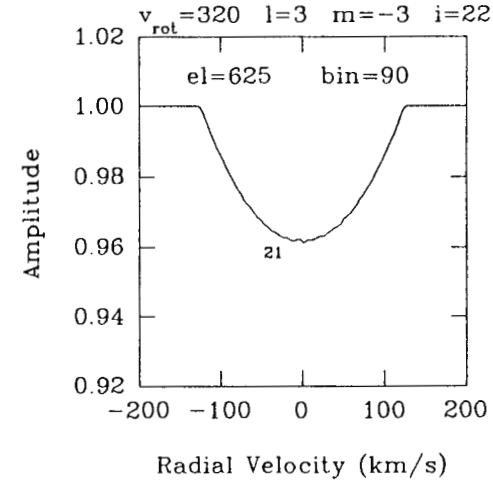
v rot =320 l=3 m=-3 i=22,5
el=625 bin=90
21
Amplitude
1.02
1.00
0.98
0.96
0.94
0.92
-200 -100 0 100 200
Radial Velocity (km/s)

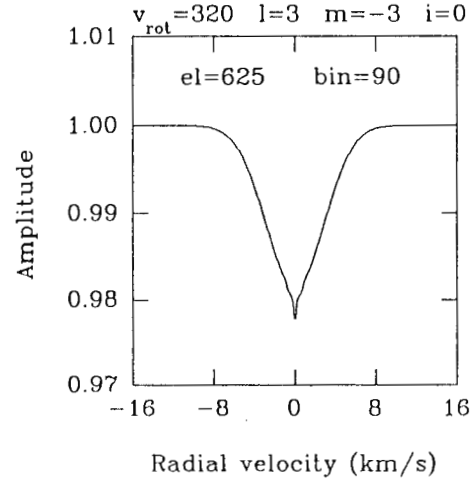
v rot =320 l=3 m=-3 i=0
el=625 bin=90
Amplitude
1.01
1.00
0.99
0.98
0.97
-16 -8 0 8 16
Radial velocity (km/s)

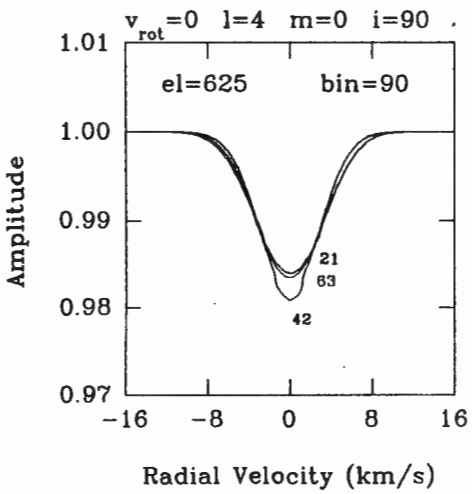
v_rot=0 l=4 m=0 i=90
el=625 bin=90
Amplitude
1.01
1.00
0.99
0.98
0.97
21
63
42
−16 −8 0 8 16
Radial Velocity (km/s)

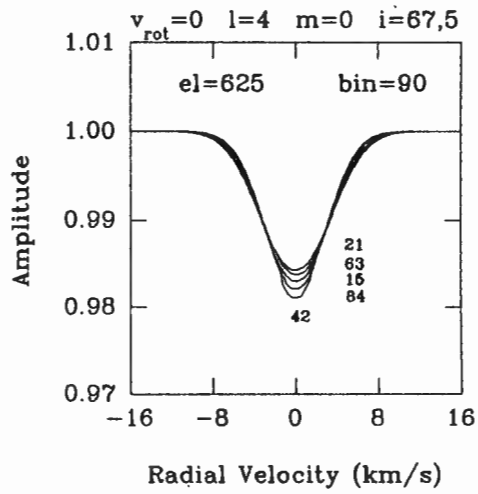
v_rot=0 l=4 m=0 i=67,5
el=625 bin=90
Amplitude
1.01
1.00
0.99
0.98
0.97
21
63
15
84
42
−16 −8 0 8 16
Radial Velocity (km/s)

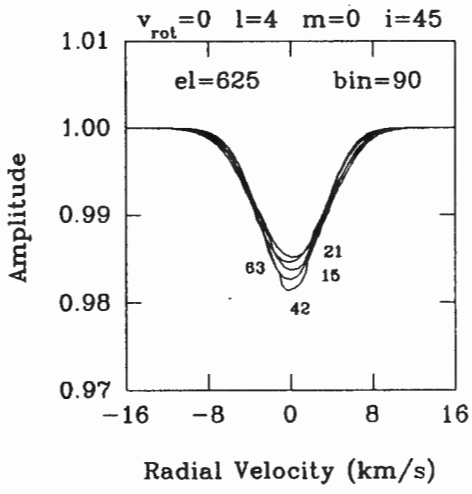
v_rot=0 l=4 m=0 i=45
el=625 bin=90
Amplitude
1.01
1.00
0.99
0.98
0.97
63
21
15
42
−16 −8 0 8 16
Radial Velocity (km/s)

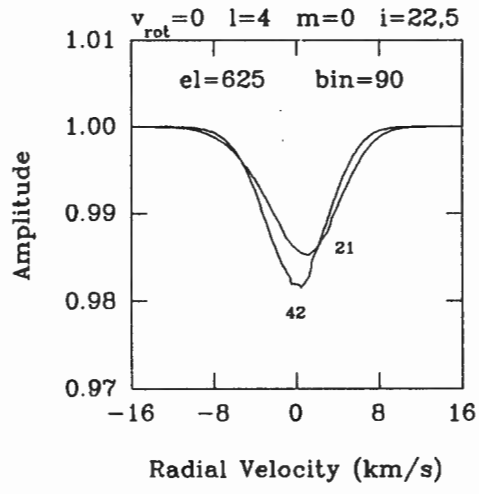
v_rot=0 l=4 m=0 i=22,5
el=625 bin=90
Amplitude
1.01
1.00
0.99
0.98
0.97
21
42
−16 −8 0 8 16
Radial Velocity (km/s)

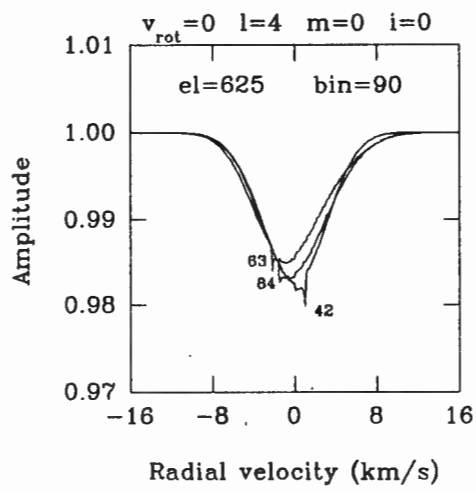
v_rot=0 l=4 m=0 i=0
el=625 bin=90
Amplitude
1.01
1.00
0.99
0.98
0.97
63
84
42
−16 −8 0 8 16
Radial velocity (km/s)

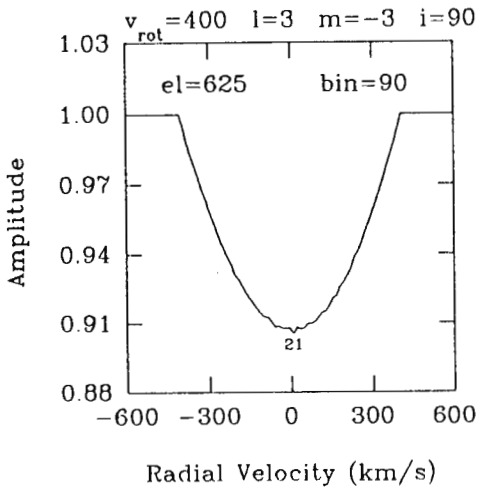
v rot =400 l=3 m=-3 i=90
el=625 bin=90
1.03
1.00
0.97
0.94
0.91
0.88
21
-600 -300 0 300 600
Amplitude
Radial Velocity (km/s)

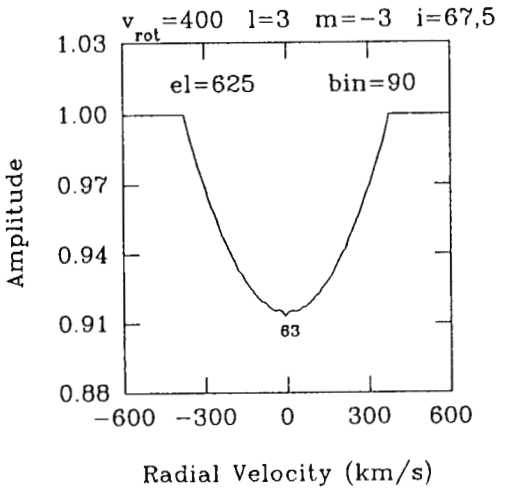
v rot =400 l=3 m=-3 i=67,5
el=625 bin=90
1.03
1.00
0.97
0.94
0.91
0.88
63
-600 -300 0 300 600
Amplitude
Radial Velocity (km/s)

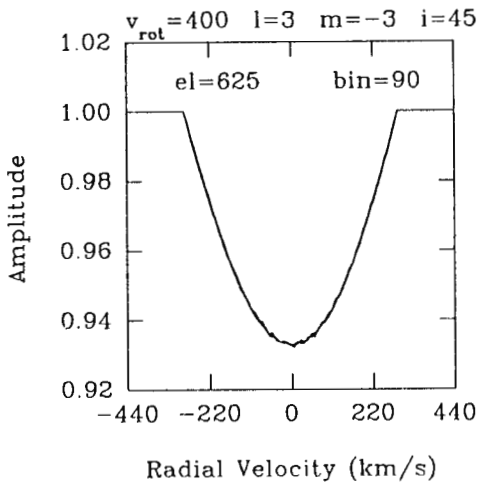
v rot =400 l=3 m=-3 i=45
el=625 bin=90
1.02
1.00
0.98
0.96
0.94
0.92
-440 -220 0 220 440
Amplitude
Radial Velocity (km/s)

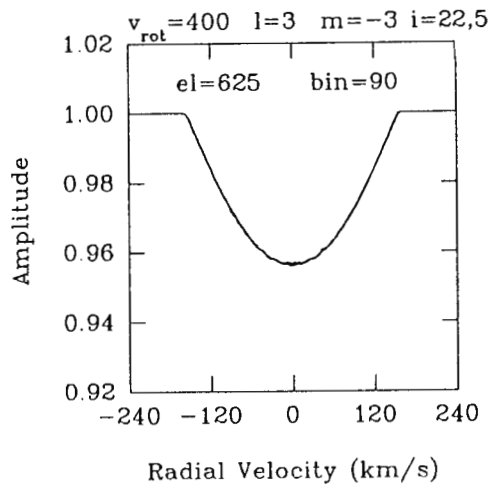
v rot =400 l=3 m=-3 i=22,5
el=625 bin=90
1.02
1.00
0.98
0.96
0.94
0.92
-240 -120 0 120 240
Amplitude
Radial Velocity (km/s)

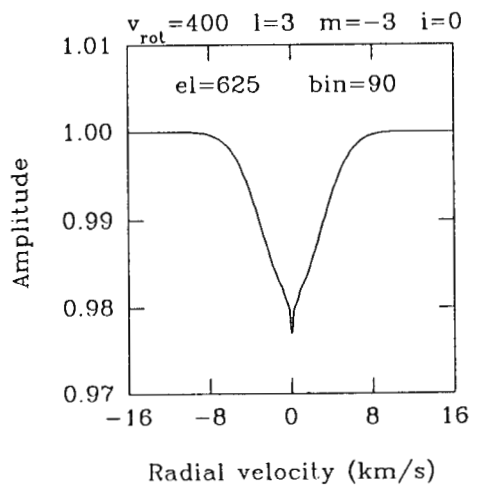
v rot =400 l=3 m=-3 i=0
el=625 bin=90
1.01
1.00
0.99
0.98
0.97
-16 -8 0 8 16
Amplitude
Radial velocity (km/s)

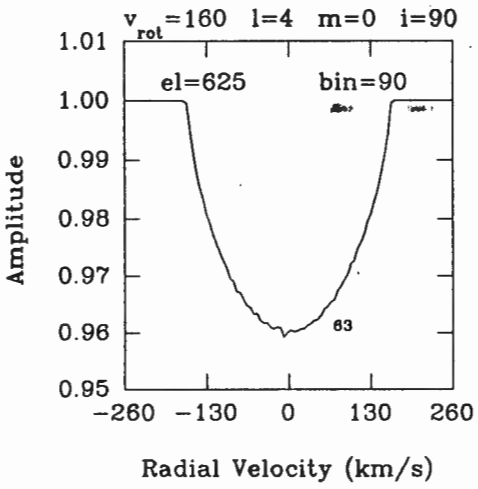
v rot =160 l=4 m=0 i=90
el=625 bin=90
63
Amplitude
1.01
1.00
0.99
0.98
0.97
0.96
0.95
−260 −130 0 130 260
Radial Velocity (km/s)

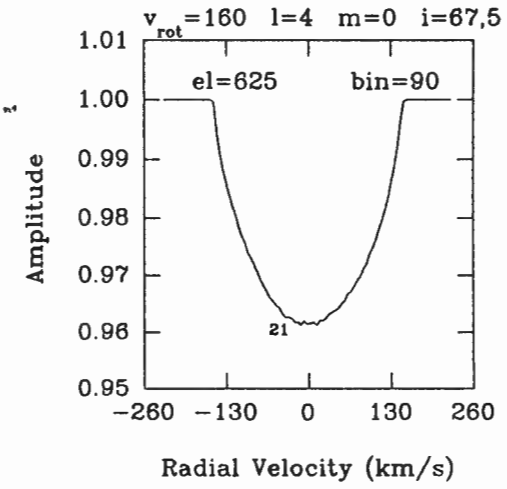
v rot =160 l=4 m=0 i=67,5
el=625 bin=90
21
Amplitude
1.01
1.00
0.99
0.98
0.97
0.96
0.95
−260 −130 0 130 260
Radial Velocity (km/s)

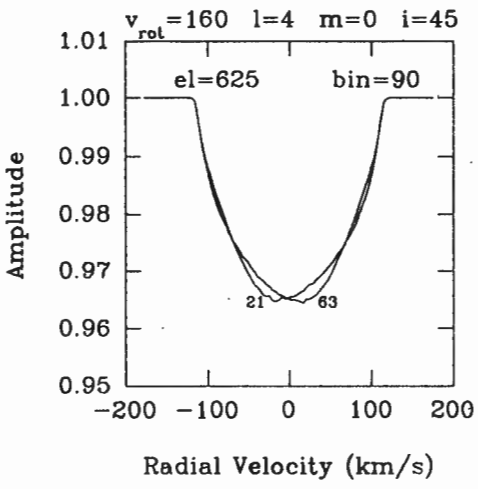
v rot =160 l=4 m=0 i=45
el=625 bin=90
21
63
Amplitude
1.01
1.00
0.99
0.98
0.97
0.96
0.95
−200 −100 0 100 200
Radial Velocity (km/s)

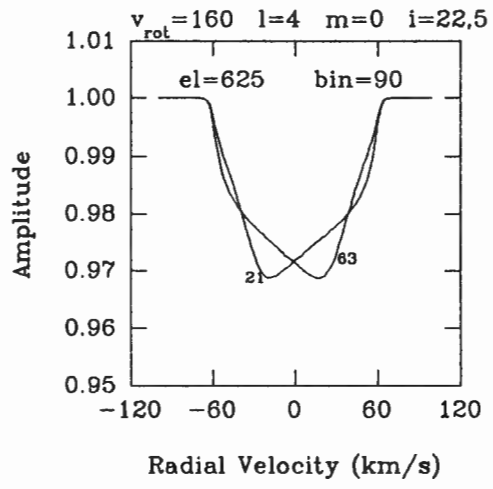
v rot =160 l=4 m=0 i=22,5
el=625 bin=90
21
63
Amplitude
1.01
1.00
0.99
0.98
0.97
0.96
0.95
−120 −60 0 60 120
Radial Velocity (km/s)

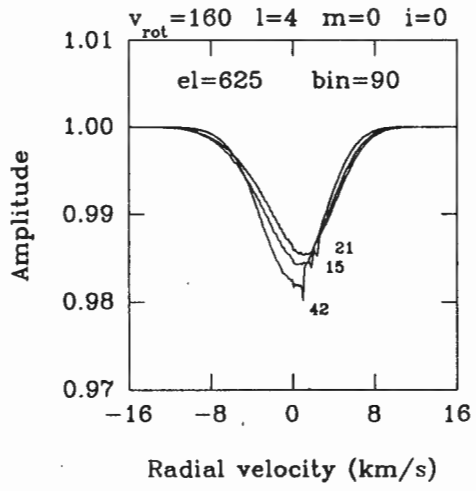
v rot =160 l=4 m=0 i=0
el=625 bin=90
21
15
42
Amplitude
1.01
1.00
0.99
0.98
0.97
−16 −8 0 8 16
Radial velocity (km/s)

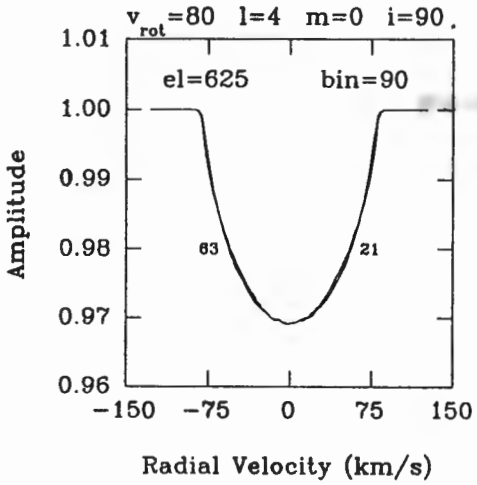
v rot =80 l=4 m=0 i=90
el=625 bin=90
63
21
Amplitude
1.01
1.00
0.99
0.98
0.97
0.96
−150 −75 0 75 150
Radial Velocity (km/s)

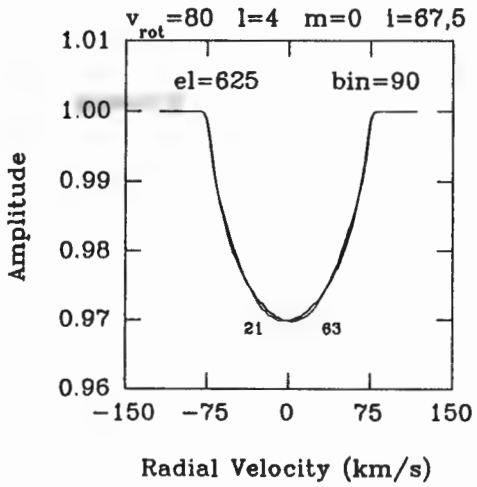
v rot =80 l=4 m=0 i=67,5
el=625 bin=90
21
63
Amplitude
1.01
1.00
0.99
0.98
0.97
0.96
−150 −75 0 75 150
Radial Velocity (km/s)

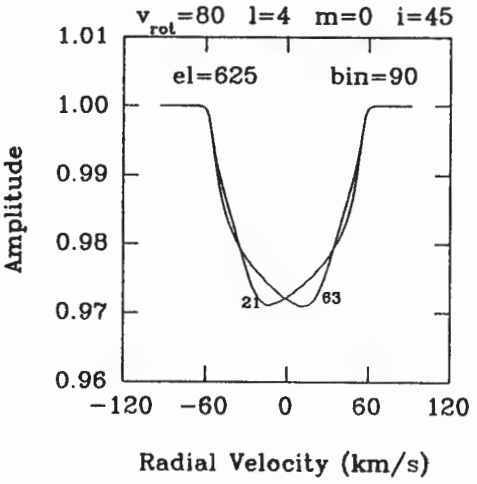
v rot =80 l=4 m=0 i=45
el=625 bin=90
21
63
Amplitude
1.01
1.00
0.99
0.98
0.97
0.96
−120 −60 0 60 120
Radial Velocity (km/s)

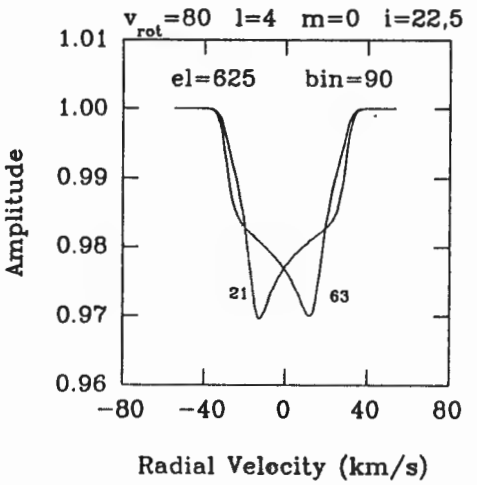
v rot =80 l=4 m=0 i=22,5
el=625 bin=90
21
63
Amplitude
1.01
1.00
0.99
0.98
0.97
0.96
−80 −40 0 40 80
Radial Velocity (km/s)

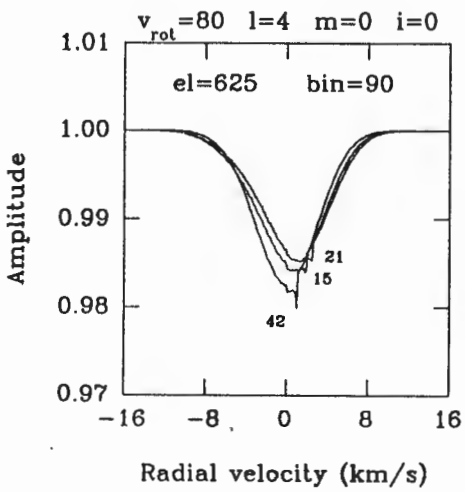
v rot =80 l=4 m=0 i=0
el=625 bin=90
21
15
42
Amplitude
1.01
1.00
0.99
0.98
0.97
−16 −8 0 8 16
Radial velocity (km/s)

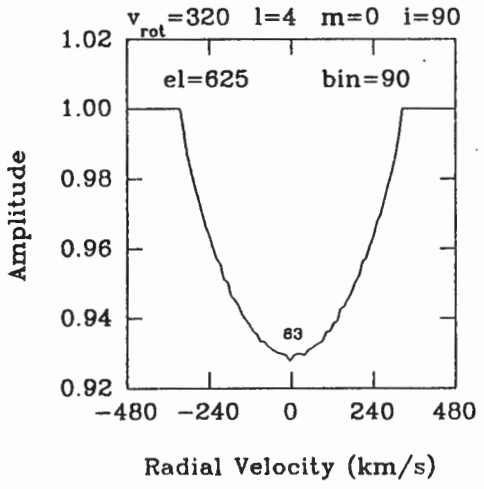
v rot =320 l=4 m=0 i=90
el=625 bin=90
Amplitude
1.02
1.00
0.98
0.96
0.94
0.92
63
−480 −240 0 240 480
Radial Velocity (km/s)

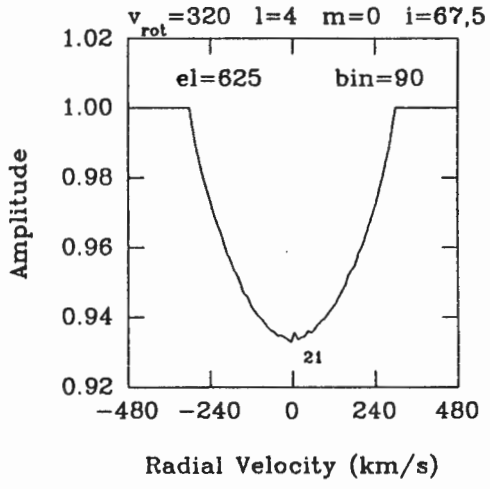
v rot =320 l=4 m=0 i=67,5
el=625 bin=90
Amplitude
1.02
1.00
0.98
0.96
0.94
0.92
21
−480 −240 0 240 480
Radial Velocity (km/s)

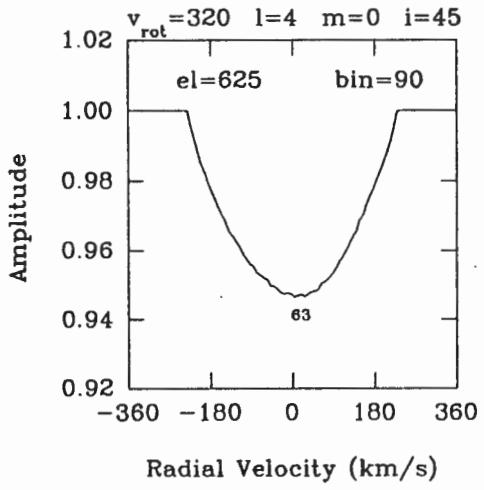
v rot =320 l=4 m=0 i=45
el=625 bin=90
Amplitude
1.02
1.00
0.98
0.96
0.94
0.92
63
−360 −180 0 180 360
Radial Velocity (km/s)

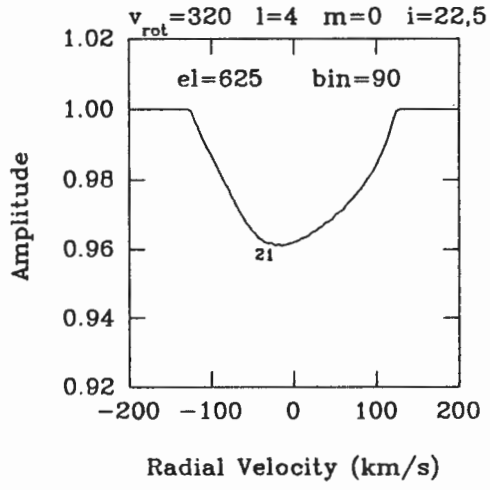
v rot =320 l=4 m=0 i=22,5
el=625 bin=90
Amplitude
1.02
1.00
0.98
0.96
0.94
0.92
21
−200 −100 0 100 200
Radial Velocity (km/s)

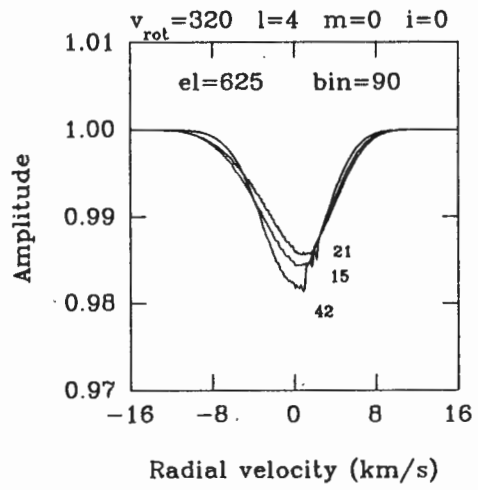
v rot =320 l=4 m=0 i=0
el=625 bin=90
Amplitude
1.01
1.00
0.99
0.98
0.97
21
15
42
−16 −8 0 8 16
Radial velocity (km/s)

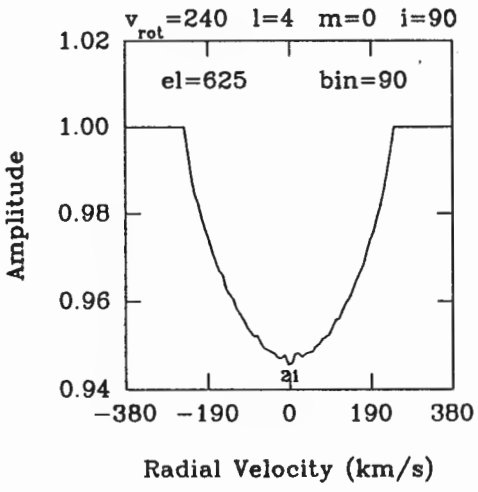
v rot =240 l=4 m=0 i=90
el=625 bin=90
Amplitude
1.02
1.00
0.98
0.96
0.94
21
−380 −190 0 190 380
Radial Velocity (km/s)

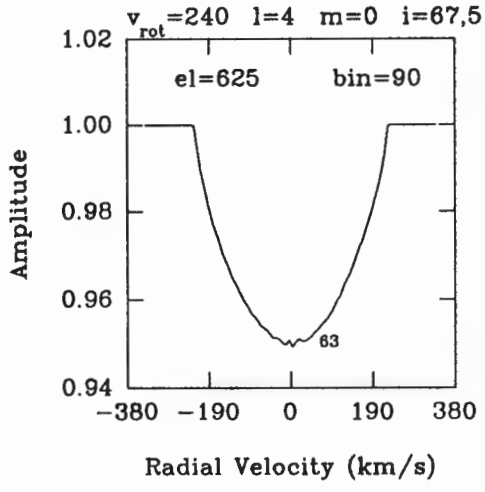
v rot =240 l=4 m=0 i=67,5
el=625 bin=90
Amplitude
1.02
1.00
0.98
0.96
0.94
63
−380 −190 0 190 380
Radial Velocity (km/s)

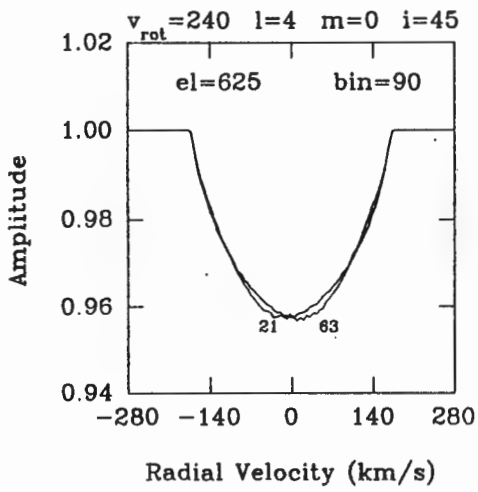
v rot =240 l=4 m=0 i=45
el=625 bin=90
Amplitude
1.02
1.00
0.98
0.96
0.94
21
63
−280 −140 0 140 280
Radial Velocity (km/s)

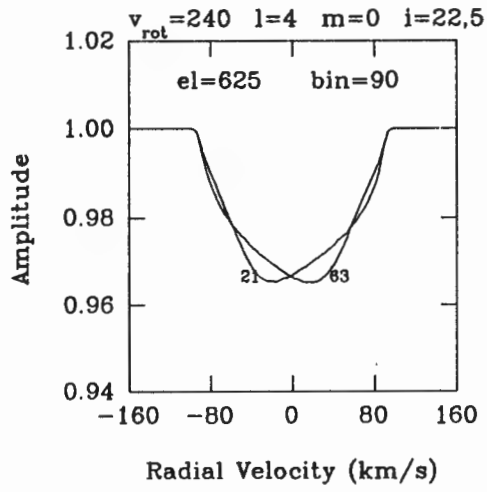
v rot =240 l=4 m=0 i=22,5
el=625 bin=90
Amplitude
1.02
1.00
0.98
0.96
0.94
21
63
−160 −80 0 80 160
Radial Velocity (km/s)

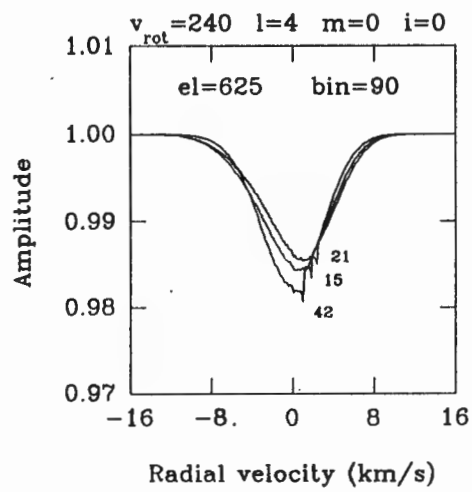
v rot =240 l=4 m=0 i=0
el=625 bin=90
Amplitude
1.01
1.00
0.99
0.98
0.97
21
15
42
−16 −8. 0 8 16
Radial velocity (km/s)

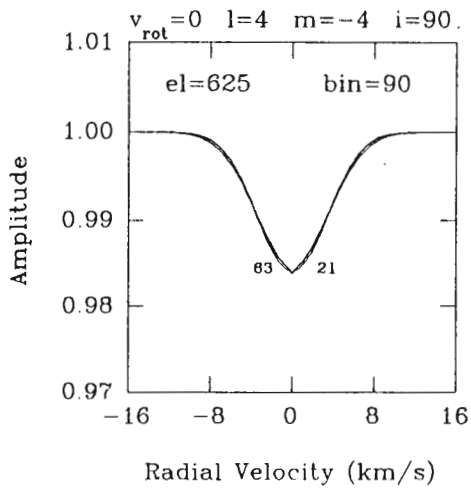
v rot =0 l=4 m=−4 i=90.
el=625 bin=90
63 21
Amplitude
1.01
1.00
0.99
0.98
0.97
−16 −8 0 8 16
Radial Velocity (km/s)

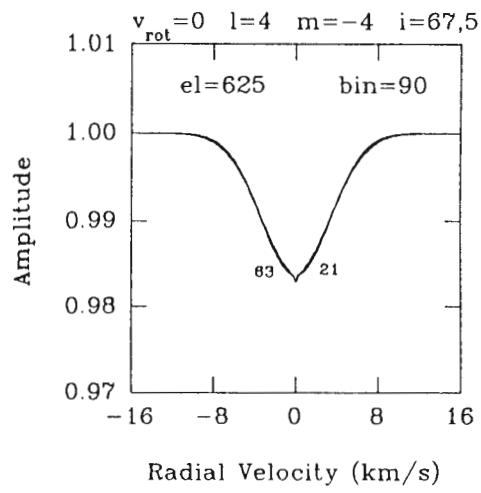
v rot =0 l=4 m=−4 i=67,5
el=625 bin=90
63 21
Amplitude
1.01
1.00
0.99
0.98
0.97
−16 −8 0 8 16
Radial Velocity (km/s)

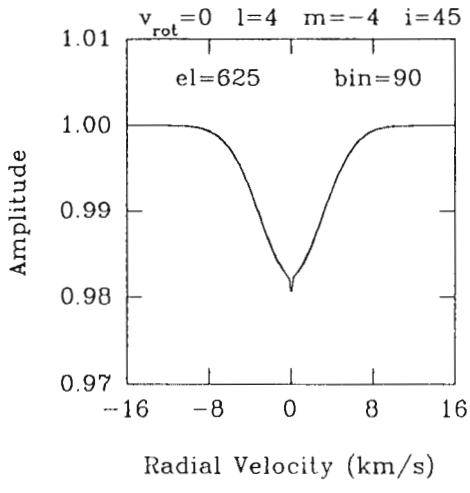
v rot =0 l=4 m=−4 i=45
el=625 bin=90
Amplitude
1.01
1.00
0.99
0.98
0.97
−16 −8 0 8 16
Radial Velocity (km/s)

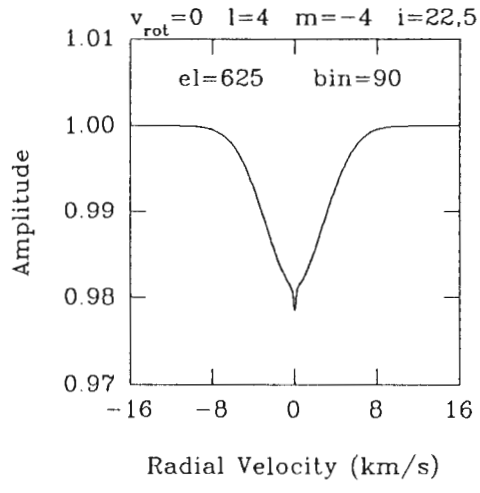
v rot =0 l=4 m=−4 i=22,5
el=625 bin=90
Amplitude
1.01
1.00
0.99
0.98
0.97
−16 −8 0 8 16
Radial Velocity (km/s)

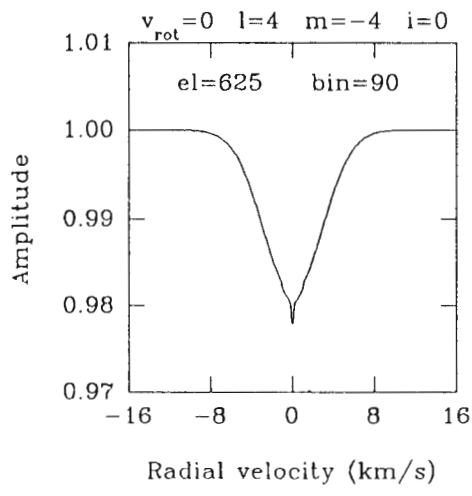
v rot =0 l=4 m=−4 i=0
el=625 bin=90
Amplitude
1.01
1.00
0.99
0.98
0.97
−16 −8 0 8 16
Radial velocity (km/s)

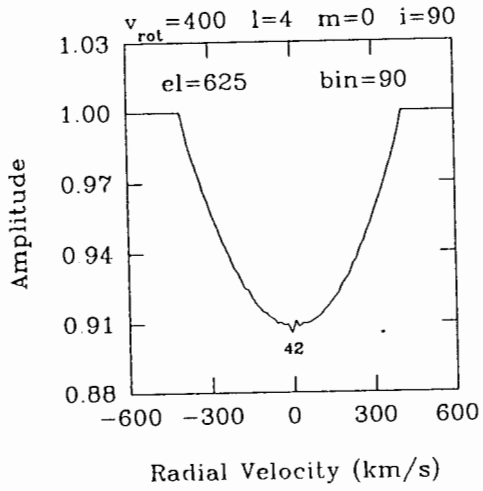
v rot =400 l=4 m=0 i=90
el=625 bin=90
1.03
1.00
0.97
0.94
0.91
0.88
Amplitude
42
−600 −300 0 300 600
Radial Velocity (km/s)

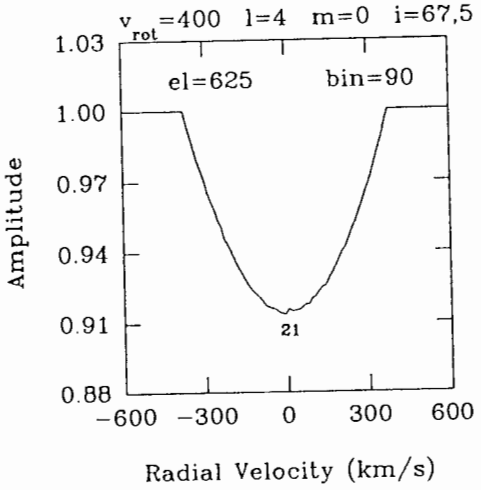
v rot =400 l=4 m=0 i=67,5
el=625 bin=90
1.03
1.00
0.97
0.94
0.91
0.88
Amplitude
21
−600 −300 0 300 600
Radial Velocity (km/s)

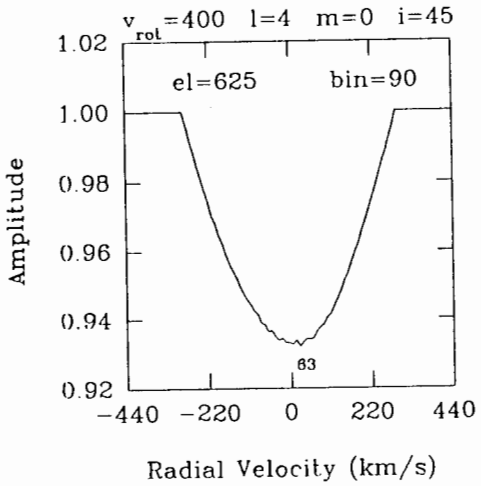
v rot =400 l=4 m=0 i=45
el=625 bin=90
1.02
1.00
0.98
0.96
0.94
0.92
Amplitude
63
−440 −220 0 220 440
Radial Velocity (km/s)

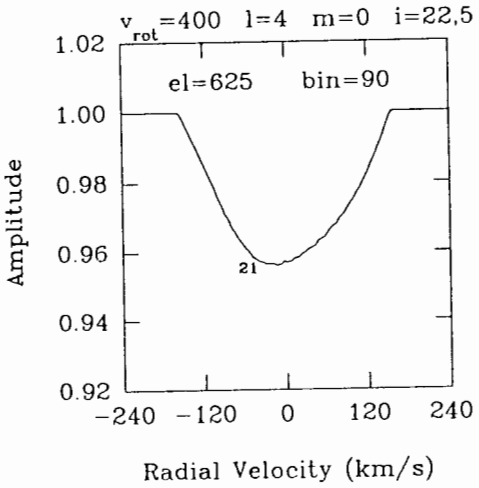
v rot =400 l=4 m=0 i=22,5
el=625 bin=90
1.02
1.00
0.98
0.96
0.94
0.92
Amplitude
21
−240 −120 0 120 240
Radial Velocity (km/s)

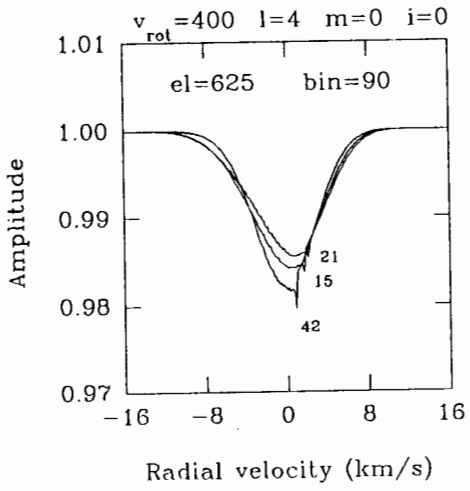
v rot =400 l=4 m=0 i=0
el=625 bin=90
1.01
1.00
0.99
0.98
0.97
Amplitude
21
15
42
−16 −8 0 8 16
Radial velocity (km/s)

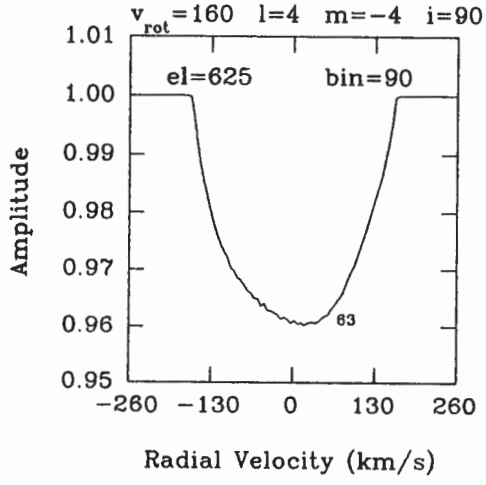
v_rot=160 l=4 m=−4 i=90
el=625 bin=90
63
Amplitude
Radial Velocity (km/s)

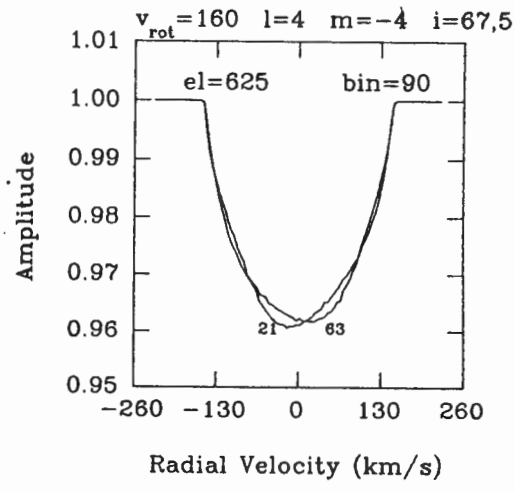
v_rot=160 l=4 m=−4 i=67,5
el=625 bin=90
21
63
Amplitude
Radial Velocity (km/s)

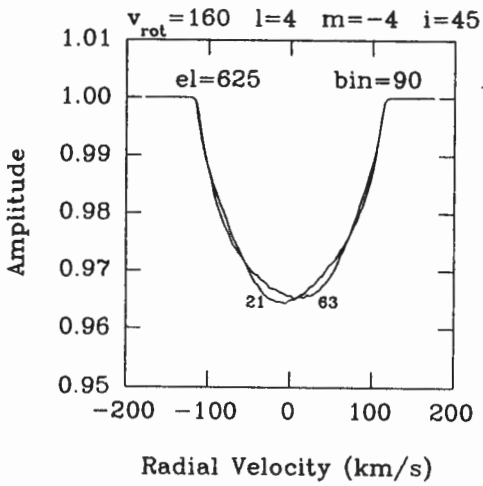
v_rot=160 l=4 m=−4 i=45
el=625 bin=90
21
63
Amplitude
Radial Velocity (km/s)

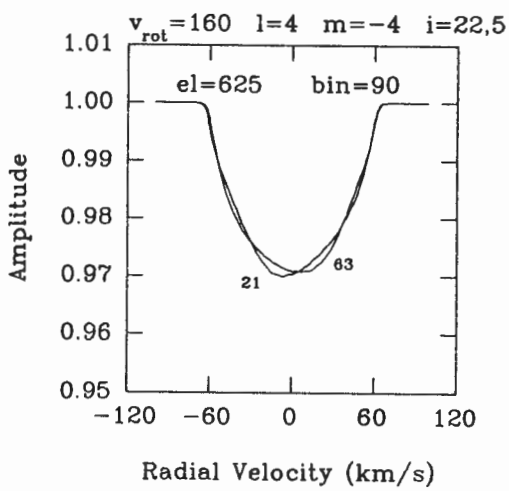
v_rot=160 l=4 m=−4 i=22,5
el=625 bin=90
21
63
Amplitude
Radial Velocity (km/s)

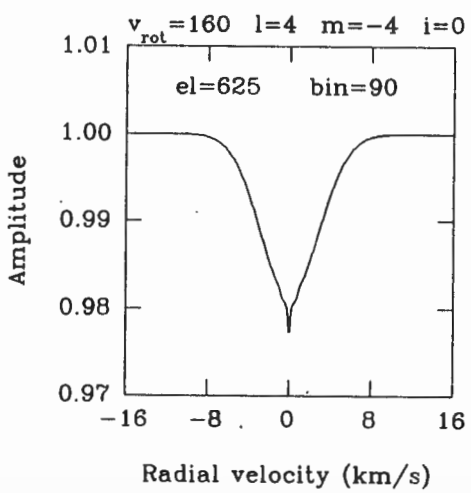
v_rot=160 l=4 m=−4 i=0
el=625 bin=90
Amplitude
Radial velocity (km/s)

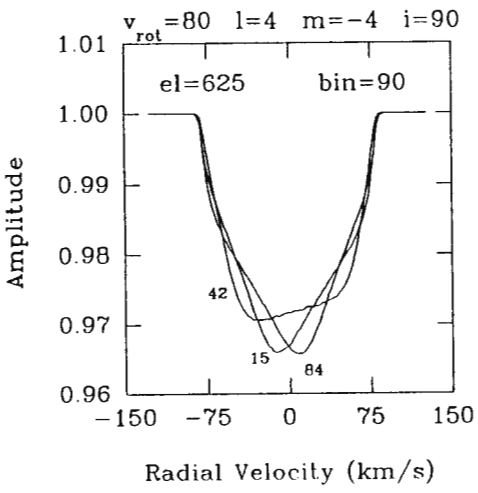
v rot =80 l=4 m=−4 i=90
el=625 bin=90
Amplitude
1.01
1.00
0.99
0.98
0.97
0.96
42
15
84
−150 −75 0 75 150
Radial Velocity (km/s)

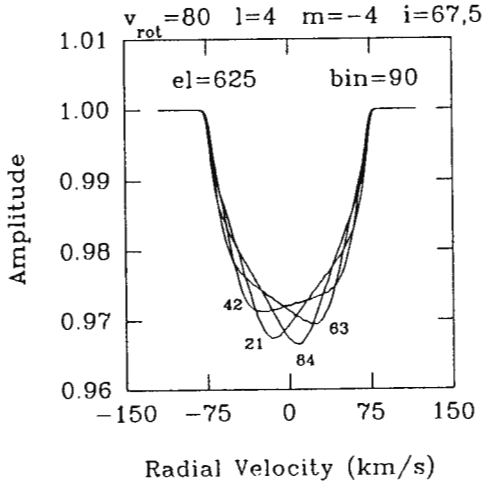
v rot =80 l=4 m=−4 i=67,5
el=625 bin=90
Amplitude
1.01
1.00
0.99
0.98
0.97
0.96
42
21
63
84
−150 −75 0 75 150
Radial Velocity (km/s)

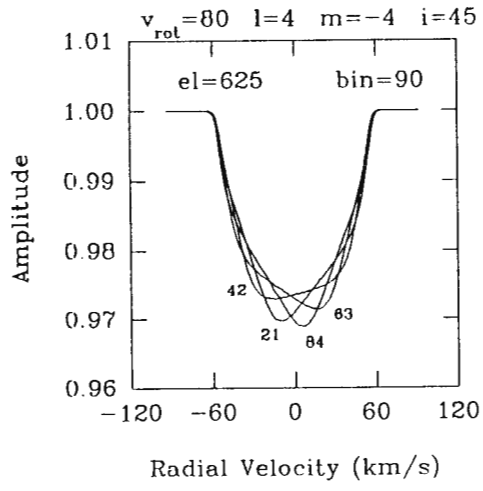
v rot =80 l=4 m=−4 i=45
el=625 bin=90
Amplitude
1.01
1.00
0.99
0.98
0.97
0.96
42
21
63
84
−120 −60 0 60 120
Radial Velocity (km/s)

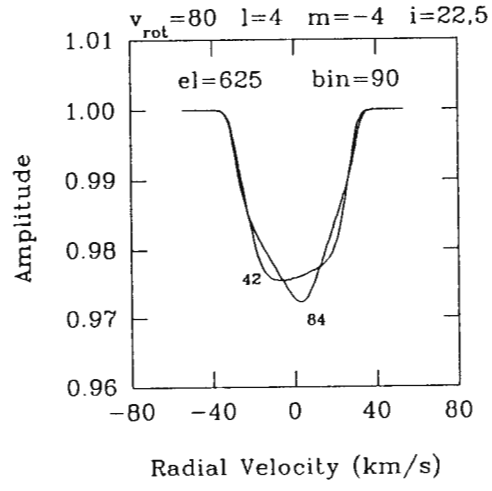
v rot =80 l=4 m=−4 i=22,5
el=625 bin=90
Amplitude
1.01
1.00
0.99
0.98
0.97
0.96
42
84
−80 −40 0 40 80
Radial Velocity (km/s)

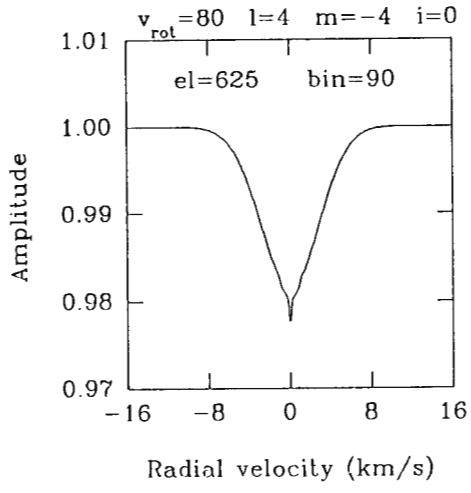
v rot =80 l=4 m=−4 i=0
el=625 bin=90
Amplitude
1.01
1.00
0.99
0.98
0.97
−16 −8 0 8 16
Radial velocity (km/s)

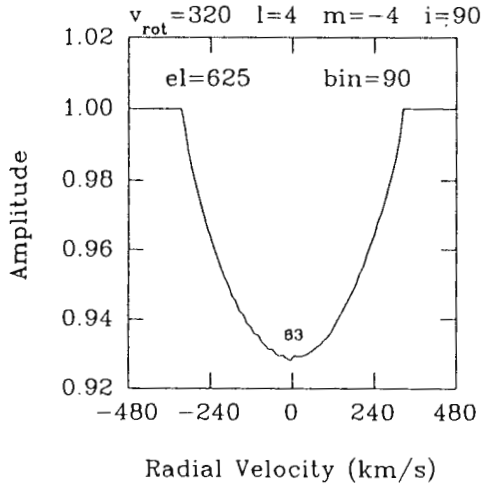
v rot =320 l=4 m=−4 i=90
el=625 bin=90
Amplitude
1.02
1.00
0.98
0.96
0.94
0.92
63
−480 −240 0 240 480
Radial Velocity (km/s)

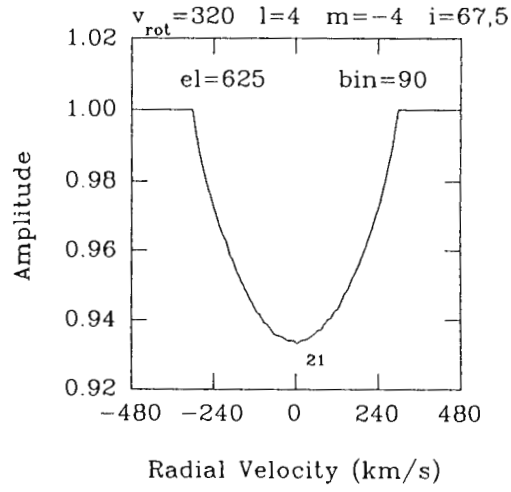
v rot =320 l=4 m=−4 i=67,5
el=625 bin=90
Amplitude
1.02
1.00
0.98
0.96
0.94
0.92
21
−480 −240 0 240 480
Radial Velocity (km/s)

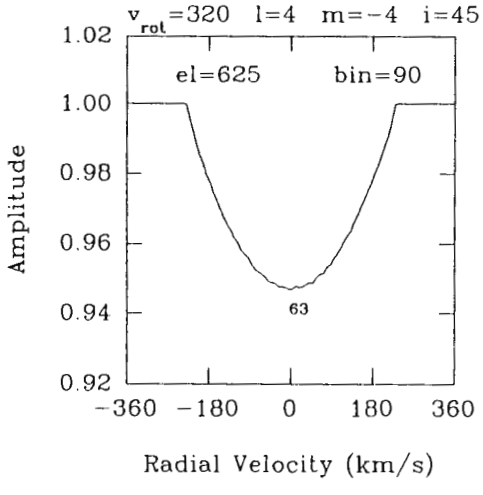
v rot =320 l=4 m=−4 i=45
el=625 bin=90
Amplitude
1.02
1.00
0.98
0.96
0.94
0.92
63
−360 −180 0 180 360
Radial Velocity (km/s)

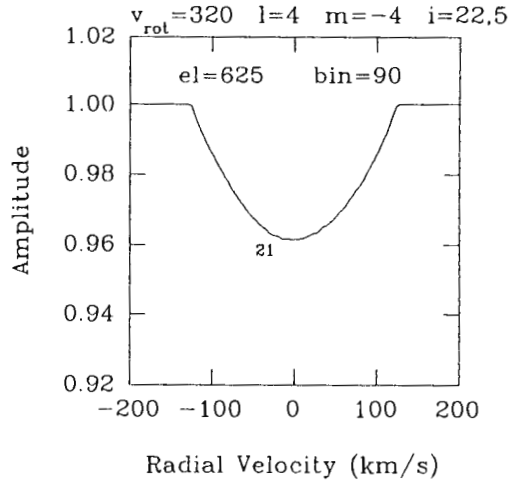
v rot =320 l=4 m=−4 i=22,5
el=625 bin=90
Amplitude
1.02
1.00
0.98
0.96
0.94
0.92
21
−200 −100 0 100 200
Radial Velocity (km/s)

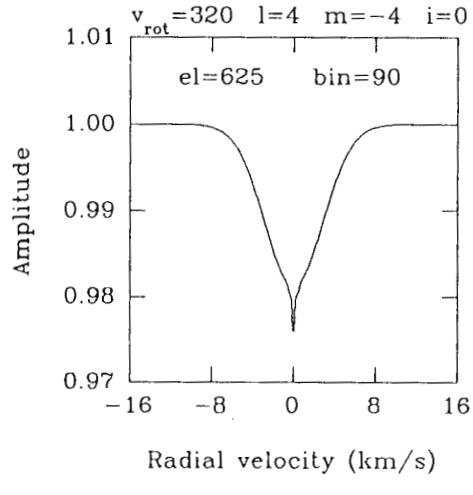
v rot =320 l=4 m=−4 i=0
el=625 bin=90
Amplitude
1.01
1.00
0.99
0.98
0.97
−16 −8 0 8 16
Radial velocity (km/s)

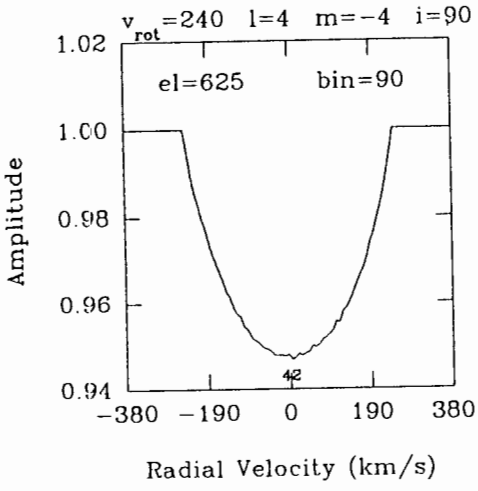
v rot =240 l=4 m=-4 i=90
el=625 bin=90
Amplitude
1.02
1.00
0.98
0.96
0.94
42
-380 -190 0 190 380
Radial Velocity (km/s)

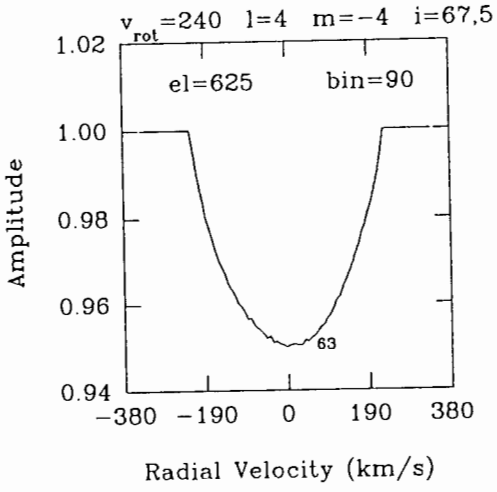
v rot =240 l=4 m=-4 i=67,5
el=625 bin=90
Amplitude
1.02
1.00
0.98
0.96
0.94
63
-380 -190 0 190 380
Radial Velocity (km/s)

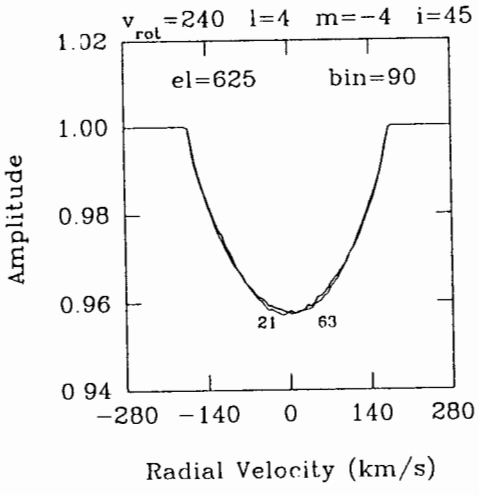
v rot =240 l=4 m=-4 i=45
el=625 bin=90
Amplitude
1.02
1.00
0.98
0.96
0 94
21 63
-280 -140 0 140 280
Radial Velocity (km/s)

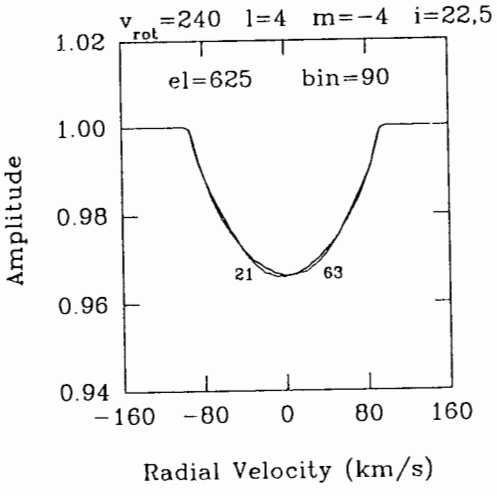
v rot =240 l=4 m=-4 i=22,5
el=625 bin=90
Amplitude
1.02
1.00
0.98
0.96
0.94
21 63
-160 -80 0 80 160
Radial Velocity (km/s)

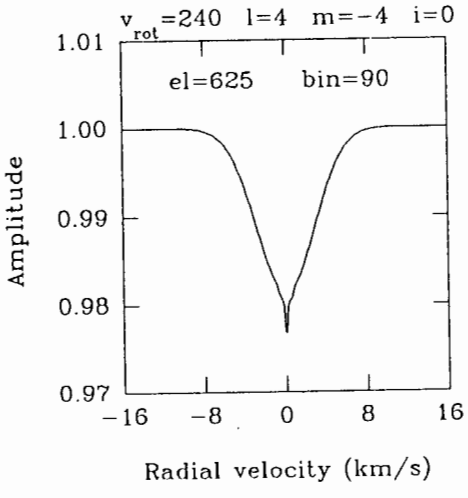
v rot =240 l=4 m=-4 i=0
el=625 bin=90
Amplitude
1.01
1.00
0.99
0.98
0.97
-16 -8 0 8 16
Radial velocity (km/s)

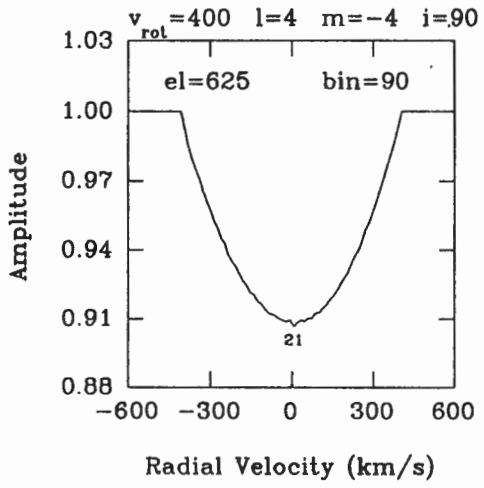
v rot =400 l=4 m=−4 i=90
el=625 bin=90
1.03
1.00
0.97
0.94
0.91
0.88
21
−600 −300 0 300 600
Amplitude
Radial Velocity (km/s)

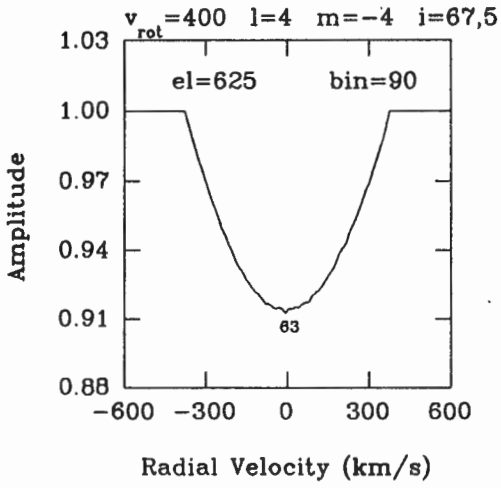
v rot =400 l=4 m=−4 i=67,5
el=625 bin=90
1.03
1.00
0.97
0.94
0.91
0.88
63
−600 −300 0 300 600
Amplitude
Radial Velocity (km/s)

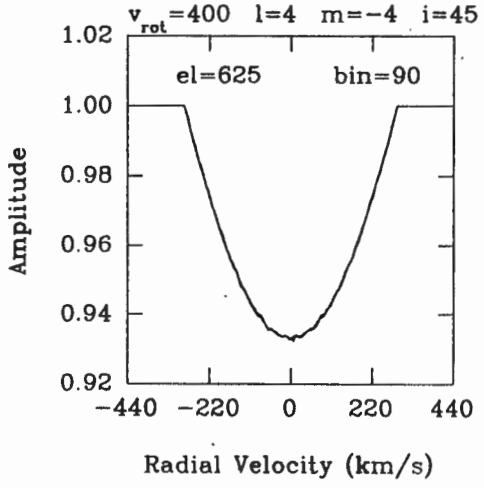
v rot =400 l=4 m=−4 i=45
el=625 bin=90
1.02
1.00
0.98
0.96
0.94
0.92
−440 −220 0 220 440
Amplitude
Radial Velocity (km/s)

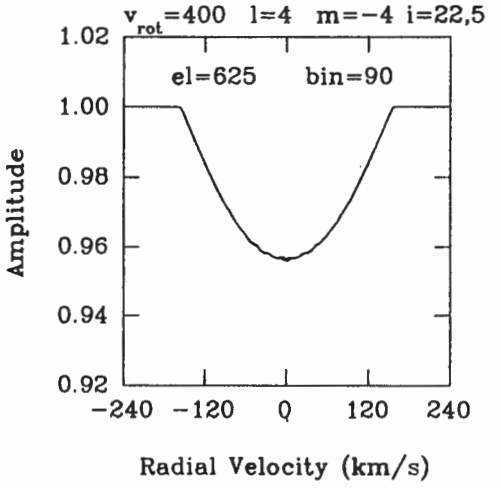
v rot =400 l=4 m=−4 i=22,5
el=625 bin=90
1.02
1.00
0.98
0.96
0.94
0.92
−240 −120 0 120 240
Amplitude
Radial Velocity (km/s)

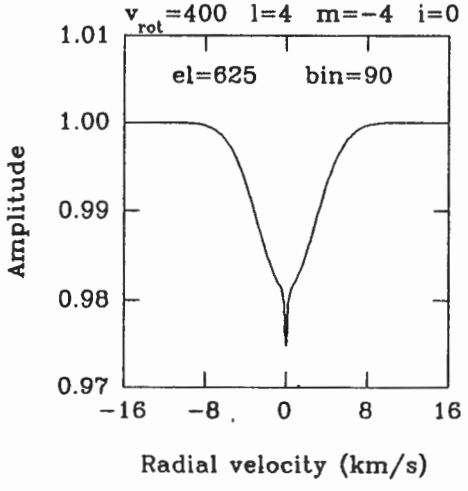
v rot =400 l=4 m=−4 i=0
el=625 bin=90
1.01
1.00
0.99
0.98
0.97
−16 −8 0 8 16
Amplitude
Radial velocity (km/s)

```
*
*
*       PROGRAM RPBSTAR
*
*       THIS PROGRAM CALCULATES LIGHT CURVES, RADIAL VELOCITY
*       CURVES AND SPECTRAL LINE PROFILES FOR MODELS OF
*       NONRADIALLY OSCILLATING, ROTATING BETA CEPHEI STARS
*
*
*     .
      IMPLICIT REAL*8 (A-H,O-Z)
      REAL*8 VROTER(10), C1TAB(5), C2TAB(10), UNPERT(5,11), BIN(91)
      REAL*8 VCOUNT(90), BINMID(90)
      PARAMETER(PI=3.14159265D0)
      PARAMETER(IBIN=90)
      DATA VROTER/6.4D-4,2.54D-3,5.71D-3,1.05D-2,1.6D-2,2.33D-2,
     +  3.2D-2,4.24D-2,5.46D-2,6.89D-2/
      DATA C1TAB/0.0D0,3.0D-2,1.5D-1,1.2D-1,1.0D-1/
      DATA C2TAB/-6.4D0,0.0D0,-1.5D0,-3.5D0,-3.4D0,-1.2D0,-4.8D0,
     +  -0.73D0,-6.0D0,-0.7D0/
      DATA E,GIR,GIRP,GIH,GIHP,GAM2,OMND2,WAVLGT,UN/5.0D-3,0.0D0,0.0D0,
     + 0.0D0,0.0D0,1.66666667D0,17.9D0,4.2D-7,0.4D0/
      DATA IVROT,L,M,DFRQ,INCT,INCANG,RADIUS/80,8,-8,6.D0,36,250,5.D6/
      OPEN(60,FILE='/u/engelca/litxp288')
      OPEN(62,FILE='/u/engelca/prfxp288')
*
*
*     INITIAL DEFINITIONS AND ASSIGNMENTS
*
*
      TEMPER=21100.D0
      H1=1.0D0-UN
      H2=UN
      C1=C1TAB(L+1)
      IC21=2*L+1
      IC22=IC21+1
      XM2=M*M
      C2=C2TAB(IC21)+C2TAB(IC22)*XM2
      FP=L*(L+1)/OMND2-4.0D0-OMND2
      BBX=1.4388D-2/(WAVLGT*TEMPER)
      FT=(GAM2-1.0D0)*FP/GAM2
      BBODY=BBX*DEXP(BBX)/(DEXP(BBX)-1.0D0)
      FLC=BBODY*FT
      OMEGAZ=2.0D0*PI*DFRQ/8.64D4
      COMEGA=IVROT/5.0D6
      OMP=(C1-1.0D0)*COMEGA*M
      OMPP=(COMEGA*COMEGA)*C2/OMEGAZ
      OMEGA=OMEGAZ+OMP+OMPP
      OMRATO=COMEGA/OMEGAZ
      VOTERM=(-VOMEGA)-COMEGA*M
      IEREL=IVROT/40
      IF(IVROT.NE.0)ER=VROTER(IEREL)
      IF(IVROT.EQ.0)ER=0.0D0
      ER2=ER*ER
      ER3=ER*ER2
      ER4=ER*ER3
      ER5=ER*ER4
      EP=E*(0.2D0)*2.D0*M*OMRATO
      EH=0.558D-1*E
      EHP=EH*(0.2D0)*2.D0*M*OMRATO
      IFCLMM=IFAC(L-M)
      IFCLPM=IFAC(L+M)
      TNLM=DSQRT((2.0D0*L+1.D0)/(4.0D0*PI)*IFCLMM/IFCLPM)*(-1)**M
      TNLM2=TNLM*TNLM
```

APPENDIX 3

This appendix contains the Fortran code developed to calculate the observable characteristics of a rotating β Cephei star, as discussed in chapter 7, as well as the code used to model thermal broadening into the calculated spectral line profiles, as discussed in chapter 9.

```
      CPHO2=CPHO*CPHO
      CTH=(-SAI)*STHO*SPHO-CAI*CTHO
      STH2=CAI2*STHO2*SPHO2+SAI2*CTHO2-2.D0*SAI*CAI*CTHO*
     +   STHO*SPHO+STHO2*CPHO2
      STH=DSQRT(STH2)
      CPH=STHO*CPHO/STH
      SPH=(SAI*CTHO-CAI*STHO*SPHO)/STH
      OBSR=SAI*STH*SPH-CAI*CTH
      OBST=SAI*CTH*SPH+CAI*STH
      OBSP=SAI*CPH
      P20=1.5D0*CTH*CTH-0.5D0
      P202=P20*P20
      P203=P202*P20
      P204=P203*P20
      P205=P204*P20
      DP20=-3.0D0*STH*CTH
      DP202=DP20*DP20
      AIX=PI-AI
*
      TPLM=POLG(L,M,CTH,STH)*ECEPCP(M,CPH,SPH,E,EP,OMEGA,T,GIR,
     +                              GIRP)
      TPLMS=POLG(L,M,CTH,STH)*ESEPSP(M,CPH,SPH,E,EP,OMEGA,T,
     +                               GIR,GIRP)
      TDPLM=DPOLG(L,M,CTH,STH)*ECEPCP(M,CPH,SPH,E,EP,OMEGA,T,
     +                                GIR,GIRP)
      PLM2=(POLG(L,M,CTH,STH))**2*(2.0D0*E*EP*((CMP(M,CPH,SPH)*
     +       CMP(M,CPH,SPH)-SMP(M,CPH,SPH)*SMP(M,CPH,SPH))*
     +       DCOS(2.D0*OMEGA*T+GIR+GIRP)-2.D0*SMP(M,CPH,SPH)*
     +       CMP(M,CPH,SPH)*DSIN(2.D0*OMEGA*T+GIR+GIRP))+E*E*
     +       ((CMP(M,CPH,SPH)*
     +       CMP(M,CPH,SPH)-SMP(M,CPH,SPH)*SMP(M,CPH,SPH))*
     +       DCOS(2.D0*OMEGA*T+2.0D0*GIR)-2.D0*SMP(M,CPH,SPH)*
     +       CMP(M,CPH,SPH)*DSIN(2.D0*OMEGA*T+2.D0*GIR))+EP*EP*
     +       ((CMP(M,CPH,SPH)*
     +       CMP(M,CPH,SPH)-SMP(M,CPH,SPH)*SMP(M,CPH,SPH))*
     +       DCOS(2.D0*OMEGA*T+2.D0*GIRP)-2.D0*SMP(M,CPH,SPH)*
     +       CMP(M,CPH,SPH)*DSIN(2.D0*OMEGA*T+2.D0*GIRP)))
      PLMS2=(POLG(L,M,CTH,STH))**2*(2.0D0*E*EP*(2.D0*SMP(M,CPH,
     +SPH)*CMP(M,CPH,SPH)*DCOS(2.D0*OMEGA*T+GIR+GIRP)+(CMP(M,
     +CPH,SPH)*CMP(M,CPH,SPH)-SMP(M,CPH,SPH)*SMP(M,CPH,SPH))*
     +DSIN(2.D0*OMEGA*T+GIR+GIRP))+E*E*(2.D0*SMP(M,CPH,
     +SPH)*CMP(M,CPH,SPH)*DCOS(2.D0*OMEGA*T+2.D0*GIR)+(CMP(M,
     +CPH,SPH)*CMP(M,CPH,SPH)-SMP(M,CPH,SPH)*SMP(M,CPH,SPH))*
     +DSIN(2.D0*OMEGA*T+2.D0*GIR))+EP*EP*(2.D0*SMP(M,CPH,
     +SPH)*CMP(M,CPH,SPH)*DCOS(2.D0*OMEGA*T+2.D0*GIRP)+(CMP(M,
     +CPH,SPH)*CMP(M,CPH,SPH)-SMP(M,CPH,SPH)*SMP(M,CPH,SPH))*
     +DSIN(2.D0*OMEGA*T+2.D0*GIRP)))
      VPLMS=TPLMS
      VPLMSH=POLG(L,M,CTH,STH)*ESEPSP(M,CPH,SPH,EH,EHP,OMEGA,T,
     +                                GIH,GIHP)
      VPLMS0=POLG(L,M,CTH,STH)*ESIN(M,CPH,SPH,E,OMEGA,T,GIR)
      VPLSH0=POLG(L,M,CTH,STH)*ESIN(M,CPH,SPH,EH,OMEGA,T,GIH)
      VPLMH=POLG(L,M,CTH,STH)*ECEPCP(M,CPH,SPH,EH,EHP,OMEGA,T,
     +                               GIH,GIHP)
      VPLM0=POLG(L,M,CTH,STH)*ECOS(M,CPH,SPH,E,OMEGA,T,GIR)
      VPLMH0=POLG(L,M,CTH,STH)*ECOS(M,CPH,SPH,EH,OMEGA,T,GIH)
      DPLMSH=DPOLG(L,M,CTH,STH)*ESEPSP(M,CPH,SPH,EH,EHP,OMEGA,
     +                                 T,GIH,GIHP)
      DPLSH0=DPOLG(L,M,CTH,STH)*ESIN(M,CPH,SPH,EH,OMEGA,T,GIH)
      DPLMH0=DPOLG(L,M,CTH,STH)*ECOS(M,CPH,SPH,EH,OMEGA,T,GIH)
*
*
*     FLUX TERM
*
```

```
      BINT1=DBLE(IBIN/2)
      BINT2=DBLE(IBIN)
      BINT3=BINT2/1.5D0
*
*
*     DEFINE INITIAL VALUES AND INCREMENTS OF ITERATION VARIABLES
*
*
      AI=(9.0D1)*PI/1.8D2
      AIINT=PI/8.0
      TINT=2.4*PI/(OMEGA*INCT)
      THINT=PI/INCANG
      PHINT=PI/INCANG
*
*
*     DETERMINE RANGE AND START ITERATIONS
*
*
      ILIMTH=INCANG/2
      ILIMPH=2*INCANG
      GIRD=GIR*1.8D2/PI
      GIRPD=GIRP*1.8D2/PI
      WRITE(60,1000)IVROT,DFRQ,INCT*10/12,INCANG**2,E,GIRD,GIRPD,TEMPER,
     +  OMND2,UN,EP,EH,EHP,GIH,GIHP,IBIN
        IANGI=1
        DO 100 I=1,5
          VSINI=DSIN(AI)*IVROT
          DO 80 I5=1,IBIN+1
            IF(IVROT.NE.0)BIN(I5)=1.5D0*VSINI*((I5-1)/BINT1-1.D0)
            IF(IVROT.EQ.0)BIN(I5)=0.6D1*((I5-1)/BINT1-1.D0)
            IF(DSIN(AI).LT.1.D-1)BIN(I5)=0.6D1*((I5-1)/BINT1-1.D0)
   80   CONTINUE
        IF(IVROT.NE.0)BININC=1.5D0/BINT2*VSINI
        IF(IVROT.EQ.0)BININC=0.6D1/BINT2
        IF(DSIN(AI).LT.1.D-1)BININC=0.6D1/BINT2
        DO 85 I6=1,IBIN
          BINMID(I6)=BIN(I6)+BININC
   85   CONTINUE
        AIDEG=1.8D2-AI*1.8D2/PI
        WRITE(60,1005)L,M,AIDEG
        UNPRTL=2.724368D0
        T=0.0D0
        ITIME=1
        SAI=DSIN(AI)
        CAI=DCOS(AI)
        SAI2=SAI*SAI
        CAI2=CAI*CAI
        DO 110 I1=1,INCT
          XLUMT=0.D0
          VRADT=0.D0
          TH=0.0D0+0.5*THINT
          DO 90 IV=1,IBIN
            VCOUNT(IV)=0.D0
   90     CONTINUE
          DO 120 I2=1,ILIMTH
            PH=0.0D0+0.5*PHINT
            STHO=DSIN(TH)
            CTHO=DCOS(TH)
            STHO2=STHO*STHO
            CTHO2=CTHO*CTHO
            DO 130 I3=1,ILIMPH
              SPHO=DSIN(PH)
              CPHO=DCOS(PH)
              SPHO2=SPHO*SPHO
```

```
*     VARIATION IN B MAGNITUDE
*
*
          XMAGN=-1.08574*DLOG(XLUMT/UNPRTL)
          WRITE(60,1020)T,XMAGN,VRADT*UNPRTL/XLUMT
          IF(ITIME.EQ.7)THEN
            DO 115 IW=1,IBIN
              WRITE(62,1025)BINMID(IW),1.0D0-(VCOUNT(IW))/XLUMT
  115       CONTINUE
          ENDIF
          XMAGN=0.0D0
          T=T+TINT
          ITIME=ITIME+1
          IF(ITIME.EQ.8)ITIME=1
  110   CONTINUE
        AI=AI+AIINT
        IANGI=IANGI+1
  100 CONTINUE
 1000 FORMAT(' ',20X,'LTEXP: OUTPUT OF ALLEXP.F'//' ROTATION SPEED: ',
     + I3,' KM/S',5X,'PULSATION FREQUENCY: ',F6.3,' CYCLES PER DAY'/
     + ' NUMBER OF POINTS IN ONE CYCLE: ',I3,5X,'NUMBER OF AREA ELEMENTS
     +: ',I5/' RADIAL PULSATION AMPLITUDE: ',F6.4,5X,'PULSATION PHASE: '
     + ,F6.3,5X/' PHASE OF ROTATIONAL CORRECTION: ',F6.3,5X,
     + 'TEMPERATURE: ',F8.1/' DIMENSIONLESS FREQUENCY SQUARED: ',
     + F7.3,5X,'LIMB-DARKENING COEFF: ',F5.3/' EP: ',F8.5,5X,'EH: ',
     + F8.5,5X,'EHP: ',F8.5,5X/' HORIZONTAL PULSATION PHASE: ',F6.3,
     + 5X,'PHASE OF ROT. CORRECTION: ',F6.3/' NUMBER OF BINS: ',I3///
     + ' ',3X,'TIME',7X,'MAGNITUDE VARIATION',5X,'RADIAL VELOCITY'/)
 1005 FORMAT(' '/' ',25X,'(L =',I2,3X,'M =',I3,3X,'INCLINATION ANGLE=',
     +F7.2,')'/)
 1020 FORMAT(' ',F10.3,5X,E14.7,5X,E14.7)
 1025 FORMAT(' ',F12.7,5X,E14.7)
      END
*
*
*     FUNCTION SUBROUTINES:
*
*
*
*     POLG(NEW)
*
*
      REAL*8 FUNCTION POLG(L,M,CTH,STH)
      IMPLICIT REAL*8 (A-H, O-Z)
      IF(L.EQ.0.AND.M.EQ.0)POLG=1.0D0
      IF(L.EQ.1.AND.M.EQ.-1)POLG=STH*(-0.5D0)
      IF(L.EQ.1.AND.M.EQ.0)POLG=CTH
      IF(L.EQ.1.AND.M.EQ.1)POLG=STH
      IF(L.EQ.2.AND.M.EQ.-2)POLG=0.125D0*STH**2
      IF(L.EQ.2.AND.M.EQ.-1)POLG=STH*CTH*(-0.5D0)
      IF(L.EQ.2.AND.M.EQ.0)POLG=1.5D0*CTH**2-0.5D0
      IF(L.EQ.2.AND.M.EQ.1)POLG=3.0D0*STH*CTH
      IF(L.EQ.2.AND.M.EQ.2)POLG=3.0D0*STH**2
      IF(L.EQ.3.AND.M.EQ.-3)POLG=STH**3*(-1.0D0/48.0D0)
      IF(L.EQ.3.AND.M.EQ.-2)POLG=CTH*STH**2*0.125D0
      IF(L.EQ.3.AND.M.EQ.-1)POLG=(5.0D0*CTH**2-1.0D0)*STH*(-0.125D0)
      IF(L.EQ.3.AND.M.EQ.0)POLG=2.5D0*CTH**3-1.5D0*CTH
      IF(L.EQ.3.AND.M.EQ.1)POLG=1.5D0*(5.0D0*CTH**2-1.0D0)*STH
      IF(L.EQ.3.AND.M.EQ.2)POLG=1.5D1*CTH*STH**2
      IF(L.EQ.3.AND.M.EQ.3)POLG=1.5D1*STH**3
      IF(L.EQ.4.AND.M.EQ.-4)POLG=(1.0D0/384.0D0)*STH**4
      IF(L.EQ.4.AND.M.EQ.-3)POLG=(-1.0D0/48.0D0)*STH**3*CTH
      IF(L.EQ.4.AND.M.EQ.-2)POLG=(1.0D0/48.0D0)*STH**2*(7.0D0*
     +  CTH**2-1.0D0)
```

```
*
            FLUX=1.0D0+FLC*(TNLM*TPLM-ER*P20)
*
*
*     LIMB-DARKENING TERM
*
*
            DARCX1=1.0D0+ER*2.0D0*P20+ER2*(3.0D0*P202-0.5D0*DP202)+
     +        ER3*(2.0D0*P203-3.0*P20*DP202)+ER4*P204*(-76.5D0)
     +        -2.0D0*TNLM*TPLM+ER*TNLM*(-6.0D0*P20*TPLM+DP20*
     +        TDPLM)+ER3*TNLM*3.6D2*P203*TPLM+ER5*1.35D2*P205
            DARCX2=TNLM2*PLM2
            DARCPX=DARCX1-DARCX2*XM2/STH2
            H31=((1.0D0+2.0D0*TNLM*TPLM)*(1.0D0-2.0D0*ER*P20)+ER2*
     +        P202)*OBSR
            H32=(ER*DP20-TNLM*TDPLM-ER2*P20*DP20+ER*TNLM*(P20*TDPLM+
     +        DP20*TPLM))*OBST
            H33=(TNLM*TPLMS*(1.0D0-ER*P20)+TNLM2*PLMS2)*OBSP*M
            HTOT=H1+H2*DARCPX*(H31+H32+H33)
*
*
*     PROJECTED SURFACE AREA TERM
*
*
            PSA=(H31+H32+H33)*STHO*THINT*PHINT
*
*
*     TOTAL LUMINOSITY TERM
*
*
             XLUM=DABS(FLUX*HTOT*PSA)
             XLUMT=XLUMT+XLUM
*
*
*     RADIAL VELOCITY
*
*
             VRR=RADIUS*TNLM*(VOTERM*VPLMS+COMEGA*M*VPLMSH-XM2*COMEGA*
     +         OMRATO*C1*VPLSH0-2.D0*COMEGA*OMRATO*STH*(STH*VPLMS0+CTH*
     +         DPLSH0))
             VRT=RADIUS*TNLM*(VOTERM*(DPLMSH-2.D0*M*OMRATO*C1*DPLSH0+
     +         2.D0*M*OMRATO*CTH/STH*VPLSH0)+COMEGA*M*CTH/STH*(VPLMSH-
     +         2.D0*M*OMRATO*C1*VPLSH0)+2.D0*COMEGA*OMRATO*CTH*(STH*
     +         VPLMS0+CTH*DPLSH0))
             VRP=RADIUS*TNLM*VOTERM*(M/STH*(VPLMH-2.D0*OMRATO*M*C1*
     +         VPLMH0)+2.D0*OMRATO*(STH*VPLM0+CTH*DPLMH0))+RADIUS*
     +         COMEGA*STH
             VRAD=VRR*OBSR+VRT*OBST+VRP*OBSP
             VRADW=VRAD*XLUM/UNPRTL
             VRADT=VRADT+VRADW
             IF(ITIME.EQ.7)THEN
               DO 140 I4=1,IBIN
                 IF(VRAD.GT.BIN(I4).AND.VRAD.LE.BIN(I4+1))VCOUNT(I4)=
     +             VCOUNT(I4)+XLUM
  140          CONTINUE
             ENDIF
             XLUM=0.0D0
             VRAD=0.D0
             PH=PH+PHINT
  130      CONTINUE
           TH=TH+THINT
  120    CONTINUE
*
*
```

```
      IF(IX.LE.2)GO TO 510
      IFAC=IX
      ITEL=IX-2
      DO 500 IB=1,ITEL
        IFAC=IFAC*(IX-IB)
  500 CONTINUE
 1100 FORMAT(' ',5X,'YOU ARE ATTEMPTING TO CALCULATE THE FACTORIAL OF A
     +  NEGATIVE NUMBER'/)
  510 END
*
*
*     TRIGONOMETRIC FUNCTIONS
*
*
*
      REAL*8 FUNCTION ECEPCP(M,CPH,SPH,A,B,X,T,G,GP)
      IMPLICIT REAL*8 (A-H,O-Z)
      ECEPCP=A*(CMP(M,CPH,SPH)*DCOS(X*T+G)-SMP(M,CPH,SPH)*DSIN(X*T+G))
     +    +B*(CMP(M,CPH,SPH)*DCOS(X*T+GP)-SMP(M,CPH,SPH)*DSIN(X*T+GP))
      END
*
      REAL*8 FUNCTION ESEPSP(M,CPH,SPH,A,B,X,T,G,GP)
      IMPLICIT REAL*8 (A-H,O-Z)
      ESEPSP=A*(SMP(M,CPH,SPH)*DCOS(X*T+G)+CMP(M,CPH,SPH)*DSIN(X*T+G))
     +  +B*(SMP(M,CPH,SPH)*DCOS(X*T+GP)+CMP(M,CPH,SPH)*DSIN(X*T+GP))
      END
*
      REAL*8 FUNCTION ECOS(M,CPH,SPH,A,X,T,G)
      IMPLICIT REAL*8 (A-H,O-Z)
      ECOS=A*(CMP(M,CPH,SPH)*DCOS(X*T+G)-SMP(M,CPH,SPH)*DSIN(X*T+G))
      END
*
      REAL*8 FUNCTION ESIN(M,CPH,SPH,A,X,T,G)
      IMPLICIT REAL*8 (A-H,O-Z)
      ESIN=A*(SMP(M,CPH,SPH)*DCOS(X*T+G)+CMP(M,CPH,SPH)*DSIN(X*T+G))
      END
*
      REAL*8 FUNCTION CMP(M,CPH,SPH)
      IMPLICIT REAL*8 (A-H,O-Z)
      IF(M.EQ.0)CMP=1.0D0
      IF(M.EQ.1)CMP=CPH
      IF(M.EQ.-1)CMP=CPH
      IF(M.EQ.2)CMP=CPH**2-SPH**2
      IF(M.EQ.-2)CMP=CPH**2-SPH**2
      IF(M.EQ.3)CMP=4.0D0*CPH**3-3.0D0*CPH
      IF(M.EQ.-3)CMP=4.0D0*CPH**3-3.0D0*CPH
      IF(M.EQ.4)CMP=8.0D0*(CPH**4-CPH**2)+1.0D0
      IF(M.EQ.-4)CMP=8.0D0*(CPH**4-CPH**2)+1.0D0
      IF(M.EQ.-7)CMP=6.4D1*CPH**7-1.12D2*CPH**5+5.6D1*CPH**3-7.0D0*CPH
      IF(M.EQ.-8)CMP=1.28D2*CPH**8-2.56D2*CPH**6+1.6D2*CPH**4-3.2D1*
     +               CPH**2+1.0D0
      END
*
      REAL*8 FUNCTION SMP(M,CPH,SPH)
      IMPLICIT REAL*8 (A-H,O-Z)
      IF(M.EQ.0)SMP=0.0D0
      IF(M.EQ.1)SMP=SPH
      IF(M.EQ.-1)SMP=(-SPH)
      IF(M.EQ.2)SMP=2.0D0*SPH*CPH
      IF(M.EQ.-2)SMP=(-2.0D0*SPH*CPH)
      IF(M.EQ.3)SMP=3.0D0*SPH-4.0D0*SPH**3
      IF(M.EQ.-3)SMP=(-3.0D0*SPH+4.0D0*SPH**3)
      IF(M.EQ.4)SMP=4.0D0*SPH*CPH-8.0D0*SPH**3*CPH
      IF(M.EQ.-4)SMP=(-4.0D0*SPH*CPH+8.0D0*SPH**3*CPH)
```

```
      IF(L.EQ.4.AND.M.EQ.-1)POLG=-0.125D0*STH*(7.0D0*CTH**3
     +  -3.0D0*CTH)
      IF(L.EQ.4.AND.M.EQ.0)POLG=0.125D0*(35.0D0*CTH**4-30.0D0*
     +  CTH**2+3.0D0)
      IF(L.EQ.4.AND.M.EQ.1)POLG=0.5D0*STH*(35.0D0*CTH**3-15.0D0*CTH)
      IF(L.EQ.4.AND.M.EQ.2)POLG=7.5D0*STH**2*(7.0D0*CTH**2-1.0D0)
      IF(L.EQ.4.AND.M.EQ.3)POLG=105.0D0*STH**3*CTH
      IF(L.EQ.4.AND.M.EQ.4)POLG=105.0D0*STH**4
      IF(L.EQ.8.AND.M.EQ.-8)POLG=(1.0D0/10321920.0D0)*STH**8
      IF(L.EQ.8.AND.M.EQ.-7)POLG=(-1.0D0/322560.0D0)*STH**7*CTH
      END
*
*
*     DPOLG
*
*
      REAL*8 FUNCTION DPOLG(L,M,CTH,STH)
      IMPLICIT REAL*8 (A-H, O-Z)
      IF(L.EQ.0.AND.M.EQ.0)DPOLG=0.0D0
      IF(L.EQ.1.AND.M.EQ.-1)DPOLG=CTH*(-0.5D0)
      IF(L.EQ.1.AND.M.EQ.0)DPOLG=-STH
      IF(L.EQ.1.AND.M.EQ.1)DPOLG=CTH
      IF(L.EQ.2.AND.M.EQ.-2)DPOLG=0.25D0*STH*CTH
      IF(L.EQ.2.AND.M.EQ.-1)DPOLG=0.5D0*(STH**2-CTH**2)
      IF(L.EQ.2.AND.M.EQ.0)DPOLG=(-3.0D0)*CTH*STH
      IF(L.EQ.2.AND.M.EQ.1)DPOLG=3.0D0*(CTH**2-STH**2)
      IF(L.EQ.2.AND.M.EQ.2)DPOLG=6.0D0*STH*CTH
      IF(L.EQ.3.AND.M.EQ.-3)DPOLG=STH**2*CTH*(-1.0D0/16.0D0)
      IF(L.EQ.3.AND.M.EQ.-2)DPOLG=0.25D0*CTH**2*STH-0.125D0*STH**3
      IF(L.EQ.3.AND.M.EQ.-1)DPOLG=1.25D0*CTH*STH**2-0.625D0*CTH**3+
     +                     0.125D0*CTH
      IF(L.EQ.3.AND.M.EQ.0)DPOLG=1.5D0*STH-7.5D0*CTH**2*STH
      IF(L.EQ.3.AND.M.EQ.1)DPOLG=7.5D0*CTH**3-15.0D0*CTH*STH**2-
     +                    1.5D0*CTH
      IF(L.EQ.3.AND.M.EQ.2)DPOLG=3.0D1*STH*CTH**2-1.5D1*STH**3
      IF(L.EQ.3.AND.M.EQ.3)DPOLG=4.5D1*STH**2*CTH
      IF(L.EQ.4.AND.M.EQ.-4)DPOLG=(1.0D0/9.6D1)*STH**3*CTH
      IF(L.EQ.4.AND.M.EQ.-3)DPOLG=(1.0D0/4.8D1)*STH**4-(1.0D0/1.6D1)*
     +                     STH**2*CTH**2
      IF(L.EQ.4.AND.M.EQ.-2)DPOLG=(7.0D0/2.4D1)*(STH*CTH**3-CTH*
     +                     STH**3)-(1.0D0/2.4D1)*STH*CTH
      IF(L.EQ.4.AND.M.EQ.-1)DPOLG=0.875D0*(3.0D0*CTH**2*STH**2-CTH**4)
     +                     +0.375D0*(CTH**2-STH**2)
      IF(L.EQ.4.AND.M.EQ.0)DPOLG=7.5D0*CTH*STH-1.75D1*CTH**3*STH
      IF(L.EQ.4.AND.M.EQ.1)DPOLG=1.75D1*(CTH**4-3.0D0*CTH**2*STH**2)+
     +                    7.5D0*(STH**2-CTH**2)
      IF(L.EQ.4.AND.M.EQ.2)DPOLG=1.05D2*(STH*CTH**3-CTH*STH**3)-1.5D1*
     +                    STH*CTH
      IF(L.EQ.4.AND.M.EQ.3)DPOLG=1.05D2*(3.0D0*STH**2*CTH**2-STH**4)
      IF(L.EQ.4.AND.M.EQ.4)DPOLG=4.2D2*STH**3*CTH
      IF(L.EQ.8.AND.M.EQ.-8)DPOLG=(1.0D0/1.290240D6)*STH**7*CTH
      IF(L.EQ.8.AND.M.EQ.-7)DPOLG=(1.0D0/322560.0D0)*STH**8-
     +                     (1.0D0/4.6080D4)*STH**6*CTH**2
      END
*
*
*     IFAC
*
*
      INTEGER FUNCTION IFAC(IX)
      IF(IX.LT.0)WRITE(*,1100)
      IF(IX.EQ.0)IFAC=1
      IF(IX.EQ.1)IFAC=1
      IF(IX.EQ.2)IFAC=2
```

```
*
*
*       PROGRAM CONVOL
*
*       THIS PROGRAM CONVOLVES SPECTRAL LINE PROFILE OUTPUT
*       FROM PROGRAM RPBSTAR WITH A GAUSSIAN THERMAL
*       BROADENING PROFILE
*
*
      IMPLICIT REAL*8 (A-H,O-Z)
      REAL*8 SPEED(2250),AMP(2250),ACNT(2250),XNORM(2250),ACNTX(25,75),
     +   ACNTY(25,75),SPEEDX(25,75),SPEEDY(25,75),INUM(25)
      PARAMETER(PI=3.14159265D0)
      OPEN(50,FILE='/u/engelca/pnfxp430')
      OPEN(51,FILE='/u/engelca/pgnfx430')
      ROOTPI=DSQRT(PI)
      DO 95 MX=1,25
        DO 96 MY=1,75
              ACNTX(MX,MY)=0.0D0
 96     CONTINUE
 95   CONTINUE
      DO 97 MV=1,25
        DO 98 MW=1,75
              ACNTY(MV,MW)=0.0D0
 98     CONTINUE
 97   CONTINUE
      DO 100 I=1,25
         DO 110 J=1,90
            JI=90*(I-1)+J
            READ(50,1000)SPEED(JI),AMP(JI)
            ACNT(JI)=0.0D0
110      CONTINUE
         VINT=SPEED(JI-1)-SPEED(JI-2)
         IX=9.0D0/VINT
         INUM(I)=IX
         DO 112 LX=1,IX
            SPEEDX(I,LX)=SPEED(90*(I-1)+1)-9.0D0+VINT*(LX-1)
            SPEEDY(I,LX)=SPEED(90*I)+VINT*LX
112      CONTINUE
         DO 120 JJ=1,90
            JI=90*(I-1)+JJ
            XNORM(JI)=0.25D0*(1.0D0-AMP(JI))*VINT/ROOTPI
            JK=90*I
            DO 125 K=JI,JK
               DSPEED=(SPEED(K)-SPEED(JI))/4.0D0
               DSPD2=DSPEED*DSPEED
              IF(DSPEED.LT.16.0D0)ACNT(K)=ACNT(K)+XNORM(JI)/DEXP(DSPD2)
125         CONTINUE
            JL=90*(I-1)+1
            DO 130 L=JL,JI
               DSPEED=(SPEED(JI)-SPEED(L))/4.0D0
               DSPD2=DSPEED*DSPEED
              IF(DSPEED.LT.16.0D0)ACNT(L)=ACNT(L)+XNORM(JI)/DEXP(DSPD2)
130         CONTINUE
            DO 127 LA=1,IX
               DSPEED=(SPEEDX(I,LA)-SPEED(JI))/4.0D0
               DSPD2=DSPEED*DSPEED
              IF(DSPEED.LT.16.0D0)ACNTX(I,LA)=ACNTX(I,LA)+XNORM(JI)/
     +          DEXP(DSPD2)
               DSPEED=(SPEEDY(I,LA)-SPEED(JI))/4.0D0
               DSPD2=DSPEED*DSPEED
              IF(DSPEED.LT.16.0D0)ACNTY(I,LA)=ACNTY(I,LA)+XNORM(JI)/
     +          DEXP(DSPD2)
127         CONTINUE
```

```
 IF(M.EQ.-7)SMP=(-6.4D1)*(CPH**6*SPH-CPH**4*SPH)-1.2D1*CPH**2*
+      SPH+5.0D0*SPH-2.0D1*SPH**3+1.6D1*SPH**5
 IF(M.EQ.-8)SMP=(1.6D2*CPH**5-1.28D2*CPH**7-5.6D1*CPH**3+1.6D1*
+                CPH)*SPH+(3.2D1*SPH**5-4.0D1*SPH**3)*CPH
 END
```

```
120      CONTINUE
100   CONTINUE
      DO 133 I=1,25
         DO 135 J=1,INUM(I)
            WRITE(51,1010)SPEEDX(I,J),1.0D0-ACNTX(I,J)
135      CONTINUE
         DO 136 JJ=90*(I-1)+1,90*I
            WRITE(51,1010)SPEED(JJ),1.0D0-ACNT(JJ)
136      CONTINUE
         DO 138 JK=1,INUM(I)
            WRITE(51,1010)SPEEDY(I,JK),1.0D0-ACNTY(I,JK)
138   CONTINUE
133   CONTINUE
1000  FORMAT(' ',F12.7,5X,E14.7)
1010  FORMAT(' ',F12.7,5X,E14.7)
      END
```

HAGAR THE HORRIBLE — by Dik Browne

In emulation of CK